Enhancing Mine Subsidence Prediction and Control Methodologies for Long-term Landscape Stability.

Final Report

Submitted to

OSMRE, Pittsburgh Center

By

Dr. Michael Karmis,
Stonie Barker Professor, Department of Mining and Minerals Engineering & Director,
Virginia Center for Coal and Energy Research
Virginia Tech

and

Dr. Zacharias Agioutantis, Ph.D.

Blacksburg, Virginia

March 2009

Table of Contents

1. Executive Summary 10
2. Introduction and Objectives 10
3. Approach 11
4. Objective I: Develop and Improve Subsidence Engineering Parameters 13
4.1 Review of Previous Research 13
4.2 Implemented Methodology 14
4.3 Validation of Method 14
4.4 Case Studies 16
4.4.1 NA-1 Case Study (Northern Appalachia) 16
4.4.2 NA-2 Case Study (Northern Appalachia) 19
4.4.3 NA-3 Case Study (Northern Appalachia) 24
4.4.4 IL-1 Case Study (Illinois) 30
4.4.5 IL-2 Case Study (Illinois) 36
4.4.6 AL-1 Case Study (Alabama) 40
4.5 Discussion 44
5. Objective II: Improve Prediction Methodologies 46
5.1 Modeling the Dynamic Deformations 46
5.1.1 Basic Concepts 46
5.1.2 Implemented Methodology 51
5.1.3 Validation of Method 54
5.1.4 NA-2 Dynamic Case Study (Northern Appalachia) 55
5.1.5 IL-1 Dynamic Subsidence Case Study (Illinois/Indiana) 65
5.1.6 Discussion 71
5.1.7 Other Dynamic Deformation Indices 72
5.2 Subsidence Prediction in Areas of Steeply Sloping Terrain/Steeply Dipping Seams 73
5.2.1 Review of Previous Research 73
5.2.2 Subsidence in Steeply Sloping Terrain 74
5.2.3 Subsidence over Steeply Dipping Seams 79
5.2.4 Implemented Methodology 80
5.2.5 Validation of Method 82
5.2.6 Discussion 84
5.3 Improvement of Calibration Procedures 85
5.3.1 Review of Previous Research 85
5.3.2 Implemented Methodology 88
5.3.3 Validation of Method 88
5.3.4 NA-2 Calibration Case Study (N. Appalachia) - Transverse Line 88
5.3.5 NA-2 Calibration Case Study (N. Appalachia) - Longitudinal Line 91
5.3.6 NA-1 Calibration Case Study (N. Appalachia) 93
5.3.7 Location Angles 95
5.3.8 Discussion 95
6. Objective III: Apply subsidence methodology for landscape stability and control 99
6.1 Previous Research 99

6.2 Deformation and Damage 99
6.3 Classification of Damage 101
6.4 Damage Prediction 104
6.5 Mitigation of Expected Damage 105
7. Objective IV: Assess long-term stability 107
7.1 Assessing Long-term Landscape Stability 107
7.1.1 Phases of Mining-Induced Deformation 107
7.1.2 Prediction and Assessment of Long-term Landscape Stability 109
7.1.3 Mechanisms Affecting Long-Term Stability 113
7.2 Implemented Methodology 116
7.3 Validation of Method 119
7.4 Discussion 126
8. Objective V: To disseminate project results 128
8.1 Awareness of the engineering and regulatory community 128
8.2 Project Showcase 128
8.3 Progress Meeting 128
8.4 Project Presentation 128
8.5 Paper presentation 128
8.6 Short Course to OSM personnel 129
9. Summary of Deliverables 130
9.1 Detailed project report 130
9.2 Software Enhancements 130
9.3 Updated User's Guide 131
9.4 Updated online Help File 131
9.5 Resource Files 131
9.5 Short Course Material 131
10. Recommendations 133
11. References 135

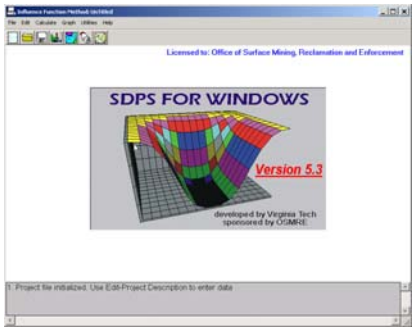

List of Figures

Figure 1: Mine plan and prediction point locations for NA-1 Case Study 16
Figure 2: Graphical display of predicted and measured subsidence profiles after calibration 18
Figure 3: Original scanned image of mine plan showing panel, transverse monitoring line, and longitudinal monitoring line. Mining progressed from left to right (Coal mine in Northern Appalachia, reprinted with company permission, mine location and company name confidential).....20
Figure 4: Mine plan and monitoring points for transverse and longitudinal lines as imported into SDPS. 20
Figure 5: Transverse Line - matched predicted and measured subsidence profiles 23
Figure 6: Longitudinal Line – matched predicted and measured subsidence profiles 23
Figure 7: Scanned image of hand-drawn version of Panel 1 North with digitized panel and points. The monitoring points are located along a road above the mine. 25
Figure 8: Scanned image of hand-drawn version of Panel 3 North with digitized panel and points. 25
Figure 9: Panel 1 North – Mine plan and prediction point locations in SDPS.....26
Figure 10: Panel 3 North – Mine plan and prediction point locations in SDPS. Note use of variable edge effect. 26
Figure 11: Panel 1 North - matched predicted and measured subsidence profiles 29
Figure 12: Panel 3 North - matched predicted and measured subsidence profiles 29
Figure 13: Monument Line 5 - Scanned image of mine map with digitized panels and points. The map was retrieved from company information (The American Coal Company, Galatia Mine, Harrisonburg, Illinois) submitted to the Illinois Department of Natural Resources, Office of Mines and Minerals for permit application in 1989. 31
Figure 14: Monument Line 6 - Scanned image of mine map with digitized panels and points. The map was retrieved from company information (The American Coal Company, Galatia Mine, Harrisonburg, Illinois) submitted to the Illinois Department of Natural Resources, Office of Mines and Minerals for permit application in 1989. 31
Figure 15: Monument Line 5 - Mine plan and prediction point locations in SDPS 32
Figure 16: Monument Line 6 - Mine plan and prediction point locations in SDPS 32
Figure 17: Monument Line 5 - matched predicted and measured subsidence profiles 34
Figure 18: Monument Line 6 – matched predicted and measured subsidence profiles 35

Figure 19: IL-2 Case Study Pin Line 1 - Scanned image of mine map with digitized panels and points. (Coal mine in Illinois, reprinted with company permission, mine location and company name confidential).....37
Figure 20: Pin Line 1 - Mine plan and prediction point locations in SDPS 37
Figure 21: Matched predicted and measured subsidence profiles.....39
Figure 22: Scanned image of mine map with digitized panels and points. The map was provided to Dr. Michael Karmis of the Center for Coal and Energy Research at Virginia Polytechnic and State University by Jim Walter Resources (#5 Mine, East Brookwood, Alabama, 2001) 41
Figure 23: Mine plan and prediction point locations in SDPS.....41
Figure 24: Matched predicted and measured subsidence profiles.....43
Figure 25: Dynamic subsidence as a moving “wave” accompanied by both tensile and compressive strains (after Geddes and Cooper, 1962). 47
Figure 26: Expected subsidence of a surface point over time as a mine face progresses toward, underneath, and past the point. Image modified from National Coal Board (1975). 47
Figure 27: Jarosz, et al. (1990) confirmed three phases of subsidence development and produced a conceptual subsidence development plot. Image modified from Jarosz, et al. (1990). 48
Figure 28: In 1957, Wardell demonstrated a “consistent travelling ground strain profile” for dynamic subsidence. Image modified from Wardell (1957) in Whittaker and Reddish (1989). 50
Figure 29: Comparison of predicted dynamic subsidence for same point with varying advance rates.....53
Figure 30: Monitoring points used for dynamic prediction-measured subsidence comparison. Mine map base from coal mine in Northern Appalachia.....55
Figure 31: Representation of mine panel with edge effect and dynamic subsidence prediction point. 56
Figure 32: NA-2 Dynamic Case Study - SDPS Project Description Screen.....57
Figure 33: NA-2 Dynamic Case Study – Dynamic Options Screen.....57
Figure 34: NA-2 Dynamic Case Study – Prediction Points Management Screen58
Figure 35: NA-2 Dynamic Case Study – Subsidence Development Data.....58
Figure 36: NA-2 Dynamic Case Study – Surface Deformation Development Calculation Screen.....59
Figure 37: Comparison of dynamic subsidence prediction with measured subsidence values at Point 0 60
Figure 38: Dynamic subsidence prediction using a 37 ft/day average advance rate 61
Figure 39: Dynamic subsidence prediction using a 19 ft/day average advance rate 62
Figure 40: Comparison of dynamic subsidence prediction with measured subsidence values for Points 0 through 750E.....65
Figure 41: Map showing Point 1P-1 on Monument Line 5. Mine map from The American Coal Company, Galatia Mine, Harrisonburg, Illinois, submitted to the Illinois Department of Natural Resources, Office of Mines and Minerals for permit application in 1989.....66

Figure 42: IL-1 Dynamic Case Study – SDPS Project Description Screen 67
Figure 43: IL-1 Dynamic Case Study – Dynamic Options Screen.....68
Figure 44: IL-1 Dynamic Case Study – Prediction Points Management Screen .68
Figure 45: IL-1 Dynamic Case Study – Subsidence Development Data.....69
Figure 46: Representation of mine panel with edge effect and dynamic subsidence prediction point. 69
Figure 47: Comparison of dynamic subsidence prediction with measured subsidence values at Point 1P-1.....71
Figure 48: Dynamic and final strain prediction. Red line corresponds to the end of main phase of subsidence development.....73
Figure 49: Components of horizontal strain and ground strain in sloping terrain 81
Figure 50: Contoured map of horizontal strain and subsidence over the end of synthesized mine panel. Horizontal strain contours assume a threshold value of 1.5 x 10^{-3}. 83
Figure 51: Contoured map of ground strain and subsidence over the end of synthesized mine panel. Horizontal strain contours assume a threshold value of 1.5 x 10^{-3}. Note the more pronounced upslope migration of tensile ground strain due to the steeply-sloping topography (as compared to horizontal strain in previous Figure).....83
Figure 52: Combination of contoured ground strain and horizontal strain maps, with subsidence. 84
Figure 53: NA-2 - Transverse Line - Graphical display of predicted and measured subsidence profiles after calibration.....89
Figure 54: NA-2 - Transverse Line - Graphical display of predicted and measured strain profiles after calibration.....90
Figure 55: Longitudinal Line - Graphical display of predicted and measured subsidence profiles after calibration.....91
Figure 56: Longitudinal Line - Graphical display of predicted and measured strain profiles after calibration.....92
Figure 57: Graphical display of predicted and measured subsidence profiles after calibration 93
Figure 58: NA-1 Case Study - Graphical display of predicted and measured strain profiles after calibration.....94
Figure 59: Definition of characteristics angles 95
Figure 60: Calculation of the Location Angle 97
Figure 61: Two-dimensional representation of differences in components used to calculate horizontal strain and ground strain.....117
Figure 62: Plan view of grid pattern used to calculate ground strain at one point (red) in three-dimensional space. Ground strain at each point in a grid is calculated by taking into account all adjacent points. 118
Figure 63: Risk assessment map showing combination of predicted horizontal and ground strain with surface structures. 120
Figure 64: Basic illustration of risk-based analysis showing high-risk zones resulting from “worst case” scenario of collapse of all weakened pillars. Zones of tension and compression exceeding a threshold strain value of 1.5 x 10^{-3} are labeled. A predicted subsidence contour of -0.05 feet is also

shown. 121
Figure 65: Map illustrating the position of the previously mined section in relation to the boundary of planned surface development (reprinted with company permission, mine location and company name confidential).....122
Figure 66: Contoured threshold values (in this case, 1.5 x 10^{-3}) of horizontal and ground strain expected considering a “worst case” scenario of collapse of all existing pillars. 123
Figure 67: Map showing combination of threshold strain values and boundary of planned surface development. High-risk zones are those where overlap occurs. 123
Figure 68: Vector map indicating the direction of predicted horizontal surface point movement as a result of subsidence.....124
Figure 69: Layout and contoured values for example comparison of predicted ground strain values with predicted subsidence values for various seam depths.....125
Figure 70: Example comparison of predicted ground strain values with predicted subsidence values for various seam depths. A threshold strain value of 1.5 x 10^{-3} is indicated to provide an estimate of the “threshold” subsidence value. 126
Figure 71: Booth at ASMR meeting in Richmond, VA, June 2008. 129
Figure 72: Access to the Resource File menu 131

List of Tables

Table 1: NA-1 Case Study, measured subsidence values 17
Table 2: Calibration parameters for NA-1 Case Study 18
Table 3: Measured Subsidence Values for NA-2 Case Study, Transverse Line .21
Table 4: Measured Subsidence Values for NA-2 Case Study, Longitudinal Line 21
Table 5: Transverse Line - calibration parameters.....23
Table 6: Longitudinal Line - calibration parameters 24
Table 7: Panel 1 North - Measured subsidence values.....27
Table 8: Panel 3 North - Measured subsidence values.....28
Table 9: Panel 1 North – calibration parameters.....29
Table 10: Panel 3 North - calibration parameters.....30
Table 11: Monument Line 5 – Measured Subsidence Note – Reverse numbering matches numbering on SDPS mine plan 32
Table 12: Monument Line 6 – Measured Subsidence.....33
Table 13: Monument Line 5 - calibration parameters.....35
Table 14: Monument Line 6 - calibration parameters.....35
Table 15: Measured subsidence data for Pin Line 1 38
Table 16: Calibration parameters.....39
Table 17: Measured subsidence values.....42
Table 18: Calibration parameters.....43
Table 19: Average advance rate calculations using all available data 60
Table 20: Average advance rate calculations after elimination of highest and

lowest estimated advance rates....62
Table 21: Measured dynamic subsidence values and distances between mine face and surface points....64
Table 22: Measured dynamic subsidence values and distances between mine face and surface points....70
Table 23: Transverse Line - Calibration parameters....89
Table 24: NA-2 Transverse Line – Calibration parameters....90
Table 25: Comparison of subsidence – strain calibration parameters for NA-2 - Transverse Line....90
Table 26: Longitudinal Line – Calibration parameters....91
Table 27: Longitudinal Line - Calibration parameters....92
Table 28: Comparison of subsidence – strain calibration parameters for NA-2 – Longitudinal Line....93
Table 29: Calibration parameters....94
Table 30: NA-1 Case Study - Calibration parameters....94
Table 31: Comparison of subsidence – strain calibration parameters for NA-1 case study line....95
Table 32: Classification of damage caused by subsidence-related horizontal ground movements by Orchard, presented in Geddes and Cooper (1962)101
Table 33: National Coal Board classification of subsidence damage based on strain and building length....102
Table 34: Comparison and combination of damage classification schemes as presented by Karmis, et al. (1994)....103
Table 35: Classes of damage and suggested threshold (damage limit) values of horizontal strain and angular distortion(Karmis, et al., 1994)....103

Abbreviations

Symbol	Definition of abbreviations
w	panel width
h	panel depth
w/h	width to depth ratio of a panel
%HR	percent hardrock in the overburden (defined as the sum of the strong rocks -- e.g., sandstone, limestone -- having a minimum thickness of 5 feet, expressed as a percentage of the total overburden thickness.)
Smax	maximum subsidence
m	seam thickness
Smax/m	subsidence factor
Tanb	Tangent of influence angle

1. Executive Summary

The purpose of this research project and report was to a) to develop and improve subsidence engineering parameters, b) to improve prediction methodologies, c) to apply subsidence methodology for landscape stability and control, d) to assess long-term stability, and e) to disseminate project results. In order to accomplish the objectives of the projects, case studies were collected and analyzed for static and dynamic conditions, the model for the dynamic analysis was updated, new models were developed for landscape stability and control and for long term stability and a number of new tools and functions were developed and incorporated into the Surface Deformation Prediction System (SDPS) software package. Finally the results of this research effort were integrated into the revised SDPS User's Manual which includes examples for all new functions and tools.

2. Introduction and Objectives

The authors have been actively involved in intensive research and application development concerning ground deformations over underground coal mines for over 20 years. One of the results of this activity is the development and continued enhancement of the Surface Deformation Prediction System (SDPS) software package, for predicting ground movements above undermined areas as well as for addressing mine stability issues. The SDPS methodology is used widely by the mining industry and state and federal agencies for subsidence planning, prediction and control. These calculations are based on several empirical relationships, developed through the statistical analysis of data from a number of case studies derived from the U.S. Coalfields.

The objectives of this research were as follows:

1. <u>To develop and improve subsidence engineering parameters</u>. The original database used in by OSMRE was compiled over 25 years ago and included only the Eastern US Coalfields. Recently, subsidence engineering parameters were developed for the central and western US coalfields; however, gaps in the database for the eastern coalfields were not addressed. It was proposed that data would be collected in order to

enhance the database of the regional subsidence engineering parameters. Data collection would include published and unpublished case studies and data analysis would focus on the improvement of characteristic parameters.

2. To improve prediction methodologies. Prediction methodologies available in the SDPS package are mainly based on the influence function method. Although these methodologies have been enhanced since the initial release of the package in 1989, there is further room for improvement. It was proposed that better methodologies for dynamic deformations, for subsidence and strain calibrations would be investigated and developed. In addition it was proposed that the potential of secondary sliding of the surface layers in steep terrain, due to subsidence trough development, would be addressed.
3. To apply subsidence methodology for landscape stability and control. Damage to surface structures is mainly caused by tilt, angular, bending, horizontal strains, or the combined action of these effects. Damage classification systems have been proposed depending on the type of building and foundation. It was proposed that limiting values for horizontal strain, curvature, and slope due to underground mining would be correlated so that control measures can be uniformly applied when necessary.
4. To assess long-term stability. A variety of tools to assess stability of underground workings exist as standalone software or as separate modules within software packages. It was proposed that a methodology would be developed to allow the user to directly evaluate long-term stability at the mine level so that landscape stability can be evaluated.
5. To disseminate project results. It was proposed that a comprehensive user's guide would be developed to aid in the implementation of a uniform approach towards subsidence/ground-deformation analysis. In addition, a training course would be held for the benefit of OSMRE personnel to update them on new technologies and methodologies developed through this project.

3. Approach

The approach to this research consisted of the following steps:

1. Data collection
2. Reduction of data for static and dynamic analysis
3. Influence Function Method validation with new case studies
4. Development of a model for the dynamic analysis
5. Development of a model for landscape stability and control
6. Development of a model for long term stability
7. Development of new tools and functions
8. Software enhancement to incorporate new features and to allow for the analysis of case study data
9. Analysis and processing of collected data using the enhanced software
10. Dissemination of results

These accomplishments for each objective are explained in detail in the following sections. Screen shots in a form of a step by step guide to applying the Influence Function program to many of the analyzed case studies are given in Figures in the Appendices.

4. Objective I: Develop and Improve Subsidence Engineering Parameters

4.1 Review of Previous Research

As a result of the empirical nature of many subsidence prediction techniques, such as the influence function used by SDPS, the amount of reliable data upon which subsidence relationships are based is a limiting factor. Therefore, more data results in better defined regional and/or site-specific empirical parameters. In turn, better subsidence parameters result in more accurate subsidence predictions and more applicable mitigation efforts.

In the 1980's, prompted by increasing mine subsidence-related problems and regulatory requirements, intense subsidence research efforts were carried out by government agencies, coal companies, and academic institutions in the United States (Schilizzi, et al. 1986). One such effort, involving the initial collection of subsidence data from 32 longwall panels and 60 room-and-pillar mines, was completed by Virginia Tech. Analysis of the initial data resulted in the decision to use the profile function method and the influence function method to develop a subsidence prediction system specific to the Appalachian coal region (Schilizzi, et al. 1986). Of the initial collected data, approximately 25 longwall panels and 21 room-and-pillar mines were used for the project. Due to limitations of the initial data collected, researchers at Virginia Tech implemented a very detailed subsidence and strain monitoring program over active mines in Virginia. Following a more recent update in 2003, the SDPS database consists of data from 35 longwall mines and 21 room-and-pillar mines.

The active mine monitoring program completed by Virginia Tech included approximately sixteen room and pillar mines and seven longwall mines. The active mines monitored, and the monitoring techniques employed were chosen based on a set of fairly strict criteria to ensure accurate, yet practical collection of data. The criteria included both mining and site/geological parameters. Preference was given to sites with supercritical width to depth ratio (greater than 1.2), with limited influence from nearby mining, and with easier accessibility (Schilizzi, et al. 1986). The monitoring program used approximately 1,200 stations, each consisting of either a two or five feet long steel bar monument (Schilizzi, et al. 1986). The monuments were placed in longitudinal and

transverse line orientations that extended over the mines as well as far beyond the expected extent of subsidence influence. Monitoring (utilizing a “total station” or digital computer tacheometer with built-in electronic distance measurement device) of the monuments began well before mining impacts (to establish solid baseline conditions) and continued at regular intervals until mining had passed and significant subsidence movements ceased (Schilizzi, et al. 1986).

In addition to developing profile function and influence function subsidence prediction systems based on the collected data, the researchers at Virginia Tech stressed the fact that rational and realistic solutions to subsidence-related problems require continued monitoring of additional case studies (Schilizzi, et al. 1986).

4.2 Implemented Methodology

The current research builds upon the original database of subsidence case studies that was created by Virginia Tech in the 1980’s. New case studies have been collected and analyzed by comparing the SDPS predictions for each area with measured data. For each new case study, the mining and geologic conditions have been documented. The parameters required by SDPS to make subsidence predictions have been extracted from the site specific information. Actual measured data has also been entered into SDPS to allow for direct comparison of predicted versus measured values. Selection of new case study data was completed based, as closely as possible, on the same criteria used by the original Virginia Tech research. Due to some difficulty in obtaining subsidence case study data, not all case studies fit the most desirable criteria. As in the original study, preference was given to longwall panels with supercritical width to depth ratios and to panels not significantly influenced by nearby mining. However, restrictions on data necessitated exceptions to the criteria.

4.3 Validation of Method

Validation and enhancement of the influence function method of subsidence prediction are accomplished through evaluation of additional case study data. Nine different lines of measured subsidence from six different case study areas in three different states (Northern Appalachia, Illinois/Indiana, and Alabama) are included in this research. Case studies from Northern Appalachia are referred to as NA-1, NA-2, and NA-3. Case studies from Illinois/Indiana are referred to as

IL-1 and IL-2. The case study from Alabama is referred to as AL-1. Additional case study data was collected; however, a significant portion of it proved to be unreliable, inapplicable, or incomprehensible. Validation/enhancement is achieved by comparing SDPS-predicted subsidence measurements with actual field-measured subsidence.

Prediction curves are compared with measured data using the percent error calculated by SDPS. The program evaluates various combinations of tangent of the influence angle (Tan b) and subsidence factor (max subsidence/extraction thickness) based on the restrictions outlined in the Subsidence Calibrations Options window (the Subsidence Calibrations Options windows for each of the following case studies are included in Appendix I and referenced throughout the case study discussions). Put very simply, SDPS performs numerous iterations as it back-calculates to try to fit the predicted curve to the measured subsidence curve. For each iteration (combination of tangent of the influence angle (Tan b) and subsidence factor), an error index is calculated using the following equation (Agioutantis and Karmis, 2005):

$$\%\ \text{error} = \frac{\sum_{i=1}^{n}(|\text{calculated subsidence} - \text{measured subsidence}|)}{\sum_{i=1}^{n}|\text{measured subsidence}|} \times 100\% \quad [1]$$

The combination that produces the lowest error is chosen and displayed. Adjustment of Tan b and the subsidence factor control the modeling of the subsidence magnitude. Adjustment of the edge effect controls the position of the inflection point of subsidence in relation to the side of the panel (Agioutantis, 2008).

In general, the case studies include:

- ✓ A brief overview of the location and general characteristics of the mine,
- ✓ Mention of any special conditions,
- ✓ Description of the case study analysis,
- ✓ Figures showing the actual mine layout and prediction point locations (and figures showing the components as they appear after being entered/imported into SDPS),
- ✓ Tables of the measured subsidence values along the monument lines,
- ✓ The calibration parameters (Tan b, S_{max}/m, and edge effect adjustment) obtained using the SDPS iterative calibration function,

- ✓ A graph that visually compares predicted subsidence with measured subsidence, and
- ✓ A discussion of the results of the comparison of predicted to measured values.

Additional figures showing SDPS screen shots for each step are included in Appendix I. Many of the figures in Appendix I are referenced throughout the text.

4.4 Case Studies

4.4.1 NA-1 Case Study (Northern Appalachia)

This case study involves data from above a longwall panel in a mine in Northern Appalachia. The data for this mine is of moderate to good quality. The average extraction thickness for the mine is 6.5 feet. Average seam depth is estimated to be 305 feet. The percentage of hardrock in the overburden is 34 percent, as provided by the coal company. The panel has an approximate width to depth ratio of 3.28 (1000 ft/305 ft), which classifies it as supercritical. An initial estimate of subsidence factor was calculated to be 53.8 percent (3.5 feet/6.5 feet) (Appendix I, Figure 2). For confidentiality, the scanned image of the mine map used for this case study is not provided. Figure 1 shows the mine plan and points after being imported into SDPS.

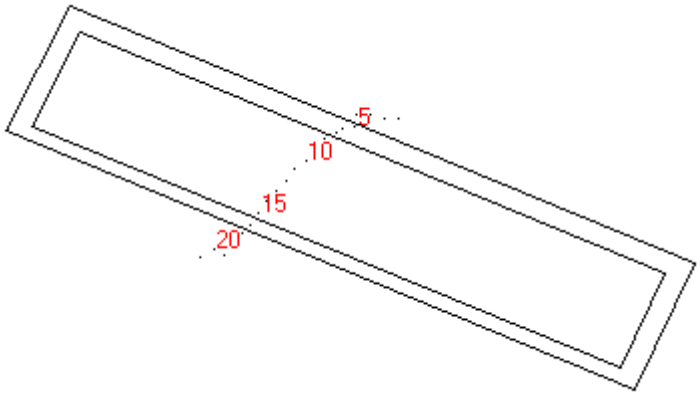

Figure 1: Mine plan and prediction point locations for NA-1 Case Study

As is evident from Figure 1, variable edge effect offset distances were applied to the panel (Appendix I, Figures 4-6). An edge effect offset of 150 feet was applied to the northwest, northeast, and southeast sides of the panel. An offset of 100 feet was applied to the southwest edge of the panel. The final edge effect offsets

were found during the calibration process by observing the graphical “best fit” and adjusting the offsets accordingly. For the final calibration run, the edge effect calibration function was set to “Apply Edge Effect as Defined in Mine Plan” (therefore “locking in” the variable edge effects) (Appendix I, Figure 10).

Measured subsidence values (Table 1) were entered into the Scattered Prediction Points Management screen (Appendix I, Figure 7). Once all measured data and known mine parameters were entered into SDPS, the Subsidence Calibration function of SDPS was used to find the combination of influence angle, subsidence factor, and edge effect that most closely matched predicted values of subsidence with measured values of subsidence.

Table 1: NA-1 Case Study, measured subsidence values

Point	Measured Subsidence (ft)	Point	Measured Subsidence (ft)
1	0.07	12	-3.5
2	0.08	13	-3.38
3	0.24	14	-3.23
4	0.16	15	-2.74
5	0.16	16	-0.07
6	-0.33	17	0.04
7	-1.31	18	0.11
8	-2.74	19	0.12
9	-3.24	20	0.12
10	-3.36	21	0.12
11	-3.38		

The “best fit” subsidence parameters, resulting from matching predicted values with measured values, are shown graphically in Figure 2 and the three lowest-error iterations are listed in Table 2.

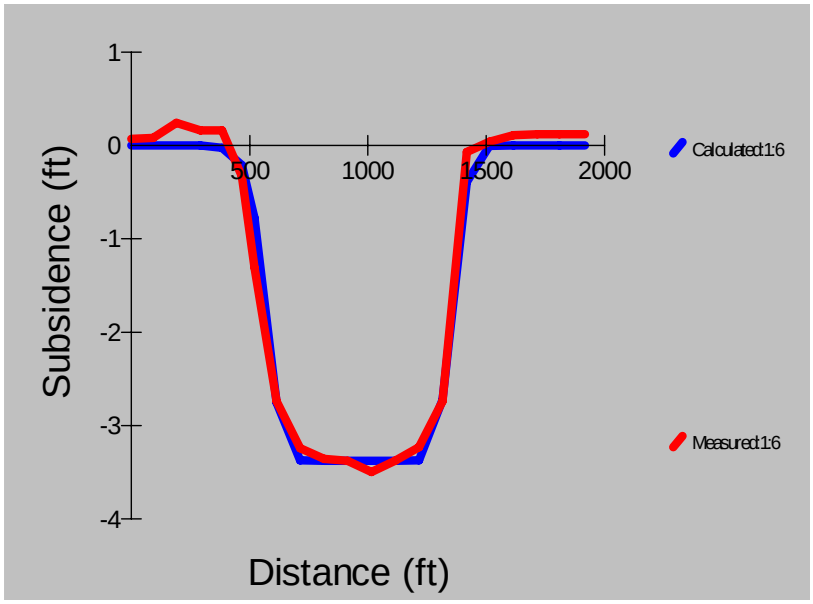

Figure 2: Graphical display of predicted and measured subsidence profiles after calibration

Table 2: Calibration parameters for NA-1 Case Study

Rank	Iteration Number	Tangent of Influence Angle (Tanb)	Subsidence Factor (Smax/m)	Edge Effect Offset (ft)	Total Error	Percent Error
1	6	2.50	52	150	6.664	7.90
2	5	2.40	52	150	6.877	8.15
3	7	2.60	52	150	6.949	8.24

As indicated, predicted values were calibrated to measured values with only 7.90% error. This case study further validates the influence function prediction method utilized by SDPS. Some of the error may be attributable to the positive measured subsidence values on the outer edges of the subsidence basin. Positive subsidence, or upsidence, means that the ground has actually moved upward due to the ground deformation. Positive subsidence has been observed on the edges of the subsidence trough in other case studies. The influence function used by SDPS is not designed to predict positive subsidence values and, therefore, does not match the predicted curve to the measured data in these areas.

4.4.2 NA-2 Case Study (Northern Appalachia)

This case study pertains to data collected in the mid-1980's over a longwall mine in Northern Appalachia. Data for this mine was collected along both a transverse line and a longitudinal line. Default values for the tangent of the influence angle, strain coefficient, and time coefficient were initially used for both lines (Appendix I, Figures 12 and 22). Depth to seam ranges from 698 feet to 827 feet according to data for the transverse line and from 695 feet to 767 feet for the longitudinal line. However, these depths are not completely accurate because only an average elevation was known for the mine. The average extraction height is 6.5 feet, as provided by the company. A percent hardrock value of 50% was used for both lines in this case. For the transverse line, an initial estimate of the subsidence factor was calculated by dividing the maximum measured subsidence by the average extraction height (3.06 ft/6.5 feet = 0.47). The estimated subsidence factor for the longitudinal line is (3.48 ft/6.5 ft = 0.53). Based on these two estimates, an initial subsidence factor of 0.50 was used for both the transverse and longitudinal lines (Appendix I, Figures 13 and 23). The panel monitored is classified as a subcritical panel, having an approximate width to depth ratio of 0.86 (630 feet/730 feet). Despite its subcritical status, the mine was included as a case study due to its abundance of well documented measured data (both measured subsidence and measured strain).

A paper copy of the mine plan, showing both the transverse and longitudinal monument lines, was scanned using a desktop scanner. The scanned image was imported into AutoCAD using the "Image Manager" function and was scaled to match the original document. Figure 3 shows the original scanned image. Mining direction was from left to right.

The outline of the longwall panel was digitized and saved on its own AutoCAD layer. The width of the extracted panel was digitized to include, not only the width of the panel, but also the width of the entries immediately adjacent to the panel. The digitized panel outline was imported into SDPS. For this case study, locations of the monitoring points were input manually into SDPS (Appendix I, Figures 17 and 26). Figure 4 shows the mine plan and monitoring points for both the transverse line (top) and longitudinal line (bottom).

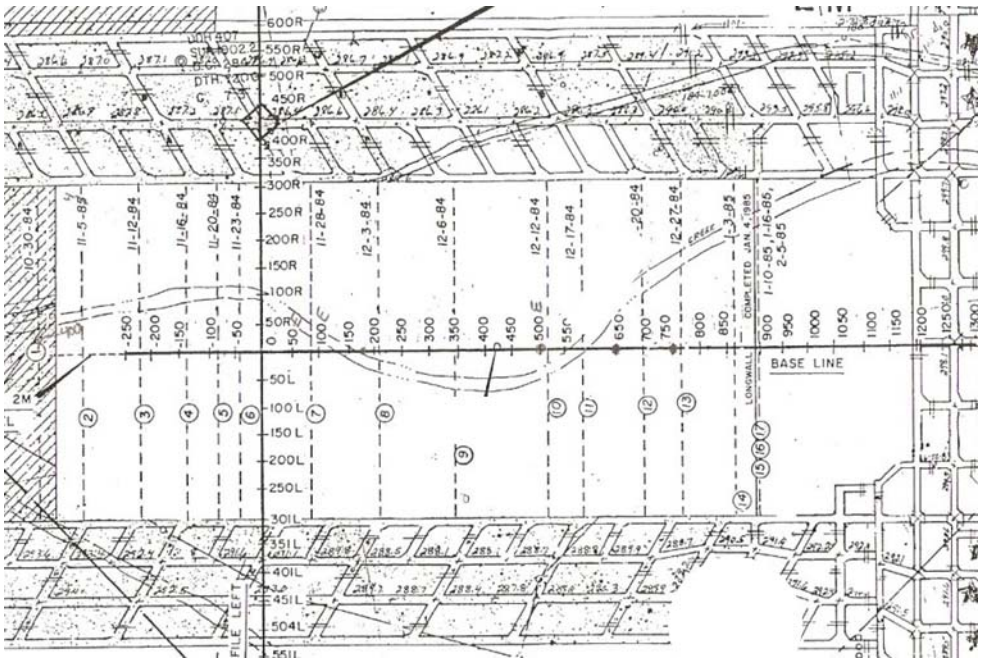

Figure 3: Original scanned image of mine plan showing panel, transverse monitoring line, and longitudinal monitoring line. Mining progressed from left to right (Coal mine in Northern Appalachia, reprinted with company permission, mine location and company name confidential)

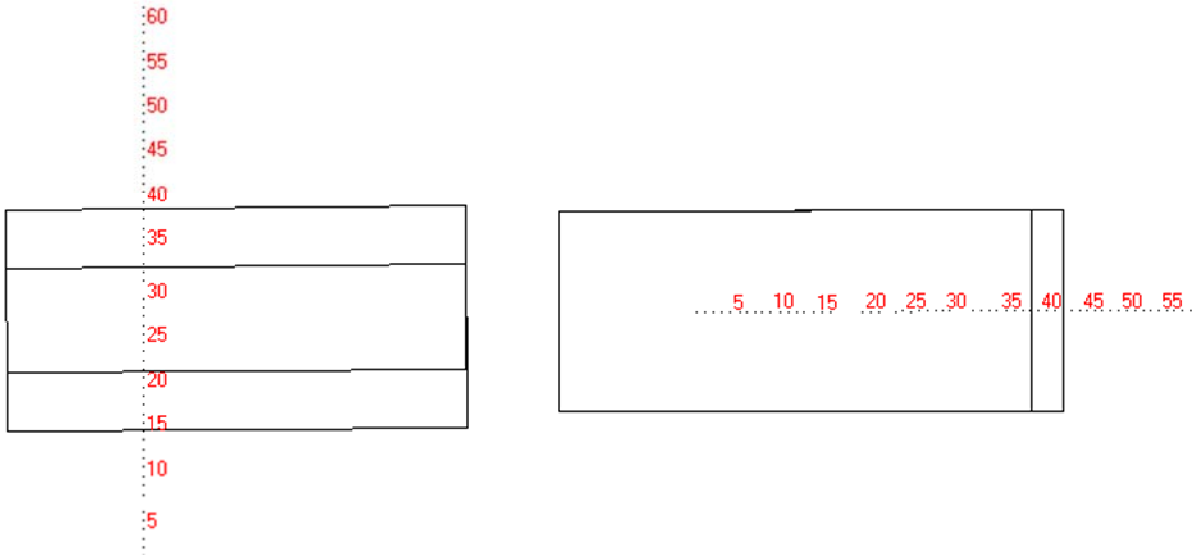

Figure 4: Mine plan and monitoring points for transverse and longitudinal lines as imported into SDPS.

Edge effect offsets for the transverse and longitudinal lines were initially estimated to be approximately 100 to 110 feet based on measurements of panel

width and depth (Appendix I, Figures 15, 16 and 25). However, suggested edge effect offsets resulting from the iterative calibration process are 167 feet (Table 5) for the transverse line and 218 feet (Table 6) for the longitudinal line.

The measured subsidence values to which the SDPS predicted values were calibrated are presented in Table 3 for the transverse line and Table 4 for the longitudinal line. The measured subsidence values reflect the final subsidence measured at all points following the passing of the longwall.

Table 3: Measured Subsidence Values for NA-2 Case Study, Transverse Line

Point	Measured Subsidence (ft)	Point	Measured Subsidence (ft)	Point	Measured Subsidence (ft)
1	0.03	22	-1.72	43	-0.05
2	0.04	23	-2.14	44	-0.05
3	0.05	24	-2.49	45	-0.03
4	0.05	25	-2.82	46	-0.04
5	0.05	26	-3	47	-0.02
6	0.06	27	-3.06	48	-0.01
7	0.06	28	-3	49	0.01
8	0.05	29	-2.86	50	-0.01
9	0.09	30	-2.66	51	0.01
10	0.03	31	-2.27	52	-0.01
11	-0.02	32	-1.95	53	-0.01
12	-0.05	33	-1.62	54	0
13	-0.08	34	-1.28	55	0
14	-0.11	35	-0.95	56	0
15	-0.16	36	-0.61	57	0
16	-0.23	37	-0.43	58	0.04
17	-0.32	38	-0.28	59	0.03
18	-0.43	39	-0.19	60	0.02
19	-0.62	40	-0.13	61	0
20	-0.92	41	-0.13	62	0
21	-1.3	42	-0.07		

Table 4: Measured Subsidence Values for NA-2 Case Study, Longitudinal Line

Point	Measured Subsidence (ft)	Point	Measured Subsidence (ft)	Point	Measured Subsidence (ft)
1	-3.21	21	-3.43	41	-0.22
2	-3.17	22	-3.41	42	-0.19
3	-3.24	23	0	43	-0.16

4	-3.21	24	-3.48	44	-0.14
5	-3.19	25	-3.44	45	-0.12
6	-3.15	26	-3.45	46	-0.1
7	-3.05	27	-3.42	47	-0.09
8	-2.99	28	-3.39	48	-0.09
9	-3.01	29	-3.31	49	-0.08
10	-3	30	-3.19	50	-0.06
11	-3.01	31	-3.06	51	-0.06
12	-3.03	32	-2.42	52	-0.06
13	-3.02	33	-2.1	53	-0.06
14	-3.04	34	-1.76	54	-0.04
15	-3.11	35	-1.42	55	-0.05
16	-3.22	36	-1.1	56	-0.03
17	-3.39	37	-0.81	57	-0.03
18	0	38	-0.6	58	-0.01
19	0	39	-0.43	59	0
20	-3.46	40	-0.29		

The calibration function of SDPS was used to better match predicted subsidence values with measured values for each line. Figure 5 and Table 5 indicate the calibration parameters for the transverse line and Figure 6 and Table 6 indicate the calibration parameters for the longitudinal line. Figures 18 through 21 in Appendix I provide the subsidence calibration options yielding the calibrated results for the transverse line. Appendix I, Figures 27 through 30 show the calibration settings for the longitudinal line.

The calibration results for the two lines yield similar tangent of influence angle (Tanb) values and similar subsidence factors (Smax/m). This is not uncommon for two lines over the same panel. The difference in calibrated edge effect offset between the two lines may be a result of the orientation of the lines with respect to direction of mining or local geologic conditions. Despite the slightly higher percentage error for the transverse line, and the undulation of the measured data in the longitudinal line (Figure 6), this case study further validates the influence function prediction technique.

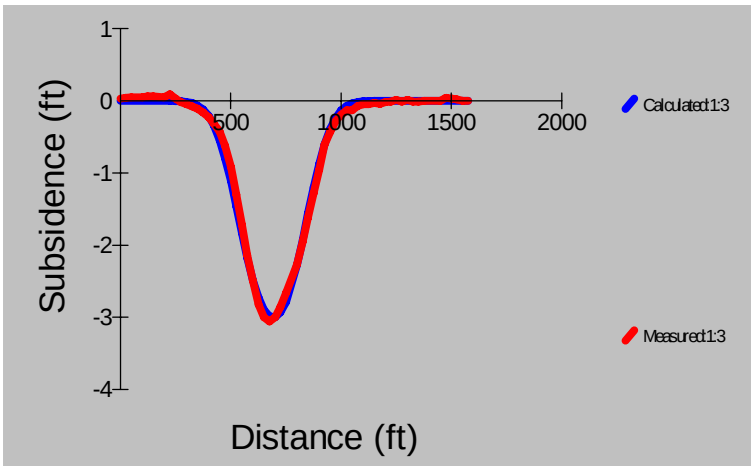

Figure 5: Transverse Line - matched predicted and measured subsidence profiles

Table 5: Transverse Line - calibration parameters

Rank	Iteration Number	Tangent of Influence Angle (Tanb)	Subsidence Factor (Smax/m)	Edge Effect Offset (ft)	Total Error	Percent Error
1	856	3.00	53.0	167.00	10.895	13.21
2	371	3.00	52.0	163.00	10.962	13.29
3	492	3.00	52.0	164.00	10.977	13.31

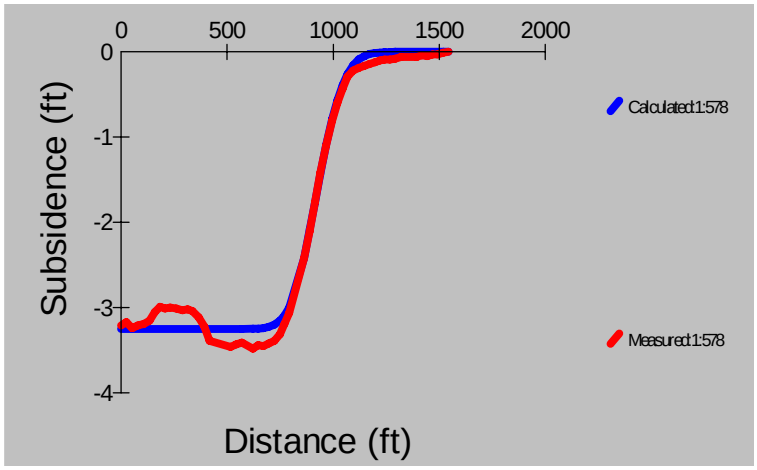

Figure 6: Longitudinal Line – matched predicted and measured subsidence profiles

Table 6: Longitudinal Line - calibration parameters

Rank	Iteration Number	Tangent of Influence Angle (Tanb)	Subsidence Factor (Smax/m)	Edge Effect Offset (ft)	Total Error	Percent Error
1	963	3.10	49.0	218.00	29.332	9.50
2	897	3.10	49.0	216.00	29.333	9.50
3	969	3.20	49.0	218.00	29.362	9.51

4.4.3 NA-3 Case Study (Northern Appalachia)

This case study involves calibration of SDPS predictions with measured subsidence values from two longwall panels in Northern Appalachia. The panels are designated as Panel 1 North and Panel 3 North. One line of measured subsidence data was collected for each of the two panels. The measured subsidence values were collected as part of an investigation concerning possible damage to a waterline due to undermining. As shown in Figures 31 and 40 of Appendix I, regional default values for tangent of influence angle, strain coefficient, and time coefficient were used for both panels. The hardrock for both was estimated to be approximately 21 percent based on a nearby drill hole log (Appendix I, Figures 31 and 40). The estimated subsidence factors are 85% (4.68 feet maximum observed subsidence/5.5 feet extraction height x 100%) for Panel 1 North and 80.9% (4.45 feet maximum observed subsidence/5.5 feet extraction height x 100%) for Panel 3 North (Appendix I, Figures 32 and 41). Width to depth ratios for Panel 1 North and Panel 3 North are 1.84 (885 feet/ 480 feet) and 2.78 (890 feet/ 320 feet), respectively.

Due to the very large scale and relatively low quality of the maps included with this case study, no scan of the original map is provided. Instead, each original map was scaled down and redrawn by hand to allow for a scanned version to be imported into AutoCAD. Figure 7 and Figure 8 show scans of the hand-drawn maps with digitized panels and points.

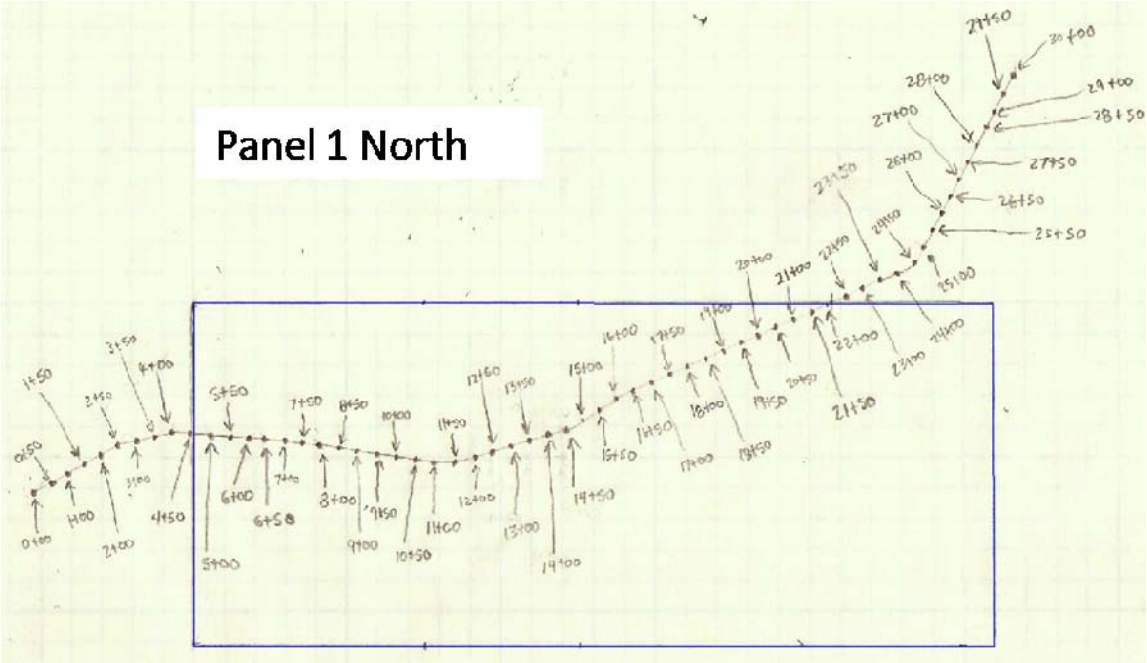

Figure 7: Scanned image of hand-drawn version of Panel 1 North with digitized panel and points. The monitoring points are located along a road above the mine.

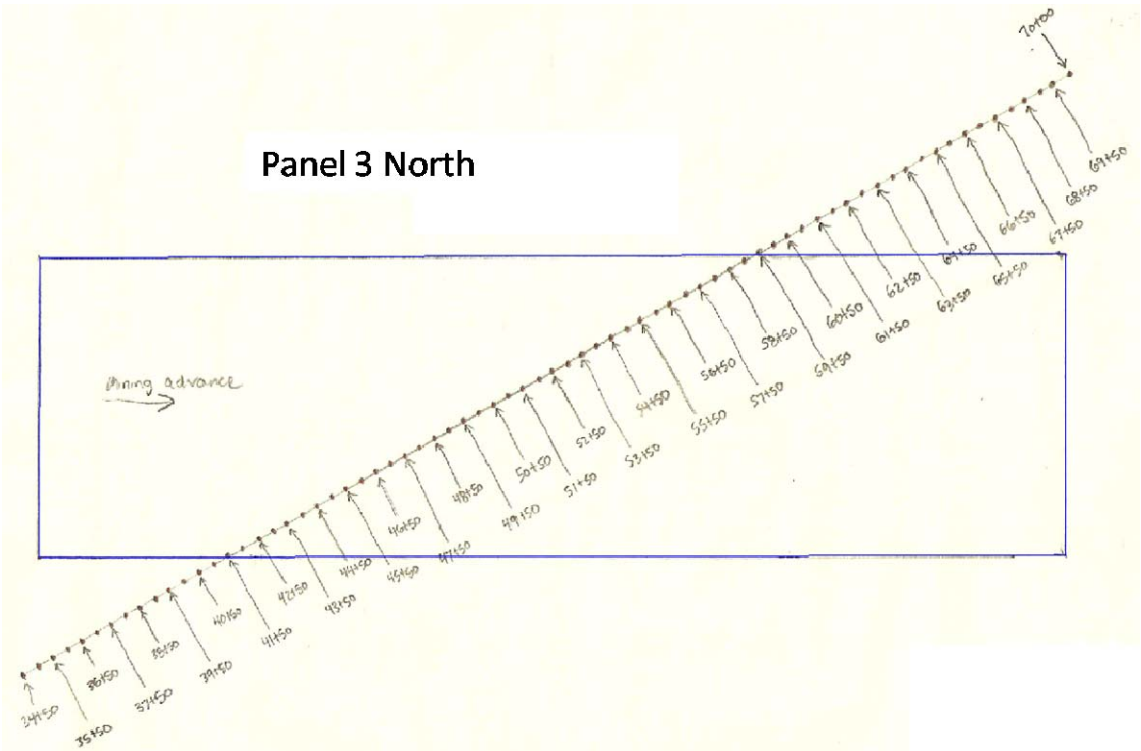

Figure 8: Scanned image of hand-drawn version of Panel 3 North with digitized panel and points.

Panel and Points AutoCAD layers for each panel were imported into SDPS. Figure 9 shows the panel and points for Panel 1 North and Figure 10 shows the panel and points for Panel 3 North. The edge effect offsets are also represented in the figures. An average edge effect value is applied to all sides of Panel 1 North. In contrast, variable edge effect offset distances are applied to Panel 3 North. This is a result of numerous attempts to match measured values with predicted values using the iterative calibration function. The need for variable edge effect offsets is likely a result of influence from an additional panel located just south of Panel 3 North. The additional panel was not included in the case study due to insufficient data.

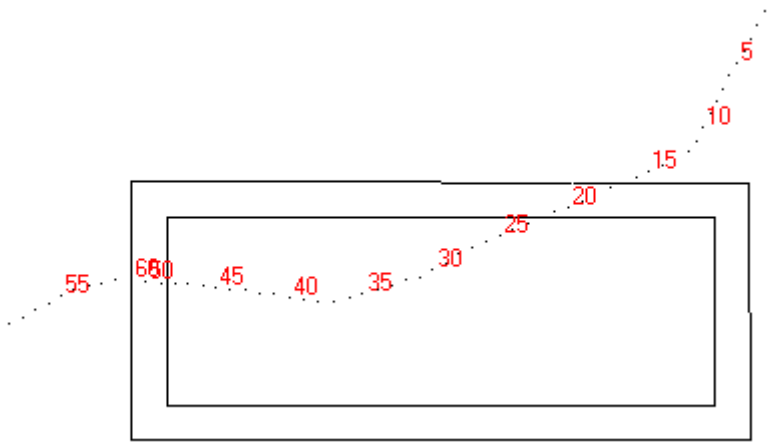

Figure 9: Panel 1 North – Mine plan and prediction point locations in SDPS

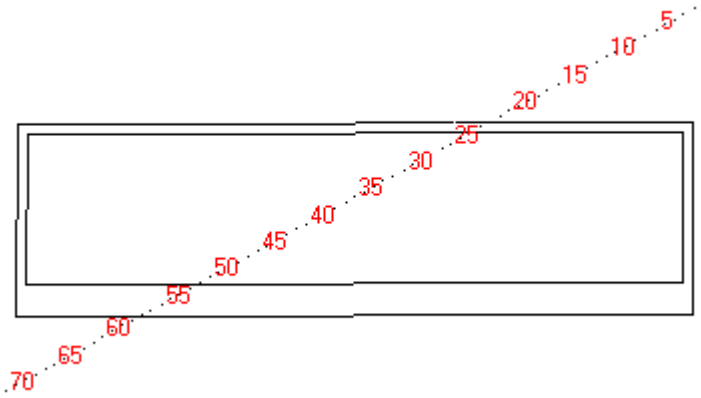

Figure 10: Panel 3 North – Mine plan and prediction point locations in SDPS. Note use of variable edge effect.

Table 7 and Table 8 list the measured subsidence values for Panel 1 North and

Panel 3 North, respectively. Figure 11 and Table 9 indicate the results of the calibration procedures for Panel 1 North. Panel 3 North results are indicated in Figure 12 and Table 10. Calibration resulted in similar values for tangent of influence angle (Tanb) for the two panels (2.80 for Panel 1 North and 3.20 for Panel 3 North). Both calibrations resulted in a subsidence factor (Smax/m) of approximately 80%. The calibrated edge effect for Panel 1 North is 132 feet, which is just slightly greater than the average of 118 feet estimated prior to calibration. The post-calibration edge effect indicated for Panel 3 North (45 feet) in Table 10 reflects only one of the edge effect values applied to that panel. Note that the edge effect was restricted to be "as defined in mine plan" for Panel 3 North (Appendix I, Figure 48). The ability to assign variable edge effect values and keep these values constant is a relatively new feature of SDPS that provides more flexibility, and ultimately results in more accurate model calibration.

Table 7: Panel 1 North - Measured subsidence values

Point	Measured Subsidence (ft)	Point	Measured Subsidence (ft)	Point	Measured Subsidence (ft)
1	0.06	22	-1.83	43	-4.68
2	0.04	23	-2.62	44	-4.51
3	0.03	24	-3.16	45	-4.45
4	0.05	25	-3.43	46	-4.13
5	0.02	26	-3.61	47	-3.59
6	0.03	27	-3.75	48	-2.59
7	0.03	28	-4.26	49	-1.44
8	0.02	29	-4.36	50	-0.75
9	0.03	30	-4.31	51	0
10	0.02	31	-4.4	52	-0.25
11	0	32	-4.43	53	-0.22
12	-0.01	33	-4.44	54	-0.2
13	-0.02	34	-4.43	55	-0.17
14	-0.04	35	-4.47	56	-0.16
15	-0.07	36	-4.45	57	-0.15
16	-0.09	37	-4.42	58	-0.15
17	-0.19	38	-4.34	59	-0.13
18	-0.28	39	-4.48	60	-0.47
19	-0.47	40	-4.59	61	-0.12
20	-0.48	41	-4.61		
21	-1.04	42	-4.65		

The errors associated with the calibrations from both panels are very low (both <

9%, with Panel 1 North calibrating to less than 6% error), indicating that the influence function method of SDPS is able to accurately represent measured subsidence data. This case study further validates the influence function technique of SDPS.

Table 8: Panel 3 North - Measured subsidence values

Point	Measured Subsidence (ft)	Point	Measured Subsidence (ft)	Point	Measured Subsidence (ft)
1	0	26	-3.83	51	-0.91
2	0.02	27	-3.95	52	-0.41
3	0.02	28	-3.98	53	-0.15
4	0.03	29	-4	54	-0.04
5	0.03	30	-4.12	55	0
6	0.03	31	-4.16	56	0
7	0.03	32	-4.27	57	0.02
8	0.03	33	-4.41	58	0.01
9	0.03	34	-4.43	59	0.01
10	0.02	35	-4.34	60	0.03
11	0.02	36	-4.33	61	-0.01
12	0.01	37	-4.34	62	0
13	0.01	38	-4.4	63	0.01
14	-0.01	39	-4.45	64	0
15	-0.03	40	-4.24	65	0.01
16	-0.06	41	-4.37	66	0
17	-0.08	42	-4.38	67	0.01
18	-0.15	43	-4.39	68	0
19	-0.22	44	-4.42	69	-0.01
20	-0.35	45	-4.18	70	0
21	-0.53	46	-3.88	71	-0.8
22	-1.49	47	-3.46	72	0.03
23	-2.46	48	-3.43		
24	-3.23	49	-2.85		
25	-3.64	50	-1.72		

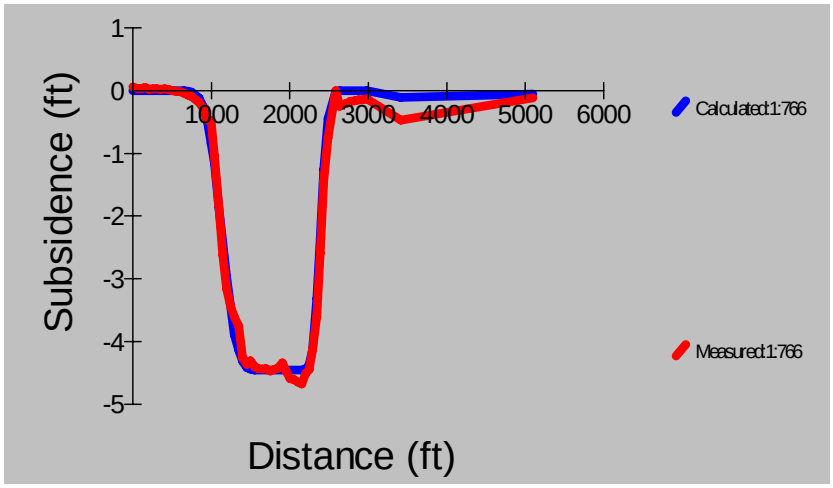

Figure 11: Panel 1 North - matched predicted and measured subsidence profiles

Table 9: Panel 1 North – calibration parameters

Rank	Iteration Number	Tangent of Influence Angle (Tanb)	Subsidence Factor (Smax/m)	Edge Effect Offset (ft)	Total Error	Percent Error
1	887	2.80	81	132	27.352	5.96
2	656	2.90	81	130	27.359	5.96
3	777	2.90	81	131	27.395	5.97

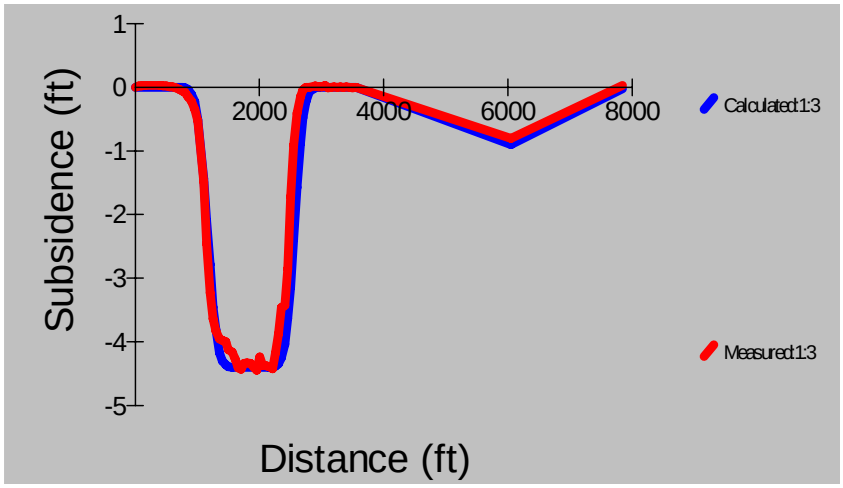

Figure 12: Panel 3 North - matched predicted and measured subsidence profiles

Table 10: Panel 3 North - calibration parameters

Rank	Iteration Number	Tangent of Influence Angle (Tanb)	Subsidence Factor (Smax/m)	Edge Effect Offset (ft)	Total Error	Percent Error
1	3	3.20	80	45	40.043	8.98
2	1	3.00	80	45	40.060	8.99
3	2	3.10	80	45	40.061	8.99

4.4.4 IL-1 Case Study (Illinois)

This case study involves data collected from two monitoring lines (Monument Line 5 and Monument Line 6) over longwall panels in the Number 5 coal seam of Illinois. The data in this case study was of only moderate to poor quality. Width to depth ratios for the panels indicate that both are supercritical. The Monument Line 5 panel has a width to depth ratio of about 1.21 (667 feet/550 feet) and the Monument Line 6 panel has a width to depth ratio of about 1.45 (844 feet/582 feet). An average coal thickness of 9.5 feet, found in handwritten notes from the coal company, was used for the case study (Appendix I, Figures 51 and 60). 50% hardrock was assumed in both cases due to a lack of data (Appendix I, Figures 50 and 59). The estimated subsidence factor for Monument Line 5 is 56% (5.33 feet/9.5 feet x 100%), and 47% (4.47 feet/9.5 feet x 100%) for Monument Line 6 (Appendix I, Figures 51 and 60).

Available mine maps were scanned with a desktop scanner and imported into AutoCAD. The scanned maps were scaled, and each panel and monitoring point locations were digitized. Figure 13 shows the mine and points for Monument Line 5 and Figure 14 shows the mine and points for Monument Line 6.

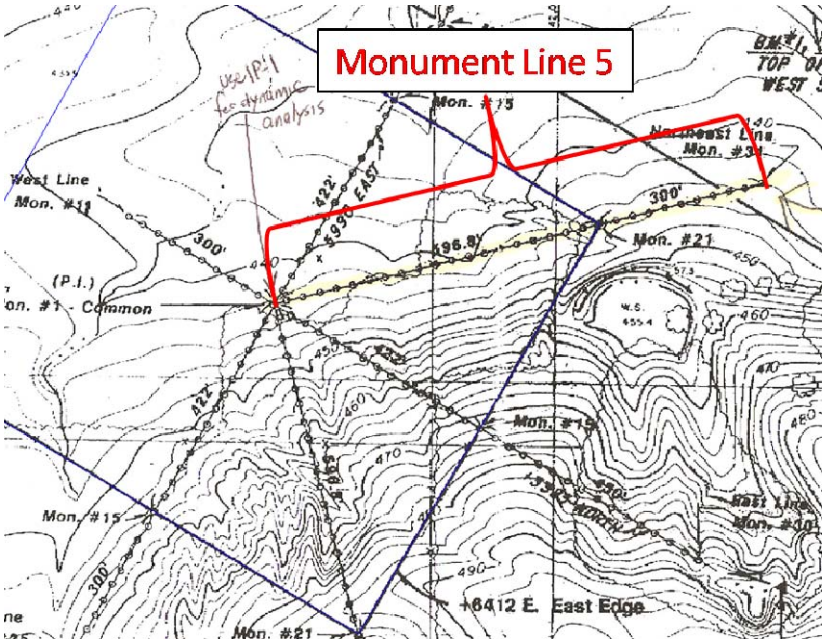

Figure 13: Monument Line 5 - Scanned image of mine map with digitized panels and points. The map was retrieved from company information (The American Coal Company, Galatia Mine, Harrisonburg, Illinois) submitted to the Illinois Department of Natural Resources, Office of Mines and Minerals for permit application in 1989.

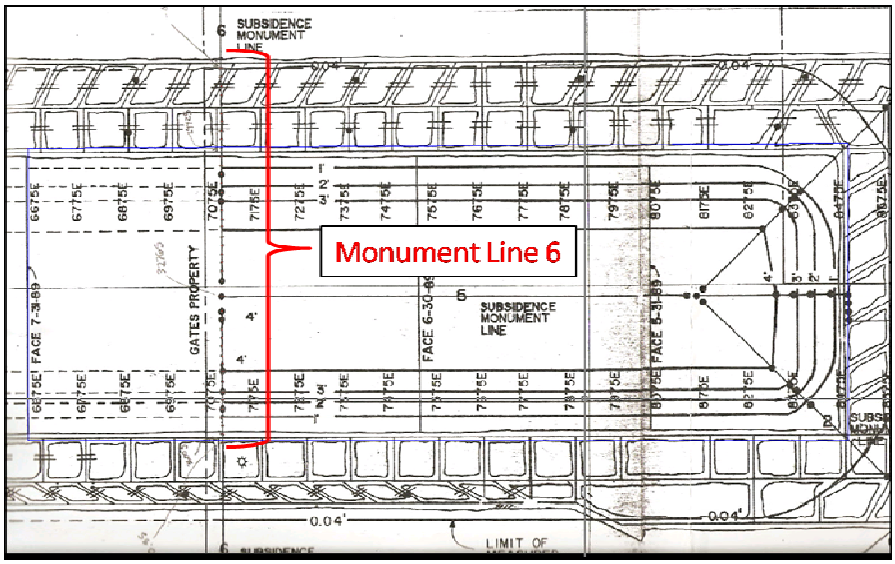

Figure 14: Monument Line 6 - Scanned image of mine map with digitized panels and points. The map was retrieved from company information (The American Coal Company, Galatia Mine, Harrisonburg, Illinois) submitted to the Illinois Department of Natural Resources, Office of Mines and Minerals for permit application in 1989.

For each monument line, the digitized panel and points were imported into

SDPS. Figure 15 and Figure 16 show the SDPS representations of Monument Line 5 and Monument Line 6, respectively. An average edge effect of 138 feet was initially applied to the panels for both Monument Line 5 and Monument Line 6 (Appendix I, Figures 53 and 62).

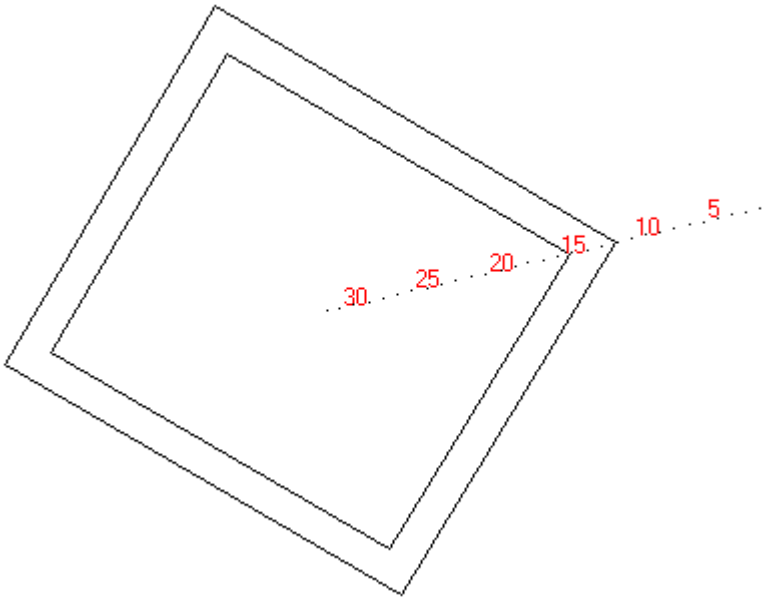

Figure 15: Monument Line 5 - Mine plan and prediction point locations in SDPS

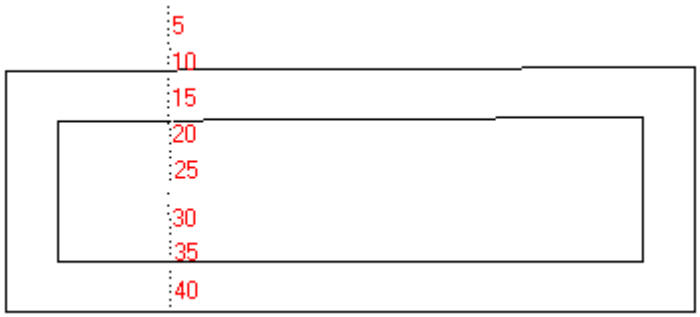

Figure 16: Monument Line 6 - Mine plan and prediction point locations in SDPS

Measured subsidence data for Monument Line 5 and Monument Line 6 is included in Table 11 and Table 12, respectively. The measured data was entered into SDPS.

Table 11: Monument Line 5 – Measured Subsidence Note – Reverse numbering matches

numbering on SDPS mine plan

Point	Measured Subsidence (ft)	Point	Measured Subsidence (ft)
31	-0.3	15	-1.08
30	-0.23	14	-1.86
29	-0.18	13	-2.84
28	-0.15	12	-3.74
27	-0.12	11	-4.27
26	-0.1	10	-4.53
25	-0.09	9	-4.69
24	-0.09	8	-4.9
23	-0.1	7	-5.12
22	-0.09	6	-5.18
21	-0.11	5	-5.25
20	-0.12	4	-5.18
19	-0.14	3	-5.27
18	-0.2	2	-5.26
17	-0.29	1	-5.33
16	-0.45		

Table 12: Monument Line 6 – Measured Subsidence

Point	Measured Subsidence (ft)	Point	Measured Subsidence (ft)
1	-0.01	22	-4.02
2	-0.06	23	-4.02
3	-0.06	24	-4.03
4	-0.06	25	-4.06
5	-0.08	26	-4.1
6	-0.09	27	-4.15
7	-0.11	28	-4.24
8	-0.14	29	-4.36
9	-0.17	30	-4.45
10	-0.25	31	-4.47
11	-0.46	32	-4.46
12	-0.68	33	-4.37
13	-1.21	34	-4.21
14	-1.92	35	-3.93
15	-2.64	36	-3.33
16	-3.26	37	-2.52
17	-3.63	38	-1.69

18	-3.84	39	-1
19	-3.97	40	-0.61
20	-4.05	41	-0.43
21	-4.02	42	-0.35

Calibration parameters are presented in Figure 17 and Table 13 for Monument Line 5 and in Figure 18 and Table 14 for Monument Line 6. It is important to note the differences in calibration parameters that exist between Monument Line 5 and Monument Line 6. The calibration parameters for Monument Line 5 suggest a tangent of the influence angle (Tan b) of 2.0 and an edge effect offset of 250 feet. Tan b = 2.0 is very low compared to the average value of Tan b = 3.5 for previously analyzed Illinois data, established by previous studies of Illinois subsidence during the development of SDPS. Similarly, an edge effect of 250 feet is unusually high (and may have been higher if not restricted during the calibration procedure, see Figure 57 in Appendix I). The calibration of Monument Line 6 yields parameters more common to Illinois subsidence, a Tan b of 4.60 and an edge effect offset of 85 feet. Such a large difference in calibration parameters between measurement lines located so close together may suggest that an anomalous geologic condition exists. The difference may also be an indication of limitations of the prediction program or attributable to human error associated with the calibration process. The difference may also be a result of the unusual orientation of Monument Line 5 with respect to the panel (see Figure 13). Monument Line 6 is aligned as a transverse profile of the panel, a more common alignment for measuring subsidence.

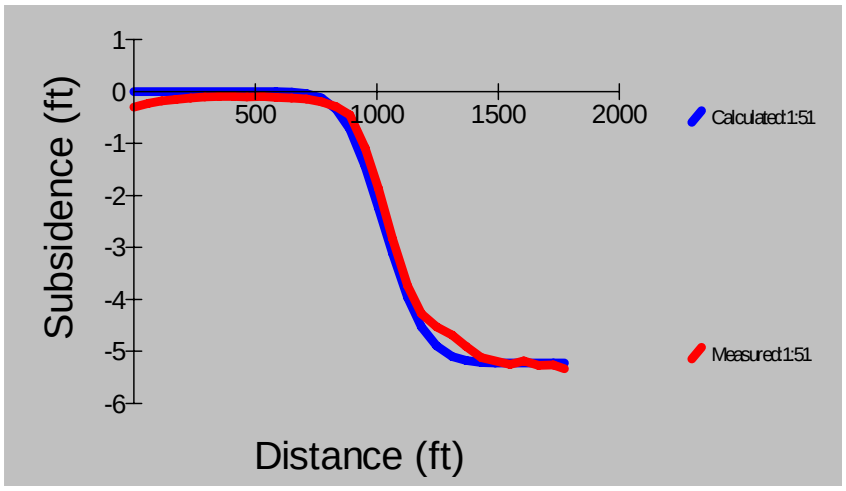

Figure 17: Monument Line 5 - matched predicted and measured subsidence profiles

Table 13: Monument Line 5 - calibration parameters

Rank	Iteration Number	Tangent of Influence Angle (Tanb)	Subsidence Factor (Smax/m)	Edge Effect Offset (ft)	Total Error	Percent Error
1	51	2.00	55	250	19.694	6.49
2	50	2.00	55	249	19.949	6.58
3	49	2.00	55	248	20.197	6.66

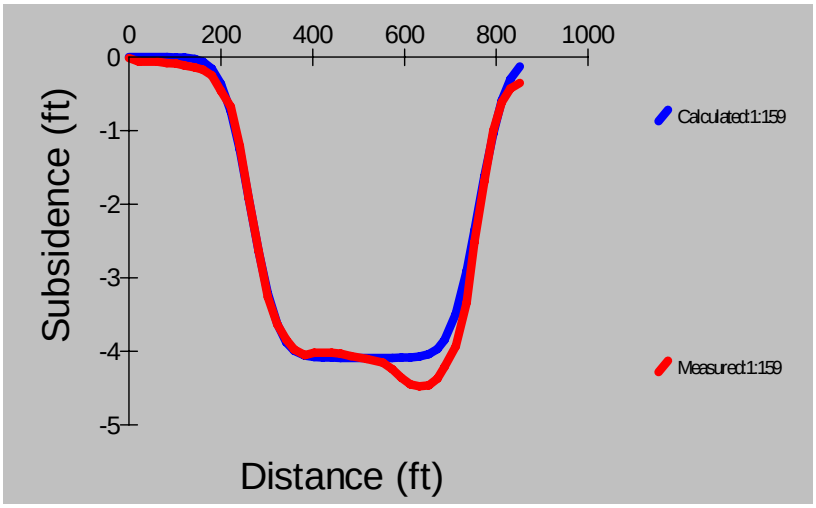

Figure 18: Monument Line 6 – matched predicted and measured subsidence profiles

Table 14: Monument Line 6 - calibration parameters

Rank	Iteration Number	Tangent of Influence Angle (Tanb)	Subsidence Factor (Smax/m)	Edge Effect Offset (ft)	Total Error	Percent Error
1	159	4.60	43	85	26.065	7.05
2	171	4.90	43	85	26.250	7.10
3	167	4.80	43	85	26.256	7.10

The calibration parameters for Monument Line 6 (only 7.05% error) are similar to previous results obtained from studies of Illinois subsidence, and serve to further validate the influence function method utilized by SDPS. The results for

Monument Line 5 also indicate that SDPS is able to match the predicted subsidence with measured subsidence (only 6.49% error). However, the results of Monument Line 5 also raise some questions due to inconsistency with previously determined subsidence parameters typical for Illinois.

4.4.5 IL-2 Case Study (Illinois)

This case study involves data from above a longwall mine in south central Illinois. The mine is located adjacent to, and beneath, a lake. The lake is the centerpiece of a very active recreation area. The data was collected as part of a study to minimize the subsidence effects of high extraction mining of the Herrin (#6) coal seam. The lake is situated over part of the largest low sulfur coal reserve in Illinois (Powell, et al. 1992). Deposits of the Herrin (#6) coal are at a depth of about 600 to 700 feet beneath the lake. The coal ranges from 6 feet thick to 11 feet thick in the area of the lake (Powell, et al. 1992). An extraction thickness of 10 feet was used for calibration purposes. A value of 20% hardrock for the area is reported by Powell, et al. (1992) and used for calibration (Appendix I, Figure 68).

The case study involves a subsidence measurement line that traverses two adjacent panels. Considering each panel separately, the width to depth ratio is approximately 0.89 (611 ft/687 ft) indicating that the panels are subcritical. There is a 180 feet thick barrier between the panels, the presence of which is very pronounced in the subsidence data. Therefore, the panels could not be considered as a single subsidence trough. A pre-calibration subsidence factor of 50% was used for both panels (Appendix I, Figures 69 and 70). The pre-calibration estimate of the subsidence factor for the left panel is 51% (5.12 feet/10 feet x 100%) and 48% (4.83 feet/ 10 feet x 100%) for the right panel.

The original mine map was scanned with a desktop scanner and imported into AutoCAD. Two panels and the points along Pin Line 1 were digitized. The scanned mine map with digitized components is shown in Figure 19. An average edge effect offset of 108 feet was originally applied to all sides of both of the panels (Appendix I, Figures 72 and 73). This edge effect offset was estimated based on an average panel width of 611 feet and an average depth of 687 feet.

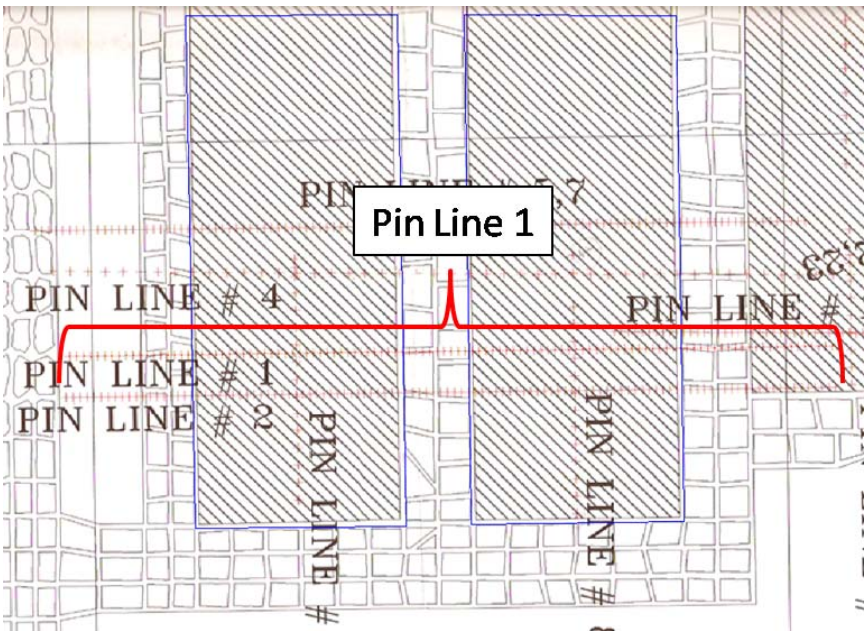

Figure 19: IL-2 Case Study Pin Line 1 - Scanned image of mine map with digitized panels and points. (Coal mine in Illinois, reprinted with company permission, mine location and company name confidential).

The digitized points and panels were imported into SDPS. Figure 20 shows the mine plan (including applied edge effect offsets) and prediction points as imported into SDPS.

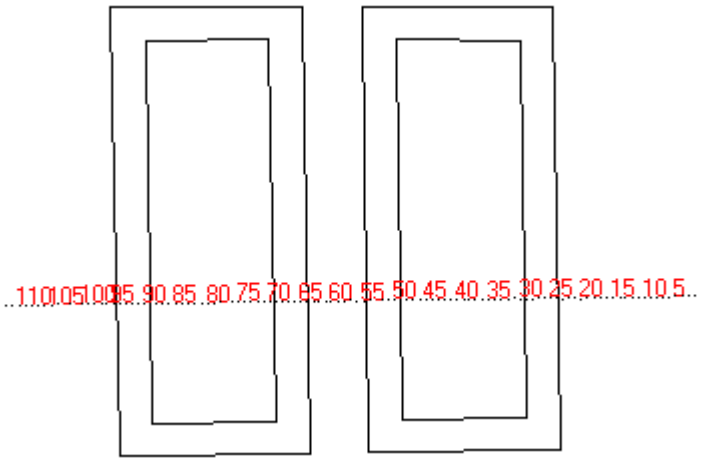

Figure 20: Pin Line 1 - Mine plan and prediction point locations in SDPS

Measured subsidence data used for this case study is provided in Table 15.

Table 15: Measured subsidence data for Pin Line 1

Point	Measured Subsidence (ft)	Point	Measured Subsidence (ft)	Point	Measured Subsidence (ft)
1	0	39	-4.97	77	-4.76
2	0	40	-4.91	78	-4.52
3	0	41	-4.82	79	-4.83
4	0	42	-4.67	80	-4.72
5	0	43	-4.42	81	-4.58
6	0	44	-4.02	82	-4.41
7	0	45	-3.29	83	-4.13
8	0	46	-2.43	84	-3.72
9	0	47	-1.61	85	-3.25
10	-0.04	48	-0.91	86	-2.73
11	-0.11	49	-0.54	87	-2.16
12	-0.12	50	-0.33	88	-1.55
13	0.04	51	-0.24	89	-0.47
14	-0.13	52	-0.2	90	-0.3
15	-0.14	53	-0.19	91	-0.23
16	-0.15	54	-0.18	92	-0.19
17	-0.16	55	-0.16	93	-0.15
18	-0.17	56	-0.15	94	-0.13
19	-0.19	57	-0.14	95	-0.1
20	-0.22	58	-0.14	96	-0.09
21	-0.24	59	-0.17	97	-0.08
22	-0.27	60	-0.15	98	-0.07
23	-0.3	61	-0.18	99	-0.05
24	-0.36	62	-0.37	100	-0.04
25	-0.44	63	-0.2	101	-0.02
26	-0.54	64	-0.13	102	-0.03
27	-0.73	65	-0.5	103	-0.02
28	-1.17	66	-0.25	104	-0.03
29	-2.04	67	-0.53	105	-0.02
30	-2.93	68	-1.25	106	-0.01
31	-3.65	69	-2.09	107	-0.01
32	-4.22	70	-2.83	108	-0.01
33	-4.65	71	-2.9	109	0
34	-4.92	72	-3.82	110	-0.01
35	-5.06	73	-4.1	111	0.01
36	-5.12	74	-4.3		
37	-5.12	75	-4.55		

Point	Measured Subsidence (ft)	Point	Measured Subsidence (ft)	Point	Measured Subsidence (ft)
38	-5.03	76	-4.73		

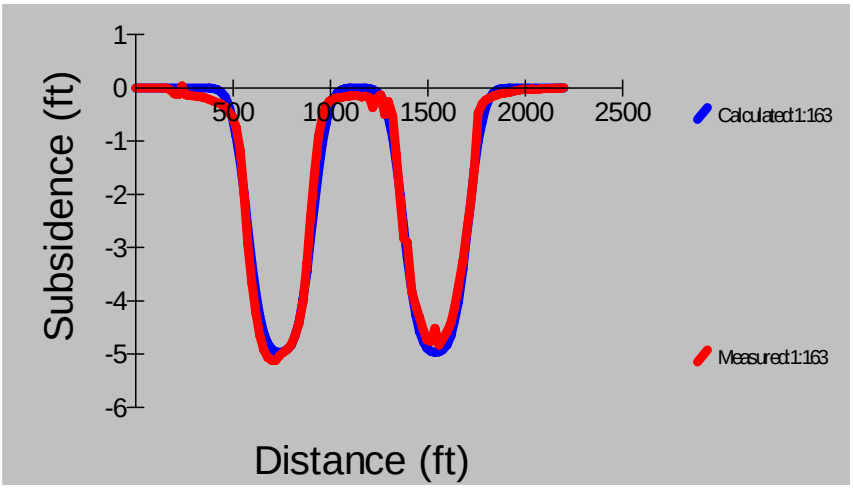

Figure 21: Matched predicted and measured subsidence profiles

Table 16: Calibration parameters

Rank	Iteration Number	Tangent of Influence Angle (Tanb)	Subsidence Factor (Smax/m)	Edge Effect Offset (ft)	Total Error	Percent Error
1	163	4.50	50	137	56.468	8.71
2	266	4.80	48	140	56.609	8.73
3	231	4.70	48	139	56.747	8.76

Figure 21 and Table 16 display the matched subsidence profile lines and the calibration parameters, respectively. The restrictions applied to the calibration are provided in Figures 75 through 78 in Appendix I. The calibrated value of Tan b is slightly higher than the typical Tan b of 3.5 established for subsidence in Illinois by studies conducted during the initial development of SDPS. The calibration-derived subsidence factor is exactly the same as the pre-calibration estimate, and the calibrated edge effect is only slightly higher than the pre-calibration estimate. Despite the subcritical subsidence classification, the calibration yields a relatively low error (8.71 %), further validating the influence function method utilized by SDPS.

4.4.6 AL-1 Case Study (Alabama)

This case study is involves measured final subsidence values from above a longwall mine near Alabama Highway 216. The data was collected along the roadway where it passes over top (or very nearby to) four longwall panels. The data used for this case study was only of moderate quality. If only individual panels are considered for this case study, the width to depth ratio is approximately 0.49 (970 ft/2000 ft), which suggests a subcritical situation. However, if the four panels are considered together, the width to depth ratio is 2.26 (4515 ft/2000 ft), and the panel is considered supercritical. While the presence of the barriers between the pillars can be identified to some degree in the measured subsidence data, the overall shape of the subsided area appears to act much like one basin (see Figure 24). To acknowledge the presence of the barrier pillars, the calibration was completed using four separate parcels (panels).

Average elevations were estimated for all monitoring points, and for the mine itself, using a limited number of drill hole logs. Drill hole logs suggest highly variable estimates of percent hardrock. A value of 80% hardrock was used (Appendix I, Figure 79). The average coal thickness in the mine was estimated using drilling records to be around 6.38 feet (Appendix I, Figure 80). The pre-calibration estimate of subsidence factor is 54% (3.43 feet/6.38 feet x 100%) and was applied to all four panels (Appendix I, Figures 80 through 83).

The relatively large scale of the initial mine map required photocopying at a reduced scale to create a map that could be scanned with a desktop scanner. The scanned image was imported into AutoCAD and scaled appropriately. Four longwall panels and all monitoring points were digitized as shown in Figure 22.

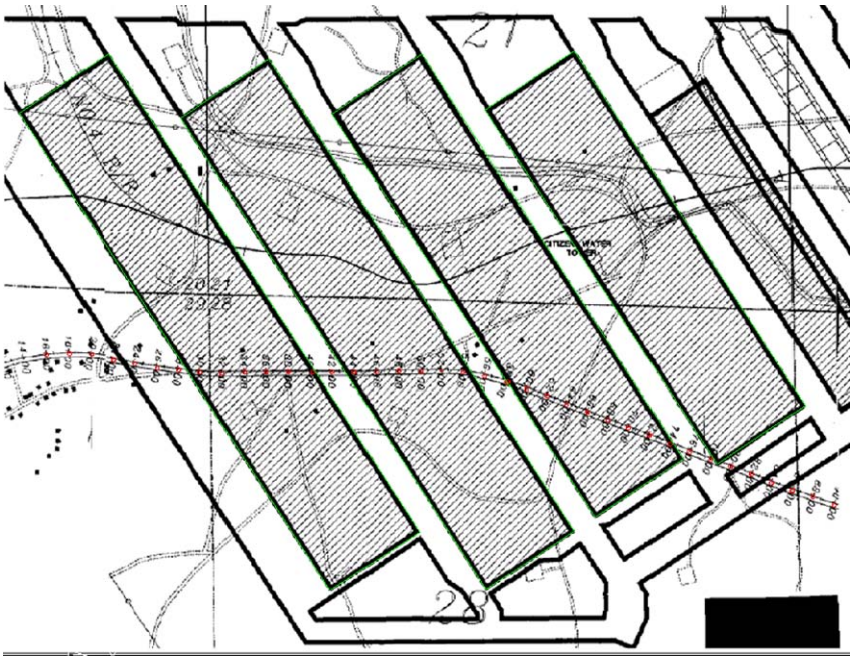

Figure 22: Scanned image of mine map with digitized panels and points. The map was provided to Dr. Michael Karmis of the Center for Coal and Energy Research at Virginia Polytechnic and State University by Jim Walter Resources (#5 Mine, East Brookwood, Alabama, 2001)

.

The digitized panels and point were imported into SDPS (Figure 23).

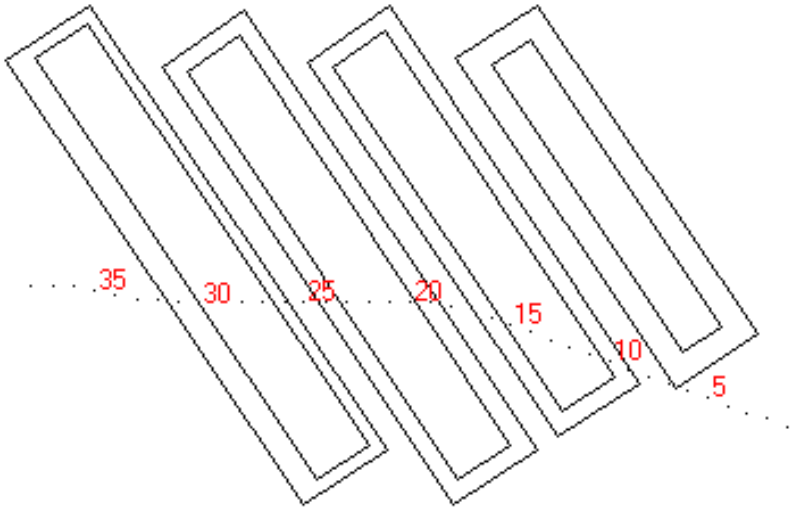

Figure 23: Mine plan and prediction point locations in SDPS

As indicated in Figure 23, variable edge effect offset distances were applied to the panels. The edge effects specified in the mine plan were used for calibration (Appendix I, Figures 85 through 92). Figure 96 of Appendix I indicates the SDPS setting that forces the calibration function to use the edge effect “AS defined in mine plan”. Edge effect adjustments to each panel were made manually by observing the graphical comparison of predicted versus measured profile curves during the iterative calibration process.

The measured final subsidence values for this case study are provided in Table 17.

Table 17: Measured subsidence values

Point	Measured Subsidence (ft)	Point	Measured Subsidence (ft)
1	-0.2	21	-3.36
2	-0.24	22	-3.26
3	-0.26	23	-2.84
4	-0.31	24	-2.61
5	-0.36	25	-2.6
6	-0.46	26	-2.72
7	-0.6	27	-2.67
8	-0.57	28	-3.21
9	-1.1	29	-2.74
10	-1.46	30	-1.55
11	-2.12	31	-0.4
12	-3.11	32	-0.08
13	-3.43	33	-0.12
14	-2.93	34	-0.13
15	-3.4	35	-0.14
16	-2.58	36	-0.13
17	-2.58	37	-0.09
18	-2.57	38	-0.09
19	-2.68		
20	-2.99		

Figure 24 displays the matched subsidence profiles and Table 18 displays the calibration parameters. The calibrated Tanb of 2.10 is very close to the average Tan b for the eastern U.S. (2.31), as defined by previous studies. The calibration-derived subsidence factor value of 88% is consistent with the pre-calibration estimate (80%). 15.48% error is relatively high compared to many of

the other case studies, but this particular case study is somewhat more complicated than others due to the number of panels, irregular orientation of the monitoring line with respect to the panels, use of an average value to represent depth of the mine, and the fact that the monitoring points were located along a highway where they may have been affected by unknown variables. The relatively excessive depth of this mine (approximately 2000 feet) is also likely to be a contributing factor leading to the higher error involved with this case study calibration. Most of the data upon which SDPS is based was measured over shallower mines.

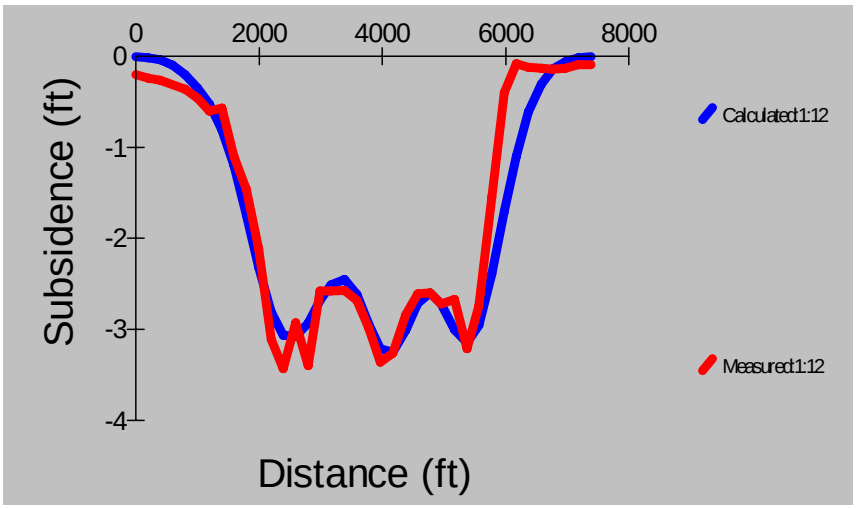

Figure 24: Matched predicted and measured subsidence profiles

Table 18: Calibration parameters

Rank	Iteration Number	Tangent of Influence Angle (Tanb)	Subsidence Factor (Smax/m)	Edge Effect Offset (ft)	Total Error	Percent Error
1	12	2.10	88.0	250	25.593	15.48
2	13	2.10	89.0	250	25.973	15.71
3	2	2.00	86.0	250	26.195	15.85

The right side of the subsidence profile in Figure 24 (which corresponds to the left side of the monitoring points in Figure 23) appears to be the source of much of the calibration error. Appendix I, Figure 86 indicates that an edge effect of 250 feet was applied to the left side of the left-most panel (edge effect was held to “as

defined in mine plan" during calibration). Numerous manual adjustments of the edge effect at this location were completed during the calibration process, with the current model being the best fit possible. Overall, this case study serves as a good example of the ability to account for multiple variables associated with more complicated subsidence scenarios using SDPS.

4.5 Discussion

The case studies presented in this section confirm the validity of the subsidence prediction methodology of SDPS and demonstrate the ability of the methodology to accommodate various subsidence scenarios. In most cases, the influence function methodology is able to fit prediction profiles to measured profiles with less than 10% error. It should be emphasized that when measured values are not available for calibration, the operation can use default values for subsidence engineering parameters for predictions. However, when measurements are available, then site specific values can be determined and subsequently applied to predict surface deformations at neighboring locations. The case studies also demonstrate the flexibility of the influence function, as a powerful tool for a comprehensive analysis of ground movements due to underground mining.

As demonstrated by the case studies, the influence function can achieve accurate calibration despite a lack of abundant data. The case studies also demonstrate the various ways in which data and maps can be input to the program (scans of original maps, reduced photocopies, hand-drawn to scale maps). Furthermore, accurate model calibration is achieved over single panels, as well as over numerous adjacent panels. Calibrated tangent of influence angle (Tan b) values can be compared to previously-determined, regional Tan b values to assess the validity of the calibrations. Differences in Tan b and subsidence factor values for measurement lines in the same area or over the same mine can also be used to identify questionable data or anomalies, whether geologic or otherwise.

The flexibility of the influence function method of SDPS is further exemplified in many of the case studies by the ability to assign variable edge effects to different sides of a single panel. This option allows for more accurate calibration where nearby excavations or anomalous geologic conditions may affect one or more sides of a panel differently. The manually-defined edge effects are held constant

for computer-driven calibration procedures and can be adjusted based on evaluation of calibration results and site-specific features.

Some of the error associated with calibrated results is undoubtedly a result of measurement error. Other errors may be attributable to site-specific anomalous conditions that must be evaluated separately for each case. In case study NA-1, some of the error appears to be a result of the inability of the SDPS influence function methodology to account for positive values of subsidence (upsidence, or where the ground has moved upward as a result of ground deformation). In AL-1, the greater depth of the mine relative to the majority of mines evaluated for the development of SDPS may have some effect on the accuracy of the calibration.

The collection and calibration of subsidence case study data form the basis of key relationships used by the influence function of SDPS. The case studies discussed in this chapter further validate the method, while also providing insight into some of the limitations of the methodology.

5. Objective II: Improve Prediction Methodologies

5.1 Modeling the Dynamic Deformations

5.1.1 Basic Concepts

An understanding of the difference between final, or static, subsidence and dynamic subsidence must be established in order to properly assess almost any mine subsidence issue. In general, the dynamic subsidence differs from the final subsidence in that it is the subsidence movements that occur as mining progresses toward, beneath, and past a point on the surface. In contrast, static or final subsidence relates to the degree of subsidence that occurs at a given point on the surface after the mining has passed the point and no further subsidence-related movements are expected to occur. The distinction between dynamic and static states of subsidence is very important because the distribution of strains, and therefore damage potential, for each condition is significantly different. When evaluating an area to be undermined, it is important that mining engineers assess the damage potential from both dynamic and static subsidence. The final, static subsidence trough that develops over a mined area will have permanent effects on the surface structures located near the edges of the subsidence basin due to tensional strains. Depending on the size and depth of the mine, an additional amount of area within the subsidence basin may be affected by compression. In the case of dynamic subsidence, the majority of surface area within the final subsidence basin will experience both tensile and compressive strains as mining progresses. Surface structures may be damaged by both tension and compression. A basic diagram depicting the concept of a moving “wave” of subsidence, accompanied by both tensile and compressive strains, is presented in Figure 25.

The concept of dynamic subsidence is not new. Dixon (1885) recognized “the existence of a leading and following wave of disturbance” associated with underground mining. Other researchers also noticed similar phenomena, and in 1948, Perz made one of the earliest attempts to mathematically describe the characteristics of dynamic subsidence (Whittaker and Reddish, 1989). Perz (1948) created an early form of a subsidence time development plot that indicates the percentage of total subsidence of a single point on the surface over time, after initial undermining of the point.

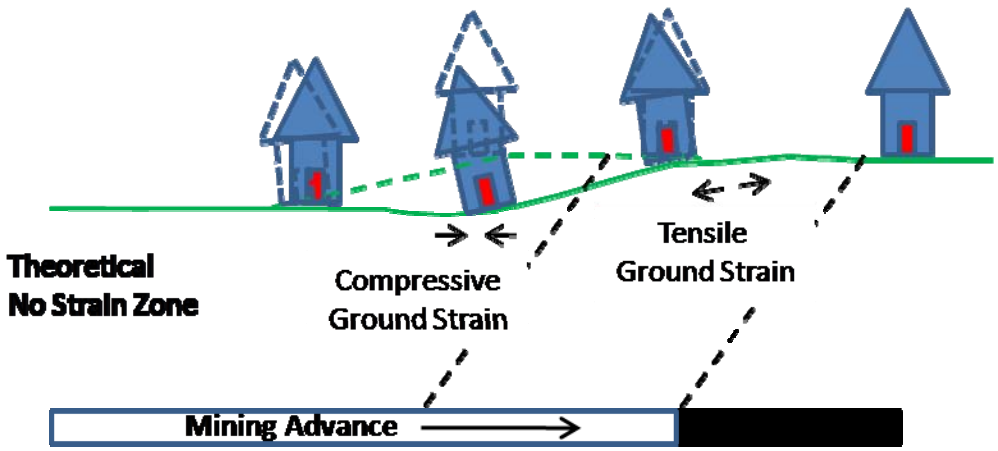

Figure 25: Dynamic subsidence as a moving "wave" accompanied by both tensile and compressive strains (after Geddes and Cooper, 1962).

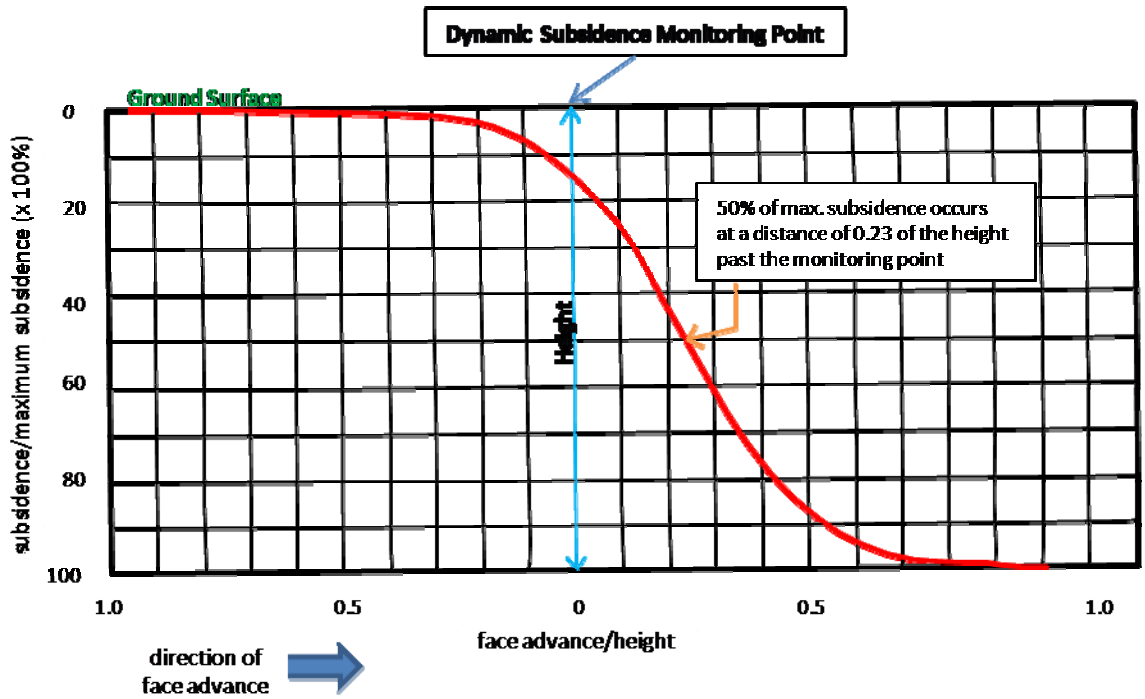

Figure 26: Expected subsidence of a surface point over time as a mine face progresses toward, underneath, and past the point. Image modified from National Coal Board (1975).

More recent work associated with subsidence development plots has been completed. Two noteworthy publications include National Coal Board (1975) and Jarosz, et al. (1990). The Subsidence Engineers' Handbook by the National Coal Board (1975) includes analyses of numerous dynamic subsidence case studies from England. Figure 26 displays the vertical subsidence (expressed as a percentage of the total subsidence at the point) expected with regard to the position of a moving longwall face (expressed as ratio of face distance from the surface point to coal seam depth). Movement of the longwall face progresses

from in front of the surface point (left side of Figure 26), under the surface point (0 on the x-axis), and past the surface point (right side of Figure 26).

As shown in Figure 26, data collected by the National Coal Board indicates that the subsidence at a given surface point will be 15.5% of the final expected subsidence at that point when the mine face is directly beneath the surface point. The figure also indicates that 50% of the final expected subsidence will occur at the surface point when the mine face has passed the point by a distance of 0.23 x the depth of cover (or thickness of overburden). In the same way, 97.5% of final expected subsidence is likely to occur when the mine face has advanced 0.7 x the depth of cover. The type of plot shown in Figure 26 is a very important tool for workers seeking to mitigate the effects of dynamic subsidence. While the subsidence development plot in the Subsidence Engineers' Handbook is derived from data collected in English coalfields, the concept of the plot is easily transferrable to other areas, provided that adequate data is available.

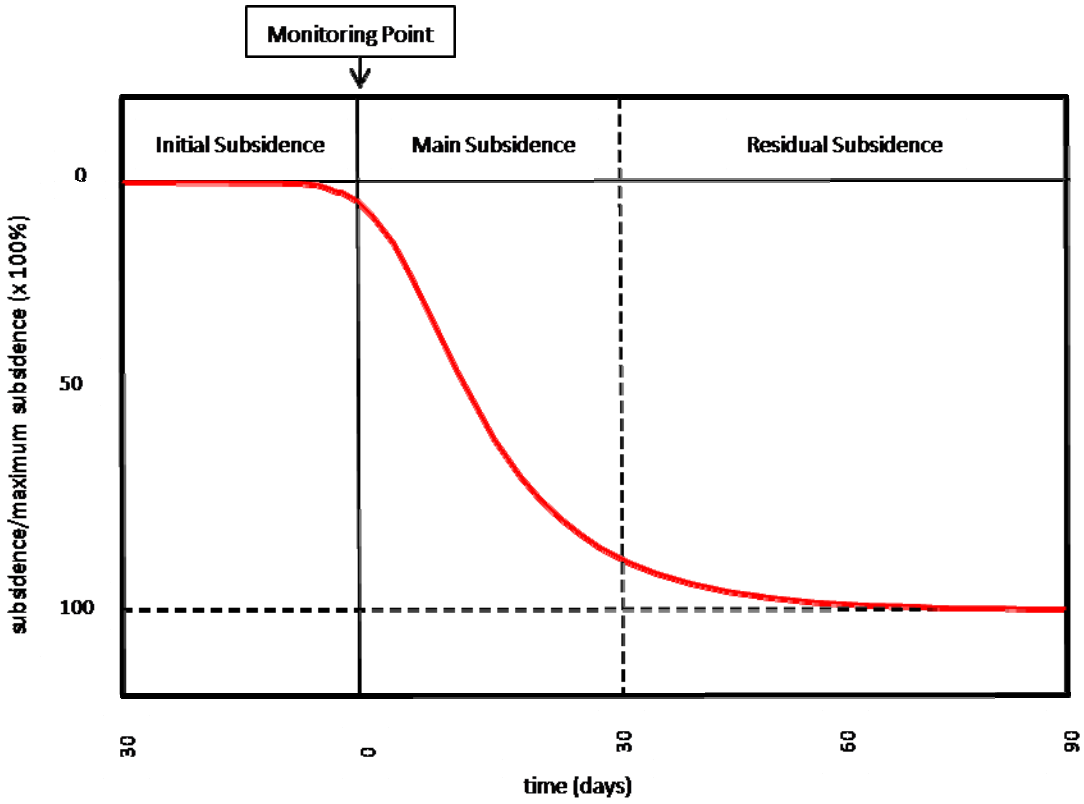

Figure 27: Jarosz, et al. (1990) confirmed three phases of subsidence development and produced a conceptual subsidence development plot. Image modified from Jarosz, et al. (1990).

Jarosz, et al. (1990) confirmed three separate phases of subsidence development which they refer to as initial, main, and residual. Using this concept, they produced their own conceptual subsidence development plot using data from the Appalachian coalfields in the United States (Figure 27).

With the intention of obtaining the means to predict dynamic subsidence, Jarosz, et al. (1990) reviewed numerous mathematical functions relating subsidence and time. They stated that it is important that the final form of a time-subsidence equation be based on the same type of equation used to describe the final state of subsidence. Since they were interested in creating a time-subsidence equation to predict dynamic subsidence related to the final subsidence predicted by SDPS, they chose the subsidence equation proposed by Knothe (1953) that uses the influence function based on the normal distribution of influences. Jarosz, et al. (1990) used the Knothe (1953) methodology to develop a conceptual solution for longwall mining of a rectangular excavation panel with one advancing side. The mathematics developed by Knothe (1953) and adapted by Jarosz, et al. (1990) form the basis for the dynamic subsidence development function recently implemented into SDPS. An additional result of the work done by Jarosz, et al. (1990) is an equation for approximating the time required for dynamic movements to reach the end of the main phase of subsidence (phase 2). Accurate prediction of the end of the main phase of subsidence is particularly important for subsidence mitigation activities and for planning development of surface structures on recently undermined land. For example, placing buildings over undermined areas prior to the completion of the main phase of subsidence may result in avoidable damage. Further discussion of the methodology by Knothe (1953) and Jarosz, et al. (1990) is provided in section 5.1.2.

In addition to a traveling “wave” of observed vertical displacement due to subsidence, progression of other subsidence parameters, such as ground strain, are also recognized. Wardell (1957) was one of the first to demonstrate a “consistent travelling ground strain profile” for dynamic subsidence (Figure 28), a very significant step toward understanding the differences between static and dynamic subsidence and the associated damage potential.

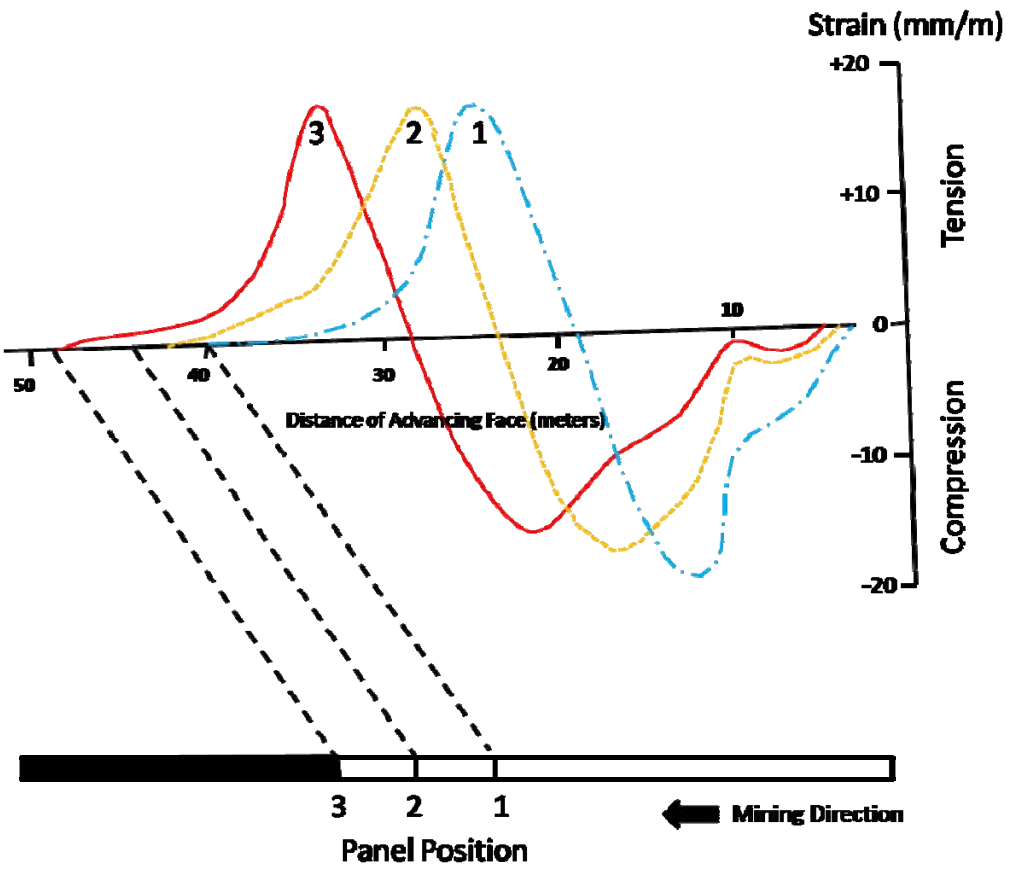

Figure 28: In 1957, Wardell demonstrated a "consistent travelling ground strain profile" for dynamic subsidence. Image modified from Wardell (1957) in Whittaker and Reddish (1989).

The ability to predict dynamic subsidence parameters, particularly strains, allows for minimization and efficient mitigation of damage to surface structures. Luo, et al. (2005) as well as many others demonstrate the importance of predicting dynamic movements related to subsidence. For example, Luo, et al. (2005) presents a case study in which a large, long warehouse-like building was successfully protected from dynamic subsidence damage. Expected characteristics of the dynamic subsidence were calculated, critical strength values for sections of the building were estimated, and mitigation techniques were employed to lessen the expected damage. In this particular case, the long building was actually cut into sections, which were then wrapped in cables. The mitigation efforts allowed the individual sections of the building to ride over the "wave" of subsidence and avoid damage due to angular distortion, ground strain, and differential settling (Luo, et al. 2005).

Preusse, et al. (2003) also presents a case in which the dynamic characteristics of surface deformation were successfully predicted to mitigate the degree of

damage to a 24-inch pipeline carrying numerous hydrocarbons. Instead of securing or modifying surface structures to withstand the effects of the dynamic deformations, the face advance rate of the mining was adjusted to decrease the maximum induced surface strains. Other examples of prediction and mitigation to lessen the effects of both final and dynamic ground deformation movements are included in Section 6.

5.1.2 Implemented Methodology

The methodology discussed by Jarosz, et al. (1990), and based on Knothe (1953), has been implemented into SDPS to enable the prediction of dynamic subsidence experienced by surface points as longwall mining approaches, passes, and moves away. The basic time-subsidence function proposed by Knothe (1953) is:

$$\acute{S}(t) = c[S^f(t) - S(t)] \qquad [1]$$

Where,

$S^f(t)$ = final subsidence,

c = time coefficient, and

$S(t)$ = subsidence at time t.

(Knothe, 1953, as presented in Jarosz, et al., 1990)

As shown in Figure 27, the methodology by Jarosz, et al. (1990) includes three phases of subsidence development (initial, main, and residual). In the Appalachian region, the main and residual phases of subsidence are believed to often constitute approximately 90% of the total subsidence (Jarosz, et al., 1990). Using the relationship by Knothe (1953), and an influence function for final subsidence at a point above a panel, Jarosz, et al. (1990) developed the following equation for calculating subsidence development due to undermining by a longwall panel. The equation assumes that the longwall panel has a constant width and that the extraction advances at a constant rate.

$$S(x_t, x_o, y_1, y_2, z, \Delta t) = S^f(x_t, x_o, y_1, y_2, z) -$$
$$- \exp\left(\frac{u_z^2}{4\pi}\right) \exp\left(\frac{u_z x_t}{r_z}\right) S^f(x_t + \frac{r_z u_z}{2\pi}, x_o + \frac{r_z u_z}{2\pi}, y_1, y_2, z) +$$
$$+ \Delta S^f(x_t, x_o, y_1, y_2, z)[1 - \exp(-c\Delta t)] \qquad [2]$$

Where,

$x_t = x_0 + vt$,

x_0 = the starting x-coordinate for the advancing panel (assumed to be 0),

v = the rate of advance of mining (assumed to be constant),

t = the time since mining began,

x_1 and x_2 = x-coordinates for the advancing panel,

y_1 and y_2 = define the width of the advancing panel (assumed to be constant),

z = value defining the depth of mining,

Δt = time since excavation time stopped (Δt = 0 for advancing faces),

S^f = final subsidence at time t,

$u_z = -\frac{c_z r_z}{v}$,

c_z = time coefficient for horizon z,

r_z = the radius of influence at the z horizon (ground surface), and

$\frac{r_z u_z}{2\pi}$ = magnitude of translation used to calculate subsidence due to advancing longwall (see discussion below). (Jarosz, et al., 1990)

The first part of the equation represents final, asymptotic subsidence at a point. Subsidence development at the point while the face is moving (constant velocity) is represented by the first two parts of the equation. Finally, the residual subsidence, or the subsidence development between the time at which the face stops and the time when the maximum subsidence is reached, is represented by the entire equation (Jarosz, et al., 1990).

To calculate the subsidence due to the advancing longwall at a given point, the methodology proposed by Jarosz, et al. (1990) evaluates the effects of extraction at an offset panel location. For any actual panel location, the method calculates the predicted effects of subsidence from a panel position offset a distance equal

to $\frac{V_x U_x}{2\pi}$ in the opposite direction of mining advance (second part of equation 2). The offset distance is referred to as the magnitude of translation. Prediction of subsidence due to an advancing longwall panel involves numerous calculations of predicted subsidence for translated panel positions corresponding to each actual panel location. The calculations reduce the final subsidence for each face location according to the influence of the offset (or translated) panel location. The overall effect of the translations is that the higher the advance rate, the greater the effective edge effect (combination of static edge effect and offset distance due to panel advance). Figure 29 illustrates the difference between predicted dynamic subsidence for an advance rate of 20 feet/day as compared to predicted subsidence for an advance rate of 30 feet/day. As is evident from the figure, a more rapid face advance rate (30 feet/day) yields less subsidence than a slower face advance rate (20 feet/day), for the same face location. This relationship causes the inflection point of the dynamic subsidence curve (which defines the offset distance due to panel advance) to be located further from the actual panel location, therefore increasing the offset distance due to panel advance.

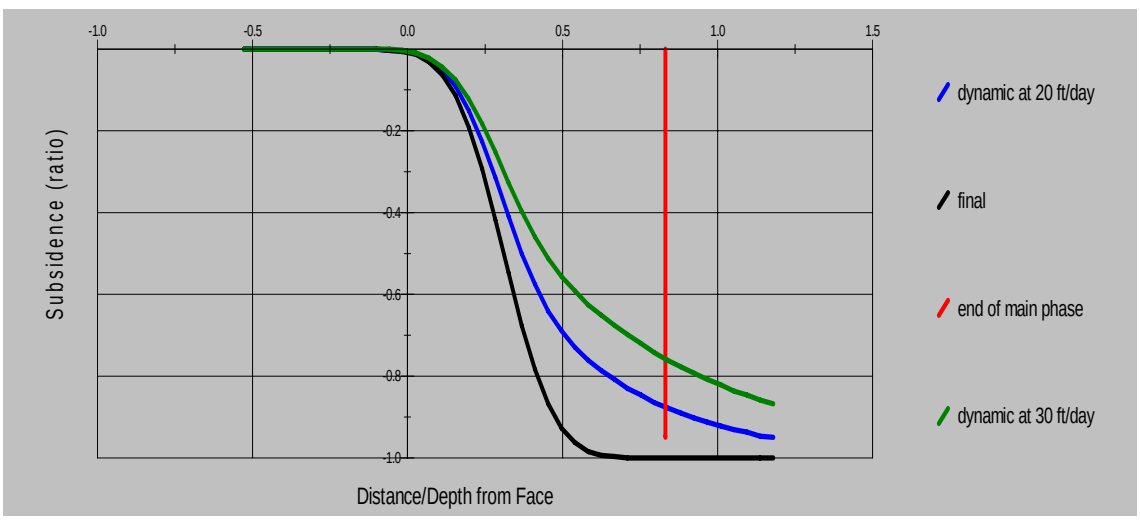

Figure 29: Comparison of predicted dynamic subsidence for same point with varying advance rates.

Jarosz, et al. (1990) also proposes a method for estimating the time required for the main subsidence phase to cease as the panel moves away from the surface point. The basic relationship is:

$$\Delta t \cong \frac{r}{v} + \frac{1}{c} \qquad [3]$$

Where

$\Delta t =$ time period of main subsidence phase (see Figure 27)

r = range of influence of the panel

v = speed of extraction

c = time coefficient (Jarosz, et al., 1990)

The main phase of dynamic subsidence development is believed to include approximately 75% of total subsidence (Jarosz, et al., 1990). Therefore, an estimate of the end of the main phase can be useful for planning post-mining surface development and for determining the likelihood that post-mining damage is related to mining.

5.1.3 Validation of Method

The following dynamic subsidence case studies were completed to test the validity of the methodology proposed by Jarosz, et al. (1990). The work involves data collected from case studies NA-2 and IL-1. More information regarding the case studies is available in Section 4. For validation, measured dynamic subsidence data is compared to the predicted dynamic subsidence curve generated for each case study. For case study data to be used for comparison, it must include multiple subsidence measurements taken over time at an established monument point as the longwall panel advanced toward, beneath, and beyond the point. The location of the longwall face with respect to the monument point and the date must also be known for each measurement. Ideally, measurements at the point should have started before the longwall was close enough to have caused any movements at the point.

Subsidence parameters determined by calibration with measured final subsidence data (Section 4) are used for dynamic subsidence prediction. For each case, the predicted (blue line) and measured (green line) dynamic subsidence movements are compared graphically. On each graph, the monument point is located at x = 0. Values on the y-axis indicate magnitude of subsidence, with y = 0 being the pre-mining location of the surface points. Negative x values are used to indicate the location of the panel in front of the point (as it approaches). Positive values on the x-axis indicate the distance of

the panel past the point (as the panel moves away and the point has been undermined).

The graphical outputs also include a predicted final subsidence line (black). The vertical distance between the predicted dynamic subsidence line and the predicted final subsidence line at any point indicates the expected residual subsidence possible at the point if the panel was to stop at that position relative to the point. A vertical line (red) is included to indicate the location of the advancing face past the monument point at which the main phase of subsidence is estimated to be complete. Screen shots of the SDPS windows used for dynamic subsidence prediction are included in Appendix II. Appendix II is referenced throughout the text to facilitate description of the procedures followed for each case study.

5.1.4 NA-2 Dynamic Case Study (Northern Appalachia)

The details of this case study are available in the previous chapter. Prediction of dynamic subsidence was done on six points as shown in Figure 30.

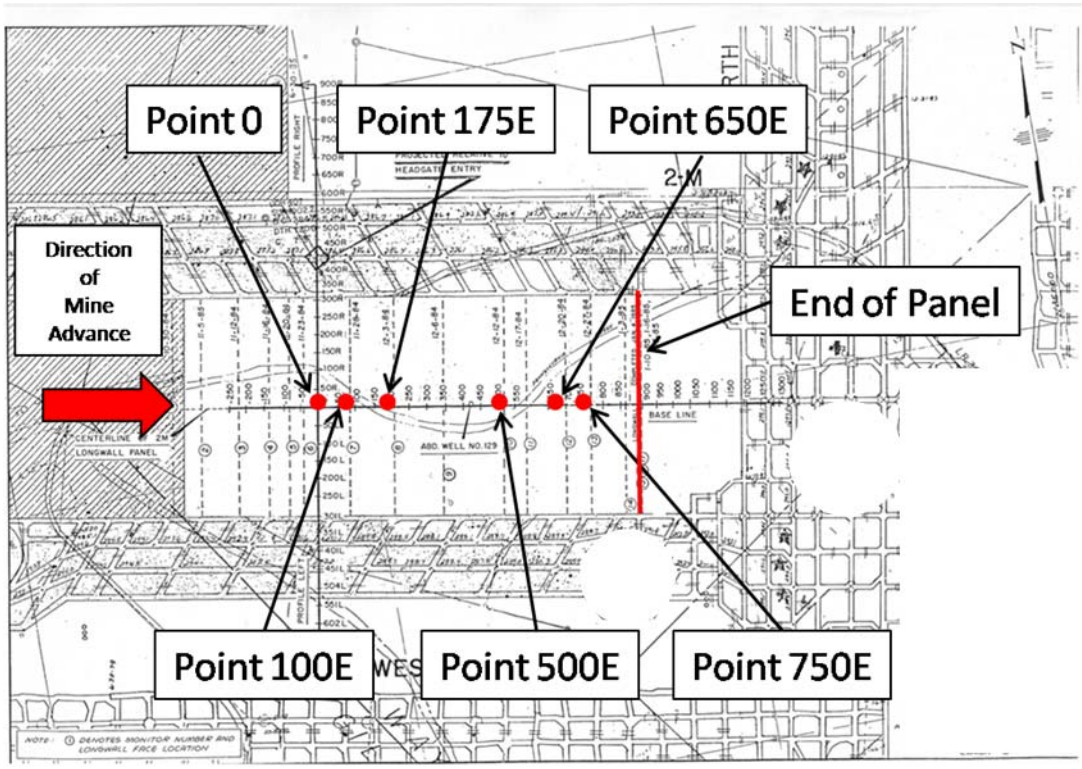

Figure 30: Monitoring points used for dynamic prediction-measured subsidence comparison. Mine map base from coal mine in Northern Appalachia

.
Figure 31 shows a surface point and an approaching longwall mine panel with edge effect as it is shown in SDPS. Each of the points in this case study was modeled as shown in Figure 31.

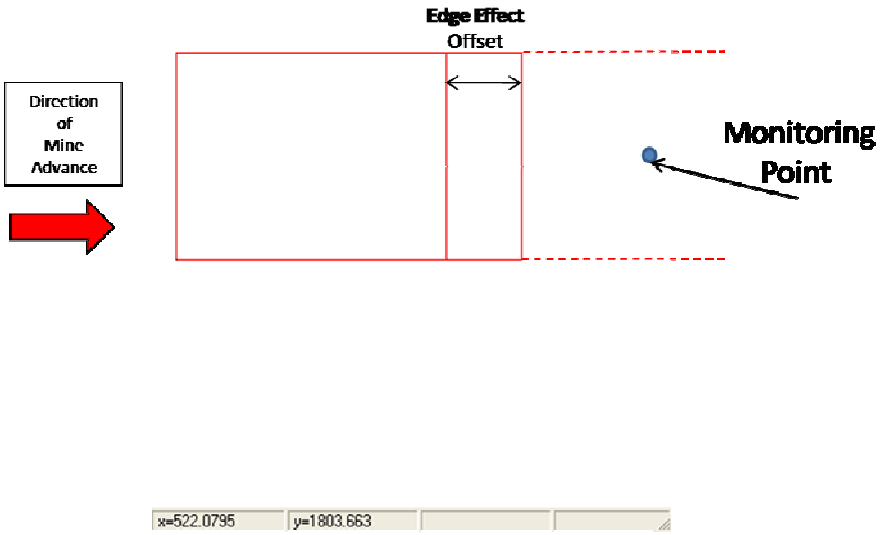

Figure 31: Representation of mine panel with edge effect and dynamic subsidence prediction point.

Subsidence parameters for this dynamic case study come directly from the results of the calibration procedures completed in Section 4. Figure 32 shows that the tangent of the influence angle used for this case is the same (3.10) as the value resulting from calibration (Table 6). An average rate of panel advance of 19 feet/day was calculated using data available from the coal company (Figure 33). Figure 33 also indicates other settings used for the dynamic prediction, as well as an animation of the advancing panel used to confirm the settings prior to running the model.

The measured dynamic subsidence development data, to which predicted values are compared, is provided in the upper left column of Table 21. Entry of the measured dynamic subsidence data is done using the Subsidence Development Data option from the Prediction Points Management screen (Figure 34 and Figure 35). The data includes the measured subsidence and the location of the face relative to the monitoring point/prediction point.

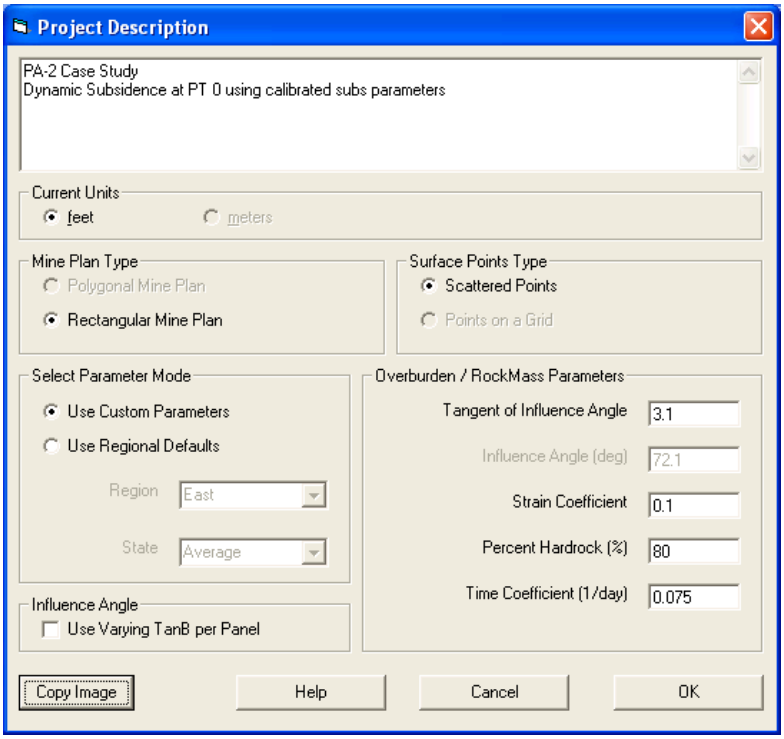

Figure 32: NA-2 Dynamic Case Study - SDPS Project Description Screen

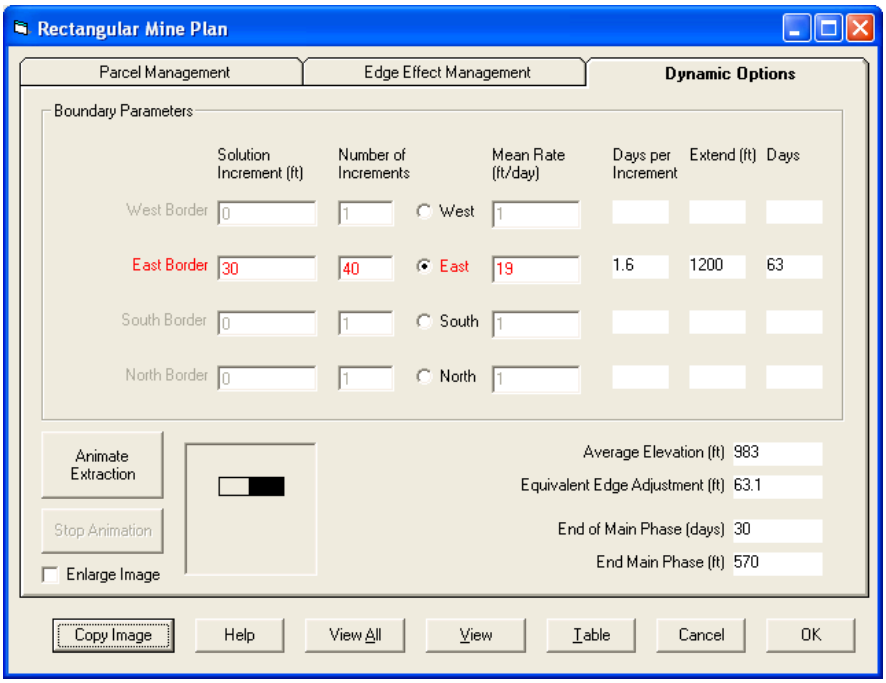

Figure 33: NA-2 Dynamic Case Study – Dynamic Options Screen

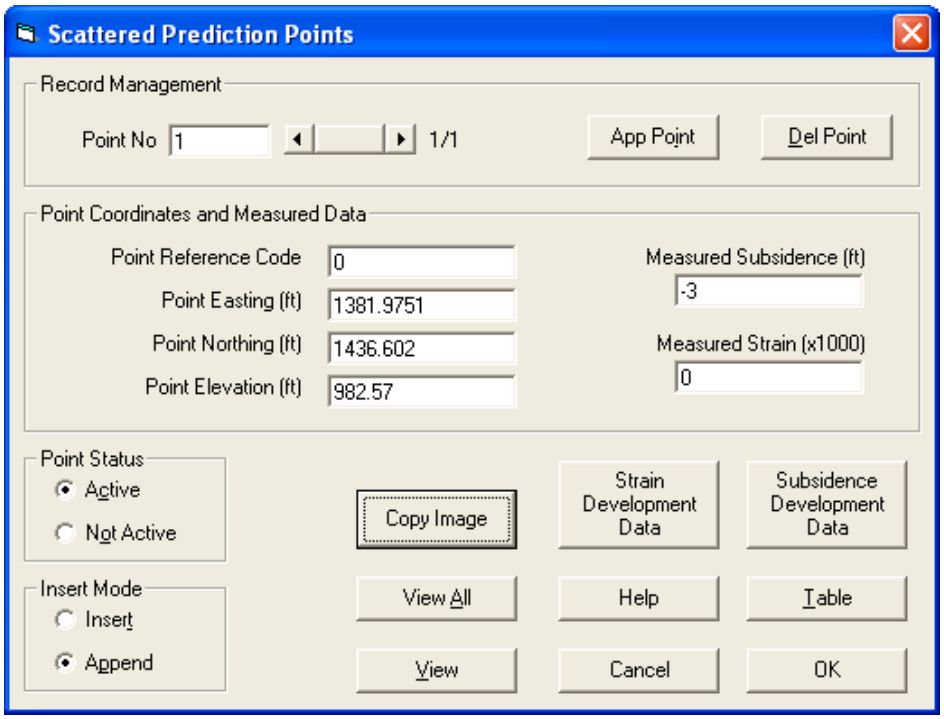

Figure 34: NA-2 Dynamic Case Study – Prediction Points Management Screen

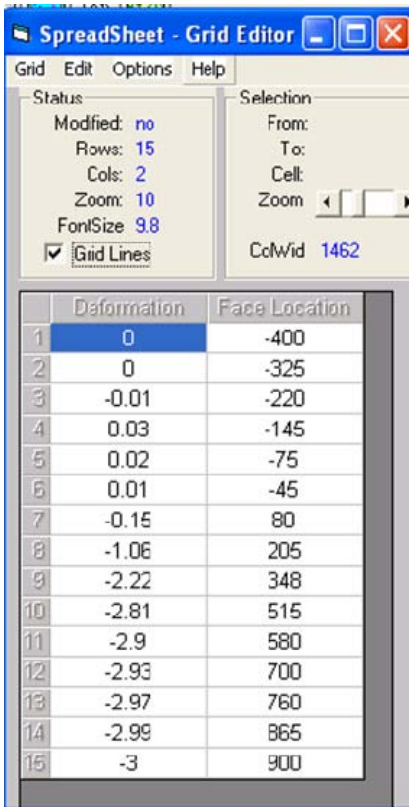

	Deformation	Face Location
1	0	-400
2	0	-325
3	-0.01	-220
4	0.03	-145
5	0.02	-75
6	0.01	-45
7	-0.15	80
8	-1.06	205
9	-2.22	348
10	-2.81	515
11	-2.9	580
12	-2.93	700
13	-2.97	760
14	-2.99	865
15	-3	900

Figure 35: NA-2 Dynamic Case Study – Subsidence Development Data

Calculation of predicted dynamic development is initiated using the Calculate –

Development of Deformations option from the main SDPS menu. Figure 36 indicates the calculation settings used for this case study. To compare the predicted values with measured subsidence values, a graph is generated. The Graph Options section shown in Figure 36 provides options for graph generation. The distance of the face relative to the point may be shown as a fraction of the depth of the mine and the deformations may be shown as a fraction of the maximum subsidence at the point. For the purposes of this discussion, the graphs show the subsidence in feet relative to the pre-mining ground elevation. Similarly, the relative distance of the face from the monitoring/prediction point is indicated as feet in front of the point (negative x-axis) and feet past the point (positive x-axis).

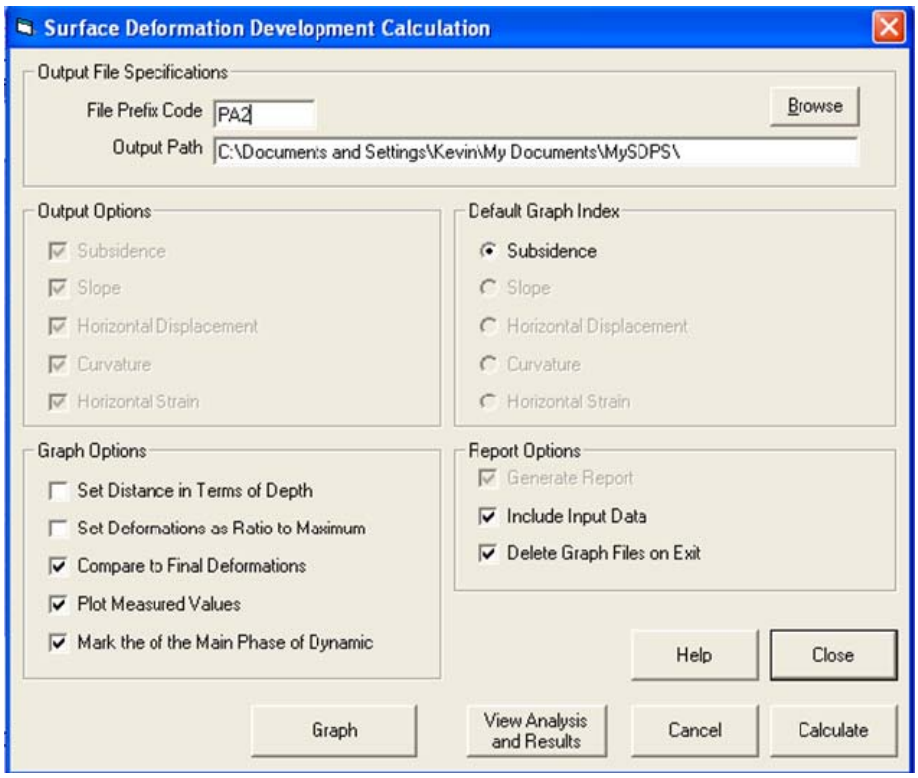

Figure 36: NA-2 Dynamic Case Study – Surface Deformation Development Calculation Screen

The results of dynamic subsidence prediction and comparison with measured values for Point 0 (Figure 30) is shown in Figure 37. The graph includes the predicted final subsidence at Point 0 as related to the position of the face, as well as the calculated estimate of the end of the main phase of subsidence. The comparison in Figure 37 shows very good correlation of predicted and measured subsidence values for face distances greater than 300 feet past the point. While

the predicted and measured values do not appear to correlate as closely for face distances closer than 300 feet past the point, it is important to note that the measured values are limited in number and it is possible that more frequent measurements during the early phase of subsidence development may have resulted in better correlation.

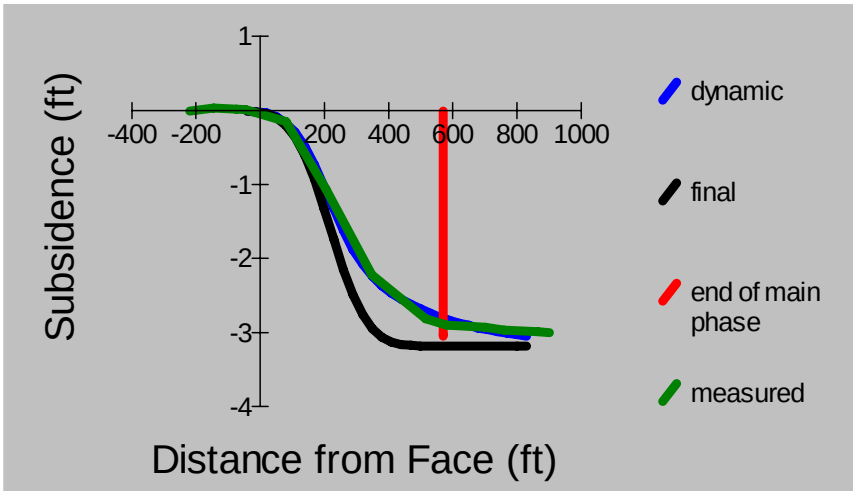

Figure 37: Comparison of dynamic subsidence prediction with measured subsidence values at Point 0

The correlation of predicted values with measured values, as shown in Figure 37, is important for assessing the affects that dynamic development of subsidence will have on surface structures. However, the limitations of the prediction methodology must be understood. The following two examples use the abundance of data available for case study NA-2 to demonstrate how rate of face advance can have significant effects on dynamic development predictions.

The face advance rates for the NA-2 mine are summarized in Table 19. The rates were calculated by measuring the distance between known face locations and dividing by the time difference between the two face locations. The result of dynamic subsidence prediction for Point 0 using a 37 ft/day average advance rate (as calculated in Table 19) is shown in Figure 38.

Table 19: Average advance rate calculations using all available data

	face advance distance (ft)	time to advance distance (day)	advance rate (ft/day)
10/30/1984			
11/5/1984	75	6	12.5
11/12/1984	105	7	15

	face advance distance (ft)	time to advance distance (day)	advance rate (ft/day)
11/16/1984	75	4	19
11/20/1984	70	4	18
11/23/1984	30	3	10
11/28/1984	125	5	25
12/3/1984	125	5	25
12/6/1984	143	3	48
12/12/1984	167	6	28
12/17/1984	65	5	13
12/20/1984	120	3	40
12/27/1984	60	7	9
1/3/1985	105	7	15
1/4/1985	35	7	5
		average	**37**

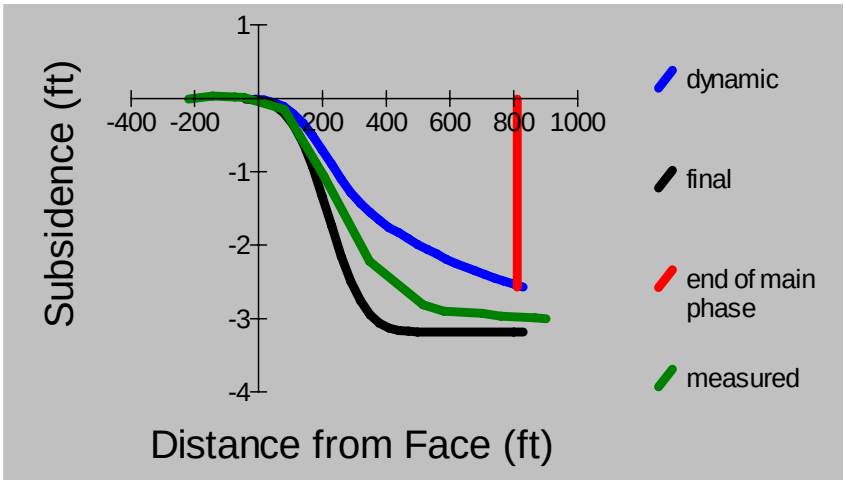

Figure 38: Dynamic subsidence prediction using a 37 ft/day average advance rate

Using a 37 ft/day average advance rate, the measured data does not fit very well with the predicted dynamic subsidence. In an attempt to decrease the range of estimated advance rates and produce better correlation of measured and predicted values, the highest and lowest advance rates were eliminated and the average advance rate for the face was recalculated. Table 20 displays the changes and the new average advance rate of 19 ft/day, and Figure 39 shows the resulting fit of predicted data with measured data.

Table 20: Average advance rate calculations after elimination of highest and lowest estimated advance rates.

	face advance distance (ft)	time to advance distance (day)	advance rate (ft/day)
10/30/1984			
11/5/1984	75	6	12.5
11/12/1984	105	7	15
11/16/1984	75	4	19
11/20/1984	70	4	18
11/23/1984	30	3	10
11/28/1984	125	5	25
12/3/1984	125	5	25
12/6/1984	143	3	(48)
12/12/1984	167	6	28
12/17/1984	65	5	13
12/20/1984	120	3	40
12/27/1984	60	7	9
1/3/1985	105	7	15
1/4/1985	35	7	(5)
		average	**19**

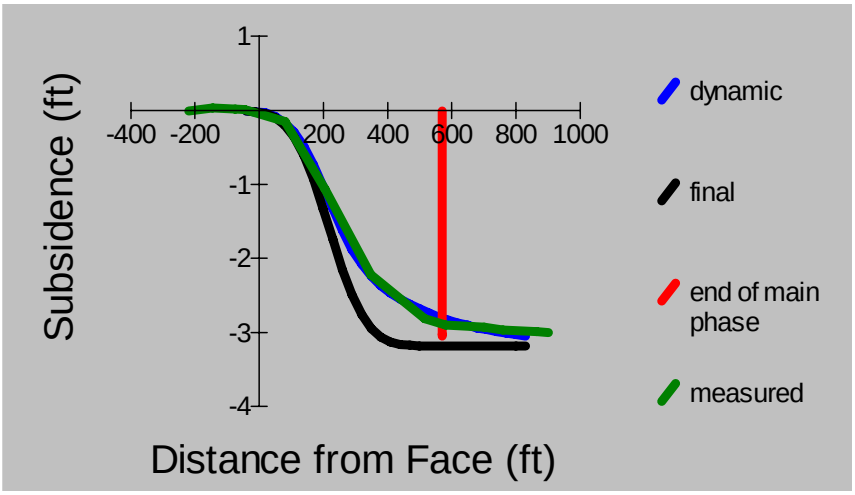

Figure 39: Dynamic subsidence prediction using a 19 ft/day average advance rate

As is evident, because the current methodology assumes a constant rate of panel advance, advance rate significantly affects the accuracy of dynamic subsidence prediction. For this reason, quality monitoring of face advance rate and careful assessment of data to be used for calculating average advance rates are necessary for accurate dynamic subsidence prediction.

The next example also illustrates the importance of careful assessment of the mining sequence when evaluating the validity of dynamic subsidence predictions. Table 19 provides measured dynamic subsidence data for each monitoring point shown in Figure 30. All monitoring points are located along the same longitudinal profile line over the NA-2 panel. The predictions are based on an average face advance rate of 19 ft/day. Graphs comparing the predicted and measured dynamic subsidence development values for each point are presented in Figure 40. There is good correlation for Point 0 and Point 100E. However, the correlation between predicted and measured values is poor beginning at Point 175E. In fact, the measured values actually begin to correlate very well with predicted final subsidence for Point 500E, Point 650E, and Point 750E. One possible reason for the discrepancies between predicted and measured values at Points 500E, 650E, and 750E may be the greater deviation of advance rate from the calculated average of 19 ft/day (Table 19 and Table 20). Also, the calculated advance rates for the panel just before it reached its end decreased significantly (9 ft/day and 5 ft/day). The slower advance rates (compared to the average of 19 ft/day) near the end of the panel may have allowed the surface to settle to final subsidence levels while the panel was still nearby. Good correlation between the measured values and the predicted final subsidence may suggest that very little residual subsidence is likely near the end of a panel as it slows down.

The previous examples suggest that care must be taken when assessing the reliability of dynamic subsidence predictions. In particular, calculations of average face advance rate must be done carefully. The prediction methodology assumes a constant rate of advance. Therefore, subsidence over panels with more constant advance rates, or over sections of panels with advance rates closer to the panel average, is likely to correlate better with predicted values. When dealing with panels that have inconsistent face advance rates, it may be better to make predictions for small intervals of the panel, each with its own average advance rate.

Table 21: Measured dynamic subsidence values and distances between mine face and surface points

Measured Deformation at Point 0 (ft)	Distance between Mine Face and Monitoring Point (ft)	Measured Deformation at Point 100E (ft)	Distance Between Mine Face and Monitoring Point (ft)	Measured Deformation at Point 175E (ft)	Distance Between Mine Face and Monitoring Point (ft)
0	-400	0	-500	0	-575
0	-325	-0.01	-425	-0.01	-500
-0.01	-220	0.01	-320	0.01	-395
0.03	-145	0.04	-245	0.04	-320
0.02	-75	0.05	-175	0.04	-250
0.01	-45	0.04	-145	0.03	-220
-0.15	80	0.01	-20	0.01	-95
-1.06	205	-0.29	105	-0.11	30
-2.22	348	-1.39	248	-0.85	173
-2.81	515	-2.61	415	-2.62	340
-2.9	580	-2.83	480	-3.03	405
-2.93	700	-2.9	600	-3.17	525
-2.97	760	-2.97	660	-3.27	585
-2.99	865	-2.99	765	-3.32	690
-3	900	-3.01	800	-3.35	725
		-3.02	801	-3.36	726
		-3.04	802	-3.39	727
Measured Deformation at Point 500E (ft)	Distance Between Mine Face and Monitoring Point (ft)	Measured Deformation at Point 650E (ft)	Distance Between Mine Face and Monitoring Point (ft)	Measured Deformation at Point 750E (ft)	Distance Between Mine Face and Monitoring Point (ft)
0	-900	0	-1050	0	-1150
0	-825	0	-975	0	-1075
0	-720	0	-870	0	-970
0	-645	0	-795	0	-895
0	-575	0	-725	0	-825
0	-545	0	-695	0	-795
0	-420	0	-570	0	-670
0	-295	0	-445	0	-545
0.01	-152	0	-302	0	-402
-0.18	15	-0.05	-135	0.01	-235
-0.35	80	-0.06	-70	-0.01	-170
-1.06	200	-0.14	50	-0.04	-50
-1.97	260	-0.32	110	-0.06	10
-2.93	365	-1.26	215	-0.32	115
-3.19	400	-1.98	250	-0.7	150
-3.24	400	-2.03	250	-0.76	150
-3.31	400	-2.1	250	-0.81	150

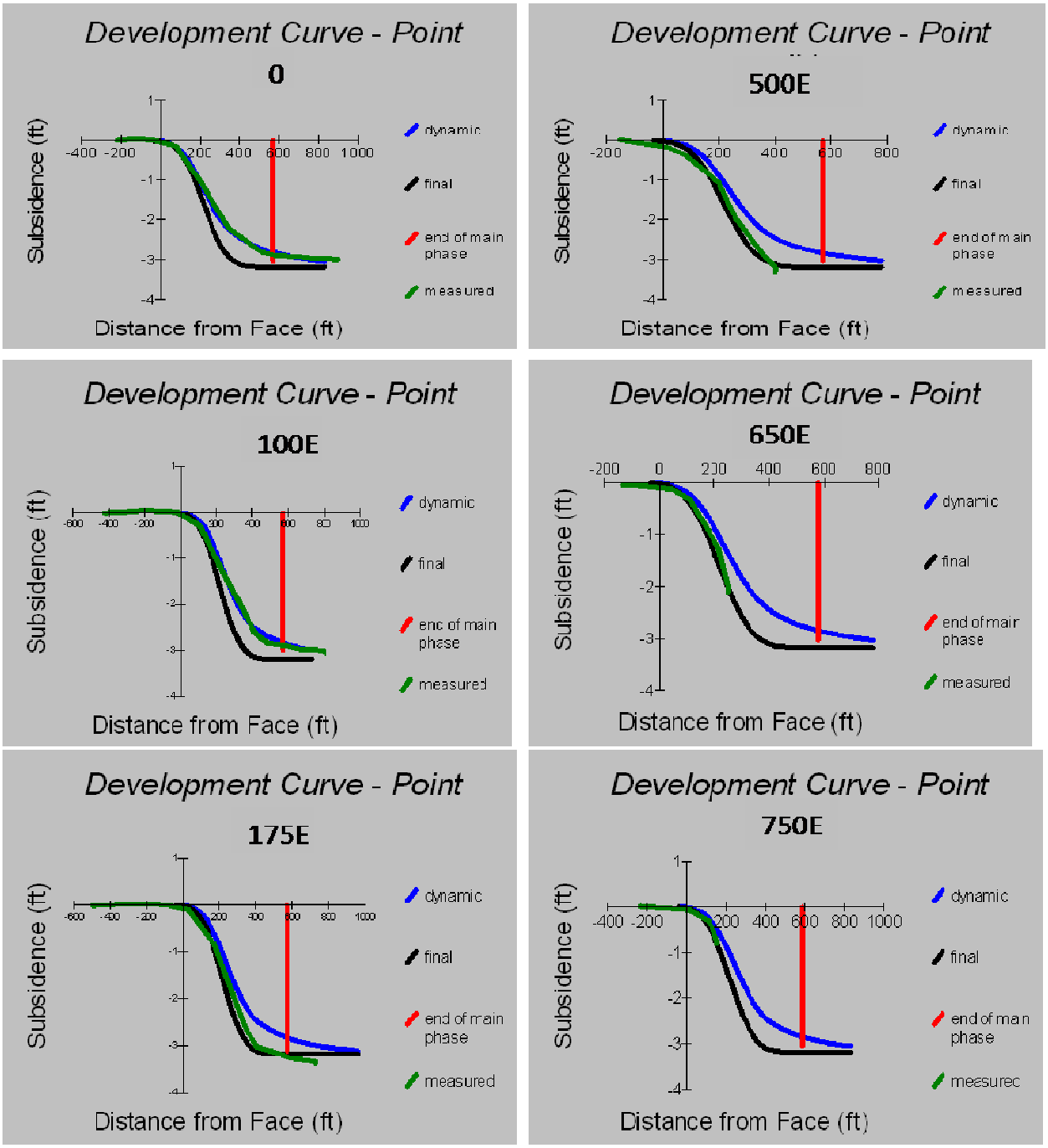

Figure 40: Comparison of dynamic subsidence prediction with measured subsidence values for Points 0 through 750E.

5.1.5 IL-1 Dynamic Subsidence Case Study (Illinois/Indiana)

This case study involves dynamic subsidence data collected on Monument Line 5 of Case Study IL-1. Details of the case study are discussed in Section 4. The

dynamic analysis was done using point 1P-1, the last point on the left side of Monument Line 5, as shown in Figure 41. Subsidence parameters from calibration exercises in Section 4 were used for the dynamic predictions (Figure 42).

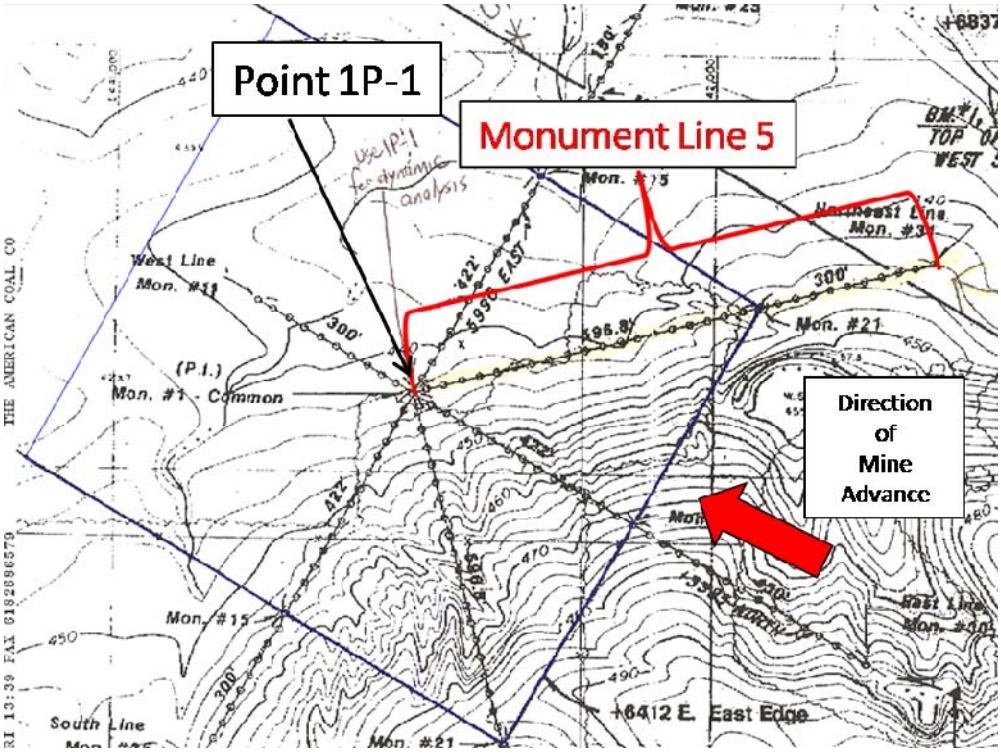

Figure 41: Map showing Point 1P-1 on Monument Line 5. Mine map from The American Coal Company, Galatia Mine, Harrisonburg, Illinois, submitted to the Illinois Department of Natural Resources, Office of Mines and Minerals for permit application in 1989.

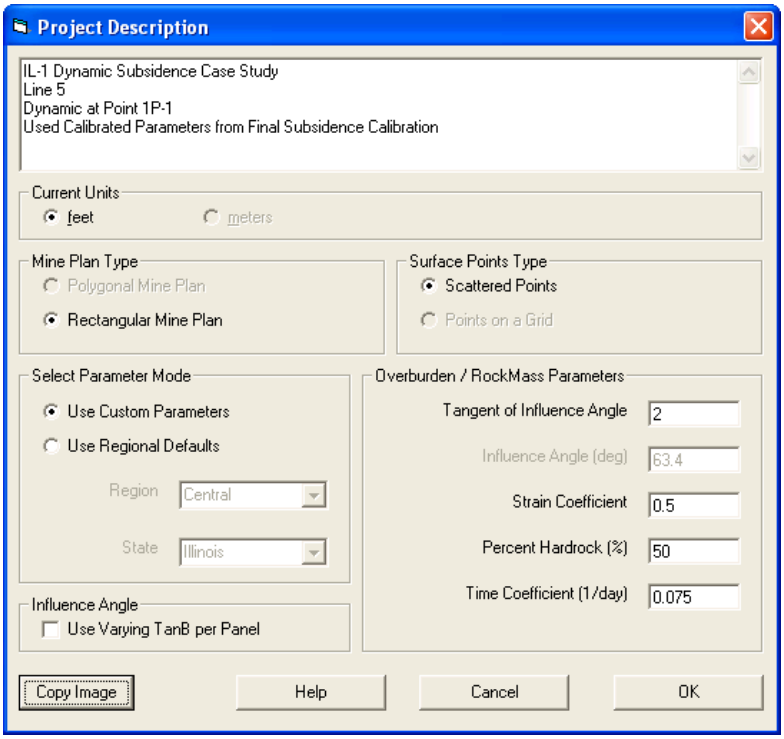

Figure 42: IL-1 Dynamic Case Study – SDPS Project Description Screen

Figure 46 displays the dynamic mine plan as input into SDPS. The orientation of the mine has been changed, but the positions of the panel and monitoring point relative to each other are the same. As evident from Figure 41, Point 1P-1 is located relatively close to the beginning of the panel. The average face advance rate, 20 ft/day was calculated based on information from the coal company. Figure 43 shows the Dynamic Options input to SDPS and an animation of the westward-advancing face. The measured dynamic subsidence data for Point 1P-1 is presented in Table 22. Figure 44 and Figure 45 display data for Point 1P-1 as input to SDPS.

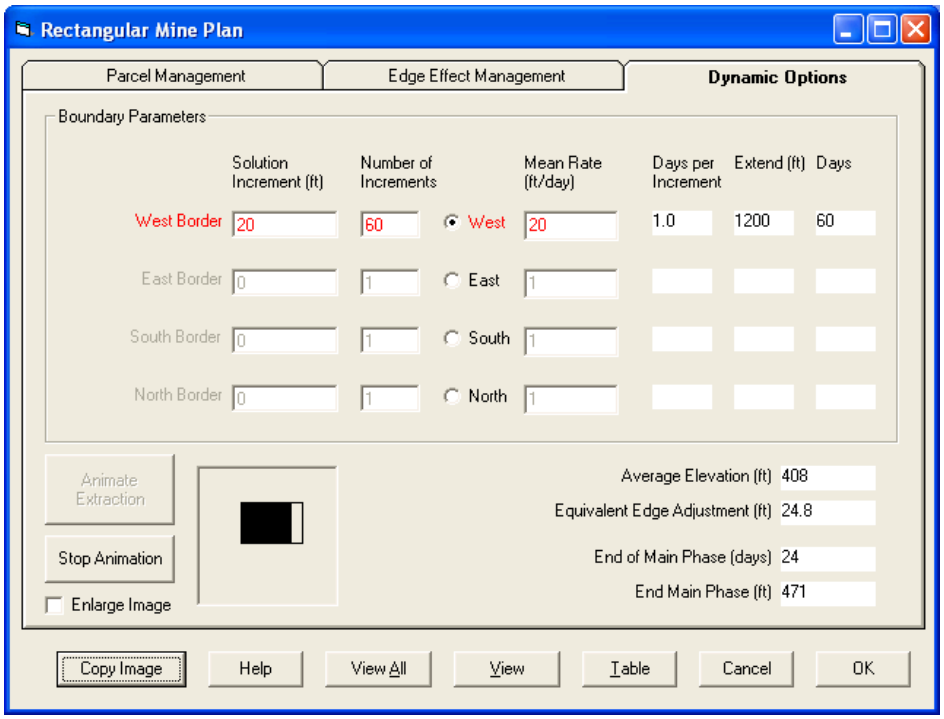

Figure 43: IL-1 Dynamic Case Study – Dynamic Options Screen

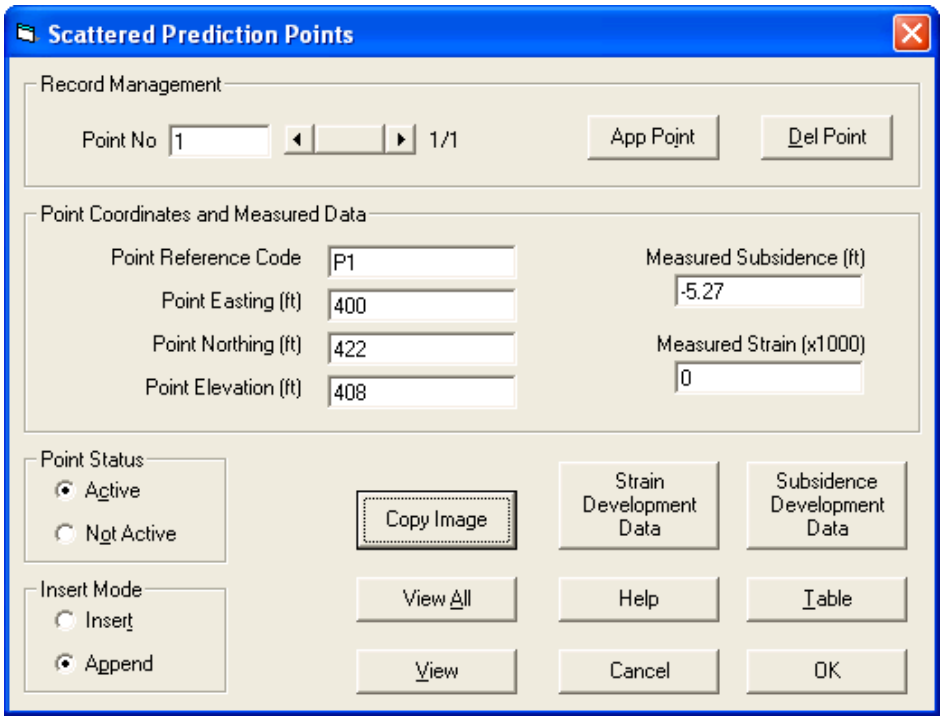

Figure 44: IL-1 Dynamic Case Study – Prediction Points Management Screen

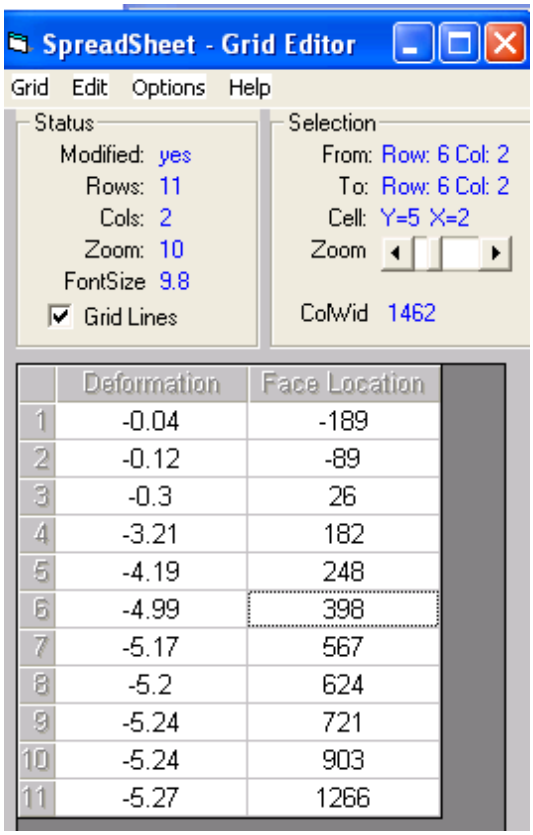

	Deformation	Face Location
1	-0.04	-189
2	-0.12	-89
3	-0.3	26
4	-3.21	182
5	-4.19	248
6	-4.99	398
7	-5.17	567
8	-5.2	624
9	-5.24	721
10	-5.24	903
11	-5.27	1266

Figure 45: IL-1 Dynamic Case Study – Subsidence Development Data

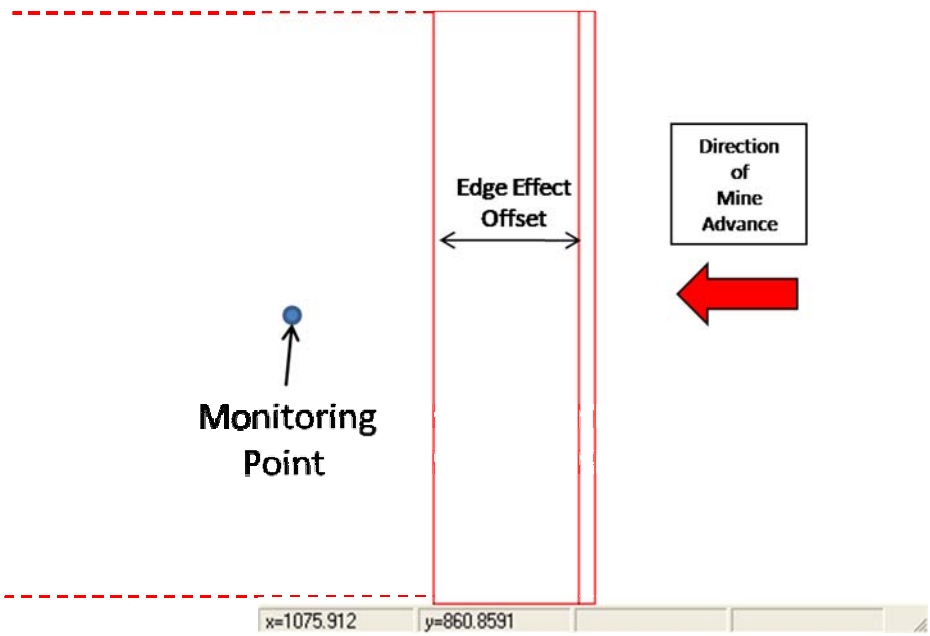

Figure 46: Representation of mine panel with edge effect and dynamic subsidence prediction point.

Figure 47 shows the results of the dynamic prediction compared to the measured data. The results indicate that the measured dynamic subsidence values actually correlate more closely with the predicted final subsidence than with the predicted dynamic subsidence. The correlation between measured dynamic subsidence and predicted final subsidence suggests that subsidence over the panel reaches final subsidence levels while the panel is still nearby (very little residual subsidence after the panel has passed). This may be a result of deviation from the average rate of face advance while the face is near the beginning edge of the panel. The results of this case study may indicate that the prediction methodology does not work well for making predictions near the beginning ends of longwall panels. At the beginning end of a panel, when the panel has not advanced a distance that is longer than its face width, the shortest dimension of the panel is actually its length. Because the methodology assumes a constant panel width (which corresponds to the actual width of the panel once it has advanced a distance that is longer than its face width), it is unable to accurately predict dynamic subsidence near the beginning of panels.

The results of this case study suggest that the methodology is unable to accurately predict dynamic subsidence development near the beginning edge of longwall panels. The case study also exemplifies the need for careful consideration of the mining layout and other special circumstances when evaluating subsidence data and prediction results.

Table 22: Measured dynamic subsidence values and distances between mine face and surface points

Measured Deformation at Point 1P-1 (ft)	Distance Between Mine Face and Monitoring Point (ft)
-0.04	189
-0.12	89
-0.3	-26
-3.21	-182
-4.19	-248
-4.99	-398
-5.17	-567
-5.2	-624
-5.24	-721
-5.24	-903
-5.27	-1266

Measured Deformation at Point 1P-1 (ft)	Distance Between Mine Face and Monitoring Point (ft)
-5.29	-1636
-5.31	-1895
-5.32	-2224
-5.32	-2937
-5.34	-3310
-5.35	-3806

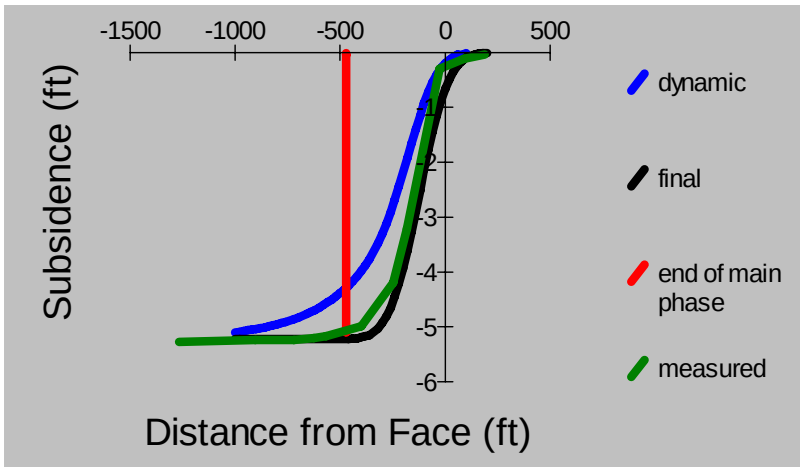

Figure 47: Comparison of dynamic subsidence prediction with measured subsidence values at Point 1P-1

5.1.6 Discussion

Data from case studies in Northern Appalachia and Illinois/Indiana provide a means for assessing the validity of the method proposed by Jarosz, et al. (1990) for predicting dynamic subsidence development at a specific point. Using SDPS, predicted values of dynamic subsidence can be visually compared to measured values of subsidence development, as well as predicted values of final subsidence. The methodology also includes a means for estimating the end of the main phase of subsidence.

In general, the case studies suggest that the prediction methodology is capable of producing dynamic subsidence predictions that are comparable to actual measured dynamic subsidence data. However, results of the case study work also suggest that the methodology does have limitations that must be understood by the user. The main limitation appears to be associated with face advance

rate. The methodology from Jarosz, et al. (1990) assumes a constant advance rate. The NA-2 case study includes two examples that illustrate how easily face advance rate can affect dynamic subsidence predictions. Problems seem to occur when localized face advance rates differ significantly from the average rate used for prediction calculations. One solution, although a potentially time-consuming one, is to evaluate smaller intervals of panel, using different average advance rates for each section.

Case study IL-1 illustrates the importance of carefully considering the mine layout and other special circumstances when predicting dynamic subsidence. The results of the IL-1 study suggest that the location of the monitoring point near the beginning of the panel cannot be accurately accounted for with the implemented methodology.

Due to limited availability of usable, measured dynamic subsidence data, only two case studies are presented. The case studies do indicate that the implemented prediction methodology has the potential to produce accurate subsidence development predictions. However, the case studies also indicate that limitations of the methodology do exist. As with any newly-implemented methodology, further validation is necessary.

5.1.7 Other Dynamic Deformation Indices

Using the same concept as in the case of subsidence dynamic analysis, the dynamic profiles for horizontal strain, tilt, curvature and horizontal displacement can be calculated. In all cases of dynamic predictions it should be noted that the dynamic component is lower than the final component of the respective deformation index. Figure 48 shows a typical example of the prediction of dynamic horizontal strains as compared to final horizontal strains.

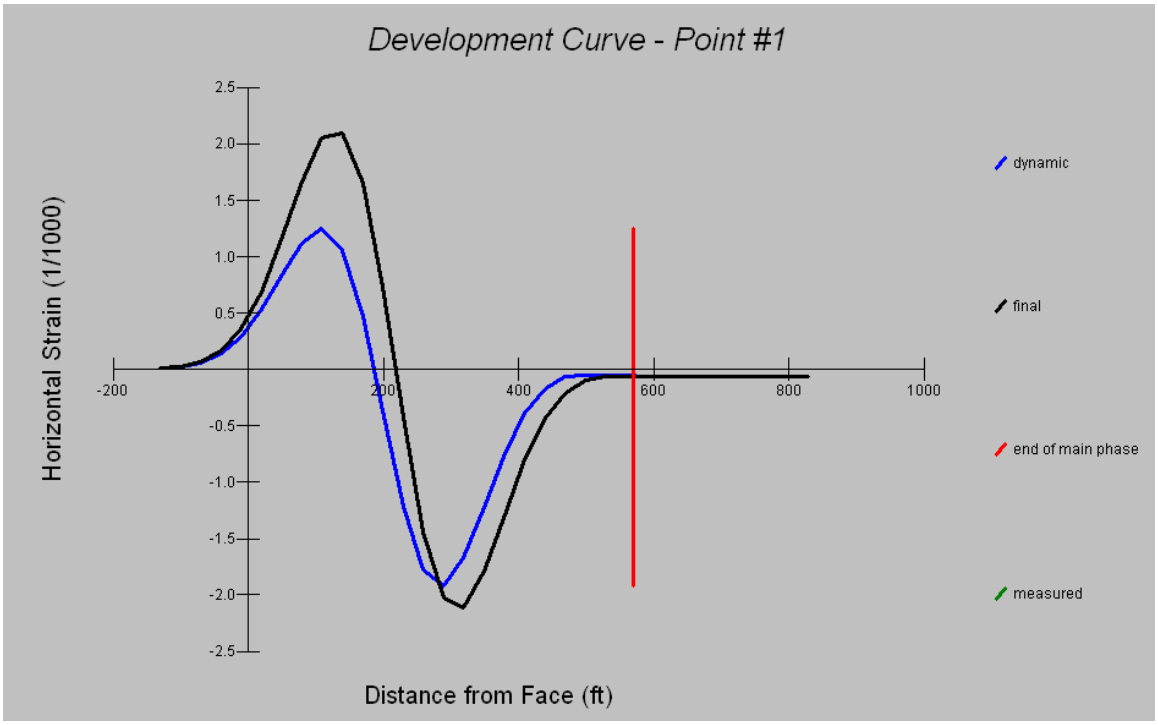

Figure 48: Dynamic and final strain prediction. Red line corresponds to the end of main phase of subsidence development.

5.2 Subsidence Prediction in Areas of Steeply Sloping Terrain/Steeply Dipping Seams

5.2.1 Review of Previous Research

For simplicity, the initial models developed for the prediction of surface subsidence due to underground mining assumed that the surface terrain above the mine was flat. Similarly, early modeling techniques assumed a flat-lying coal deposit. In many cases these assumptions are valid, but numerous researchers have documented deviation of measured subsidence values from expected subsidence values in areas of mountainous terrain. Similarly, values of subsidence associated with very steeply dipping coal seams are significantly different than values expected from flat-lying seams. Among many other factors, both scenarios involve rapidly changing overburden thicknesses. Recognizing the need for prediction techniques to account for these differences, several researchers have contributed to an evolving methodology of subsidence prediction in mountainous terrain and in areas of steep seam dip.

Because the research presented in this thesis focuses on subsidence associated with coal mining in the eastern United States, more emphasis is placed on

subsidence in steeply-sloping terrain. Seams in the coal-bearing basin deposits of the eastern U.S. have relatively low dip angles compared to areas where mine subsidence is observed to be affected by dip. Section 10.1.2 provides a brief discussion of previous work associated with subsidence over steeply-dipping seams, but no additional research on the topic was conducted for this thesis.

5.2.2 Subsidence in Steeply Sloping Terrain

In mountainous or significantly sloping terrain overlying a relatively flat coal seam, subsidence at the surface is affected by changing overburden thickness as well as subsidence-induced soil slope movements (Whittaker and Reddish, 1989). In general, factors that must be considered when assessing mining-induced subsidence in areas of steeply-sloping surface terrain include an increase in water infiltration and a decrease in slope stability due to opening of pre-existing fractures and joints in up-slope areas subjected to increased tensile strains; instability due to small changes in tilt of the ground; and enhancement of down-slope creep movement due to down-slope subsidence and soil movements (Whittaker and Reddish, 1989).

With above drainage room-and-pillar mining near the coal outcrop, thinning overburden allows for enhanced water infiltration into the mine, often resulting in collapse of the mine roof and creation of sinkholes and depressions at the surface (Whittaker and Reddish, 1989). This type of slope-related subsidence is expected where mining has taken place very close to the outcrop and is enhanced by higher extraction mining. In England, the frequency of landslides on steep slopes increased during times of industrial growth when coal mining beneath the slopes increased (Jones et al., 1992). Many of the landslides are believed to have been triggered by differential subsidence due to pillars left near the outcrop under shallow cover (Jones et al., 1992). Most of the slides are associated with movement along pre-existing geological discontinuities that were stable prior to undermining (Jones et al., 1992).

Whittaker and Reddish (1989) also discuss the effects of longwall mining under sloping terrain where the longwall panel is actually started at, or near, the outcrop of the coal seam and advanced into the mountain. In this case, the high extraction and enhanced collapse associated with longwall mining acts to destabilize the overlying slope by steepening the slope (due to subsidence-induced tilt) and creating high ground strains (Whittaker and Reddish, 1989).

While longwall mining from the outcrop of a coal seam can create extreme instability, it is not a common practice (Whittaker and Reddish, 1989).

More commonly, researchers focus investigations on predicting the effects of sloping terrain on subsidence associated with high extraction mining at significant distances from the coal seam outcrop. One of the simplest methods of predicting subsidence in sloping terrain is the empirically-based graphical projection procedure presented by National Coal Board (1975). The method simply takes empirical subsidence prediction assuming a flat surface and projects the subsidence values proportionally onto an inclined surface (Whittaker and Reddish, 1989). This method assumes a horizontal extraction horizon and an angle of draw of 35° (although the angle of draw can be modified to fit different locations). This method of predicting subsidence in steep topography has been used extensively, but has also been criticized. The method works better with panels that are sub-critical and it always increases the extent of subsidence in the upslope direction, while decreasing the extent of subsidence in the down-slope direction (Whittaker and Reddish, 1989).

Gentry and Abel (1978) compared measured subsidence parameters from the York Canyon Mine in New Mexico to subsidence parameters predicted by the methods outlined in the National Coal Board's Subsidence Engineers' Handbook. Subsidence measurements were conducted in mountainous terrain over a 550 ft wide panel in a 10 ft thick coal seam (Gentry and Abel, 1978). In general, the strains predicted by the Subsidence Engineers' Handbook were much less than the strains measured at the York Canyon Mine, suggesting that the more mountainous terrain above the New Mexico mine (compared to the flat or gentle terrain of the England coalfields) greatly affected the surface subsidence parameters (Gentry and Abel, 1978). The actual vertical subsidence in the valleys was less than predicted and actual vertical subsidence at the ridgetops was greater than predicted. The study also concluded that greatest horizontal ground movements occur when mining advances in a downslope direction, in relation to the slope of the surface topography. When considering the extent of mining subsidence in relation to sloping terrain, Gentry and Abel (1978) found that the angle of draw from the panel was greater on the upslope side of the subsidence trough than on the downslope side.

Franks and Geddes (1984) also concluded that the subsidence prediction

techniques of the National Coal Board's Subsidence Engineers' Handbook, even with the suggested modifications for prediction in steep terrain included in the handbook, were not applicable for subsidence in steep terrain because the data on which it was developed is from areas with gentle or flat-lying topography. Instead, Franks and Geddes (1984) analyzed a theoretical model using finite element numerical modeling. Franks and Geddes (1984) considered two scenarios of undermining a 35° slope, mining advancing in an upslope direction and mining advancing in a downslope direction. The finite element modeling, while based on many assumptions of rock property qualities, allowed Franks and Geddes (1984) to conclude that undermining of sloping ground has greater effects on horizontal movements and ground strains associated with subsidence than it does on subsidence-induced vertical movements or tilt.

Franks and Geddes (1986) presents additional conclusions with regard to theoretical modeling of subsidence associated with undermining of steep slopes. Regardless of the direction of mining advance, subsidence-induced horizontal movements at the slope crest tend to be 10% to 50% greater than horizontal movements expected in flat-lying terrain (Franks and Geddes, 1986). Furthermore, the inflection point of a subsidence basin in sloping terrain is always displaced downslope. By evaluating the effects of various slope angles on subsidence characteristics, Franks and Geddes (1986) found that subsidence predictions for slopes less than 15° are not significantly different than subsidence predictions for flat ground. The conclusions presented in Franks and Geddes (1984) and Franks and Geddes (1986) are important; however, the analyses were based on many assumptions and present results from modeling of subsidence associated with undermining of only a single ground slope of constant dip (modified from Sun, 1988). The analysis also fails to account for soil slope instability, an important factor to consider when assessing the manifestation of subsidence in mountainous terrain.

Jeran and Adamek (1988) recorded movements suggesting that downslope sliding of soil material on steep slopes (up to 40° in the area of study) continues after vertical movements associated with mining subsidence have ceased. The report concludes that subsidence-induced horizontal movements and tensional strains are greatly affected by steep surface slopes. In general, the downslope movement of soil, believed to be sliding along the soil-bedrock boundary, tends to increase the horizontal movements associated with mining subsidence. The

subsidence-related downslope movement of soil on steep slopes also tends to increase tensional strain in upslope areas and increase compressive strain in downslope areas (Jeran and Adamek, 1988).

The idea that horizontal movements associated with undermining of steep slopes is directly related to soil instability is further validated by Litwinowicz (1984). He found that soil strength changes as it goes through the extensional and compressional stages of mine subsidence development. The study found that increasing subsidence-induced strains cause a significant decrease in the cohesion of overlying soil. Litwinowicz (1984) presents a method of predicting the change in soil cohesion due to mining subsidence. Interestingly, the work did not indicate a significant change in the angle of internal friction of soil due to mine subsidence.

Marschalko (2004) also found evidence that mining subsidence tends to have significant effects on soil characteristics. The study found that tension zones associated with mining in an area of the Czech Republic have caused increases in soil porosity and decreases in soil consistency. The angle of internal friction of soil in the tensile subsidence zones has decreased 3 to 4 degrees and the soil cohesion has been reduced 50 to 75%. The changes in soil character due to mining subsidence, coupled with local weather patterns, is believed to be the cause of reactivation of a large, slow-moving landslide in the study area (Marschalko, 2004).

More recent development of methodology for understanding mine subsidence in steeply sloped terrain is based on subsidence-related ground movements and the effects of those ground movements on the stability of the boundary between bedrock and soil deposits. Peng and Luo (1989) presents an equation for defining the relationships between subsidence movements and slope instability. The work is based on the assumption that the higher horizontal subsidence movements measured on undermined steep slopes are all due to the downslope movement of soil on bedrock. Peng and Luo (1989) outlines a method of analysis wherein subsidence predictions are conducted using a normal subsidence prediction technique. Predicted ground strains are then compared to soil cohesion and strength parameters for the soil-bedrock boundary (using the Mohr-Coulomb failure criteria) to assess the potential for slope instability and enhanced downslope movement. The method is able to predict where sliding is

likely to occur and which way it will go, but not the extent of sliding (Peng and Luo, 1989). The calculations are based on the properties and thickness of the surface soil layer, normal subsidence prediction parameters, and topography (Peng and Luo, 1989). Properties of the soil and the soil-bedrock interface at each prediction point must be determined to produce accurate results. For small areas, these parameters may be more easily obtained, but soil thickness and other properties tend to change quickly. Therefore, accurate knowledge of soil characteristics are a limiting factor for the methodology presented in Peng and Luo (1989).

Work completed by Sun (1988); Karmis, et al. (1990); and Karmis, et al. (1991) is also based on the assumption that surface slope and topsoil stability account for large horizontal subsidence-related movements. The model assumes that movement of bedrock due to subsidence causes instability and movement at the soil-bedrock interface. Therefore, the final subsidence-induced displacement on a sloping surface is a combination of bedrock movement and downslope soil sliding (Karmis, et al., 1990). Karmis, et al. (1990) outlines basic equations that describes the interactions between slope geometry, soil layer stability, and subsidence-induced disturbance of the soil-bedrock interface. The preliminary conclusions included in Karmis, et al. (1990) state that enhanced downslope subsidence-induced movements are very significant. They also found that the inflection point for subsidence-induced strain tends to be shifted downslope when associated with steeply-sloping ground terrain. This, in turn, creates non-symmetrical magnitude changes of tensile and compressive ground strains (Karmis, et al., 1990).

Karmis, et al. (1991) completed subsidence prediction case studies based on the methodology presented in Karmis, et al. (1990) and observed that the sloping terrain methodology does yield subsidence prediction results that are closer to the measured subsidence than are regular subsidence prediction results. The results of the sloping terrain subsidence predictions are dependent upon the difference between measured and predicted horizontal displacements for each prediction point and the cohesion, angle of internal friction, cover depth, and the seepage zone depth for the soil in the prediction area (Karmis, et al., 1991). These factors are all accounted for by an empirical site parameter called $\mathbf{C_d}$. Of all the factors, $\mathbf{C_d}$ was affected most by changes in soil cohesion.

Recent development of methodologies to describe the effect of steeply sloping terrain on mine subsidence parameters, such as presented in Peng and Luo (1989); Sun (1988); Karmis, et al. (1990); and Karmis, et al. (1991) focuses on the soil-bedrock interface and the properties of the soil itself. While the methods necessitate fairly detailed, and sometimes difficult to retrieve, knowledge of soil characteristics, the potential benefits of more accurate subsidence prediction are abundant.

5.2.3 Subsidence over Steeply Dipping Seams

Steeply-dipping coal seams also affect mining-induced surface subsidence. Most of the prediction techniques for subsidence due to mining of steeply dipping seams simply involve adaptation of the normal flat seam subsidence prediction (Ren et al., 1989). Typically, the subsidence limit angles and the position of maximum vertical displacement are changed. In general, Ren et al. (1989) states that maximum subsidence is not significantly displaced due to steeply dipping coal seams if the overburden is relatively weak. Conversley, the maximum subsidence is displaced significantly in the down-dip direction when relatively strong overburden material is involved. This conclusion is very general, but it does begin to capture some of the factors that must be considered when evaluating subsidence over steeply dipping seams. Ren et al. (1989) points out that there is a very limited amount of subsidence data available for seams dipping greater than 45˚, making subsidence research for steep seams more difficult.

More recently, Torano et al. (2000) looks specifically at subsidence above very steeply dipping (70˚-90˚ dip) coal seams. When assessing mining subsidence over very steeply dipping seams, the effects of three different overlapping subsidence zones must be taken into account. Subsidence due to breaking of overburden rocks, subsidence due to breaking of mine floor rocks, and subsidence due to slippage along the coal seam-roof interface or the coal seam-floor interface must all be considered (Torano et al., 2000). Due to the complex overlapping of subsidence zones associated with very steeply-dipping coal seams, it is very possible to get tensile strains at locations other than the edges of the final subsidence basin and compressive strains at locations other than near the middle of the final subsidence basin (Torano et al., 2000). Torano et al. (2000) suggest using a profile function to calculate the probable locations of

ranges of damage-inducing values of strain from mining of very steep coal seams. In this way, areas of expected surface damage and the probability of damage at various locations can be calculated. While this method of predicting subsidence over steeply dipping coal seams has the potential to produce useful results, it necessitates numerous subsidence prediction calculations to provide data for the histograms on which the results are based. Due to the numerous calculations needed, the method is dependent on the calculation time for each subsidence prediction. For this reason, the authors suggest using only the profile function method.

5.2.4 Implemented Methodology

The more recent work by Sun (1988), Karmis, et al. (1990), Karmis, et al. (1991), and Peng and Luo (1989) suggests that the best way to approach modeling and prediction of subsidence in steeply-sloping terrain is to calculate expected subsidence movements and then evaluate the effect of those movements on soil slope stability. The bedrock-soil interface is the focus of the stability assessment because that is the surface on which additional downslope movement (sliding) is expected to occur. The detailed theory for this method can be found in the aforementioned references.

For this thesis, a lack of data related to soil characteristics and soil behavior in steeply-sloping, subsidence-affected areas in the eastern U.S. hindered further development of methodology concerning mining-induced slope instability at the bedrock-soil interface. However, this thesis does provide discussion of enhanced methodology for prediction of subsidence-induced ground strains in steeply-sloping terrain.

Ground strains differ from horizontal strains in that they account for the surface topography. Horizontal strains are calculated by considering only the horizontal component of deformation. Figure 49 illustrates the difference between horizontal strain and ground strain. A more detailed explanation of the methodology for calculating ground strain in three-dimensional space is included in section 7.2.

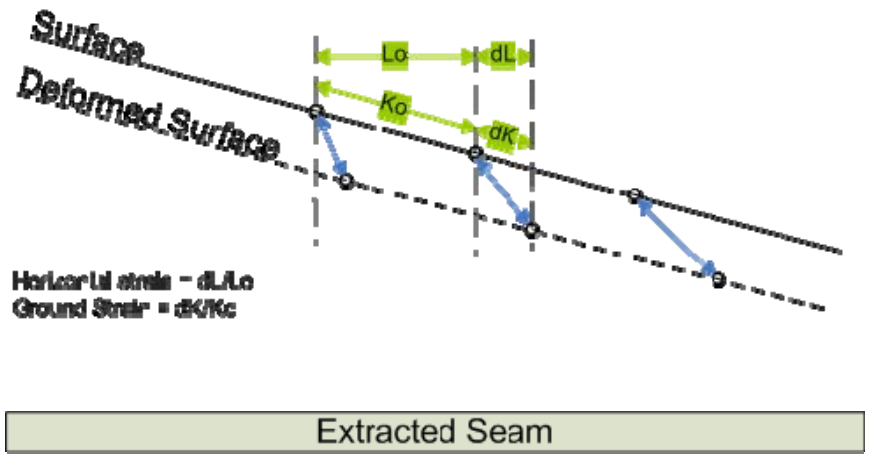

Figure 49: Components of horizontal strain and ground strain in sloping terrain

Due to the pronounced slope of the ground surface in Figure 49: Components of horizontal strain and ground strain in sloping terrain, it is easy see the difference between components used to calculate the two types of strain. However, as the slope of the ground surface flattens, horizontal strain and ground strain converge. Therefore, subsidence in flat-lying topography will theoretically produce ground strain that is equal to horizontal strain. Due to the steep topography in much of the eastern U.S. coalfields, ground strain is often much more applicable.

Figure 49 is a typical diagram used to illustrate strain along a line. Very often, predictions of strain and subsidence are calculated along cross-section lines. The most common prediction line orientations are transverse (parallel to the short axis of a panel) and longitudinal (parallel to the long axis of a panel). Enhanced methodology, developed for the current research and validated in section 5.2.5 evaluates strain at any given point by taking into account the effects of deformation on all adjacent points. The result is the ability to evaluate strain at any point, not just at points located on a cross-section line. The enhanced strain prediction approach is capable of producing plan view maps of contoured strain. In effect, the lateral distribution of ground deformation-induced strain (both ground and horizontal) can be predicted using a grid of surface points positioned over a mine. Contoured, “pseudo” three-dimensional maps of strain and subsidence are extremely helpful for engineers faced with predicting areas most likely to be affected by ground deformation movements.

With regard to accurately predicting ground strains and subsidence in areas with steep topography, the contoured maps are likely to prove themselves invaluable.

The enhanced ability to easily evaluate lateral subsidence and strain distributions that take into account surface topography provides the first step in the aforementioned methodology for assessment of soil slope movements due to undermining in steeply-sloping areas. Accurate predictions of subsidence and strain will undoubtedly lead to more accurate predictions of soil slope instability.

5.2.5 Validation of Method

To demonstrate the difference between predicted horizontal strains and predicted ground strains in steeply-sloping terrain, and to illustrate one of the benefits of contoured subsidence and strain maps, an example using synthetic mine characteristics is provided. The example involves prediction of final subsidence, horizontal strain, and ground strain over the end of a longwall mine panel. The mine panel has a width of 600 feet and an average depth of 800 feet, giving it a width to depth ratio of approximately 0.75. The extraction thickness is 5 feet. An edge effect of 140 feet is included in the model. Default values of influence angle and subsidence factor have been assumed (see Appendix IV, Figures 1 through 3). The ground surface above the mine slopes downward to the right at an angle of 30˚. Figures 4 and 5 in Appendix IV show the SDPS input for the sloping prediction grid. Calculation of predicted deformation was achieved via the Calculation Options screen (Appendix IV, Figure 6). Note that both the "Calculate Horizontal Strain" and "Calculate Ground Strain" boxes are checked. The Surfer Grid output format is used to produce files compatible with Surfer, a contouring program separate from SDPS. Contouring of predicted values is done through the Contouring option in the Graph Module (Appendix IV, Figures 7-9). Figure 8 in Appendix IV displays the chosen settings for this example. Values for horizontal and ground strain are set at 1.5×10^{-3}. The contoured results may be manipulated using the available settings in Surfer (Appendix IV, Figure 9).

Final results of the synthetic example are shown in Figure 50, Figure 51 and Figure 52. All figures show expected strains in the same sloping terrain. Figure 50 shows a relatively symmetrical expected distribution of horizontal strain above the synthetic mine panel. In contrast, Figure 51 indicates a strongly non-symmetrical distribution of expected ground strain. Figure 52 contains both the expected horizontal strain and expected ground strain, and facilitates recognition of the difference between the two.

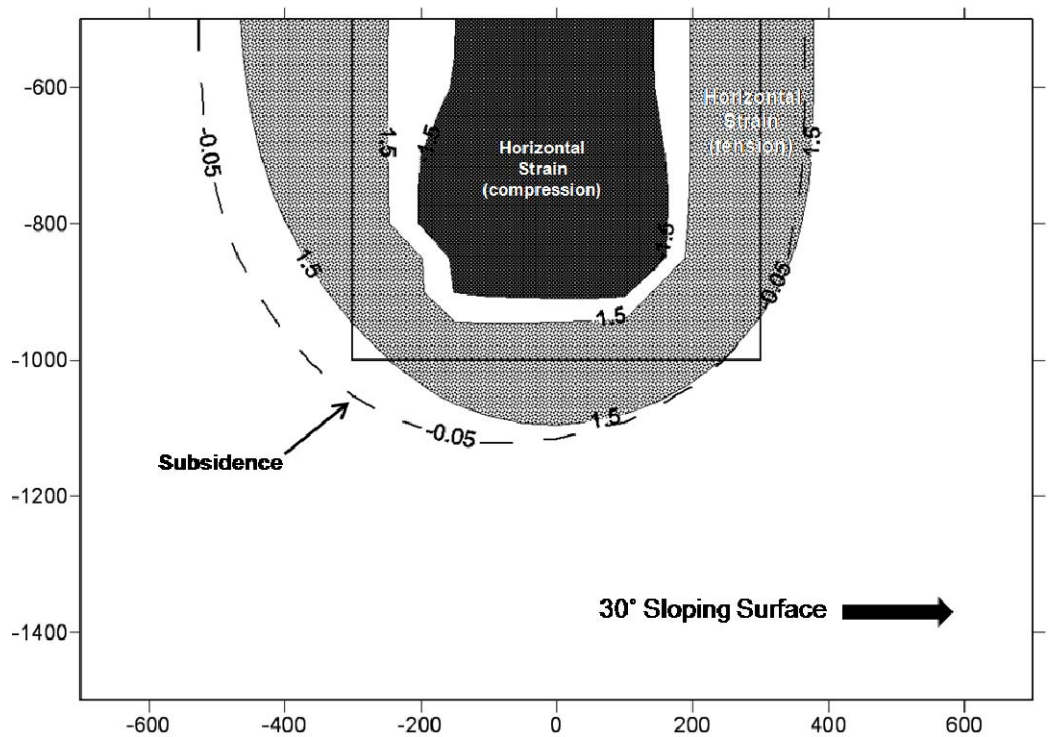

Figure 50: Contoured map of horizontal strain and subsidence over the end of synthesized mine panel. Horizontal strain contours assume a threshold value of 1.5 x 10^{-3}.

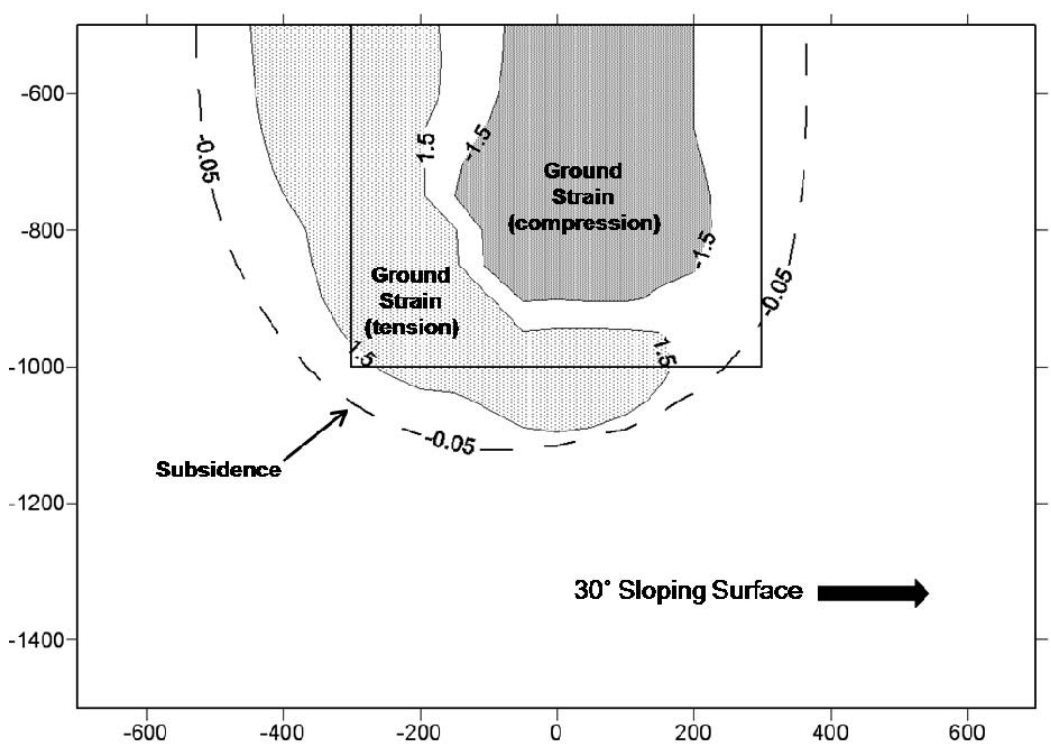

Figure 51: Contoured map of ground strain and subsidence over the end of synthesized mine panel. Horizontal strain contours assume a threshold value of 1.5 x 10^{-3}. Note the

more pronounced upslope migration of tensile ground strain due to the steeply-sloping topography (as compared to horizontal strain in previous Figure).

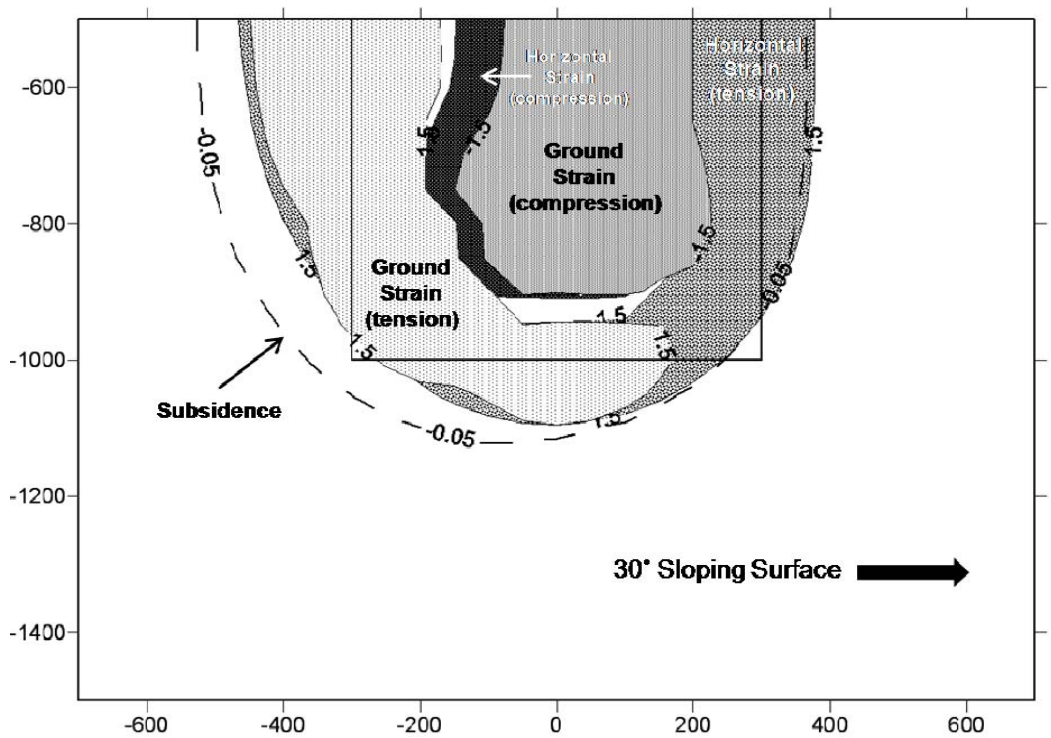

Figure 52: Combination of contoured ground strain and horizontal strain maps, with subsidence.

5.2.6 Discussion

The enhanced methodology presented and validated in this section provides a means for easily and accurately evaluating lateral distributions of ground strain and subsidence in steep topography, the first step of the most recent methodology for assessment of mining-induced soil slope movements (as discussed in Sun (1988), Karmis, et al. (1990), Karmis, et al. (1991), and Peng and Luo (1989)). While a lack of data inhibited the development of enhanced methodologies associated with soil slope stability and subsidence in this thesis, the capabilities for prediction of subsidence and strain in steep terrain have been greatly improved.

The example presented in Figure 50, Figure 51 and Figure 52 clearly exposes the significant difference between ground strain and horizontal strain in steeply-sloping topography. Ground strain is obviously much more applicable than horizontal strain when working in steep terrain. The distribution of ground strain

in the example (Figure 51) is consistent with the observations of Gentry and Abel (1978), Franks and Geddes (1986), and Karmis, et al. (1990) regarding general trends of subsidence parameters in steep terrain (see section 5.2.2).

Development of methodology for predicting and displaying strain (and subsidence) distributions in a pseudo three-dimensional, contoured manner is invaluable for engineers assessing areas likely to be damaged by ground deformation (see Section 6). Future work involving soil slope instability in steeply-sloping undermined areas will also benefit from maps of contoured ground strain and subsidence. The maps may assist engineers in assessing areas of probable slope instability, even in locations with variable soil characteristics.

5.3 Improvement of Calibration Procedures

5.3.1 Review of Previous Research

In many cases, calibration of subsidence modeling programs, such as SDPS, is based only on one kind of data. This is typically a result of lack of measured data other than vertical displacement. Often, cost inhibits the collection of various types of measured subsidence data. Having the ability to evaluate the accuracy of a model using numerous types of measured data greatly increases the quality of the model. Work presented below displays the results of a newly-implemented SDPS function allowing users to calibrate subsidence models using both vertical displacement and strain (either horizontal or ground). The importance of assessing strain when analyzing mine subsidence effects is discussed below. A brief discussion of the potential for calibration using subsidence-induced tilt measurements is subsequently. Unfortunately, availability of usable data prohibited implementation of tilt calibration capabilities for this thesis.

Strain

Knowledge of subsidence-induced strain and ground strain is essential for assessing potential surface damage. Strain is induced by non-uniform displacement (horizontal movement) (Peng, 1992). Strains may be tensile or compressive. Horizontal strain and ground strain are two of the biggest causes of structural damage due to subsidence. Very simply, “horizontal strain is the difference in horizontal displacement between two points divided by the distance between the two points” (Peng, 1992). Tensile strain (positive strain value)

occurs when the distance between two points is increased and compressive strain (negative strain value) occurs when the distnace between two points is decreased (Peng, 1992). Ground strain, in contrast to horizontal strain, takes into account topography. Ground strain can differ significantly from horizontal strain, especially in areas of high relief.

Tilt

Simply stated, tilt is rigid body rotation (Marino, 1986) or a change in vertical displacement over a horizontal distance (Powell, et al., 1986). Tilt is mathematically related to vertical subsidence in that tilt at any point along a subsidence profile is the change in subsidence over a horizontal distance (Powell, et al., 1986). Curvature is also closely related to tilt, and is defined as the change in tilt over a horizontal distance (Powell, et al., 1986). Curvature is often referred to as differential tilt and serves as an indication of the degree of bending strain on a structure. O'Connor, et al. (2001) states that humping curvature causes tensile strain and sagging curvature causes compressive strain, therefore completing the explanation of the link between vertical subsidence and tilt, and tilt and strain. Marino (1986) states that almost all foundations exposed to subsidence movements will experience tilt. Tilt may affect the aesthetics, functionality, and stability of a foundation (Marino, 1986). In general, tilt has a greater effect on foundation elements that resist yield and tend to rotate as single units (Marino, 1986). Conroy (1982) suggests that tilt and ground strain associated with mining subsidence should actually be measured more often than vertical displacement because they are the parameters responsible for the most damage.

Powell, et al. (1986) monitored the response of foundations to high extraction room-and-pillar mining in southern Illinois. A main objective of the research was to determine the capability of tiltmeters to detect and monitor subsidence movements. At the time, the U.S. Bureau of Mines was investigating the development of cost-effective, alternative subsidence monitoring methods, such as tilt. Powell, et al. (1986) found that tiltmeters are easy to use and provide significant subsidence data. The main conclusions from Powell, et al. (1986) regarding the applicability of tiltmeters to subsidence monitoring are listed below.

Tiltmeters:

- Respond accurately to changes in vertical displacement
- Show accurate magnitude and direction in response to mining sequence
- May be a good toll for assessing bending strain
- Indicate a good relationship between small changes in tilt and vertical subsidence

While Powell, et al. (1986) found that tiltmeters have the potential to be very useful for subsidence measurement, they state that the tiltmeter is not ready to replace the standard survey networks.

More recently, O'Connor, et al. (2001) reports results from a study by the Pennsylvania Department of Transportation (PennDoT) that incorporated tiltmeters, in addition to time domain reflectometry (TDR) and global positioning system (GPS) measurements, to monitor longwall mining subsidence effects on Interstate-70 in Pennsylvania. An automatic tiltmeter measurement system, utilizing a centrally-located datalogger, was set up to alert highway officials of potential driving hazards due to exceedence of threshold tilt values on the highway. In highway systems, tilt can also compromise the hydraulic performance of concrete box culverts (O'Connor, et al., 2001). Analysis of the tilt data indicates that tilt at any given point began as the longwall moved beneath an area, reached a maximum value, and then decreased as the longwall moved away from the area. The study indicates that the highway experiences much greater transient (dynamic) tilt during mining than final tilt after mining. To assess the curvature and strain experienced by the highway as mining occurred, the tilt measurements were resolved into components parallel to the centerline of the road. Maximum difference in slope between adjacent tiltmeters was then used to find peak strains. Results of the study indicate that tiltmeter measurements can be used successfully to estimate surface strains where measurement of strain over large areas would be too costly. While the researchers found the automated monitoring system used with the tiltmeters to be expensive, the cost was still less than what would have been required for strain gauges over such a large area.

While previous studies indicate at least partial success for using tiltmeters for

subsidence monitoring, it is apparent that further research into the relationship between measurements from tiltmeters and other subsidence parameters is necessary before reliable subsidence prediction can be developed. The use of alternative subsidence prediction calibration techniques, such as calibrating with tilt, may allow for cheaper and more reliable methods of collecting continuous subsidence data. More data allows researchers to have a better understanding of the relationships among subsidence parameters and increases the probability of producing more accurate subsidence prediction models.

5.3.2 Implemented Methodology

To evaluate the difference between calibration parameters for measured vertical subsidence calibration and measured ground strain calibration, case studies including both types of data were sought. Due to the expense and time associated with monitoring of strain, only three available case studies possess both measured subsidence and measured strain data. The case studies include two lines from the NA-2 case study one line from the NA-1 case study. More information regarding the case studies can be found in Section 4. For each case, calibration parameters such as tan of influence angle (Tan b), subsidence factor (Smax/m), and edge effect offset were found using both measured subsidence data and measured ground strain data. The calculations were completed using the iterative calibration function of SDPS. Comparison of the calibrated models for each case study is presented below.

5.3.3 Validation of Method

The following case studies provide comparison of calibration parameters (tangent of influence angle, subsidence factor, and edge effect adjustment) using measured subsidence data with parameters calibrated using measured ground strain data. Appendix III contains SDPS screen shots used for the case studies. Many of the figures in Appendix III are referred to in the text.

5.3.4 NA-2 Calibration Case Study (N. Appalachia) - Transverse Line

Details of the NA-2 case study are available in Section 4. Figure 1 of Appendix III displays the Prediction Points Management screen used to enter both measured subsidence and measured strain data into SDPS. Calibration options for the measured subsidence data are available in Appendix I. The strain calibration options, used to set the range of values involved in the iteration

process, are displayed in Figures 2 through 6 of Appendix III. The strain calibration is based on ground strain (Appendix III, Figure 6).

The result of model calibration using measured vertical subsidence movements, as completed in Section 4, is presented again in Figure 53 and Table 23. Parameters calibrated with measured ground strain are presented in Figure 54 and Table 24.

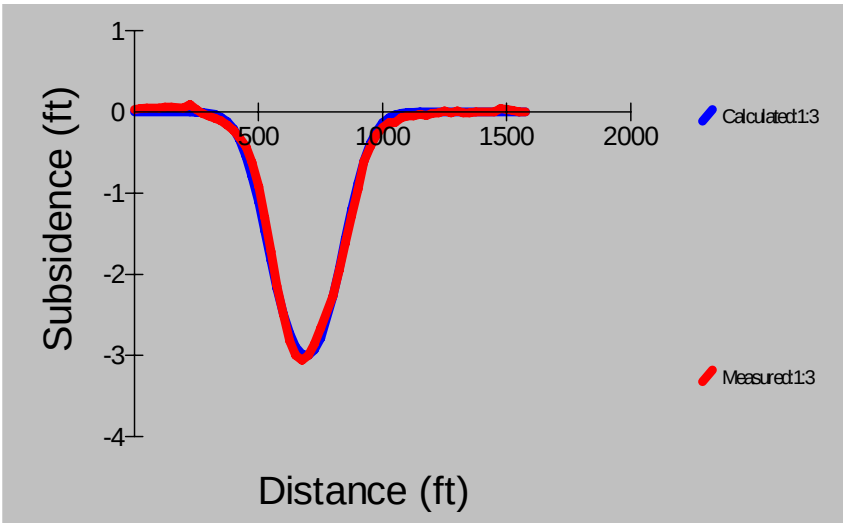

Figure 53: NA-2 - Transverse Line - Graphical display of predicted and measured subsidence profiles after calibration

Table 23: Transverse Line - Calibration parameters

Rank	Iteration Number	Tangent of Influence Angle (Tanb)	Subsidence Factor (Smax/m)	Edge Effect Offset (ft)	Total Error	Percent Error
1	856	3.00	53.0	167.00	10.895	13.21
2	371	3.00	52.0	163.00	10.962	13.29
3	492	3.00	52.0	164.00	10.977	13.31

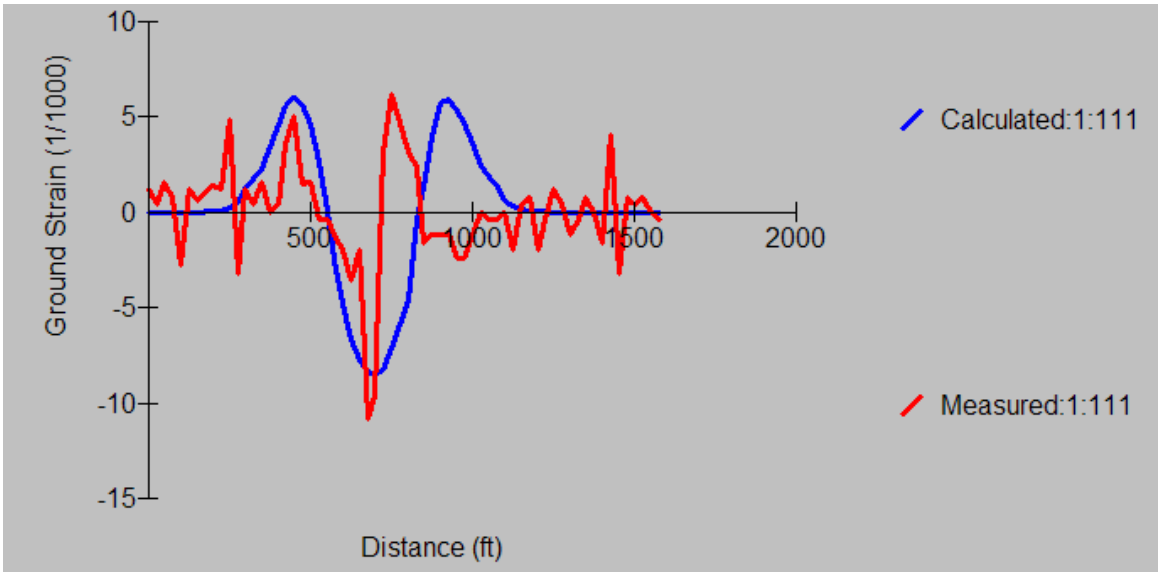

Figure 54: NA-2 - Transverse Line - Graphical display of predicted and measured strain profiles after calibration

Table 24: NA-2 Transverse Line – Calibration parameters

Rank	Iteration Number	Tangent of Influence Angle (Tanb)	Strain Coefficient (Bs)	Subsidence Factor (Smax/m)	Edge Effect Offset (ft)	Total Error	Percent Error
1	4236	3.00	0.10	45.0	165.00	109.547	23.97
2	1	3.00	0.10	45.0	160.00	109.548	23.97
3	848	3.00	0.10	45.0	161.00	109.583	23.98

Table 25 provides a comparison of the least-error calibration parameters for each type of data. The contents of Table 25 indicate that the calibration parameters using subsidence and ground strain are very similar. In this case, duplication of parameters serves to improve confidence in the calibration, demonstrating the benefit of dual calibration capabilities. The higher error associated with the strain calibration is likely a result of the difficulty of accurately measuring strain in the field. The strain calibration error may also be associated with local surface anomalies that result in deviation from normal strain distributions.

Table 25: Comparison of subsidence – strain calibration parameters for NA-2 - Transverse Line

Parameter	Subsidence Calibration	Strain Calibration

Tangent of Influence Angle (Tanb)	3.00	3.00
Subsidence Factor (Smax/m)	53.0	45.0
Edge Effect Offset (ft)	167.00	165.00
Percent Error	13.21	23.97

5.3.5 NA-2 Calibration Case Study (N. Appalachia) - Longitudinal Line

Details of this case study are included in Section 4. Figure 7 of Appendix III displays the Prediction Points Management screen used to enter measured data. Figures 8 through 12 of Appendix III provide the strain calibration settings. The final settings result from manual adjustment based on multiple calibration runs. Manual adjustment of settings is done to determine the best-fit parameters while keeping the number of computer iterations to a minimum.

Results from model calibration using measured vertical subsidence, as completed in Section 4, are presented in Figure 55 and Table 26. Calibration results using measured ground strain are presented in Figure 56 and Table 27.

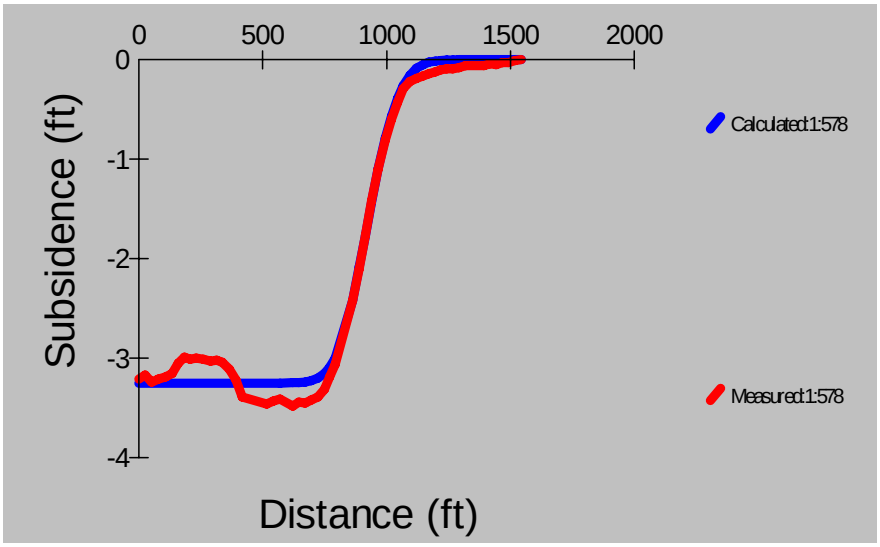

Figure 55: Longitudinal Line - Graphical display of predicted and measured subsidence profiles after calibration

Table 26: Longitudinal Line – Calibration parameters

Rank	Iteration Number	Tangent of Influence	Subsidence Factor (Smax/m)	Edge Effect Offset (ft)	Total Error	Percent Error

		Angle (Tanb)				
1	963	3.10	49.0	218.00	29.332	9.50
2	897	3.10	49.0	216.00	29.333	9.50
3	969	3.20	49.0	218.00	29.362	9.51

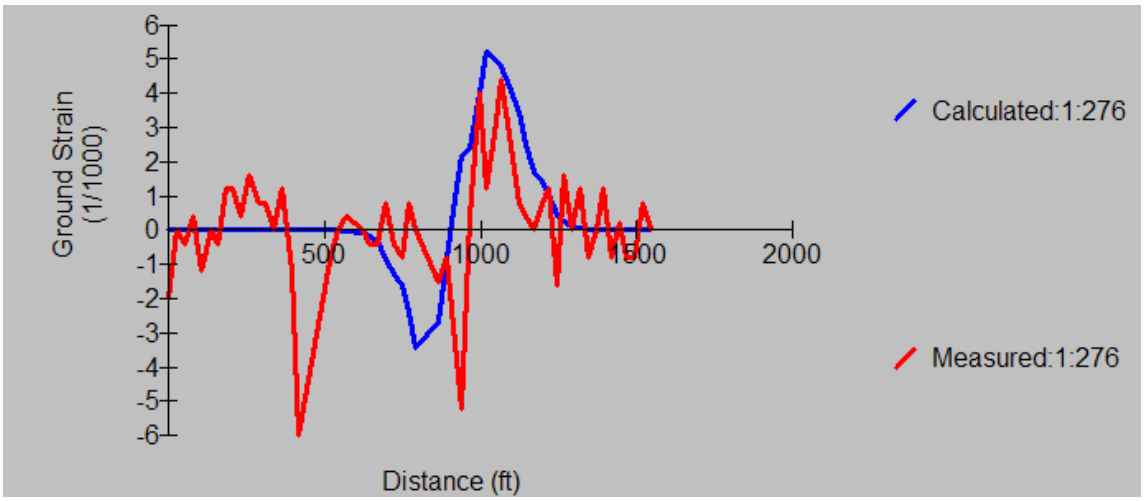

Figure 56: Longitudinal Line - Graphical display of predicted and measured strain profiles after calibration

Table 27: Longitudinal Line - Calibration parameters

Rank	Iteration Number	Tangent of Influence Angle (Tanb)	Strain Coefficient (Bs)	Subsidence Factor (Smax/m)	Edge Effect Offset (ft)	Total Error	Percent Error
1	380	3.30	0.10	45.0	192.00	58.95	36.94
2	370	3.20	0.10	46.0	192.00	59.02	36.99
3	305	3.10	0.10	47.0	190.00	59.39	37.22

Table 28 provides a comparison of subsidence parameters from measured subsidence and measured ground strain. Despite the significant error associated with the strain calibration, the parameters for the two calibration methods are similar. Values of tangent of influence angle and subsidence factor are very close. The calibrated edge effect numbers differ by 26 feet, but are still comparable. In this case, calibration of edge effect values may be complicated by the longitudinal orientation of the monument line. The subcritical nature of the panel (width to depth ratio of 0.86) may also affect the accuracy of the calibration results. Overall, the results of dual calibration for this case study strengthen confidence in the calibration parameters.

Table 28: Comparison of subsidence – strain calibration parameters for NA-2 – Longitudinal Line

Parameter	Subsidence Calibration	Strain Calibration
Tangent of Influence Angle (Tanb)	3.10	3.30
Subsidence Factor (Smax/m)	49.0	45.0
Edge Effect Offset (ft)	218	192
Percent Error	9.50	36.94

5.3.6 NA-1 Calibration Case Study (N. Appalachia)

The details of this case study are included in Section 4. The panel is classified as supercritical. Selected SDPS screen shots associated with strain calibration procedures are provided in Appendix III. As discussed in Section 4, the edge effect is restricted to "as defined in mine plan" during calibration due to the variable edge effects applied to the panel (Appendix III, Figure 16). For this reason, the calibrated edge effect values shown in the results are not applicable. Model calibration results using measured vertical subsidence are presented in Figure 57 and Table 29, and calibration results using strain are presented in Figure 58 and Table 30.

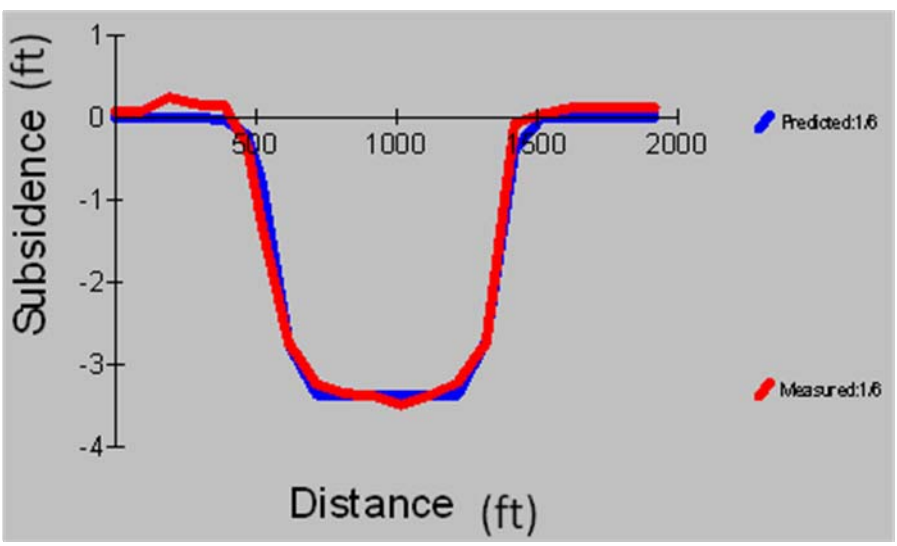

Figure 57: Graphical display of predicted and measured subsidence profiles after calibration

Table 29: Calibration parameters

Rank	Iteration Number	Tangent of Influence Angle (Tanb)	Subsidence Factor (Smax/m)	Edge Effect Offset (ft)	Total Error	Percent Error
1	6	2.50	52	150	6.664	7.90
2	5	2.40	52	150	6.877	8.15
3	7	2.60	52	150	6.949	8.24

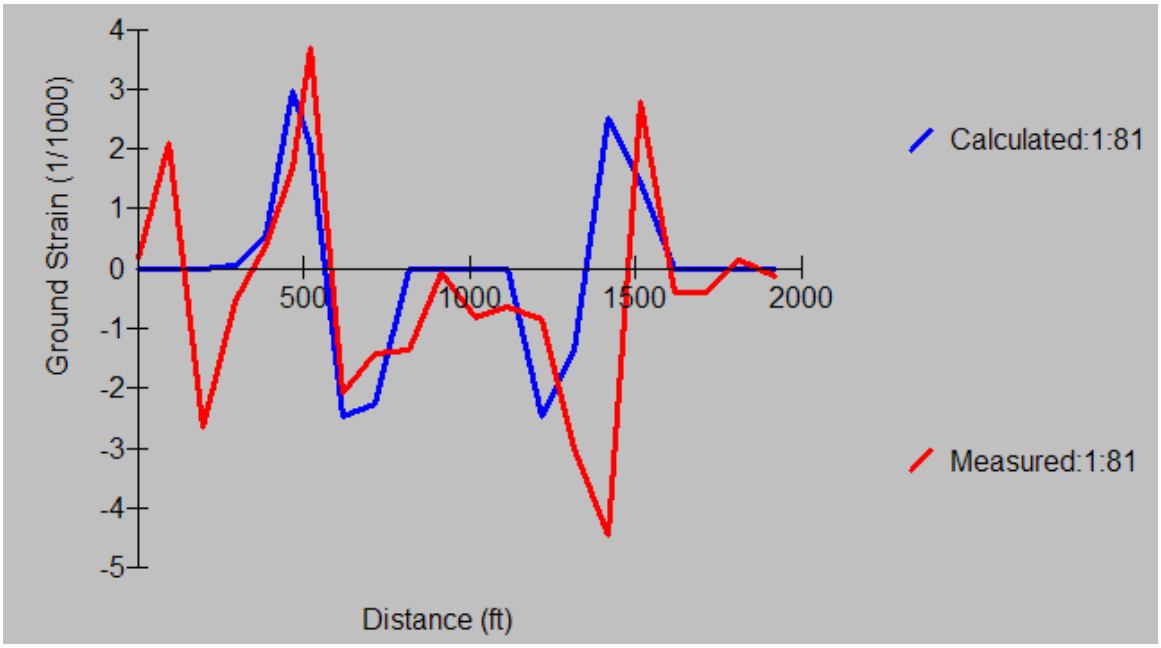

Figure 58: NA-1 Case Study - Graphical display of predicted and measured strain profiles after calibration

Table 30: NA-1 Case Study - Calibration parameters

Rank	Iteration Number	Tangent of Influence Angle (Tanb)	Strain Coefficient (Bs)	Subsidence Factor (Smax/m)	Edge Effect Offset (ft)	Total Error	Percent Error
1	326	2.70	0.15	50	153	26.351	34.80
2	235	2.70	0.15	49	152	26.375	34.83
3	417	2.70	0.15	51	154	26.410	34.88

Table 31 provides a comparison of the calibration parameters. Similar to the results of the other case studies, the Tan b and subsidence factor values for the two calibration methods are very similar. The strain calibration, once again,

results in a much more significant error factor than the subsidence calibration.

Table 31: Comparison of subsidence – strain calibration parameters for NA-1 case study line

Parameter	Subsidence Calibration	Strain Calibration
Tangent of Influence Angle (Tanb)	2.50	2.70
Subsidence Factor (Smax/m)	52	50
Edge Effect Offset (ft)	150	153
Percent Error	7.90	34.80

5.3.7 Location Angles

The angle of Draw (γ) is defined as the angle between the vertical at the panel edge and the line connecting this edge (or rib) with the surface point that defines the termination of subsidence trough (i.e., zero subsidence). Since the subsidence profile diminishes to extremely small values, far before it reaches the edge of the subsidence basin, it follows that this angle is of limited value in subsidence control (Peng, 1992). Furthermore, the concept of "zero" subsidence is rather difficult to measure or apply. A better approach, often used in subsidence work, is to define a minimum, "measurable", subsidence level as the zero reference point.

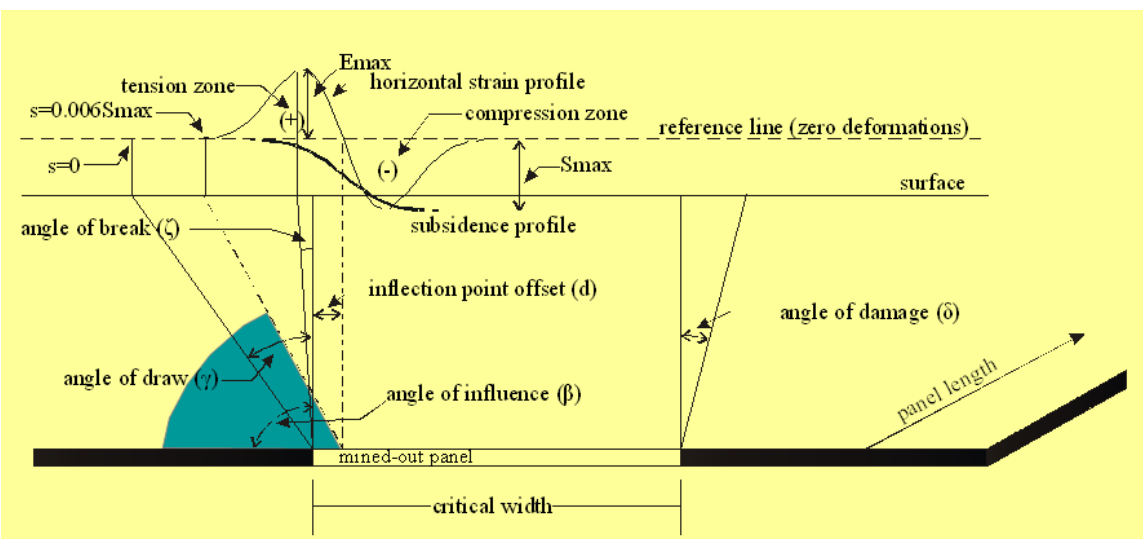

Figure 59: Definition of characteristics angles

5.3.8 Discussion

Results of the case studies suggest that subsidence and strain calibration

methods often yield similar calibration parameters (Tan b, subsidence factor, and edge effect adjustment). In all cases, the subsidence-calibrated models have significantly lower error. More significant error associated with strain calibration may be a result of the difficulty associated with measuring strain values in the field and the difficulty of modeling strain. Measured strain values may also be more susceptible to local surface anomalies in the measured area. The subcritical state of some of the case study panels may also have an effect on the accuracy of the calibration.

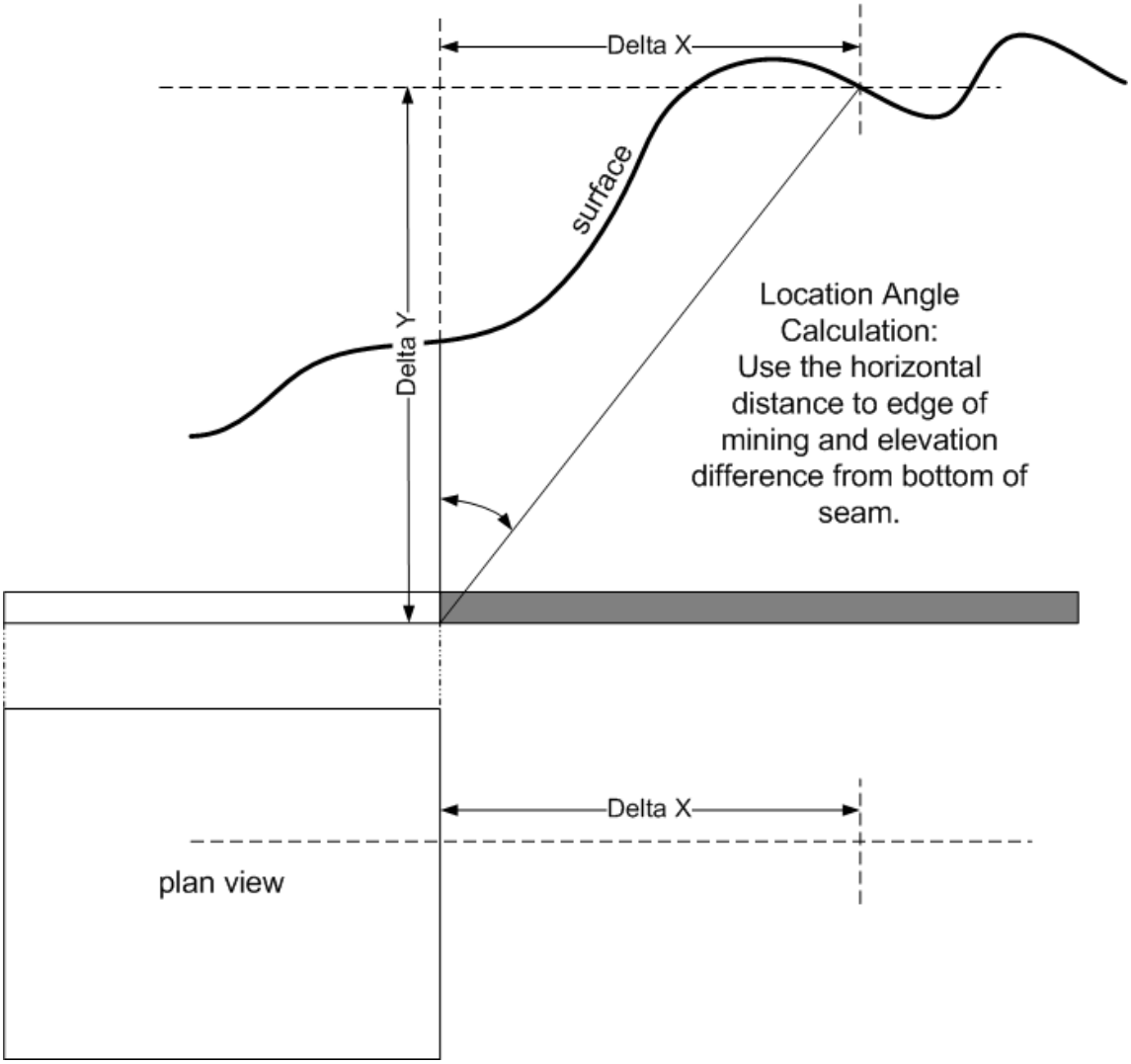

Figure 60: Calculation of the Location Angle

Regardless of the potential error associated with the calibrations, the calibration parameters from the two types of data are similar. The potential to conduct dual calibration provides researchers with more confidence in calibration parameters to be used for prediction models. The capability may also be used to detect errors in data collection.

While the case studies presented only compare subsidence and strain calibration methods, the potential also exists for using other measured parameters for calibration purposes. Section 5.3.1 provides discussion of using measured tilt values for calibration. The collection of measured data associated with ground deformation due to mining is often expensive and time consuming. However, the

data is necessary for prediction and mitigation purposes. Variable calibration capabilities may allow subsidence engineers to get the necessary data for prediction model calibration by using the least expensive, most efficient measured data.

6. Objective III: Apply subsidence methodology for landscape stability and control

6.1 Risk- Based Assessment of Mine Planning and Long-term Landscape Stability

6.1 Previous Research

Subsidence engineers must not only understand the mechanisms of subsidence, but also the effects of subsidence on surface structures and other entities at or near the ground surface. It is damage to property at the ground surface that likely prompted the initial in-depth studies of mine subsidence, and it is property damage (or the potential for property damage) that continues to drive current mine subsidence research. Gray (1992) points out that mining engineers evaluating alleged mining subsidence-related damage must also be aware of the potential for structural damage to homes due to poor engineering, poor construction, deterioration, neglect, and misuse. Types of movement associated with subsidence from underground mining may also be associated with unstable slopes, erosional processes, frost action, shrink-swell actions of clayey materials, and settlement under surface loads (Gray, 1992). Mining engineers must be aware of the possibility of alternative causes for ground movement to be able to correctly identify the subsidence-related movements. The first step to dealing with any potential subsidence-related damage situation is to establish a clear definition of what the term “damage” means in each case (Bruhn, 1992). Often times, solutions to subsidence-related damage problems require multidisciplinary studies that account for overall structural behavior and site specific details (Bruhn, 1992). Assessing current subsidence-related problems, as well as planning for potential future subsidence-related problems, necessitates the integration of geotechnical, civil, and mining engineering principles (Luxbacher, 1992).

6.2 Deformation and Damage

Various aspects of ground deformation, such as tension, compression, shear, tilt, curvature, angular distortion, bending, and horizontal strain, have been identified to be responsible for the majority of subsidence-related damage (modified from Singh, 1992). While most aspects of subsidence are readily understood, a few

require further explanation. Tilt is defined as a rigid body motion (also see discussion in Section 5.3); horizontal strain is defined as the change in horizontal length between two points divided by the original horizontal distance between the two points, while ground strain takes into account topography (see Section 5.2); curvature is the derivative of the slope of the subsidence trough; and angular distortion is the ratio of the differential displacement and the horizontal distance between two points (Triplett, et al. 1992).

In general, mining-related ground movements cause rotations and deformations of building foundations. As the degree of deformation increases, the strength and deformability of the foundation is tested (Marino, 1986). The superstructure (upper part of building) is indirectly affected by ground movements by way of the foundation (Marino, 1986). This implies that interaction at the ground-foundation interface of subsidence-affected buildings plays a significant role in determining the magnitude of effects experienced by both the foundation and the superstructure. However, due to the overwhelming number of possible combinations of soil type and foundation type, prediction methods for subsidence-induced damage typically assume that the structure moves with the ground (Marino, 1986).

Various subsidence researchers have reported correlations between aspects of subsidence movement and surface structure damage. Geddes and Cooper (1962) found relationships between the length of a building, the horizontal ground strain, and the damage to the building. Marino (1986) states that the ratio of building length to building width determines the probability and magnitude of the type of deformation that will occur. Conroy and Gyarmaty (1982) found that tilt and ground strain are responsible for the most damage and argue that more effort should be put into measurement of tilt and ground strain, rather than vertical displacement. Similarly, Triplett, et al. (1992) found a strong correlation between ground surface curvature (related to ground strain) and damage to house foundations. Karmis, et al. (1994) uses horizontal strain, angular distortion, and curvature to assess surface damage from mining subsidence. Boone (1996) reports that ground curvature is a main cause of cracks in houses, but notes that angular distortion is more readily measured. Luo, et al. (2003) also uses critical values of strain, curvature, and slope to assess potential damage due to subsidence.

6.3 Classification of Damage

To assess the damage to surface structures, and the correlation of damage to ground strains and other aspects of subsidence, it is necessary to classify the various degrees of observed damage. Many authors have compiled subsidence damage observations and constructed various forms of damage criteria. Classification of subsidence damage can be approached by assessing the actual severity of structural damage or by evaluating the value of the damage-causing subsidence parameters, such as ground strain, in the affected area (Triplett, et al., 1992). Many classification schemes provide correlations of measured subsidence parameters with characteristics of observed surface structure damage. Geddes and Cooper (1962) presents a classification by Orchard of damage caused by horizontal ground movements associated with mining subsidence (Table 32). The table presents suggested correlations between ground strain and typical damage observed in houses in England that were not specially designed to accommodate horizontal ground movements from mining subsidence.

Table 32: Classification of damage caused by subsidence-related horizontal ground movements by Orchard, presented in Geddes and Cooper (1962)

Ground Strain	Class of Damage	Description of Typical Damage
Up to 0.1%	Very slight or negligible	Fine cracks in plaster. Perhaps isolated slight fracture in building not visible externally.
0.1% to 0.2%	Slight	Several slight fractures showing inside building. Doors and windows may stick. Repairs to plastered walls and ceilings may be necessary.
0.2% to 0.3%	Appreciable	Slight fractures visible externally. Doors and windows stick.
0.3% to 0.4%	Severe	Service pipes broken. Open fractures in walls. Window and door frames distorted. Some loss of bearing in beams. If compression damage – overlapping of roof joints and lifting of brickwork with open horizontal fractures.
0.5%	Very Severe	Building may require partial or complete re-building. Roof and floor beams lose bearing and walls lean badly and have to be supported. Windows broken and distorted. Severe buckling and bulging of roof and walls under compression.

In 1975, the National Coal Board (NCB) produced a general guide for predicting the intensity of subsidence damage. It is noted that “accurate prediction also depends upon an expertise difficult to reduce to quantitative terms and which can

only be acquired from a wide experience with buildings of various age and type of construction" (NCB, 1975). The main factors considered for the NCB's damage classification scheme are strain and building length. The NCB damage classification scheme is presented in Table 33. The NCB classification scheme is very similar to that presented by Orchard in Geddes and Cooper (1962).

Table 33: National Coal Board classification of subsidence damage based on strain and building length

Change of Length of Structure	Class of Damage	Description of Typical Damage
Up to 0.03 meters	1.Very slight or negligible	Hair cracks in plaster. Perhaps isolated slight fracture in the building, not visible outside.
0.03 to 0.06 meters	2. Slight	Several slight fractures showing inside the building. Doors and windows may stick slightly. Repairs to decoration probably necessary.
0.06 to 0.12 meters	3. Appreciable	Slight fracture showing on outside of building (or one main fracture). Doors and windows sticking; service pipes may fracture.
0.12 to 0.18 meters	4. Severe	Service pipes disrupted. Open fractures requiring rebonding and allowing weather into the structure. Window and door frames distorted; floors sloping noticeably; walls leaning or bulging noticeably. Some loss of bearing in beams. If compressive damage, overlapping of roof joints and lifting of brickwork with open horizontal fractures.
More than 0.18 meters	5. Very Severe	As above, but worse, and requiring partial or complete rebuilding. Roof and floor beams lose bearing and need shoring up. Windows broken with distortion. Severe slopes on floors. If compressive damage, severe buckling and bulging of the roof and walls.

Karmis, et al. (1994) compared damage criteria suggested by multiple authors in order to define ranges of threshold damage values. Karmis, et al. (1994) notes that the damage criteria presented by NCB (1975), while widely used, ignores the construction materials, design, shape, and age of the structure experiencing the damage. In order to establish threshold values of ground movement parameters which describe a particular severity damage level, three prominent damage classification schemes were compared and then combined (Karmis, et al. 1994). The damage classification schemes by NCB (1975), Bruhn et al. (1982), and Bhattacharya and Singh (1985)/ Singh (1992) are presented in a combined format Table 34), as provided in Karmis, et al. (1994). The table compares the NCB classification with the Bruhn et al. (1982) and Bhattacharya and Singh (1985)/ Singh (1992) classifications, focusing on characteristics of damage

observed to a common brick/masonry low-rise structure (Karmis, et al. 1994). The first column of Table 34 includes ranges of strain from NCB (1975). The second column provides an approximate conversion from NCB classes of damage to damage severity levels presented by Bruhn et al. (1982) to classes of building damage by Bhattacharya and Singh (1985)/ Singh (1992). The damage severity levels, created by Bruhn et al. (1982) for the Northern Appalachian coalfields, are part of Bruhn's "Severity Index System" (SIS) and relate to severity index numbers. The severity index numbers, based on documentation of repairs required to basements (Bruhn et al., 1982), are presented in the third column of Table 34. The classes of building damage by Bhattacharya and Singh (1985)/ Singh (1992), and designated as the "Damage Classification System" (DCS), are based on information collected from numerous countries. The DCS system summarizes building categories, movement types, and ranges of damage limits associated with mining subsidence (Bhattacharya and Singh, 1985/ Singh, 1992).

Table 34: Comparison and combination of damage classification schemes as presented by Karmis, et al. (1994)

Change of Length of Structure (according to NCB (1975)	Class of Damage or Severity Level (comparative/comprehensive scheme by Bhattacharya and Singh (1985)/ Singh (1992)) **NCB System→SIS→DCS**	Severity Index (after Bruhn et al., 1982)
Up to 0.1 ft (30.5 mm)	Negligible→Slight→Architectural	0-1
From 0.1 ft (30.5 mm) to 0.2 (61 mm)	Slight→Moderate→Functional	1-2
From 0.2 ft (61 mm) to 0.4 ft (122 mm)	Appreciable→Moderate→Functional	1-2
From 0.4 ft (122 mm) to 0.6 ft (183 mm)	Severe→Severe→Structural	2-4
Over 0.6 ft (183 mm)	Very Severe→Very Severe→Structural	4-5

After establishing equivalencies among the damage classifications presented by NCB (1975), Bruhn et al. (1982), and Bhattacharya and Singh (1985)/ Singh (1992), Karmis, et al. (1994) uses measured values of horizontal strain and angular distortion from Singh (1992) to define ranges of subsidence parameter values associated with each class of damage. Table 35 summarizes the ranges of strain and distortion values associated with each combined damage class.

Table 35: Classes of damage and suggested threshold (damage limit) values of horizontal

strain and angular distortion(Karmis, et al., 1994)

Class of Damage or Severity Level (comparative/comprehensive scheme by Bhattacharya and Singh (1985)/ Singh (1992)) **NCB System→SIS→DCS**	Horizontal Strain (suggested damage limit values after Singh, 1992)	Angular Distortion (suggested damage-limit values after Singh, 1992)
Negligible→Slight→Architectural	0.5×10^{-3}	1.0×10^{-3}
Slight→Moderate→Functional	$1.5\text{-}2.0 \times 10^{-3}$	$2.5\text{-}3.0 \times 10^{-3}$
Appreciable→Moderate→Functional	$1.5\text{-}2.0 \times 10^{-3}$	$2.5\text{-}3.0 \times 10^{-3}$
Severe→Severe→Structural	3.0×10^{-3}	7.0×10^{-3}
Very Severe→Very Severe→Structural	$>3.0 \times 10^{-3}$	$>7.0 \times 10^{-3}$

Establishment of the ranges of threshold damage values for each class of damage allowed Karmis, et al. (1994) to define ranges of subsidence parameters that correspond to a threshold, above which structural damage due to mine subsidence is likely and below which structural damage is unlikely. Because horizontal strain data is most abundant, it is considered the predominant damage index. The threshold value range for horizontal strain is 1.5×10^{-3} to 3.0×10^{-3} (Karmis, et al. 1994). A value of 1.5×10^{-3} is used as a default for the case studies included in this thesis. Other threshold value ranges, such as those for angular distortion, curvature and slope, were also defined by Karmis, et al. (1994). However, it is noted that the values are based on significantly less data than the horizontal strain values.

6.4 Damage Prediction

Relying on the concept that mine subsidence damage to surface structures is most closely related to horizontal strain and ground strain, many researchers have attempted to predict damage using predicted strain values. In attempting to predict damage from strain, researchers found that different structures may have different reactions to strain. In order to take into account both subsidence-induced horizontal/ground strains and possible surface structure damage, Reddish, et al. (1996) coupled a subsidence prediction system with an “expert-based” system. The duel program calculates strain values for undermined areas and assesses the potential for surface structure damage through a series of “if-then” questions, the answers of which are analyzed by the “expert based” system

(Reddish, et al. 1996). The questions are related to expected threshold strain values for each surface structure and other variables affecting the transmission of the ground strain into the structures. The three most vital components to the assessment process are mining factors, site factors, and structural factors (Reddish, et al. 1996). The end result is a certainty value related to how much damage each structure may experience. The program is a risk based system that provides subsidence engineers with the probability of occurrence, and degree of occurrence, of subsidence-related damage.

Karmis, et al. (1994) also presents a risk based system of damage assessment based on the concept of a damage angle, defined as a "critical value of the angle of deformation at which surface structures can be maintained without some defined degree of damage". More importantly, the damage angle is determined based on the distribution of threshold values for damage-causing subsidence parameters. Case studies in section 6 exemplify the use of threshold values to determine high risk areas that can be described with damage angles. Using a damage angle (based on threshold parameter values) to define potential areas of damage due to mining accounts for both ground movement and surface structure response by considering mining conditions, geological conditions, and damage intensity levels (Karmis, et al. 1994).

6.5 Mitigation of Expected Damage

By predicting potential subsidence-induced effects, engineers have the ability to conduct mitigation efforts to lessen the predicted damages. Luo, et al. (2003) presents a very simple, yet successful, systematic approach to subsidence mitigation. First, the expected subsidence parameters must be calculated. Next, the subsidence parameters, such as ground strain and angular distortion, are compared to the critical deformation values for potentially effected structures. If the subsidence effects are expected to be greater than the strengths of the surface structures, mitigation must work to decrease the discrepancy (Luo, et al. 2003). Potential mitigation techniques include better mine planning, reduction of the transmission of strain from the ground to structures, and reinforcement of structures (Luo, et al. 2003). More specifically, trenches are often dug around structures to decrease the transmission of strain and cables may be placed on buildings to reinforce the structure as it experiences differential subsidence movements (Luo, et al. 2003). In addition, Luo, et al. (1992) discusses an

advanced plane fitting method of protecting the superstructure of a house from strain caused by curvature and twisting. The method involves using jacks to make height adjustments of different parts of a superstructure as mining progresses underneath. The jacks must be adjusted frequently to accommodate for subsidence-induced movement and keep the superstructure from experiencing damage-causing differential movements. Mitigation by the Luo, et al. (1992)/Luo, et al. (2003) approach has been implemented successfully and documented in numerous case studies.

When buildings are built in areas that are to be undermined, prediction of ground strains and potential damage allows engineers to design the buildings to adapt to subsidence-related movements. Two of the more unique early designs for “subsidence-proof” homes are discussed bhy Geddes and Cooper (1962). One involves building homes on movable timbers that adjust to subsidence movements without transferring the strains into the foundation. The other involves constructing rigid box frame foundations that are designed to withstand the damage-causing forces (Geddes and Cooper, 1962). While these designs for subsidence-resistant structures were not always successful, the basic concepts are still used when there is a possibility that structures will experience mine subsidence related movement. Numerous authors have addressed criteria for development in areas that are at risk of experiencing mining-induced ground deformation. A detailed discussion of the criteria is beyond the scope of this thesis.

7. Objective IV: Assess long-term stability

7.1 Assessing Long-term Landscape Stability

7.1.1 Phases of Mining-Induced Deformation

The process of classification, prediction, and mitigation of mining-induced damage is applicable to areas that are to be mined, as well as areas that have been mined in the past. The long-term stability of underground mines and the overlying landscape is dependent on multiple factors, one of the most important being the method of mining. Singh (1992) defines two main phases of subsidence associated with underground mining, an active phase and a residual phase. Jarosz, et al. (1990) recognizes three phases of subsidence, initial, active, and residual. The addition of the initial phase in the classification by Jarosz, et al. (1990) is in place because they were specifically considering the small amount of subsidence that is measured as a longwall face approaches a point on the surface. Singh (1992) considers subsidence in relation to time in a more general sense with respect to both longwall mining and room-and-pillar mining. The active and residual subsidence phases are present in both classifications because they include the majority of subsidence activity.

The active phase of subsidence is loosely defined as the subsidence that occurs during mining up until a point where the mining is not expected to have a direct relationship on the surface subsidence. The residual phase of mining subsidence begins after the active phase and can last for less than a year or extend for many decades, depending upon the mining method and other factors. In particular, for longwall mining the active phase includes the majority of the subsidence movement while the residual subsidence phase is important when considering post-mining land use and the extent of liability of underground coal mine operators for post-mining subsidence (Singh, 1992). In the case of room-and-pillar mining, the opposite is often true with the active phase being insignificant and the residual phase incorporating the most subsidence.

In addition to the different phases and durations of each phase associated with mining subsidence, the type of mining also determines the physical manifestation of the subsidence on the surface. The two main types of subsidence that occur on the surface are trough subsidence and chimney subsidence (Karfakis, 1993). Trough, or sag, subsidence may occur with both longwall and room-and-pillar

mining methods, and is more often associated with longwall mining and high extraction (second mining) room-and-pillar areas. In general, trough subsidence creates a gentle, shallow surface depression and chimney (or sinkhole-type) subsidence usually forms deeper, more steep-sided, conical (apex up) depressions (Karfakis (1993) and Dyne (1998)). A detailed description of chimney subsidence due to abandoned mines is presented in Karfakis (1993).

Longwall mining, for the most part, causes rapid subsidence of the undermined area (initial and active subsidence phases) with a less significant residual phase. Data presented in Singh (1992) from studies in the United Kingdom, France, Germany, USSR, and the United States suggests that the duration of residual subsidence associated with longwall mining is typically less than six years, very often around two years, and may be as short as a few weeks. The magnitude of residual subsidence from longwall mining is usually significantly less than 10% of the total subsidence (Singh, 1992) and is usually not as much of a concern for post-mining land use planning, compared to room-and-pillar mining.

Because the residual subsidence associated with longwall mining is relatively less significant than that associated with room-and-pillar mining, it has not been studied in great detail. However, Luo and Peng (2000) found that longwall subsidence in the eastern U.S. tends to reach a “quasi-stable” state once the longwall has advanced 0.7 to 0.94 times the overburden thickness past a given surface point. After this point, Luo and Peng (2000) found that residual subsidence may occur in the form of re-compaction of caved and fractured material in the gob area and/or slow (“creep”) deformation of the chain pillars between longwall panels. Karfakis (1993) also discusses residual subsidence over longwall panels due to compaction of rubblized gob, and points out that changes in the abundance of water in the gob greatly affect the degree of recompaction and occurrence of residual subsidence. Creep deformation of chain pillars is reported to cause more residual subsidence (as compared to re-compaction of gob material), the magnitude of the pillar creep dependent upon the original designed safety factor of the chain pillars and the mining height (Luo and Peng, 2000). Luo and Peng (2000) developed an equation based on these parameters to determine the half-life of the long-term subsidence (or expected creep of the chain pillars). The residual subsidence associated with longwall mining was not observed in every case reviewed by Luo and Peng (2000). Based on the predicted half-life of typical creeping chain pillars, they concluded

that longwall long-term subsidence is much less likely to cause damage to surface structures than room-and-pillar long-term subsidence.

In contrast to the relatively rapid subsidence induced by longwall mining, subsidence related to room-and-pillar mines may be delayed for decades and may only occur after pillars have deteriorated to the point of yielding or collapsed, or both (Singh, 1992). A common misconception is that mining subsidence associated with room-and-pillar mining may be avoidable if mines are developed with large pillars and at great depth under strata containing competent beds of rock (Singh, 1992). Research shows that the redistribution of stress associated with room-and-pillar mining causes measurable deformation in pillars, which is eventually transmitted to the ground surface. The conditions of each individual site determine the extent of subsidence, which can vary between considerable to nearly undetectable (Singh, 1992).

Factors controlling the deterioration of room-and-pillar mine systems, and therefore the amount and timing of associated subsidence are variable and must be considered for each site. The major factors include the strength of the coal, roof, and floor of the mine; the extent of natural fracturing; the presence, abundance, and variation of water in the mine; the depth of the mine workings; the appropriateness and variability of pillar sizes; the percent of the coal extracted (Singh, 1992); and the bulking capabilities of the caved material (Karfakis, 1993). Karfakis (1993) outlines the main mechanisms of failure of abandoned room-and-pillar mines. The abundance of mine water in the abandoned mine, the deterioration of the mine structures, and the development of residual mine subsidence are all very closely related. Varying levels of moisture in a mine has significant effects on the stability of the roof, pillars, and mine floor. The result is failure of the mine structure by pillar failure, roof caving, and pillar punching (due to exceedance of the mine floor bearing capacity) (Karfakis, 1993).

7.1.2 Prediction and Assessment of Long-term Landscape Stability

Because of the multiple factors affecting subsidence associated with room-and-pillar mining and the variability of conditions from mine to mine, many authors suggest that accurate predictions of long-term room-and-pillar mine stability are very difficult, if not impossible, to provide. Karfakis (1993) argues that while numerous approaches to subsidence prediction exist, they are only applicable to

active, total-extraction mining systems. However, Karfakis (1993) also notes that the probability of residual subsidence over abandoned room-and-pillar mines may be possible via subsidence mechanism modeling and/or analysis of historical data.

Despite the difficulties of predicting long-term stability of abandoned room-and-pillar mines, a few researchers have made an attempt. Taylor, et al. (2000) found empirical relationships between pillar factor of safety and time, subsidence and rock mass rating, and extent of vertical subsidence with peak pillar vertical stress. The research yielded an empirical equation for calculating “days to failure” for room-and-pillar mines in an area of coalfields in England, but it is emphasized that each mined area must be considered separately because general “rules of thumb” are not sufficient. Taylor, et al. (2000) also stresses the importance of site investigation, and provides an outline of procedures for determining the presence, extent, and stability of underground mining beneath surface areas to be developed.

Karfakis (1993) discusses the basis for a prediction method used for predicting chimney subsidence over lead and zinc mines in Poland. It involves the determination of the height of a stable pressure arch over the excavation as well as the expected volume increase (bulking capacity) of the caved roof rock. The possibility of caving is assessed by comparing the height of a stable pressure arch with both the overburden thickness and the height of rubblized roof material after bulking. Basically, the probability of occurrence of sinkhole subsidence is considered equal to the probability that caving of the roof will reach the ground surface (Karfakis, 1993).

Dyne (1998) assessed the occurrence of chimney subsidence associated with abandoned room-and-pillar mines in southwestern Pennsylvania and provides an equation for prediction of the height of a potential collapse-chimney. In the Pittsburgh, Pennsylvania, metropolitan area, Gray et al. (1977) reports that chimney mine subsidence is the most prevalent form of subsidence. The apparent randomness and unpredictability of chimney subsidence is a cause for great concern, especially in areas where populated zones overly abandoned mines (Karfakis, 1993). Collected data indicates that the average time between the abandonment of the mine and the appearance of chimney-collapse subsidence at the surface is approximately 60 years (Dyne, 1998). Dyne (1998)

also concludes that water table fluctuations and precipitation runoff are important factors leading to the collapses. The prediction equation, as provided by Dyne (1998), allows investigators to estimate the highest expected caving distance for the roof in different areas of underground room-and-pillar mines. Similar to the method discussed by Karfakis (1993), comparing the expected caving distance to the thickness of overburden between the mine and the surface allows researchers to predict where chimney-collapse subsidence is most likely to occur (Dyne, 1998). In this way, the subsidence prediction capability allows for preventative mitigation prior to subsidence-induced property damage.

Hao and Chugh (1992) discusses a methodology for predicting the likelihood of subsidence events over abandoned room-and-pillar mines in Illinois. This is accomplished using average values of geotechnical properties from nearby active mines and statistical correlations of safety factor values with subsidence incubation periods. The results suggest that larger initial safety factors usually correlate with longer subsidence incubation periods. Because estimated pillar safety factors in their study area of Illinois are usually much higher than the estimated floor safety factors, Hao and Chugh (1992) concludes that the floor will fail first, making floor safety factor the controlling variable of subsidence. This conclusion is confirmed by a graph showing significant correlation between observed subsidence incubation period and estimated floor safety factors Hao and Chugh (1992). The correlation chart is used to predict incubation periods from known floor safety factors. Hao and Chugh (1992) reports significant estimation error associated with the proposed method. There is a 67% likelihood that subsidence events will occur within 16 years of the predicted subsidence incubation period and a 95% likelihood that subsidence events will occur within 32 years of the predicted subsidence incubation period (Hao and Chugh, 1992).

Perhaps some of the most frequently-used methods for assessing underground stability are those incorporated into computer programs and made available by the National Institute for Occupational Safety and Health (NIOSH). The methods include pillar sizing equations by Bieniaski, Mark and Bieniaski, Holland, Holland and Gaddy, and Obert and Duvall. A program known as “Analysis of Longwall Pillar Stability” (ALPS) is provided for calculating stability factors of longwall pillars (NIOSH, 2007). The stability factors are useful for delineating areas with high probability of failure. Other underground stability analysis programs provided by NIOSH include “Analysis of Retreat Mining Pillar Stability” (ARMPS),

"Analysis of Retreat Mining Pillar Stability – Highwall Mining" (ARMPS – HWM), "Analysis of Horizontal Stress in Mining" (AHSM), and "Coal Mine Roof Rating" (CMRR). The programs are available from NIOSH at www.cdc.gov/NIOSH/. Discussion of the methodology behind the programs is beyond the scope of this thesis. However, the programs include full documentation and references of the employed methodologies.

Predicting the time in which underground room-and-pillar mines may collapse or sag is very difficult to accomplish. However, Newman (2003) and Karmis and Agioutantis (2004) concentrate on assessing the probability of a collapse and the associated potential damage. The methodology of Newman (2003) and Karmis and Agioutantis (2004) is a risk based assessment that can be used when considering long-term landscape stability to evaluate the potential problems that may occur over a period of time at a particular site. While designing slurry impoundments for coal refuse, engineers are often faced with the presence of abandoned underground room-and-pillar mines beneath the proposed impoundment site. The consequences of interaction between the slurry impoundment and residual subsidence in previously mined areas can be very dangerous, as well as expensive. Newman (2003) presents three case studies in which the ground strains generated from various degrees of possible future residual subsidence are predicted using SDPS. The potential interaction between the strains and the slurry impoundment are reviewed and the design of the impoundment is altered to make sure it can withstand the predicted strains. Often times, the strain analysis includes a "worst case" scenario in which all the remaining pillars in the abandoned mine collapse. The method also allows designers to predict strains generated by any combination of pillar collapse. The original safety factors for the pillars (determined using previously discussed methodology available from NIOSH) may be used initially to predict which pillars, or pillar areas, may fail first. Newman (2003) also discusses using the predicted strains from SDPS to analyze the factors of safety against outcrop barrier pillar failure. The work done by Newman (2003) and Karmis and Agioutantis (2004) incorporates a risk-based approach to long-term stability assessment. While the methodology does not predict the time of failure of underground room-and-pillar mine systems, it does allow engineers to predict the possible damages due to collapse and to design surface structures accordingly. The methodology presented by Newman (2003) and Karmis and Agioutantis (2004) is applicable to

any entity on the surface above underground room-and-pillar mines.

7.1.3 Mechanisms Affecting Long-Term Stability

While some researchers have attempted to find ways of predicting long-term stability of room-and-pillar mines, many have concentrated on understanding the mechanisms affecting stability through analysis of case studies. The basic mechanisms believed to control residual subsidence associated with room-and-pillar mines are collapse of the roof span between adjacent pillars, pillar failures (ranging from collapse of small areas to cascading pillar failures), and squeezing or crushing interactions between the pillars and the roof and/or mine floor (Singh, 1992). The fundamentals of each of these mechanisms are the same as what is considered during normal ground control design, but each must be assessed with regard to a much longer time period. As mentioned before, and evident in the following examples, there is a strong correlation between the abundance and variation of water in an abandoned mine and the degree of residual subsidence (Karfakis, 1993).

Subsidence associated with an abandoned room-and-pillar mine in Illinois was found to be a result of pillars punching into a moisture-affected claystone floor (Chugh, et al. 1988). The majority of the mine has less than 200 feet of overburden, with as much as 80 feet of the overburden being unconsolidated surficial deposits. Gradual sag subsidence, followed by more catastrophic subsidence was recorded often in valley bottoms where borehole cameras observed in-mine water and where overlying surficial deposits are significantly thicker (Chugh, et al. 1988). Both the slow, sagging subsidence and the more catastrophic subsidence events caused noticeable damage to surface structures. Differential surface sag due to isolated pillar collapses has also caused twisting damage in some homes (Chugh, et al. 1988). Because the mine floor is very moisture sensitive, researchers believe that subsidence will continue as water finds its way into more areas of the mine.

Also in Illinois, Mahar and Marino (1999) evaluated 15 years of residual subsidence data over old room-and-pillar mines that are approximately 200 feet deep with a 5.5 to 7.0 ft mining height. Despite the fact that only first mining had been undertaken, they found evidence of sagging over the mine and recorded both catastrophic and gradual failure. The gradual sag subsidence development, which is believed to be a result of pillar/floor punching and pillar crushing, is

described as behaving similar to a settlement curve for normally loaded clay. The faster, catastrophic sag measurements are attributed to pillar collapse. Although the sag development is relatively slow, Mahar and Marino (1999) found significant damage to some of the houses in the area. Survey data indicates that the sag subsidence over the mine has been occurring since first mining was completed 15 years ago. While making the measurements, it was discovered that seasonal changes in water levels, soil moisture, and temperature affected the accuracy. The rates of sag subsidence development were analyzed as feet of sag per month and a classification system, distinguishing initial, intermediate, and residual sag subsidence over room-and-pillar mines, is presented.

Residual subsidence problems associated with abandoned room-and-pillar mines in seven Wyoming counties are documented by Karfakis (1993). Sinkhole collapse subsidence, due to weak mine roof conditions and groundwater fluctuations in the mine, is the most prevalent form. However, as time progresses, additional collapses are likely to lead to trough subsidence. The mine subsidence problems were considered “an extreme danger to public health, safety, and property” and significant reclamation funding was applied to mitigation and abatement techniques in the affected areas (Karfakis, 1993).

Forrester (2004) investigated damage to a school situated only 150 feet above a coal mine in Canada that had been abandoned since 1890. The report concludes that roof material in the mine was weakened by fluctuating groundwater levels and subsequently failed.

Vasundhara, et al. (2001) assessed the influence of soft, clayey floor strata on the long-term stability of a room-and-pillar mine in Australia. In general, the study concluded that not only does clayey mine floor strata cause floor heave and rib spalling during mining, it also enhances long-term subsidence after mining. A clay unit beneath the floor was identified to have the ability change from near the strength of sandstone to the strength of soil when in contact with moisture. Long-term breakdown of the stability of the mine was attributed to differential moisture content in the clay unit beneath coal pillars as compared to beneath the floor of entryways (Vasundhara, et al. 2001). Water entering the mine over time was able to increase the moisture content of the clay in the entryway floors while not affecting the clay beneath the pillars. The differential moisture content resulted in differential strength of the clay layer, and resulted in

unstable conditions (Vasundhara, et al. 2001).

Morrison, et al. (2003) discusses cascading pillar collapse (CPC), another phenomenon that complicates the prediction of the stability of underground room-and-pillar mines. CPC is discussed in terms of hard rock mining by Morrison, et al. (2003), but it has also been observed in many room-and-pillar coal mines (Khair and Peng, 1985; Peng, 1986; Zipf, 2001). Very basically, CPC occurs when a pillar or smaller area of pillars collapses despite proper design or due to geologic conditions not accounted for by design. The collapse of the smaller pillar area causes a redistribution and addition of stress onto neighboring pillars. If the neighboring pillars cannot withstand the additional stress, they too fail and cause an increase in stress on more pillars. The “domino-failure” process continues until the collapse reaches an area that is strong enough to handle the stress increases (Zipf, 2001). CPC occurring in an old, abandoned room-and-pillar mine may lead to a worst case scenario during which all, or most, of the pillars in a large area collapse. The resultant surface subsidence will likely be much worse than that of normal residual subsidence.

The previous discussion suggests that long-term stability of mined areas and the effects of long-term subsidence are very complex issues. By studying the causes, duration, and behavior of long-term mine subsidence, researchers are acquiring the knowledge and skill to lessen damages to surface structures. In order to successfully develop surface structures in undermined areas, researchers must complete thorough pre-development investigation of previous mining activity, as well as investigation of all geological and hydrogeological characteristics that may affect the long-term stability of the mine. Detailed measurements of long-term mine subsidence behavior has allowed researchers to develop prediction techniques for various areas. However, researchers have also found that each location must be assessed individually to ensure that all relevant factors have been taken into account. Because predicting the timing of collapse of abandoned underground workings and the associated subsidence is very difficult, many researchers have focused efforts on predicting the possible effects of long-term collapse and designing surface development to endure the resultant subsidence. By coupling subsidence prediction techniques with building damage criteria, researchers can provide the relative probability and extent of subsidence damage for a given area. The successful implementation of this kind of approach to long-term landscape stability of undermined areas allows

reclaimed land to be used for development such as shopping malls, schools, residential housing, and landfills.

7.2 Implemented Methodology

The work done for this thesis has enhanced the risk-based assessment methodology of Newman (2003) and Karmis and Agioutantis (2004) that is discussed in section 7.1.2. It involves improving the ability to evaluate the distribution of damage-causing subsidence parameters to determine areas of high-risk on the ground surface above mining. More specifically, ground strain can now be calculated using any set of randomly located surface points. As mentioned previously, risk-based assessment often assumes worst case scenarios of total collapse because it provides the most conservative, safest estimate of affected area. However, the utilization of computer programs like SDPS allows engineers to analyze risk associated with any possible scenario of mine instability.

Risk-based assessment methodology is applicable to pre-mine planning and post-mine landscape stability assessment because the researcher has the ability to model and predict the outcome of any possible combination of mine conditions. The approach is adaptable to any mined area for which subsidence prediction parameters can be estimated. This makes it dominant over damage assessment methods that are designed specifically for certain areas.

Risk-based assessment begins with prediction of subsidence and strain based on evaluation of data associated with in-mine conditions. The stability of underground mine workings can be assessed using a number of pillar and roof stability methods (see discussion in section 7.1.2), as well as through consideration of anomalous geologic or hydrologic conditions. For example, the risk-based assessment approach does not directly address water infiltration, a major factor leading to mine instability, but it does provide the means for researchers to model scenarios in which pillars in certain areas of a mine are more likely to deteriorate due to mine water flux. The same approach can be employed to account for other variable geologic or hydrologic factors observed for a particular mine. For example, soft clayey floor that is likely to cause accelerated deterioration of pillars in a particular area can be accounted for by a model that assumes a greater degree of collapse in the area. Based on stability

analysis, as well as consideration of geologic and hydrologic conditions, any possible deformation scenario can be developed and modeled.

To facilitate risk-based assessment of subsidence-affected areas, an enhanced methodology that quickly calculates and contours predicted ground strain for each point on a grid (taking into account all adjacent points) has been implemented. As discussed briefly in section 5.2.4, horizontal strain and ground strain differ in that ground strain accounts for displacements in the z direction. In other words, ground strain calculations take into account topographic surface before and after deformation while horizontal strain only considers displacement in two dimensions. Figure 61 illustrates the components used to calculate horizontal strain and those used to calculate ground strain.

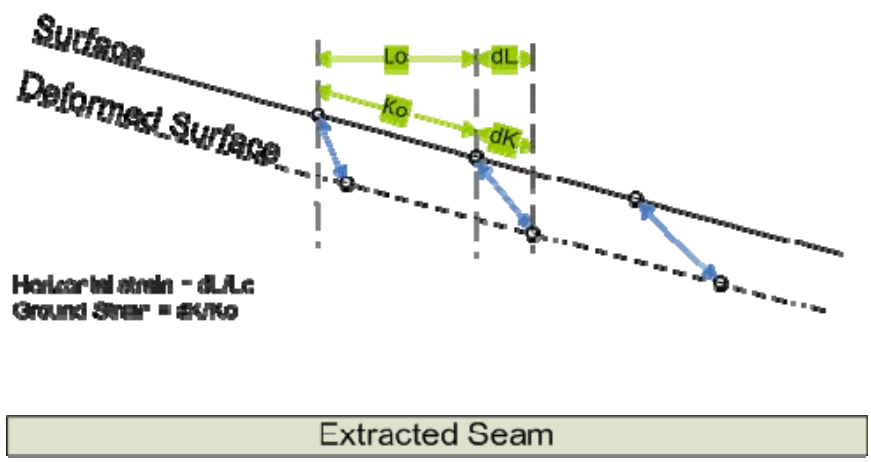

Figure 61: Two-dimensional representation of differences in components used to calculate horizontal strain and ground strain.

To be accurate, calculation of ground strain at any point must take into account the effects of all adjacent points. Figure 62 indicates the eight adjacent surface points (black) that must be considered when calculating the ground strain at a given point (red).

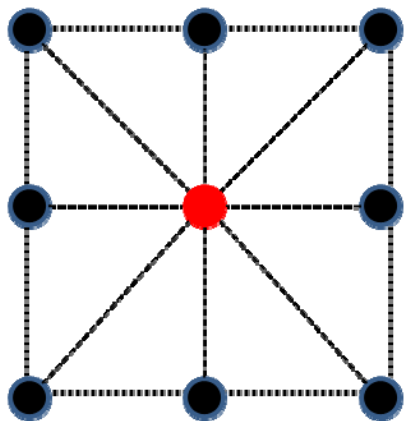

Figure 62: Plan view of grid pattern used to calculate ground strain at one point (red) in three-dimensional space. Ground strain at each point in a grid is calculated by taking into account all adjacent points.

The equation used to calculate horizontal strain between two points is provided below.

$$Horizontal\ distance\ between\ two\ points\ prior\ to\ deformation\ = l_o = \sqrt{dx^2 + dy^2}$$

$$Horizontal\ distance\ between\ two\ points\ after\ deformation = l_1 = \sqrt{(dx + ddx)^2 + (dy + ddy)^2}$$

$$\boldsymbol{Horizontal\ Strain} = \frac{(l_1 - l_o)}{l_o} = \frac{l_1}{l_o - 1} = \frac{dl}{l_o}$$

The equation for calculating ground strain at a point is provided below. It is important to remember that, for a given point, this calculation must be done considering every adjacent point.

$$Distance\ between\ two\ points\ prior\ to\ deformation\ = K_o = \sqrt{dx^2 + dy^2 + dz^2}$$

$$Distance\ between\ two\ points\ after\ deformation = K_1 = \sqrt{(dx + ddx)^2 + (dy + ddy)^2 + (dz + ddz)^2}$$

$$\boldsymbol{Ground\ Strain} = \frac{(K_1 - K_o)}{K_o} = \frac{K_1}{K_o - 1} = \frac{dK}{K_o}$$

The improved calculation techniques presented here, and implemented into SDPS for efficiency, provide engineers with the means to quickly contour damage-causing parameters (particularly ground strain) and combine the contoured maps with maps of surface development, either planned or existing.

Displaying empirically-based damage threshold values of subsidence parameters (such as ground strain and horizontal strain) for the types of structures in an affected area with maps of structures in the area, makes it possible to create maps of high-risk zones. The maps can be used by a field engineers to assess the severity of potential damage from undermining or from long-term landscape instability (risk-based analysis).

7.3 Validation of Method

To illustrate the effectiveness of the enhanced risk-based approach to assessing damage potential due to undermining, two synthetic case studies and an example of an actual case study are presented below.

Synthetic case study 1 illustrates the steps involved in conducting a basic risk-assessment analysis for two planned, adjacent longwall panels. Figures 1 through 8 of Appendix V include the SDPS screens associated with basic processing of the case study. Default subsidence prediction parameters are assumed (Appendix V, Figure 1). The panels are each 1000 feet wide and the mine is 600 feet deep. The average extraction thickness is 5 feet. An edge effect of 150 feet has been applied to all sides of each panel. Figure 2 of Appendix V shows the two panels, the edge effect, and the grid of prediction points. The prediction points are defined in Figure 5 (Appendix V). Predicted values for horizontal strain and ground strain were calculated (Appendix V, Figure 6) and threshold strain values of 1.5×10^{-3} were chosen for contouring (Appendix V, Figure 7). Figure 8 of Appendix V shows the initial contouring of strain in Surfer. The output is easily edited and can be combined with surface structure maps to determine surface areas at high risk of experiencing subsidence deformation-induced damage.

Figure 63 shows the contoured threshold strain values combined with a map showing the locations of three buildings (A-C) overlying the panel area. In this particular case, flat terrain results in ground strain nearly equal to horizontal strain. The red zone in the figure indicates the area expected to experience tensional strains exceeding 1.5×10^{-3}. Based on the overlay, the northeastern corner of Building A and the northwestern corner of Building C are expected to experience potential damage due to tensional strain.

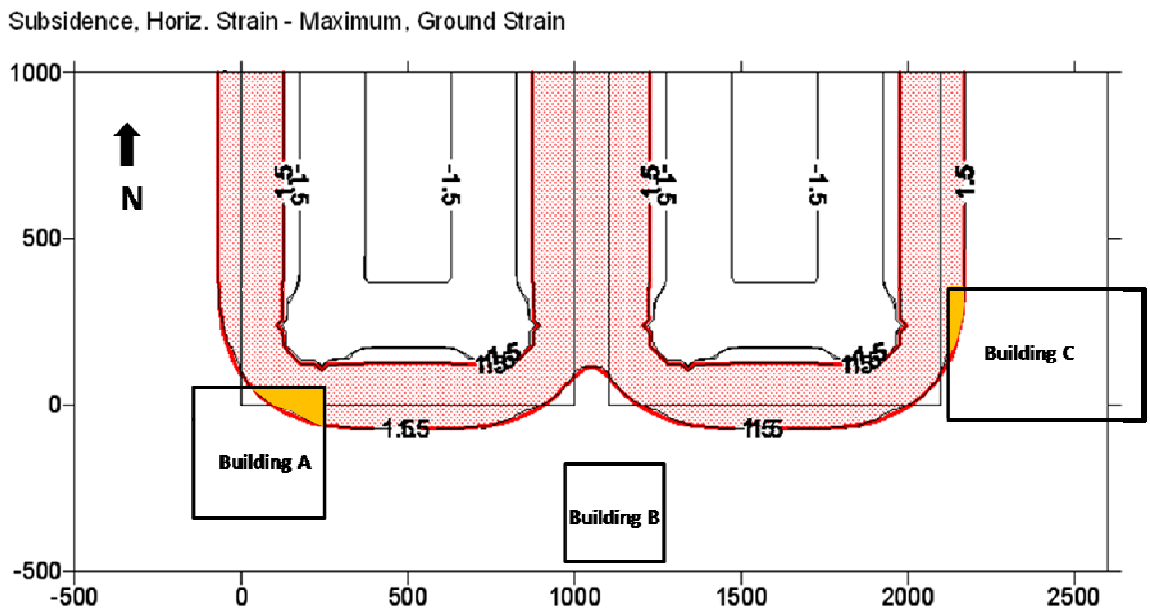

Figure 63: Risk assessment map showing combination of predicted horizontal and ground strain with surface structures.

Synthetic case study 2 is provided to outline the basic steps involved in generating a map showing high-risk zones due to collapse of weakened pillars in a previously mined room and pillar section. This case study is a basic example of risk assessment of long-term landscape stability using contoured threshold subsidence parameters (ground strain and horizontal strain). Figures 9 through 19 of Appendix V provide the components of the room and pillar setting and prediction model, including full size and weakened pillars. The depth of the mine is approximately 500 feet and the extraction thickness is set to 5 feet. Deterioration of the pillars in the weakened area may be due to partial retreat mining, observed mine water flux, or some other mine condition. Figure 10 (Appendix V) shows the weakened pillar area surrounded by full size pillars with dimensions of approximately 30 ft by 30 ft. To simulate the collapse of the weakened pillars, the subsidence factor is set to 100%. The subsidence factor for the full size pillars is set to 5%. Setup of the prediction point grid pattern is shown in Figure 16 (Appendix V). Predicted horizontal strain, ground strain, and subsidence values were calculated. A threshold strain value of 1.5 x 10^{-3} is defined in Figure 18 (Appendix V). The initial Surfer contour output is shown in Figure 19 (Appendix V).

Figure 64 indicates the zones of tensional and compressional strain exceeding the defined threshold value. A subsidence value of -0.05 feet is also indicated.

The map indicates that the southern edge of Building D is likely to experience damage from high tensional strains due to collapse of the weakened pillars. The results assume that all full size pillars will remain standing after collapse of the weakened pillars. This may not be a valid assumption and reassessment of the stability of the pillars surrounding the collapsed area may indicate the likelihood of additional failure (see discussion of cascading pillar collapse in section 7.1.3). As discussed previously, factors affecting long-term stability are very complex. The risk-assessment approach discussed in this thesis provides a means for evaluating the potential outcome of almost any combination of conditions.

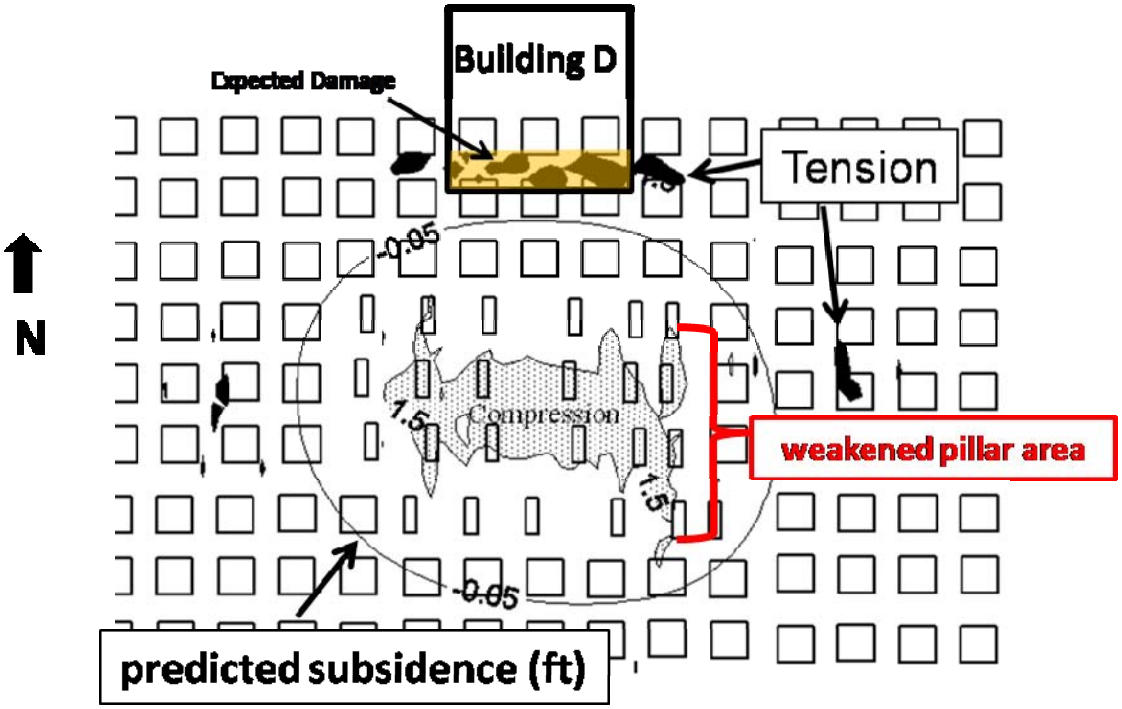

Figure 64: Basic illustration of risk-based analysis showing high-risk zones resulting from "worst case" scenario of collapse of all weakened pillars. Zones of tension and compression exceeding a threshold strain value of 1.5 x 10^{-3} are labeled. A predicted subsidence contour of -0.05 feet is also shown.

Figure 65, Figure 66, and Figure 67 illustrate the main steps of the risk assessment procedure as it was done for an actual case study involving expansion of surface development (a landfill) over part of a room and pillar mine. The SDPS screens for this case study are not included. However, the procedure for this actual case study is very similar to the previous synthetic case studies. This case study, which is presented as an example in Karmis et al, (2008), is included here to demonstrate the ability of the methodology to accommodate more complex scenarios. Figure 65 indicates the location of the mined sections

(both existing pillars and those removed during previous retreat mining activities.

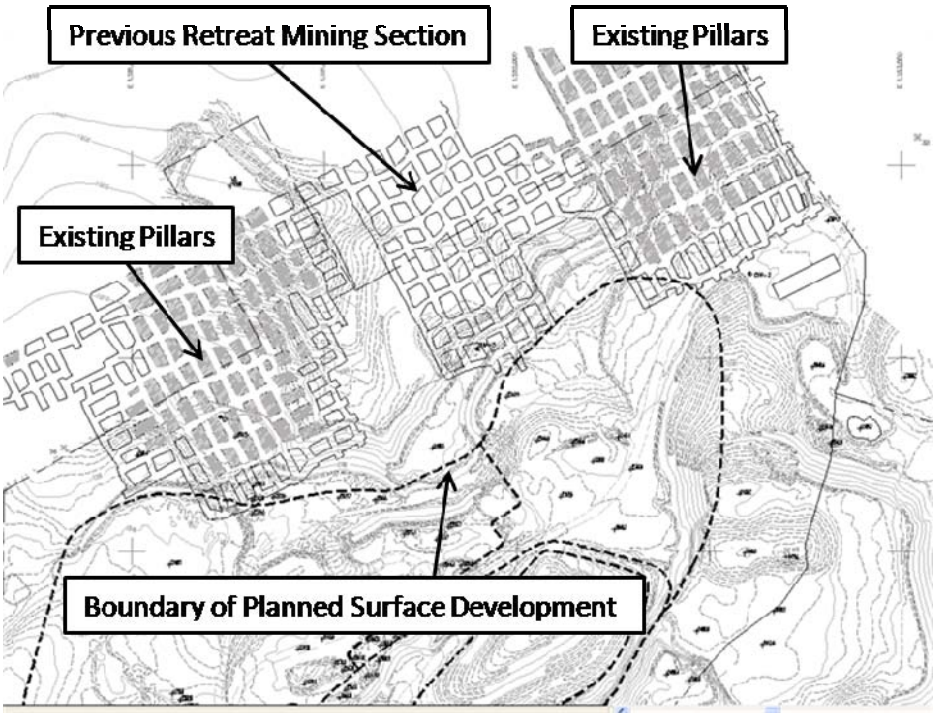

Figure 65: Map illustrating the position of the previously mined section in relation to the boundary of planned surface development (reprinted with company permission, mine location and company name confidential).

A worst case scenario is assumed wherein the existing pillars collapse and induce surface deformation. Figure 66 shows the results of calculation and contouring of horizontal strain and ground strain. Similar to the previous synthetic case studies, a threshold strain value of 1.5 x 10^{-3} is used. By combining the predicted horizontal and ground strain contours with the boundary of the planned surface development, zones of high risk for surface structures are determined (Figure 67).

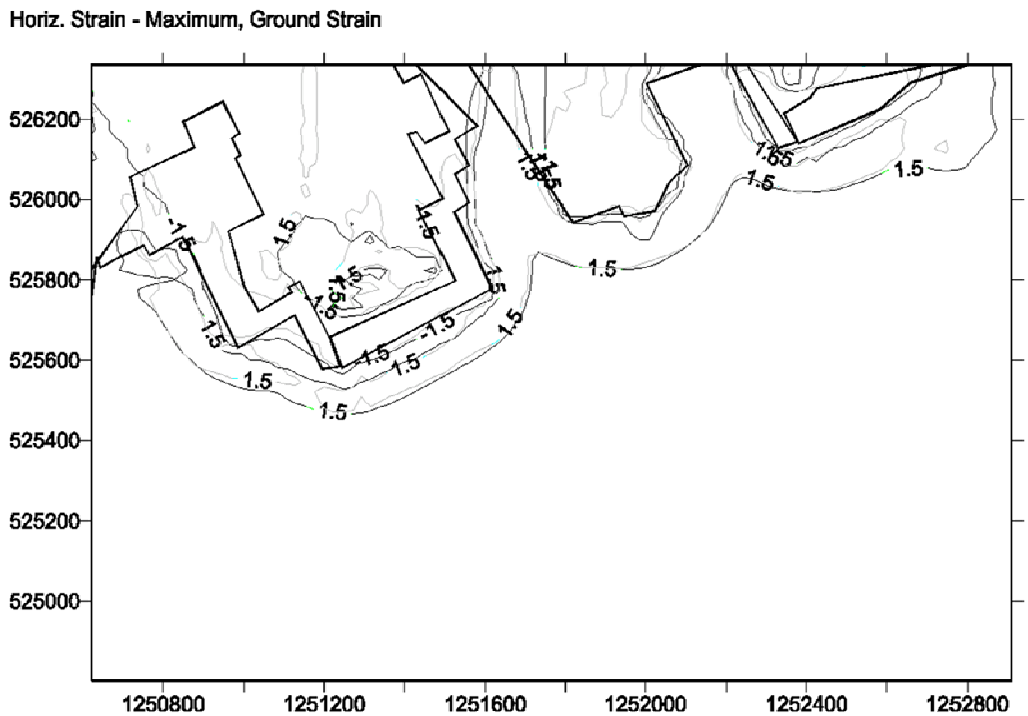

Figure 66: Contoured threshold values (in this case, 1.5 x 10^{-3}) of horizontal and ground strain expected considering a "worst case" scenario of collapse of all existing pillars.

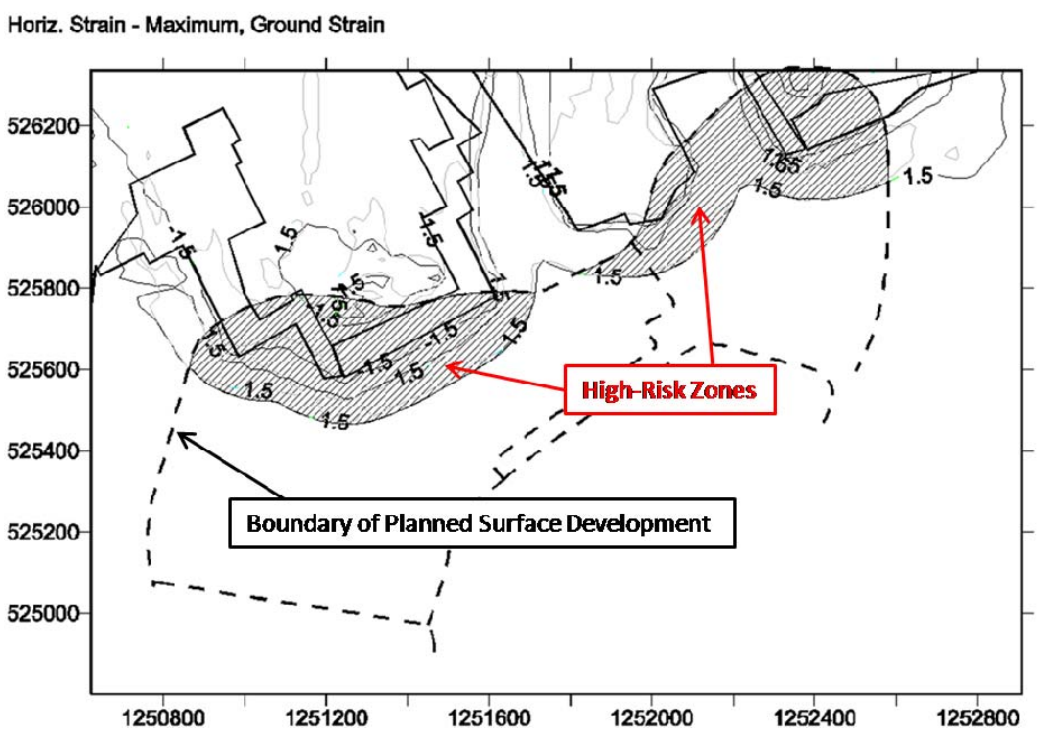

Figure 67: Map showing combination of threshold strain values and boundary of planned surface development. High-risk zones are those where overlap occurs.

In addition to providing field engineers with a means to delineate high-risk areas, contouring of predicted subsidence parameters also facilitates the creation of vector maps that indicate the direction of predicted horizontal movement of surface points due to subsidence. Figure 68 is an example of a vector map. The lengths of the arrows shown on the map indicate the relative magnitude of the displacements. The dark line indicates the position of the mined panel.

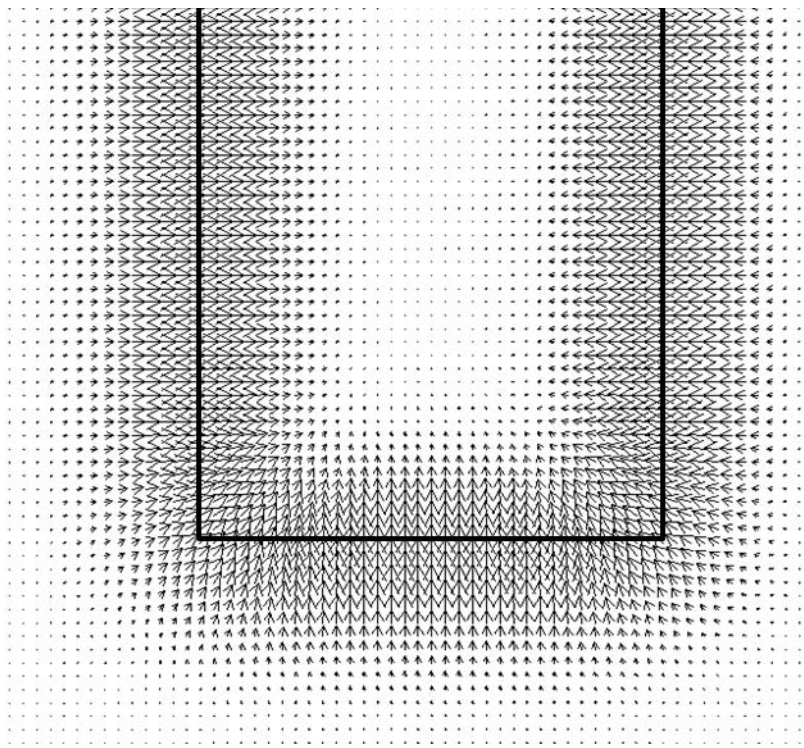

Figure 68: Vector map indicating the direction of predicted horizontal surface point movement as a result of subsidence

Contoured ground strain values also provide a way to compare distributions of predicted subsidence parameters for different scenarios. For example, by establishing a relationship between predicted subsidence and predicted ground strain for a given area, a field engineer may be able to predict the subsidence value at which the threshold ground strain value will likely be exceeded. In this way, the engineer can monitor the development of damage potential using less expensive, more common vertical displacement measurements instead of complicated strain gauges. Figure 69 provides the general layout and contoured values used to generate the graph in Figure 70. The example has an average edge effect of 140 feet and a panel width of 600 feet. The extraction thickness is five feet. Figure 69 illustrates the results of a comparison of predicted

subsidence values with predicted ground strain values for numerous seam depths. In general, the graph indicates that higher ground strain values are produced with less subsidence when mining is closer to the surface. The figure also shows the predicted subsidence values associated with a ground strain threshold value of 1.5 x 10^{-3}.

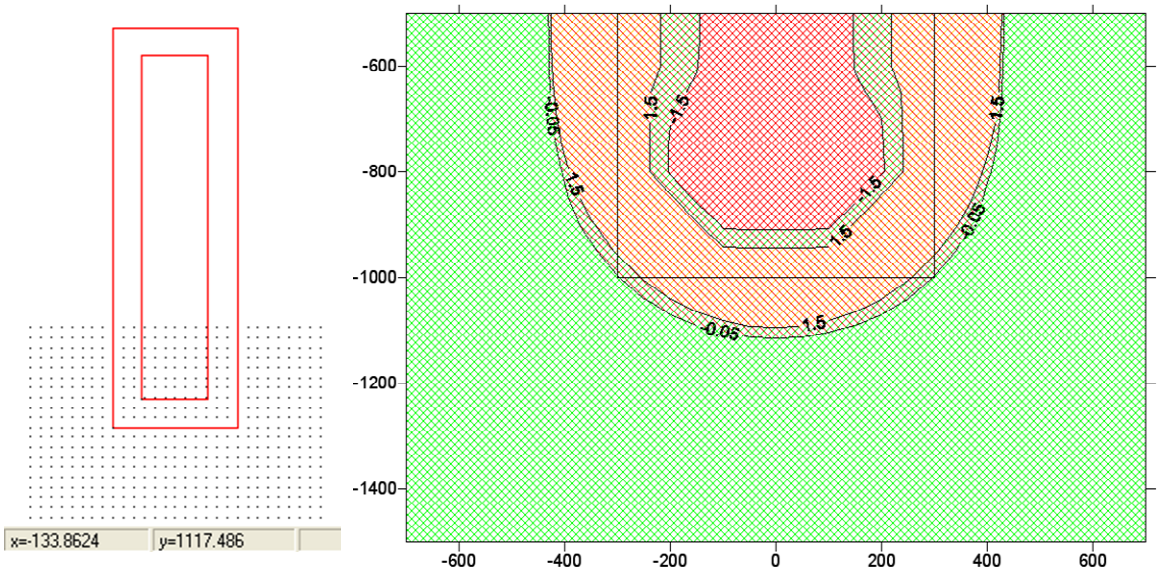

Figure 69: Layout and contoured values for example comparison of predicted ground strain values with predicted subsidence values for various seam depths

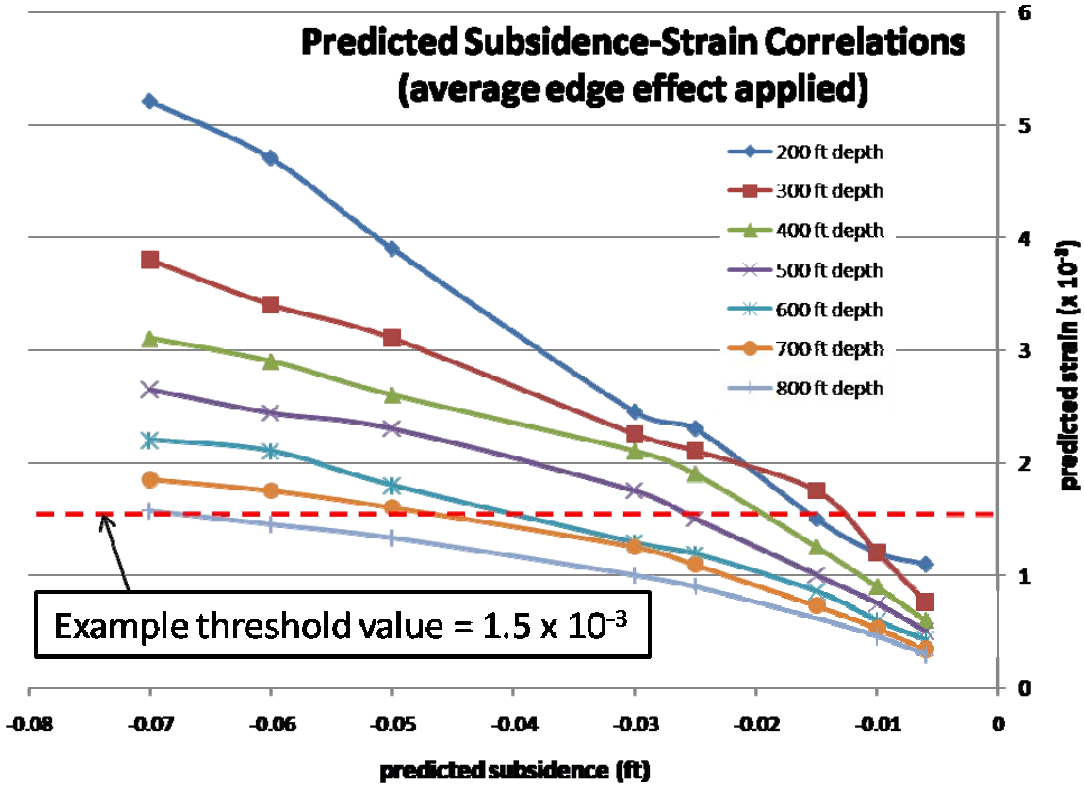

Figure 70: Example comparison of predicted ground strain values with predicted subsidence values for various seam depths. A threshold strain value of 1.5 x 10^{-3} is indicated to provide an estimate of the "threshold" subsidence value.

7.4 Discussion

This chapter discusses the types of damage-causing deformation associated with mining-related subsidence as well as classification of the induced damage. Karmis, et al. (1994) presents a risk-based system of damage assessment primarily utilizing threshold strain values (see Table 35). Threshold values were established by combining damage criteria from numerous sources. The procedure for risk-based assessment is simple. First, subsidence, horizontal strain, ground strain, and other parameters are predicted using the established influence function prediction method. Next, the predicted values are contoured. The work done for this thesis provides an enhanced methodology that allows for the contouring of important subsidence parameters. More specifically, predicted ground strain, a well established predictor of surface damage, can now be contoured and overlain on maps showing areas of planned or existing development. Areas at high risk of experiencing damage are those where

development overlaps with zones of strain that exceed the threshold value. Based on the work done by Karmis, et al. (1994), a threshold value of 1.5×10^{-3} is used for the presented case studies.

The risk-based approach to assessing damage potential is capable of providing meaningful results for both pre-mine planning and evaluation of potential damage from long-term landscape instability over previously mined areas. Similarly, the methodology can be applied to both longwall and room and pillar mines. The case studies presented in this chapter attempt to demonstrate the basic steps of the assessment procedure, as well as the adaptability of the methodology. A significant portion of the chapter discusses the complexity of the factors affecting the prediction of mine subsidence, as well as factors affecting long-term landscape stability. By using the enhanced methodology and risk-assessment approach presented in this thesis, engineers have the ability to account for numerous geologic and mining conditions when evaluating the potential for damage.

8. Objective V: To disseminate project results

Dissemination of project results was accomplished in the following ways:

8.1 Awareness of the engineering and regulatory community

Personnel from various companies, as well as OSM personnel from regional offices, were already aware of this effort as a result of the interaction during the compilation of data.

8.2 Project Showcase

The project was showcased by the Virginia Coal and Energy Center at the exhibition of the 25th Annual Meeting of the American Society of Mining and Reclamation (ASMR) which was held in Richmond VA, June 14-19, 2008. The meeting was held in conjunction with the 10th meeting of the International Affiliation of Land Reclamationists. A poster was displayed at the VCCER booth as shown in Figure 71.

8.3 Progress Meeting

A meeting between Kevin Andrews (VPI graduate student during the early stages of the project), Zach Agioutantis (VPI subcontractor for this project) and Tom Mastaller (the OSM Technical Project Officer assigned to this project) was held in August 2008, in Morgantown, WV, to discuss the progress of the project. The progress to-date was discussed a few items were clarified for both sides.

8.4 Project Presentation

A short presentation was done at the West Virginia Coal Mining Institute (WVCMI) and SME Central Appalachian Section (SMECAS) Joint Annual Meeting at The Greenbrier in White Sulphur Spring, WV in the Fall 2007. This initial presentation introduced the project, provided an explanation of the purpose of the project and outlined the overall objectives.

8.5 Paper presentation

A paper titled “Enhancing Mine Subsidence Prediction and Control Methodologies” was presented at the 27th International Conference on Ground Control in Mining held in Morgantown, WV between July 29 and July 31, 2008,

The paper is also included in the Conference proceedings (pp. 131-136).

8.6 Short Course to OSM personnel

Dr. Karmis, Dr. Agioutantis and Mr. Kevin Andrews participated in a Short Course that was conducted to OSM personnel at the OSM offices in Pittsburgh on November 13 and 14, 2008. In the short course, the latest technologies that were developed were presented and demonstrated to the attendees. A copy of the powerpoint presentation presented at the meeting is appended to this report (Appendix VI).

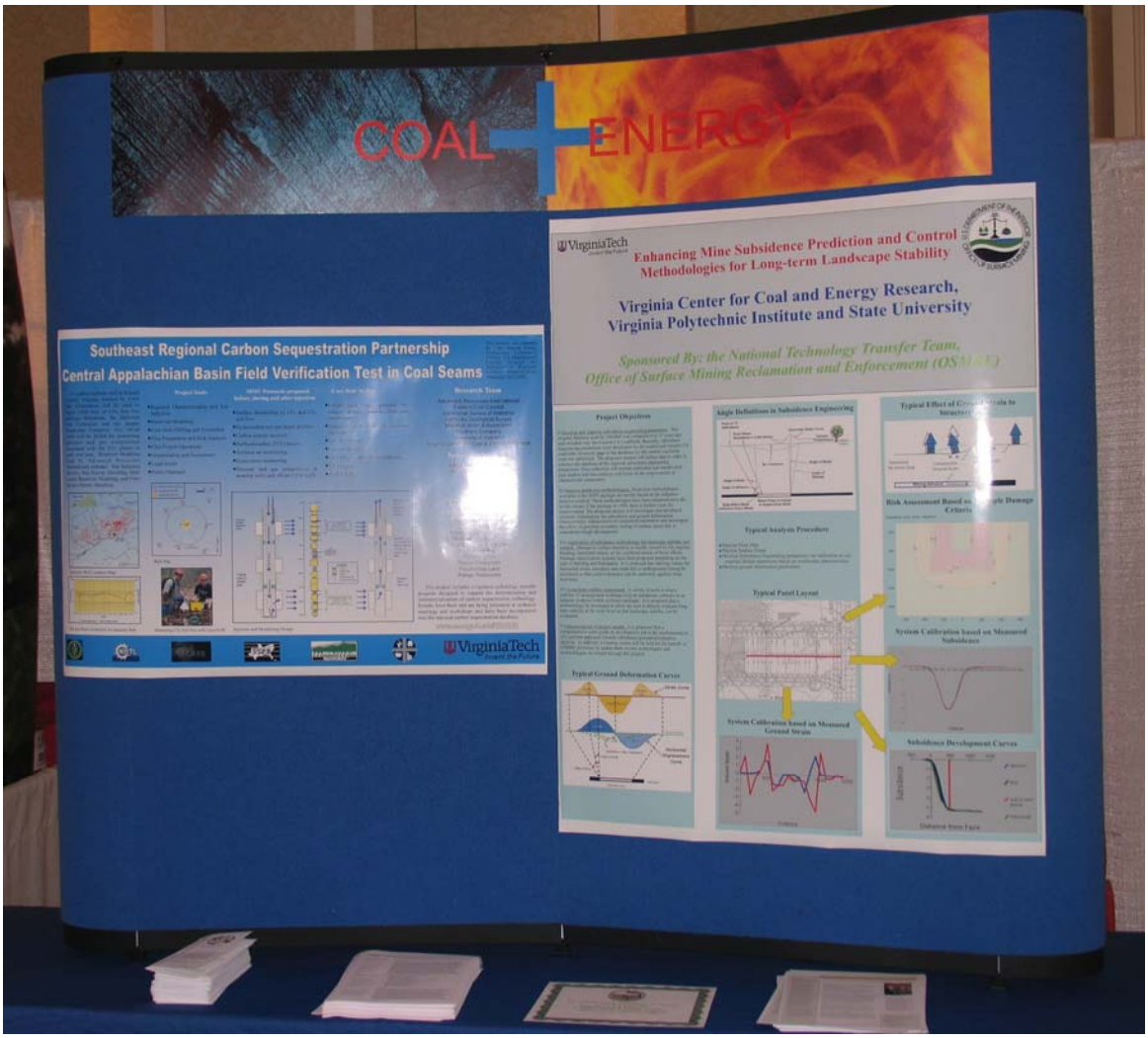

Figure 71: Booth at ASMR meeting in Richmond, VA, June 2008.

9. Summary of Deliverables

9.1 Detailed project report

The detailed project report consists of this document with its appendices

9.2 Software Enhancements

In summary, the following software enhancements were implemented in this project:

- ✓ Mine plan definition was modified to allow for long-term stability information
- ✓ The dynamic function was re-written to implement the theory by Jarosz et al (1990) for dynamic subsidence as well as calculation of dynamic slope, dynamic horizontal displacement, dynamic curvature and dynamic horizontal strain.
- ✓ The calibration procedure was enhanced to allow for:
    - o Locking of calibration parameters obtained from a subsidence profile and optional utilization of such parameters in calibration using strain profiles
    - o Option to calibrate for maximum values of horizontal or ground strain as well as for minimizing the total error during strain calibration
- ✓ The calculation procedure was enhanced to allow for calculation of ground strain for prediction points on a grid and for scattered prediction points
- ✓ A new function was added in the calculation menu for calculating long-term stability
- ✓ New contouring routines were developed utilizing the Surfer package (Golden Software)
- ✓ Contouring allows specification of damage threshold values

9.3 Updated User's Guide

The User's Guide was enhanced both by adding more examples pertaining to the use of the new / advanced features of the influence function and by adding / enhancing the theoretical sections related to the Influence Function Method.

9.4 Updated online Help File

The online Help file (which is available both as a CHM file and as a PDF file) was updated to include help material to all the new or modified form of the SDPS software.

9.5 Resource Files

A number of publications pertaining to subsidence prediction were added as resource files to the Influence Function Module. These publications as available in PDF format upon program installation (Figure 72).

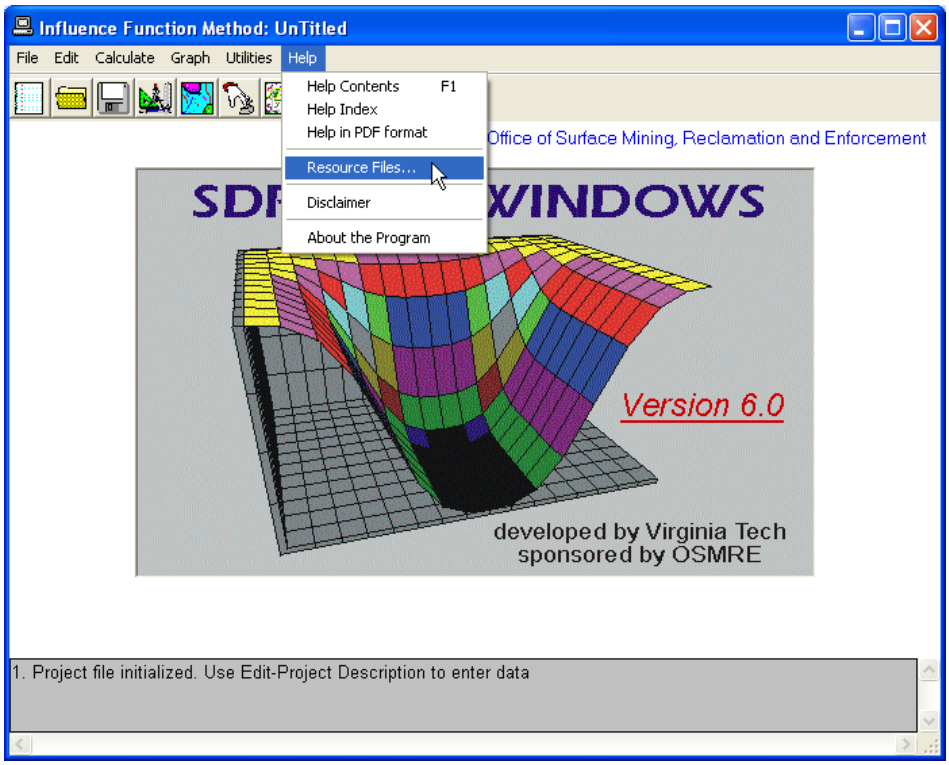

Figure 72: Access to the Resource File menu

9.5 Short Course Material

The powerpoint presentation developed for the shortcourse to OSM personnel,

delivered on November 13 and 14, 2008

10. Recommendations

During the data collection phase it became evident, that the quality and quantity of data that was needed for accurate evaluation of ground deformation parameters was available only in a few cases studies. For example, data for exact surface point locations were not always available. Instead these locations were estimated by digitizing paper maps. Also values of deformation indices with respect to face advance were not always available. It is, therefore, recommended that the data collection process should be continued, to further preview, evaluate and enhance the existing data bank.

The work done for this report represents the latest round of improvements for prediction of mine subsidence and related parameters. While a variety of enhancements have been made, future work will undoubtedly improve upon current techniques and develop new methodologies. The results presented in this thesis leave many questions to be answered and provide ideas for future subsidence work.

Perhaps one of the most important suggestions for future subsidence research is the need to place more emphasis on the standardization of techniques for measuring subsidence data associated with active mines. It is data that forms the basis of the majority of the more commonly used subsidence prediction techniques. Future validation of current methodologies using reliable data will further increase confidence in prediction models.

Collection of data associated with soil behavior in response to subsidence in steeply-sloped terrain will facilitate the development of enhanced techniques for predicting the occurrence of movements on the soil-bedrock interface. This type of research will be particularly beneficial to mines in the eastern US coalfields.

Significant enhancements may be possible for assessing high-risk areas above undermining. Linking pillar and roof stability assessment methodologies, such as those provided by NIOSH, directly into the risk-based assessment procedure using SDPS (as outlined in Section 6) would increase the speed and efficiency of assessing high risk areas. Prompt assessment is often necessary as mining continuously progresses into new areas.

Continued implementation of the most applicable methodologies in the most user-friendly computer programs will increase the likelihood that enhanced subsidence prediction methodologies, such as those presented in this report, are utilized by engineers working everyday in the industry. Furthermore, hands-on training sessions and easy-to-use instruction manuals are essential to ensure that the methodologies are used as intended.

11. References

1. Agioutantis, Z. and Karmis, M. (2005). SDPS: Surface Deformation Prediction System for Windows (Quick Reference Guide and Working Examples). Blacksburg, Virginia, USA: Department of Mining and Minerals Engineering, VPI & SU.
2. Barkley, D. (2007). Longwall Mining in Illinois: A Controversy Over Planned Subsidence of Flat Farmland. 26th International Conference on Ground Control in Mining.
3. Bauer, R.A, and Van Roosendaal, D.J. (1992). Monitoring Problems; Are We Really Measuring Coal Mine Subsidence? Proceedings of the 3rd Subsidence Workshop Due to Underground Mining, Morgantown, WV, 332-338.
4. Bhattacharya, S. and Singh, M.M., (1985). Development of Subsidence Damage Criteria. Contract No. J5120121, O.S.M.RE, U.S. Dept. of the Interior, 195 pages.
5. Boone, S. (1996). Ground-Movement-Related Building Damage. Journal of Geotechnical Engineering, November, 886-896.
6. Briggs, H. (1929). Mining Subsidence. Edward Arnold & Co.
7. Bruhn, R.W. (1992). The Tolerance of Structures to Ground Movements – Some Considerations. Proceedings of the 3rd Subsidence Workshop Due to Underground Mining, Morgantown, WV, 83-93.
8. Bruhn, R.W., McCann, W.S., Speck, R.C., and Gray, R.E. (1982). Damage to Structures Above Underground Coal Mines in the Northern Appalachian Coalfield. 1st International Conference on Stability in Underground Mining, Vancouver, Canada, 1022-1042.
9. Chugh, Y., Chandrashekhar, K., and Missavage, R. (1988). Subsidence Movements and Structural Damage Related to an Abandoned Coal Mine. Proceedings: Second International Conference on Case Histories in Geotechnical Engineering, n. 2.41, 253-261.
10. Conroy, P.J. and Gyarmaty, J.H. (1982). Planning Subsidence Monitoring Programs Over Longwall Panels. In State-of-the-Art in Ground Control in Longwall Mining and Mining Subsidence, edited by Chugh, Y., 225-233.
11. Dickinson, J. (1898). Subsidence Due to Colliery Workings. Proc. Manchester Geol. Soc., n. 25, 600.
12. Dixon, J.S. (1885). Some Notes on Subsidence and Draw. Trans. Min. Inst., Scotland, 7, pp. 224.
13. Dyne, L. (1998). The Prediction and Occurrence of Chimney Subsidence in Southwestern Pennsylvania. VT Thesis, Blacksburg, Virginia, USA: Virginia Polytechnic Institute and State University.
14. Fayol, H. (translated by Galloway, W.) (1885). Subsidences Caused by the Workings in the Mines. South Wales Institute of Engineers, v. 20, 311.
15. Flaschentrager, H. (1938). Die Kostenverteilung bei Gemeinsam Verursachten Bergschaden im Ruhrgebiet. Mitt. Markscheidew, v. 49, 95-137.
16. Forrester, D. (2004). A Case Study of Abandoned Mine Subsidence at

Dominion, Nova Scotia, Canada, 2002-2003. 23rd International Conference on Ground Control in Mining, 173-176d.

17. Franks, C. A.M. and Geddes, J.D. (1984). A Comparative Study by Numerical Modeling of Movements on Sloping Ground Due to Longwall Mining. Proceedings of the 3rd Conference on Ground Movements and Structures, Session IV, 377-396.
18. Franks, C. A.M. and Geddes, J.D. (1986). Subsidence on Steep Slopes Due to Longwall Mining. International Journal of Mining and Geological Engineering, v. 4, 291-301.
19. Geddes, J. and Cooper, D. (1962). Structures in Areas of Mining Subsidence. The Structural Engineer, 79-93.
20. Gentry, D. W. and Abel, J.F., jr. (1978). Surface Response to Longwall Coal Mining in Mountainous Terrain. Bulletin of the Association of Engineering Geologists, n. 2, 191-220.
21. Goldreich, A. (1913). Die Theorie der Bodensenkungen in Kohlengebieten. Berlin.
22. Gray, R.E. (1992). Structural Damage – Mine Subsidence, Proceedings of the 3rd Subsidence Workshop Due to Underground Mining, Morgantown, WV, 113-120.
23. Gray, R.E., Bruhn, R.W., et al. (1977). Study and Analysis of the Surface Subsidence over the Mined Pittsburgh Coalbed, Bureau of Mines Open File Report, OFR 25–78.
24. Halbaum, H.W.G. (1905). The Great Planes of Strain in the Absolute Roof of Mines. Trans. I. Min., v. 30, 175.
25. Hao, Q. and Chugh, Y.P. (1992). An Engineering Approach to Predict Subsidence likelihood Over Abandoned Coal Mines in Illinois. Proceedings of the 3rd Subsidence Workshop Due to Underground Mining, Morgantown, WV, 189-196.
26. Hausse, R. (1885). Beitrag zur Bruchttheorie Erfahrungen uber Bodensenkungen und Gebergsdruckwirkungen. Jahrbuch fur das Berg und Hutten Wesen im Konigreich Sachsen.
27. Jarosz, A., Karmis, M., and Sroka, A. (1990). Subsidence Development with Time-Experiences from Longwall Operations in the Appalachian Coalfield. International Journal of Mining and Geological Engineering, v. 8, 261-273.
28. Jeran, P. and Adamek, V. (1988). Subsidence Due to Undermining of Sloping Terrain: A Case Study, Report of Investigations 9205. United States Department of the Interior, Bureau of Mines.
29. Jones, D.B., Siddle, H.J., Reddish, D.J., and Whittaker, B.N. (1992). Landslides and Undermining: Slope Stability Interaction with Mining Subsidence Behavior. Proceedings of the 7th International Society of Rock Mechanics Congress, Aachen, 893-898.
30. Karfakis, M. (1993). Residual Subsidence Over Abandoned Coal Mines. In J. A. Hudson, Comprehensive Rock Engineering, Vol. 5: Surface and Underground Case Histories, Oxford New York Seoul Tokyo: Pergamon Press, 451-476.

31. Karmis, M. and Agioutantis, Z. (2004). A Risk Analysis Subsidence Approach for the Design of Coal Refuse Impoundments Overlying Mine Workings. Proceedings of the 8th International Symposium on Environmental Issues and Waste Management in Energy and Mineral Production (SWEMP), Antalya, Turkey, 205-210.
32. Karmis, M., Agioutantis, Z., and Jarosz, A. (1990). Recent Developments in the Application of the Influence Function Method for Ground Movement Predictions in the U.S. Mining Science and Geotechnology, v. 10, 233-245.
33. Karmis, M., Agioutantis, Z., and Jarosz, A. (1990). Subsidence Prediction in Steep Slope Terrain. Powell River Project, Annual Symposium, 43-55.
34. Karmis, M., Agioutantis, Z., and Jarosz, A. (1990). Subsidence Prediction Techniques in the United States: A State-of-the-Art Review. Mineral Resources Engineering, v. 3, n. 3, 197-210.
35. Karmis, M., Agioutantis, Z., and Jarosz, A. (1991). Subsidence Prediction in Steep Slope Terrain - Model Formulation and Application. Powell River Project, Annual Symposium, 46-54.
36. Karmis, M., Mastoris, J., and Agioutantis, Z. (1994). Potential of the "Damage Angle" Concept for Assessing Surface Impacts of Underground Mining. Transactions, Society for Mining, Metallurgy and Exploration, Inc., v. 296, 1883-1886.
37. Keinhorst, H. (1928). Bei Bodensenkungen auftretende Bodenverschiebungen und Bodenspannungen. Gluckauf, v. 64, 1141-1145.
38. Khair, A.W. and Peng, S.S. (1985). Causes and Mechanisms of Massive Pillar Failure in a Southern West Virginia Coal Mine. Mining Engineering, 323-328.
39. Knothe, S. (1953). Wplyw czasu na ksztaltowanie się niecki osiadania, Archiwum Górnictwa i Hutnictwa, Tom 1, z.1. (In Polish)
40. Knox, G. (1913). Mining Subsidence. Proc. Int. Geol. Congress, v. 12, 798.
41. Kratzsch, H. (1983). Mining Subsidence Engineering. Berlin Heidelberg New York: Springer-Verlag.
42. Lane, W.T. and Roberts, J.H. (1929). The Principles of Subsidence and the Law of Support. Alfred A. Knopf.
43. Lehmann, K. (1919). Bewegungsvorgange bei der Bildung von Pingen und Trogen. Gluckauf, v. 55, 933-942.
44. Litwinowicz, L. (1984). The Influence of Horizontal Expansion on Soil Strength in Mining Areas. Proceedings of Conference on Ground Movement, Session IV, 397-403.
45. Luo, Y. and Peng, S. (2000). Long-term Subsidence Associated with Longwall Mining - Its Causes, Development, and Magnitude. Mining Engineering, v. 52, Issue 10, 49-54.
46. Luo, Y., Peng, S., and Dutta, D. (1992) Some Mitigative Measures for Protection of Surface Structures Affected by Ground Subsidence. Proceedings of the 3rd Subsidence Workshop Due to Underground

Mining, Morgantown, WV, 129-138.
47. Luo, Y., Peng, S., and Kudlawiec, R. (2005). Mitigating Longwall Subsidence Effects on a Large Industrial Building. 24th International Conference on Ground Control in Mining, 130-136.
48. Luo, Y., Peng, S., and Miller, B. (2003). Influences of Longwall Subsidence on a Guyed Steel Tower - A Case Study. 22nd International Conference on Ground Control in Mining, 360-366.
49. Luxbacher, G.W. (1992). Subsidence Planning and Risk Assessment. Proceedings of the 3rd Subsidence Workshop Due to Underground Mining, Morgantown, WV, 100-105.
50. Mahar, J. and Marino, G. (1999). Long Term Subsidence Movements and Behavior of Subsidence-Damaged Structures. 16th Annual National Conference of the American Society for Surface Mining and Reclamation, Arizona, 495-516.
51. Marino, G.G. (1986). Interactions between Buildings and Subsidence Movements. Proceedings of the 2nd Subsidence Workshop Due to Underground Mining, Morgantown, WV, 163-180.
52. Marschalko, M. (2004). Influence of Mine Activity onto Slope Deformation in Landslide Terrain. Gornictwo i Geoinzynieria, Rok 28, Zeszyt 3, 19-26.
53. Morrison, D., Palmer, P., and Beauchamp, K. (2003). Modeling of Pillar Stability in Room and Pillar Mines. 22nd International Conference on Ground Control in Mining, 80-85.
54. National Coal Board (NCB) (1975). Subsidence Engineers' Handbook..
55. Newman, D. (2003). Rock Mechanics and the Analysis of Underground Mine Stability Adjacent to Coal Refuse Impoundments. 22nd International Conference on Ground Control in Mining, 318-325.
56. Niemczyk, O. (1949). Bergschadenkunde. Gluckauf.
57. National Institute for Occupational Safety and Health (NIOSH) (2007). ALPS Help. Help in PDF Format. 53 pages.
58. O'Connor, K., Clark, R., Whitlatch, D., and Dowding, C. (2001). Real Time Monitoring of Subsidence Along I-70 in Washington, Pennsylvania. Transportation Research Record, Journal of the Transportation Research Board, n. 1772, 32-39.
59. O' Donahue, T. (1907). Mining Formulae. Science and Art of Mining, Wigan.
60. Orchard, R. (1954). Recent Developments in Predicting the Amplitude of Mining Subsidence. Trans. R.I.C.S., v. 33, 864.
61. Orchard, R. (1956-1957). Surface Effects of Mining - the Main Factors. Trans. I. Min. E., 116, Part II, 941-955.
62. Orchard, R. (1956-1957). Surface Effects of Mining - the Main Factors. Trans. I. Min. E., 116, Part I, 942-944.
63. Peng, S. (1986). Coal Mine Ground Control. New York: Wiley.
64. Peng, S. (1992). Surface Subsidence Engineering. Littleton, CO: Society for Mining Metallurgy and Exploration, Inc.
65. Peng, S. and Luo, Y. (1989). Slope Stability under the Influence of Ground Subsidence Due to Longwall Mining. Mining Science and Technology, v.

8, 89-95.
66. Perz, F. (1948). Der Einfluss der Zeit auf die Bodenbewegung uber Abbauen. Mitt. Markscheidew, v. 55, 92-117.
67. Powell, L., Triplett, T., and Yarbrough, R. (1986). Measurement and Analysis of Foundation Tilt Results from Mine Subsidence in Southern Illinois. Proceedings of the 2nd Subsidence Workshop Due to Underground Mining, Morgantown, WV, 142-152.
68. Powell, L., Yarbrough, R., and Harp, L. (1992) Planning for Subsidence at Rend Lake, Illinois, Proceedings of Third Workshop on Surface Subsidence Due to Underground mining, Morgantown, WV, Department of Mining Engineering, West Virginia University, pp. 158-166.
69. Preusse, A., Kateloe, H., Sroka, A., and Spielberg, P. (2003). Analysis on the Dynamics of Mining Subsidence in Range of a Product Transmission Overhead Line. 22nd International Conference on Ground Control in Mining, 344-351.
70. Reddish, D., Yao, X., and Dunham, R. (1996). Risk Assessment of Surface Structural Damage Due to Mining Subsidence - An Integrated Computer-Based Approach. Mining Industry, v. 104, A139-A143.
71. Ren, G., Whittaker, B.N., and Reddish, D.J. (1989). Mining Subsidence and Displacement Prediction Using Influence Function Methods for Steep Seams. Mining Science and Technology, v. 8, 235-252.
72. Schilizzi, P., Karmis, M., and Jarosz, A. (1986). Development of Subsidence Prediction Technology from an Extensive Monitoring Program. 2nd Workshop on Surface Subsidence Due to Underground Mining, Morgantown, WV: U.S. Office of Surface Mining Reclamation and Enforcement (OSMRE) and West Virginia University, 31-41.
73. Singh, M. (1992). Mine Subsidence. In SME Mining Engineering Handbook, Littleton, Colorado: SME Inc., v. 1, 938-971.
74. Sun, W. (1988). The Effect of Slope on the Ground Movement Due to Underground Mining. Unpublished Research Report.
75. Taylor, J., Fowell, R.J., and Wade, L. (2000). Effects of Abandoned Shallow Bord-and-Pillar Coal Workings on Surface Development. Abandoned Mine Workings Section of Legacy of Mineral Extraction Conference, A140-A145.
76. Torano, J., Rodriguez, R., and Ramirez-Ovanguren, P. (2000). Probabilistic Analysis of Subsidence-Induced Strains at the Surface above Steep Seam Mining. International Journal of Rock Mechanics & Mining Sciences, v. 37, 1161-1167.
77. Triplett, T., Lin, G., Kane, W., and Bennett, R. (1992). Prediction of Coal Mine Subsidence and Implications for Structural Damage. 3rd Subsidence Workshop Due to Underground Mining, 76-82.
78. Trompeter, W.H. (1899). Die Expansivkraft im Gestein als Hauptursache der Bewegung des den Bergbau umgebenden Gebirges. Baedeker.
79. Vasundhara, G., Byrnes, R., Hebblewhite, B., and Martin, S. (2001). Long Term Stability of Mine Workings in Soft Floor Environment: Geomechanical Investigations at Cooranbong Colliery. 20th International

Conference on Ground Control in Mining, 180-183.
80. VPI (& SU) (1987). Prediction of Ground Movements Due to Underground Mining in the Eastern United States Coalfields Final Report, Contract No. J514013 to Office of Surface Mining, Reclamation and Enforcement, U.S. Department of Interior. Blacksburg, Virginia: Virginia Tech Department of Mining and Minerals Engineering.
81. Wardell, K. (1952). The Surveying Observations Required for the Determination of Ground Movements Caused by Mining. Trans. Inst. Min. Surv., v. 32, 12.
82. Wardell, K. (1953-1954). Some Observations on the Relationship between Time and Mining Subsidence. Trans. Institute Min. Eng., v. 113, 471.
83. Wardell, K. (1954). Mining Subsidence. Trans. R.I.C.S., v. 86, 53.
84. Wardell, K. (1957). The Minimisation of Surface Damage by Special Arrangement of Underground Workings. In Proceedings of the European Congress on Ground Movement, 13-19.
85. Whittaker, B.N. and Reddish, D.J. (1989). Subsidence Occurrence, Prediction, and Control, Developments in Geotechnical Engineering. Amsterdam: Elsevier.
86. Zipf, R.K., jr. (2001). Pillar Design to Prevent Collapse of Room-and-Pillar Mines. In Underground Mining Methods: Engineering Fundamentals and International Case Studies, edited by Hustrulid, W., 493-511.

Appendices

Appendix I – SDPS Screen Captures for the Analysis of Several Case Studies for Method Validation A-2

Appendix II – SDPS Screen Captures for the Prediction of Dynamic Subsidence Development A-55

Appendix III – SDPS Screen Captures for Regarding Calibration Techniques for Subsidence Prediction A-61

Appendix IV – SDPS Screen Captures for Subsidence Prediction in Areas of Steeply-Sloping Terrain A-71

Appendix V – SDPS Screen Captures for the Analysis of Risk- Based Assessment of Mine Planning and Long-term Landscape Stability A-77

Appendix VI – Powerpoint Presentation for Short Course A-88

Appendix I –

SDPS Screen Captures for the Analysis of Several Case Studies for Method Validation

NA-1 CASE STUDY (NORTHERN APPALACHIA)

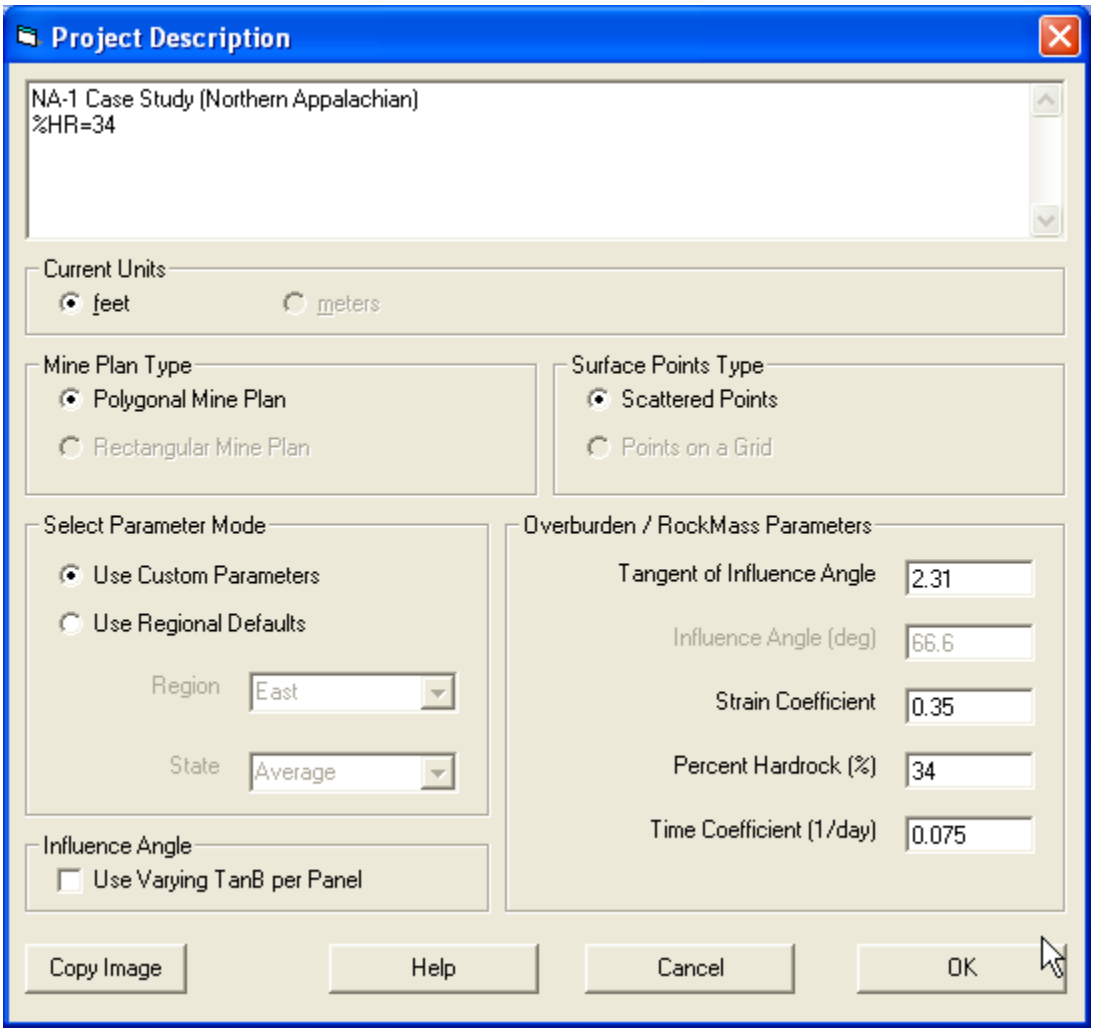

Figure 1: NA-1 Case Study – SDPS Project Description Screen

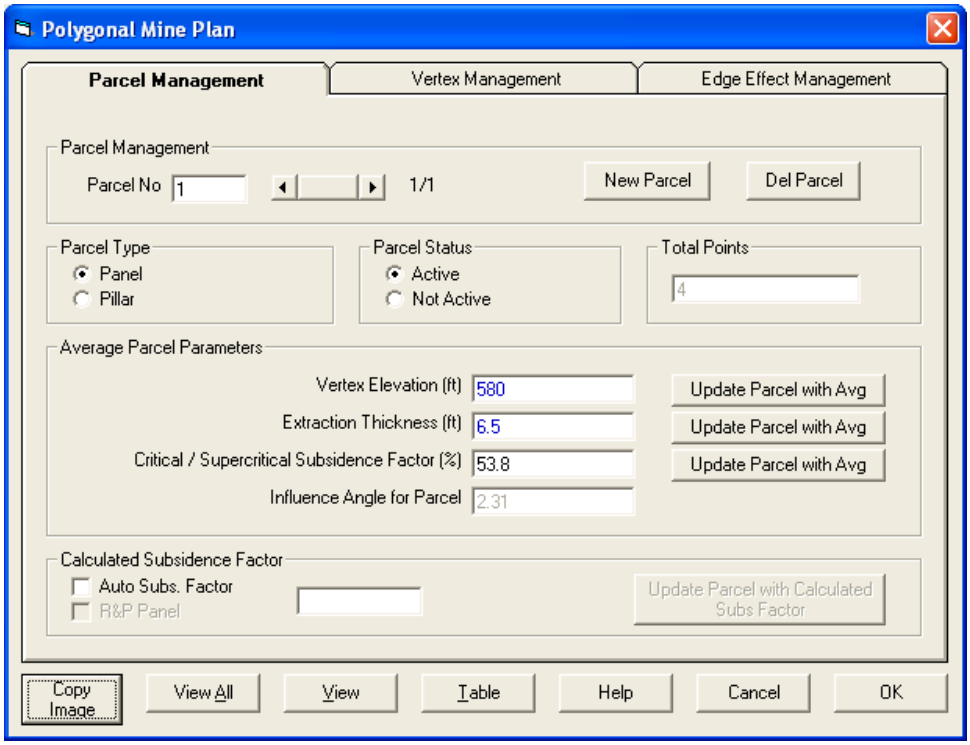

Figure 2: NA-1 Case Study – Parcel Management Screen

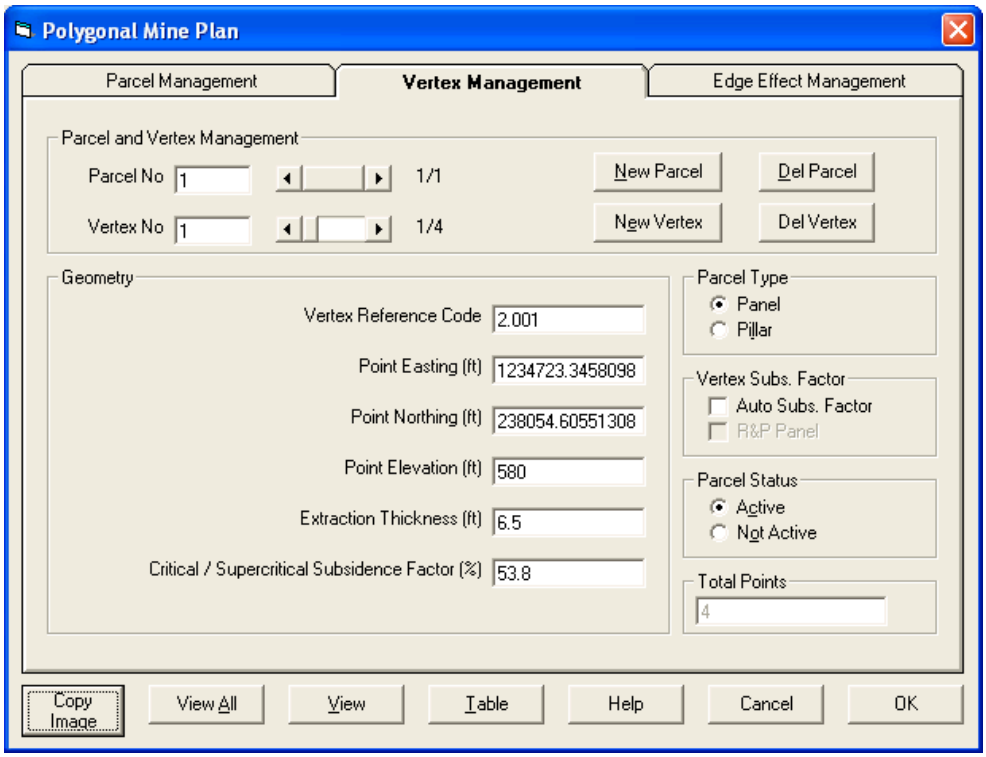

Figure 3: NA-1 Case Study – Vertex Management Screen (Only One Vertex Shown)

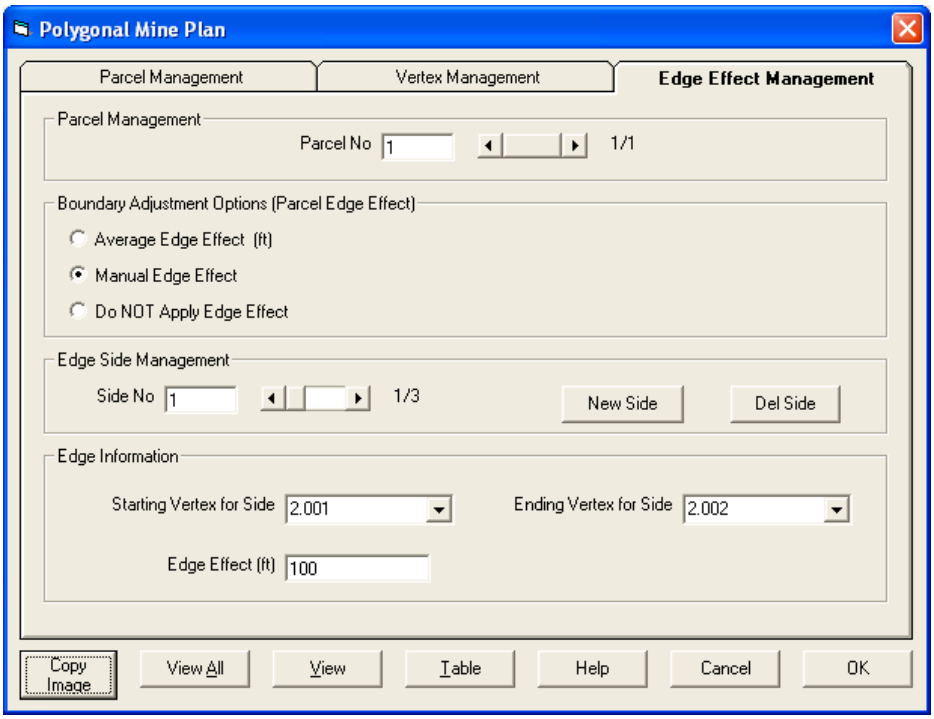

Figure 4: NA-1 Case Study – Edge Effect Management Screen, Side 1

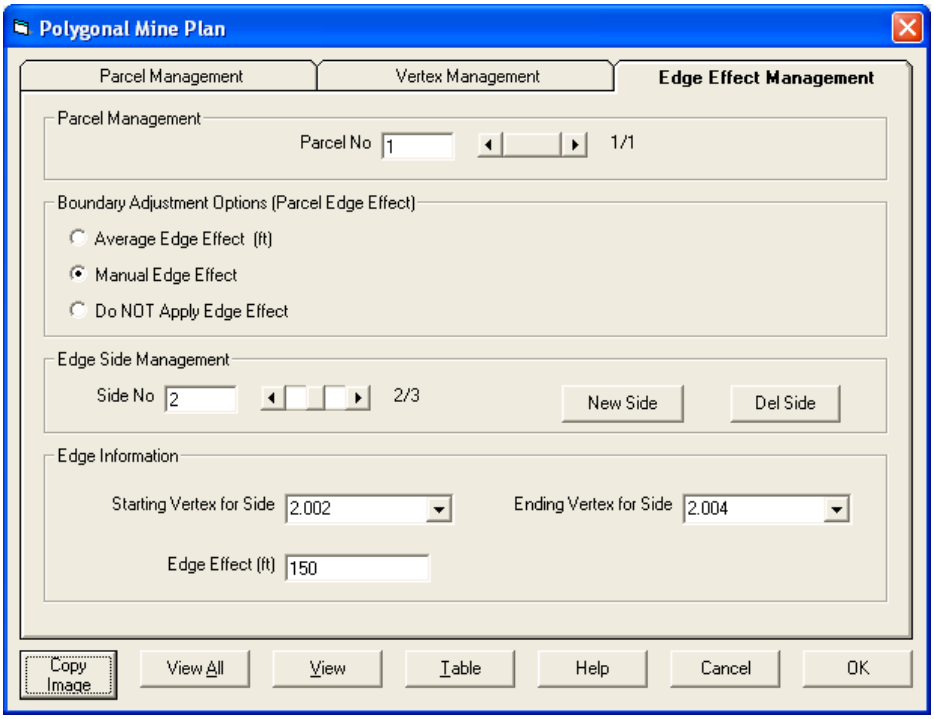

Figure 5: NA-1 Case Study – Edge Effect Management Screen, Side 2

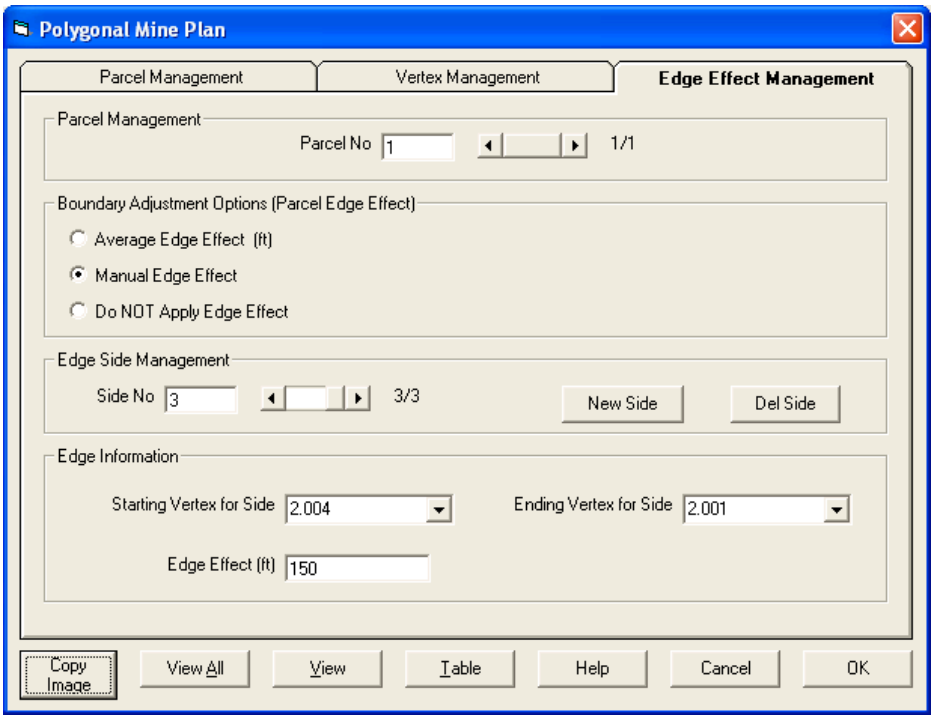

Figure 6: NA-1 Case Study – Edge Effect Management Screen, Side 3

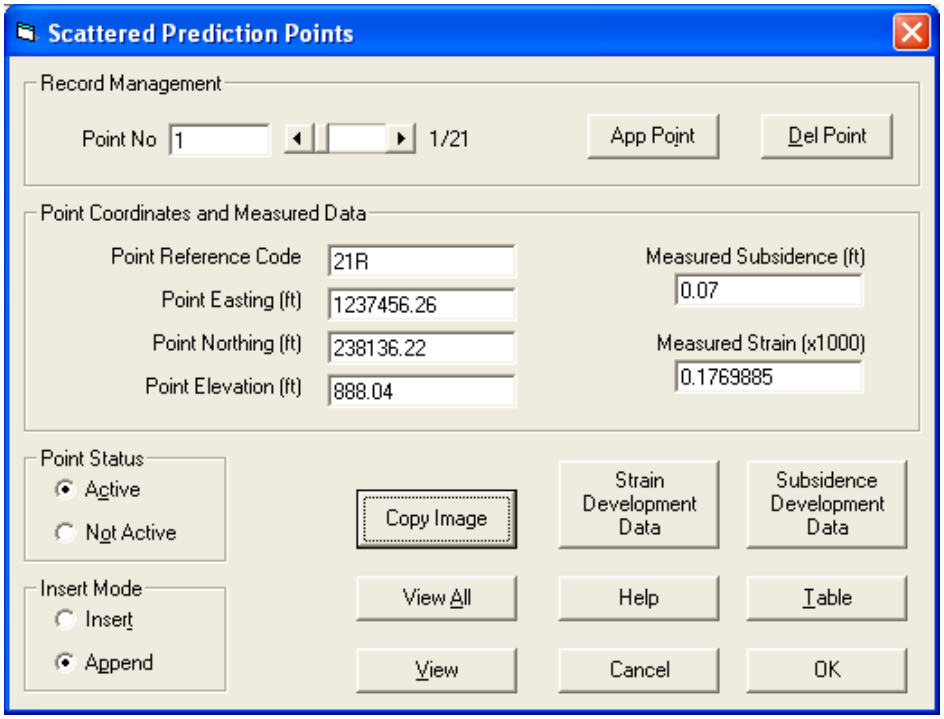

Figure 7: NA-1 Case Study –Prediction Points Management Screen (only first point shown)

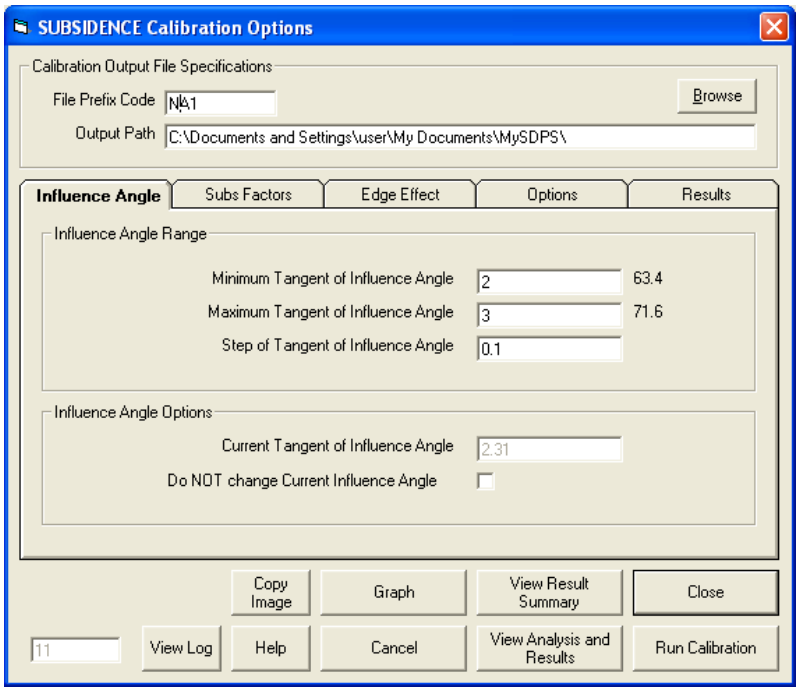

Figure 8: NA-1 Case Study – Subsidence Calibration Options Screen, Influence Angle Screen

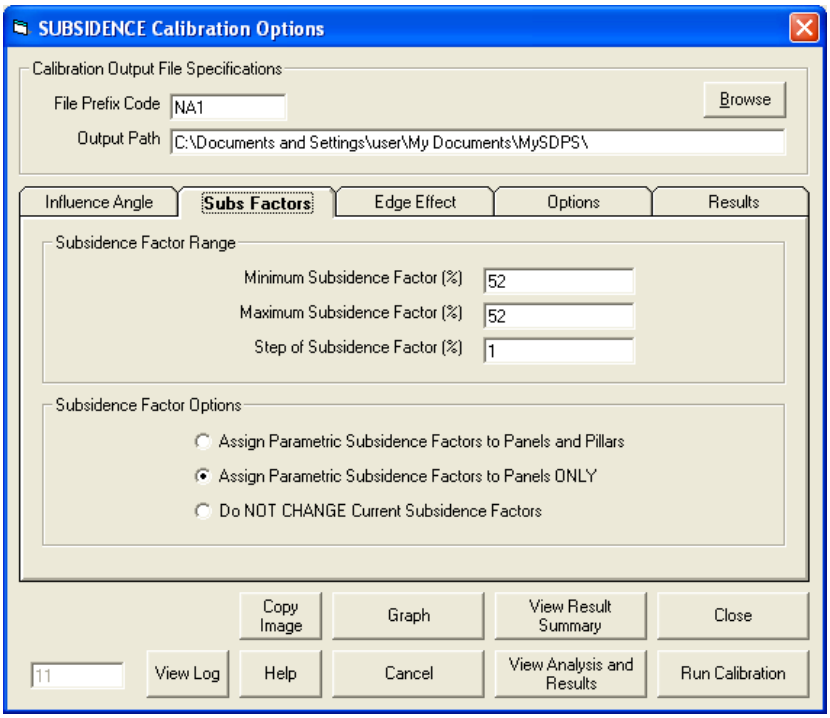

Figure 9: NA-1 Case Study – Subsidence Calibration Options Screen, Subsidence Factor Screen

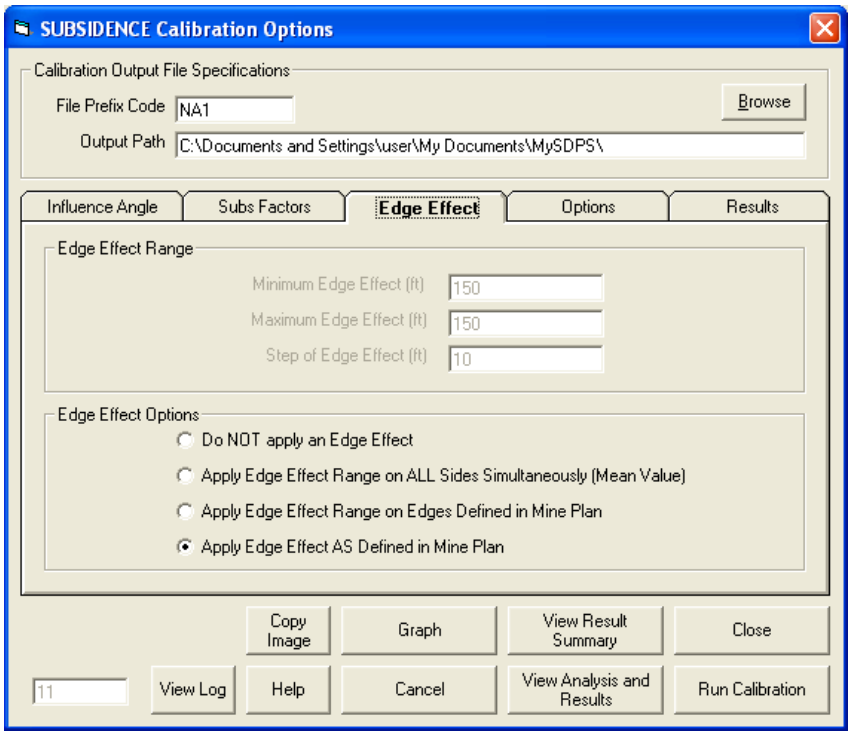

Figure 10: NA-1 Case Study – Subsidence Calibration Options Screen, Edge Effect Screen

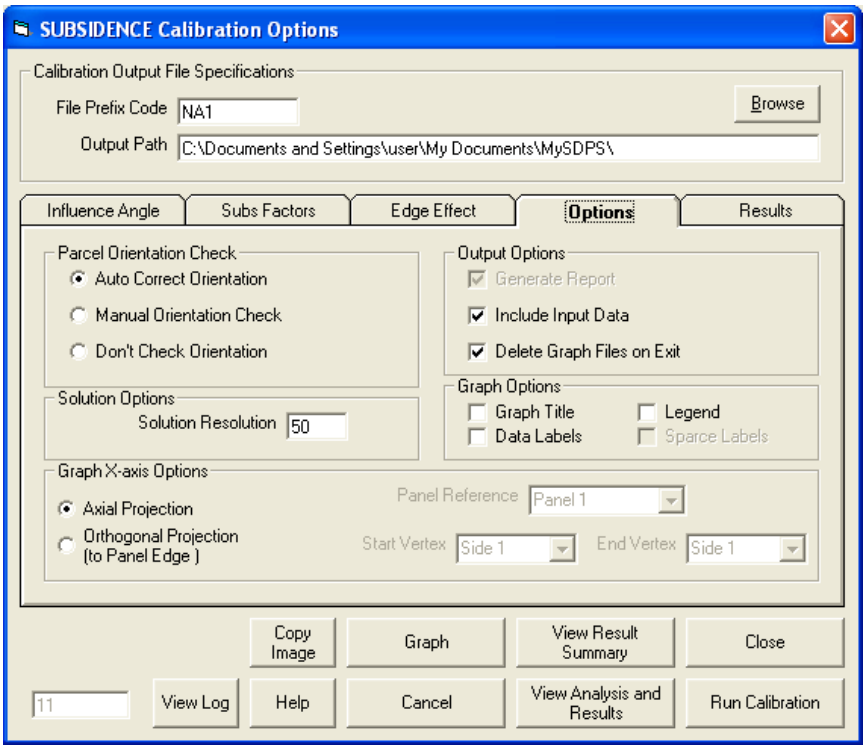

Figure 11: NA-1 Case Study – Subsidence Calibration Options Screen, Calibration Options Screen

NA-2 CASE STUDY (NORTHERN APPALACHIA) - TRANSVERSE LINE

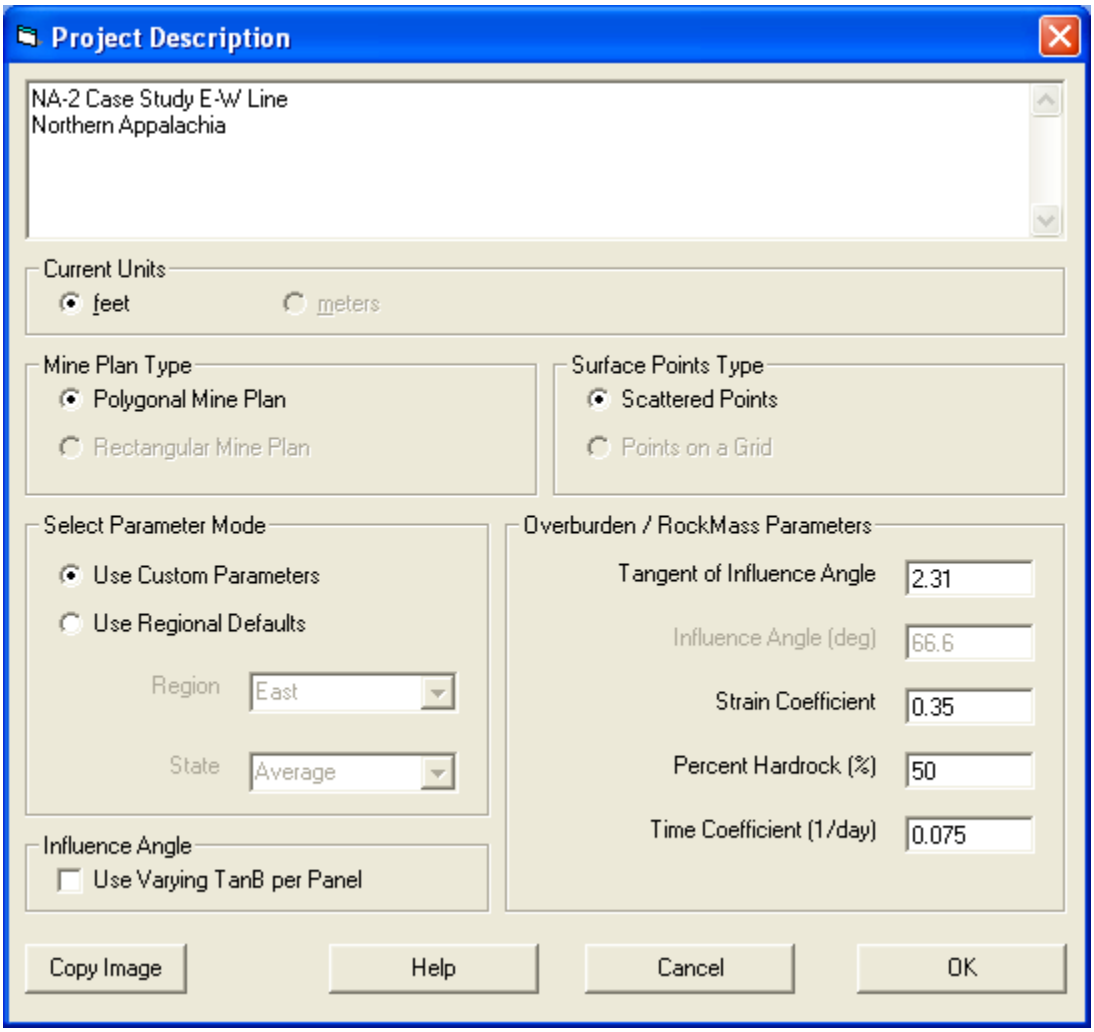

Figure 12: NA-2 Case Study, Transverse Line - SDPS Project Description Screen

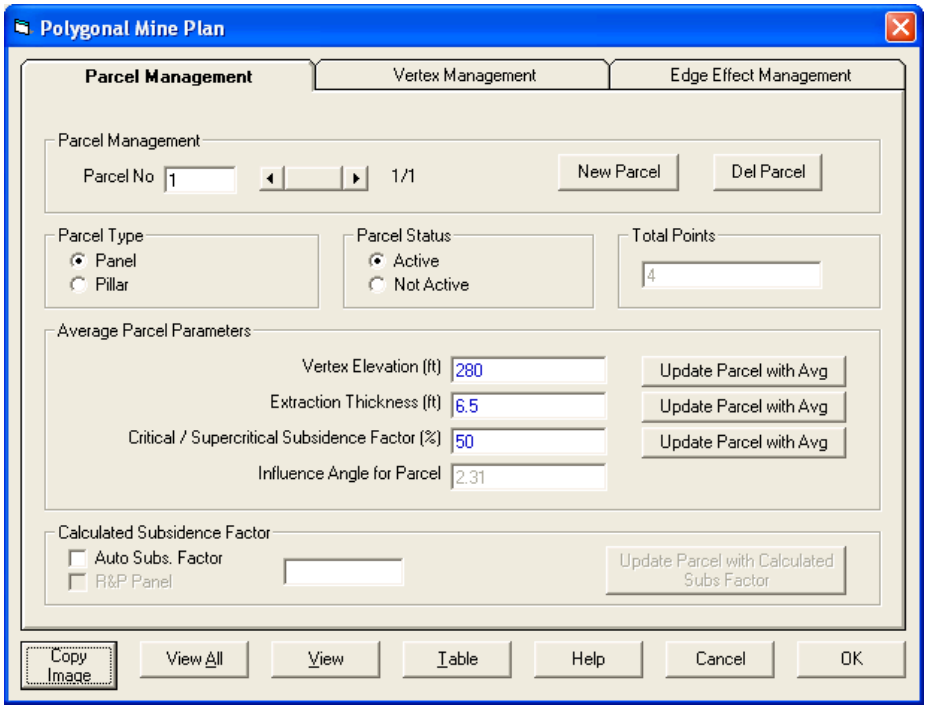

Figure 13: NA-2 Case Study, Transverse Line – Parcel Management Screen

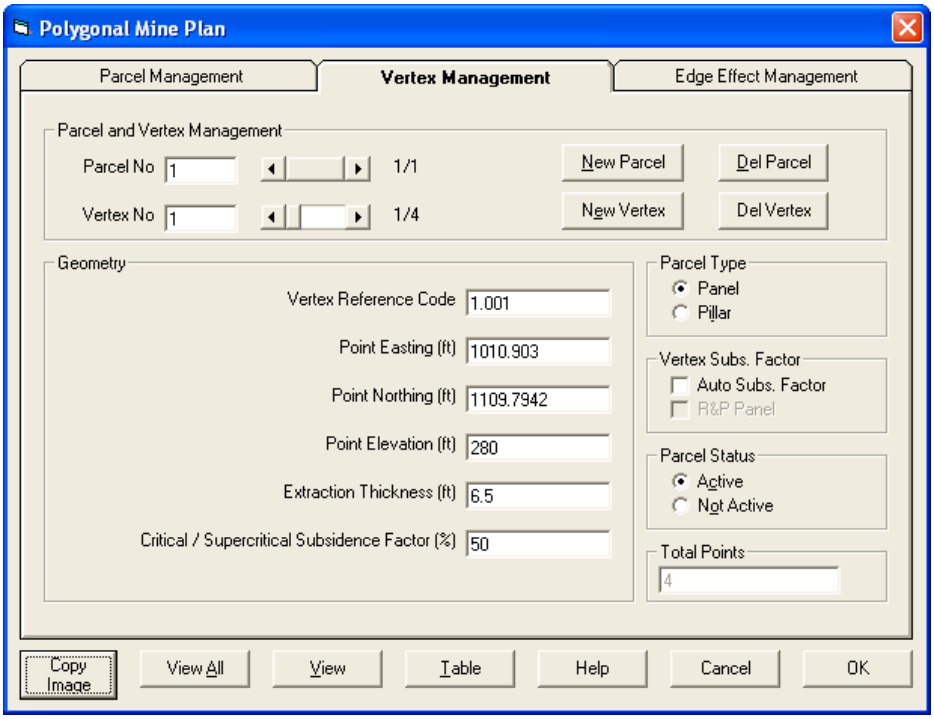

Figure 14: NA-2 Case Study, Transverse Line – Vertex Management Screen (Only One Vertex Shown)

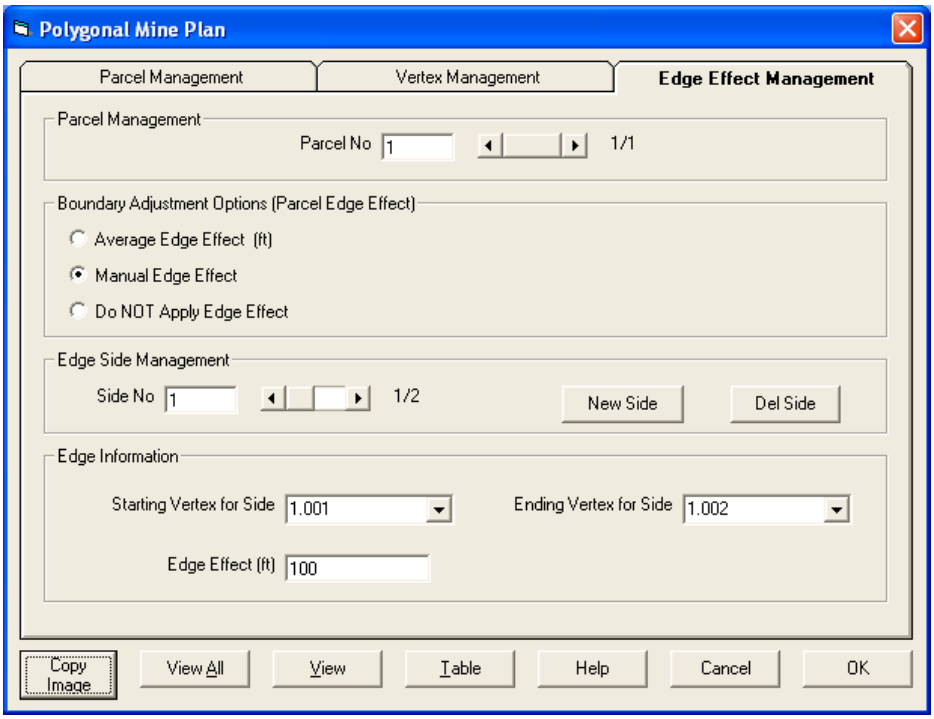

Figure 15: NA-2 Case Study, Transverse Line – Edge Effect Management Screen, Side 1

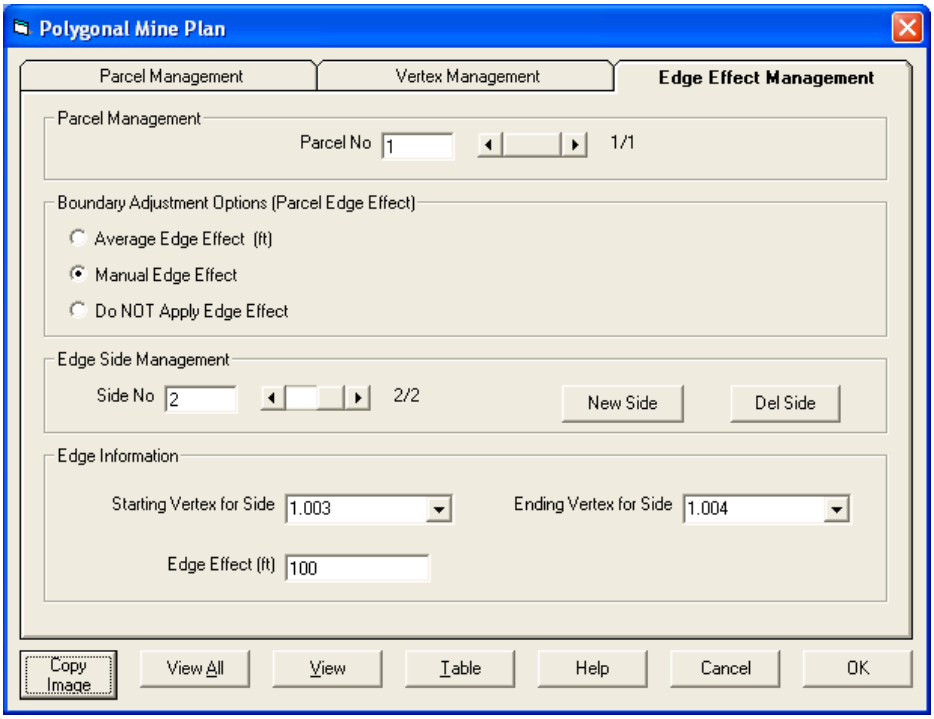

Figure 16: NA-2 Case Study, Transverse Line – Edge Effect Management Screen, Side 2

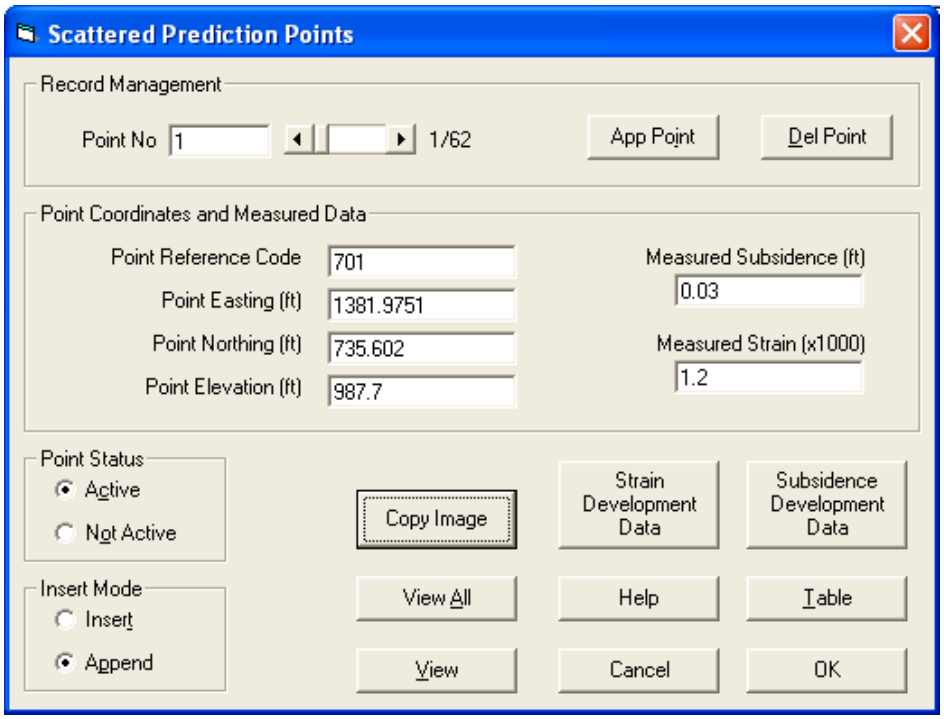

Figure 17: NA-2 Case Study, Transverse Line –Prediction Points Management Screen (only first point shown)

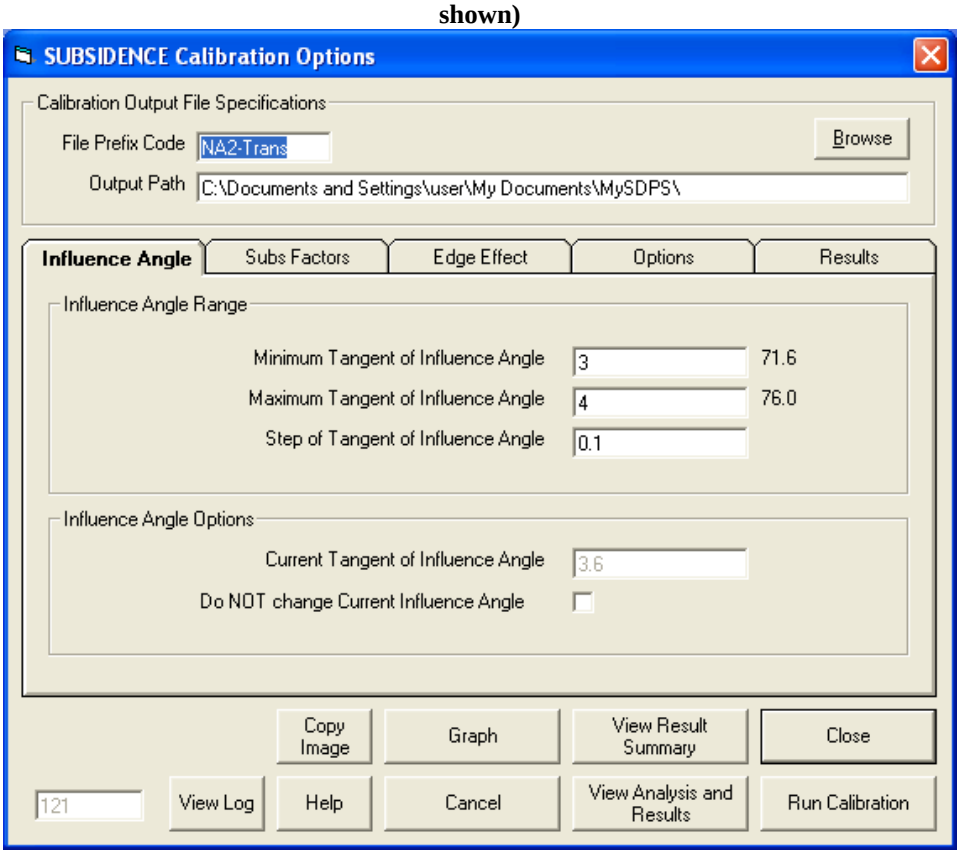

Figure 18: NA-2 Case Study, Transverse Line – Subsidence Calibration Options Screen, Influence Angle Screen

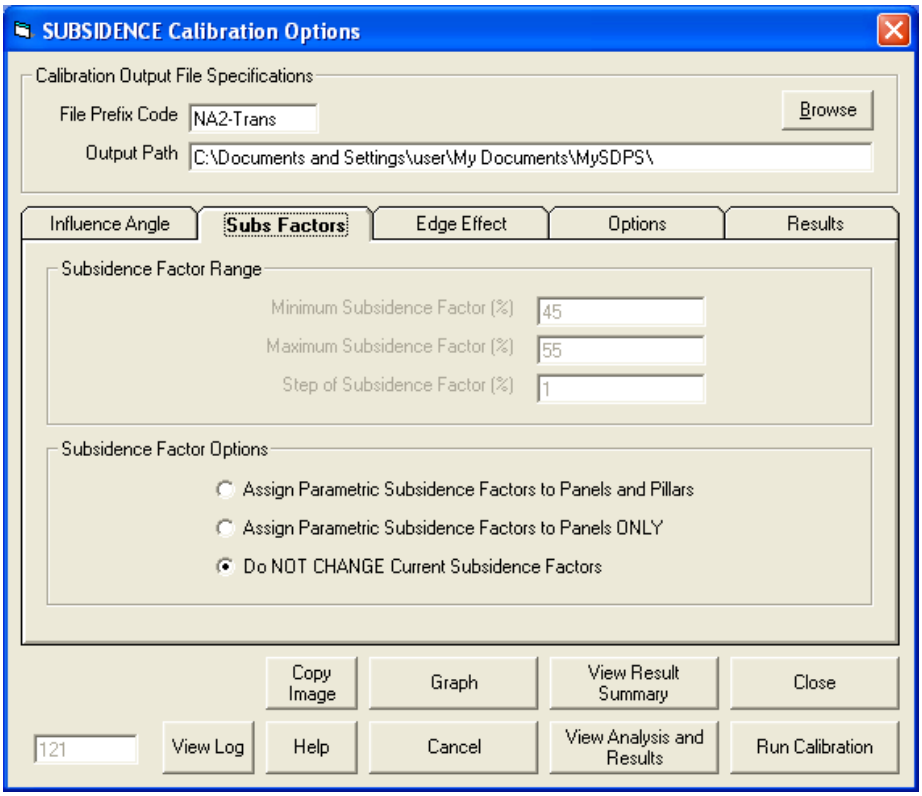

Figure 19: NA-2 Case Study, Transverse Line – Subsidence Calibration Options Screen, Subsidence Factor Screen

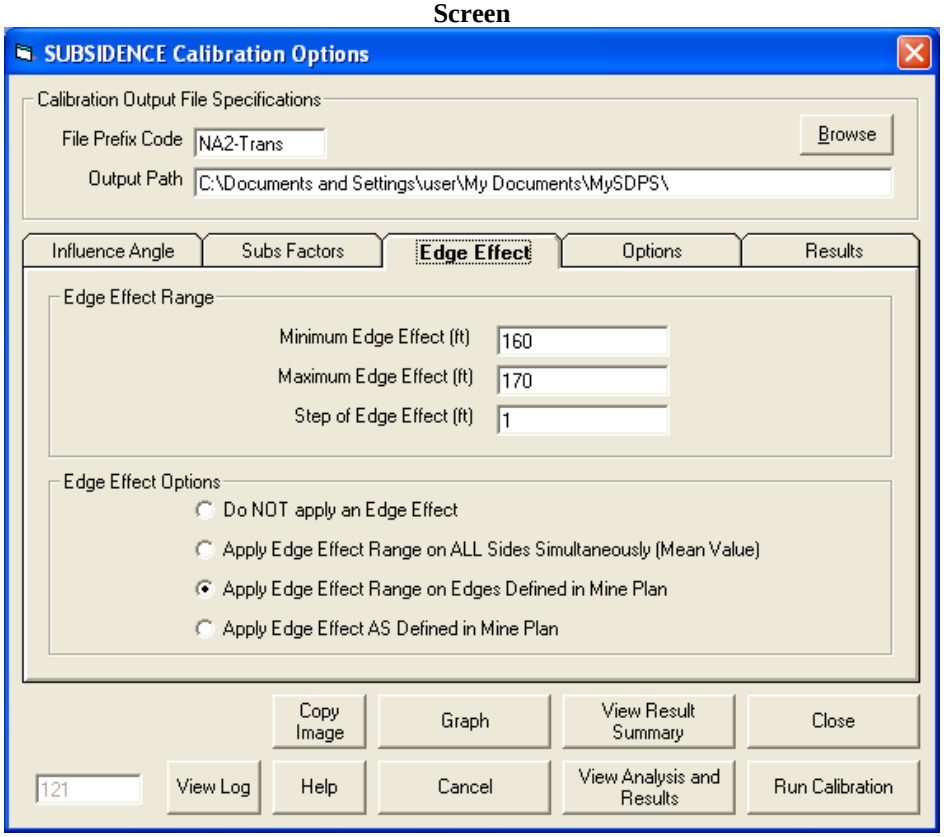

Figure 20: NA-2 Case Study, Transverse Line – Subsidence Calibration Options Screen, Edge Effect Screen

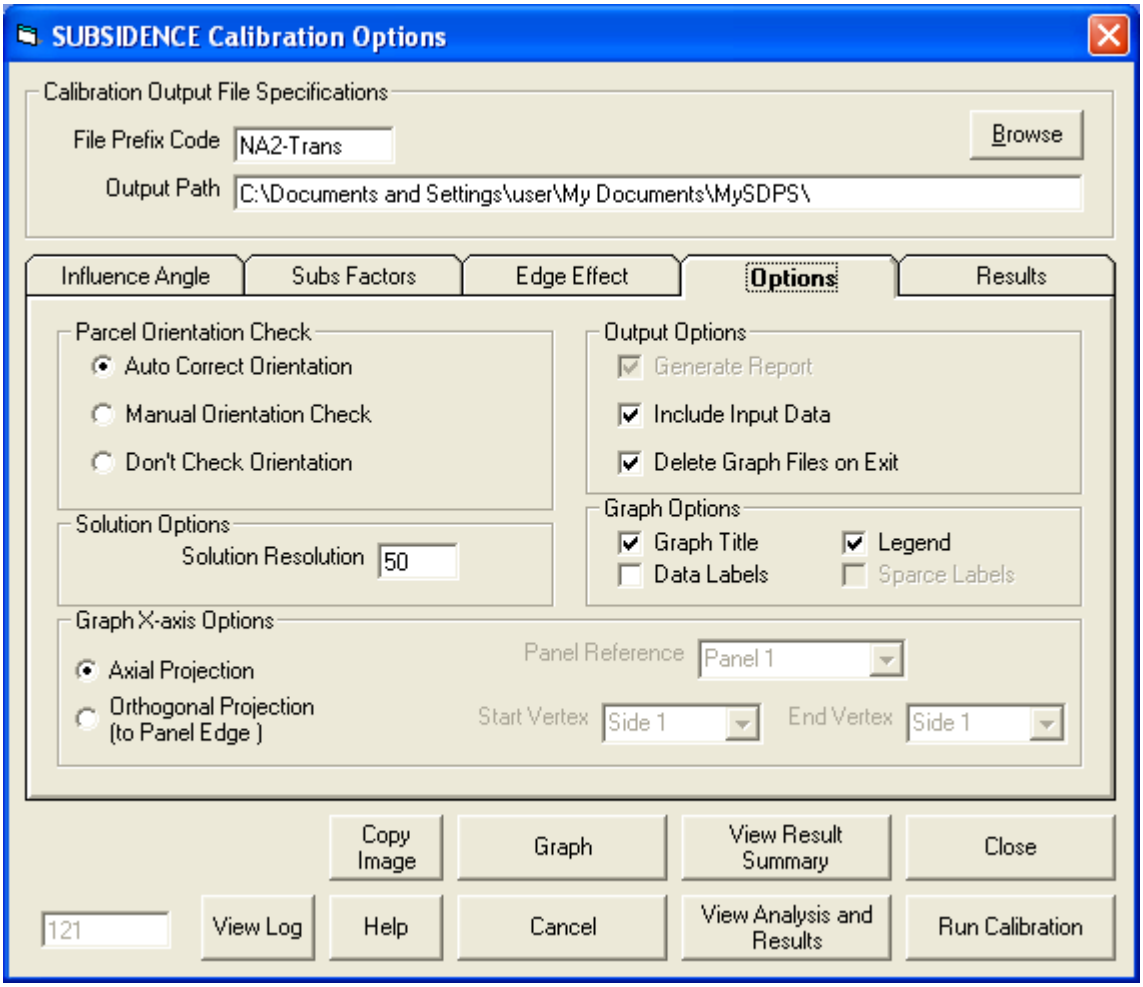

Figure 21: NA-2 Case Study, Transverse Line – Subsidence Calibration Options Screen, Calibration Options Screen

NA-2 CASE STUDY (NORTHERN APPALACHIA) - LONGITUDINAL LINE

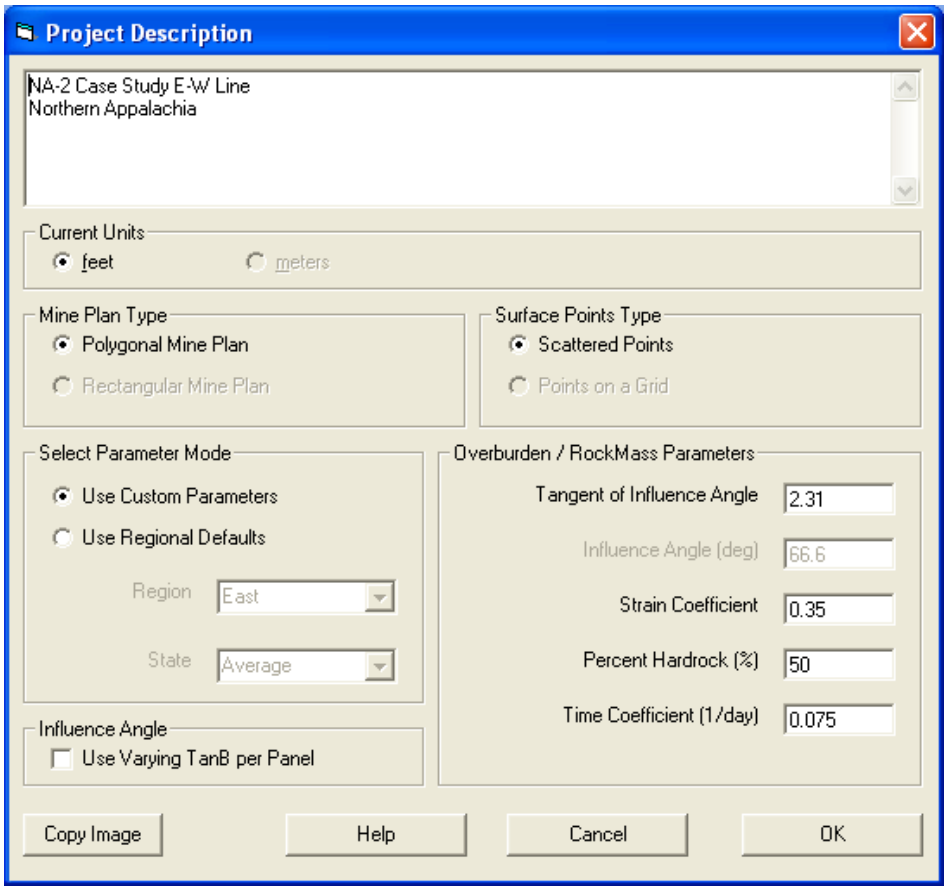

Figure 22: NA-2 Case Study, Longitudinal Line - SDPS Project Description Screen

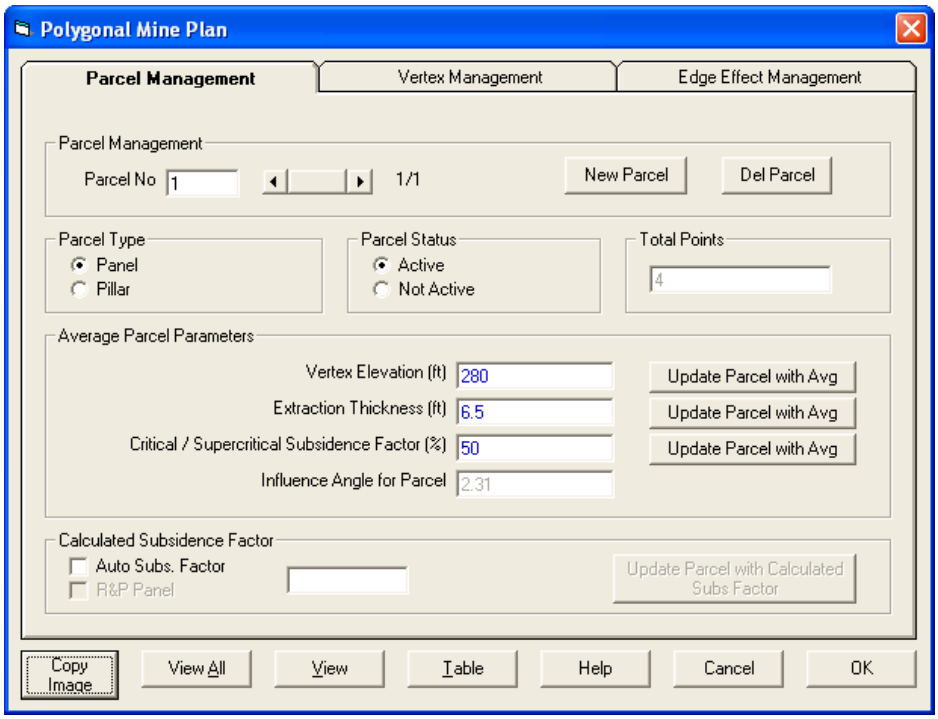

Figure 23: NA-2 Case Study, Longitudinal Line – Parcel Management Screen

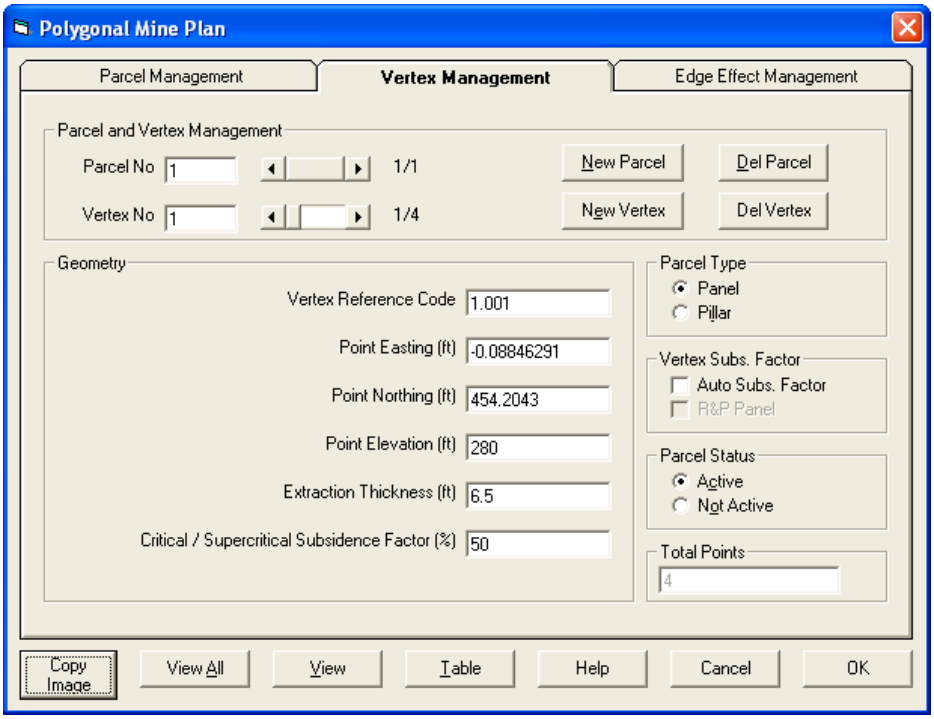

Figure 24: NA-2 Case Study, Longitudinal Line – Vertex Management Screen (Only One Vertex Shown)

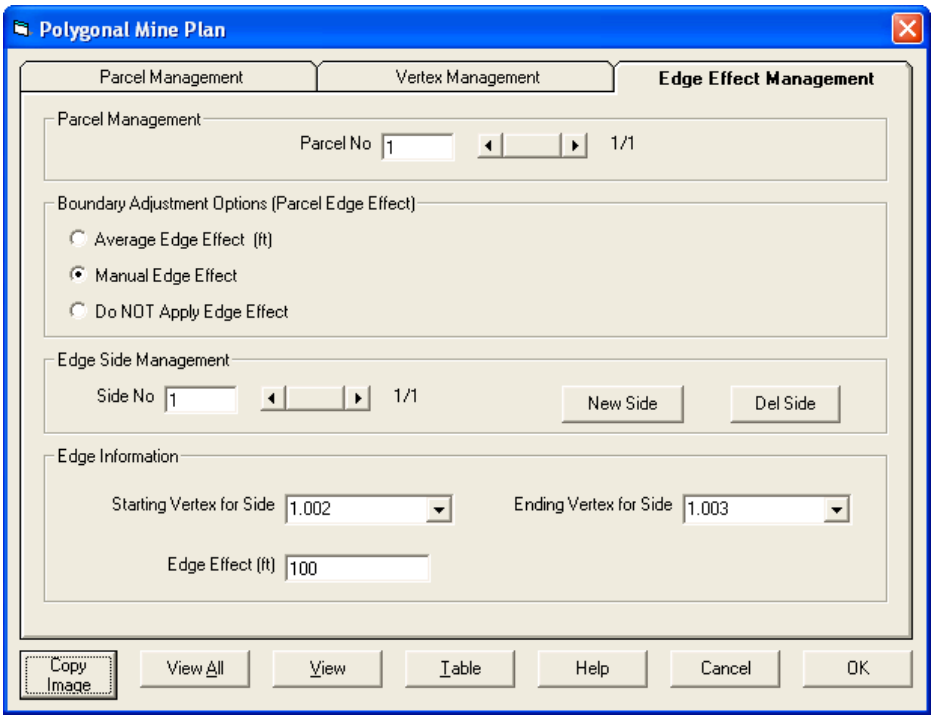

Figure 25: NA-2 Case Study, Longitudinal Line – Edge Effect Management Screen, (Only 1 Side)

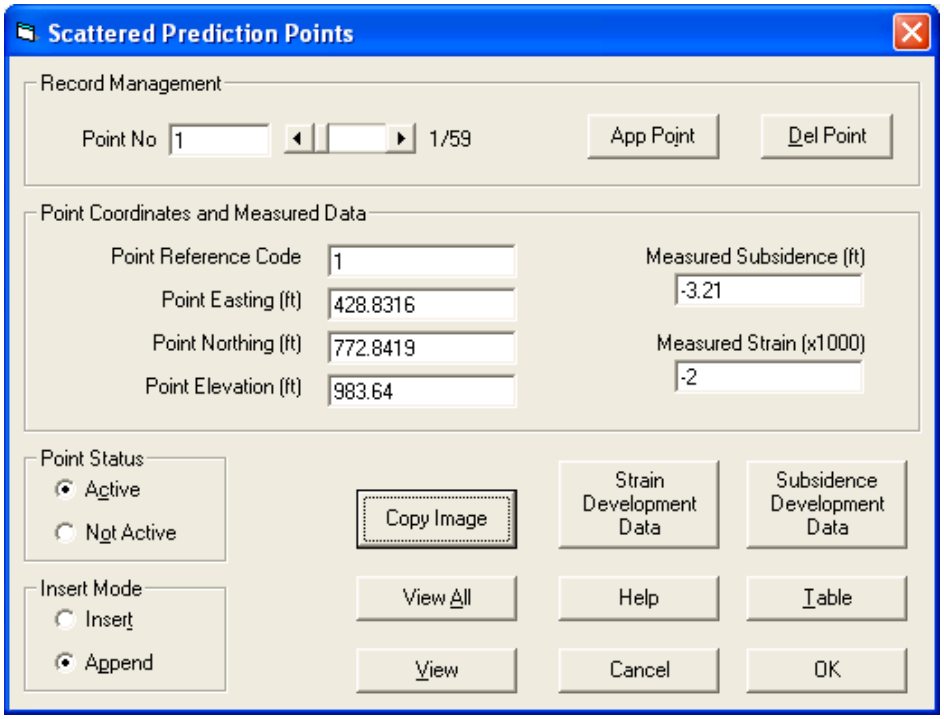

Figure 26: NA-2 Case Study, Longitudinal Line –Prediction Points Management Screen (only first point shown)

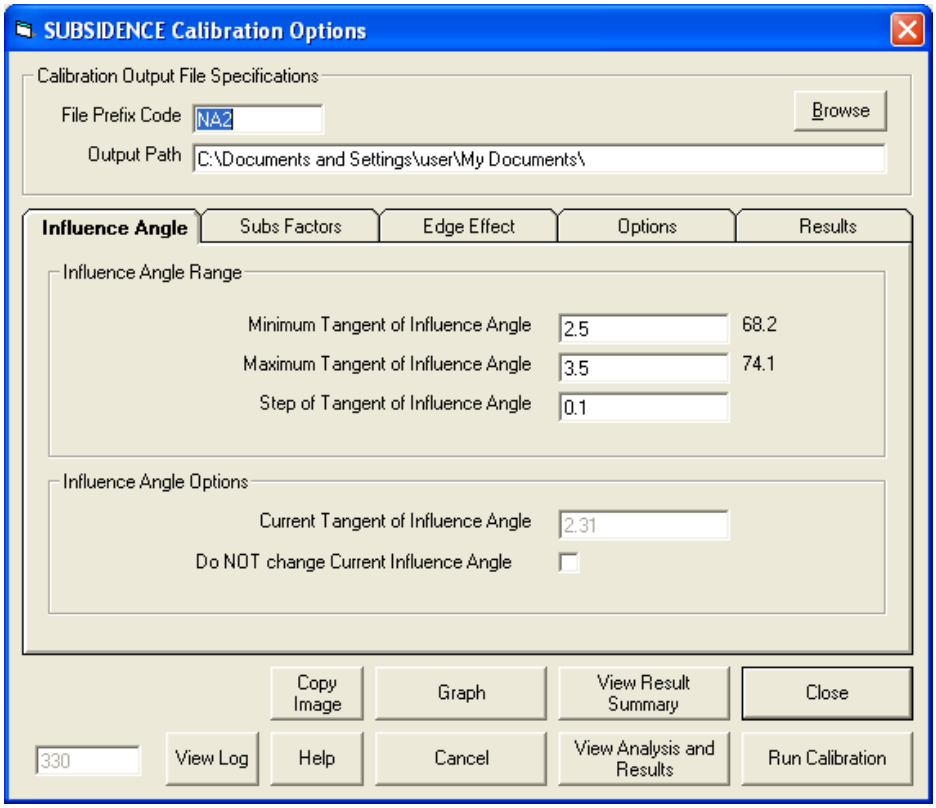

Figure 27: NA-2 Case Study, Longitudinal Line – Subsidence Calibration Options Screen, Influence Angle Screen

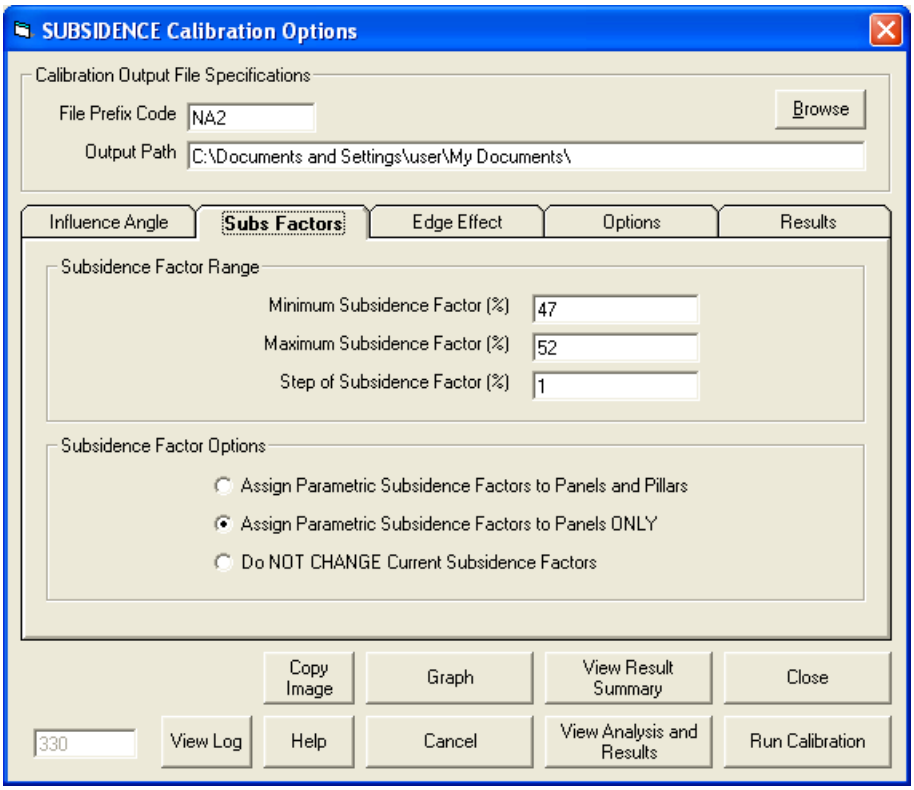

Figure 28: NA-2 Case Study, Longitudinal Line – Subsidence Calibration Options Screen, Subsidence Factor Screen

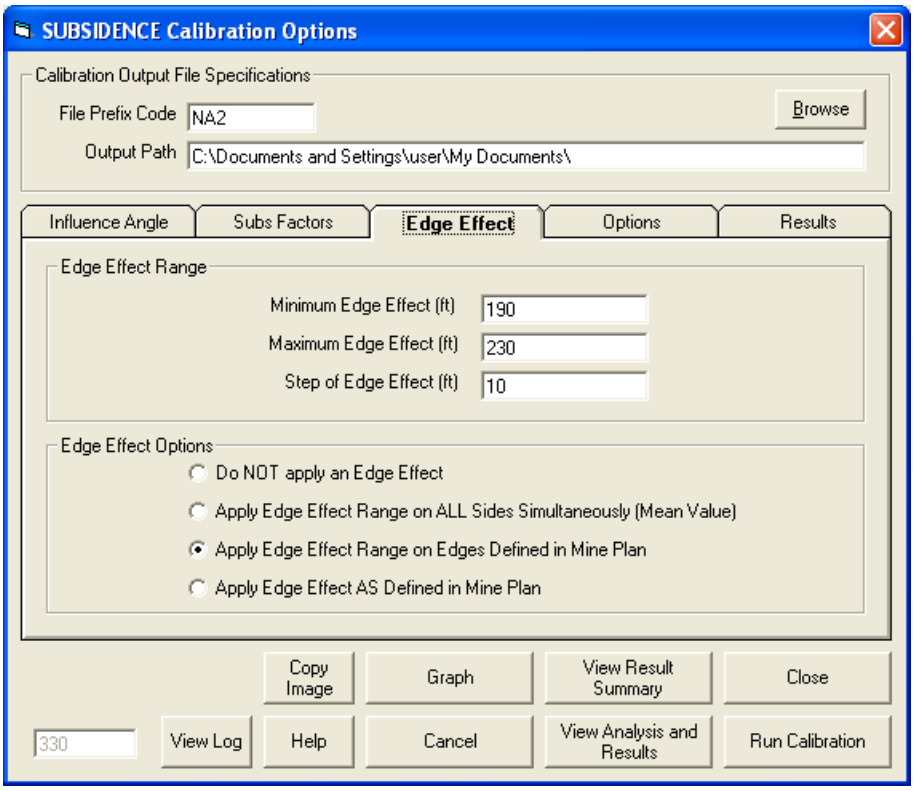

Figure 29: NA-2 Case Study, Longitudinal Line – Subsidence Calibration Options Screen, Edge Effect Screen

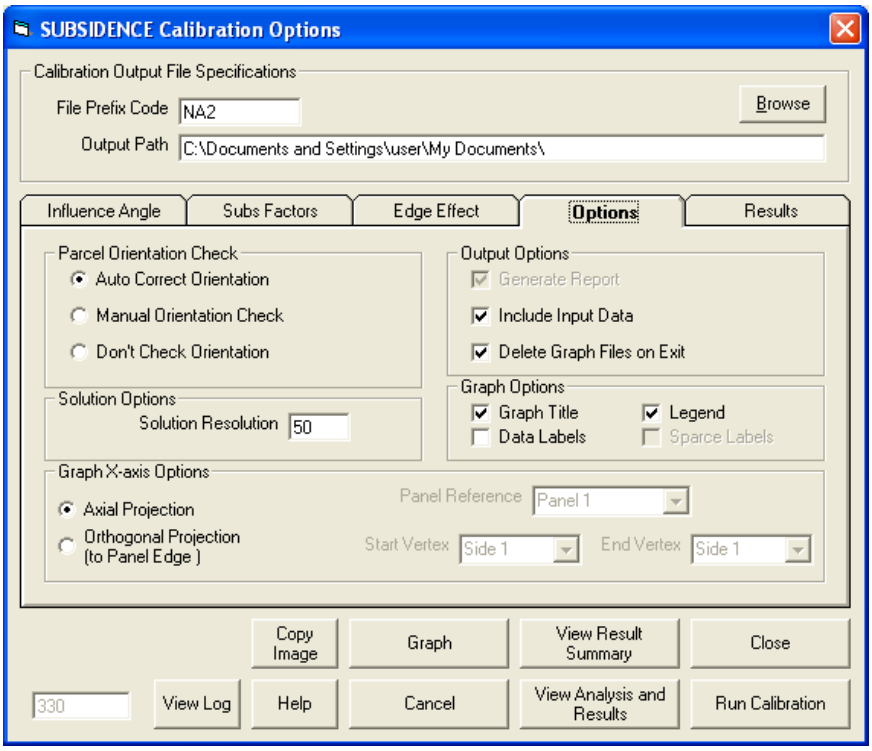

Figure 30: NA-2 Case Study, Longitudinal Line – Subsidence Calibration Options Screen, Calibration Options Screen

NA-3 CASE STUDY (NORTHERN APPALACHIA) - PANEL 1 NORTH

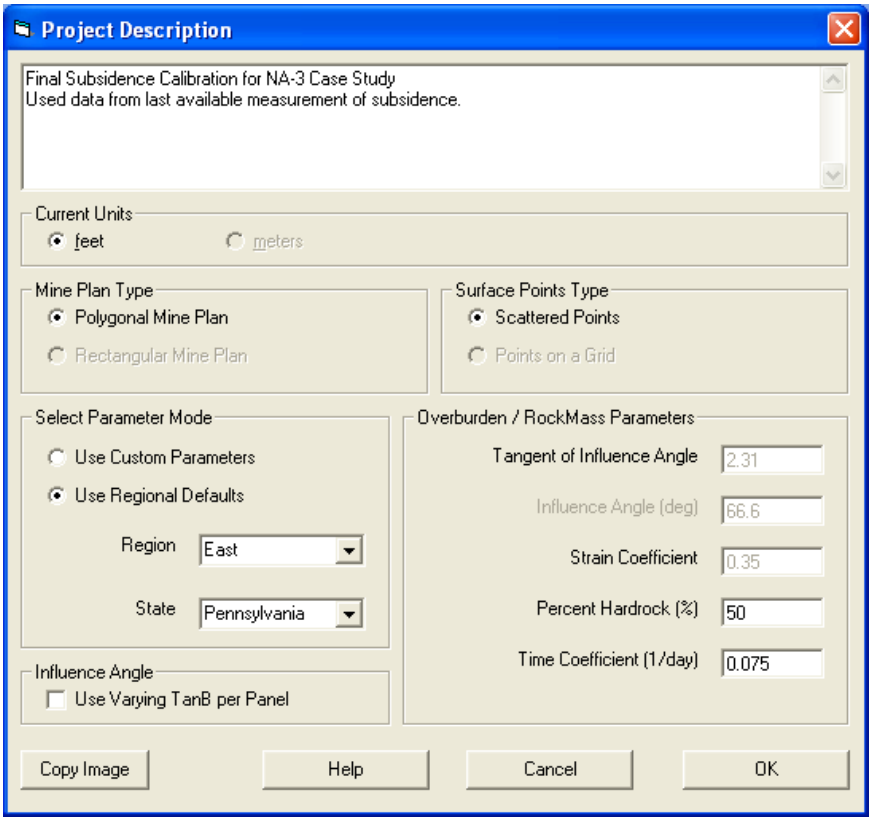

Figure 31: NA-3 Case Study, Panel 1 North - SDPS Project Description Screen

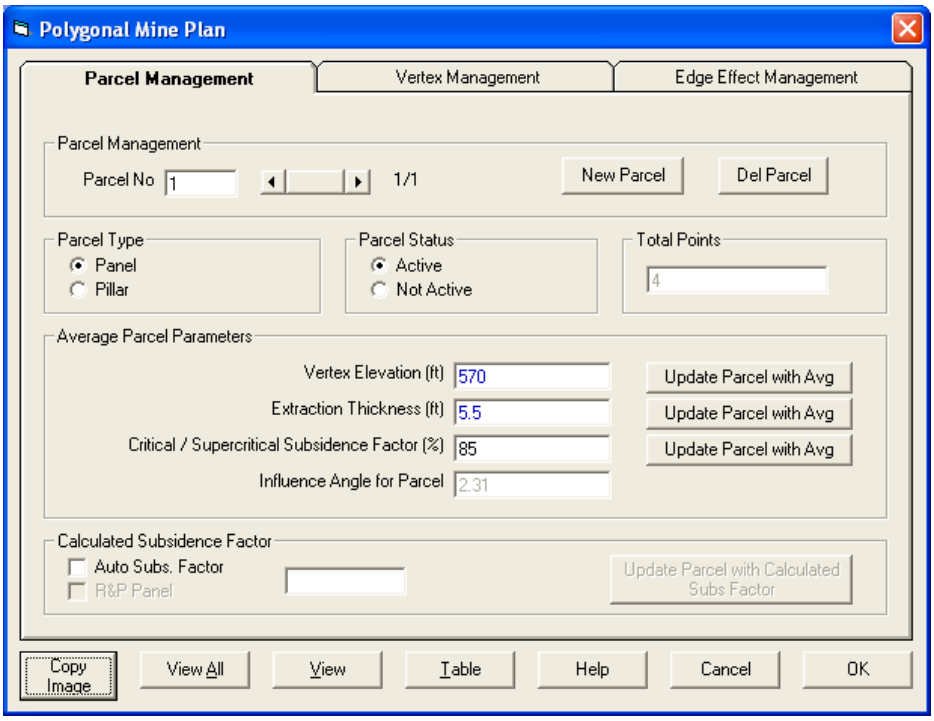

Figure 32: NA-3 Case Study, Panel 1 North - Parcel Management Screen

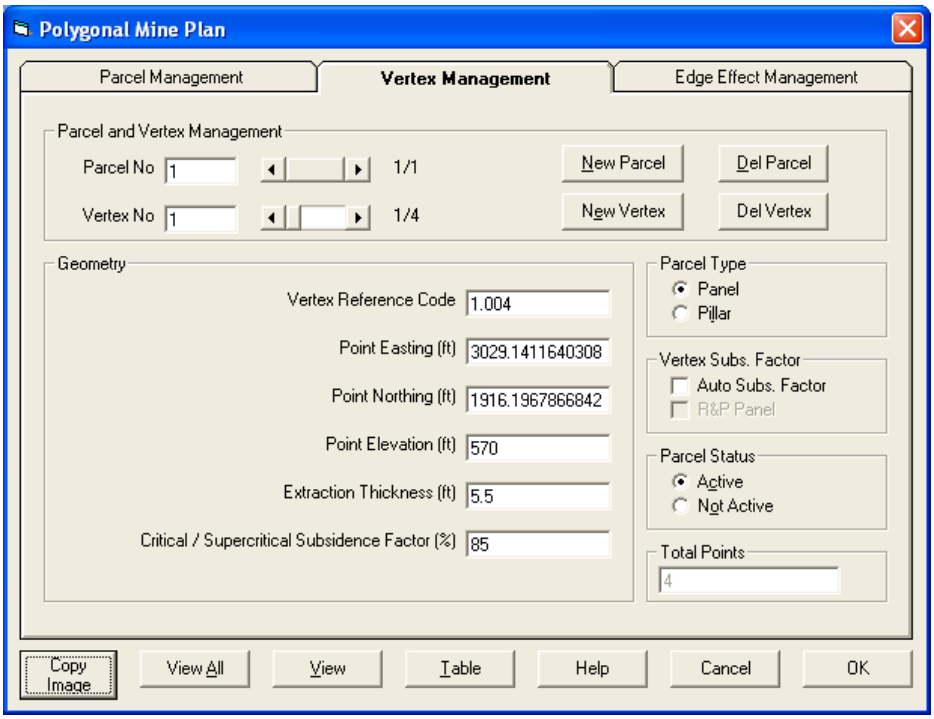

Figure 33: NA-3 Case Study, Panel 1 North - Vertex Management Screen (Only One Vertex Shown)

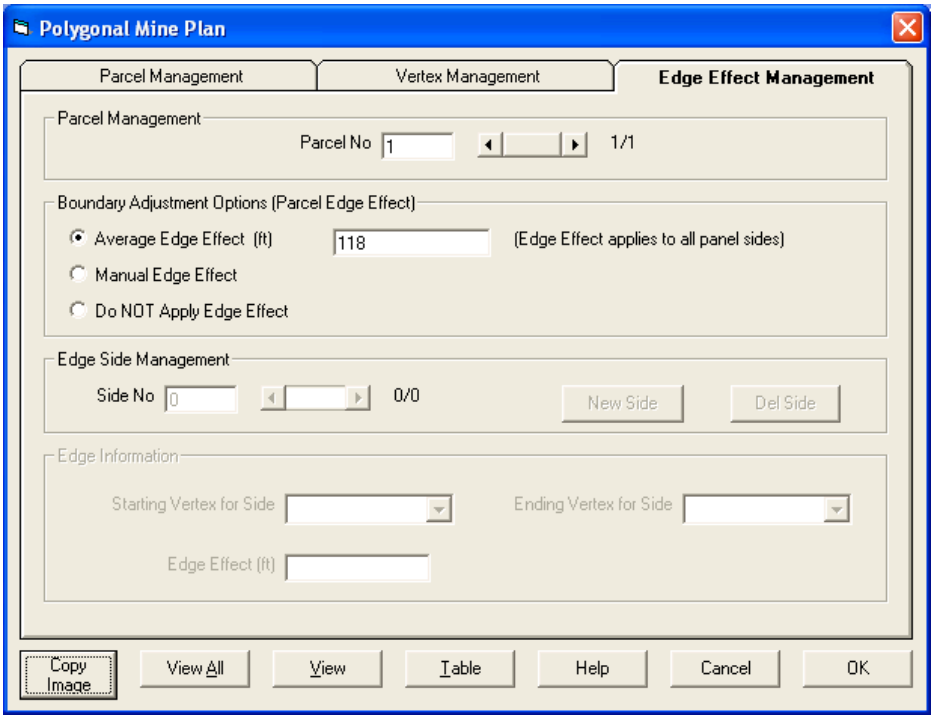

Figure 34: NA-3 Case Study, Panel 1 North - Edge Effect Management Screen

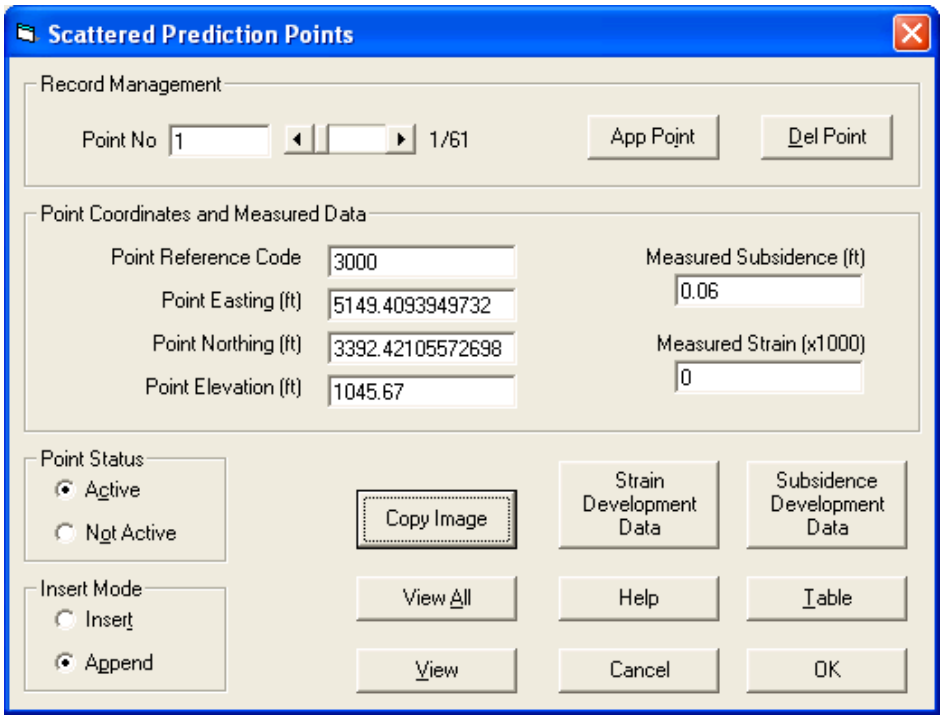

Figure 35: NA-3 Case Study, Panel 1 North - Prediction Points Management Screen (only first point shown)

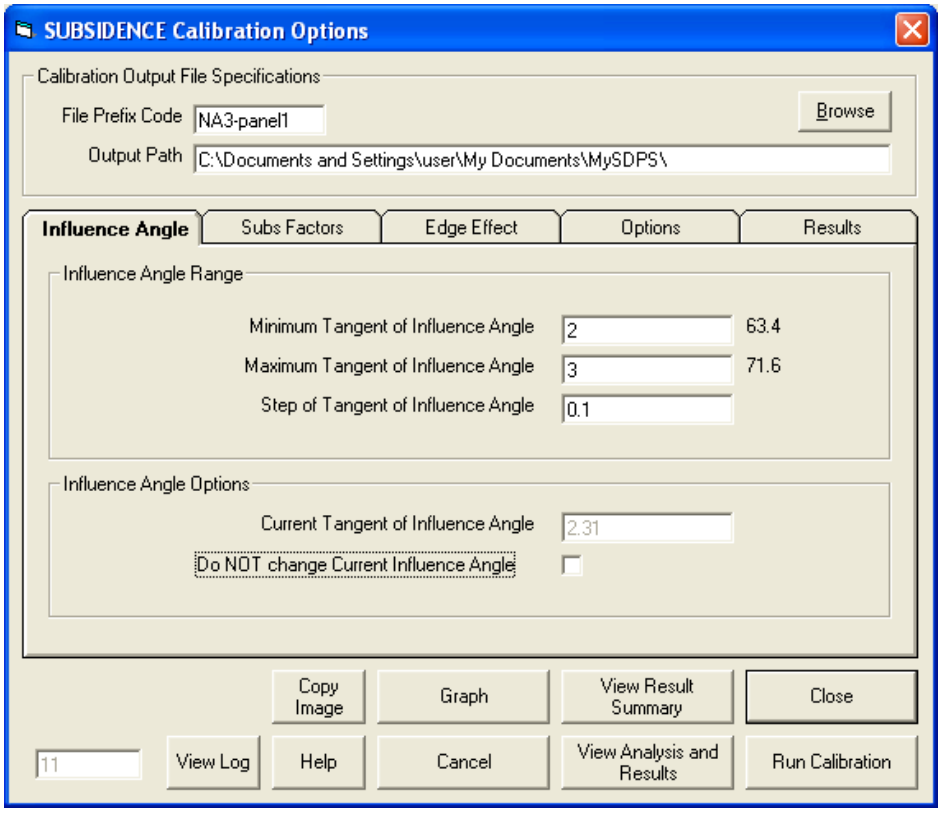

Figure 36: NA-3 Case Study, Panel 1 North - Subsidence Calibration Options Screen, Influence Angle Screen

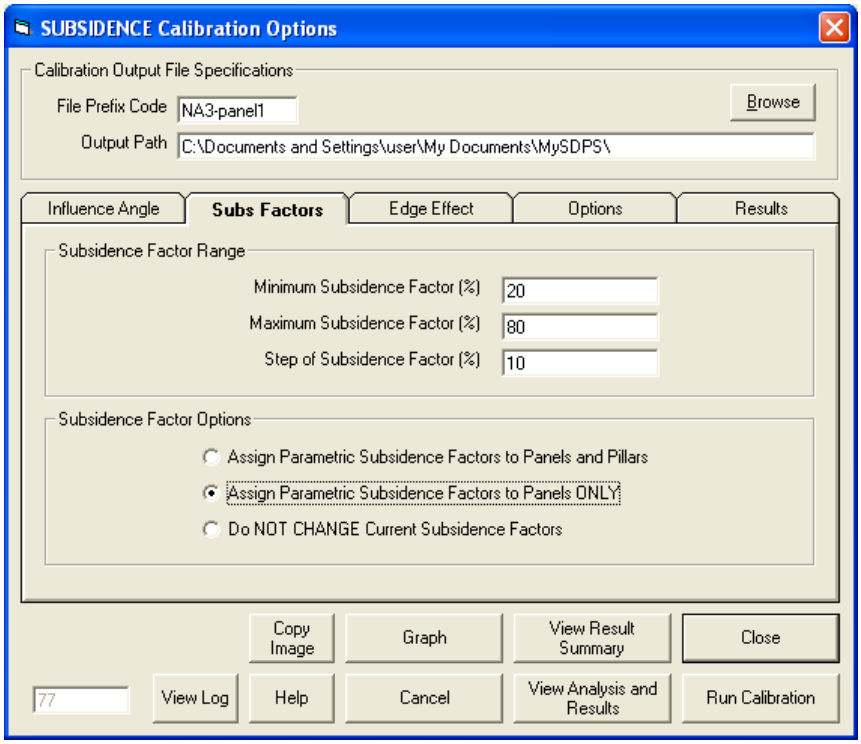

Figure 37: NA-3 Case Study, Panel 1 North - Subsidence Calibration Options Screen, Subsidence Factor Screen

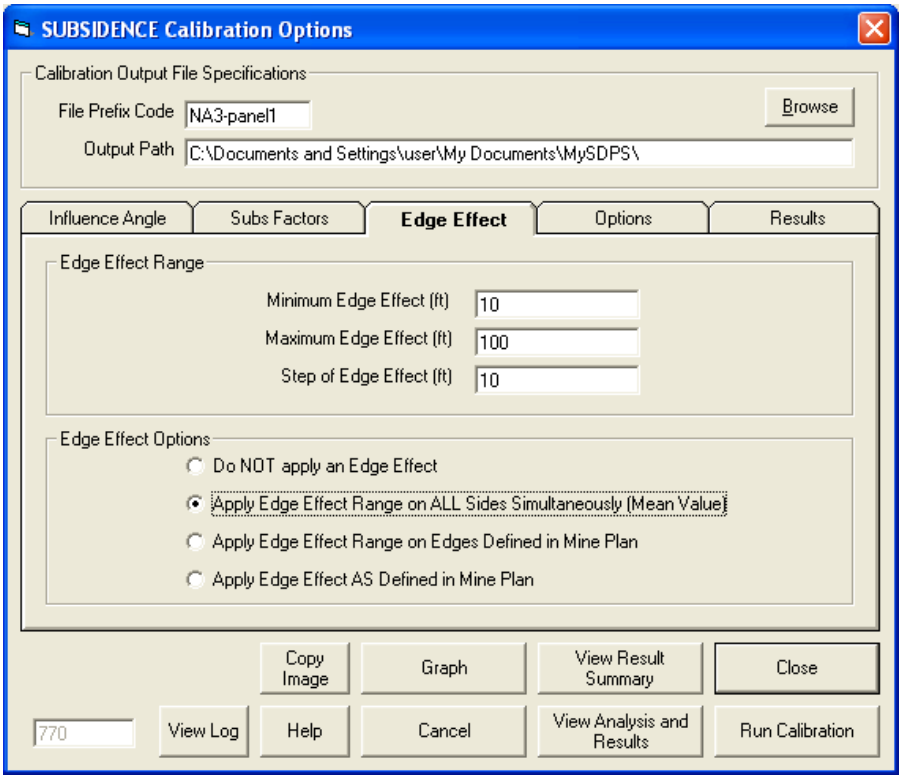

Figure 38: NA-3 Case Study, Panel 1 North - Subsidence Calibration Options Screen, Edge Effect Screen

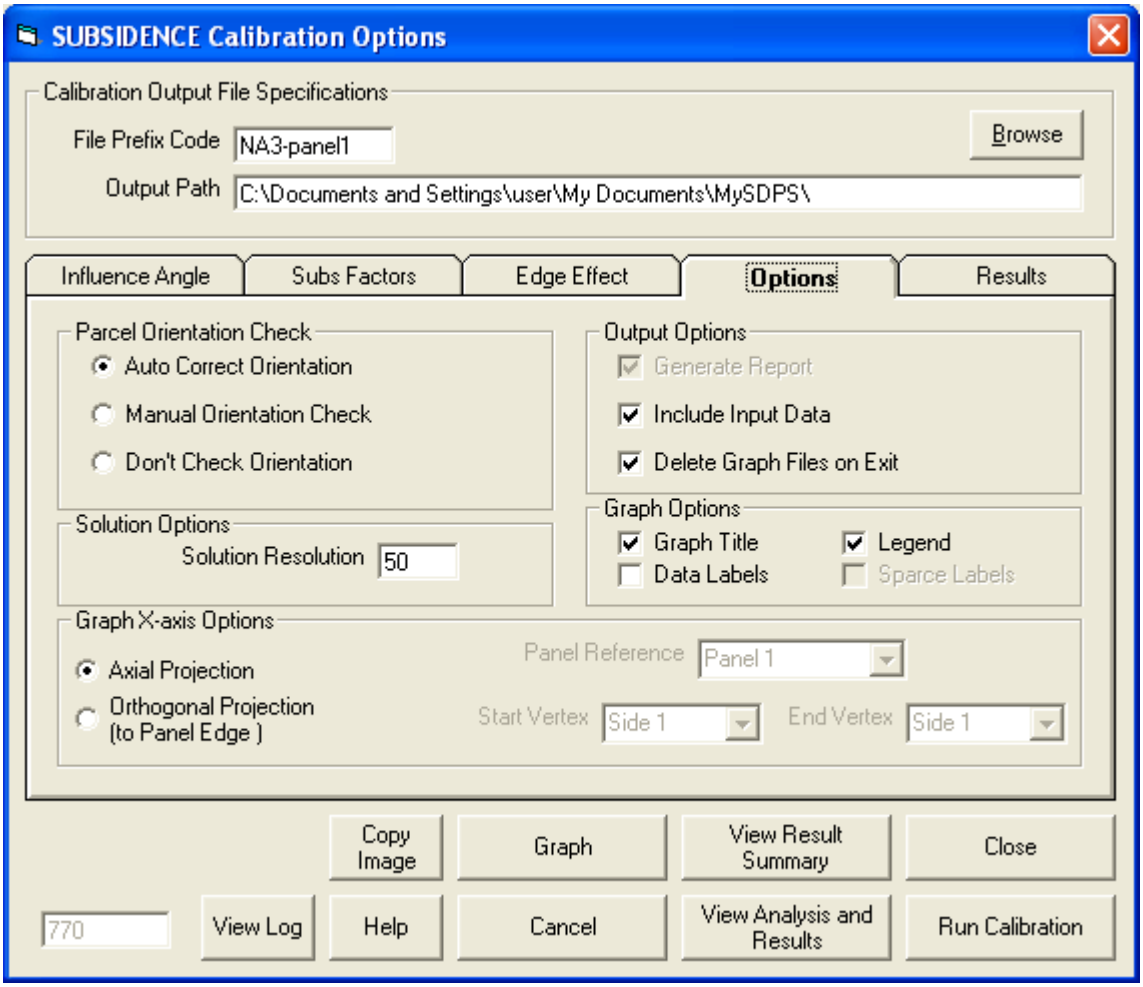

Figure 39: NA-3 Case Study, Panel 1 North - Subsidence Calibration Options Screen, Calibration Options Screen

NA-3 CASE STUDY (NORTHERN APPALACHIA) - PANEL 3 NORTH

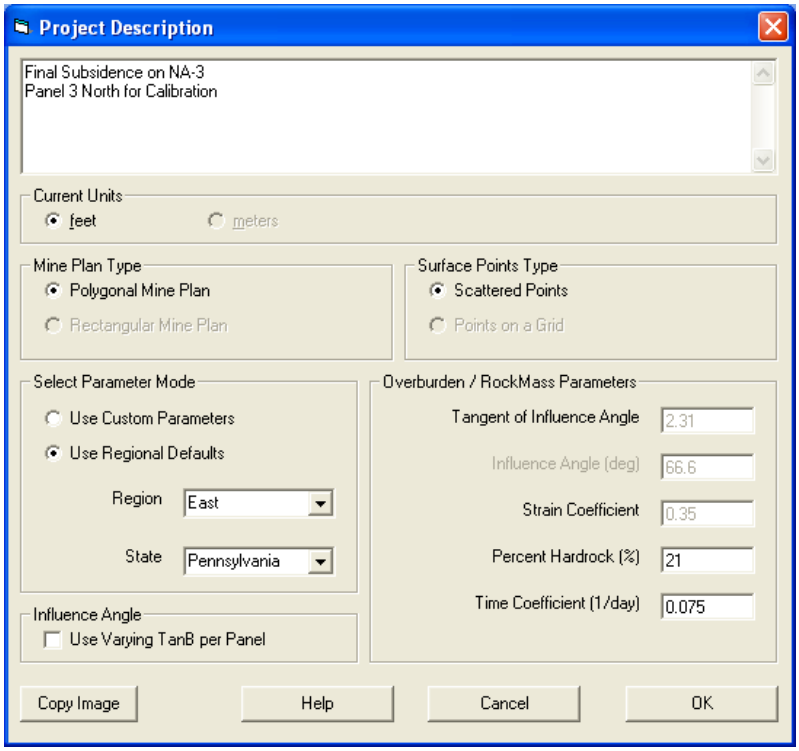

Figure 40: NA-3 Case Study, Panel 3 North - SDPS Project Description Screen

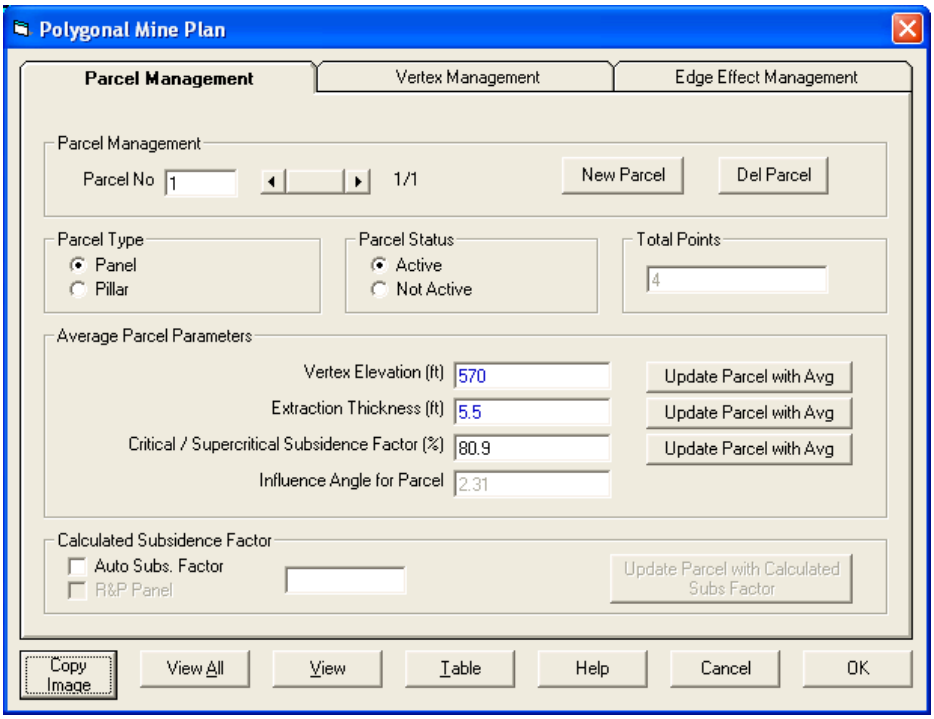

Figure 41: NA-3 Case Study, Panel 3 North - Parcel Management Screen

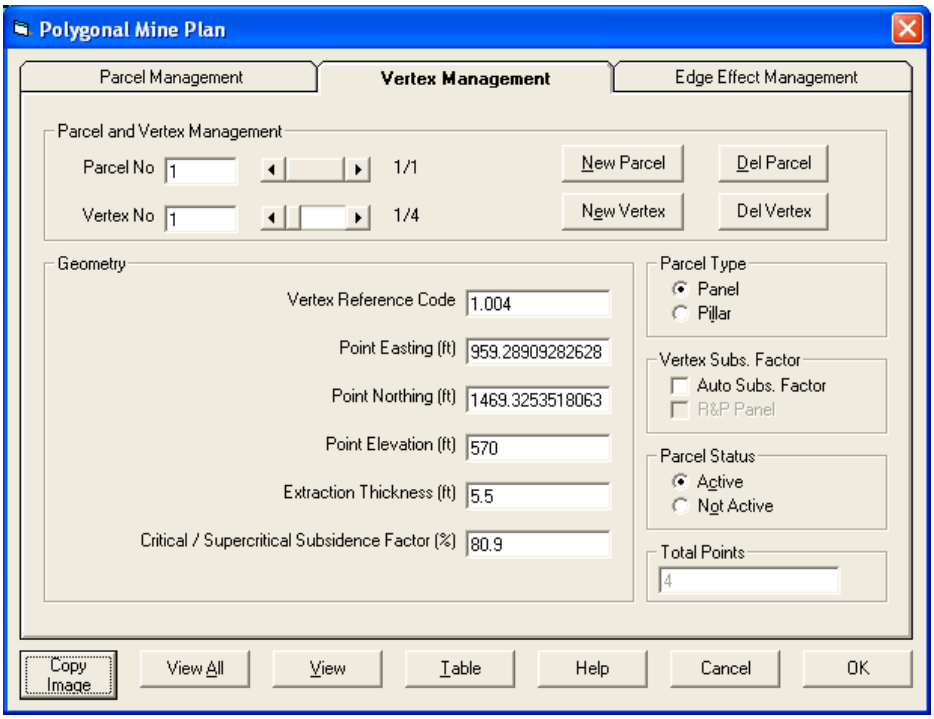

Figure 42: NA-3 Case Study, Panel 3 North - Vertex Management Screen (Only One Vertex Shown)

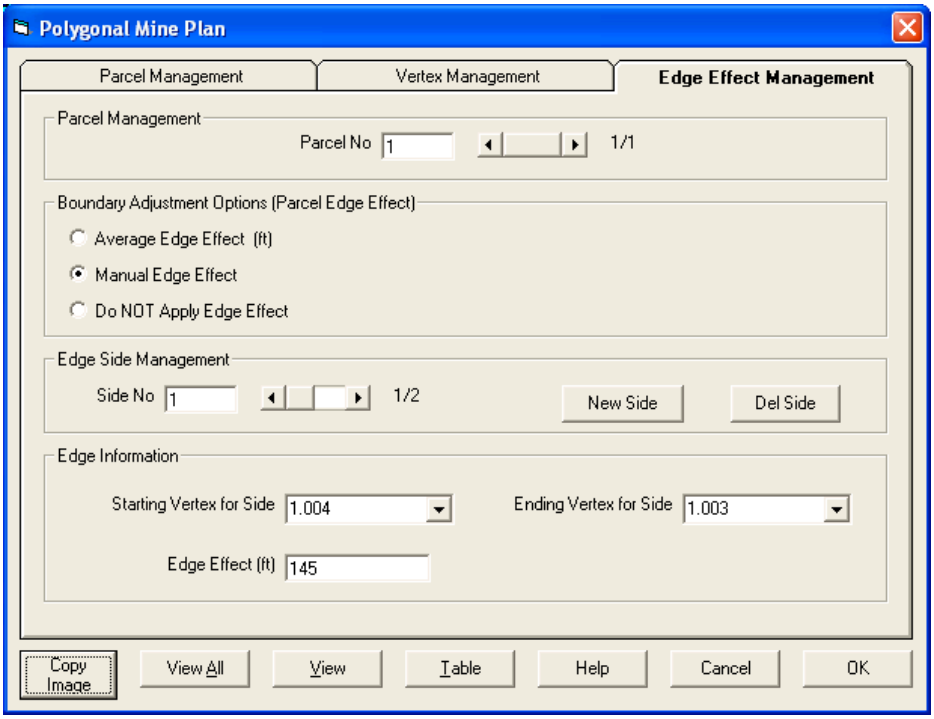

Figure 43: NA-3 Case Study, Panel 3 North - Edge Effect Management Screen, Side 1

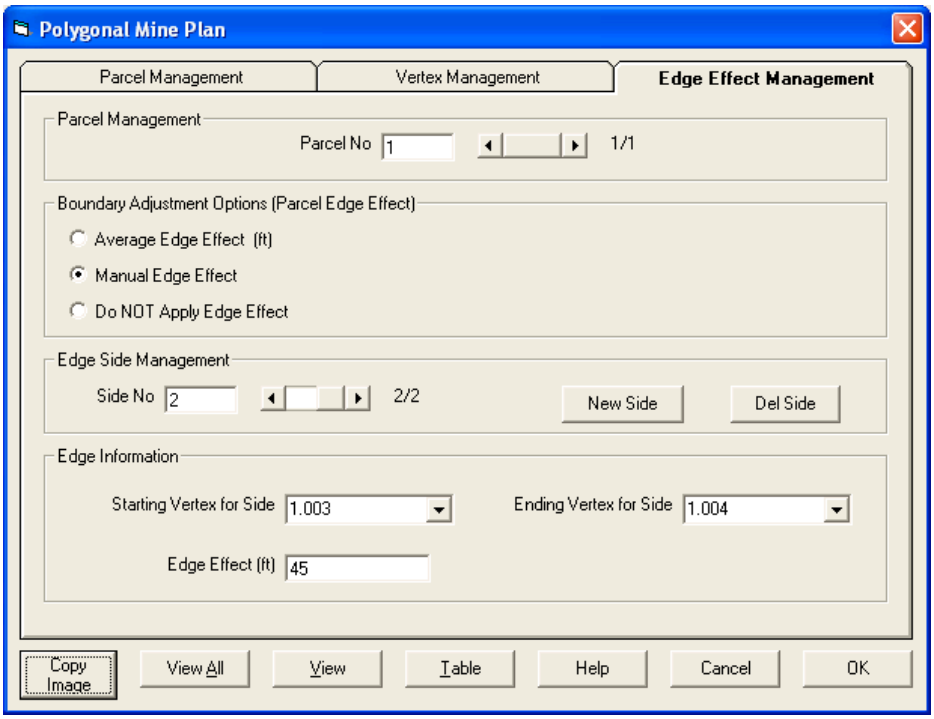

Figure 44: NA-3 Case Study, Panel 3 North - Edge Effect Management Screen, Side 2

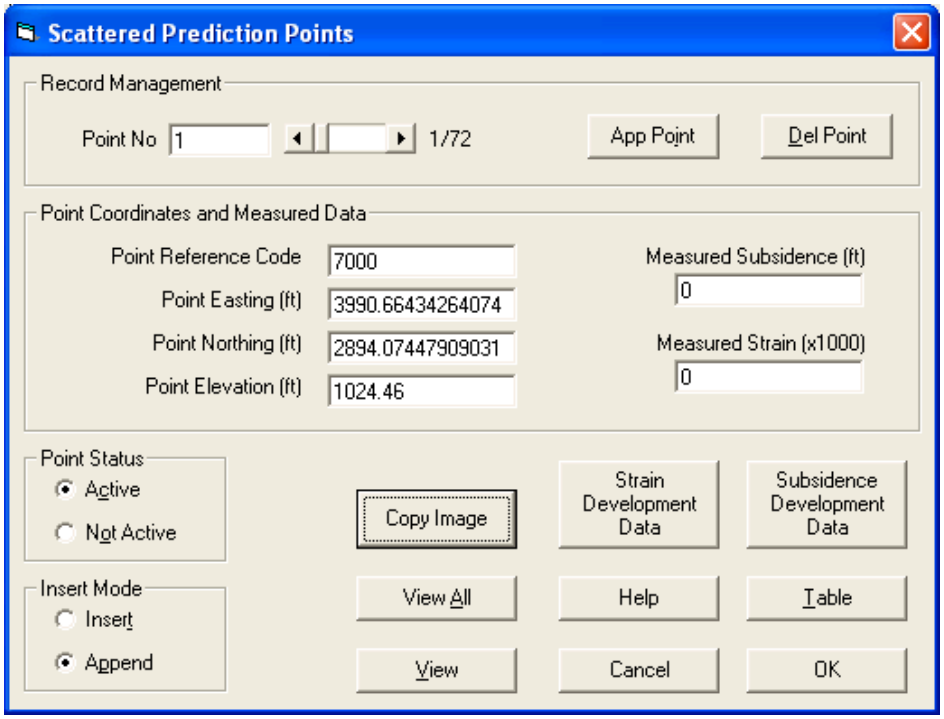

Figure 45: NA-3 Case Study, Panel 3 North - Prediction Points Management Screen (only first point shown)

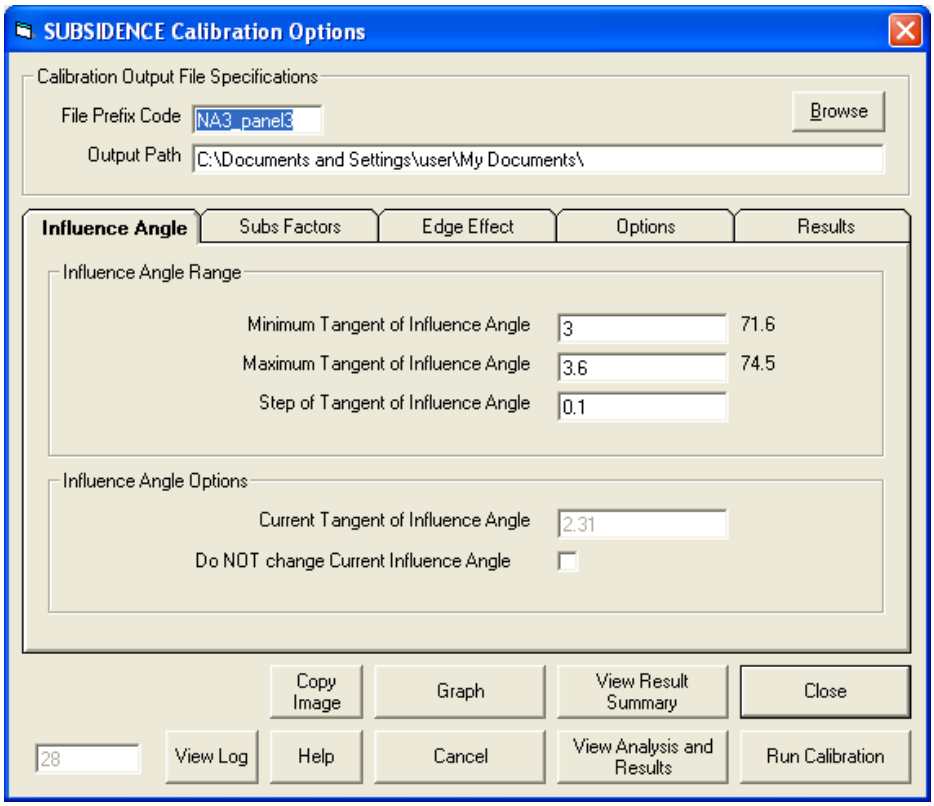

Figure 46: NA-3 Case Study, Panel 3 North - Subsidence Calibration Options Screen, Influence Angle Screen

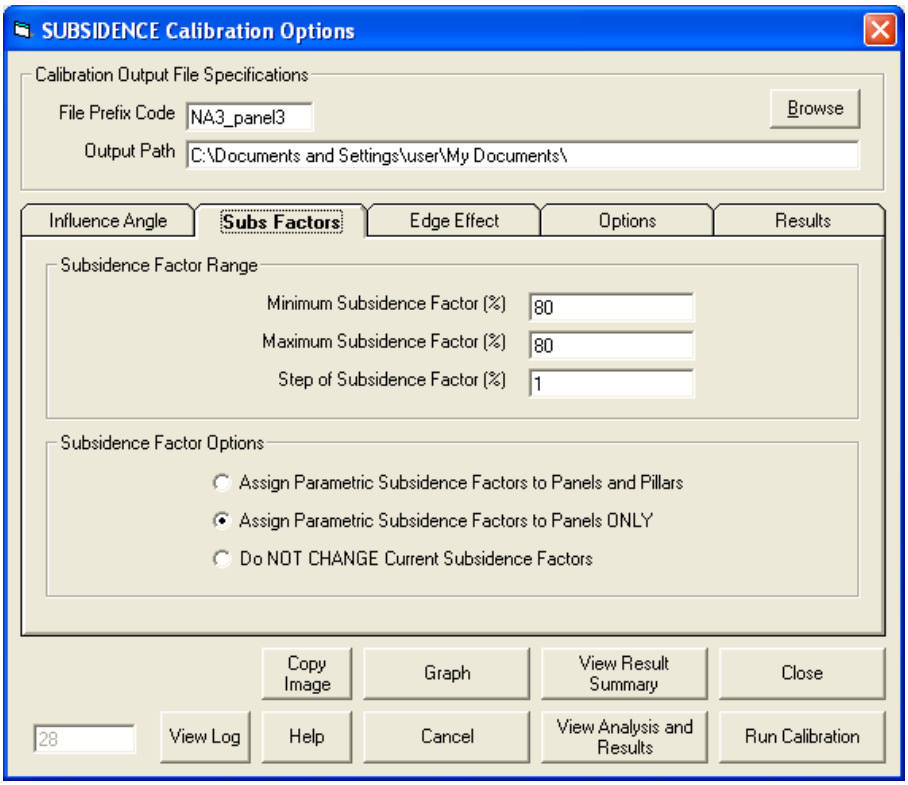

Figure 47: NA-3 Case Study, Panel 3 North - Subsidence Calibration Options Screen, Subsidence Factor Screen

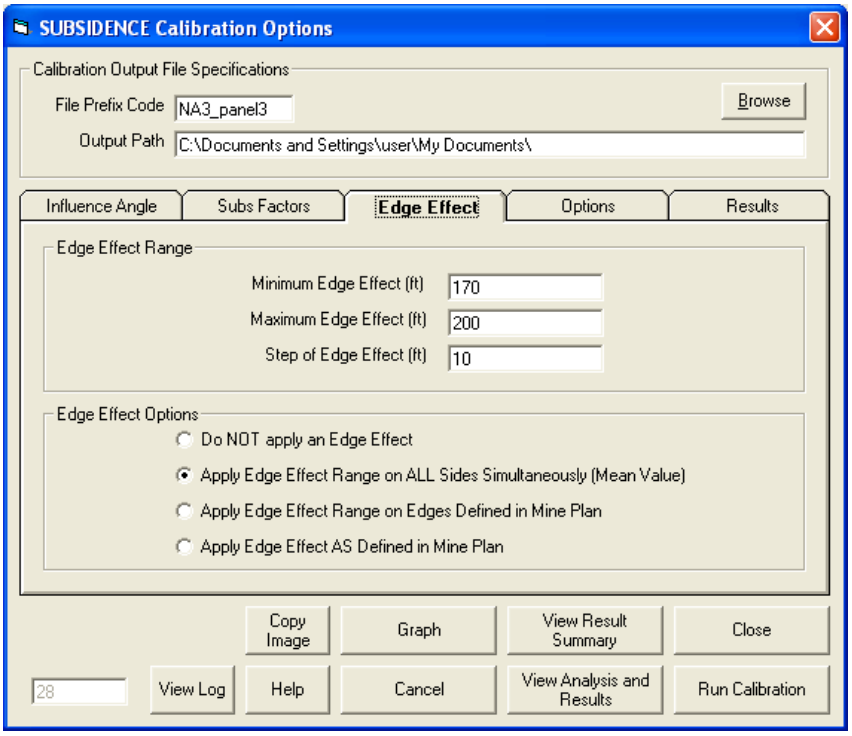

Figure 48: NA-3 Case Study, Panel 3 North - Subsidence Calibration Options Screen, Edge Effect Screen

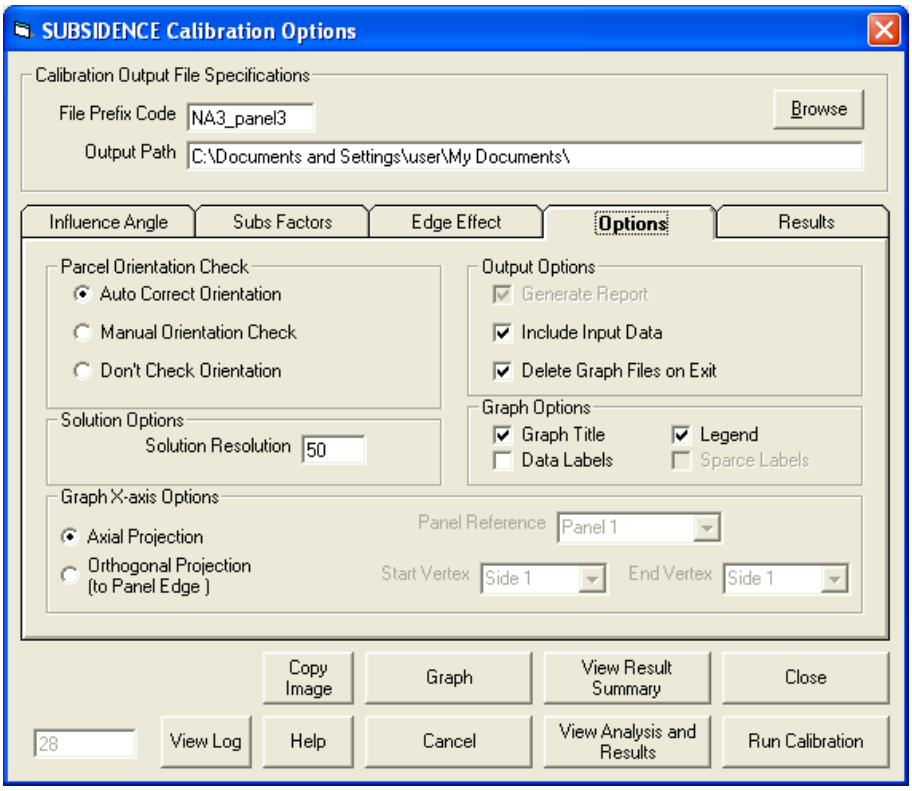

Figure 49: NA-3 Case Study, Panel 3 North - Subsidence Calibration Options Screen, Calibration Options Screen

IL-1 CASE STUDY (ILLINOIS) - MONUMENT LINE 5

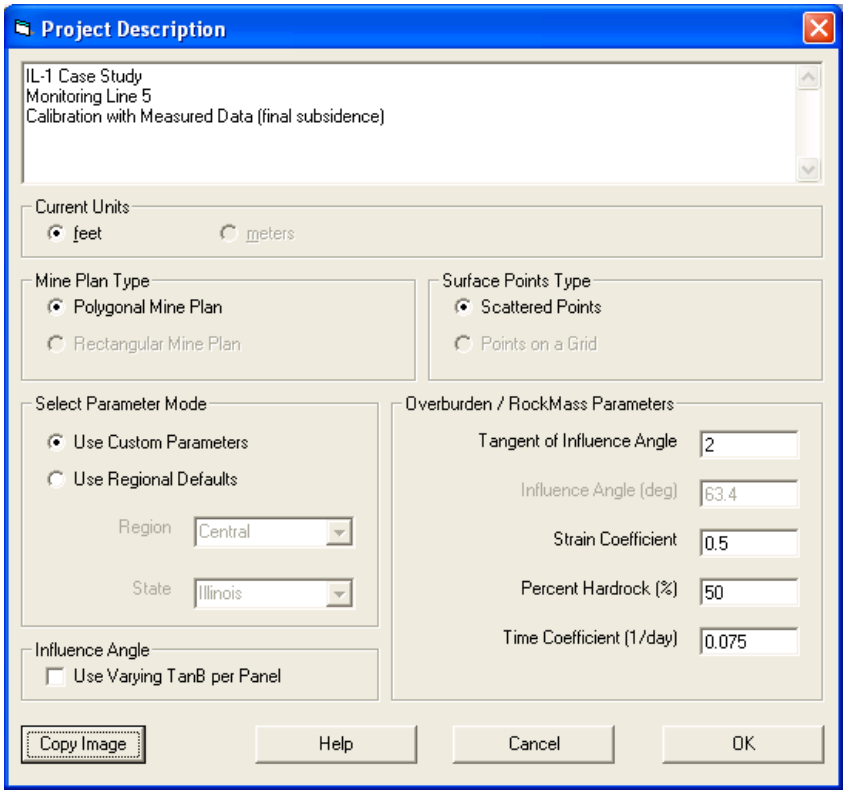

Figure 50: IL-1 Case Study, Monitoring Line 5 - SDPS Project Description Screen

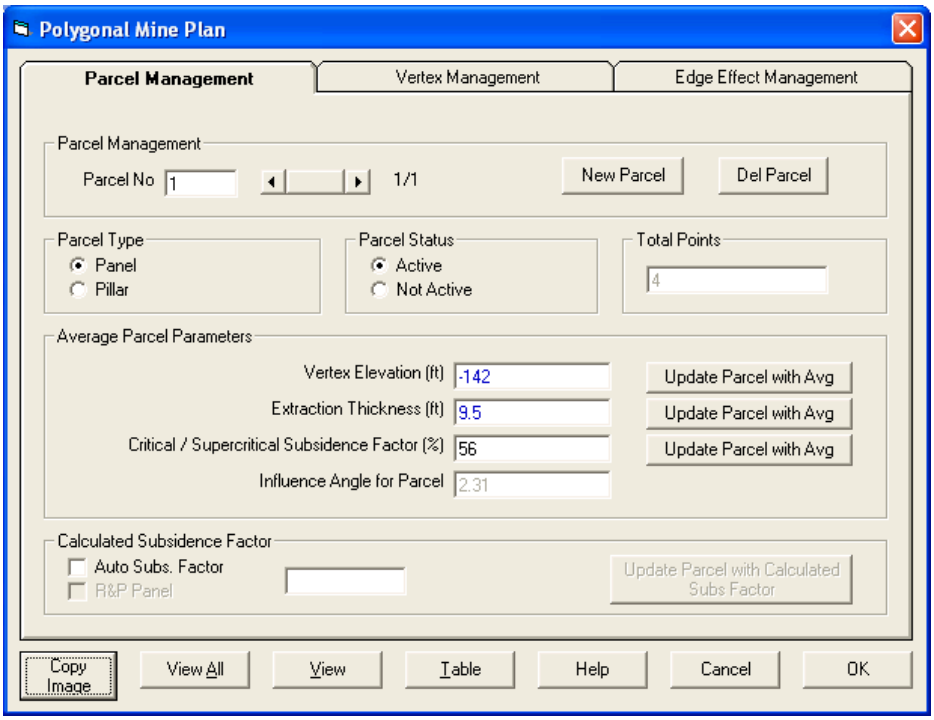

Figure 51: IL-1 Case Study, Monitoring Line 5 - Parcel Management Screen

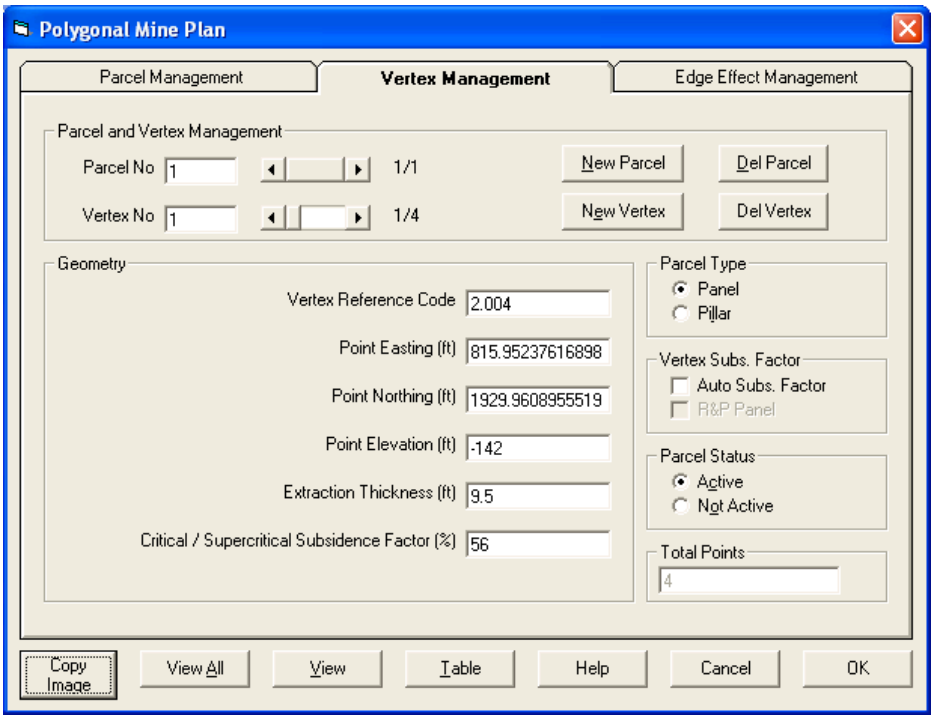

Figure 52: IL-1 Case Study, Monitoring Line 5 - Vertex Management Screen (Only One Vertex Shown)

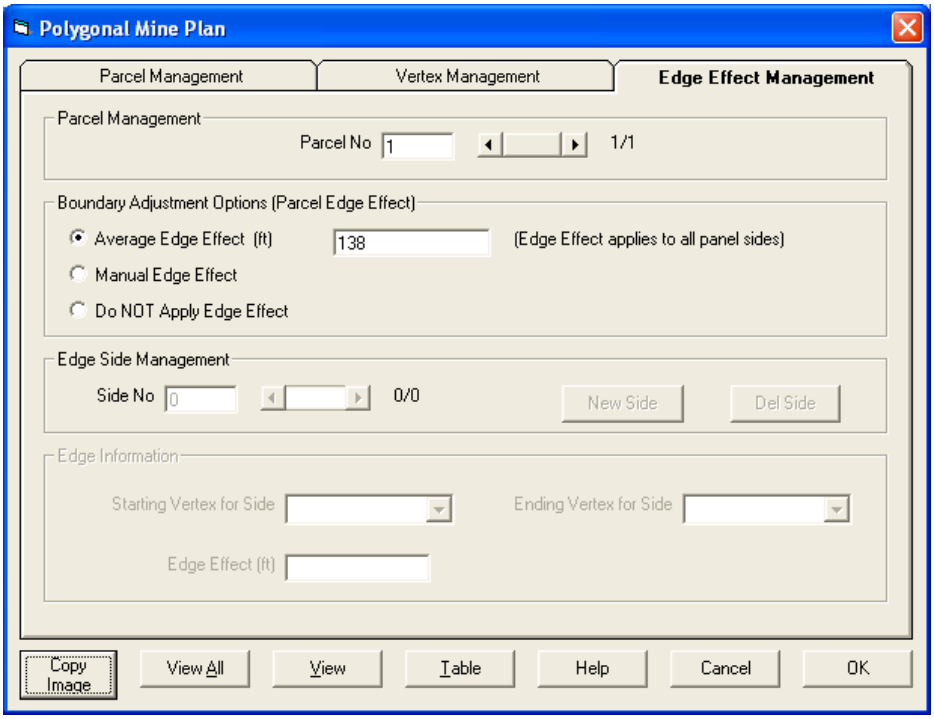

Figure 53: IL-1 Case Study, Monitoring Line 5 - Edge Effect Management Screen

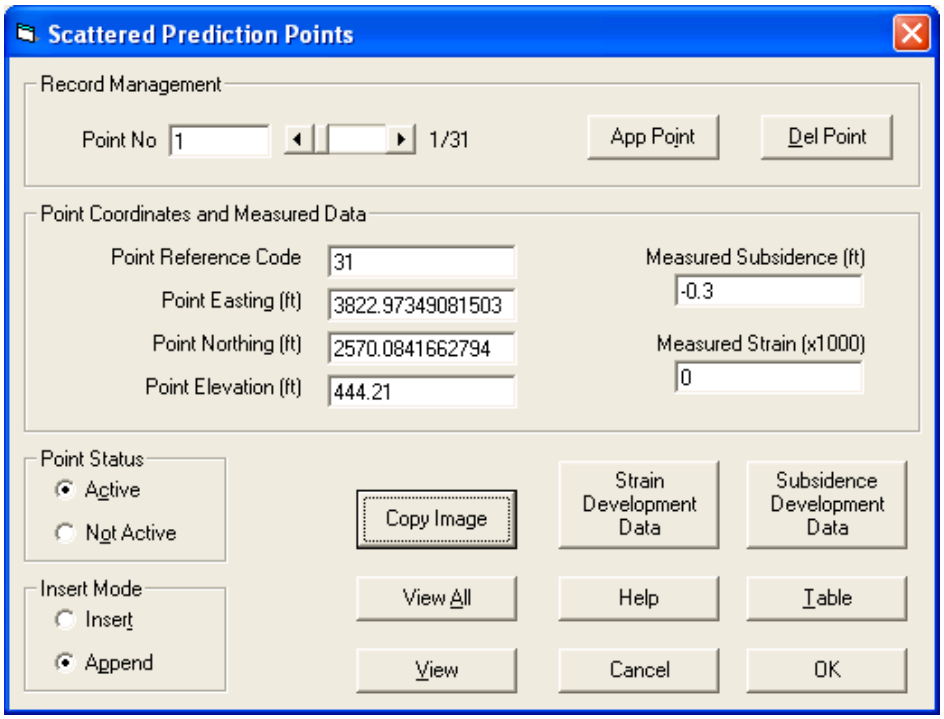

Figure 54: IL-1 Case Study, Monitoring Line 5 - Prediction Points Management Screen (only first point shown)

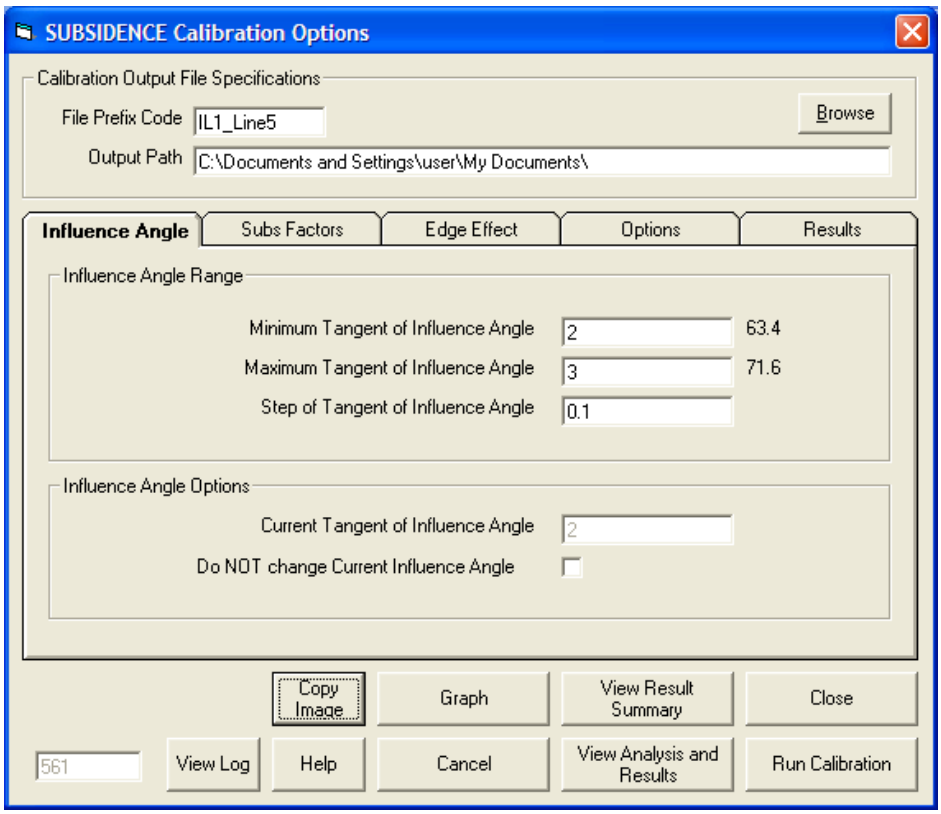

Figure 55: IL-1 Case Study, Monitoring Line 5 - Subsidence Calibration Options Screen, Influence Angle Screen

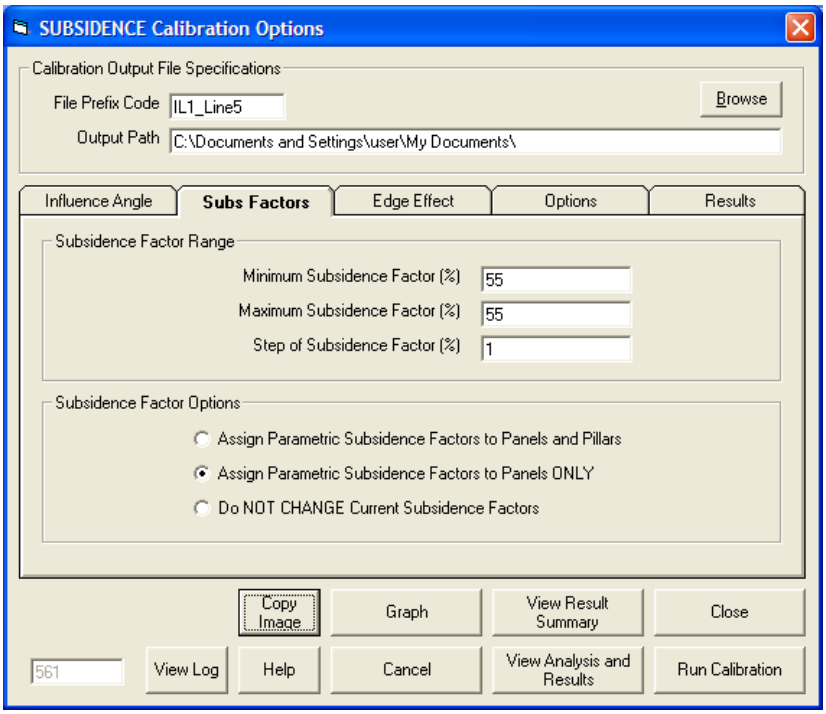

Figure 56: IL-1 Case Study, Monitoring Line 5 - Subsidence Calibration Options Screen, Subsidence Factor Screen

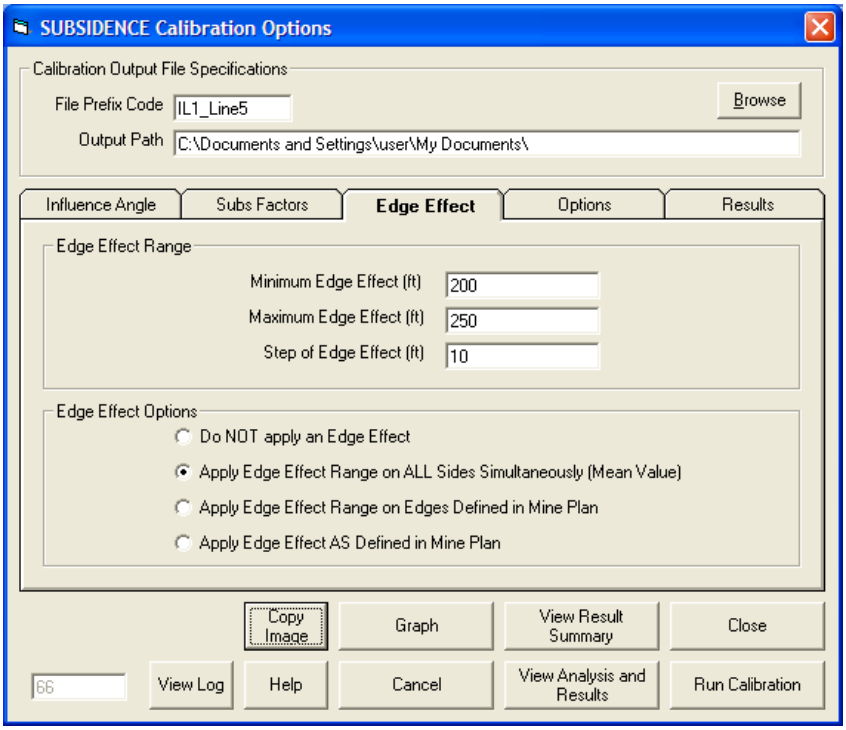

Figure 57: IL-1 Case Study, Monitoring Line 5 - Subsidence Calibration Options Screen, Edge Effect Screen

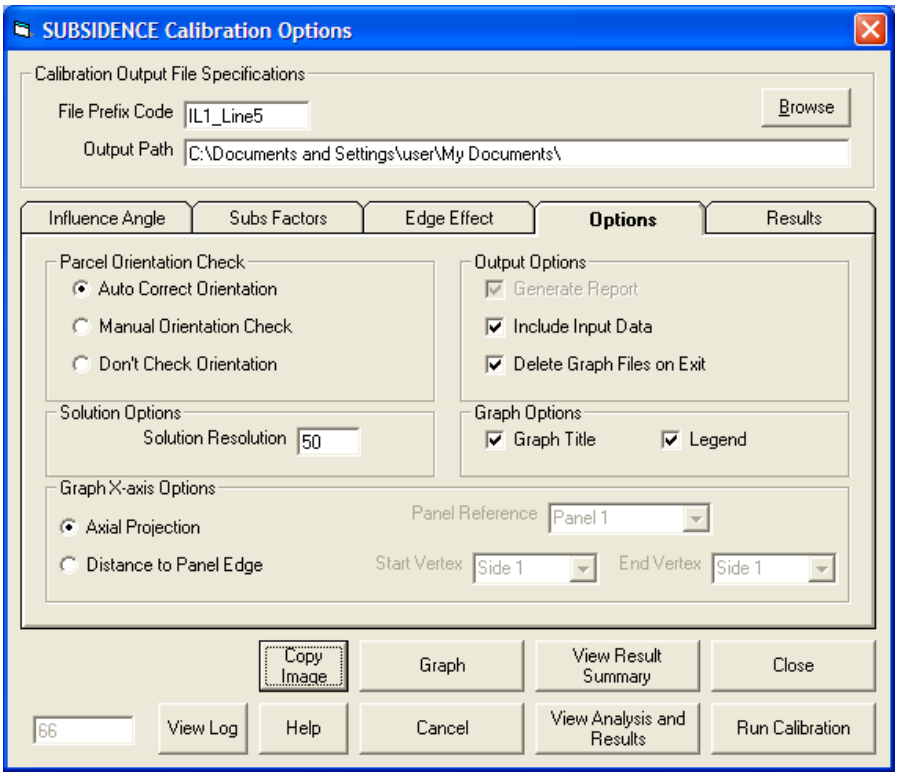

Figure 58: IL-1 Case Study, Monitoring Line 5 - Subsidence Calibration Options Screen, Calibration Options Screen

IL-1 CASE STUDY (ILLINOIS) - MONUMENT LINE 6

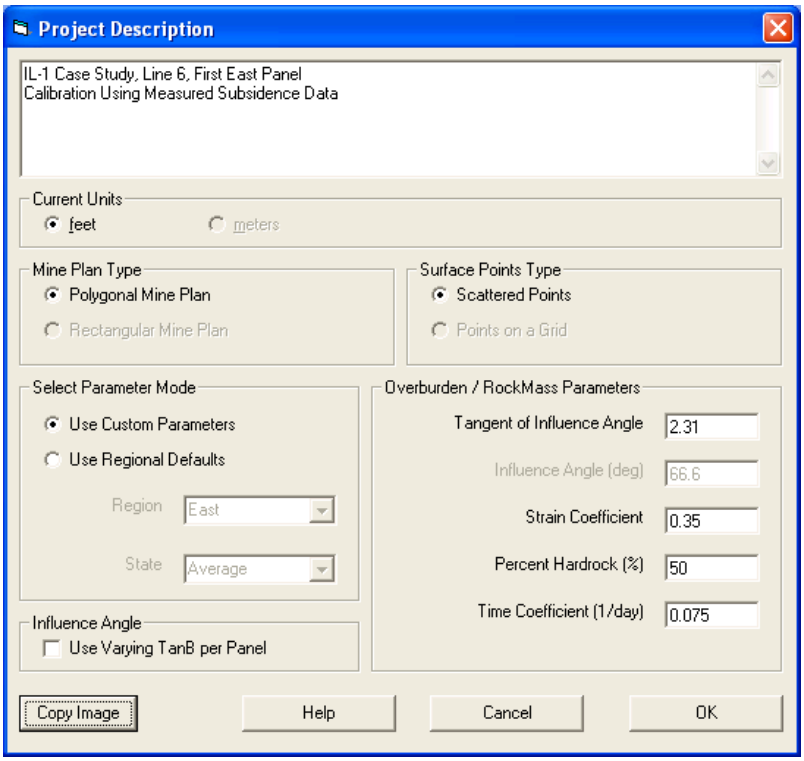

Figure 59: IL-1 Case Study, Monitoring Line 6 - SDPS Project Description Screen

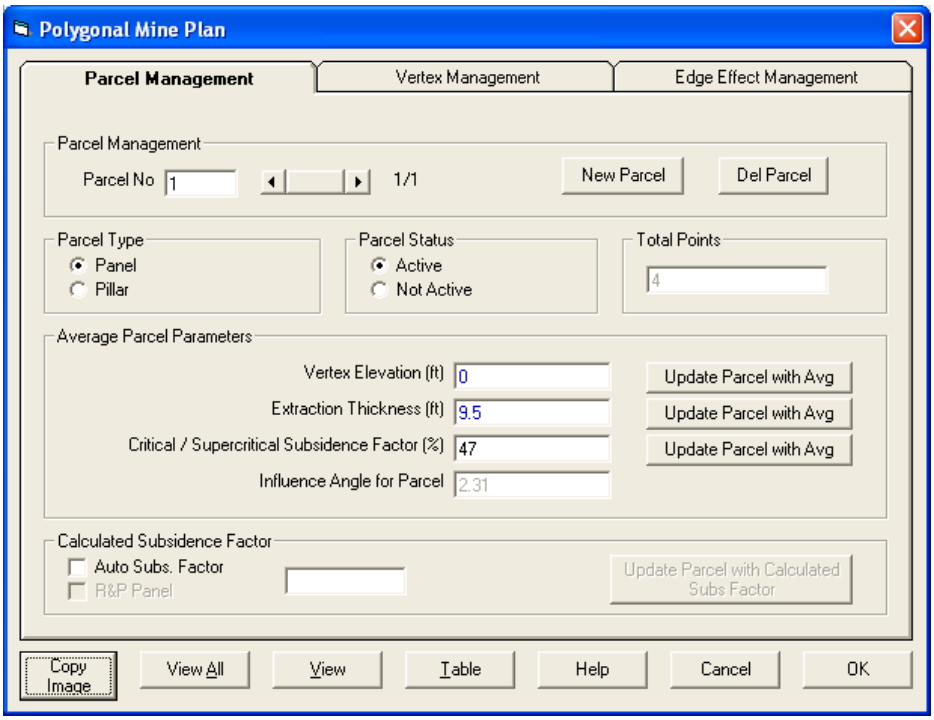

Figure 60: IL-1 Case Study, Monitoring Line 6 - Parcel Management Screen

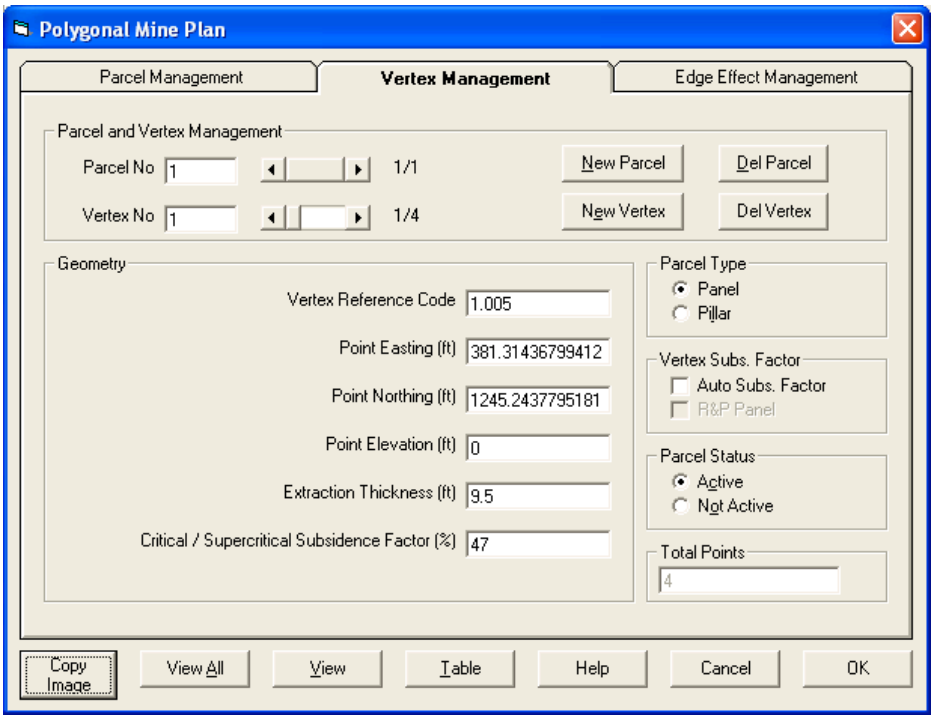

Figure 61: IL-1 Case Study, Monitoring Line 6 - Vertex Management Screen (Only One Vertex Shown)

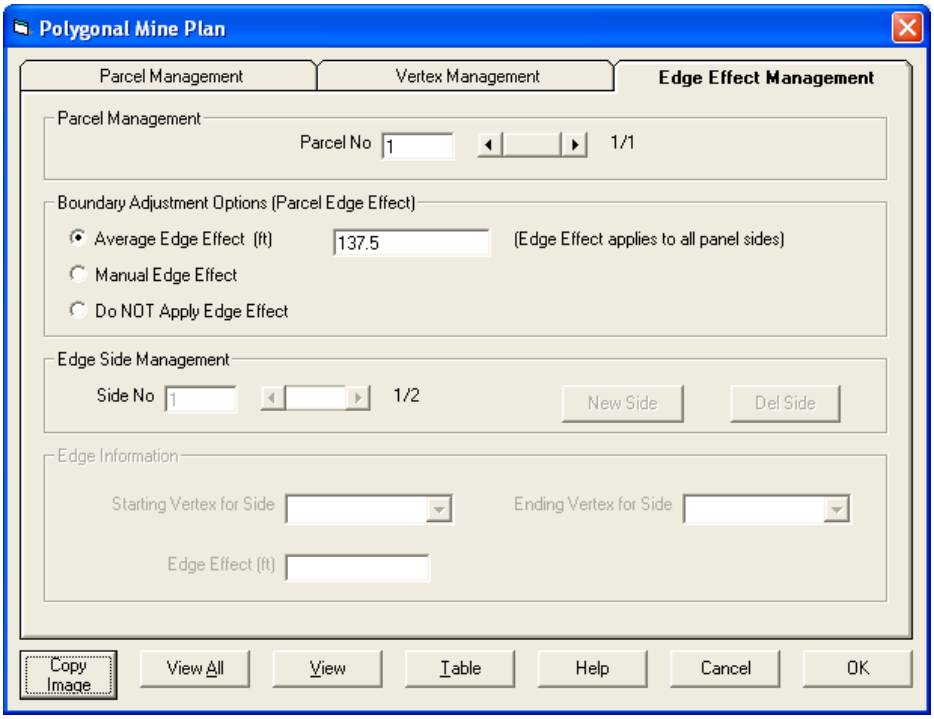

Figure 62: IL-1 Case Study, Monitoring Line 6 - Edge Effect Management Screen

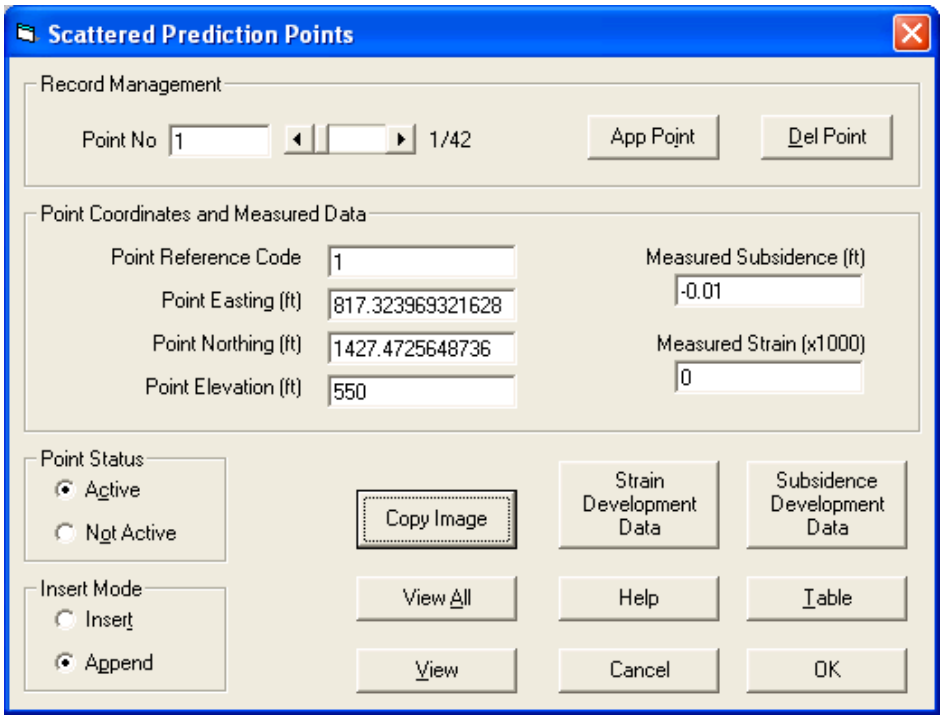

Figure 63: IL-1 Case Study, Monitoring Line 6 - Prediction Points Management Screen (only first point shown)

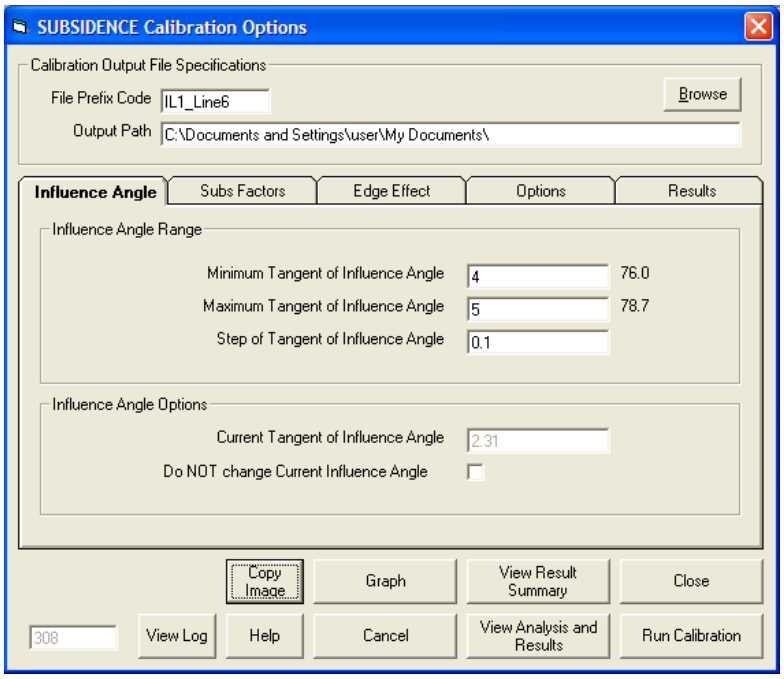

Figure 64: IL-1 Case Study, Monitoring Line 6 - Subsidence Calibration Options Screen, Influence Angle Screen

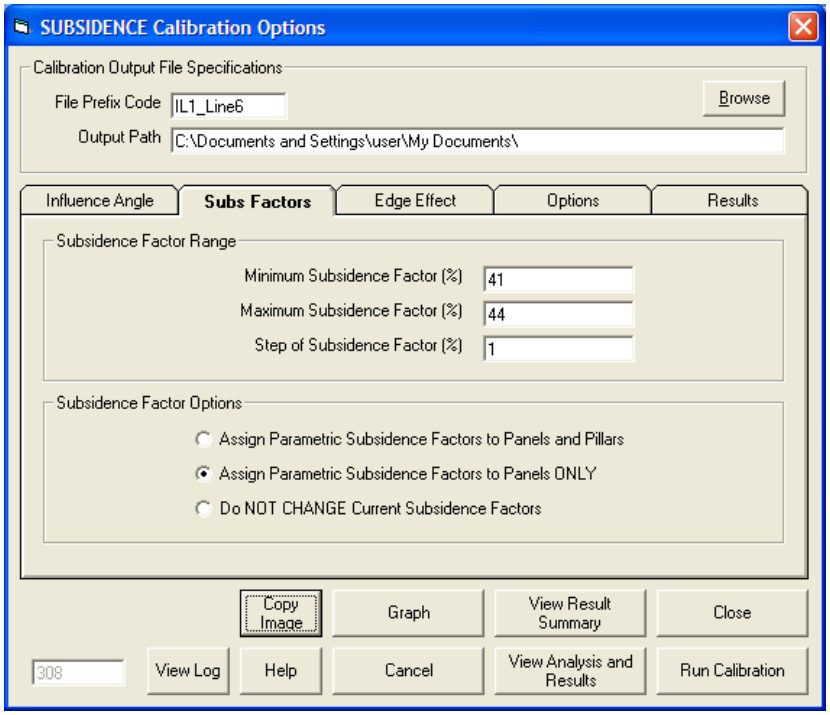

Figure 65: IL-1 Case Study, Monitoring Line 6 - Subsidence Calibration Options Screen, Subsidence Factor Screen

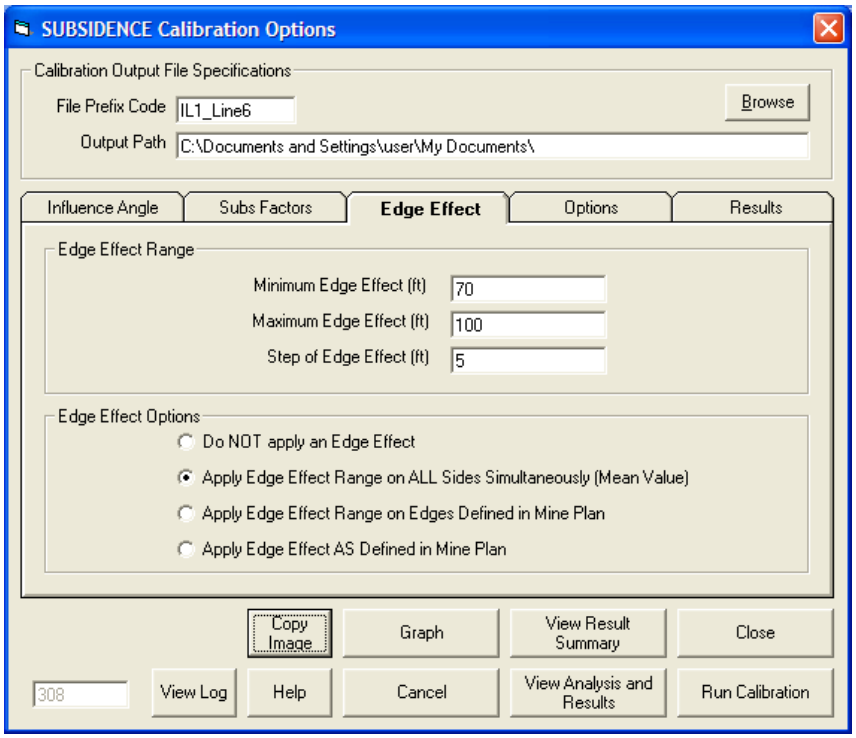

Figure 66: IL-1 Case Study, Monitoring Line 6 - Subsidence Calibration Options Screen, Edge Effect Screen

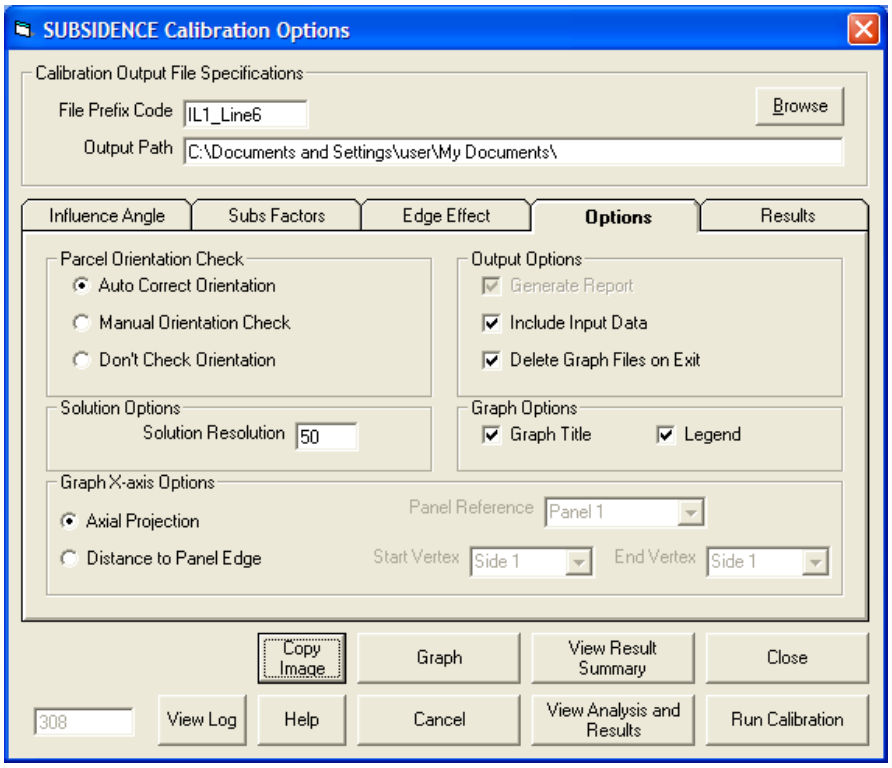

Figure 67: IL-1 Case Study, Monitoring Line 6 - Subsidence Calibration Options Screen, Calibration Options Screen

IL-2 CASE STUDY (ILLINOIS)

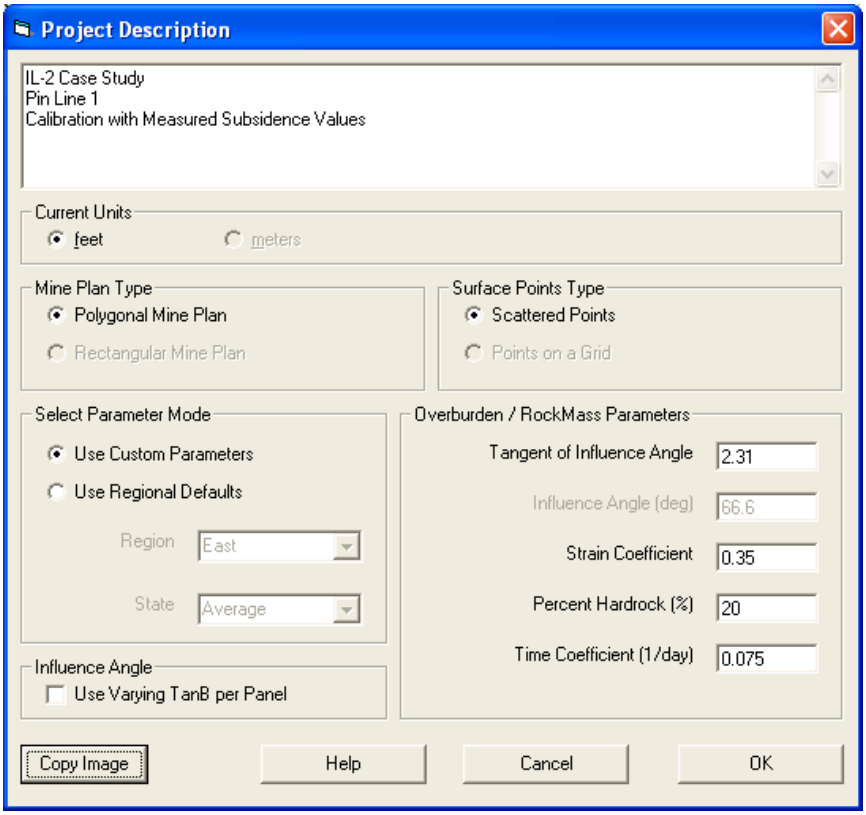

Figure 68: IL-2 Case Study - SDPS Project Description Screen

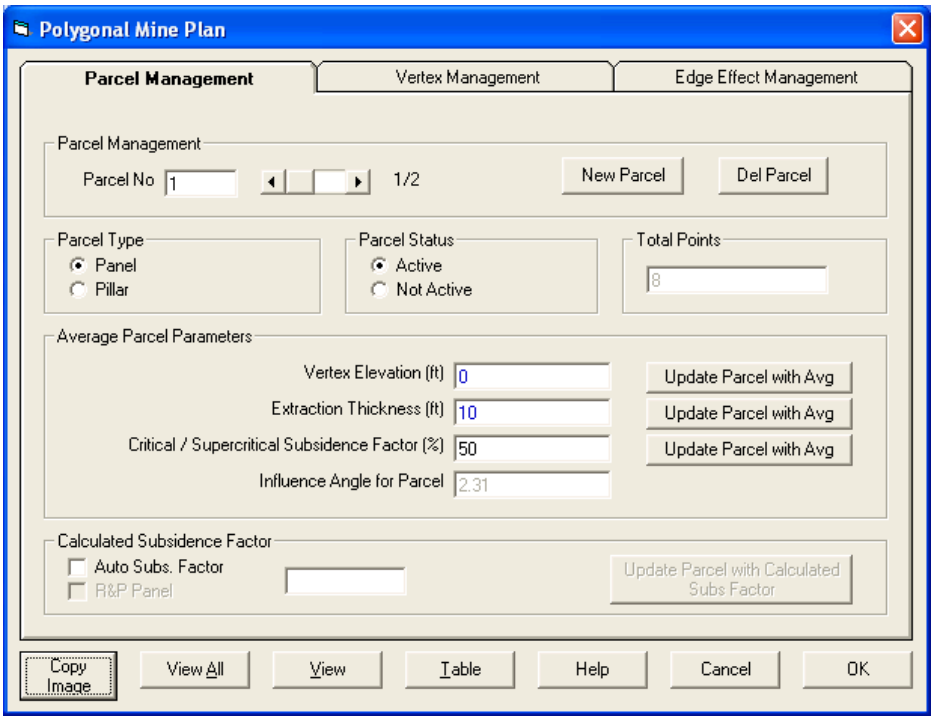

Figure 69: IL-2 Case Study - Parcel Management Screen, Parcel 1

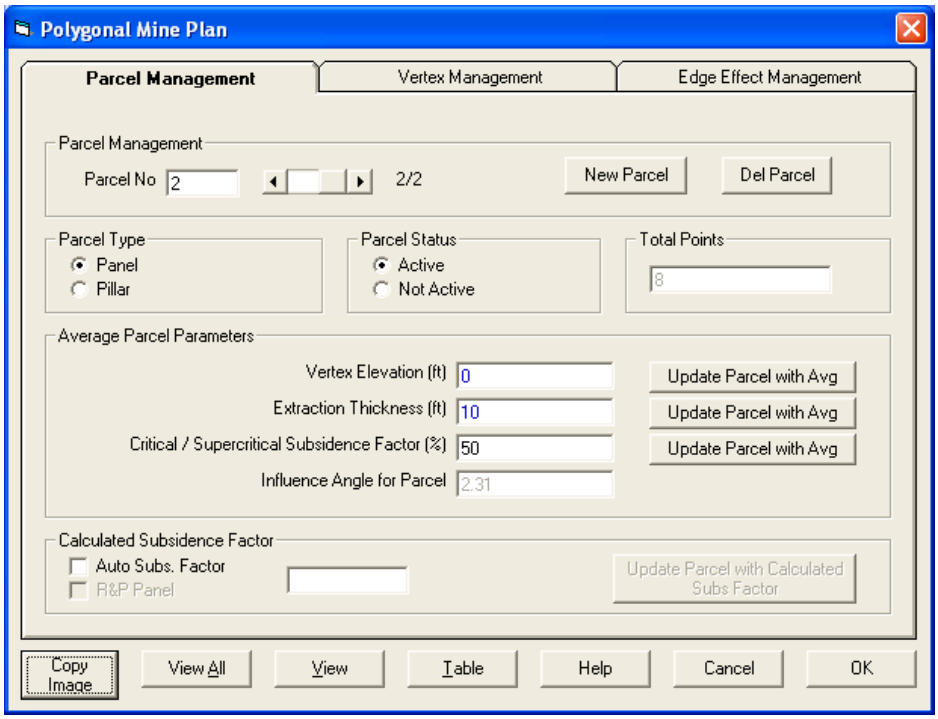

Figure 70: IL-2 Case Study - Parcel Management Screen, Parcel 2

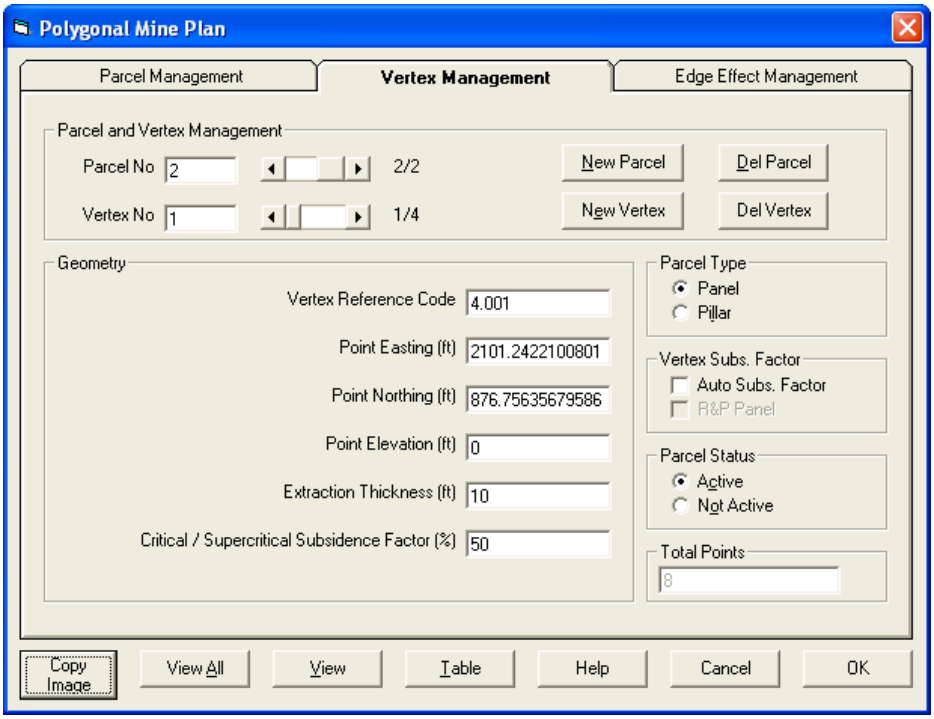

Figure 71: IL-2 Case Study - Vertex Management Screen (Only One Vertex of One Panel Shown)

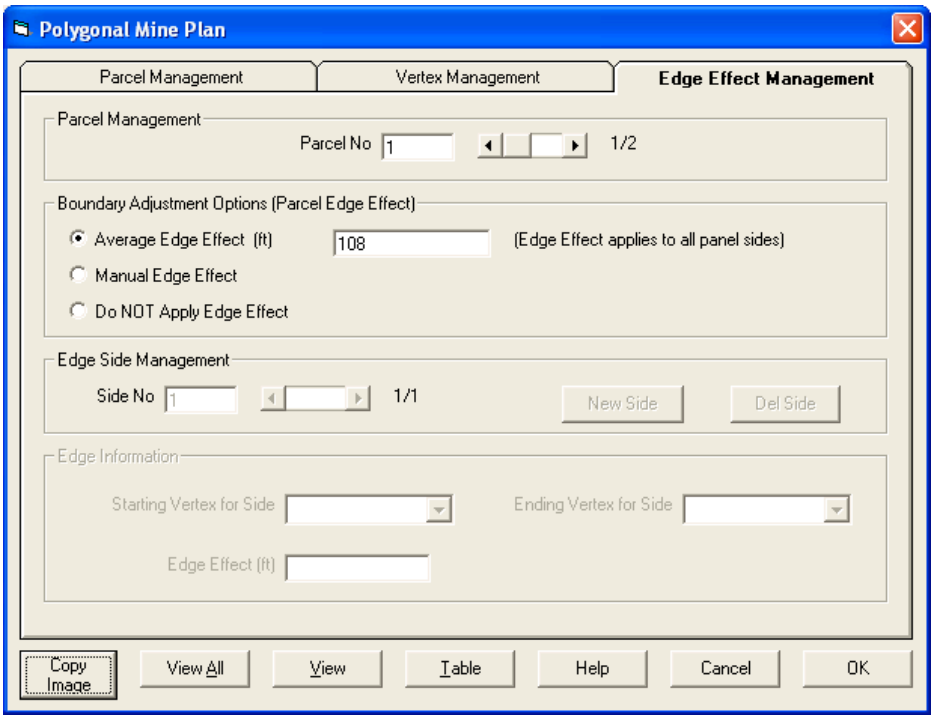

Figure 72: IL-2 Case Study - Edge Effect Management Screen, Parcel 1

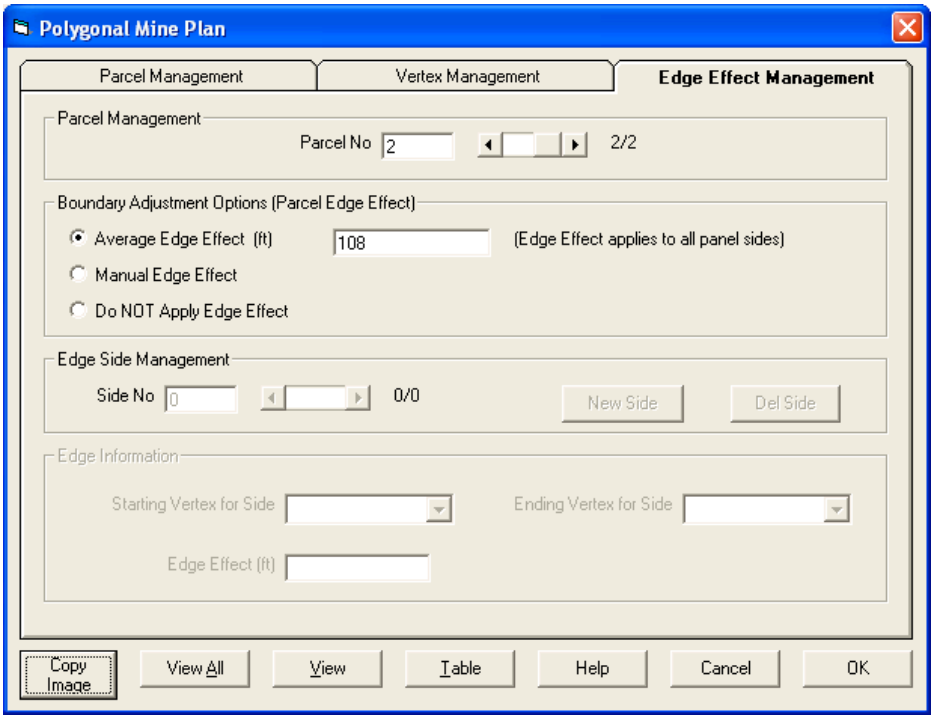

Figure 73: IL-2 Case Study - Edge Effect Management Screen, Parcel 2

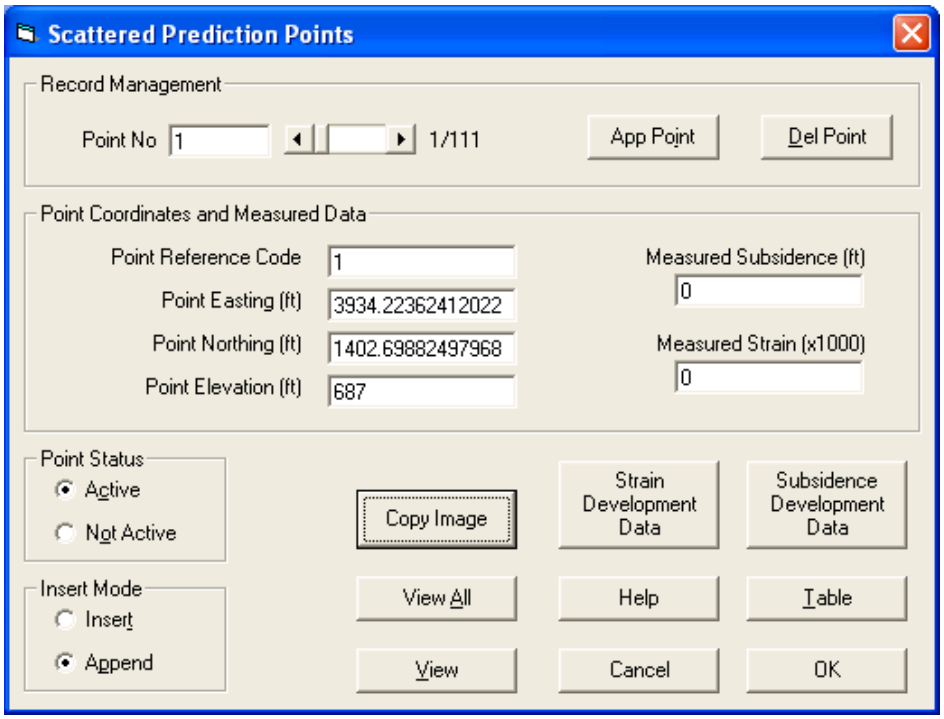

Figure 74: IL-2 Case Study - Prediction Points Management Screen (only first point shown)

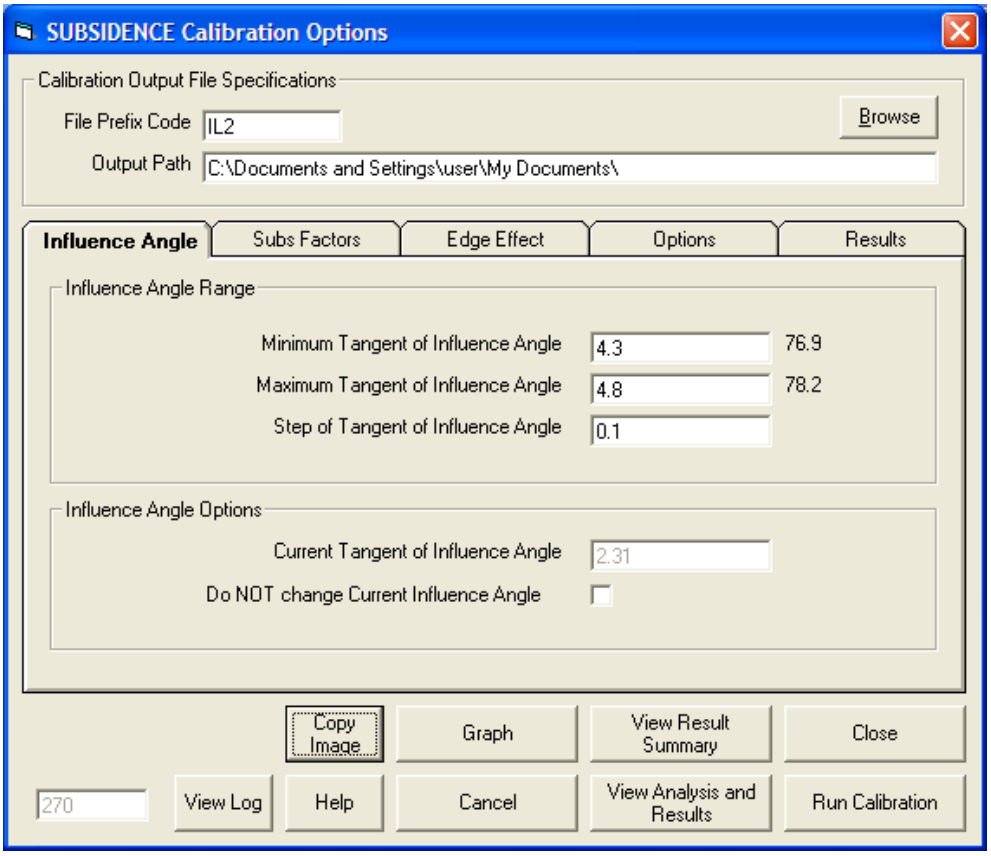

Figure 75: IL-2 Case Study - Subsidence Calibration Options Screen, Influence Angle Screen

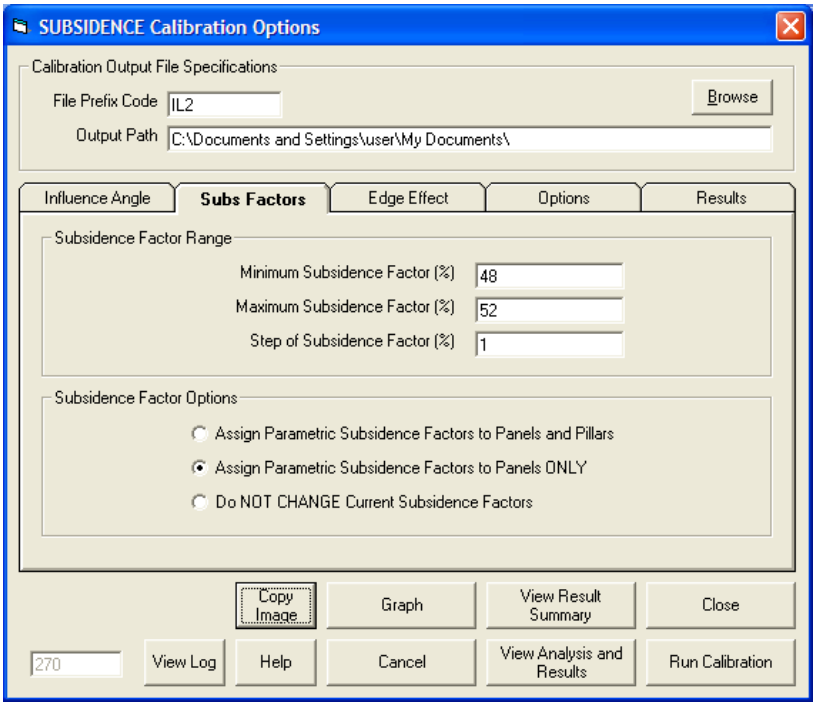

Figure 76: IL-2 Case Study - Subsidence Calibration Options Screen, Subsidence Factor Screen

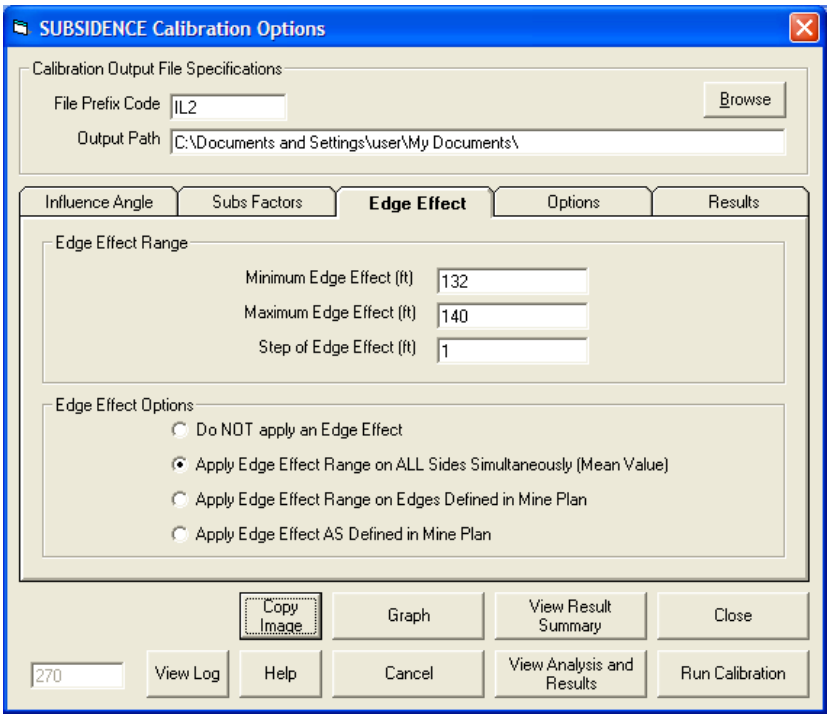

Figure 77: IL-2 Case Study - Subsidence Calibration Options Screen, Edge Effect Screen

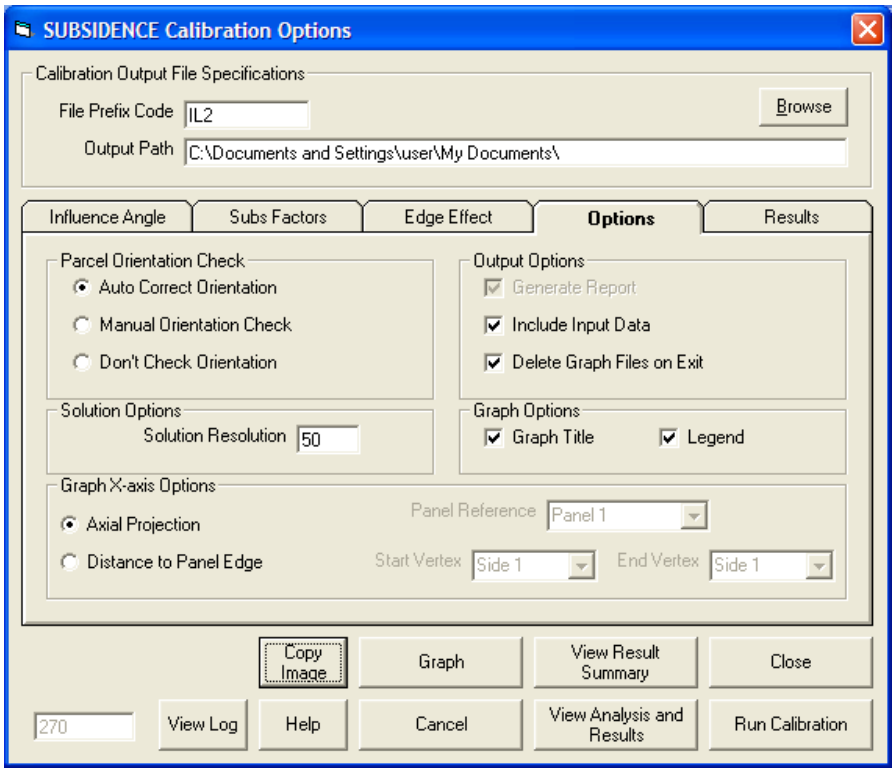

Figure 78: IL-2 Case Study - Subsidence Calibration Options Screen, Calibration Options Screen

AL-1 CASE STUDY (ALABAMA)

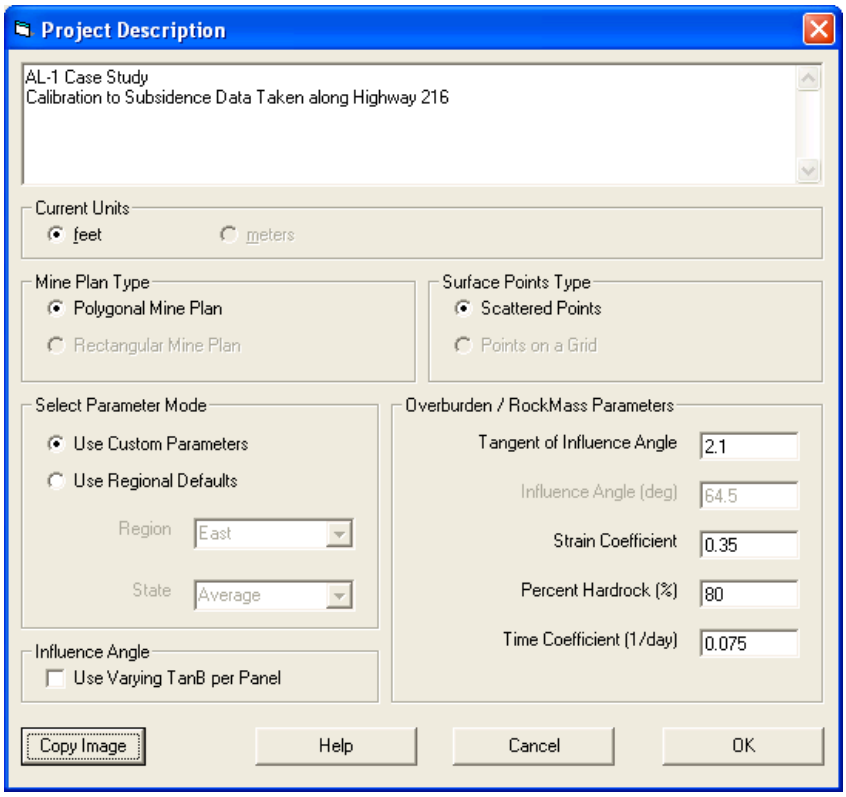

Figure 79: AL-1 Case Study - SDPS Project Description Screen

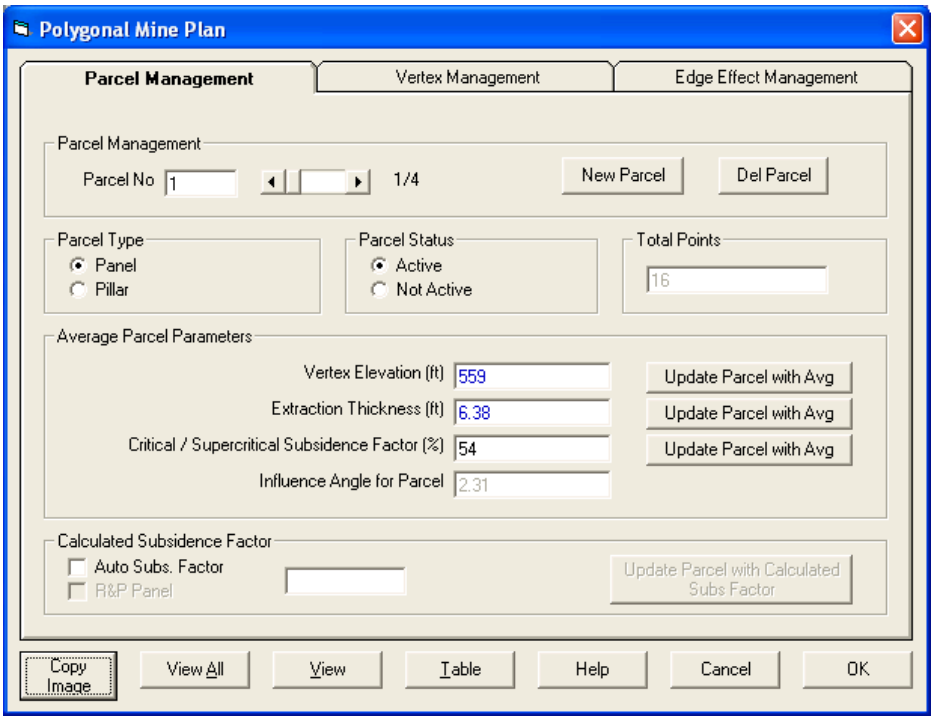

Figure 80: AL-1 Case Study - Parcel Management Screen, Parcel 1

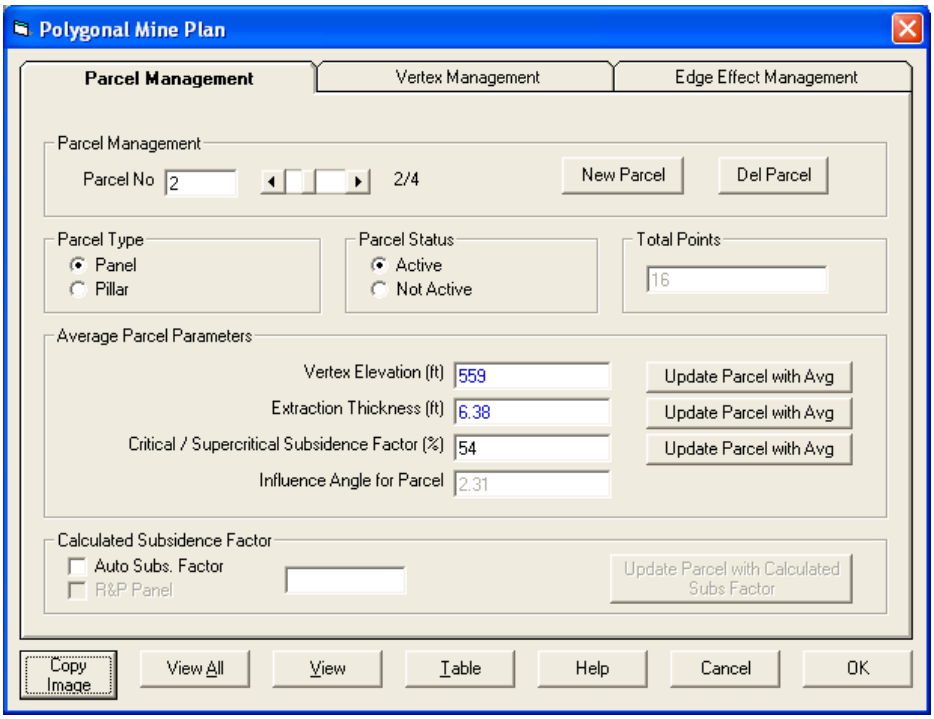

Figure 81: AL-1 Case Study - Parcel Management Screen, Parcel 2

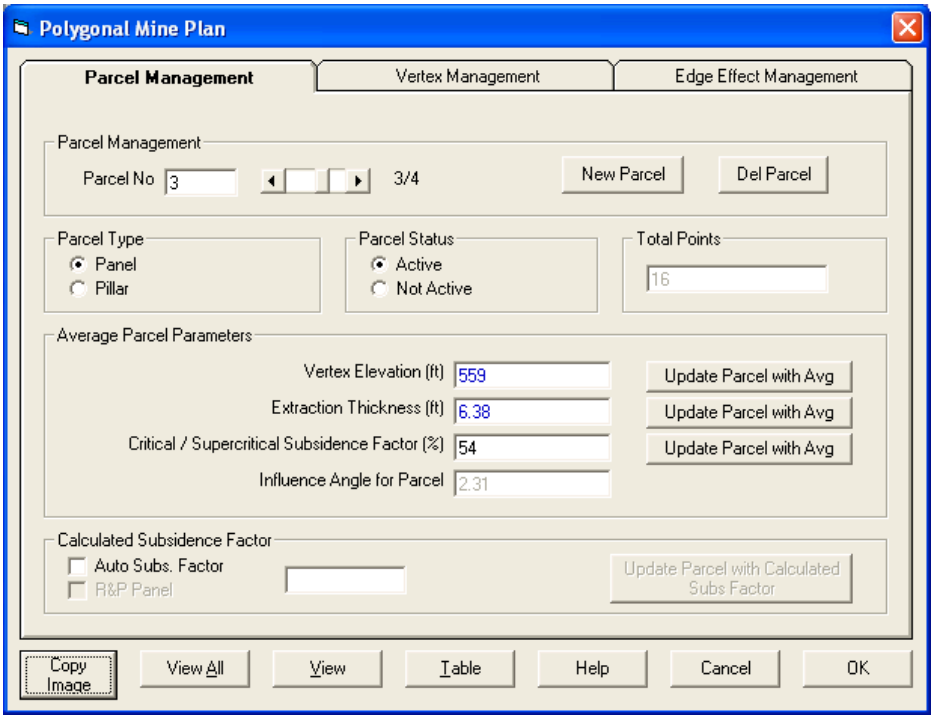

Figure 82: AL-1 Case Study - Parcel Management Screen, Parcel 3

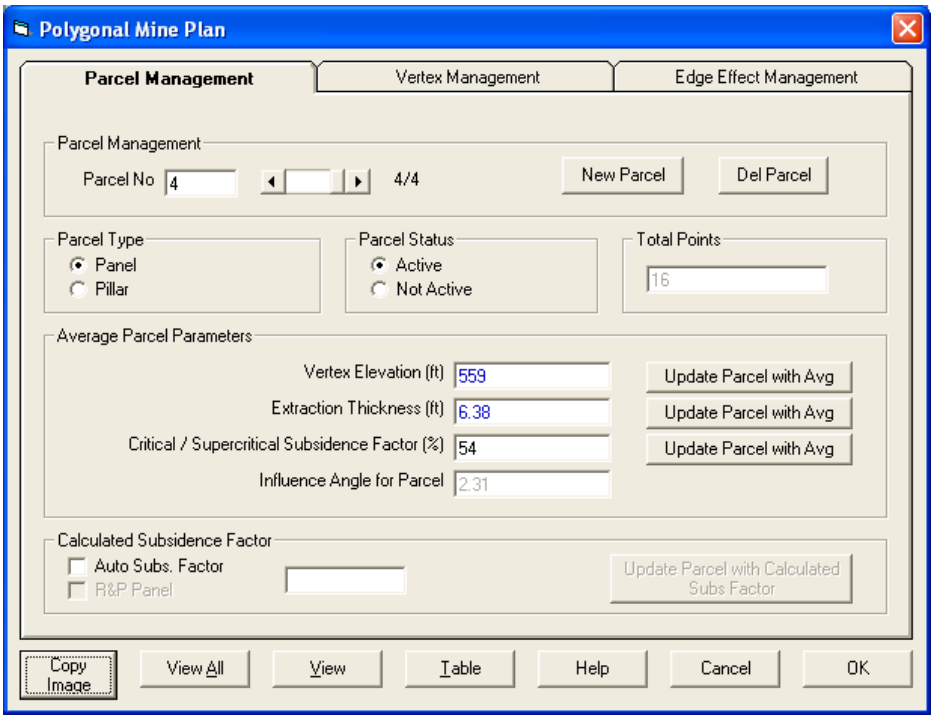

Figure 83: AL-1 Case Study - Parcel Management Screen, Parcel 4

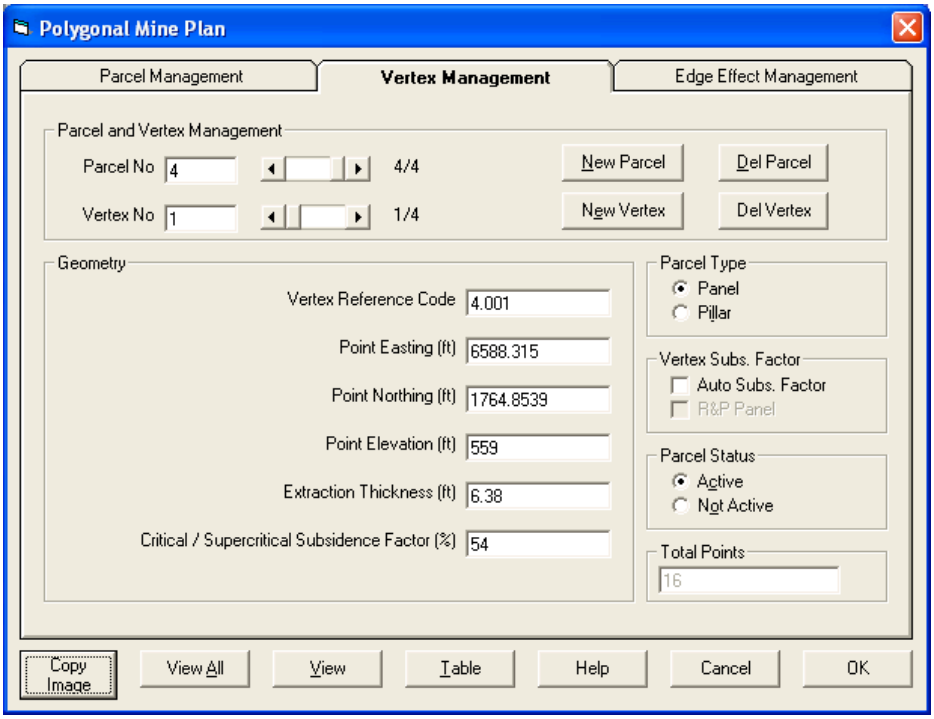

Figure 84: AL-1 Case Study - Vertex Management Screen (Only One Vertex for One Parcel Shown)

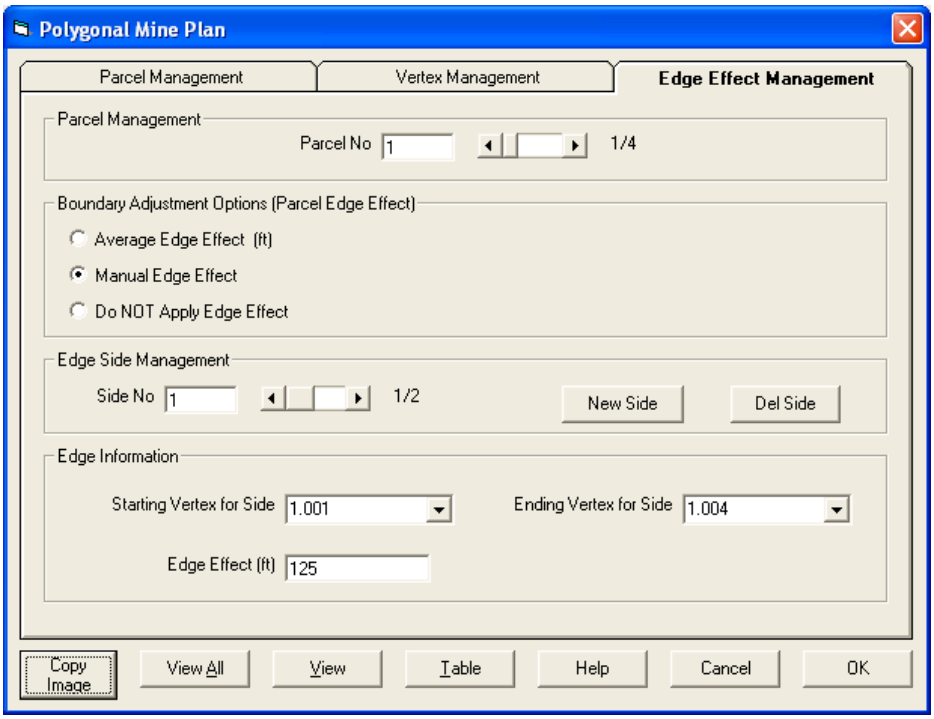

Figure 85: AL-1 Case Study - Edge Effect Management Screen, Side 1 of Parcel 1

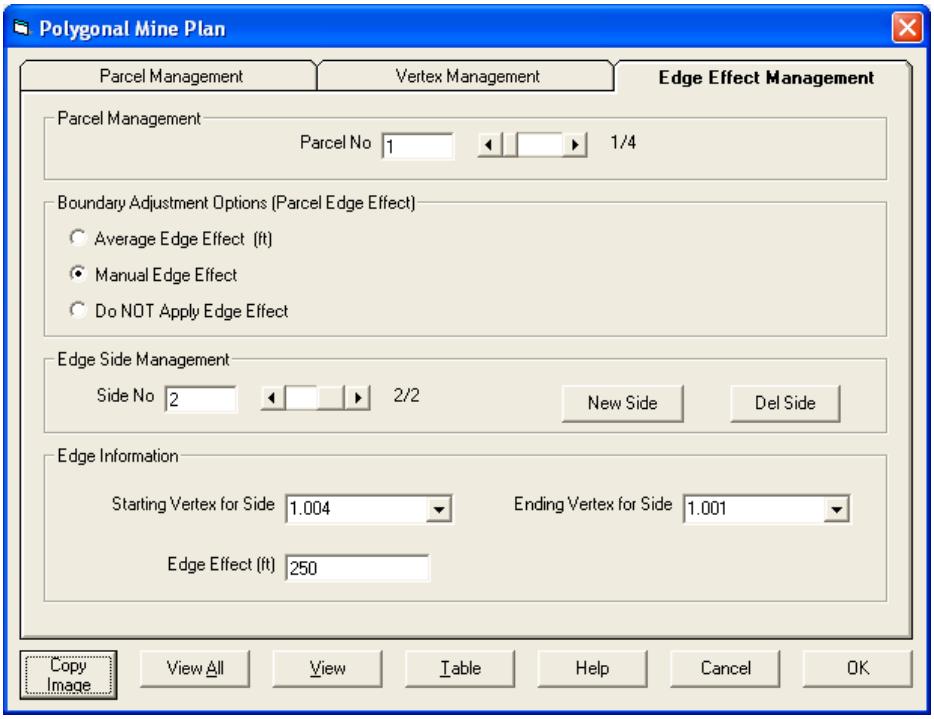

Figure 86: AL-1 Case Study - Edge Effect Management Screen, Side 2 of Parcel 1

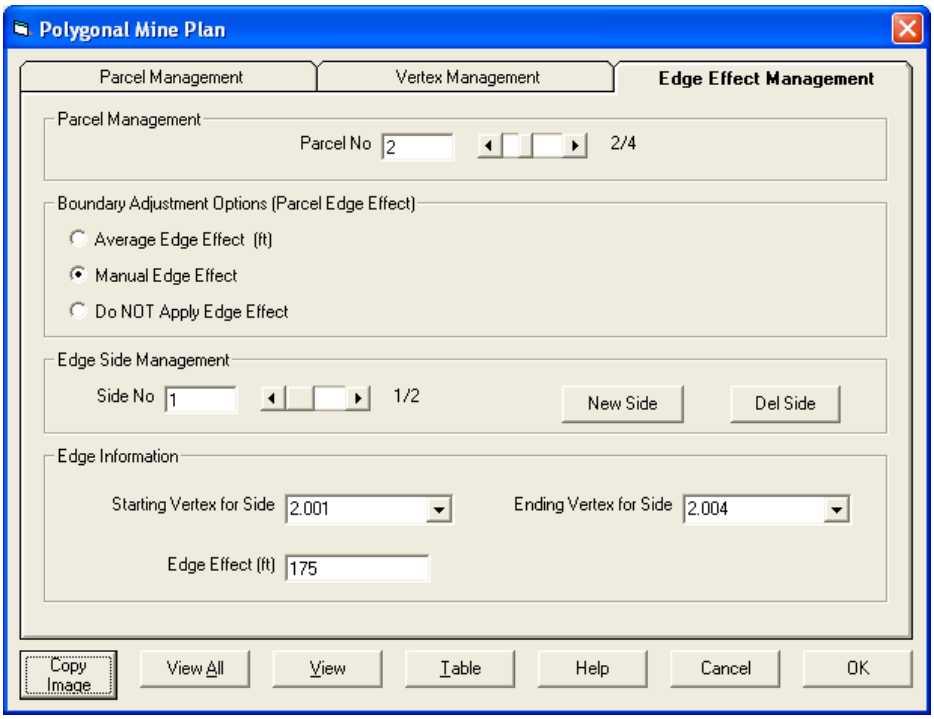

Figure 87: AL-1 Case Study - Edge Effect Management Screen, Side 1 of Parcel 2

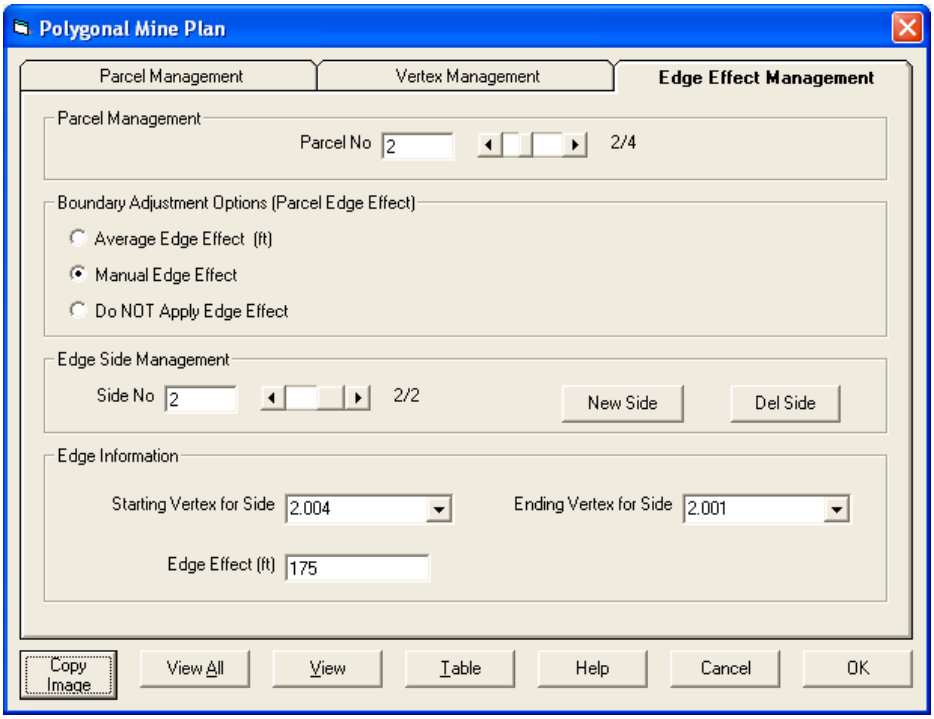

Figure 88: AL-1 Case Study - Edge Effect Management Screen, Side 2 of Parcel 2

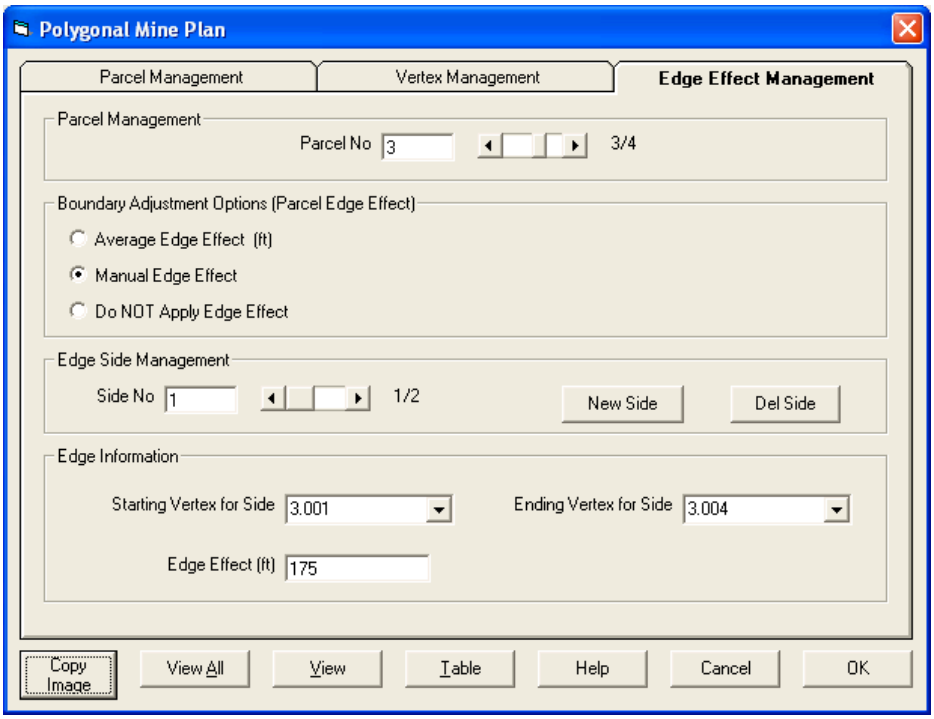

Figure 89: AL-1 Case Study - Edge Effect Management Screen, Side 1 of Parcel 3

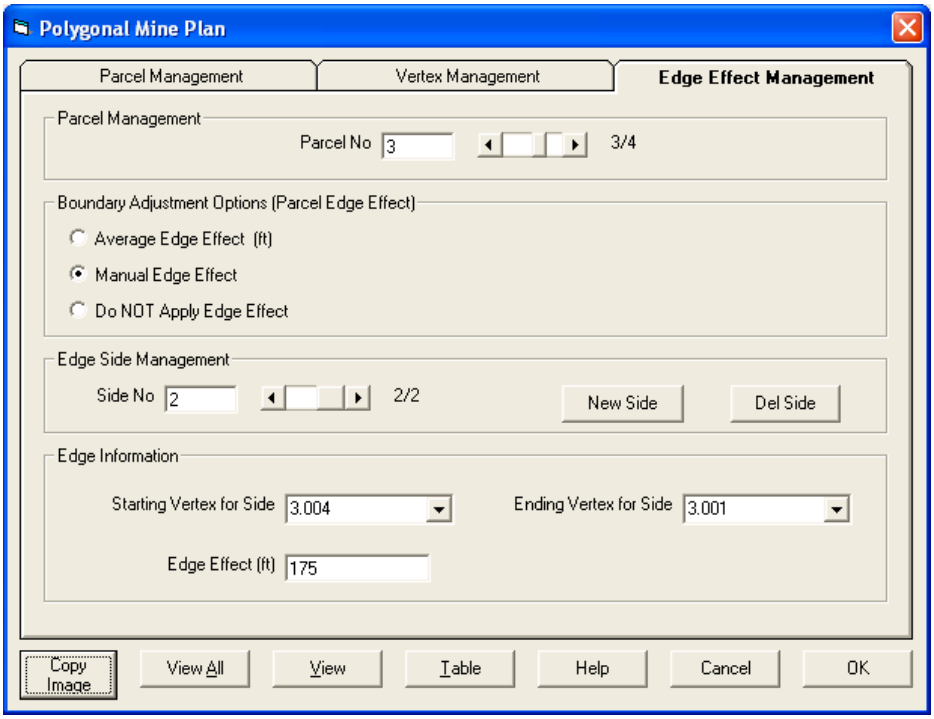

Figure 90: AL-1 Case Study - Edge Effect Management Screen, Side 2 of Parcel 3

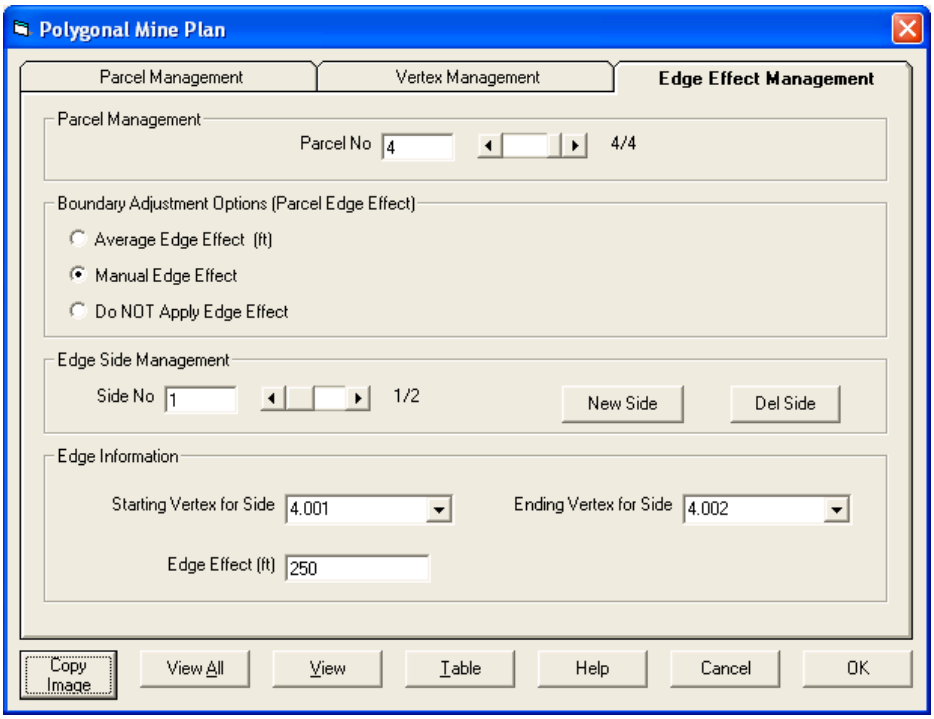

Figure 91: AL-1 Case Study - Edge Effect Management Screen, Side 1 of Parcel 4

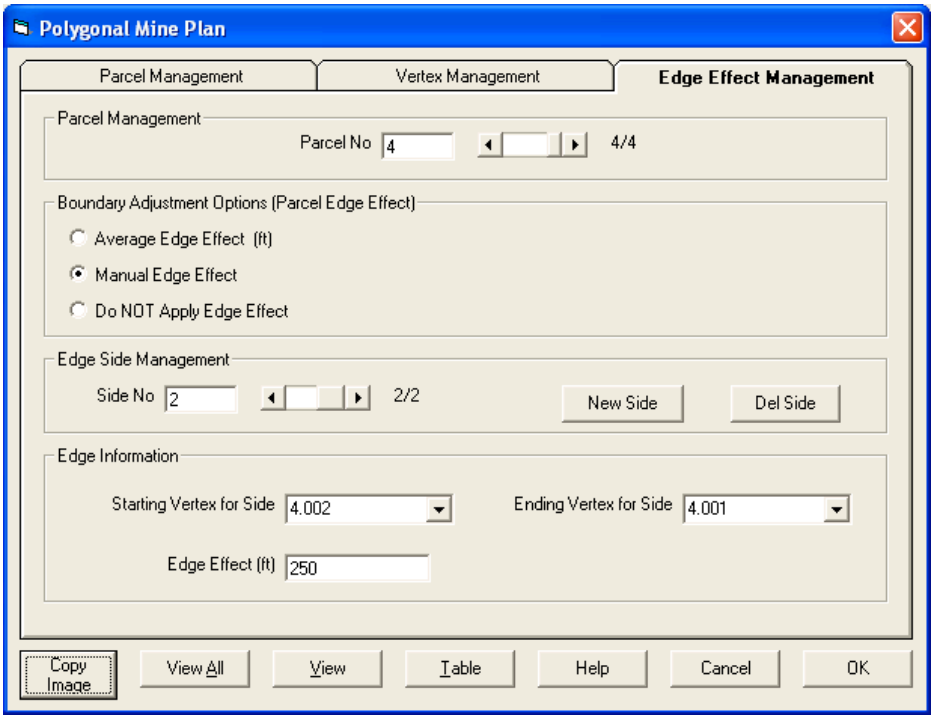

Figure 92: AL-1 Case Study - Edge Effect Management Screen, Side 2 of Parcel 4

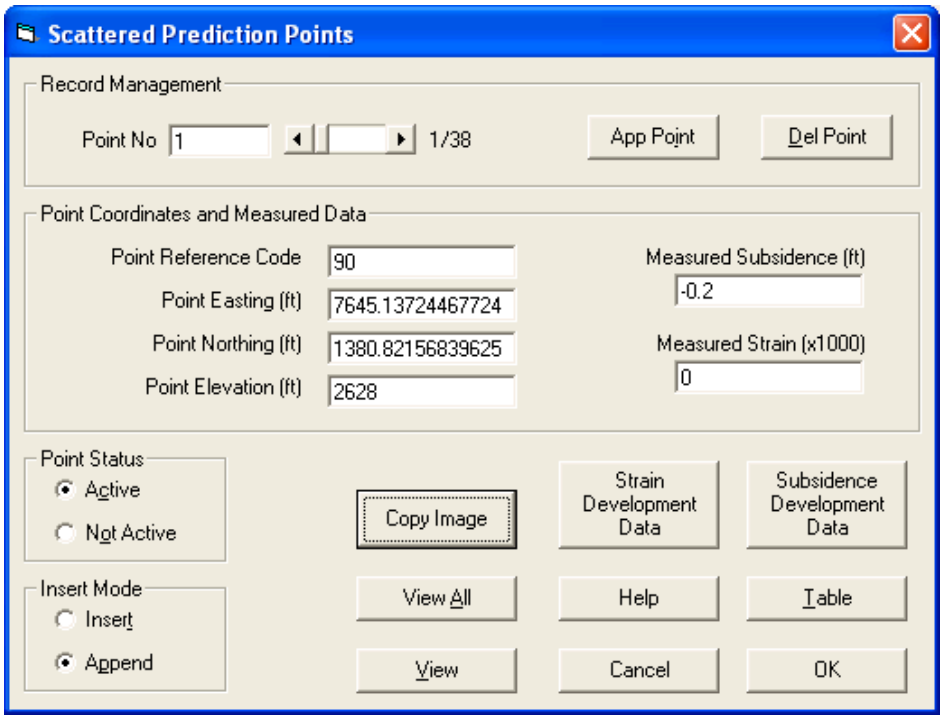

Figure 93: AL-1 Case Study - Prediction Points Management Screen (only first point shown)

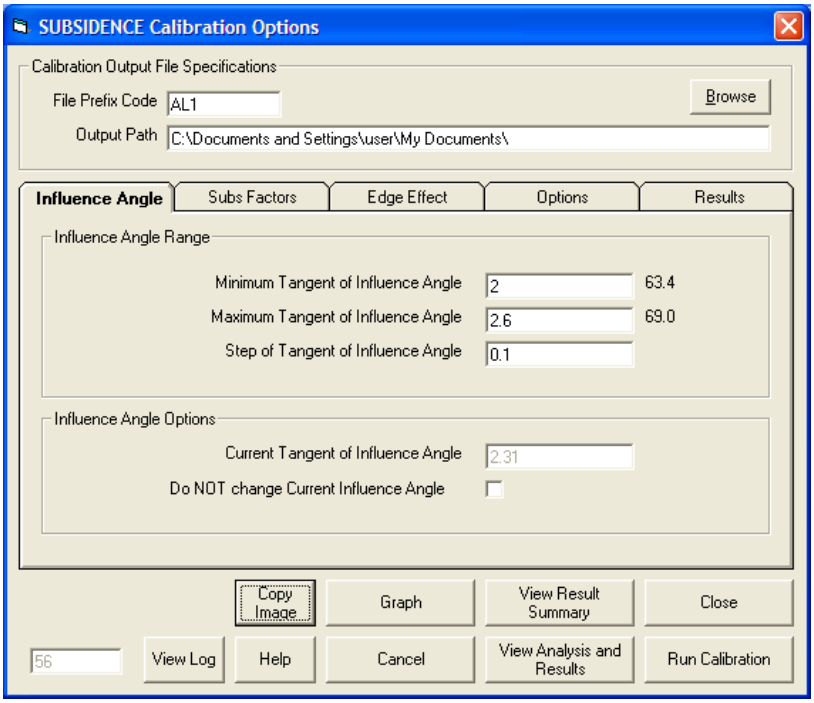

Figure 94: AL-1 Case Study - Subsidence Calibration Options Screen, Influence Angle Screen

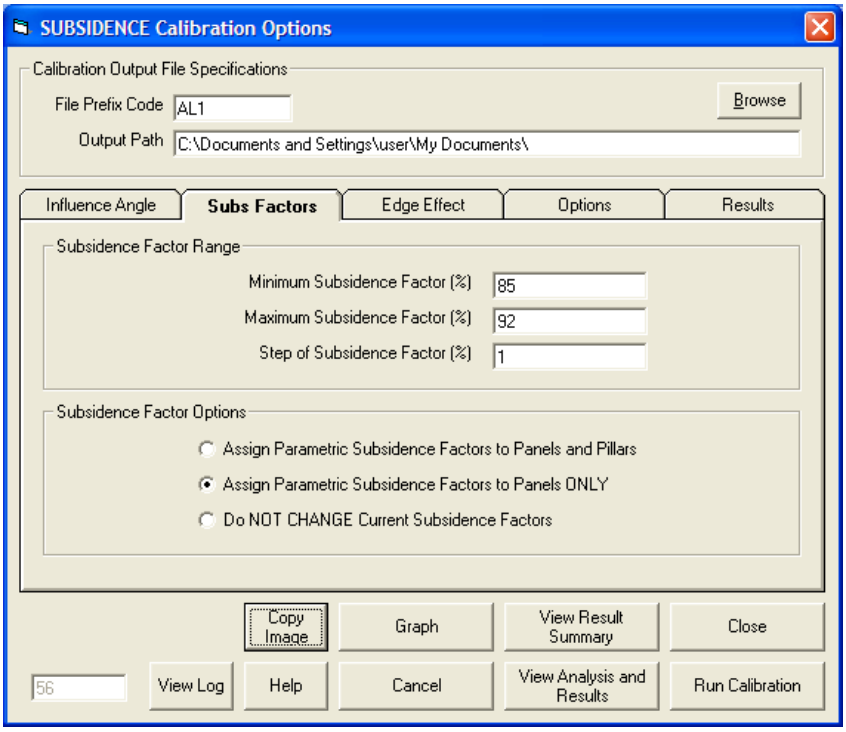

Figure 95: AL-1 Case Study - Subsidence Calibration Options Screen, Subsidence Factor Screen

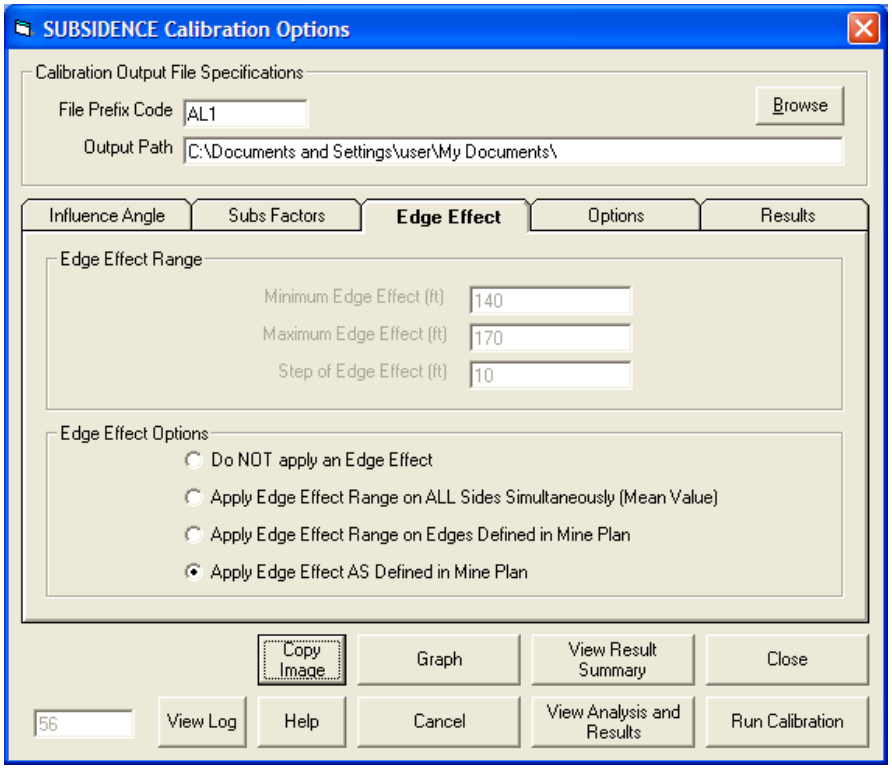

Figure 96: AL-1 Case Study – Subsidence Calibration Options Screen, Edge Effect Screen

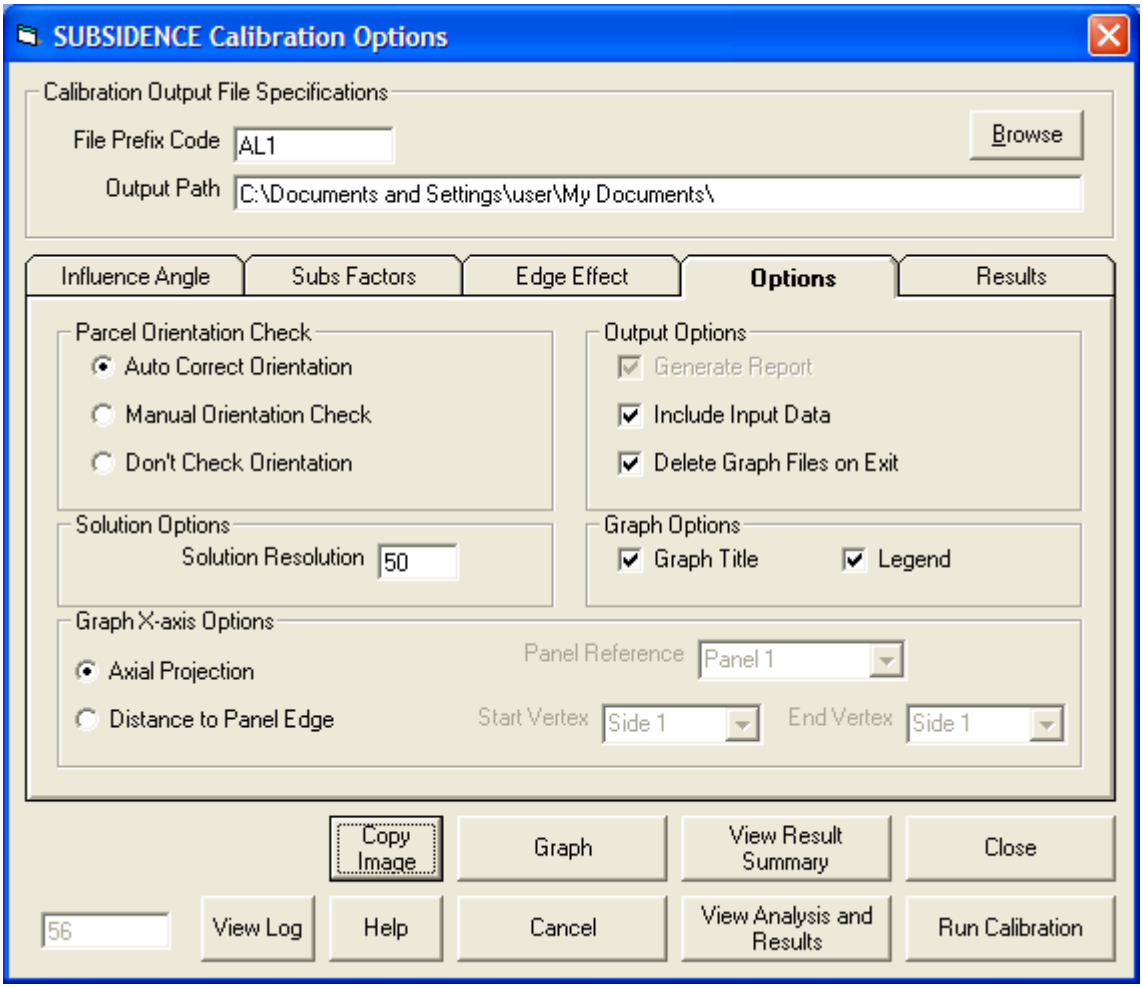

Figure 97: AL-1 Case Study - Subsidence Calibration Options Screen, Calibration Options Screen

Appendix II –

SDPS Screen Captures for the Prediction of Dynamic Subsidence Development

NA-2 Dynamic Case Study (Northern Appalachia)

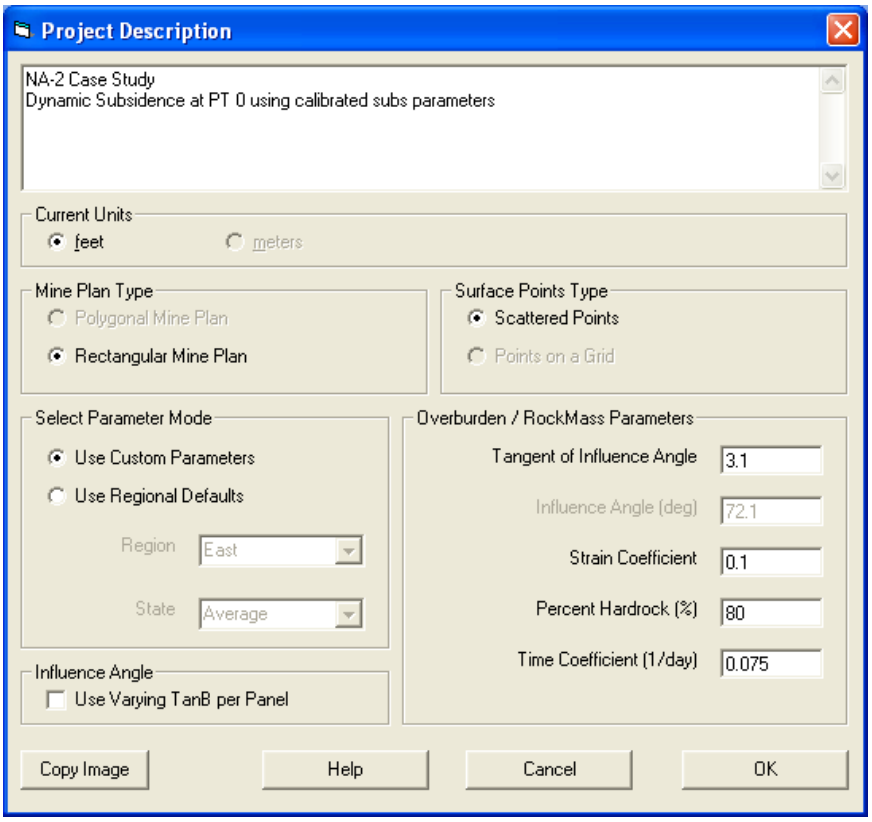

Figure 1: NA-2 Dynamic Case Study - SDPS Project Description Screen

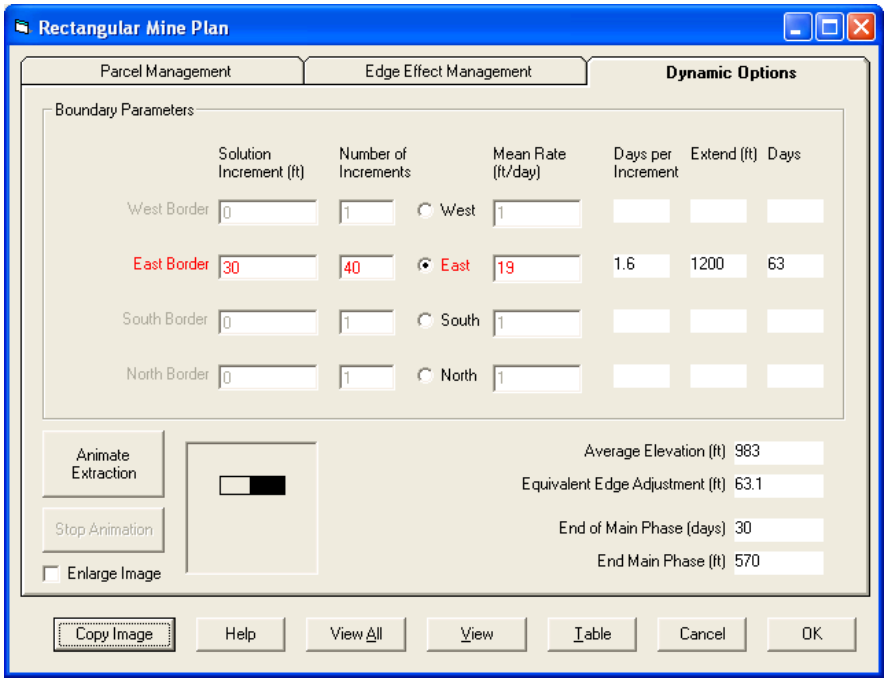

Figure 2: NA-2 Dynamic Case Study – Dynamic Options Screen

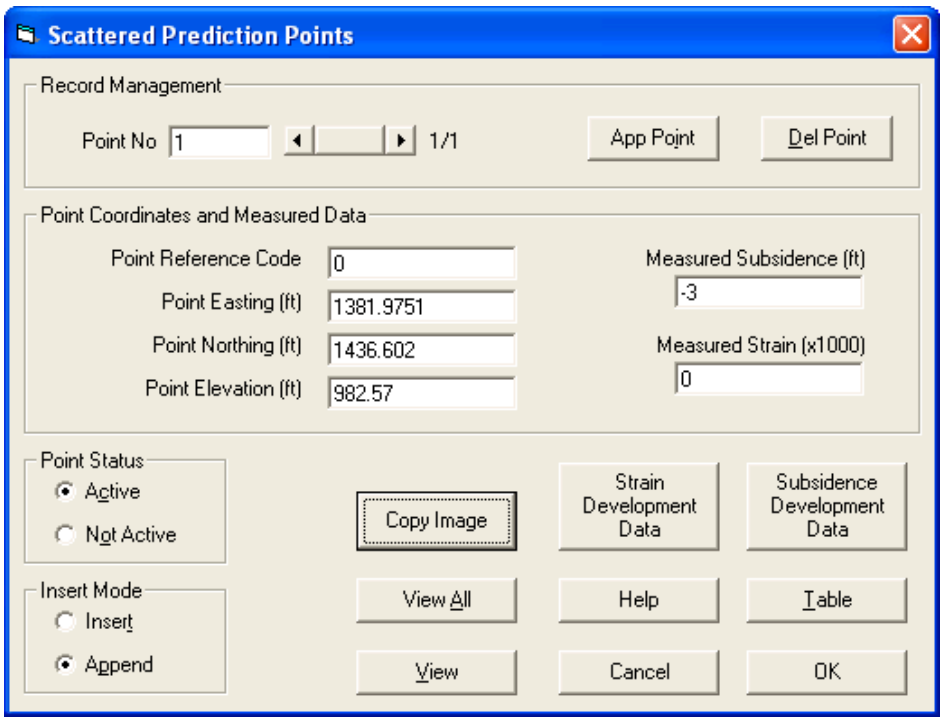

Figure 3: NA-2 Dynamic Case Study – Prediction Points Management Screen

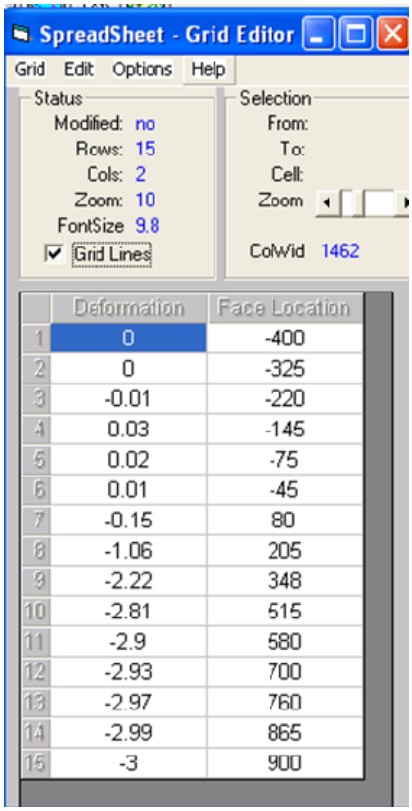

	Deformation	Face Location
1	0	-400
2	0	-325
3	-0.01	-220
4	0.03	-145
5	0.02	-75
6	0.01	-45
7	-0.15	80
8	-1.06	205
9	-2.22	348
10	-2.81	515
11	-2.9	580
12	-2.93	700
13	-2.97	760
14	-2.99	865
15	-3	900

Figure 4: NA-2 Dynamic Case Study – Subsidence Development Data

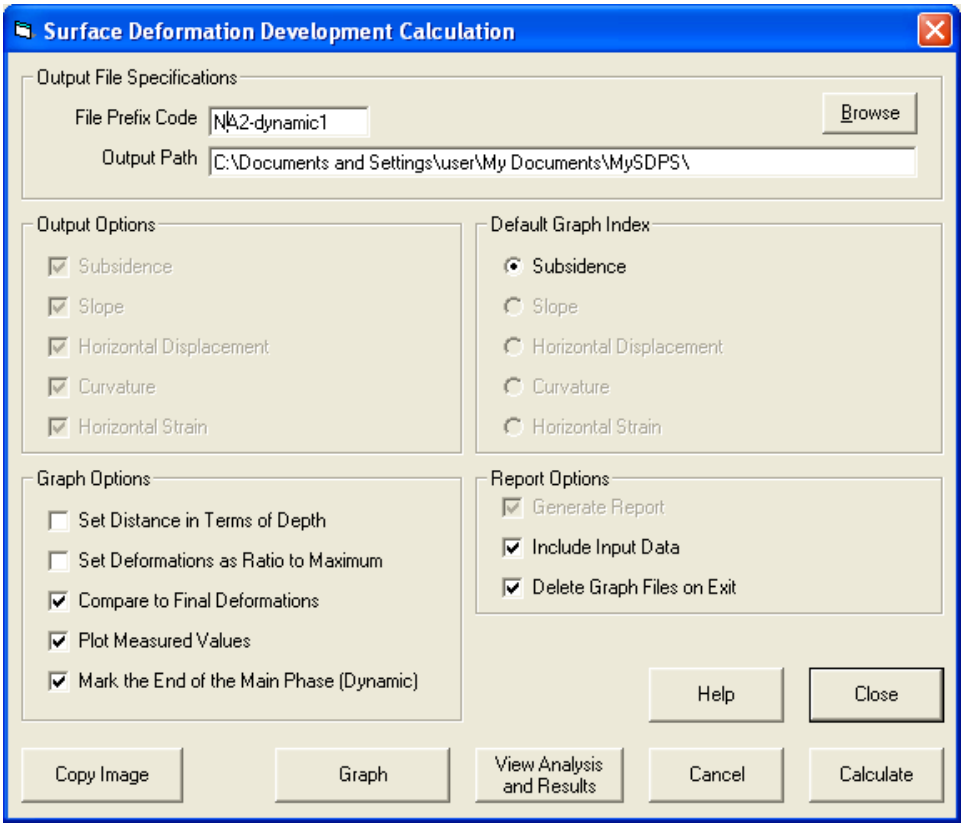

Figure 5: NA-2 Dynamic Case Study – Surface Deformation Development Calculation Screen

IL-1 DYNAMIC SUBSIDENCE CASE STUDY (ILLINOIS)

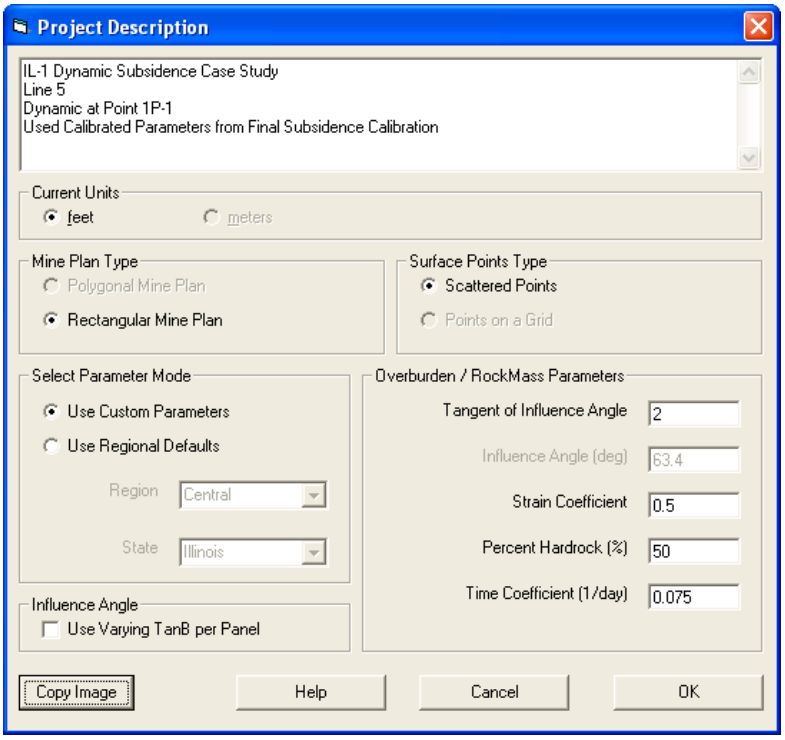

Figure 6: IL-1 Dynamic Case Study – SDPS Project Description Screen

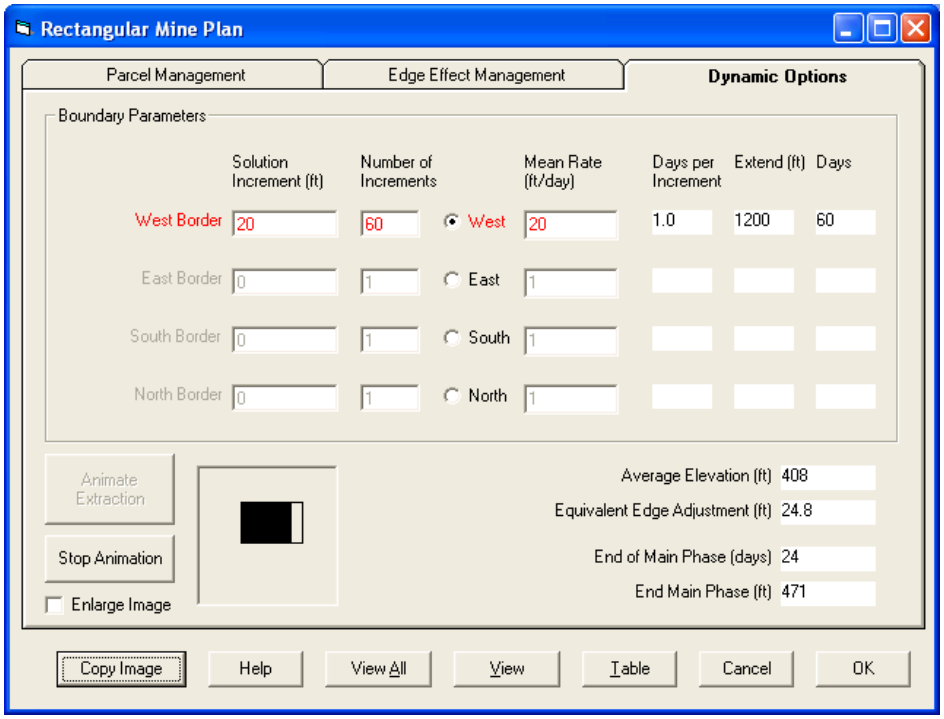

Figure 7: IL-1 Dynamic Case Study – Dynamic Options Screen

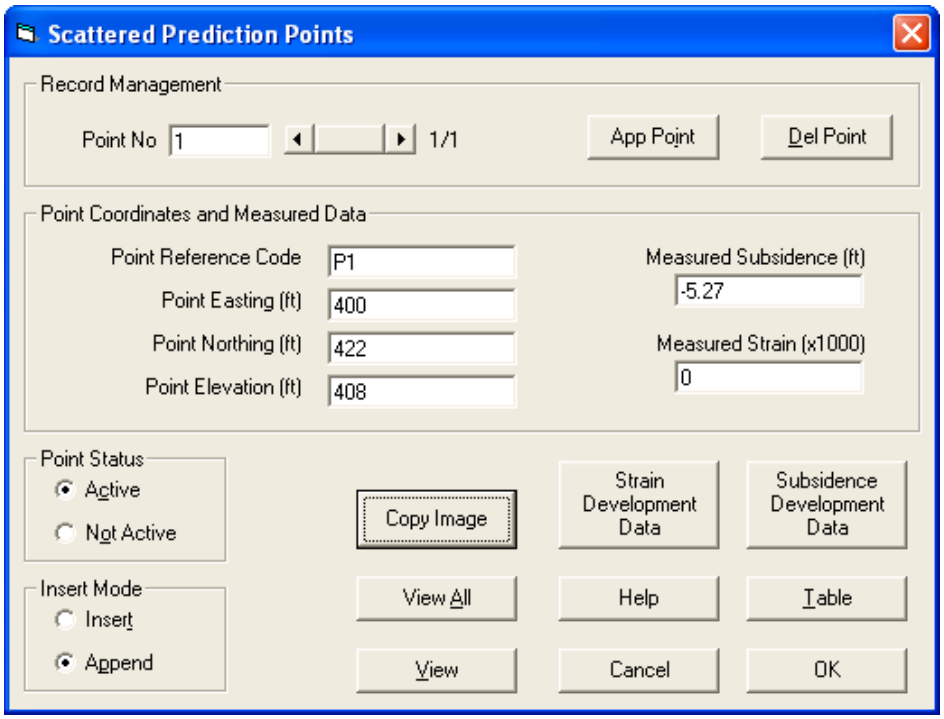

Figure 8: IL-1 Dynamic Case Study – Prediction Points Management Screen

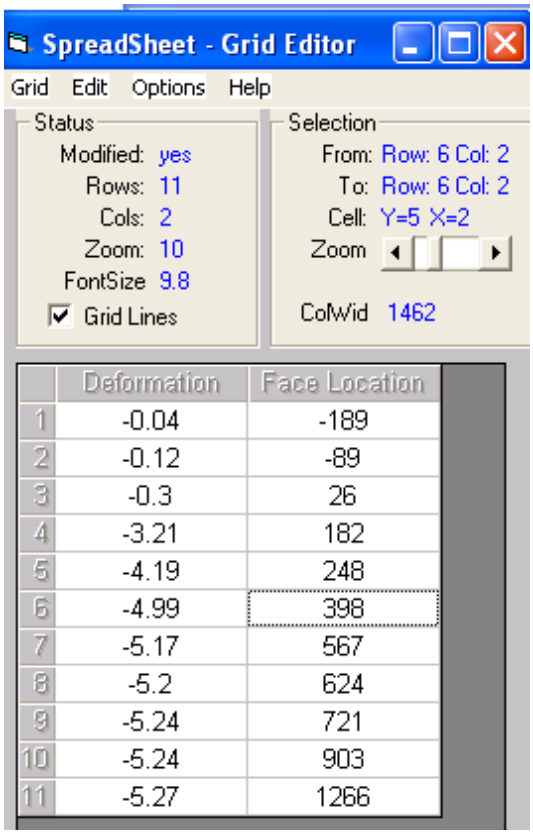

	Deformation	Face Location
1	-0.04	-189
2	-0.12	-89
3	-0.3	26
4	-3.21	182
5	-4.19	248
6	-4.99	398
7	-5.17	567
8	-5.2	624
9	-5.24	721
10	-5.24	903
11	-5.27	1266

Figure 9: IL-1 Dynamic Case Study – Subsidence Development Data

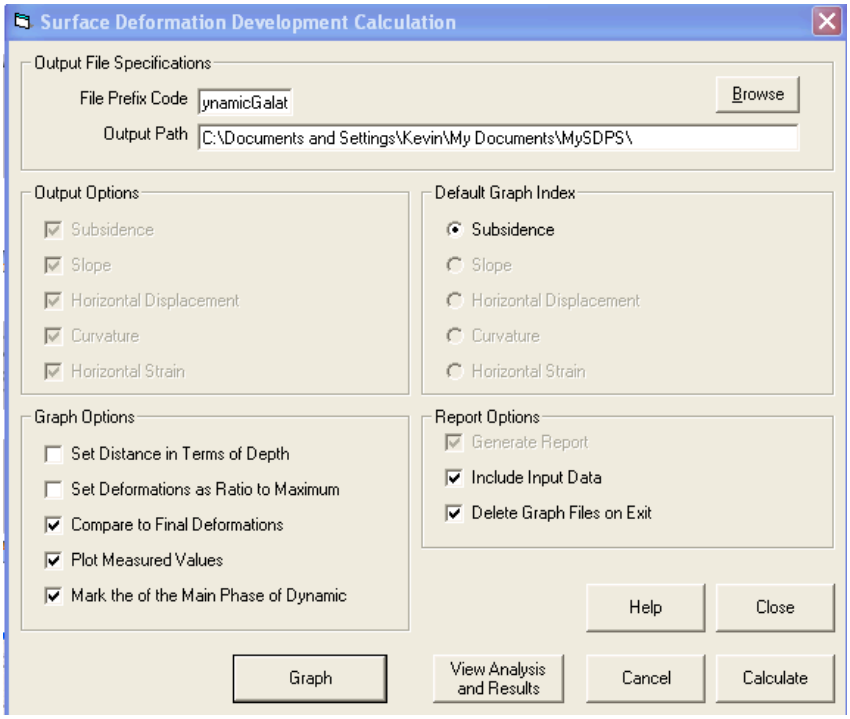

Figure 10: IL-1 Dynamic Case Study – Surface Deformation Development Calculation Screen

Appendix III –

SDPS Screen Captures for Regarding Calibration Techniques for Subsidence Prediction

NA-2 Calibration Case Study (Northern Appalachia) - Transverse Line

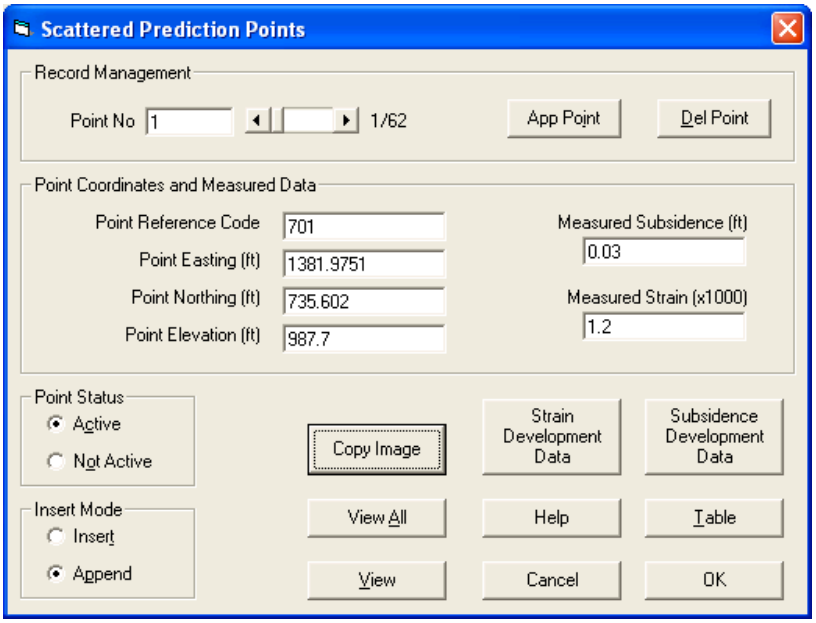

Figure 1: NA-2 Calibration Case Study, Transverse Line – Prediction Points Management Screen (only one point shown)

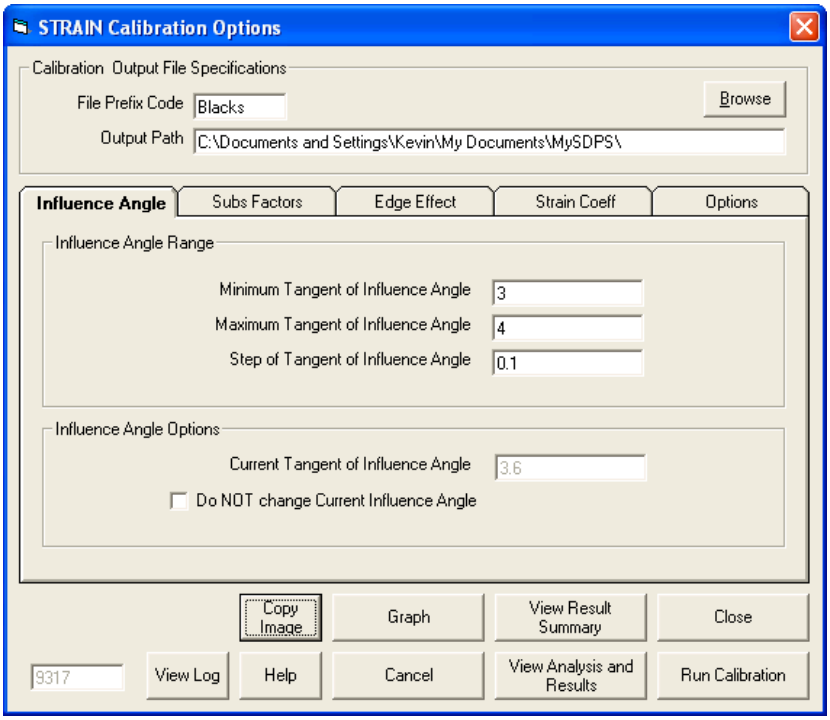

Figure 2: NA-2 Calibration Case Study, Transverse Line – Strain Calibration Options, Influence Angle Screen

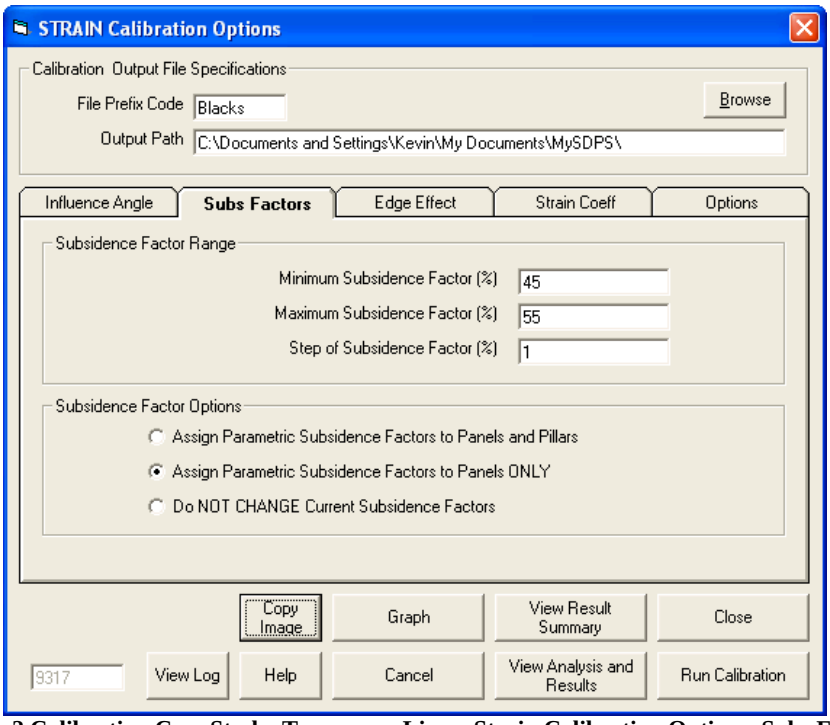

Figure 3: NA-2 Calibration Case Study, Transverse Line – Strain Calibration Options, Subs Factor Screen

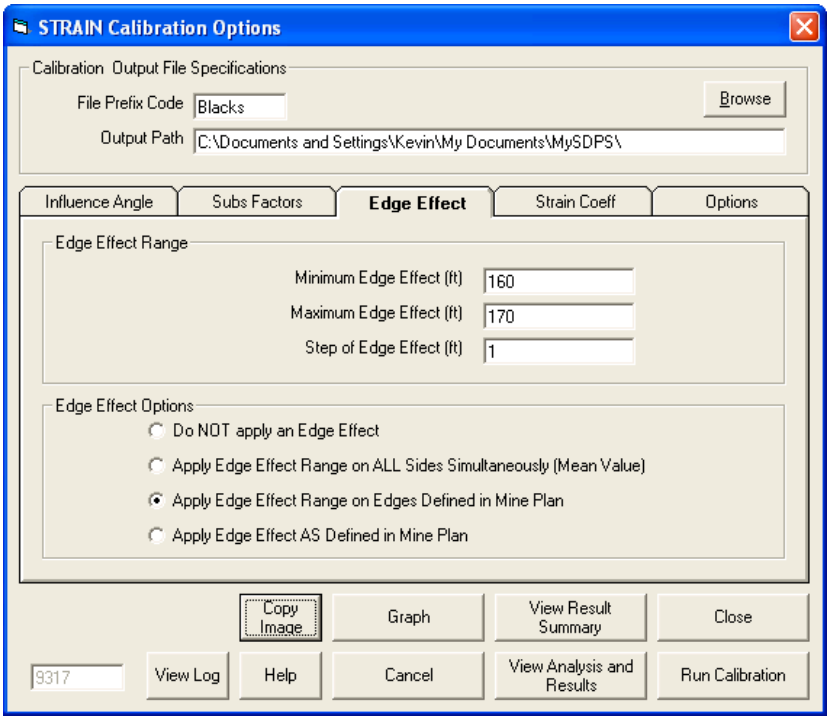

Figure 4: NA-2 Calibration Case Study, Transverse Line – Strain Calibration Options, Edge Effect Screen

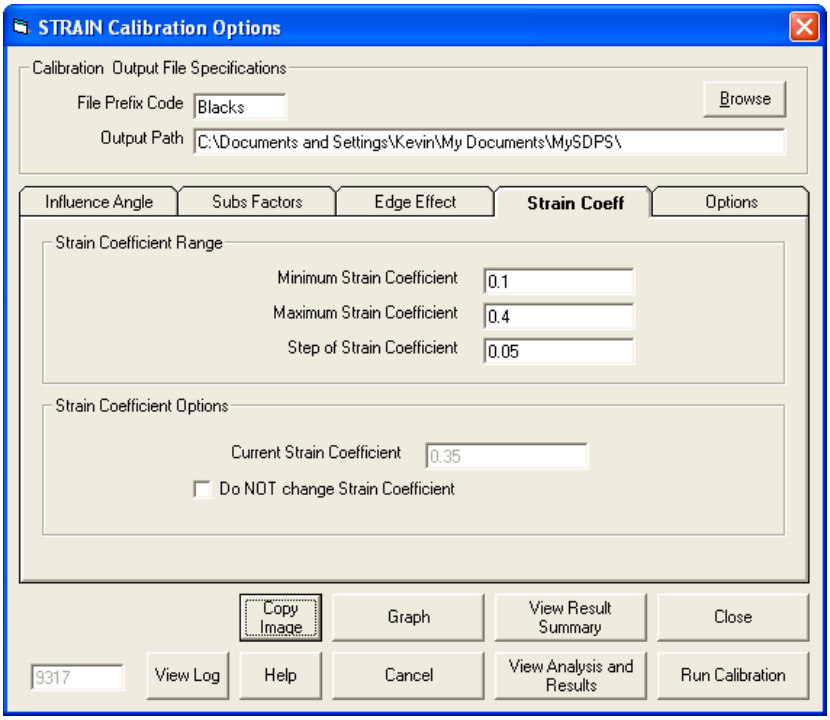

Figure 5: NA-2 Calibration Case Study, Transverse Line – Strain Calibration Options, Strain Coefficient Screen

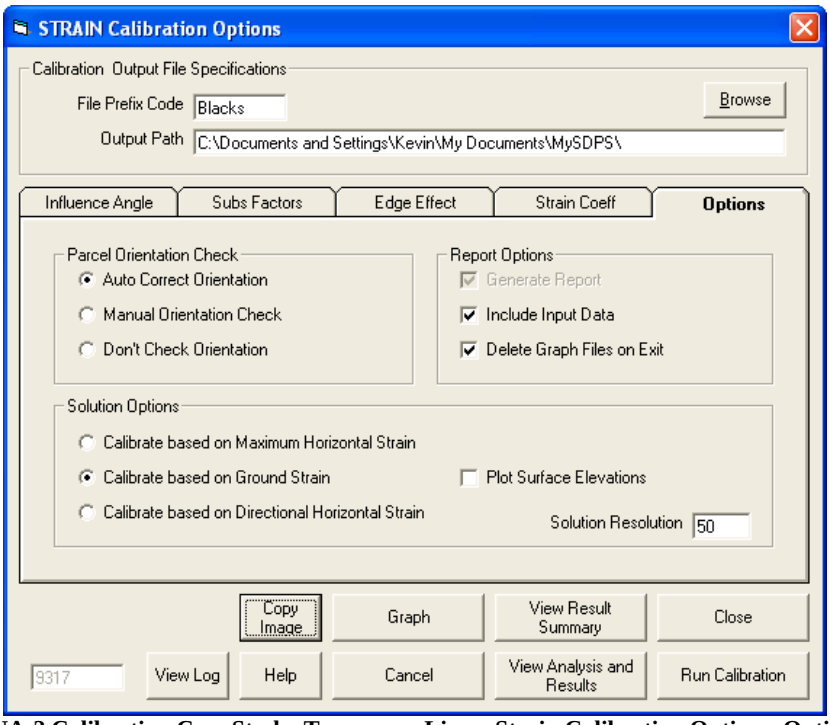

Figure 6: NA-2 Calibration Case Study, Transverse Line – Strain Calibration Options, Options Screen

NA-2 CALIBRATION CASE STUDY (NORTHERN APPALACHIA) - LONGITUDINAL LINE

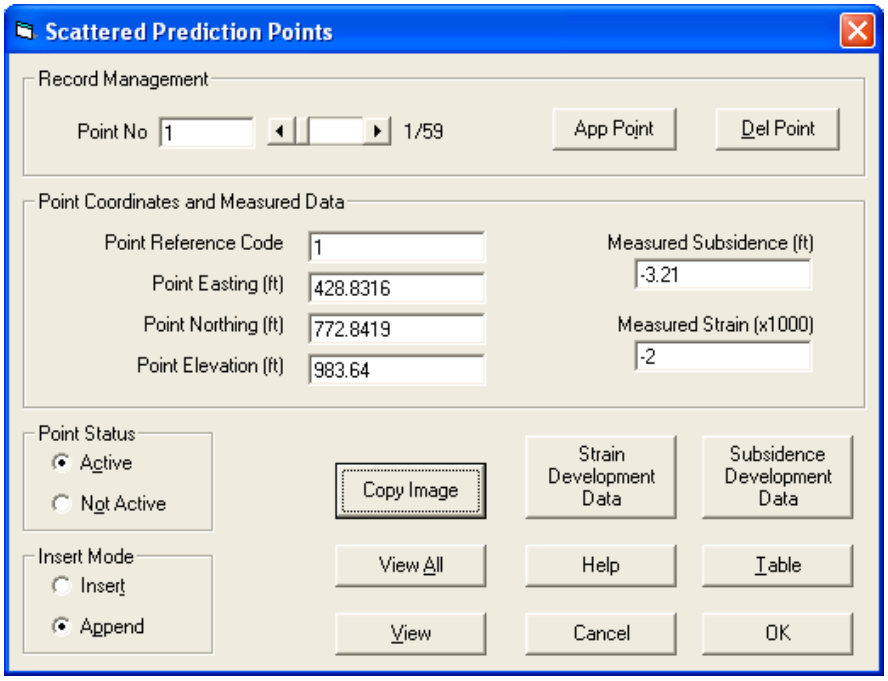

Figure 7: NA-2 Calibration Case Study, Longitudinal Line – Prediction Points Management Screen (only one point shown)

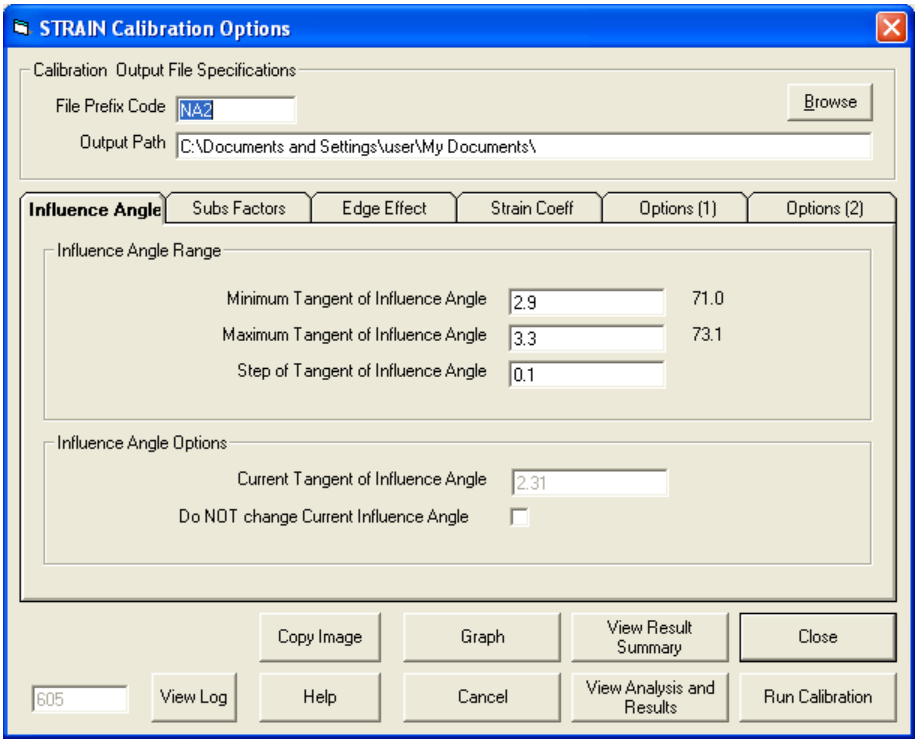

Figure 8: NA-2 Calibration Case Study, Longitudinal Line – Strain Calibration Options, Influence Angle Screen

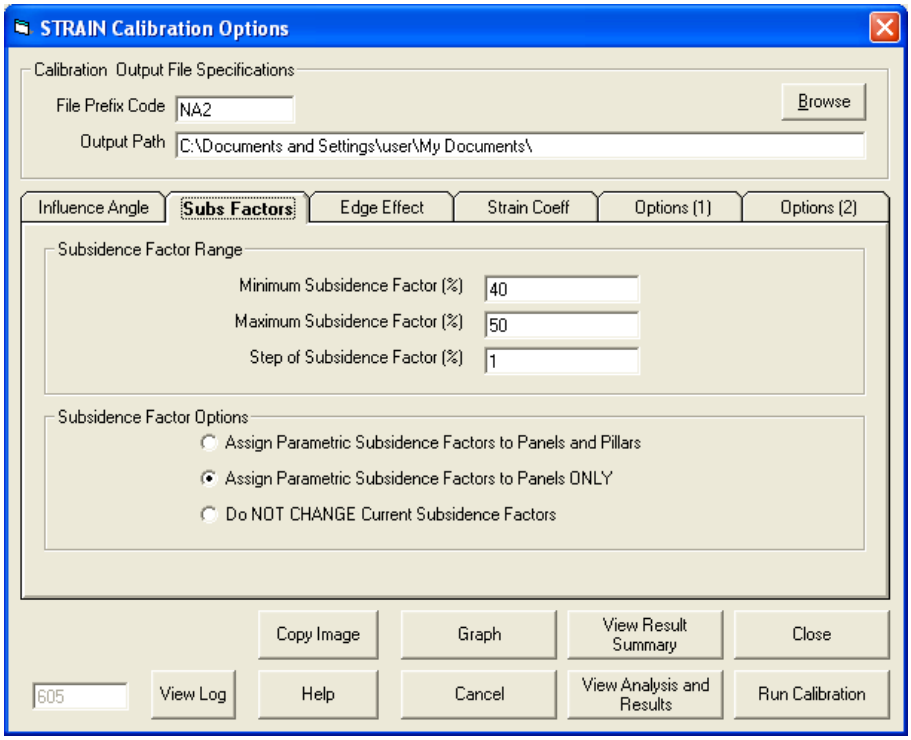

Figure 9: NA-2 Calibration Case Study, Longitudinal Line – Strain Calibration Options, Subs Factor Screen

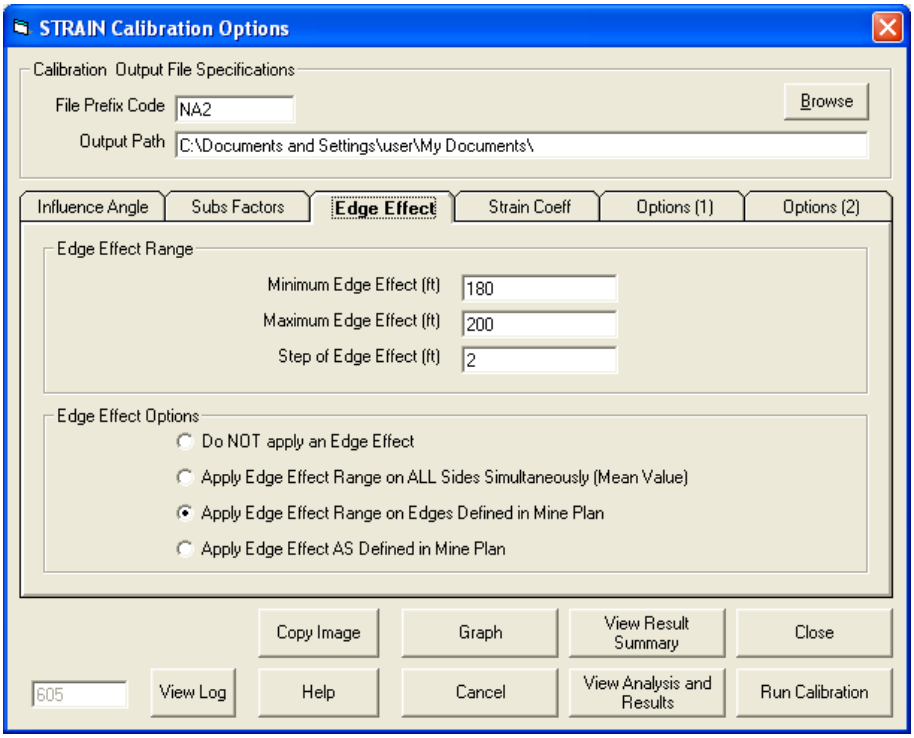

Figure 10: NA-2 Calibration Case Study, Longitudinal Line – Strain Calibration Options, Edge Effect Screen

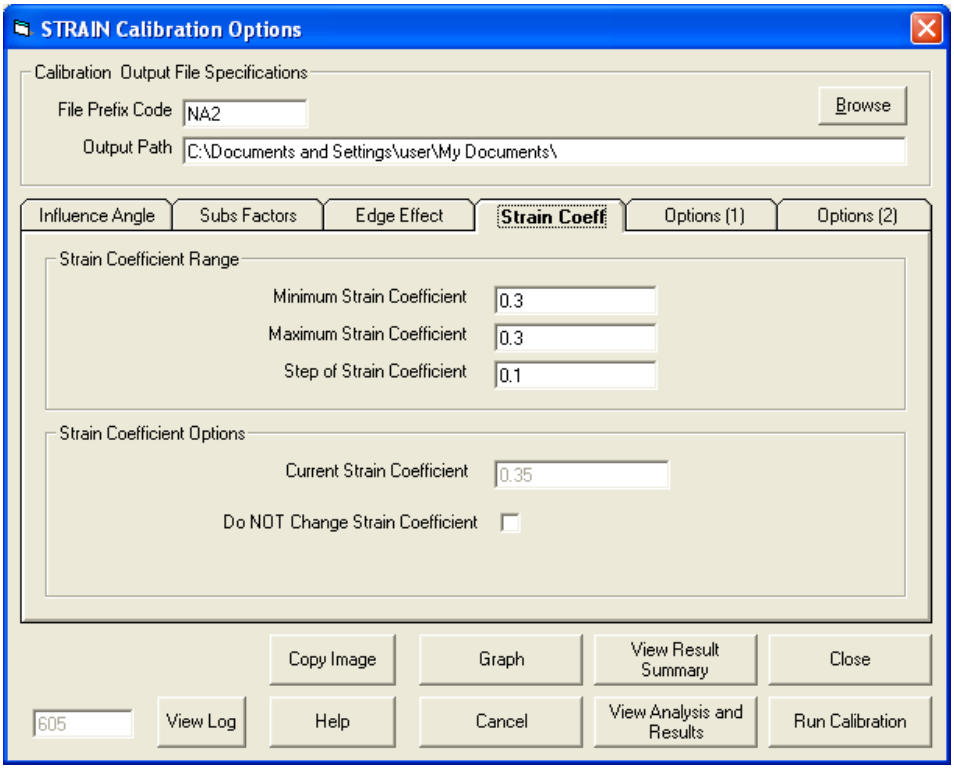

Figure 11: NA-2 Calibration Case Study, Longitudinal Line – Strain Calibration Options, Strain Coefficient Screen

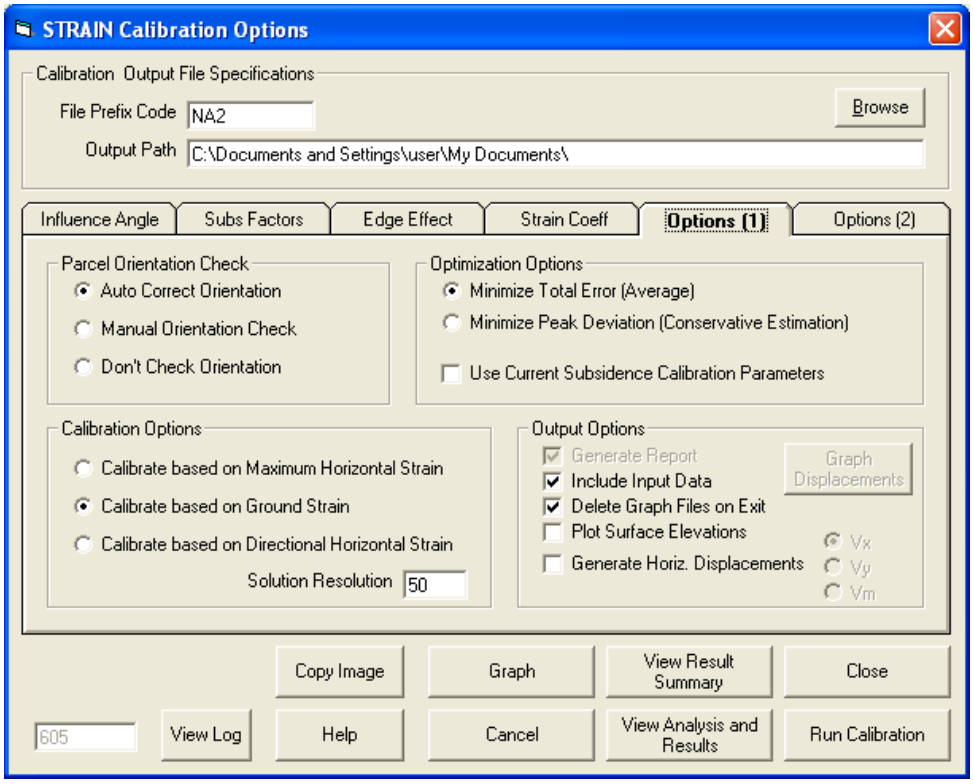

Figure 12: NA-2 Calibration Case Study, Longitudinal Line – Strain Calibration Options, Options Screen

NA-1 CALIBRATION CASE STUDY (NORTHERN APPALACHIA)

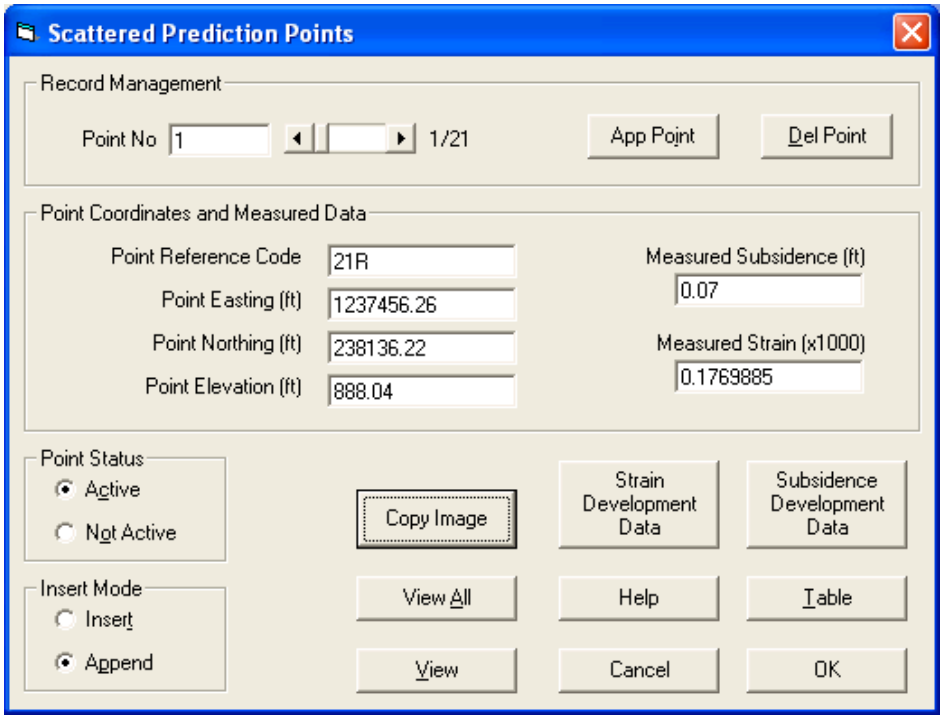

Figure 13: NA-1 Calibration Case Study – Prediction Points Management Screen

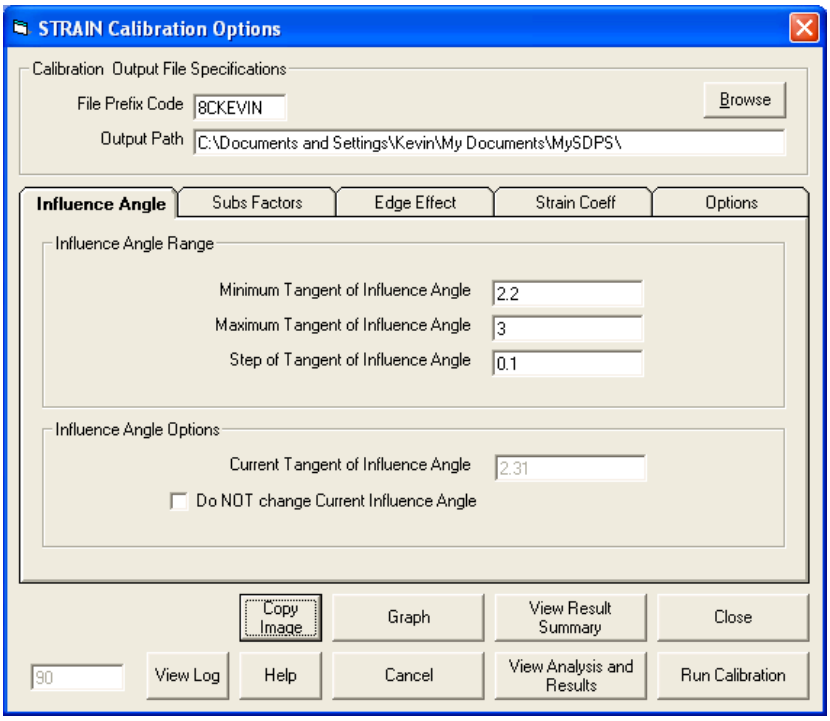

Figure 14: NA-1 Calibration Case Study – Strain Calibration Options, Influence Angle Screen

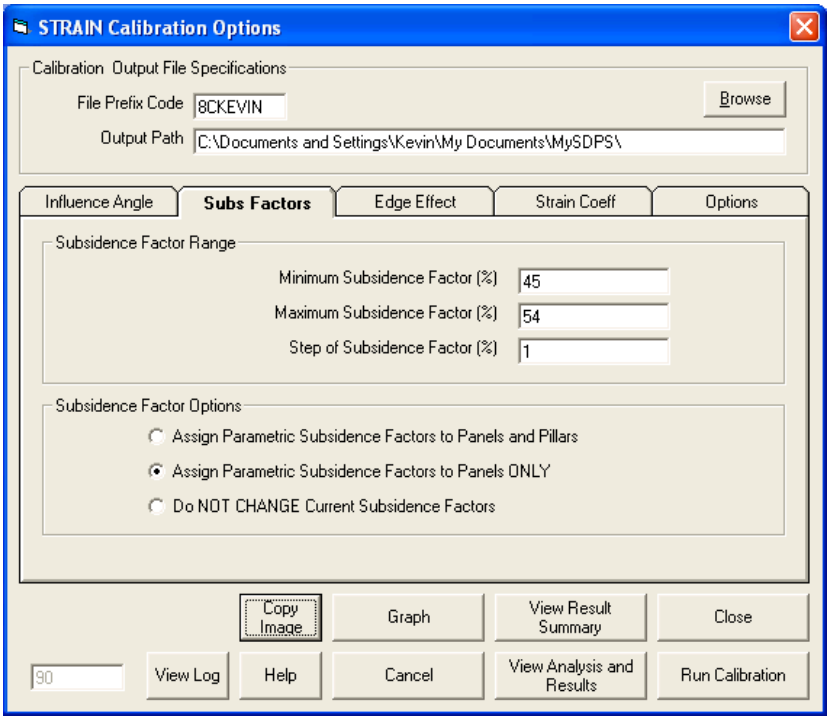

Figure 15: NA-1 Calibration Case Study – Strain Calibration Options, Subs Factor Screen

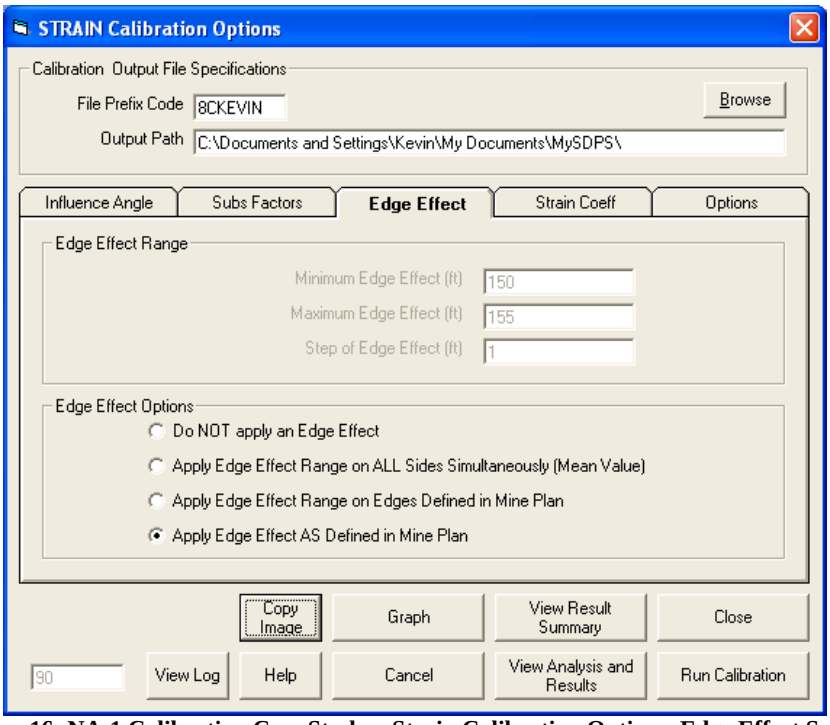

Figure 16: NA-1 Calibration Case Study – Strain Calibration Options, Edge Effect Screen

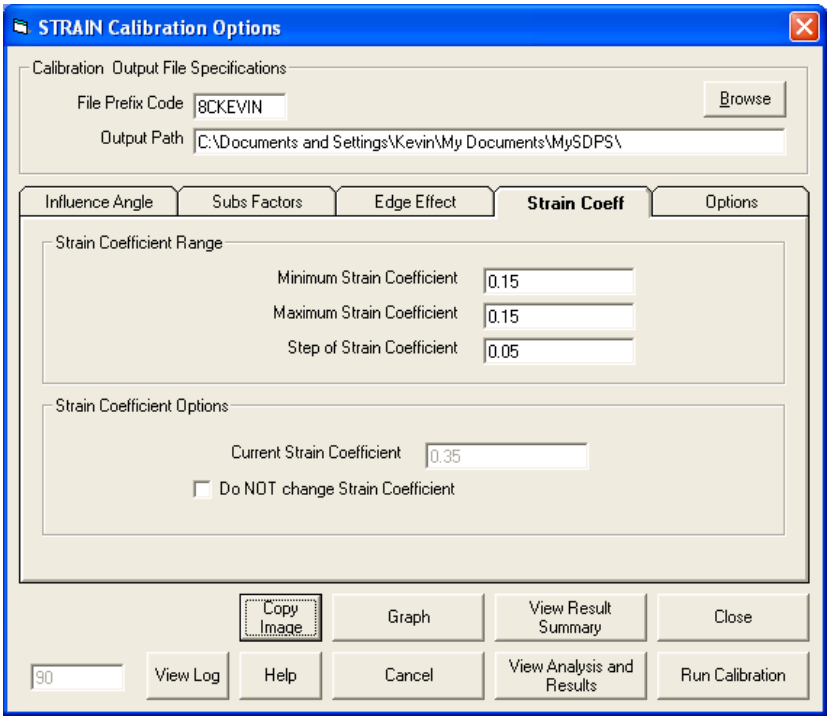

Figure 17: NA-1 Calibration Case Study – Strain Calibration Options, Strain Coefficient Screen

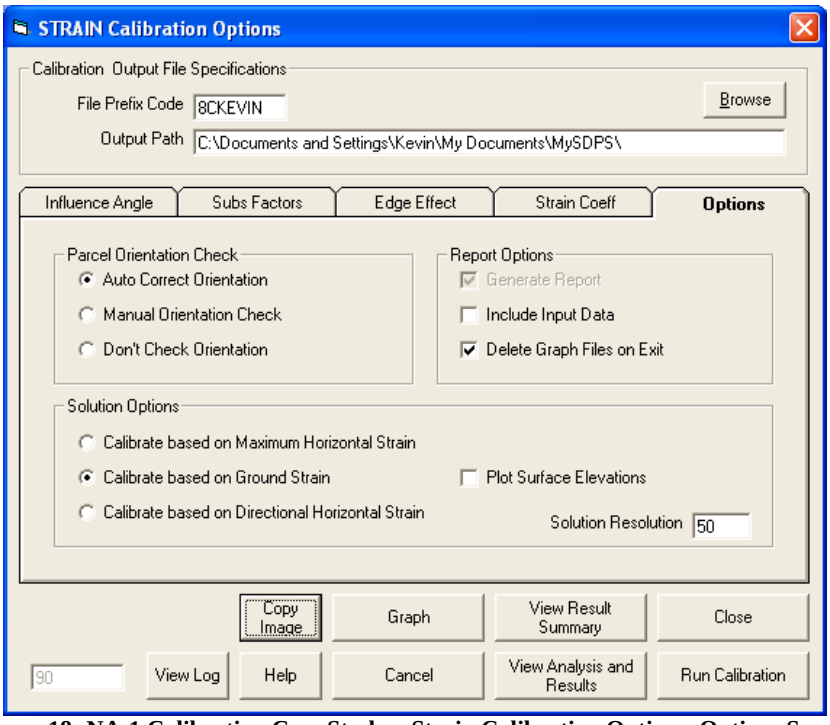

Figure 18: NA-1 Calibration Case Study – Strain Calibration Options, Options Screen

Appendix IV –

SDPS Screen Captures for Subsidence Prediction in Areas of Steeply-Sloping Terrain

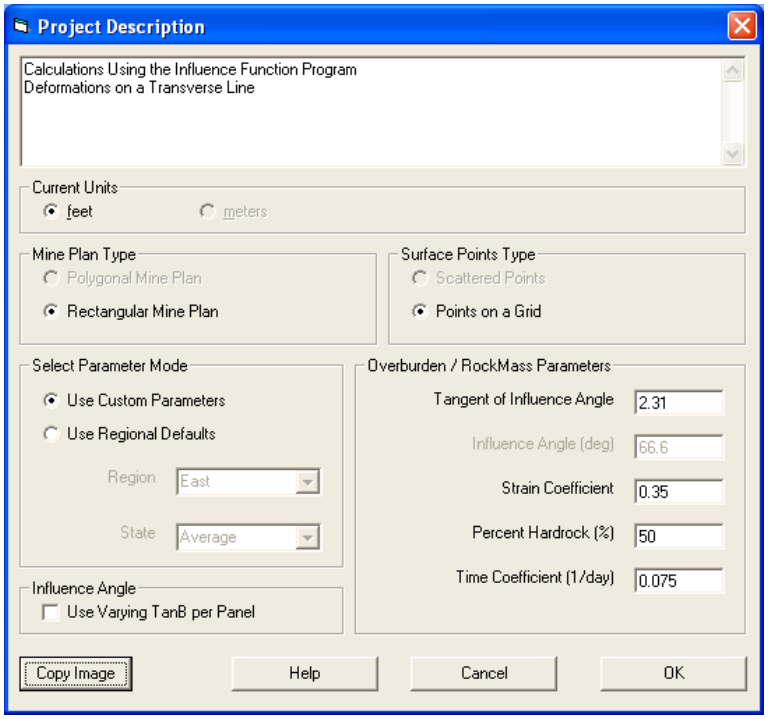

Figure 1: Steep Terrain, Synthetic Case Study – Project Description Screen

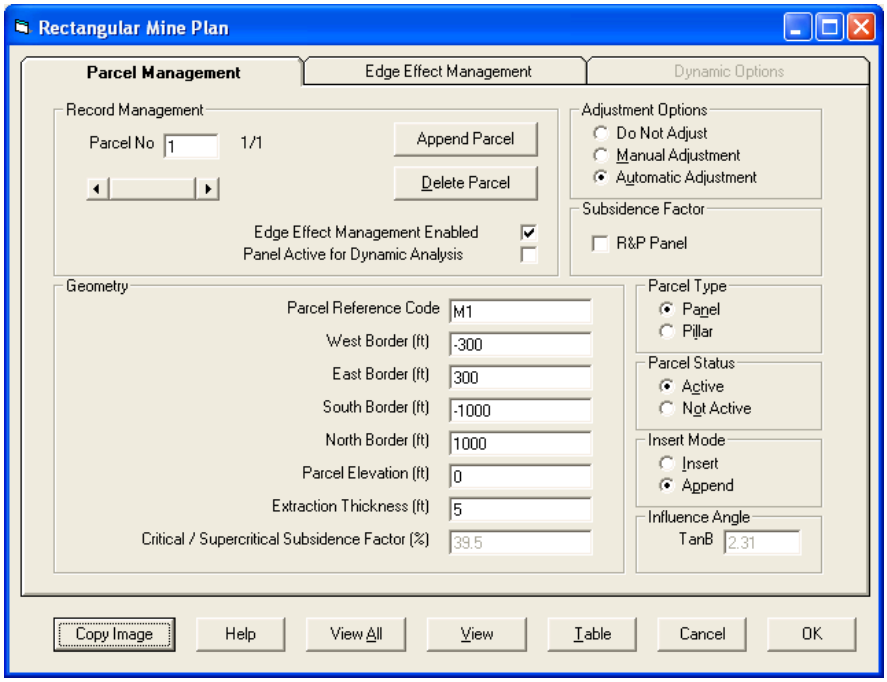

Figure 2: Steep Terrain, Synthetic Case Study – Parcel Management Screen

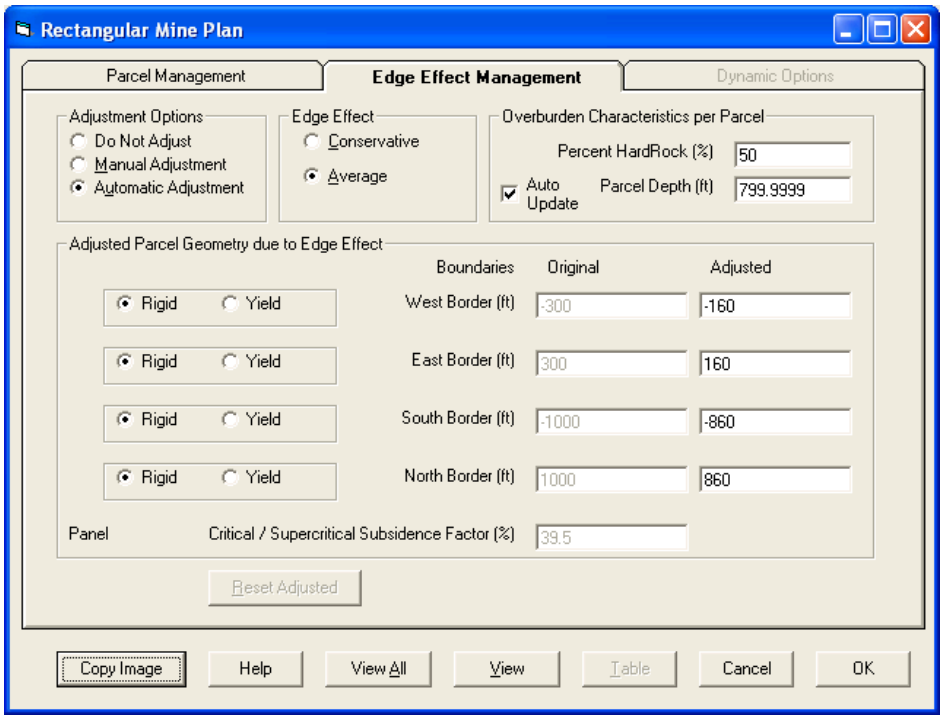

Figure 3: Steep Terrain, Synthetic Case Study – Edge Effect Management Screen

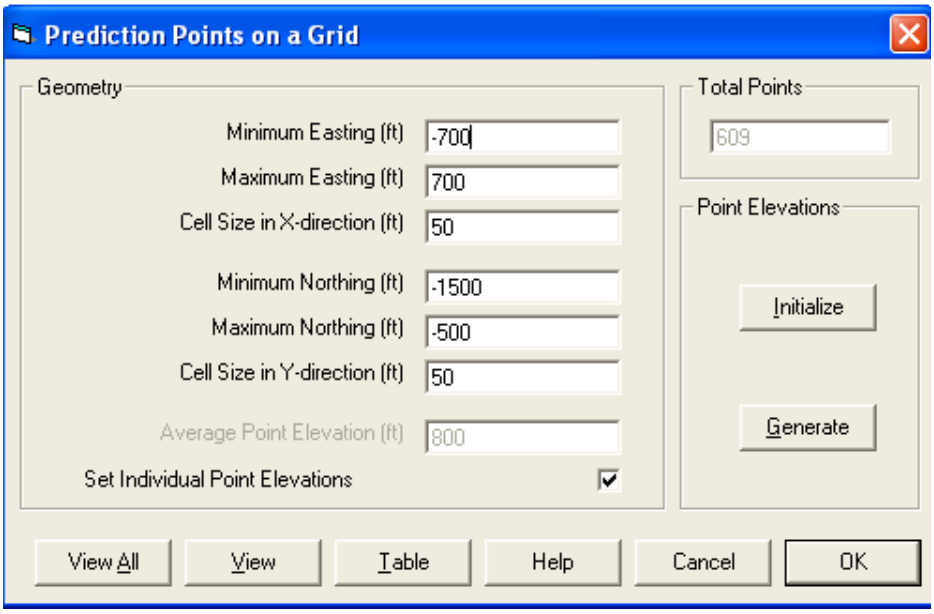

Figure 4: Steep Terrain, Synthetic Case Study – Prediction Points Management Screen

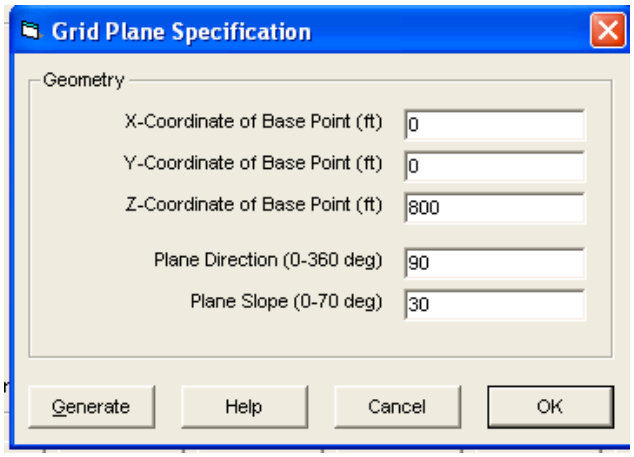

Figure 5: Steep Terrain, Synthetic Case Study – Grid Plane Specification Screen

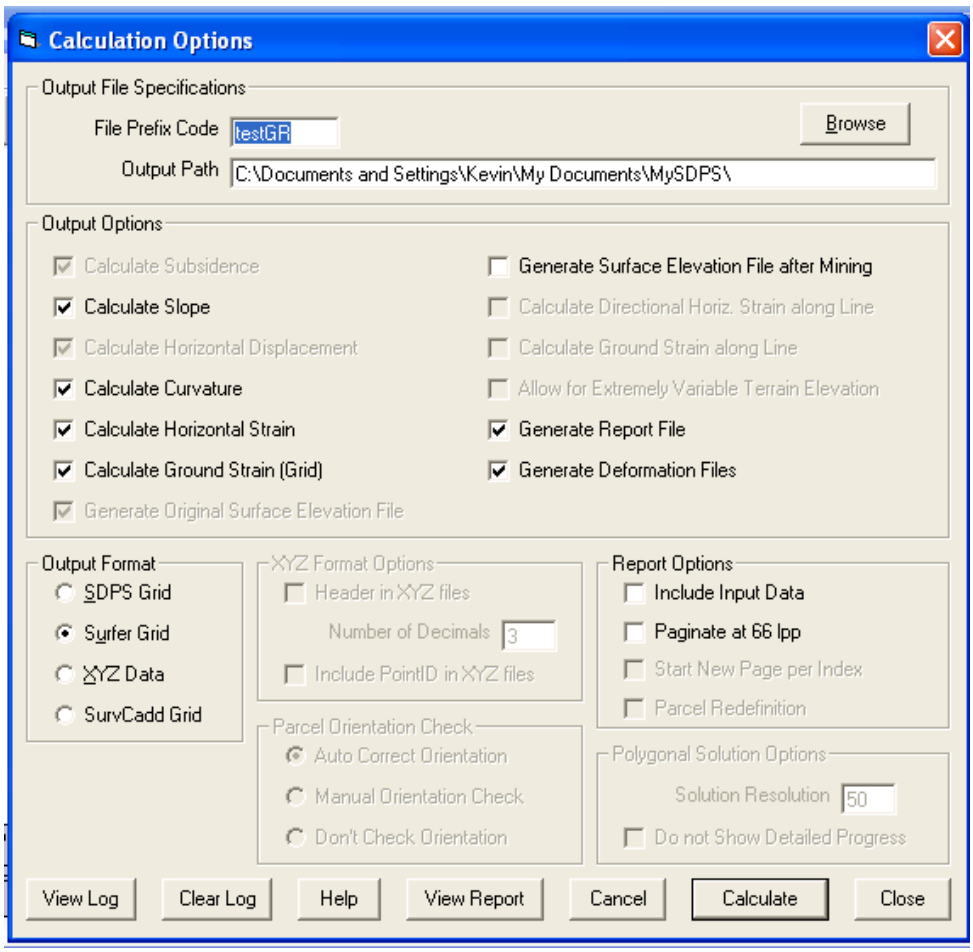

Figure 6: Steep Terrain, Synthetic Case Study – Calculation Options Screen

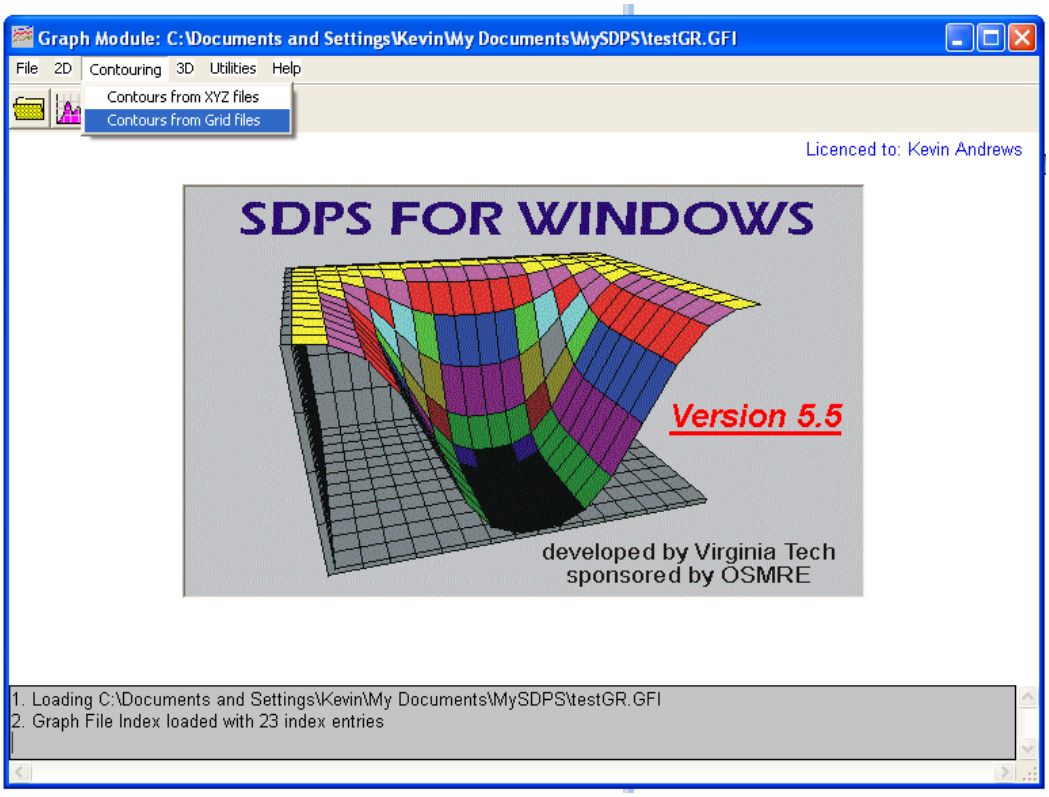

Figure 7: Steep Terrain, Synthetic Case Study – Graph Module, Menu Selection for Contouring with Surfer

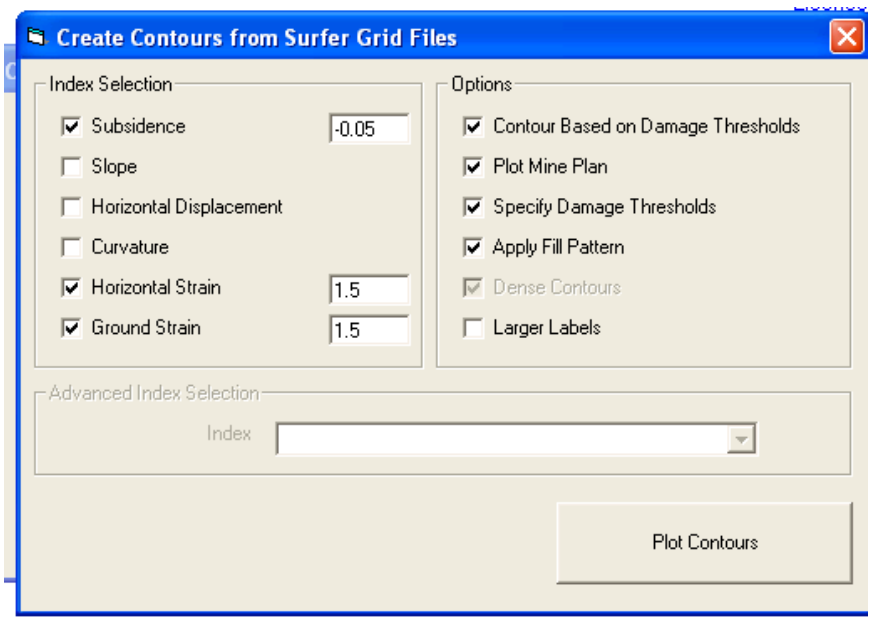

Figure 8: Steep Terrain, Synthetic Case Study – Graph Module, Menu Selection for Contouring with Surfer

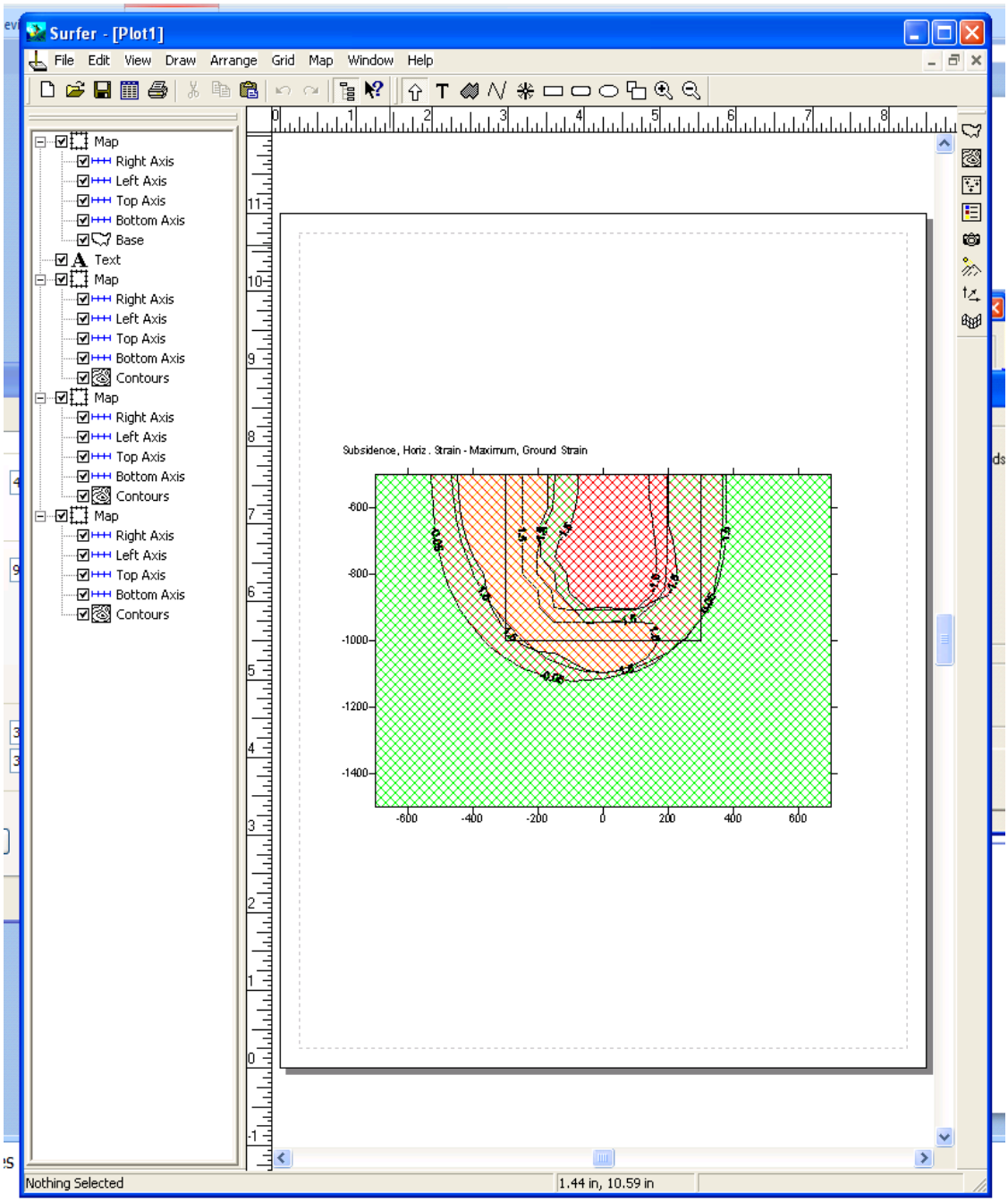

Figure 9: Steep Terrain, Synthetic Case Study – Graph Module, Menu Selection for Contouring with Surfer

Appendix V – SDPS Screen Captures for the Analysis of Risk- Based Assessment of Mine Planning and Long-term Landscape Stability

SYNTHETIC CASE STUDY 1 (BASIC RISK-ASSESSMENT OVER LONGWALL PANELS)

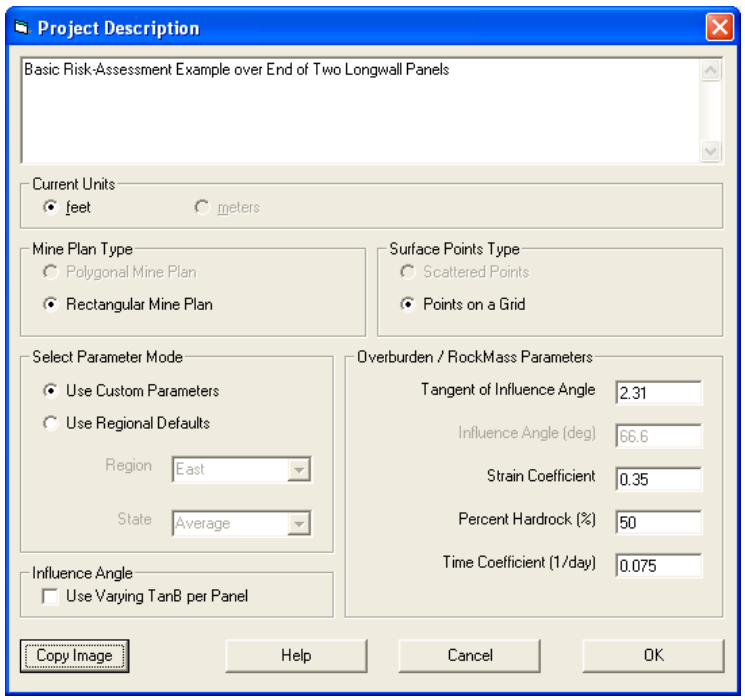

Figure 1: Risk Assessment, Basic Synthetic Case Study 1 – Project Description Screen

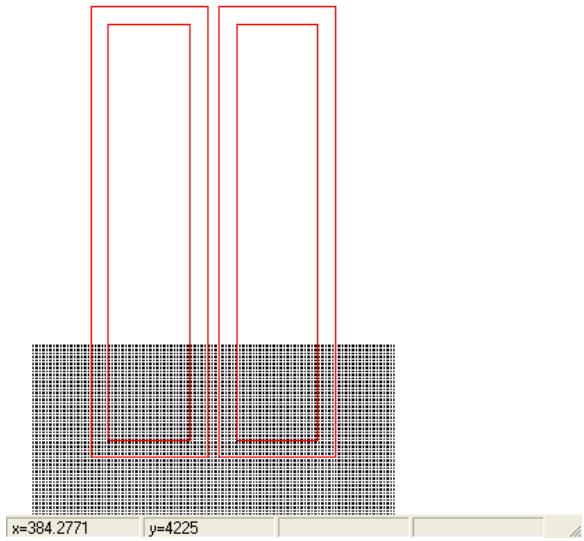

Figure 2: Risk Assessment, Basic Synthetic Case Study 1 – Basic Synthetic Mine Plan with Adjacent Panels and Prediction Point Grid

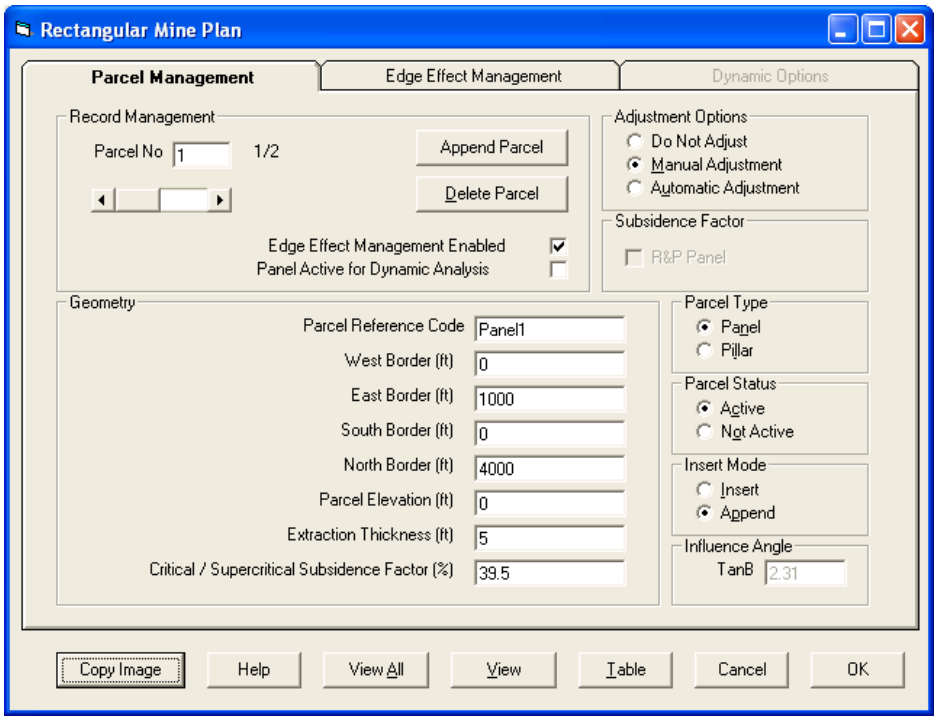

Figure 3: Risk Assessment, Basic Synthetic Case Study 1 – Parcel Management Screen, Panel 1 Only

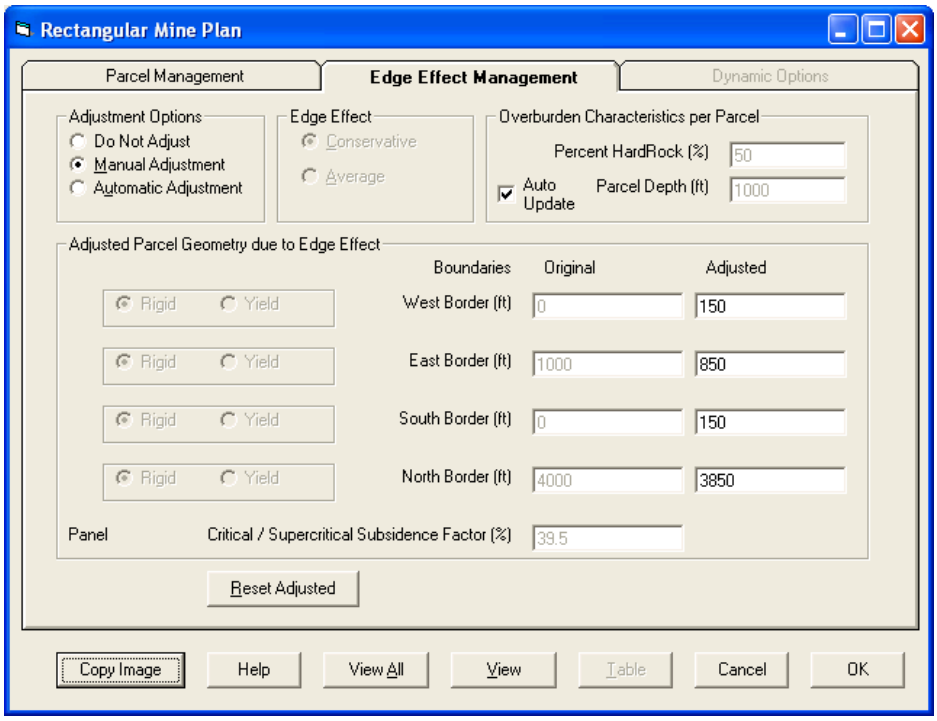

Figure 4: Risk Assessment, Basic Synthetic Case Study 1 – Edge Effect Management Screen, For Panel 1

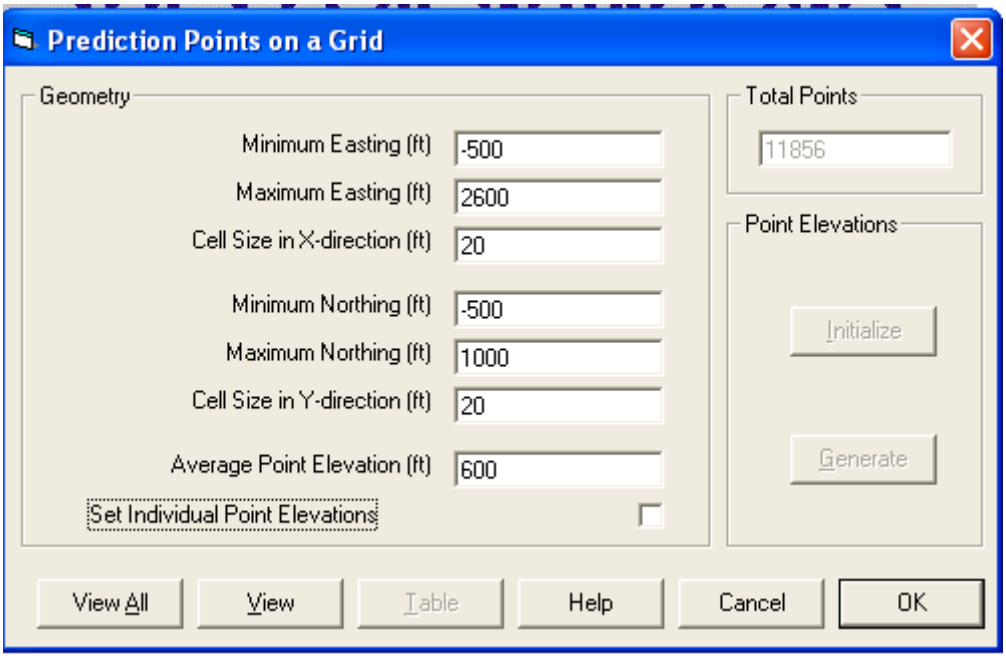

Figure 5: Risk Assessment, Basic Synthetic Case Study 1 – Prediction Points Management, Grid

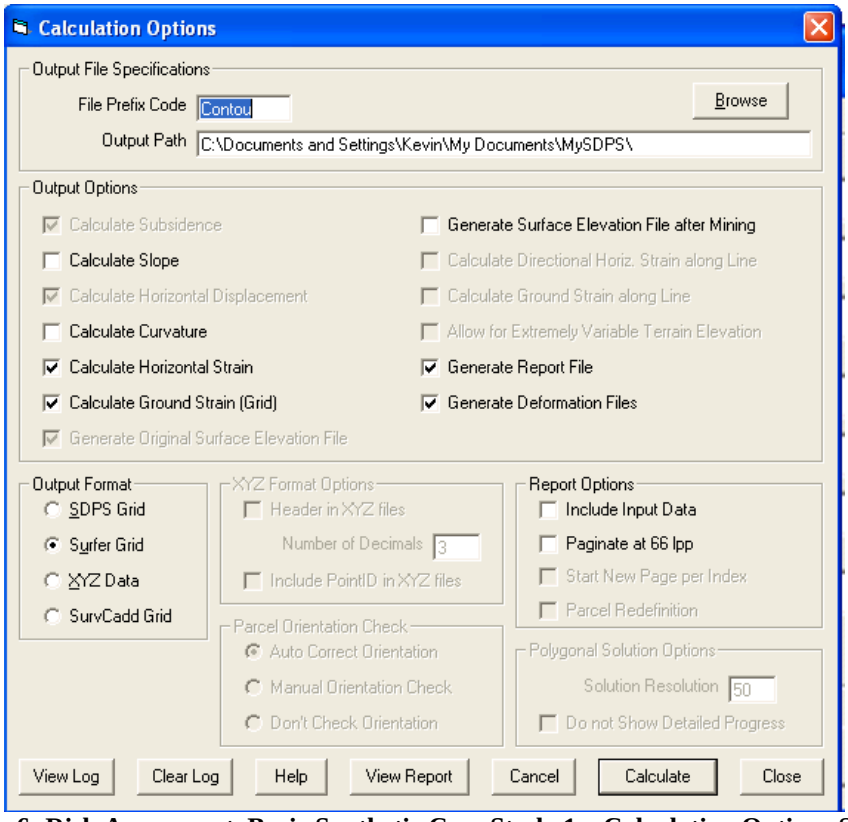

Figure 6: Risk Assessment, Basic Synthetic Case Study 1 – Calculation Options Screen

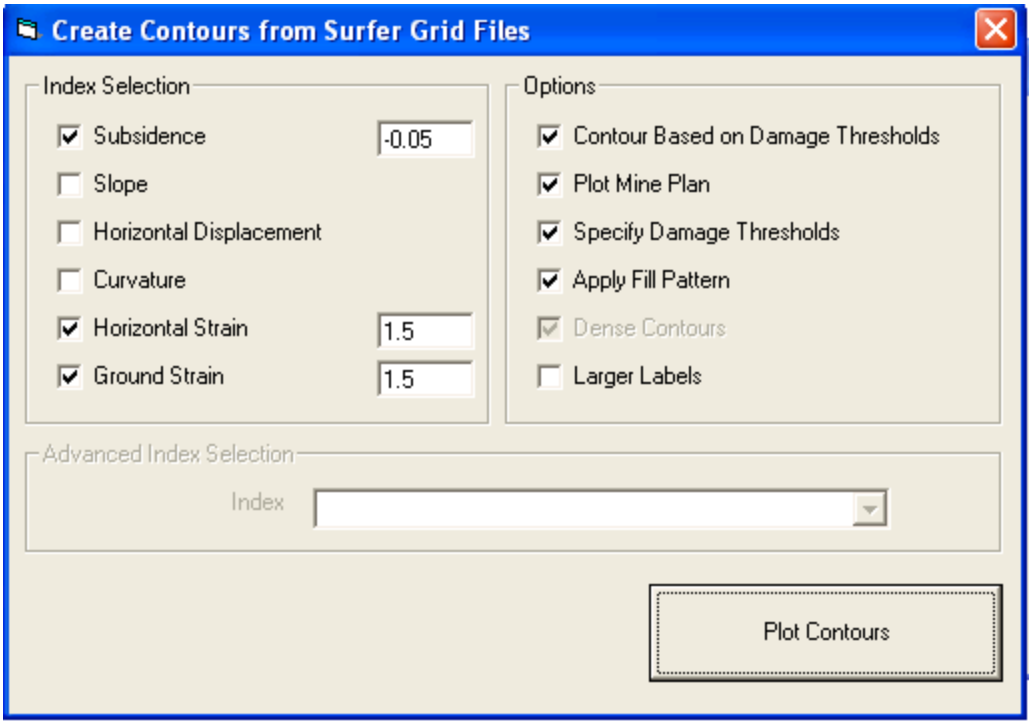

Figure 7: Risk Assessment, Basic Synthetic Case Study 1 – Grid Module, Create Contours in Surfer

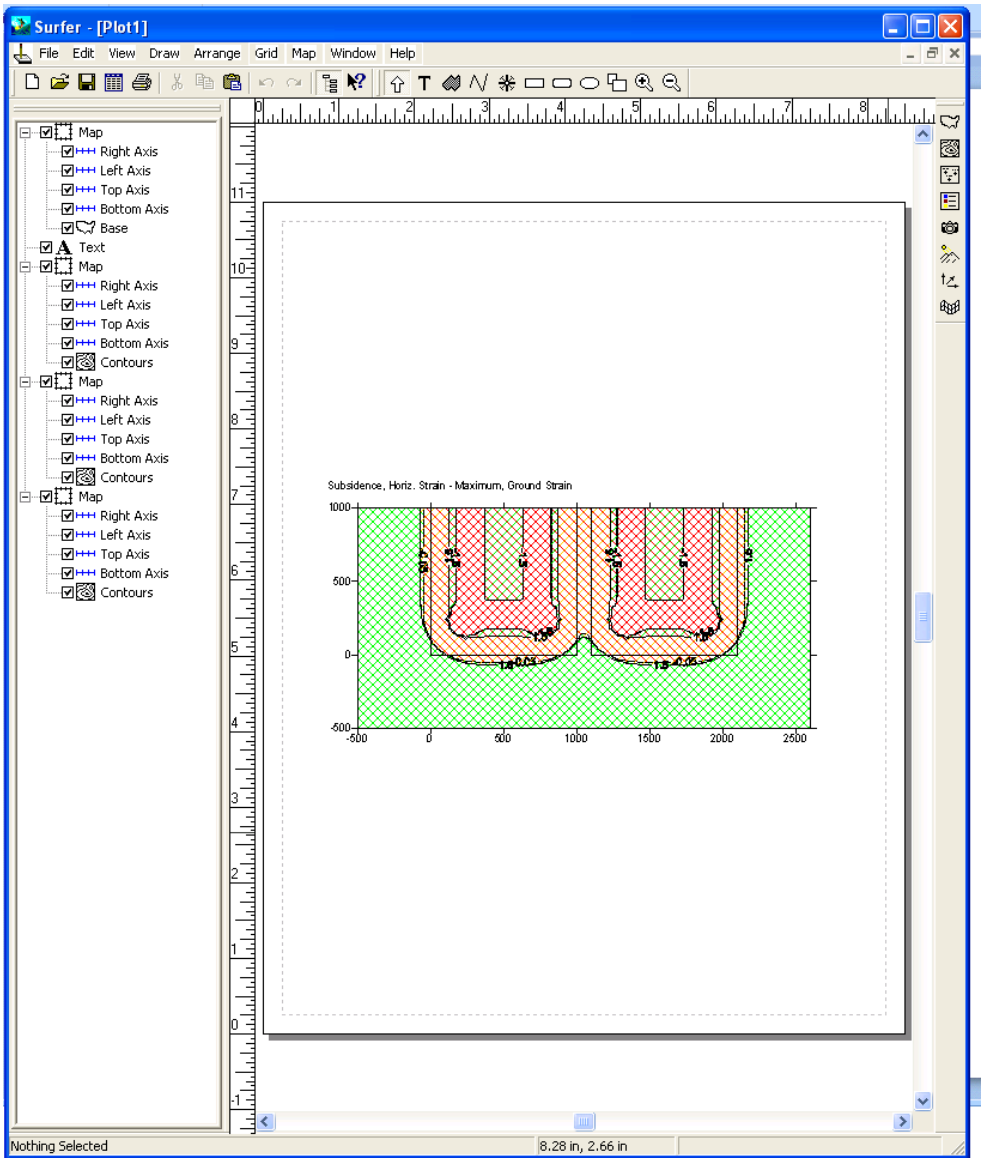

Figure 8: Risk Assessment, Basic Synthetic Case Study 1 – Initial Surfer Plot of Contoured Strain and Subsidence

SYNTHETIC CASE STUDY 2 (BASIC LONG-TERM LANDSCAPE STABILITY RISK-ASSESSMENT OVER WEAKENED PILLAR AREA IN ROOM AND PILLAR MINE)

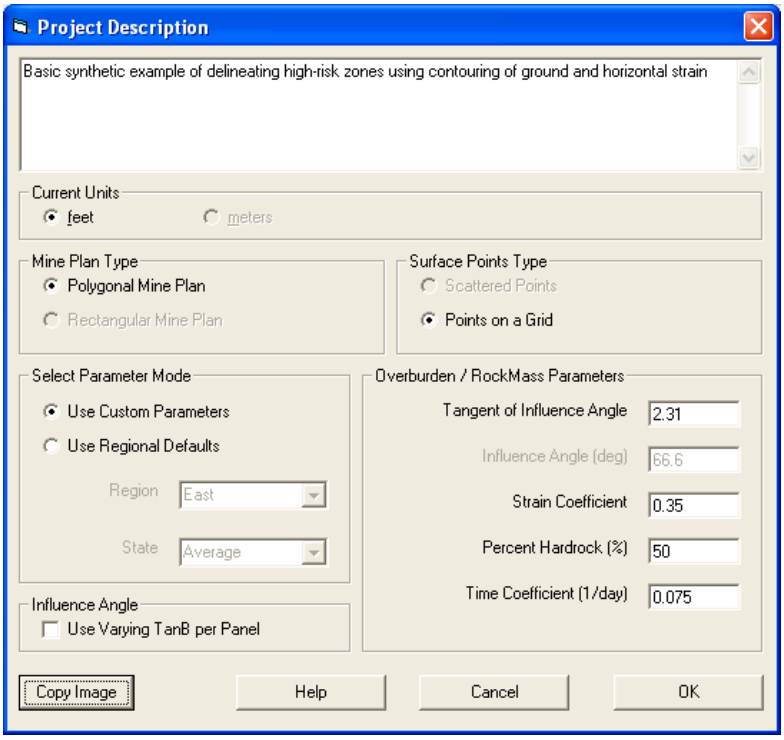

Figure 9: Risk Assessment, Basic Synthetic Case Study 2 – Project Description Screen

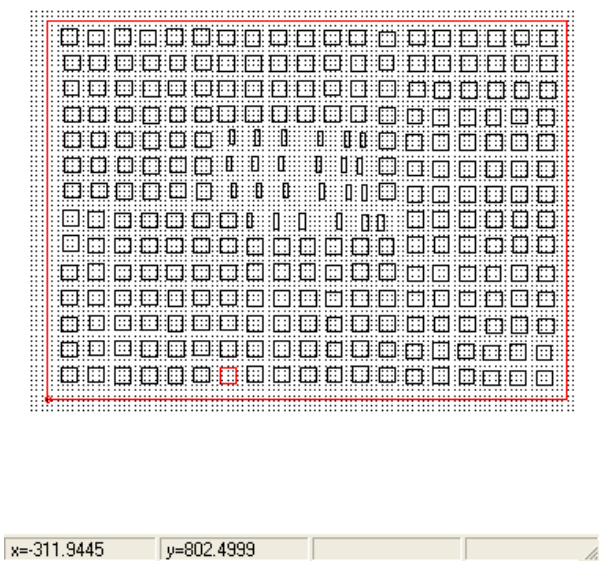

Figure 10: Risk Assessment, Basic Synthetic Case Study 2 – Basic Synthetic Mine Plan with Full-size Pillars and Weakened Pillars

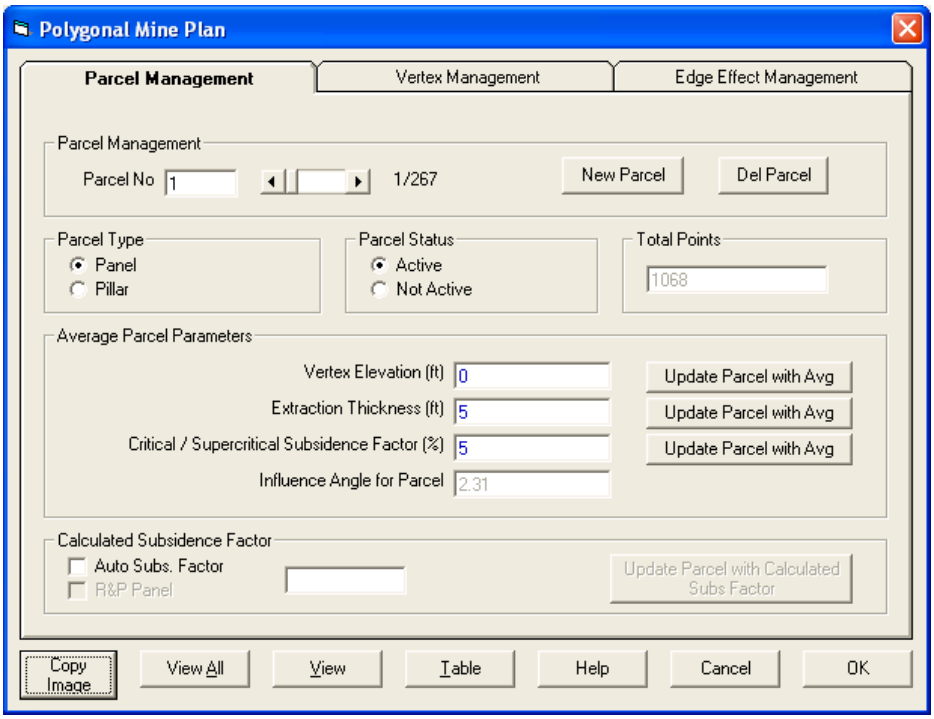

Figure 11: Risk Assessment, Basic Synthetic Case Study 2 – Parcel Management Screen, Panel

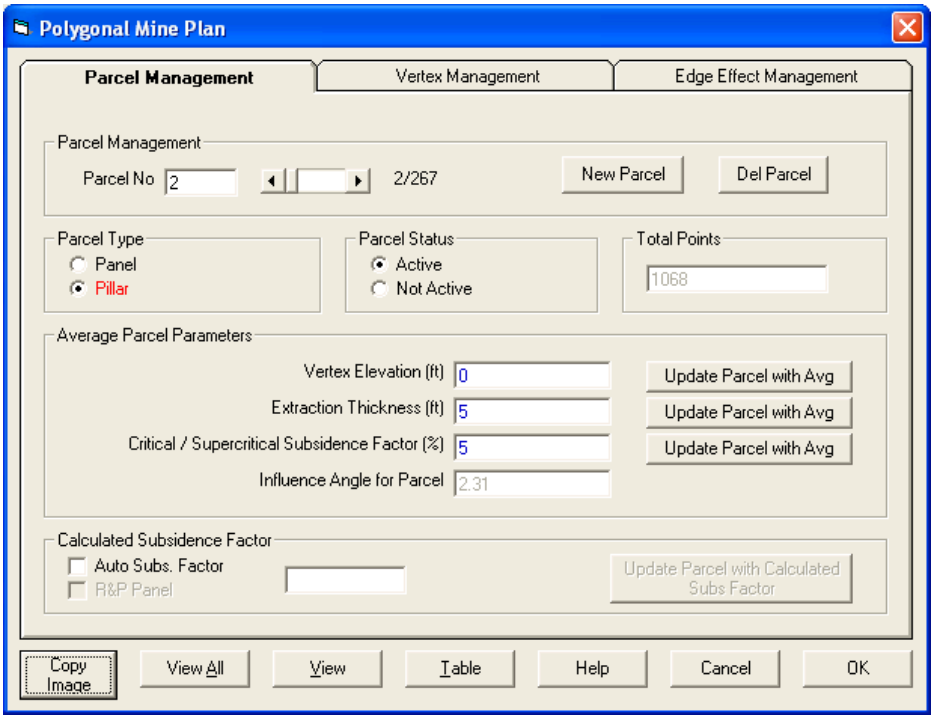

Figure 12: Risk Assessment, Basic Synthetic Case Study 2 – Parcel Management Screen, One Full-size Pillar Shown

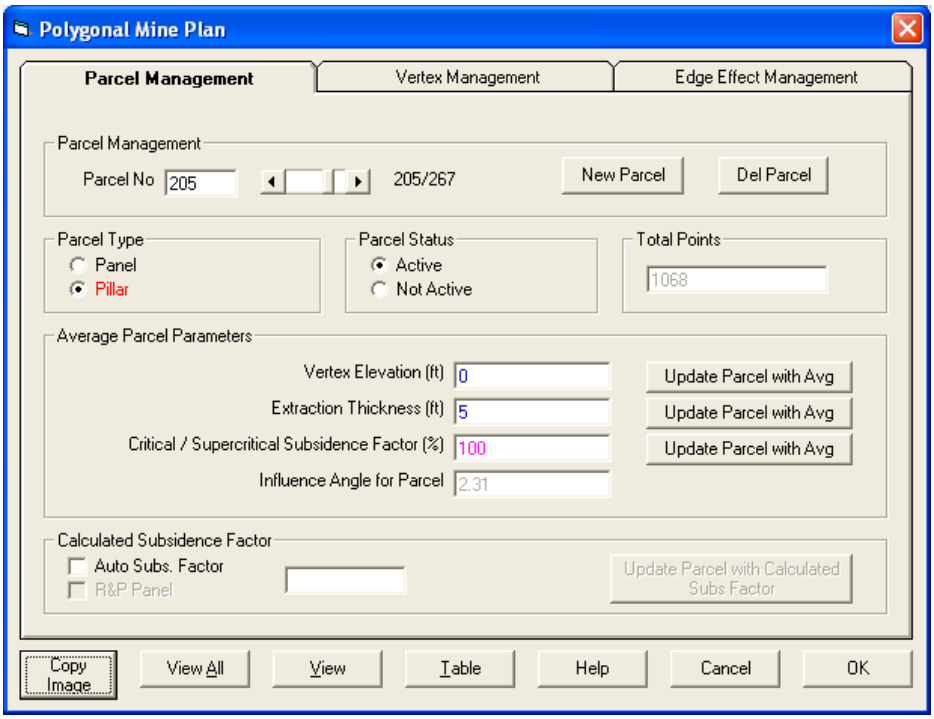

Figure 13: Risk Assessment, Basic Synthetic Case Study 2 – Parcel Management Screen, One Weakened Pillar Shown

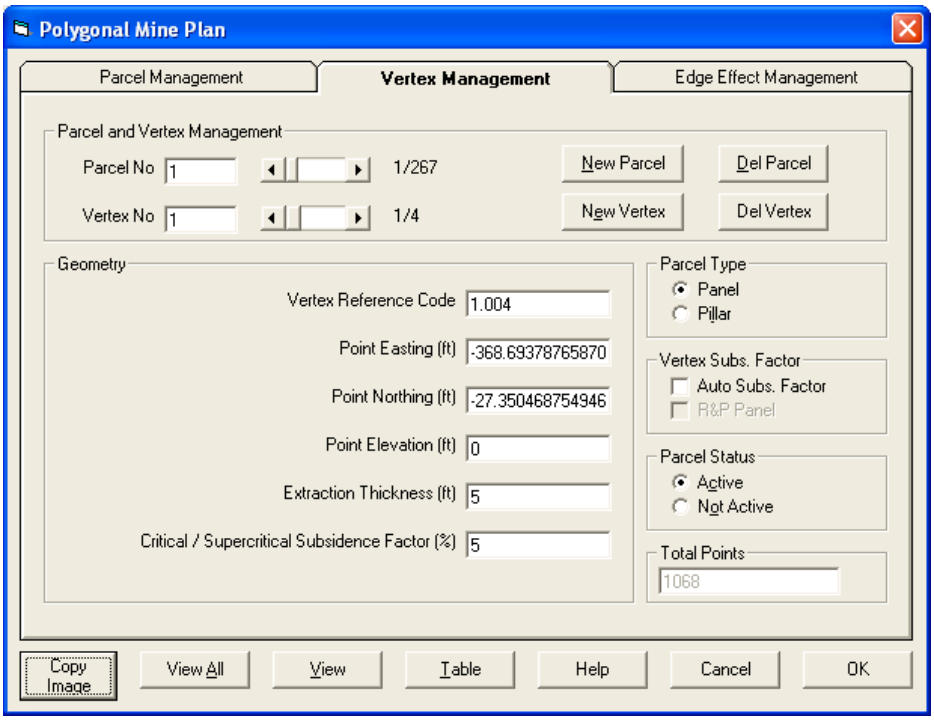

Figure 14: Risk Assessment, Basic Synthetic Case Study 2 – Vertex Management Screen, One Vertex of One Parcel Shown

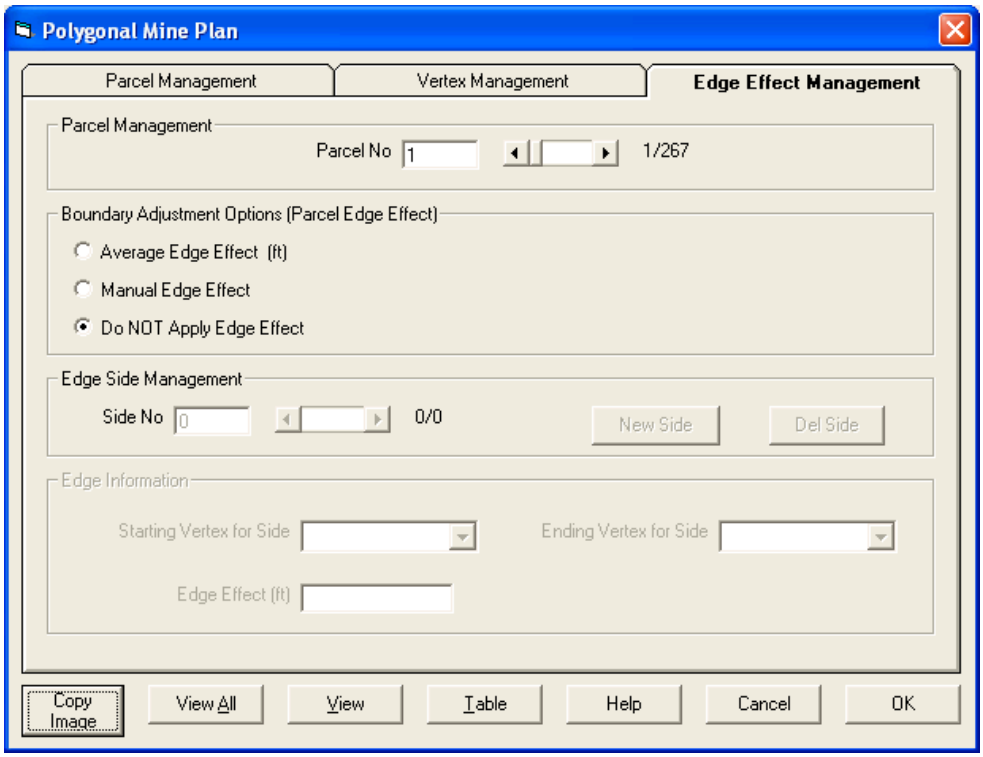

Figure 15: Risk Assessment, Basic Synthetic Case Study 2 – Edge Effect Management Screen, None Applied

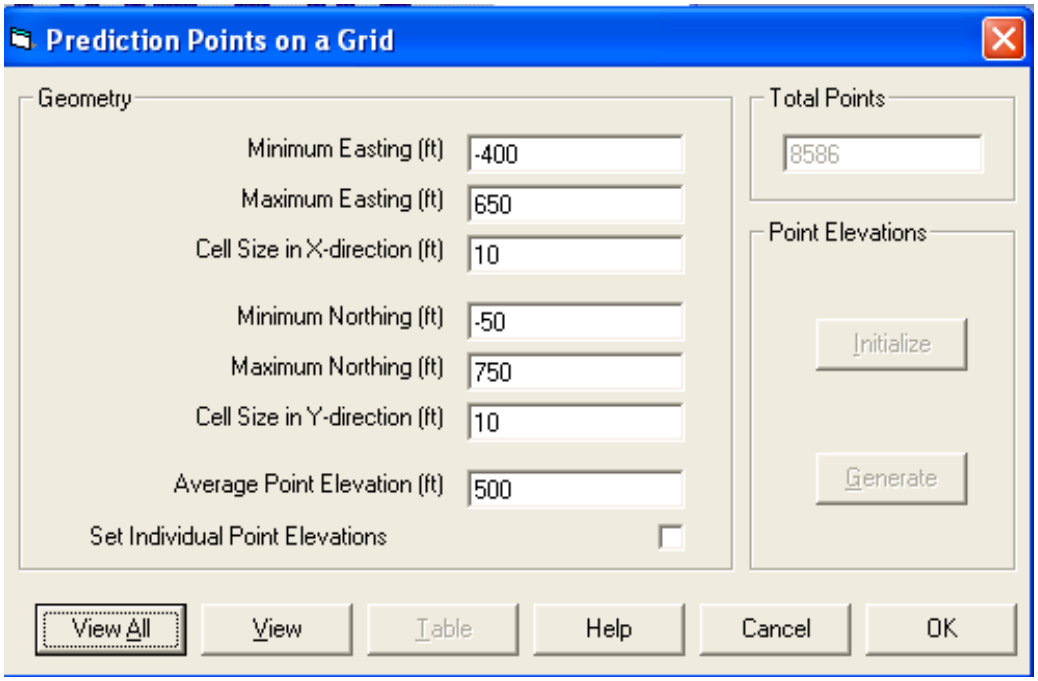

Figure 16: Risk Assessment, Basic Synthetic Case Study 2 – Prediction Points Management, Grid

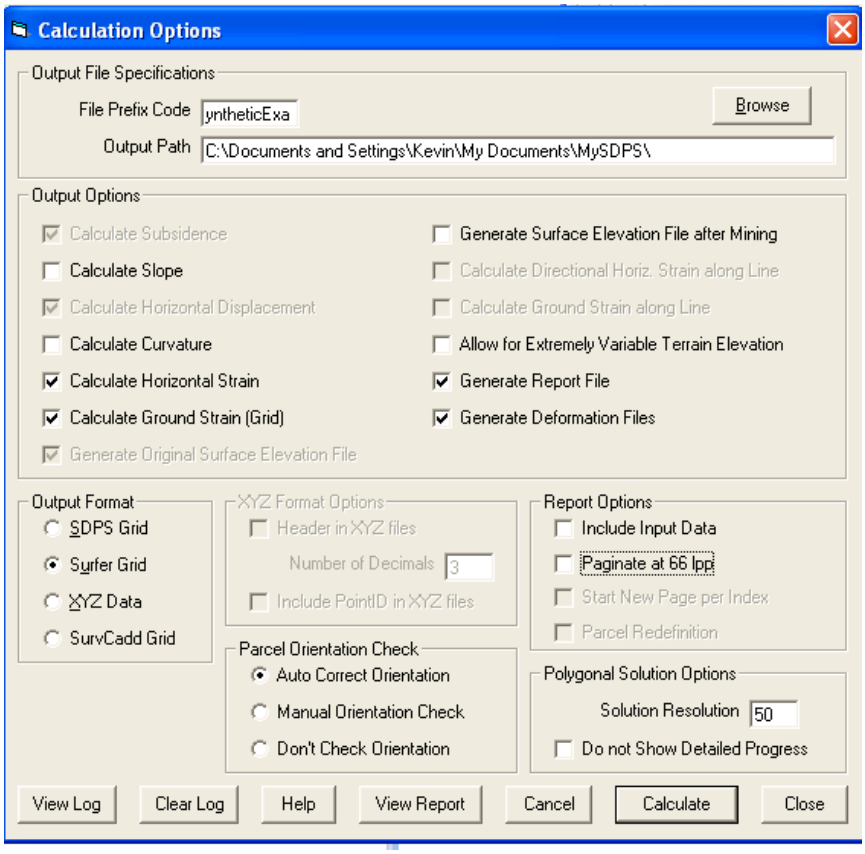

Figure 17: Risk Assessment, Basic Synthetic Case Study 2 – Calculation Options Screen

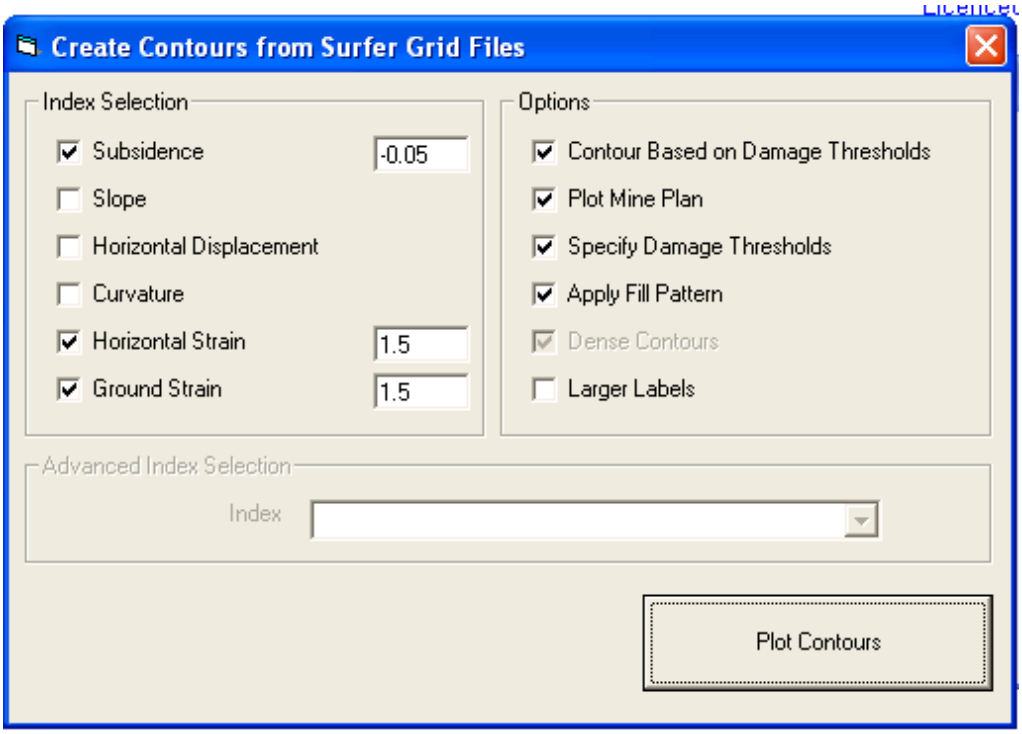

Figure 18: Risk Assessment, Basic Synthetic Case Study 2 – Grid Module, Create Contours in Surfer

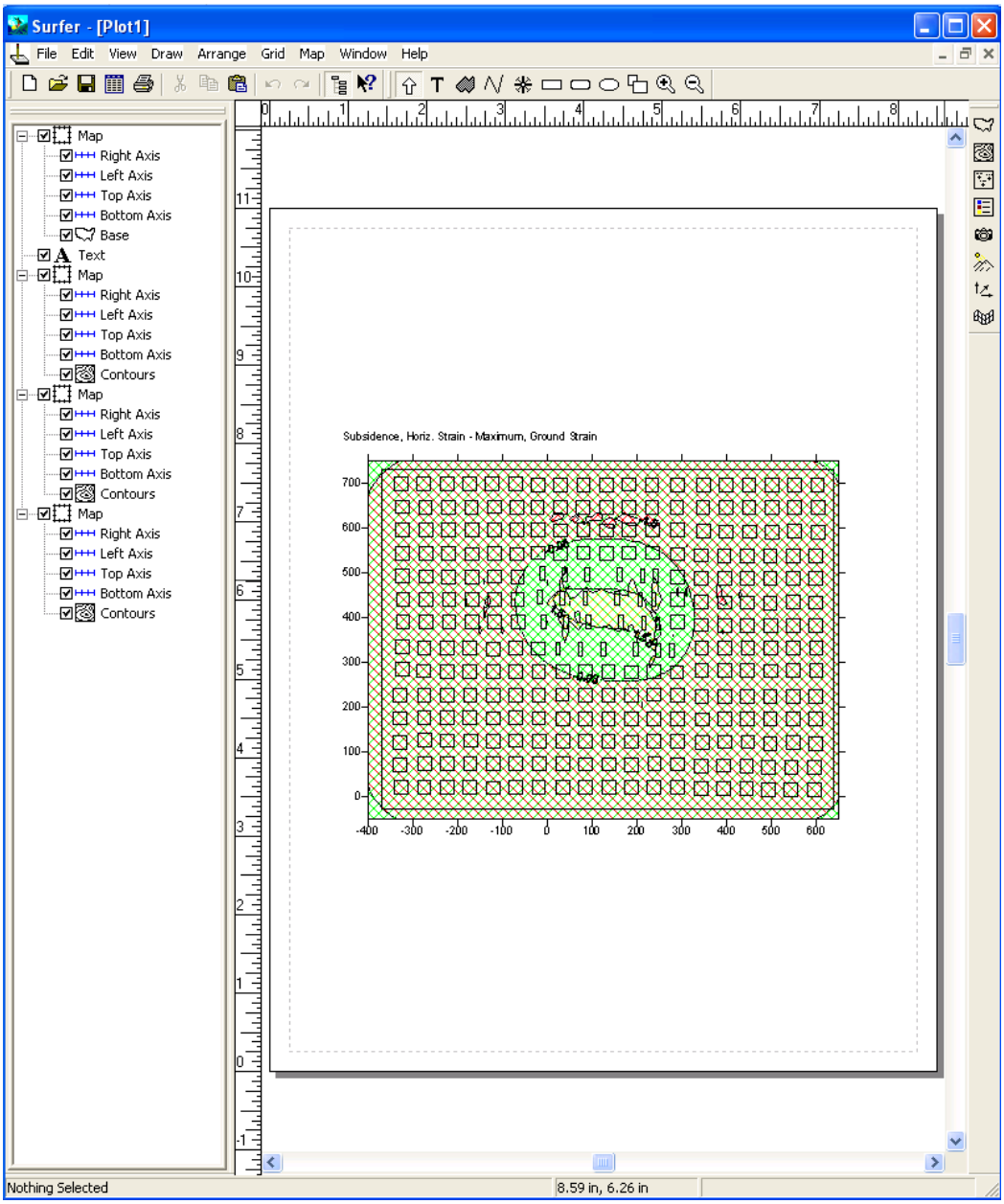

Figure 19: Risk Assessment, Basic Synthetic Case Study 2 – Initial Surfer Plot of Contoured Strain and Subsidence

Appendix VI –

Powerpoint presentation presented in a Short Course that was conducted to OSM personnel at the OSM offices in Pittsburgh on November 13 and 14, 2008

Recent Enhancement to Ground Deformation Prediction Methodology and SDPS Implementation

Pittsburgh, PA
November 13-14, 2008

M. Karmis, Z. Agioutantis, K. Andrews

Acknowledgement

- This short course is a partial requirement of the project titled “Enhancing Mine Subsidence Prediction and Control Methodologies for Long-term Landscape Stability” sponsored by the Applied Science Program of OSMRE
- Tom Mastaller is the Technical Project officer

Short Course Outline

- Review of Subsidence Fundamentals (Basic Concepts)
- SDPS Overview (Input Parameters and Software Enhancements)
- Profile Function Application - Examples
- Influence Function Application and Basic Examples
- Influence Function Application - New Approaches in Ground Deformation Assessment (Examples on Dynamic Analysis, Landscape control and Long-Term Stability)

Case Study Data

- If you have case study data with you that you would like to discuss during the short course, please provide a copy to Zach or Kevin to prepare for tomorrow.

Introduction

- The impacts of underground mining on the surface are important environmental considerations in the permission, planning and monitoring of coal mining operations
- The development of rigorous and well-accepted ground deformation prediction techniques and damage criteria for assessing mining impacts on surface structures and facilities, is the foundation of subsidence engineering and control

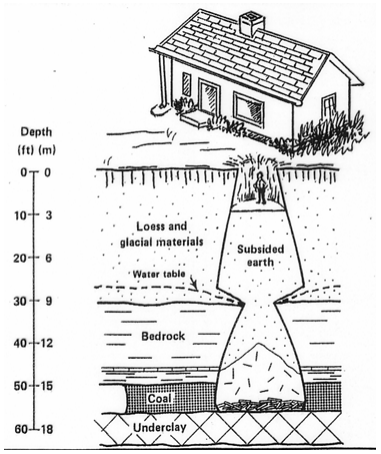

Ground Movement Predictions

- A complex task, due to the number and nature of the parameters affecting ground deformation induced by underground mining
- Important parameters include: subsidence characteristics, surface morphology, mine plan, mining sequence, coal structure characteristics, overburden lithology and type of surface facility to be protected.

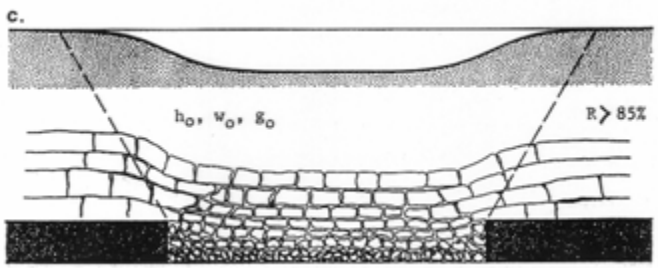

Surface Deformation Prediction Software System (SDPS)

- The Surface Deformation Prediction Software System (SDPS) is an integrated package for calculating a variety of surface deformation indices, using both the profile function and the influence function methods
- Calculations are based on several empirical relationships, developed through the statistical analysis of data from a number of case studies (VPI & SU, 1987 & 1999; Karmis et al., 1989, 1990 & 1992)

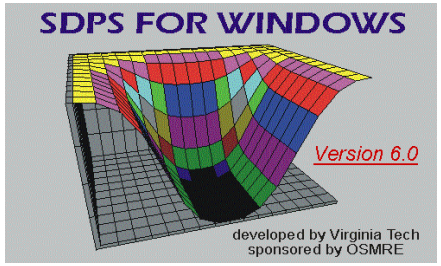

SDPS Enhancements

- SDPS has recently been enhanced following the completion of this OSMRE-sponsored project. New features include
  - Dynamic Deformations
  - Subsidence and Strain Calibration
  - Risk-Based Assessment
  - Long Term Stability

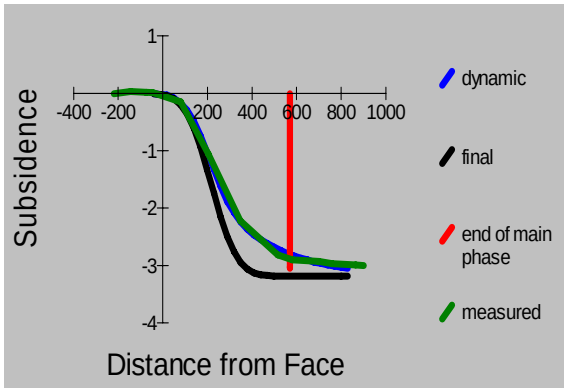

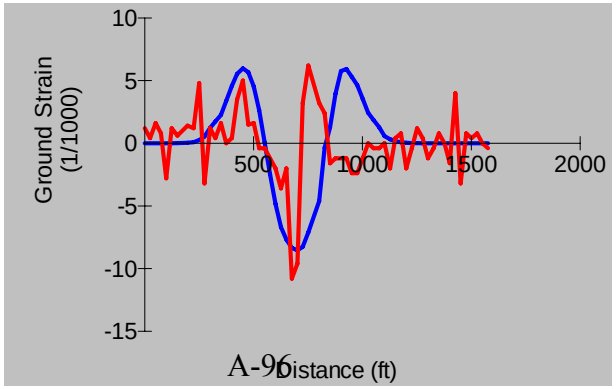

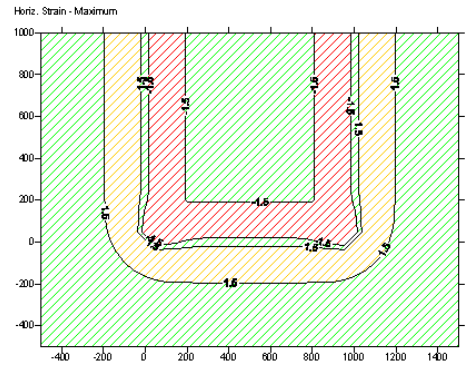

Review of Subsidence Fundamentals

- Basic Concepts
  - Characteristic angles and parameters
  - The importance of the “critical” mining area in subsidence prediction
  - Panel width in multiple panel extraction
  - Statistical correlations

Subsidence Parameters

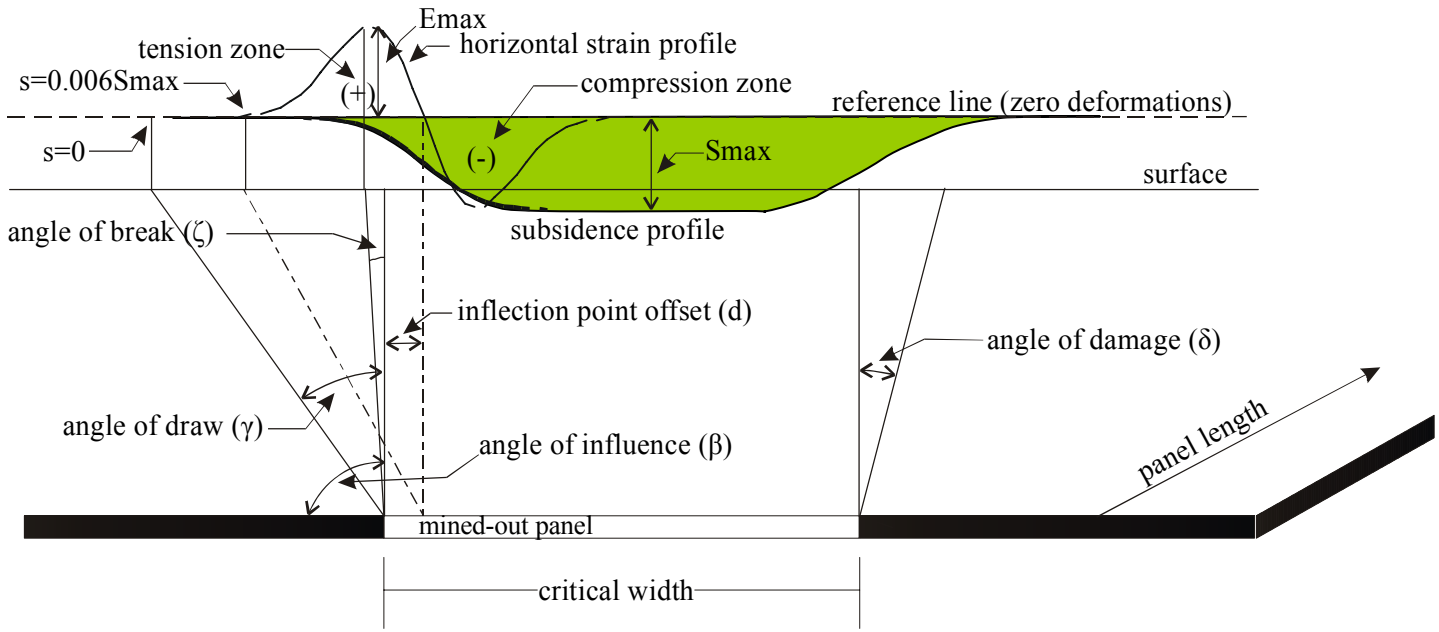

The maximum subsidence (Smax)

Subsidence Parameters

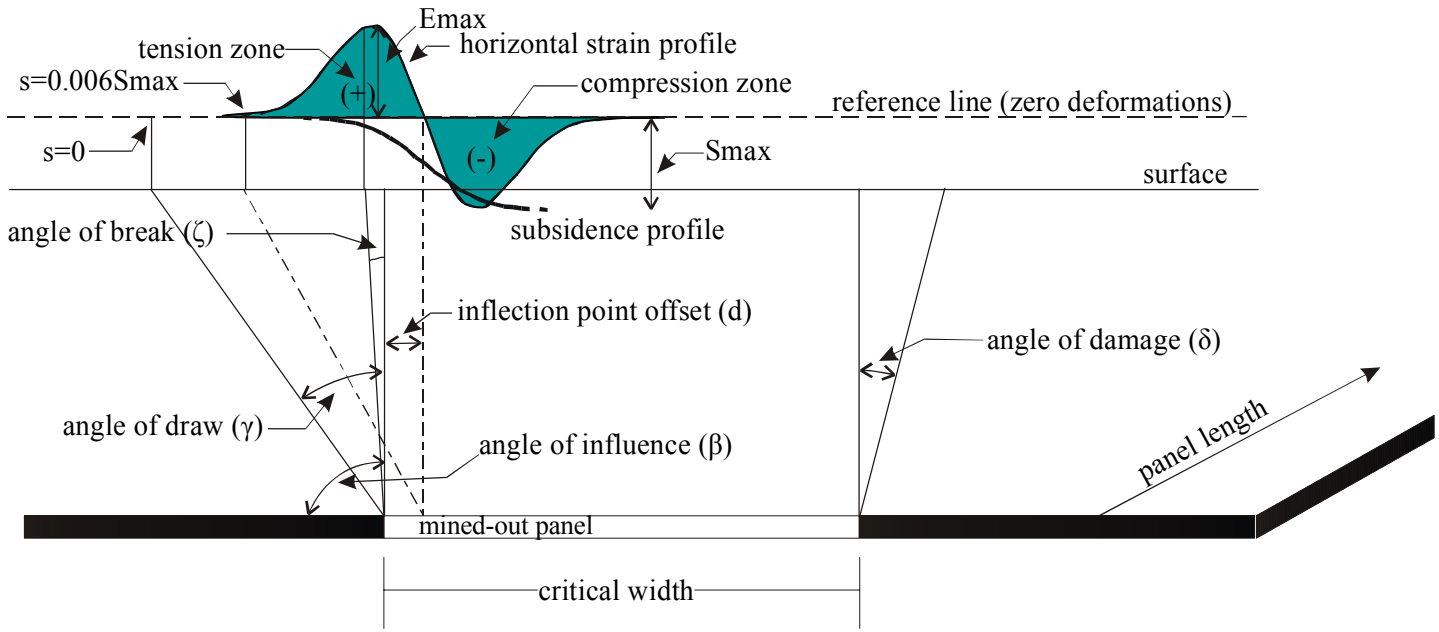

The maximum tensile and compressive strains (Emax)

Subsidence Parameters

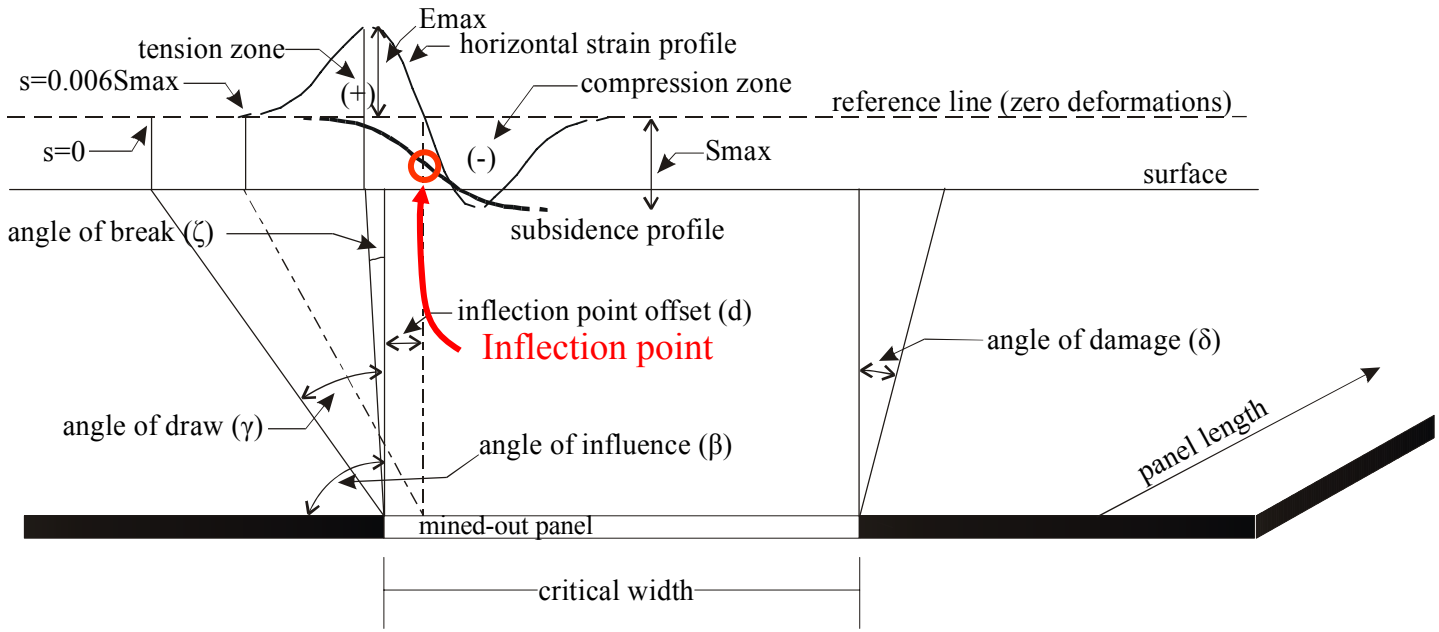

The <u>inflection point</u> corresponds to s = Smax/2 on the subsidence profile or zero curvature. This point is usually displaced from the rib of the excavation at a distance, (d) towards the panel center.

Subsidence Parameters

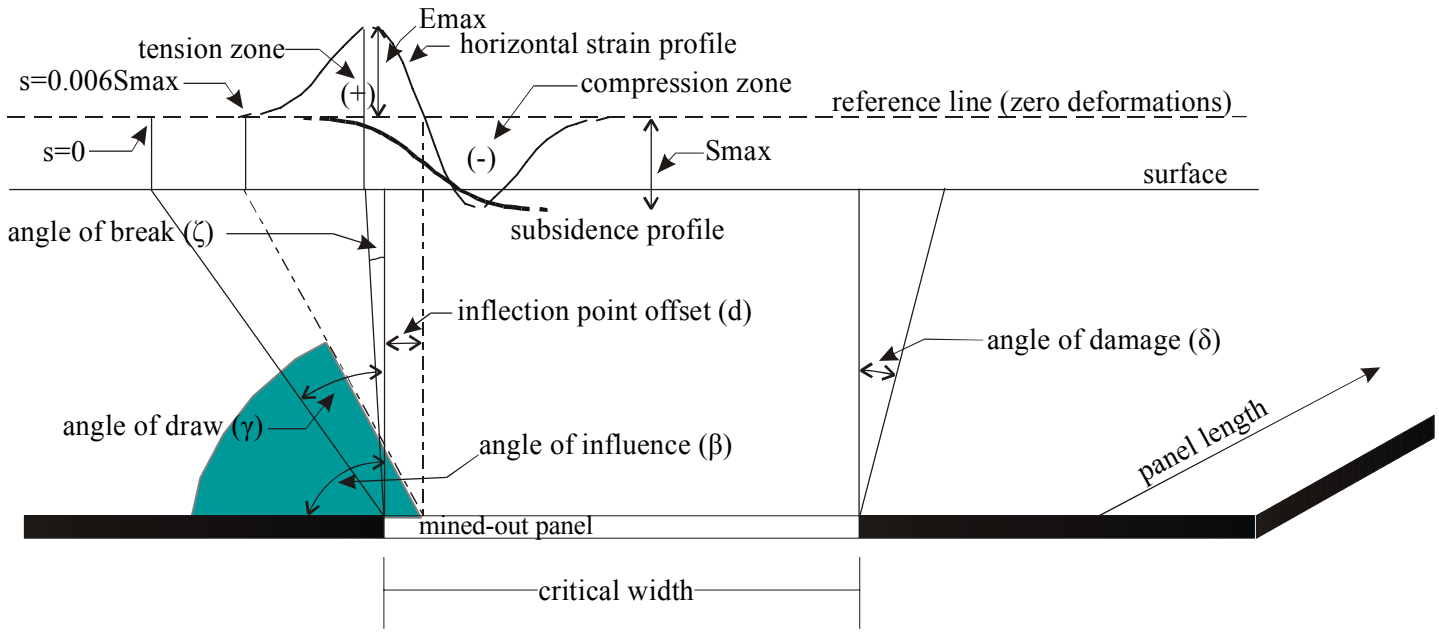

<u>Angle of Influence:</u> the angle between the horizontal and the line connecting the projection of the inflection point position of the subsidence trough, at the seam level, with the surface point of "zero influence" (i.e. defined by 0.6%Smax)

Subsidence Parameters

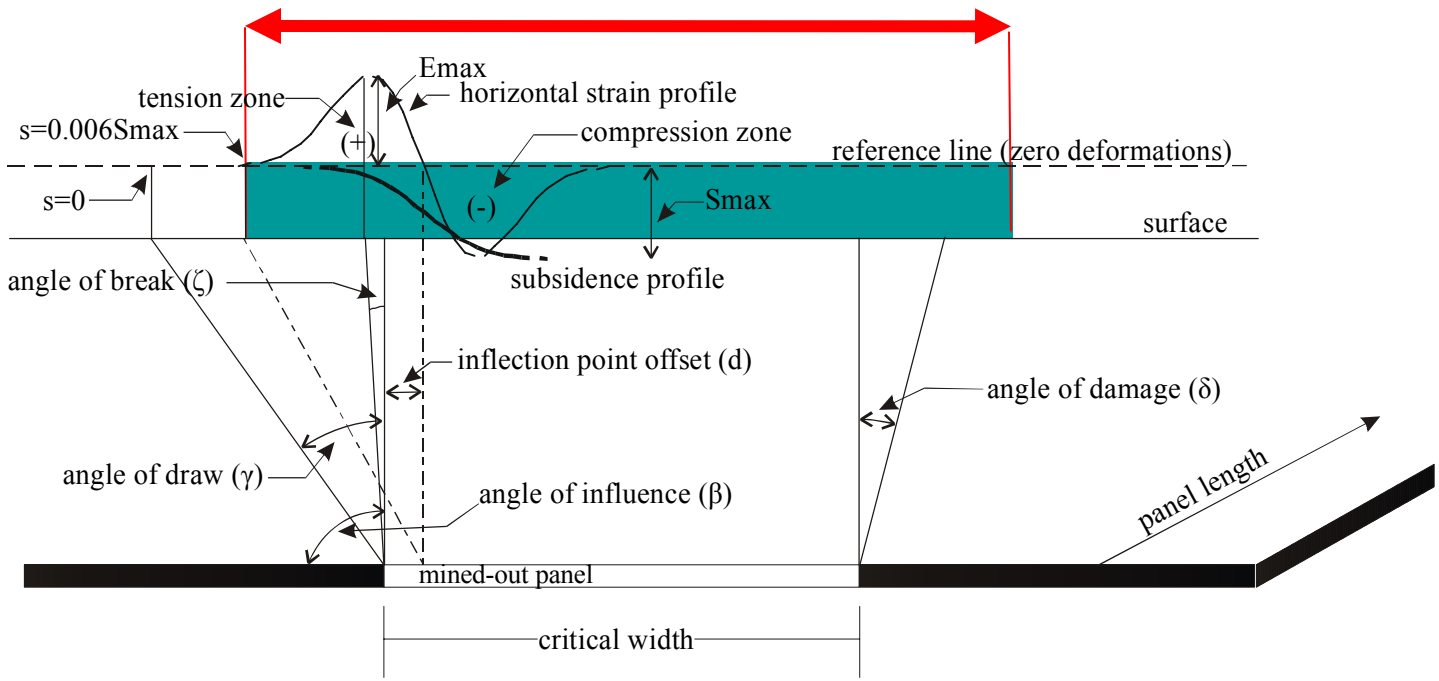

<u>Influence Area:</u> The surface area above an underground excavation within which ground movements are measurable (i.e., 0.6% Smax).

Subsidence Parameters

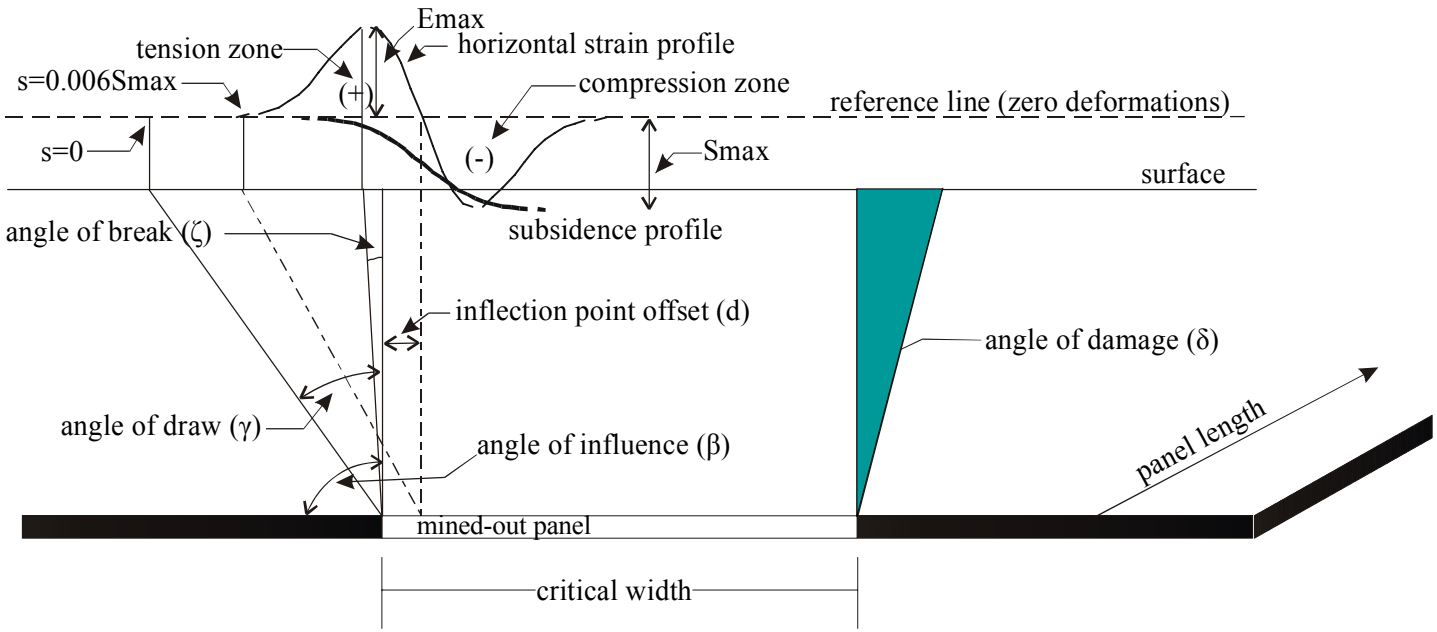

<u>Angle of damage:</u> The angle from the vertical to the point of appreciable damage on a surface structure.

Critical Extraction

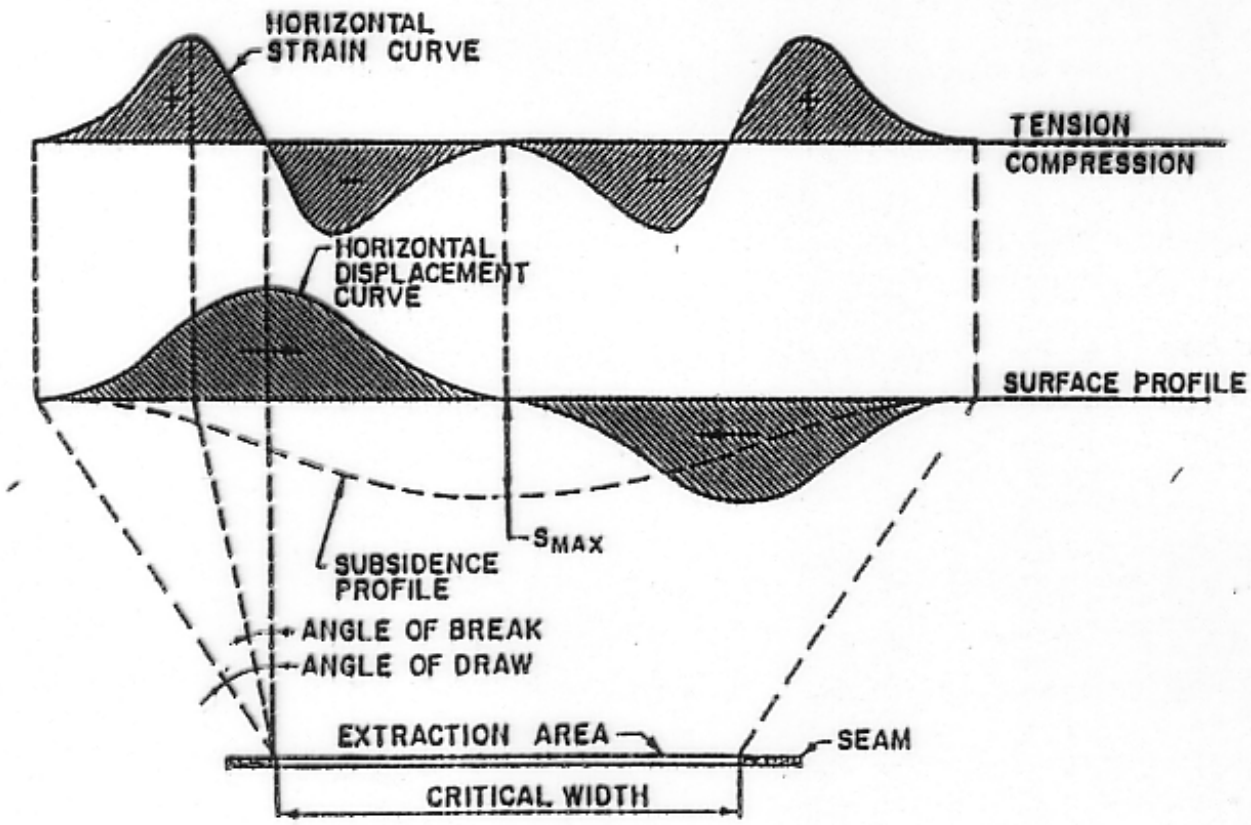

Sub-Critical Extraction

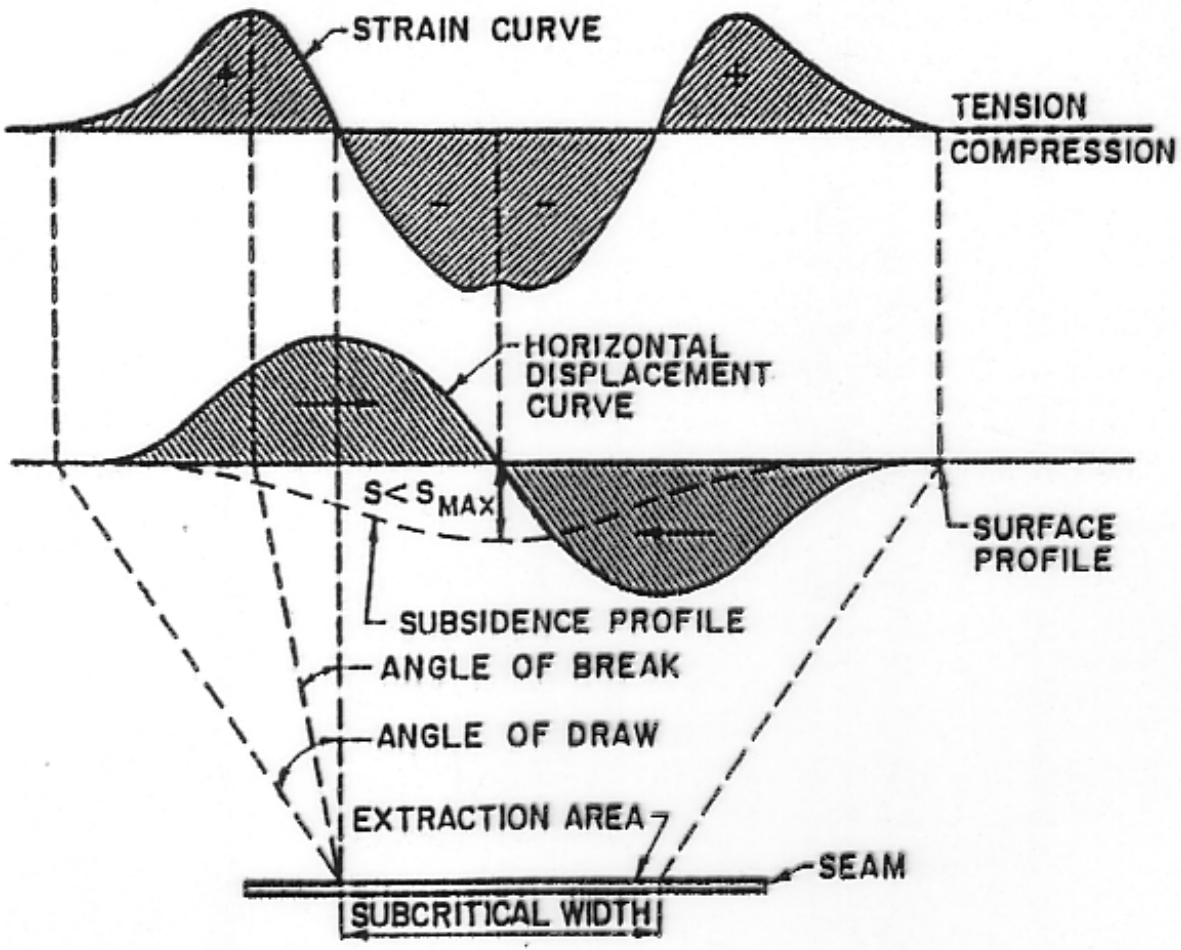

Supercritical Extraction

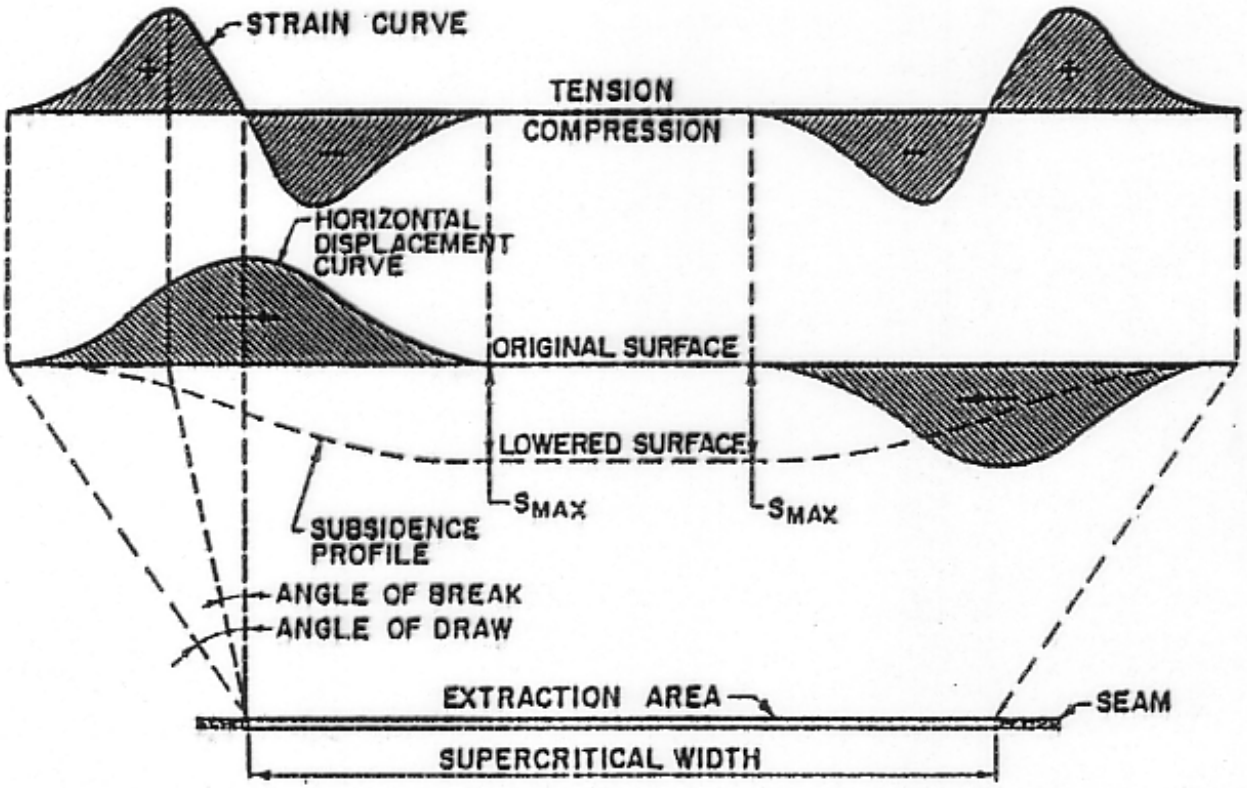

Critical and Subcritical Profiles

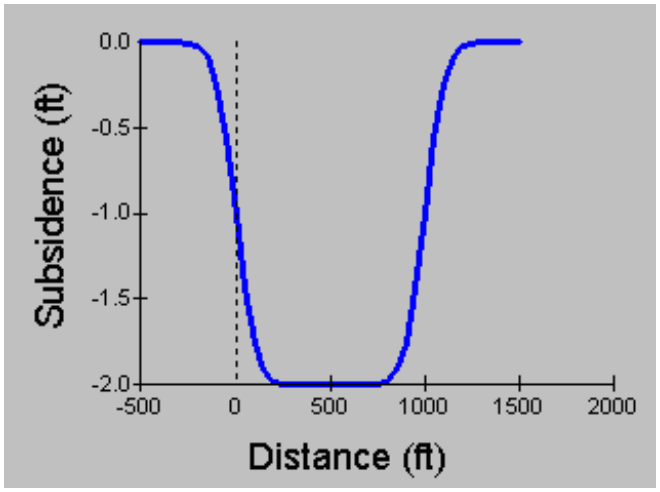

Supercritical

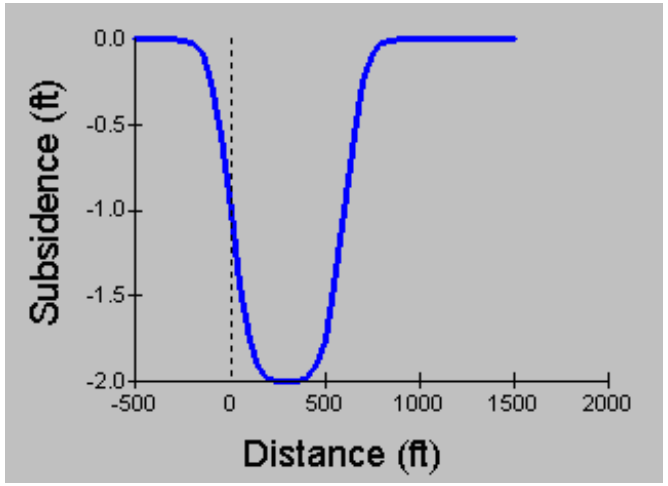

Critical

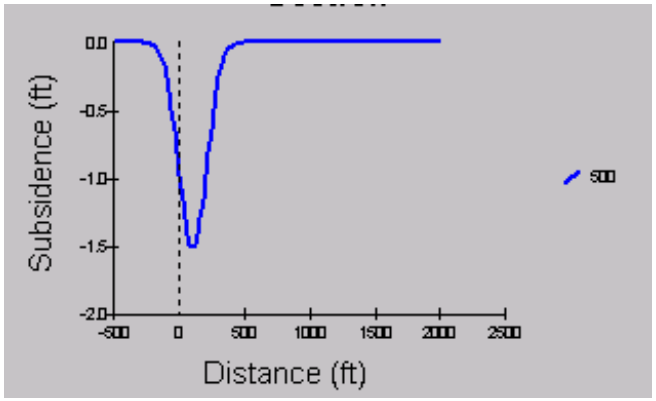

Subcritical

Critical and Subcritical Profiles

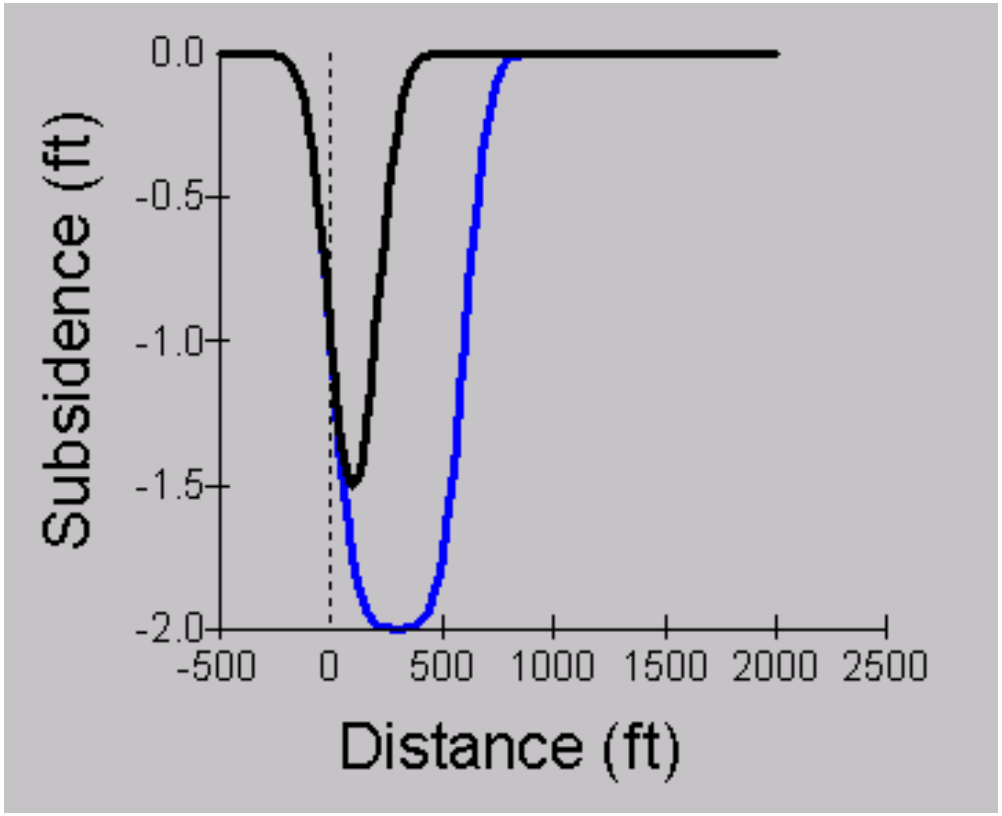

Mining Progress

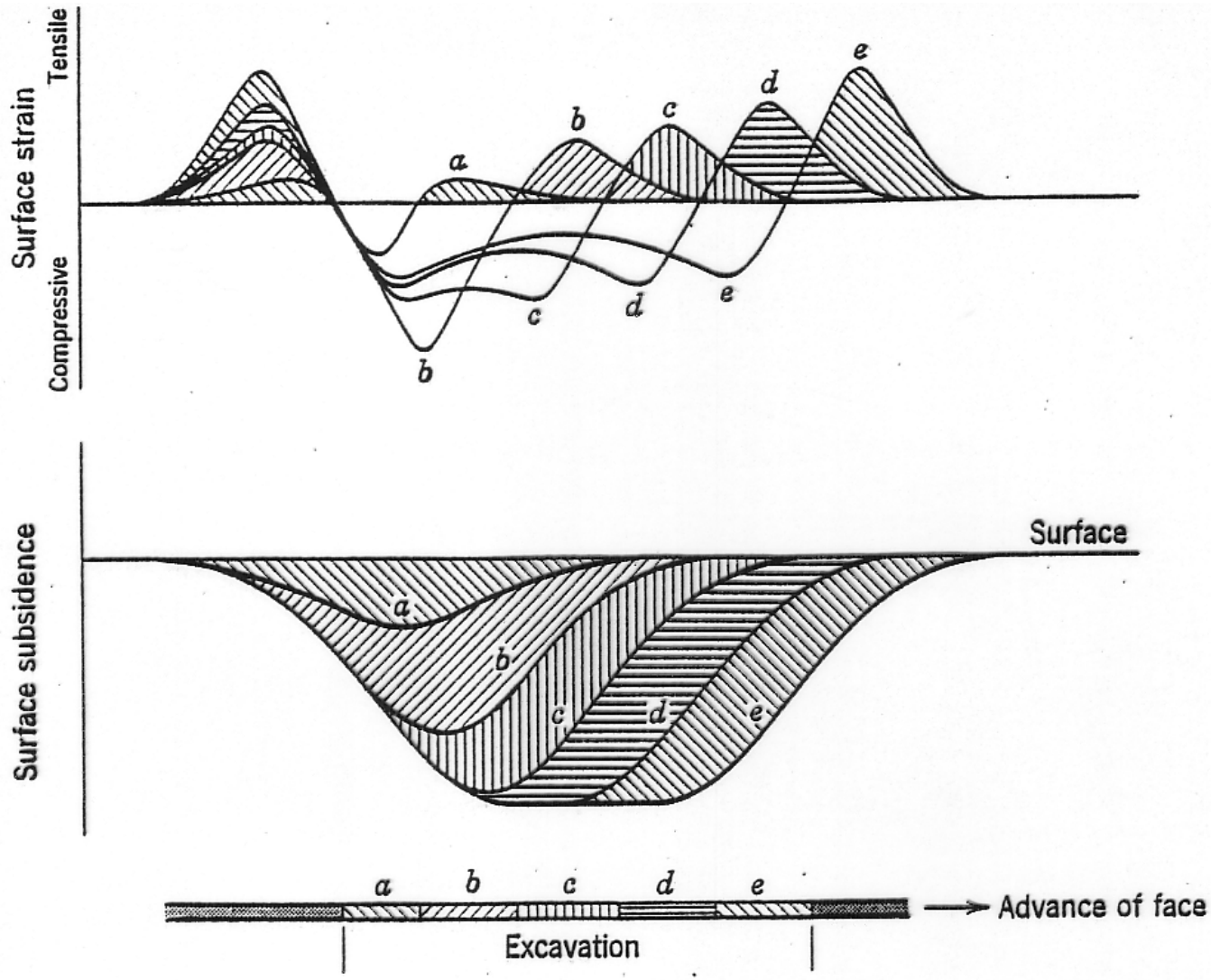

Progress of subsidence with advance of excavated area. (After Rellensmann[1])

Defining Panel Area: Single, Sub-critical, Panel

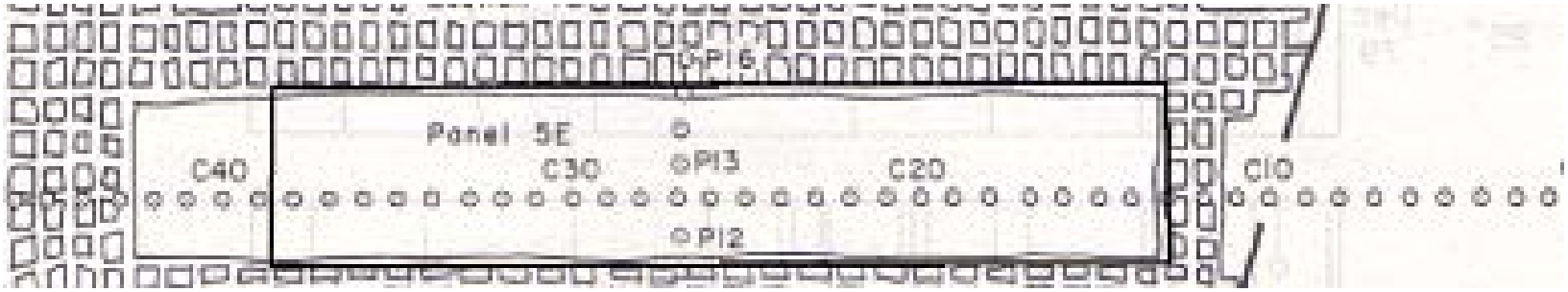

Defining Panel Area:
Multiple, Critical/Supercritical, Panels

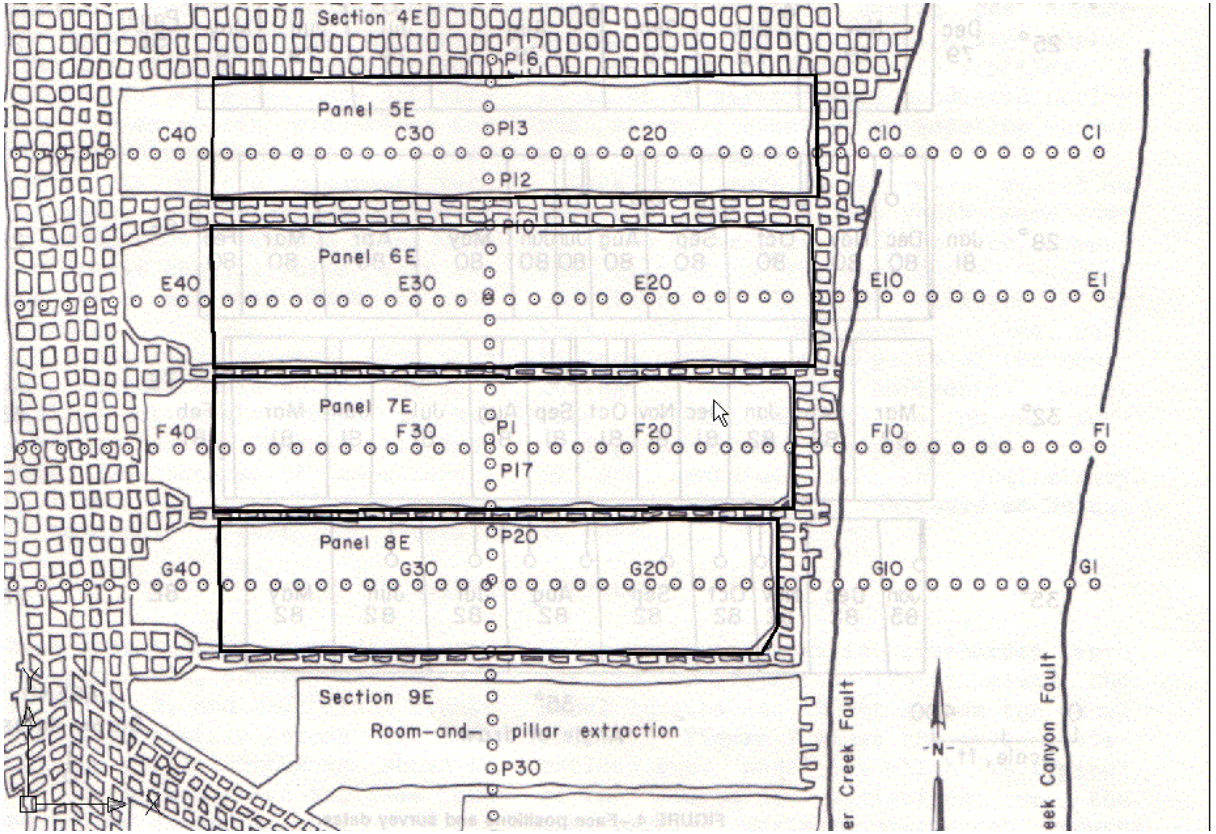

Edge Effect

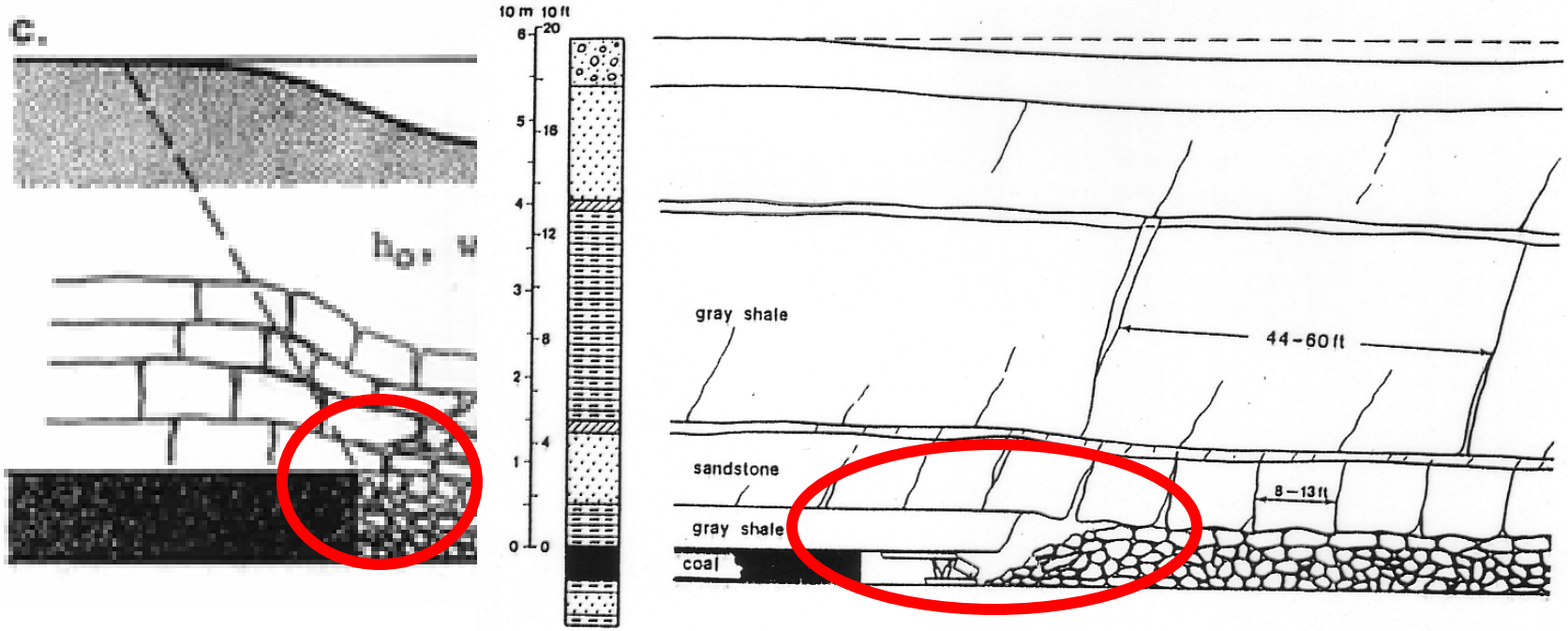

Immediate and main roof behavior in the Lower Kittanning seam.

The definition of edge effect is very important in predictions

Statistical Correlations

- Correlation of the maximum subsidence factor with the width-to-depth ratio
- Correlation of the maximum subsidence factor with %HR for critical and supercritical panels
- Correlation of the maximum subsidence factor with %HR for all W/h

Correlation of the maximum subsidence factor with the W/h

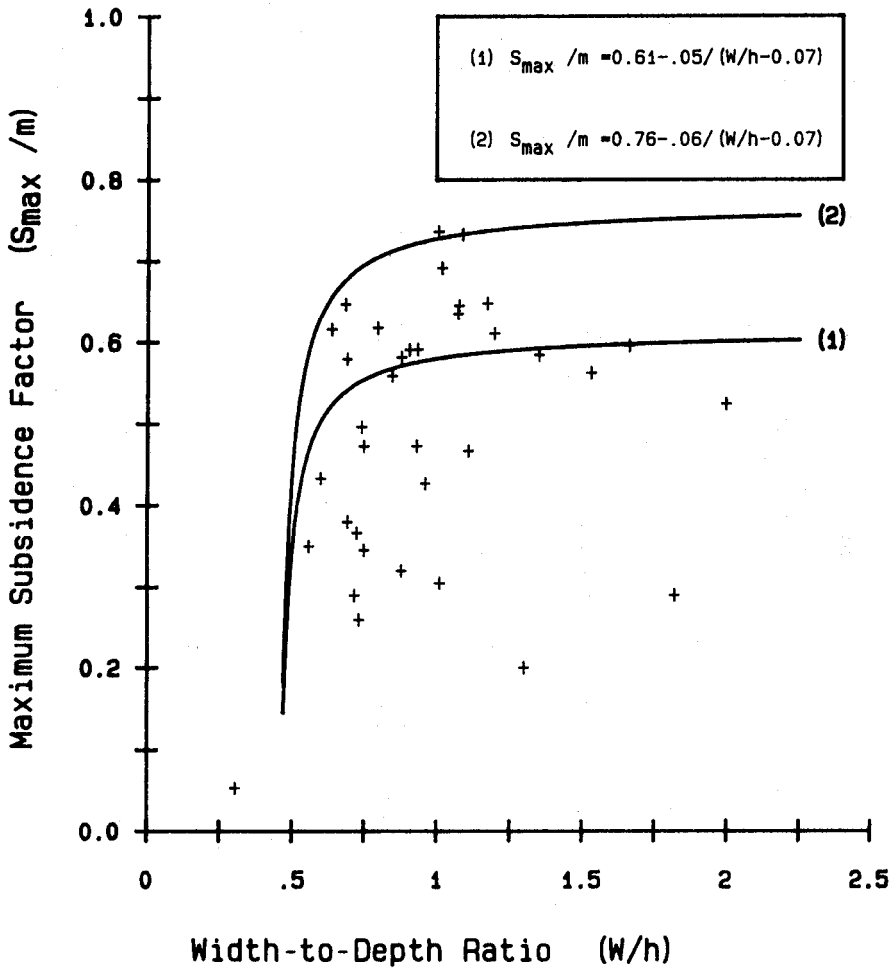

% Hardrock is Determined from Lithology

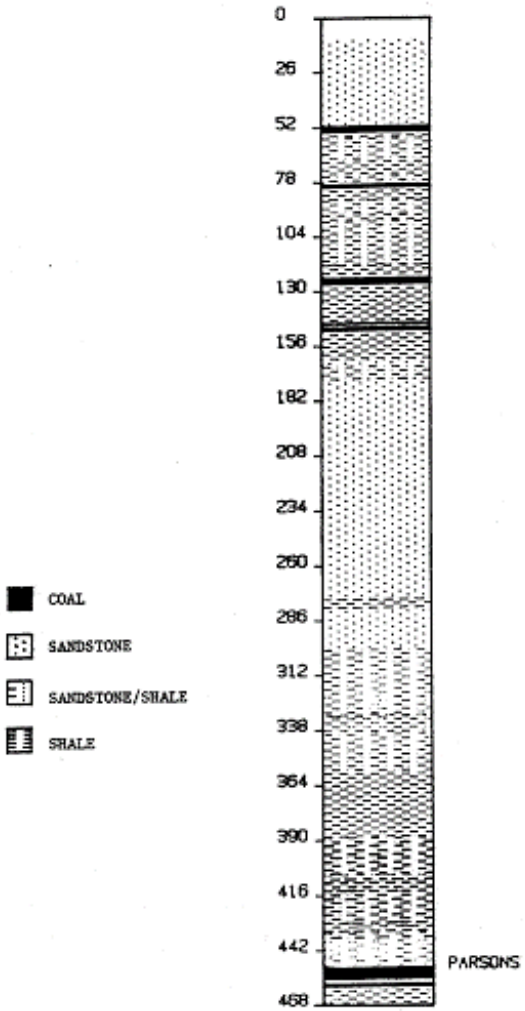

Defined, in subsidence investigations, as the sum of the strong rocks (e.g., sandstone, limestone), having a minimum thickness of 5 feet, expressed as a percentage of the total overburden thickness.

Correlation of the maximum subsidence factor with the %HR for critical and supercritical cases

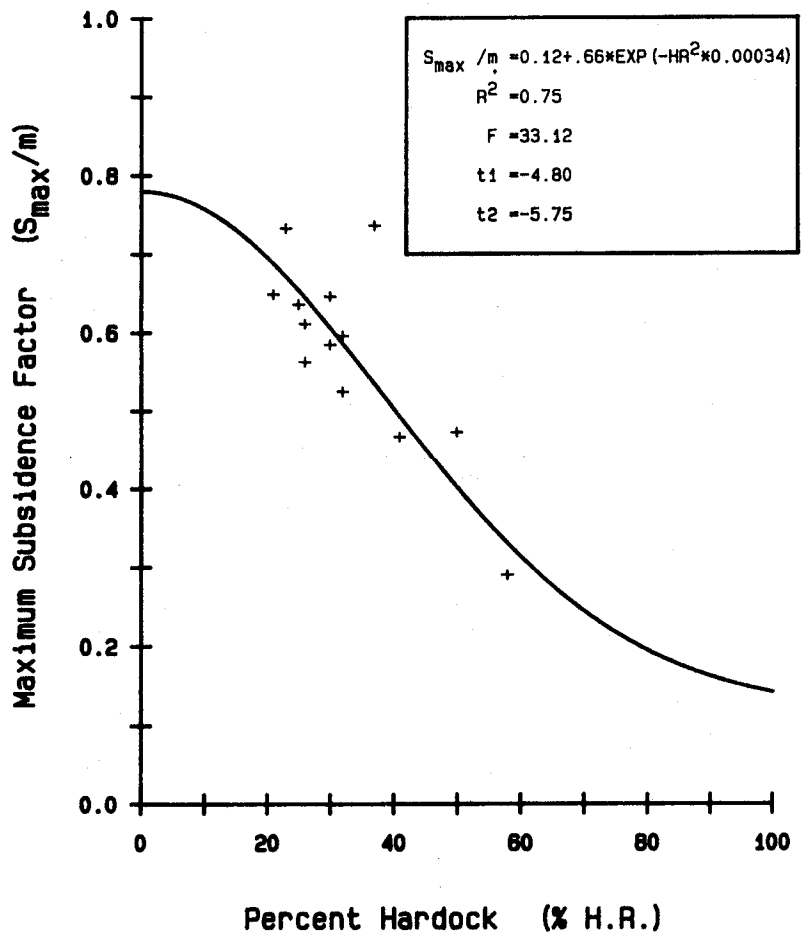

Correlation of the Smax factor with %HR for all W/h

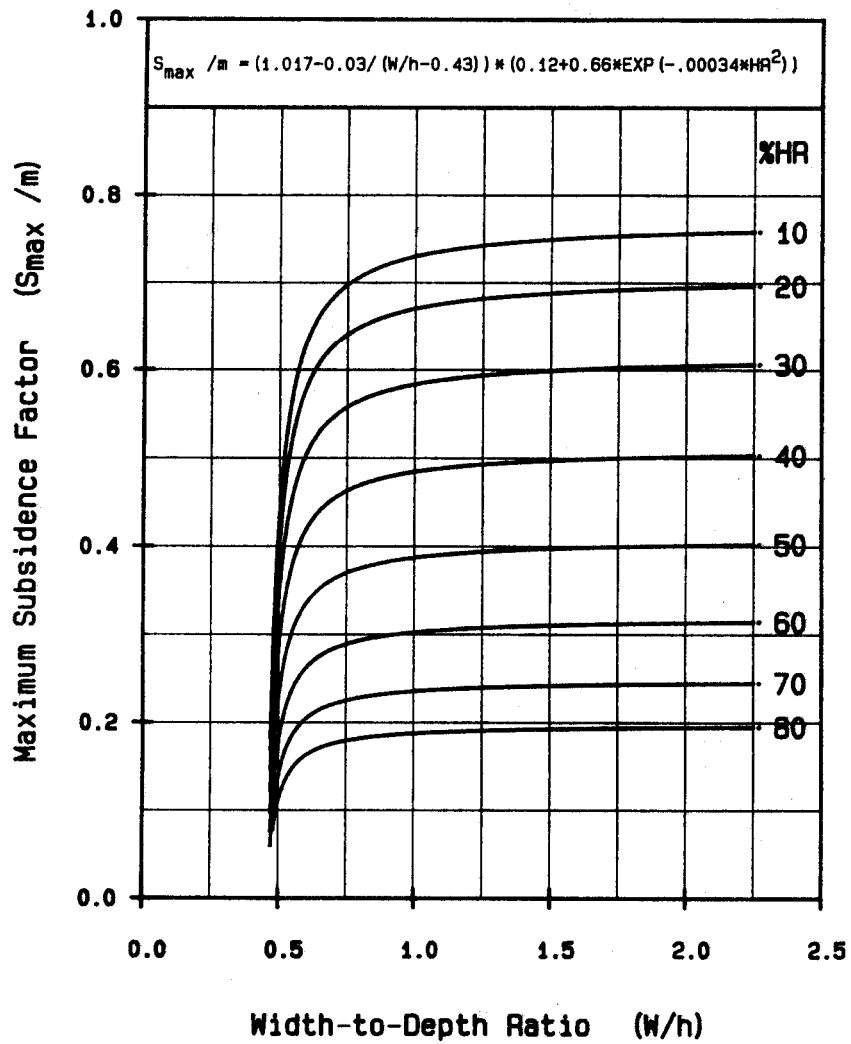

Statistical Correlations (cont'd)

- Correlation of the distance of the inflection point from the rib of the panel, with respect to the width-to-depth ratio of the panel
- Regional value for the tangent of the influence angle (tanβ) and the radius of influence
- Regional value for the horizontal strain coefficient (Bs)

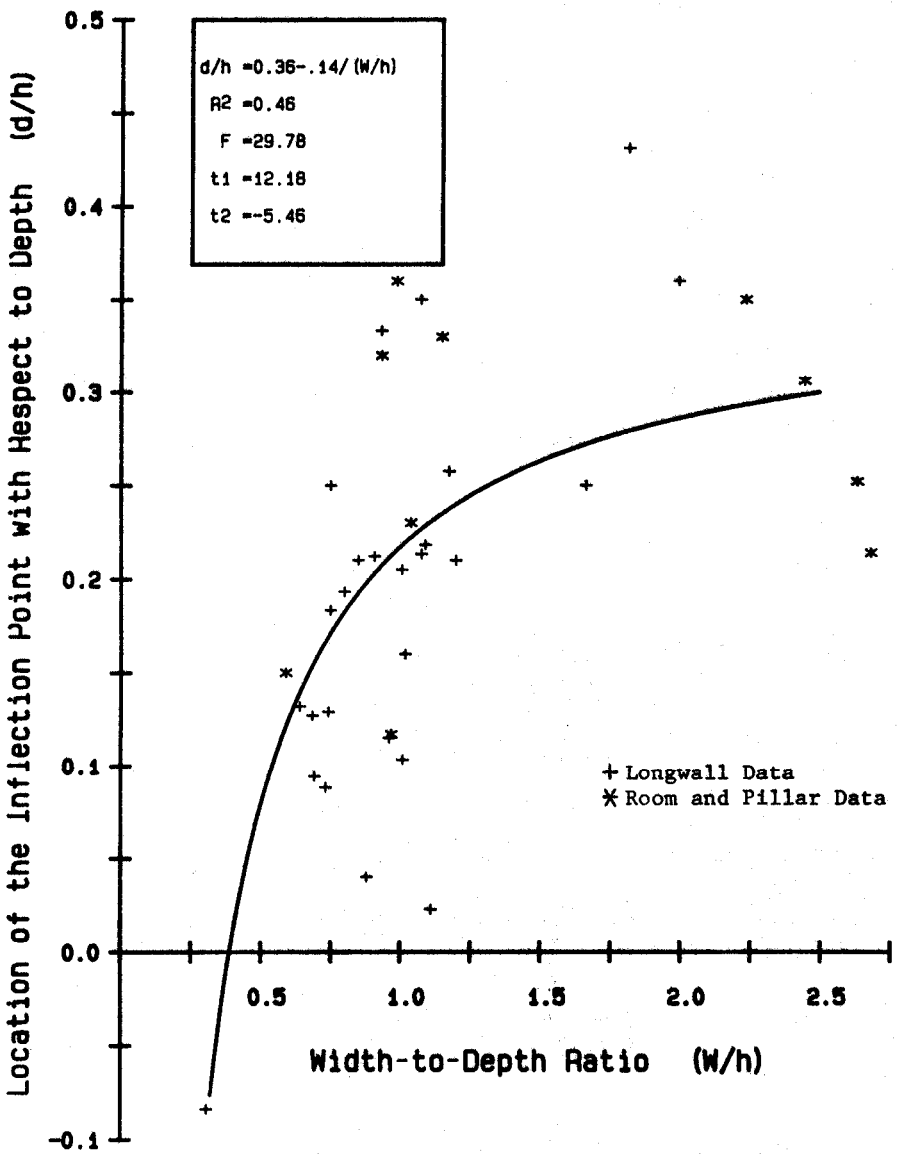

Correlation of the distance of the inflection point from the rib of the panel, with respect to the width-to-depth ratio of the panel (envelope)

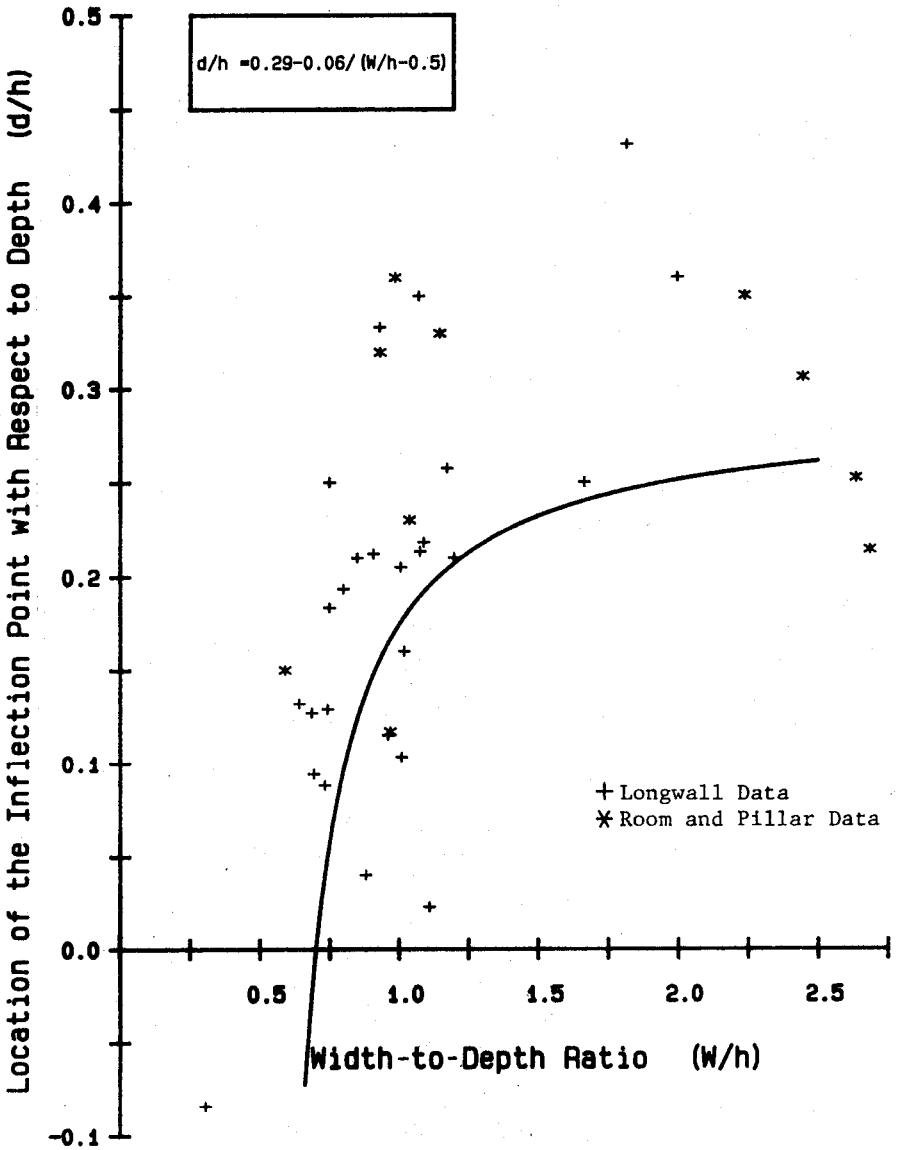

Correlation of the distance of the inflection point from the rib of the panel, with respect to the width-to-depth ratio of the panel (average)

Correlation of edge effect to W/h

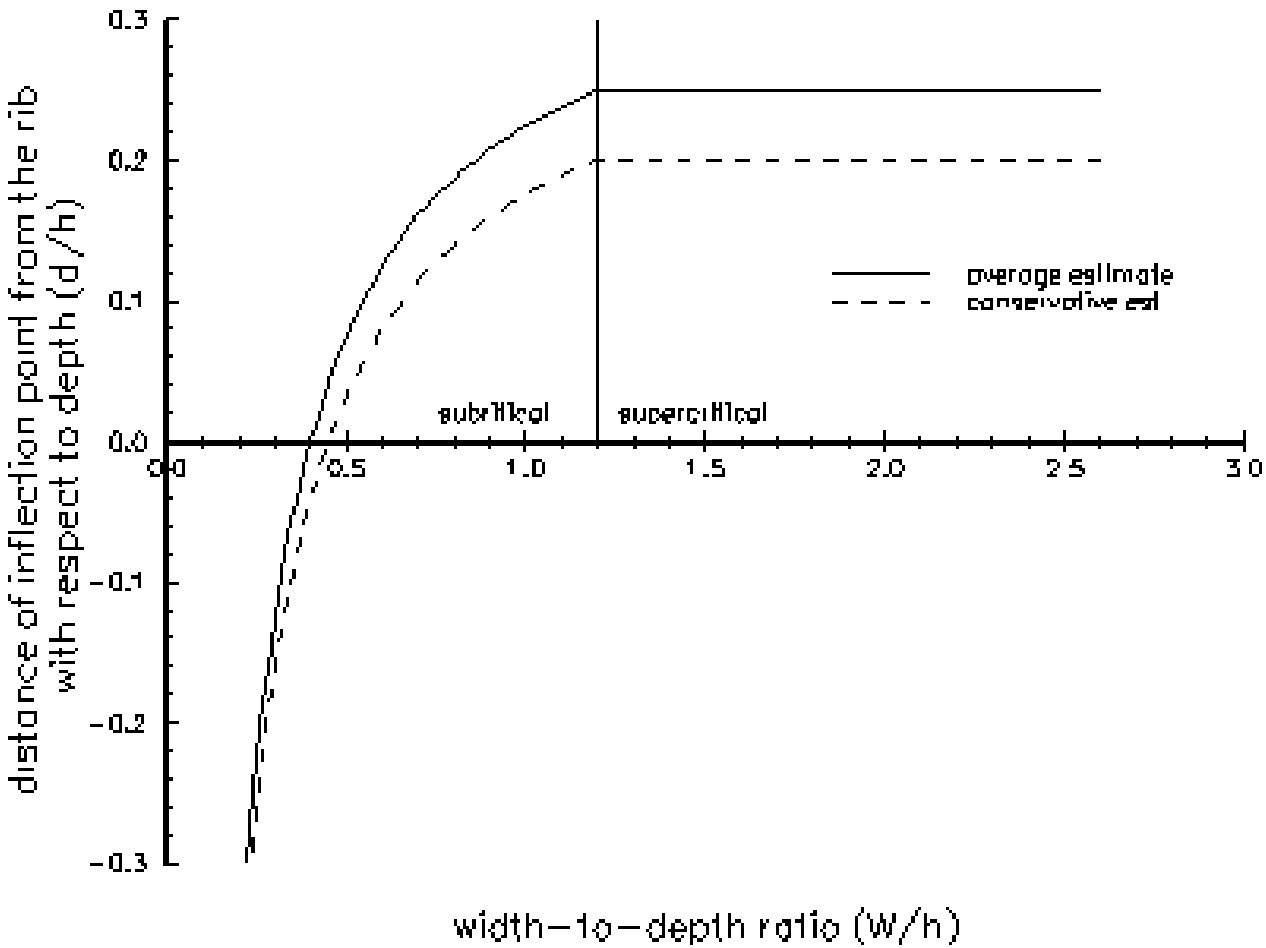

Correlation of tan(β) and Bs

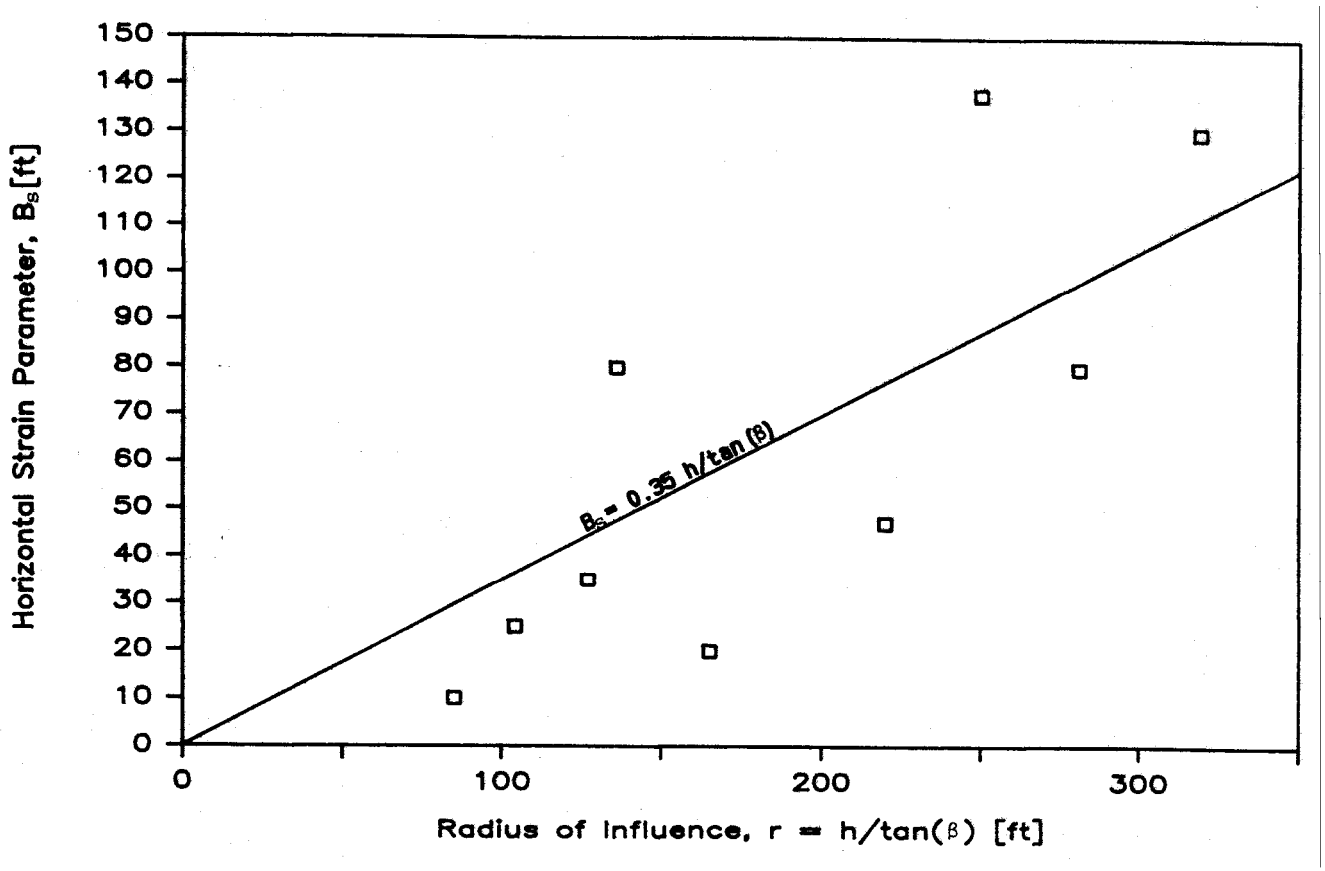

SDPS Parameters

- Required Input Parameters for Static Predictions
  - Geometry Data
  - Overburden Characteristics (Tanb,Smax,HR,Bs)
  - Mining Characteristics (d)
- Methods (Profile and Influence Function)
- Limitations and Applicability

Typical Parameters Needed for Subsidence Prediction

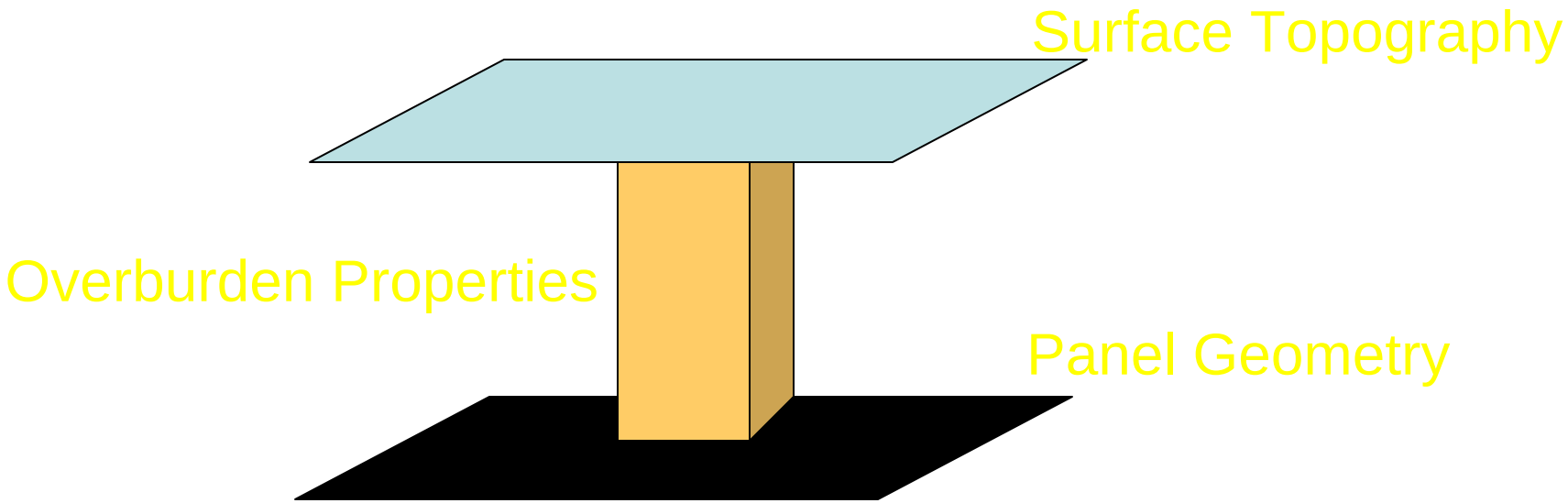

Profile Function Application and Example Problems

- Basic Predictions
  - Simple mine plan
  - Simple prediction point layout
  - Built in formulas for overburden characteristics
  - No dynamic capabilities
- New Export Capability to Excel Function

Profile Function Method

- The <u>supercritical</u> subsidence factor should be used, i.e. the subsidence factor corresponding to a supercritical geometry for the investigated site.
- Rectangular opening
- Horizontal surface
- Evenly spaced prediction points transverse to panel

Profile Function Application and Example Problems

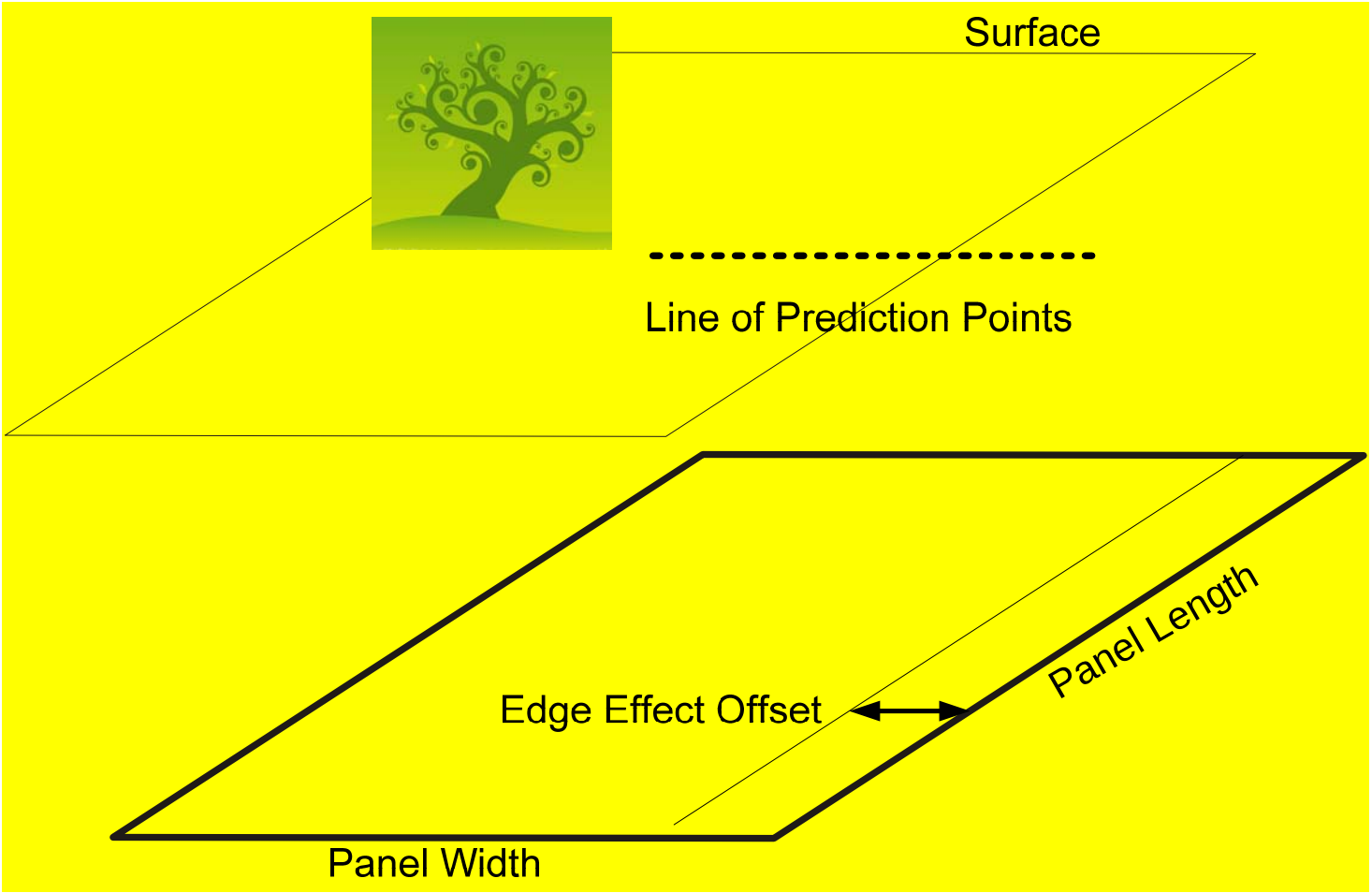

Profile Function Method

- Hands on experience

Influence Function Application – Basic Examples

- Basic Predictions
- Updates on
  - Export Capabilities
  - Contouring Procedures (Surfer 7 or 8 package by Golden Software required)

Influence Function Method

- The <u>supercritical</u> subsidence factor (Smax) should be used, i.e. the subsidence factor corresponding to a supercritical geometry for the investigated site.
- Low extraction room and pillar mines (i.e. < 50%) should show zero subsidence on the surface. User should adjust Smax to zero (0).

Concept of Influence Functions

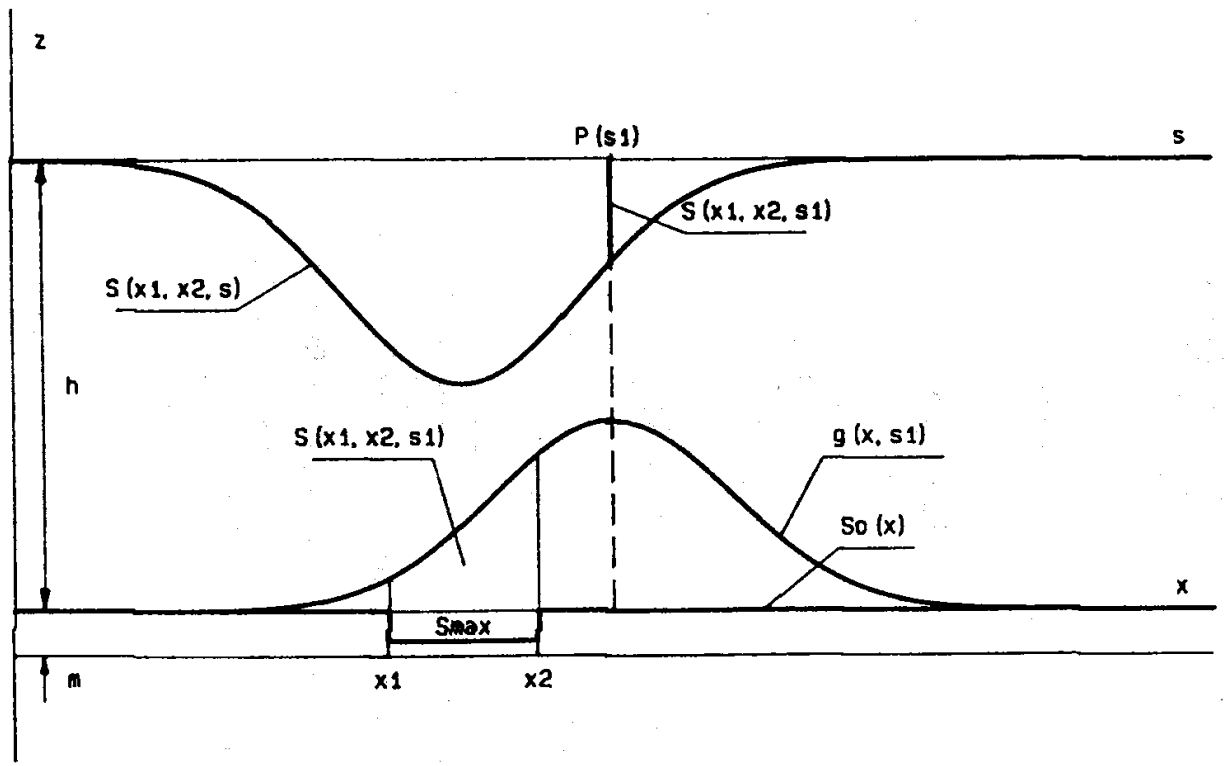

Influence Function Method

- Any mine opening (and multiple seam)
- Any surface topography (points)
- Subsidence factor, edge effect per panel
- Regional Parameters

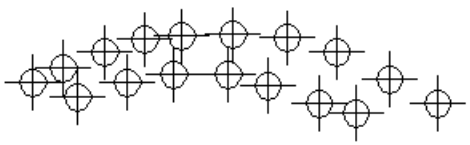

Surface Points

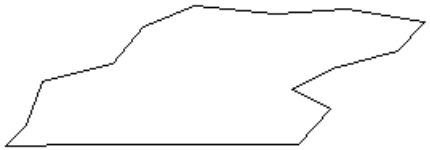

Panel(s)

Input: Mine Plan Definition

- Rectangular Mine Plan (enter throug keyboard)
- Polygonal Mine Plan
  - Enter through keyboard
  - Import from AutoCad

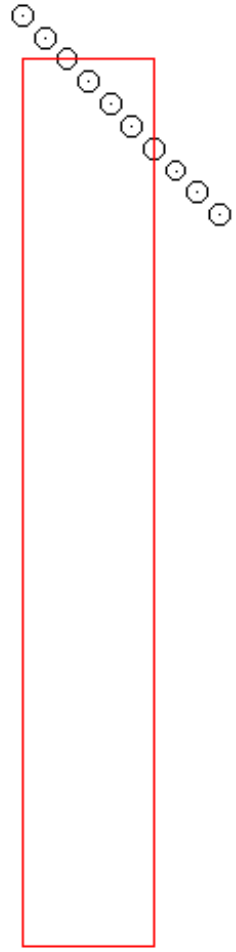

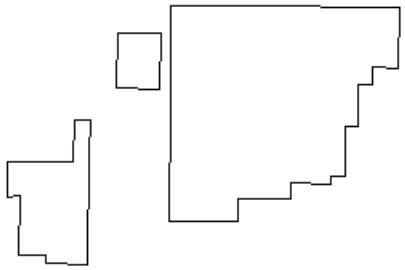

Input: Surface Point Definition

- Grid Points (enter through keyboard)
- Scattered Points
  - Enter through keyboard
  - Import from AutoCad

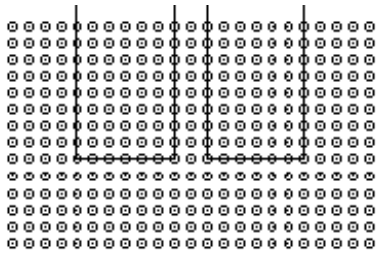

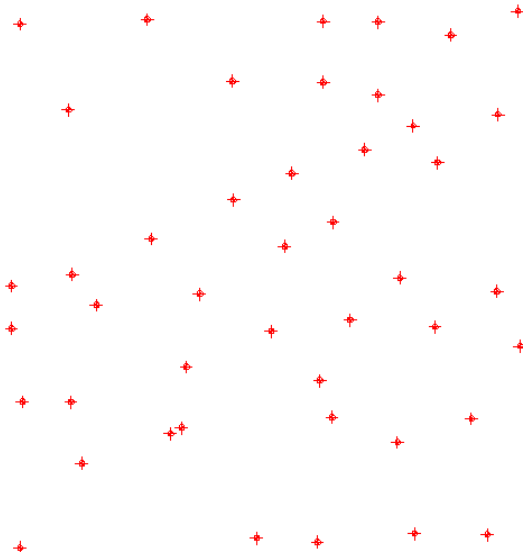

Input: Subsidence Parameter Definition

- %HR
- Supercritical Subsidence Factor (automatically determined based on %HR)
- Influence Angle
  - Set default regional value
  - Set value based on calibration
- Edge Effect (translation of Inflection Point)
- Strain Coefficient

Program Allows Site Specific or Regional Parameter Definition

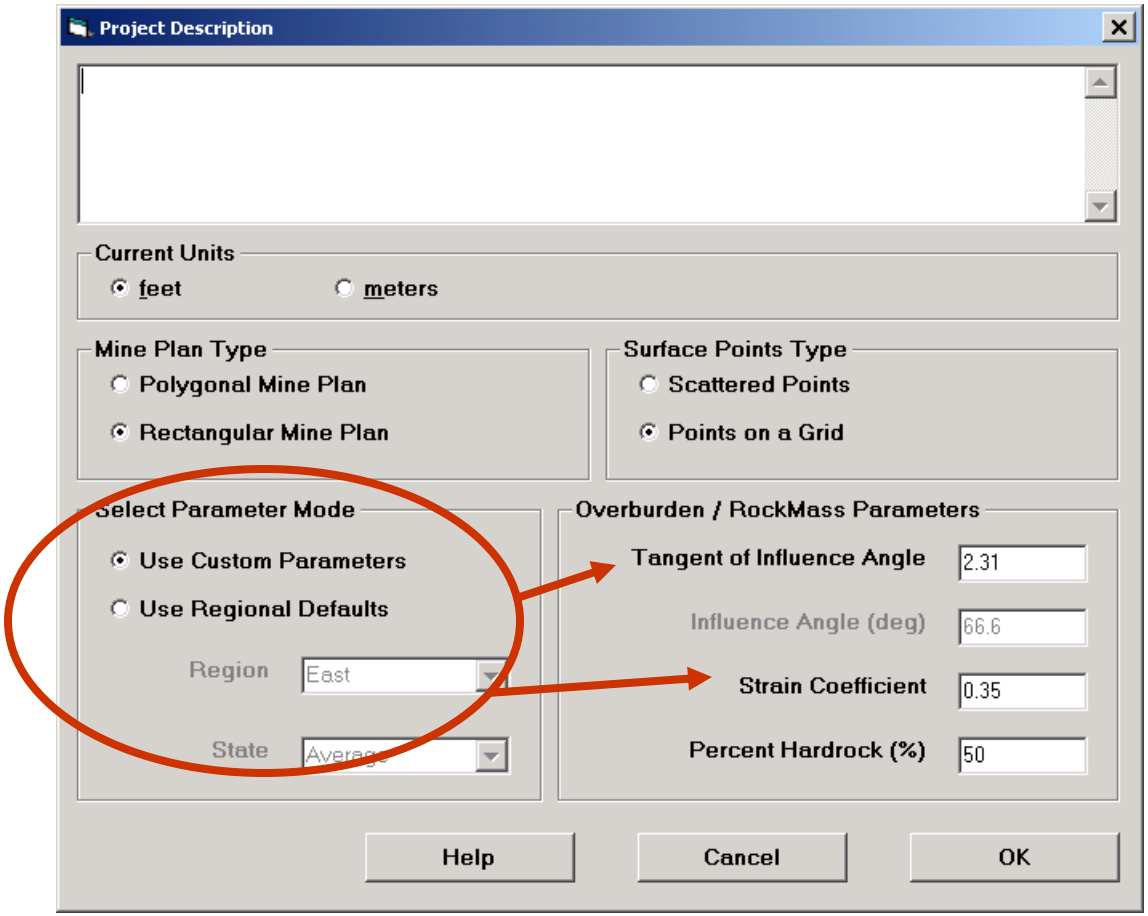

Procedure Summary

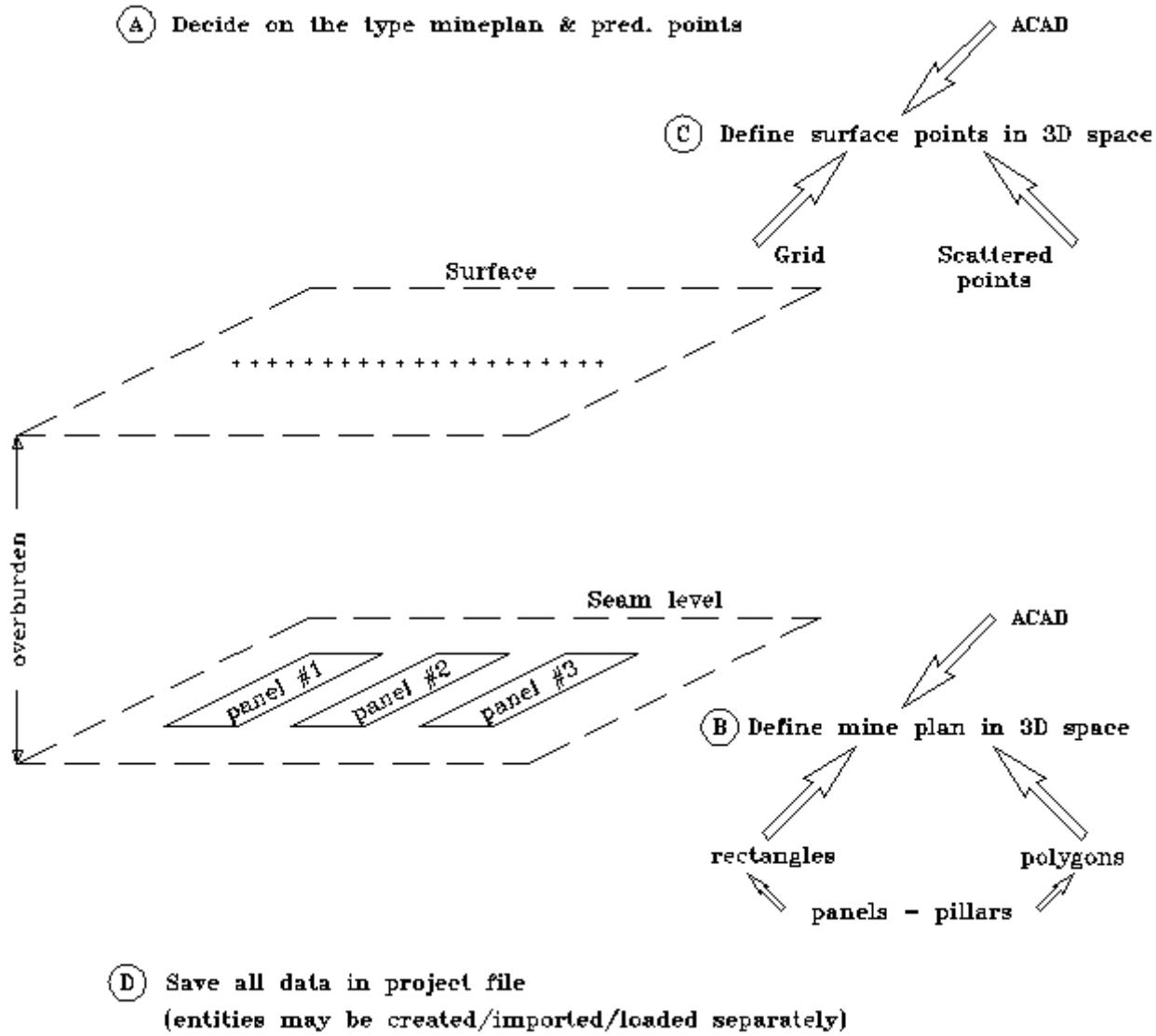

Output: Typical Deformation Indices

- Vertical displacement or subsidence
- Horizontal displacement or lateral movement
- Slope or tilt
- Horizontal strain
- Vertical curvature (or flexure)

Influence Function Method

- Hands on experience for Basic Examples
  - Rectangular Panels and Points on a Grid
  - Polygonal Panels and Scattered Points, AutoCad Interface
  - Solution Options
  - Ground Strain Calculations
  - Plotting of Deformations

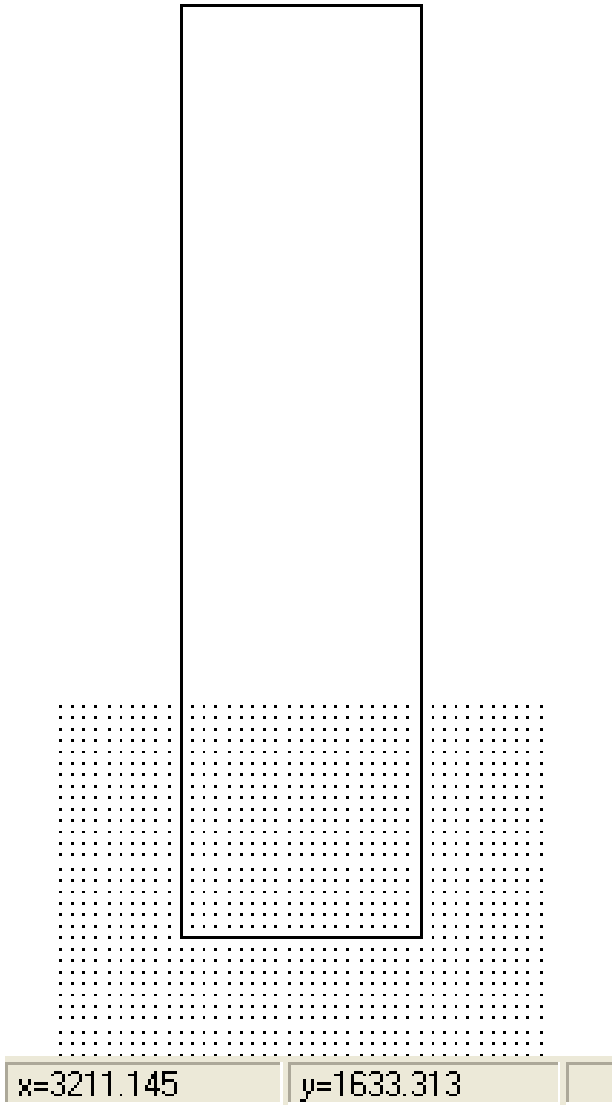

Rectangular Mine Plan and Points on a Grid

Rectangular Mine Plan and Points on a Grid – Basic Data

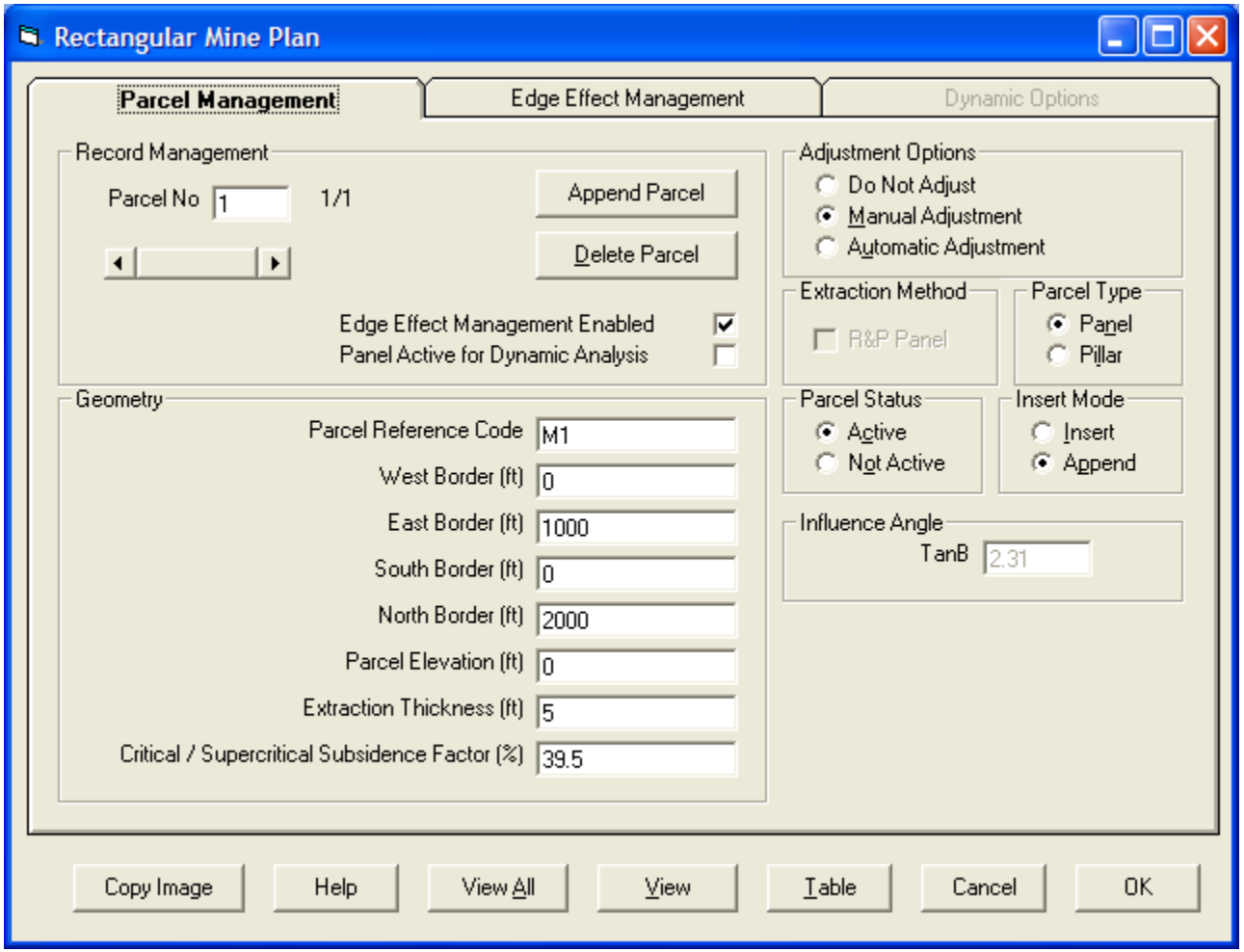

Rectangular Mine Plan and Points on a Grid – Edge Effect

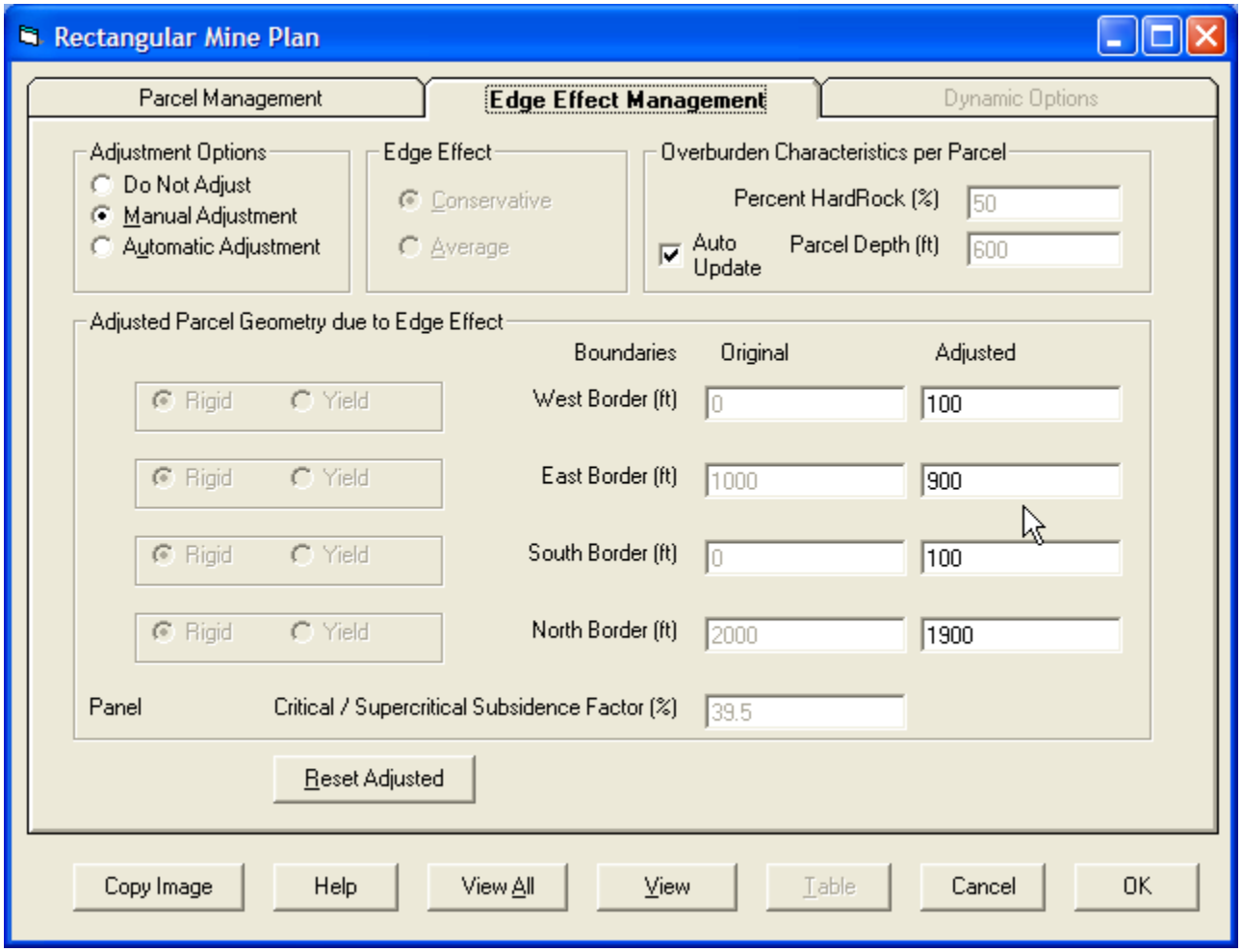

Rectangular Mine Plan and Points on a Grid – Surface Points

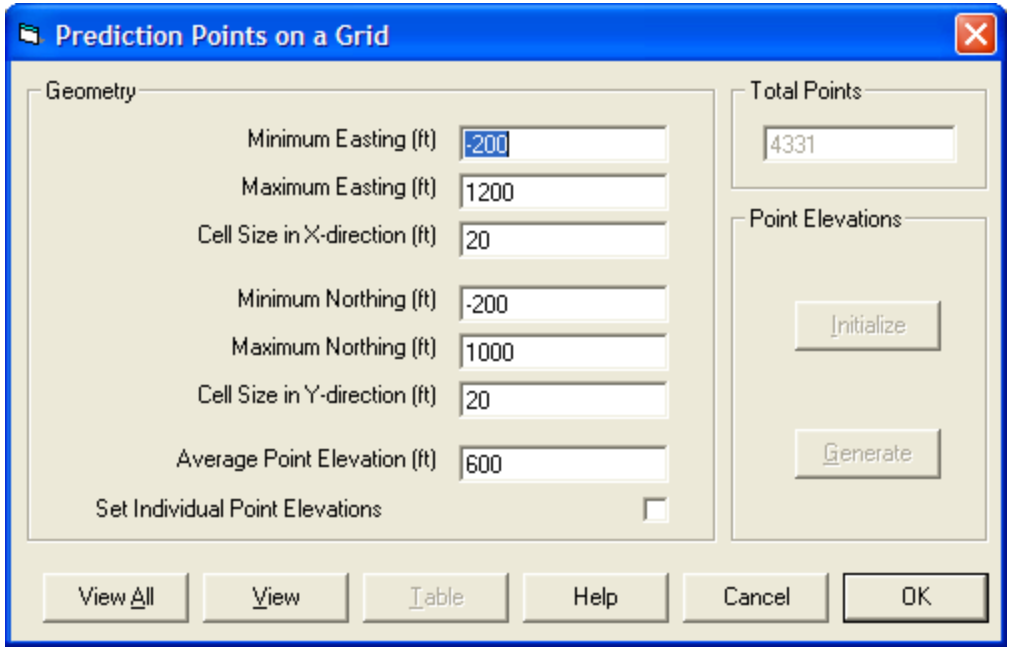

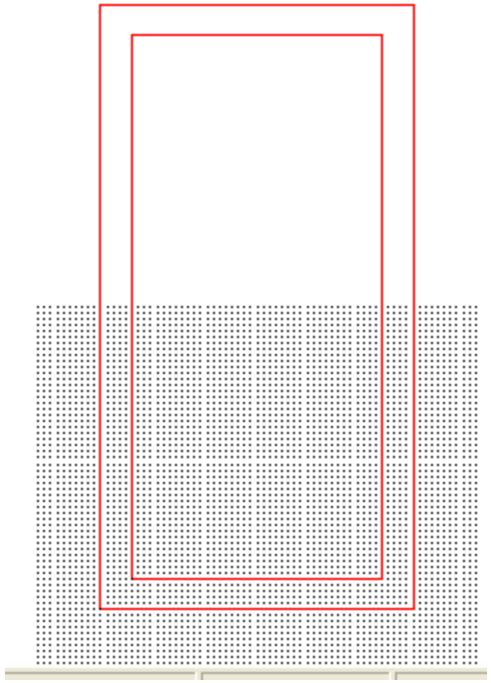

Mine Plan and Surface Points in AutoCad

Polygonal Mine Plan and Scattered Points

Warning about non-Standard AutoCad Files

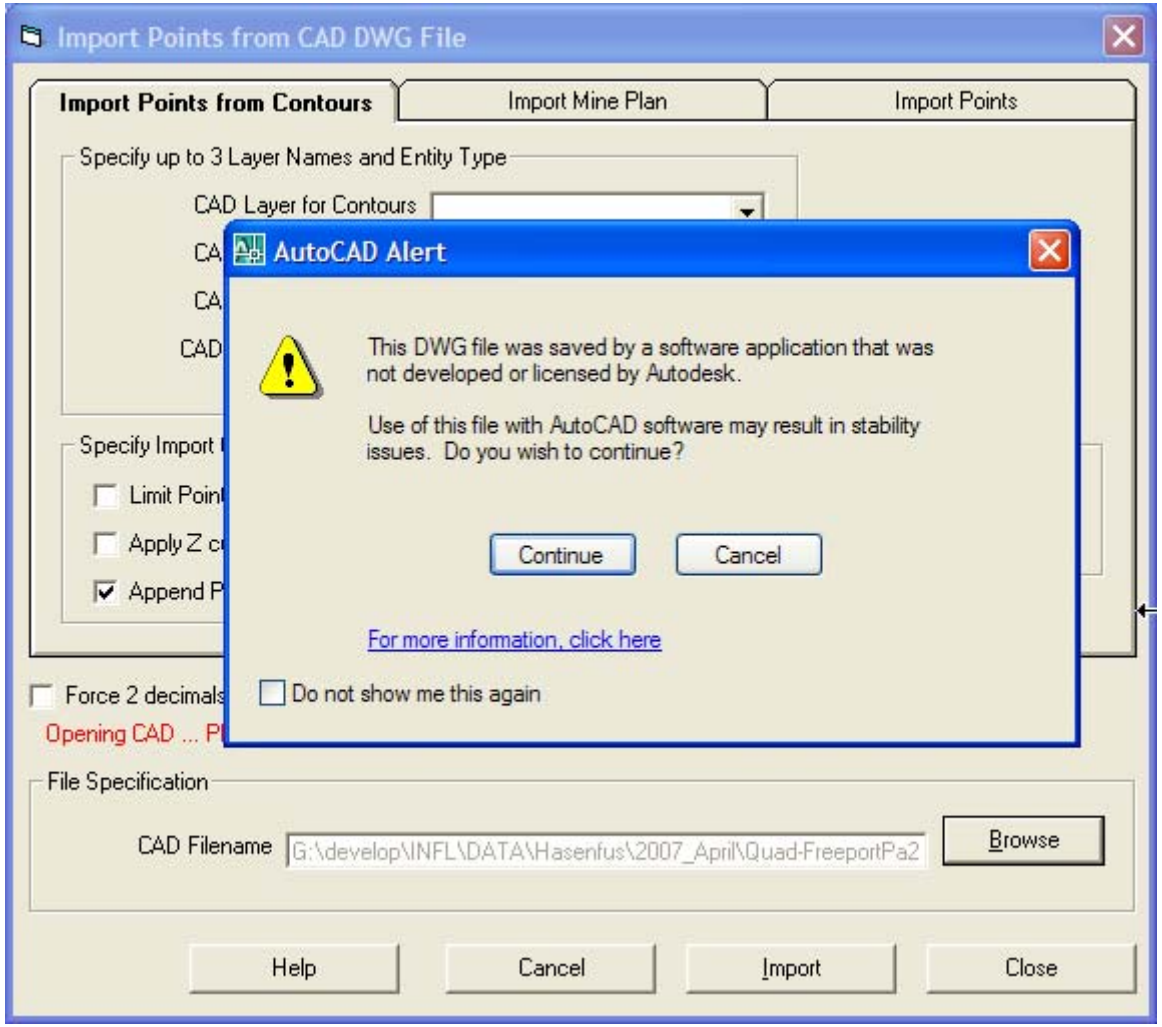

Solution Options

- Subsidence
- Slope (%)
- Horizontal Displacement
- Curvature
- Horizontal Strain (1/1000)
- Ground Strain
- Directional Strain (Axial Strain)

Correct panel orientation

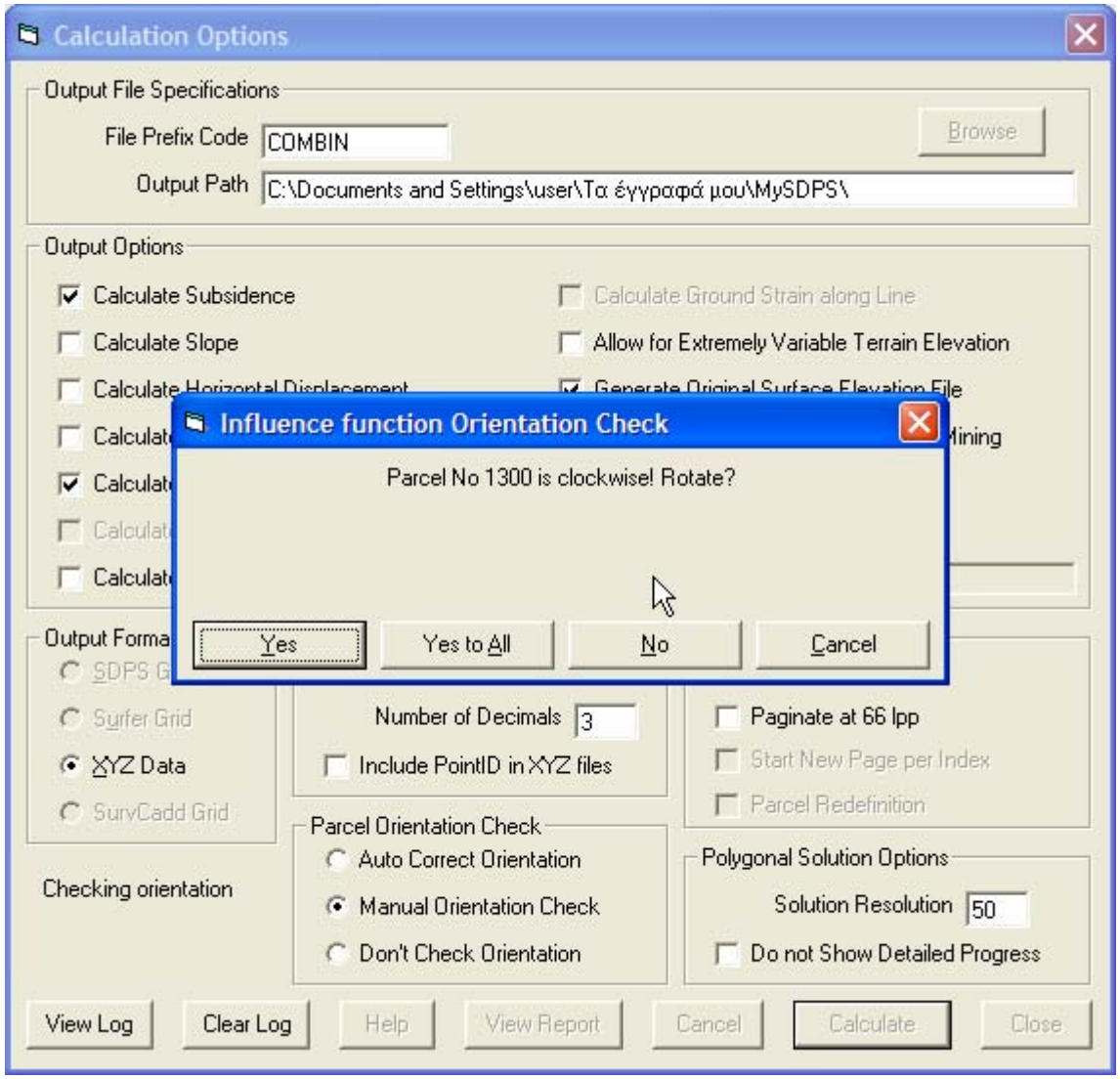

When to enable the Rough Terrain option

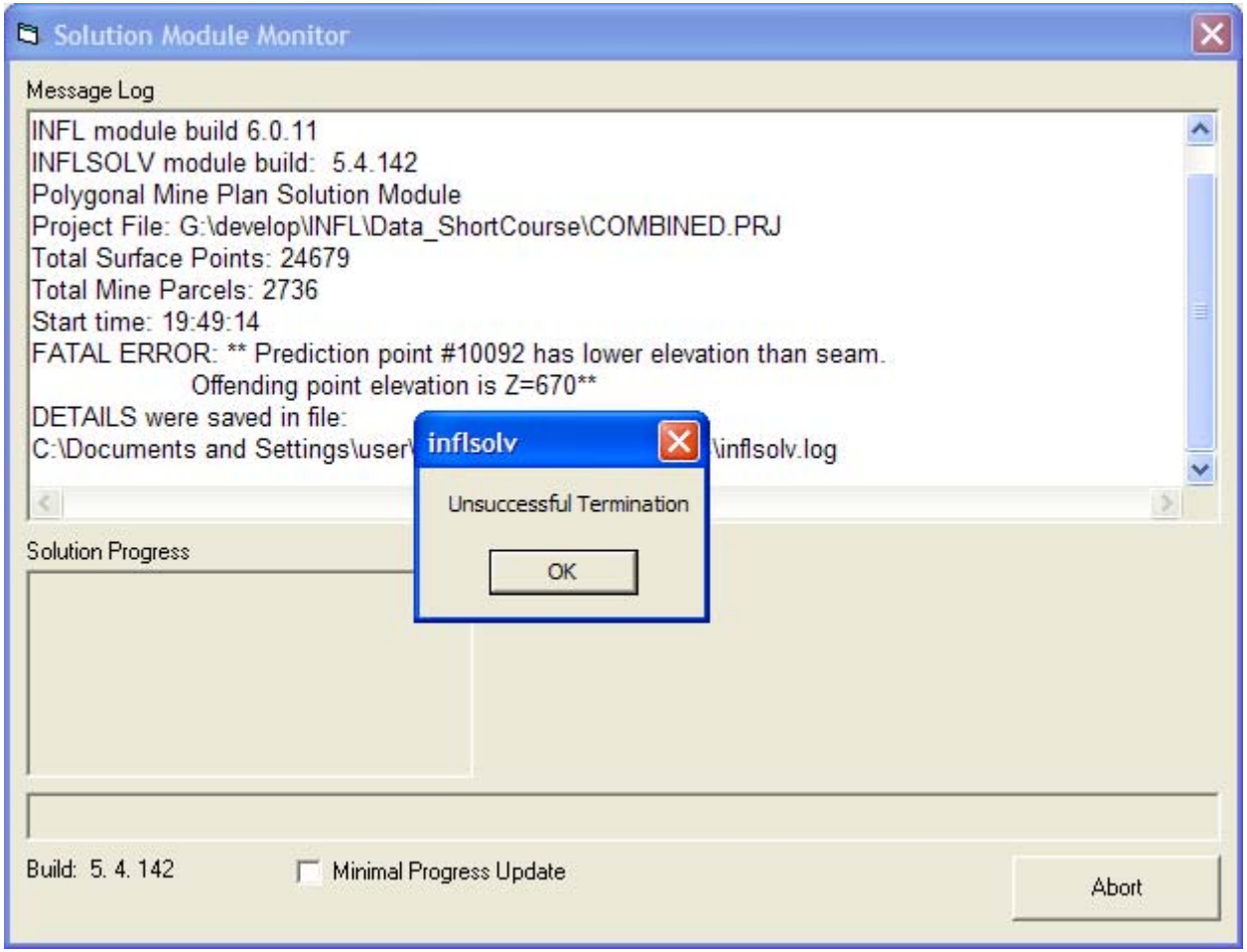

Multiple Sections

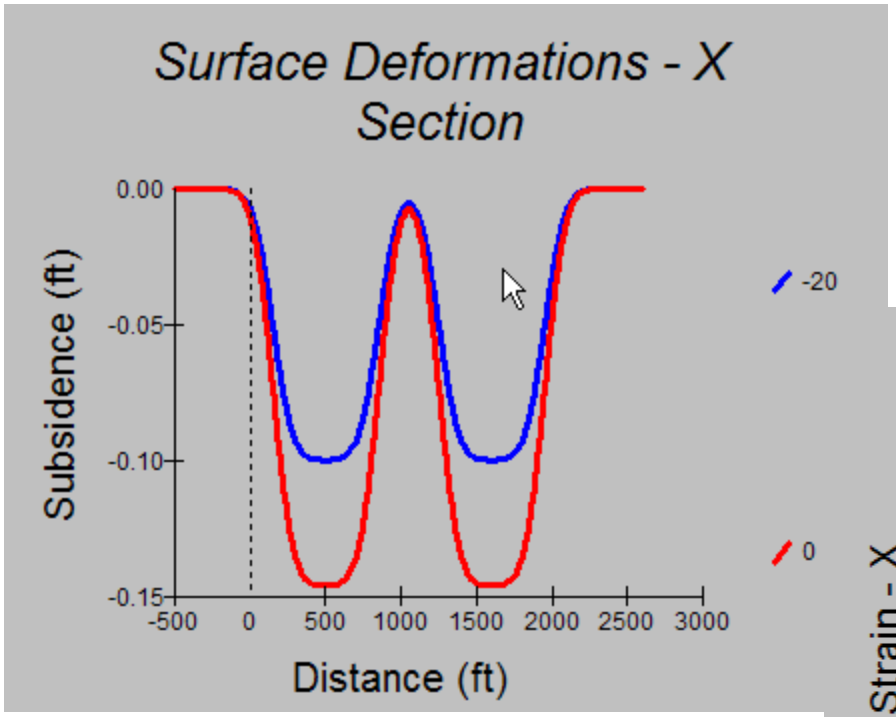

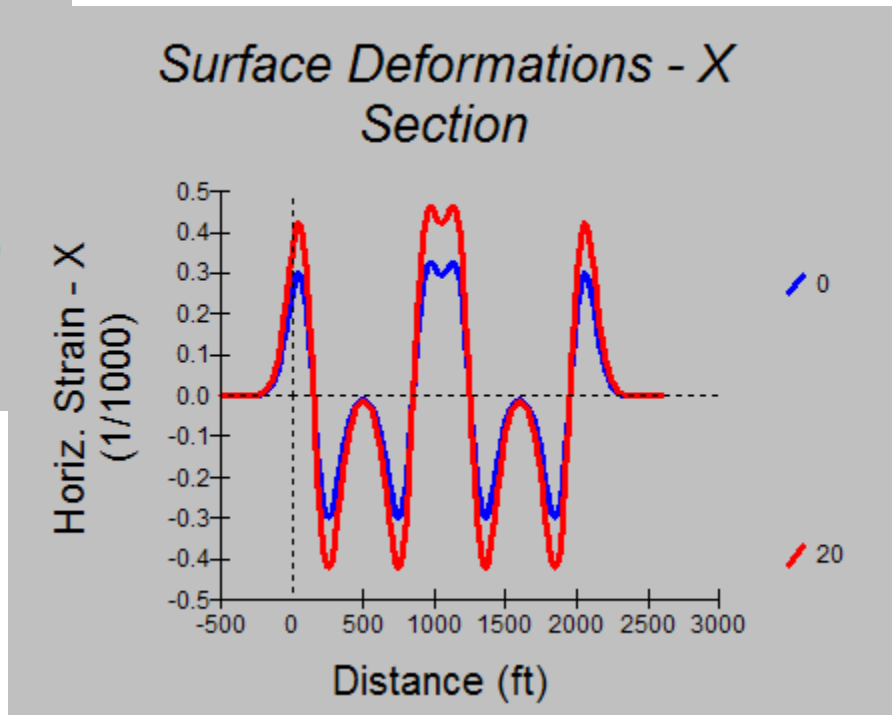

Vector Plots (for Horizontal Displacement)

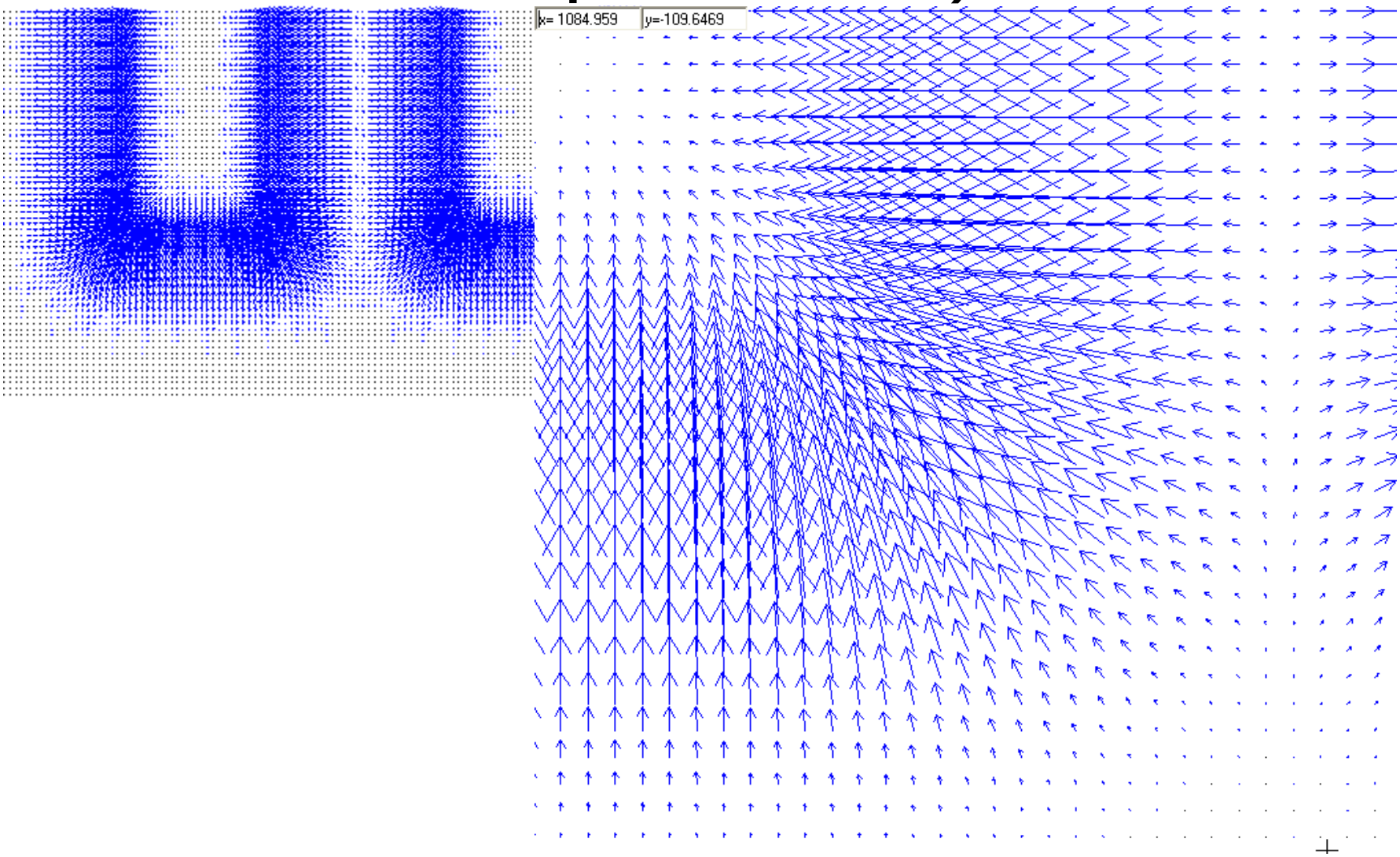

Ground Strain

Contouring of ground strain and other subsidence parameters:

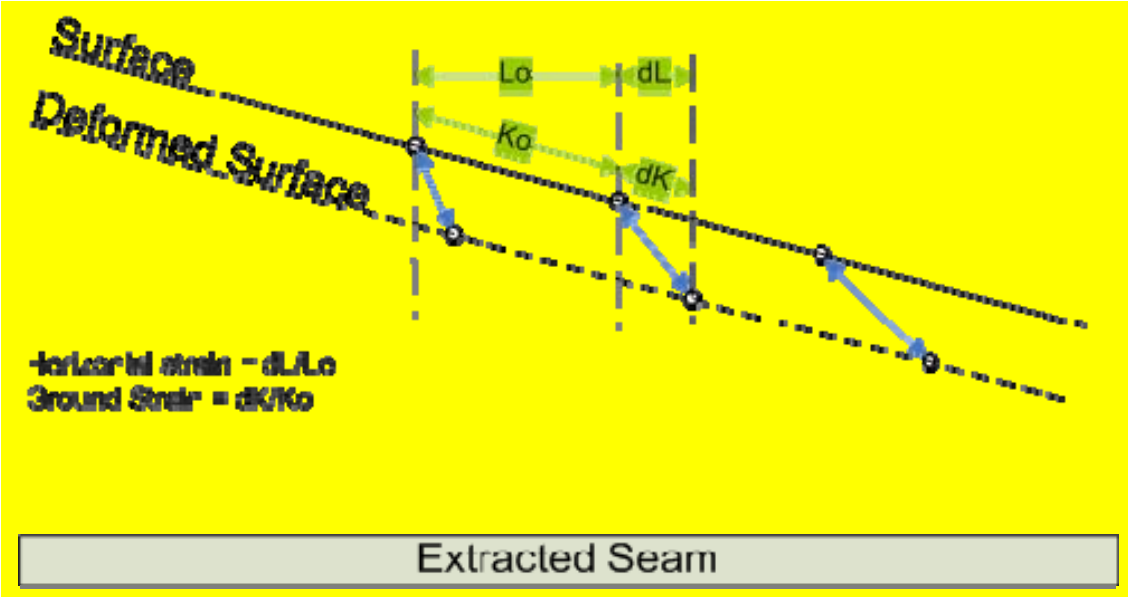

Unlike horizontal strain, ground strain takes into account the original topography of the deformed surface

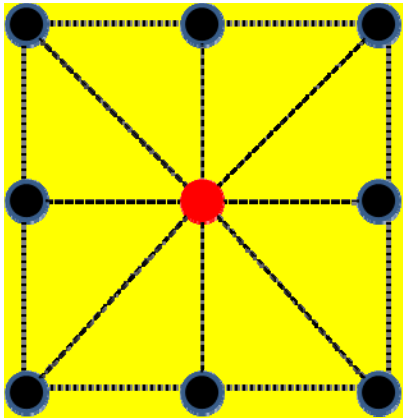

Contouring involves calculation of subsidence parameters at each point with respect to all adjacent points

Contouring (1/2)

- Grid files are needed
- If Surfer software used, then Surfer grid files should be generated
- If XYZ (scattered surface point files) are used, Grid files will automatically be generated.
- Generation employs Kriging

Contouring (2/2)

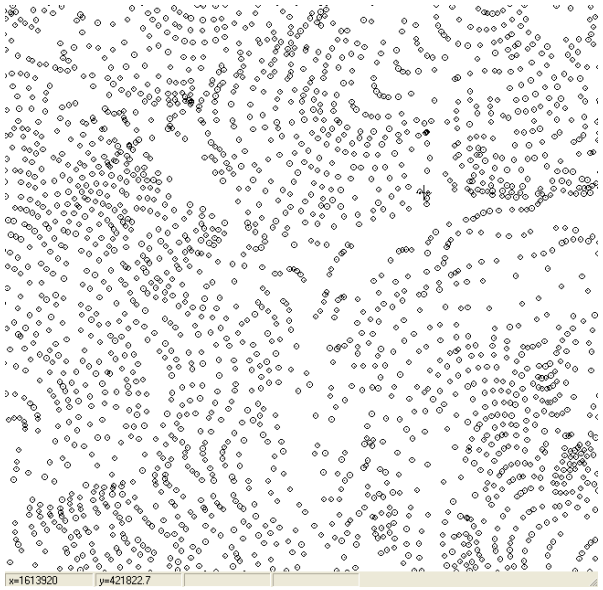

Kriging

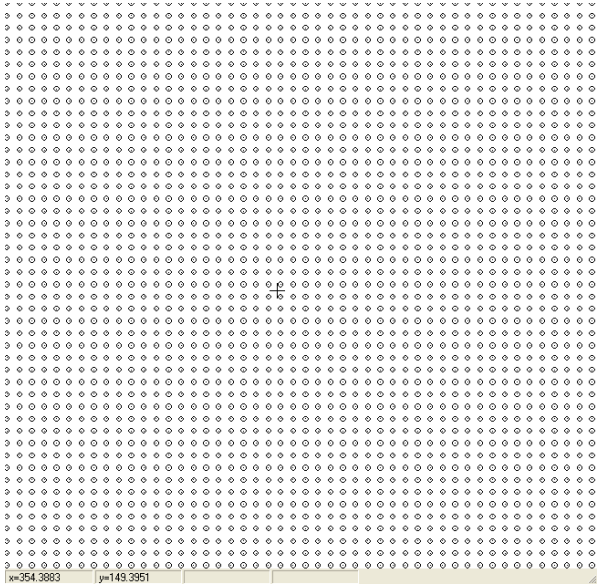

Automatically select grid size

Plot of Subsidence of a Longwall Panel for Flat Topography

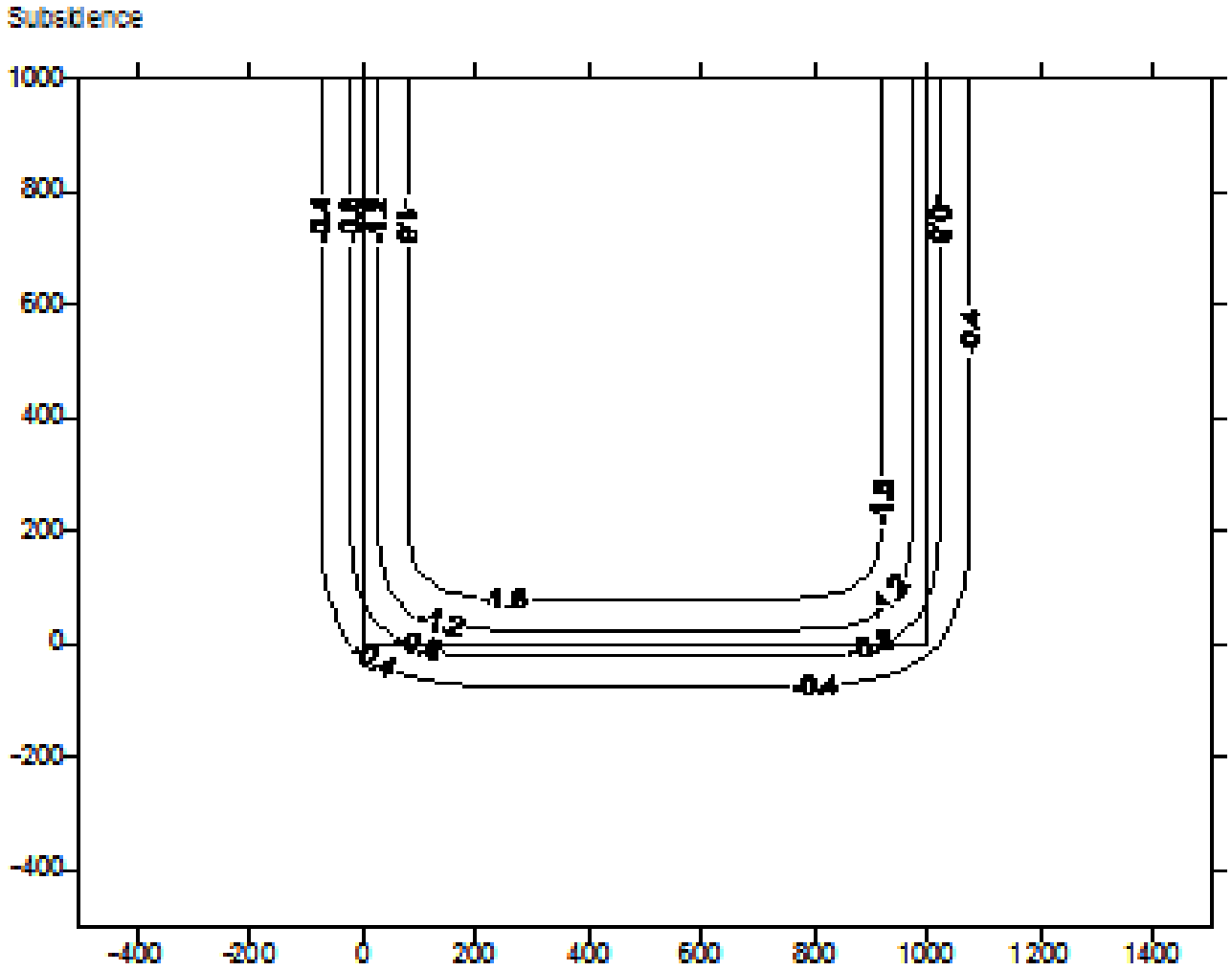

Plot of Horizontal Strain / Ground Strain for Flat Topography

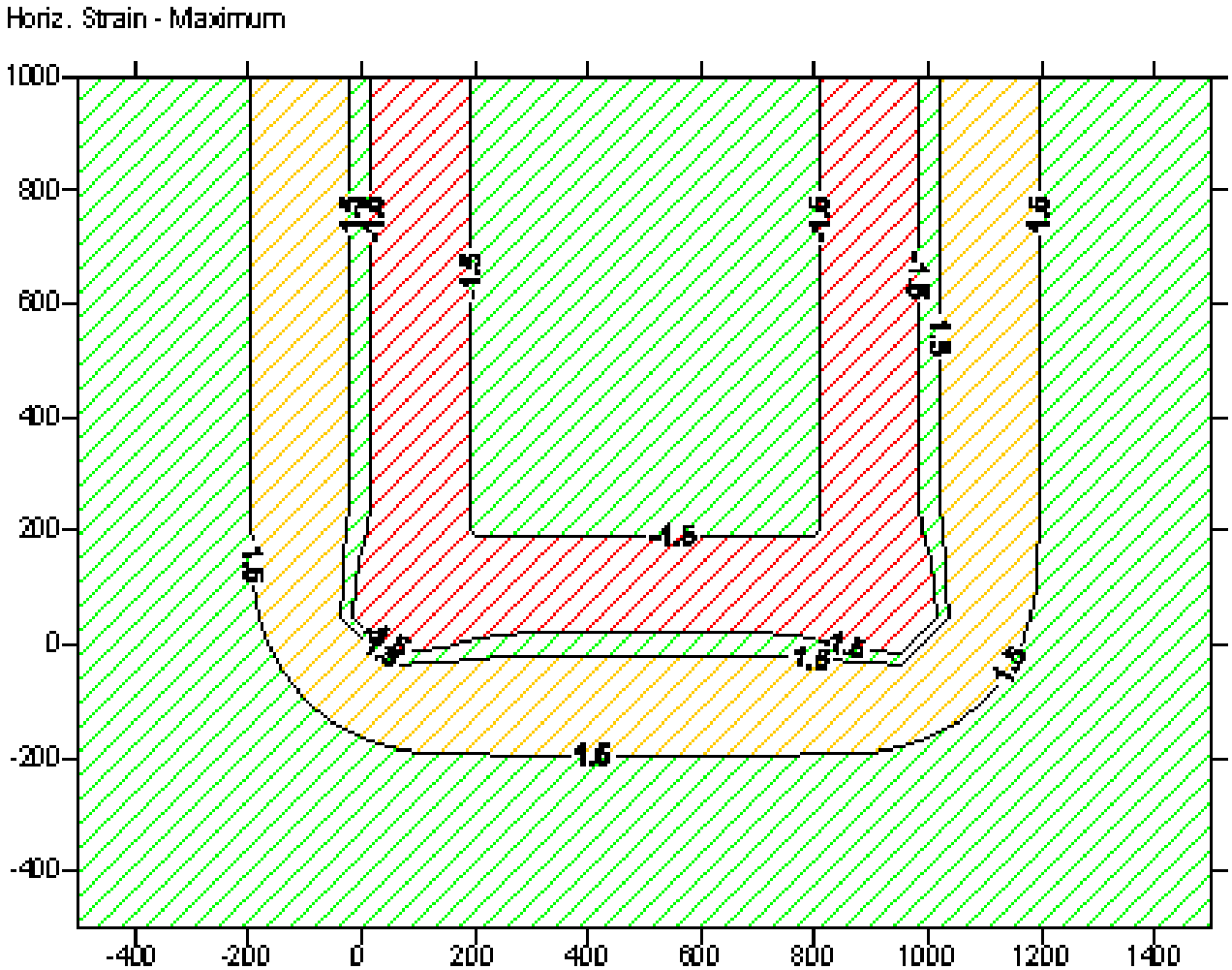

Influence Function - New Approaches in Ground Deformation Assessment

- Advanced Predictions
- Updates on
  - Dynamic Predictions
  - Calibration Procedures
  - Risk-Based Assessment for Mine Planning
  - Long-Term Stability Predictions

Dynamic Analysis

- Basics of Dynamic Analysis
- Influence of Panel Advance Rate

Panel Geometry

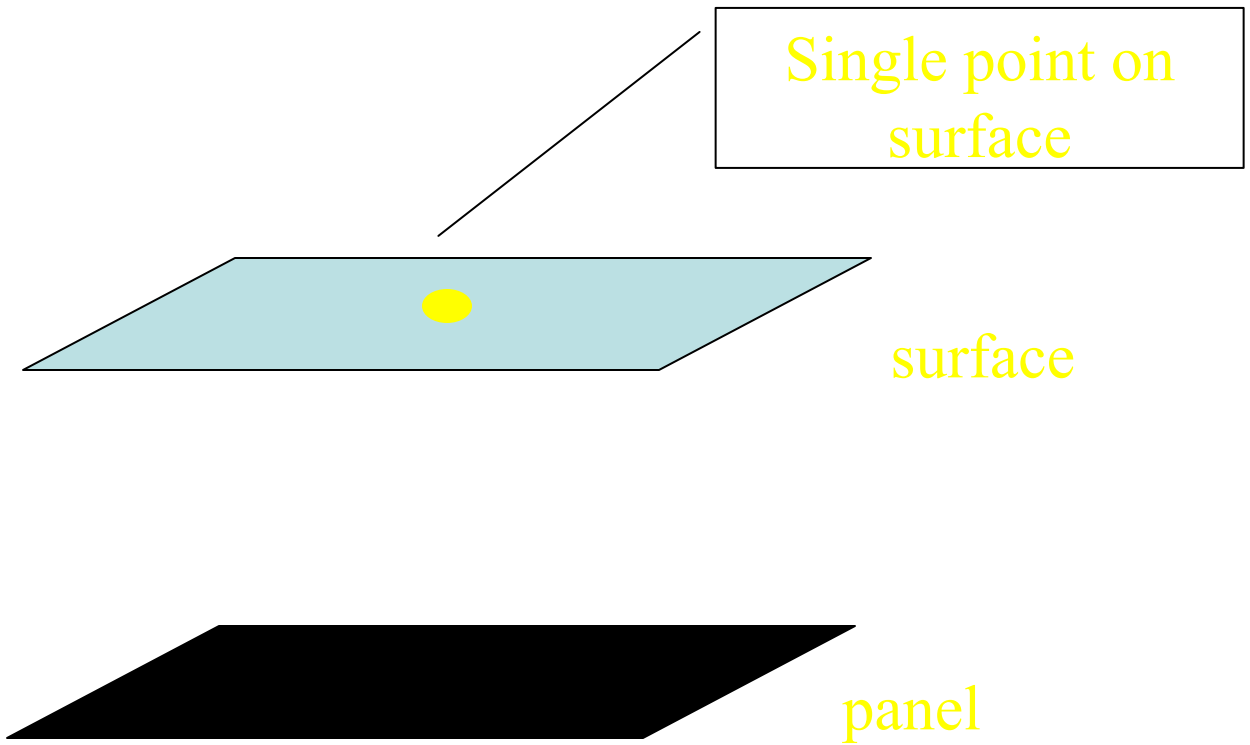

Assume Extraction Sequence of Panel

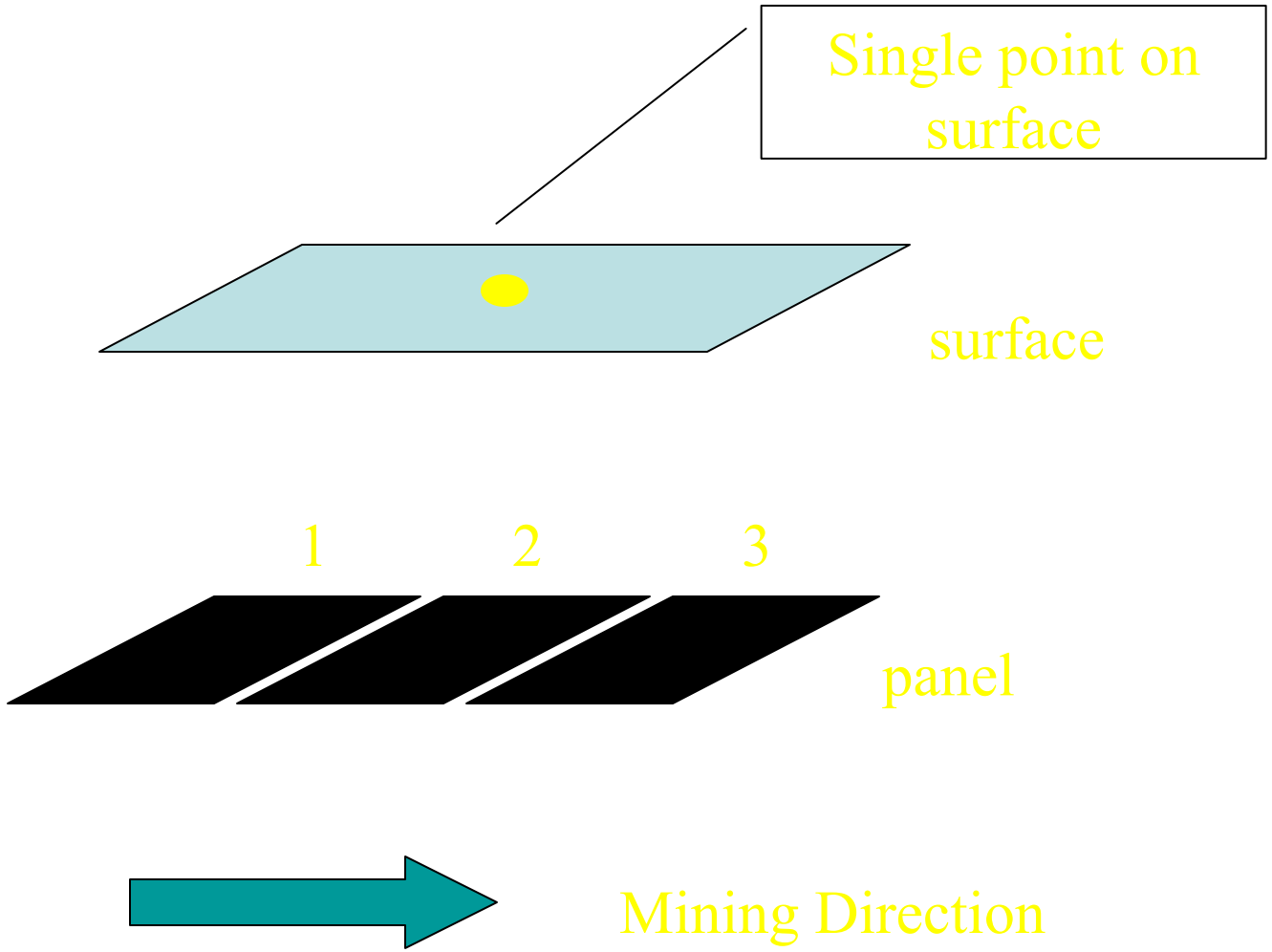

Extract parcel #1

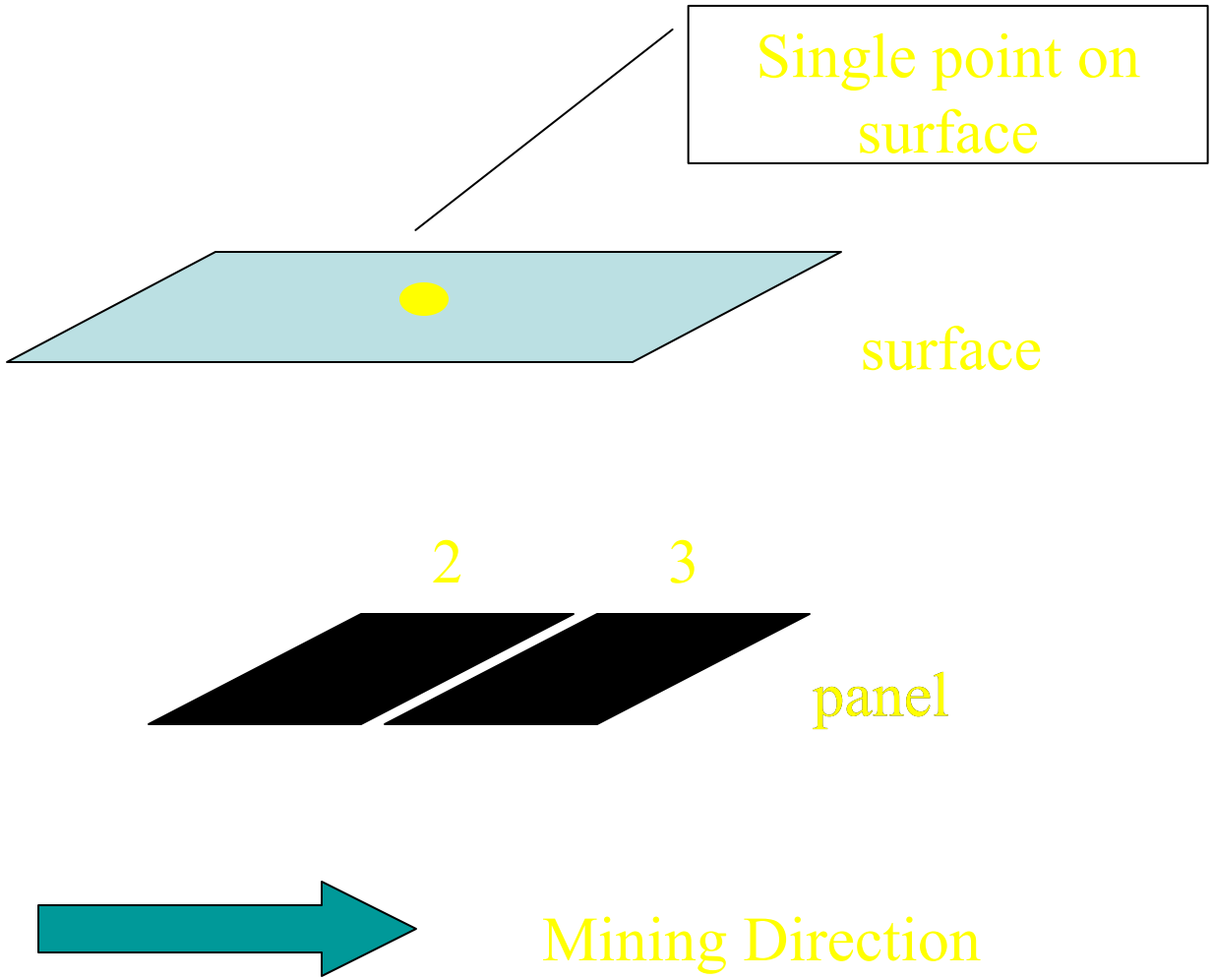

Extract parcel #2

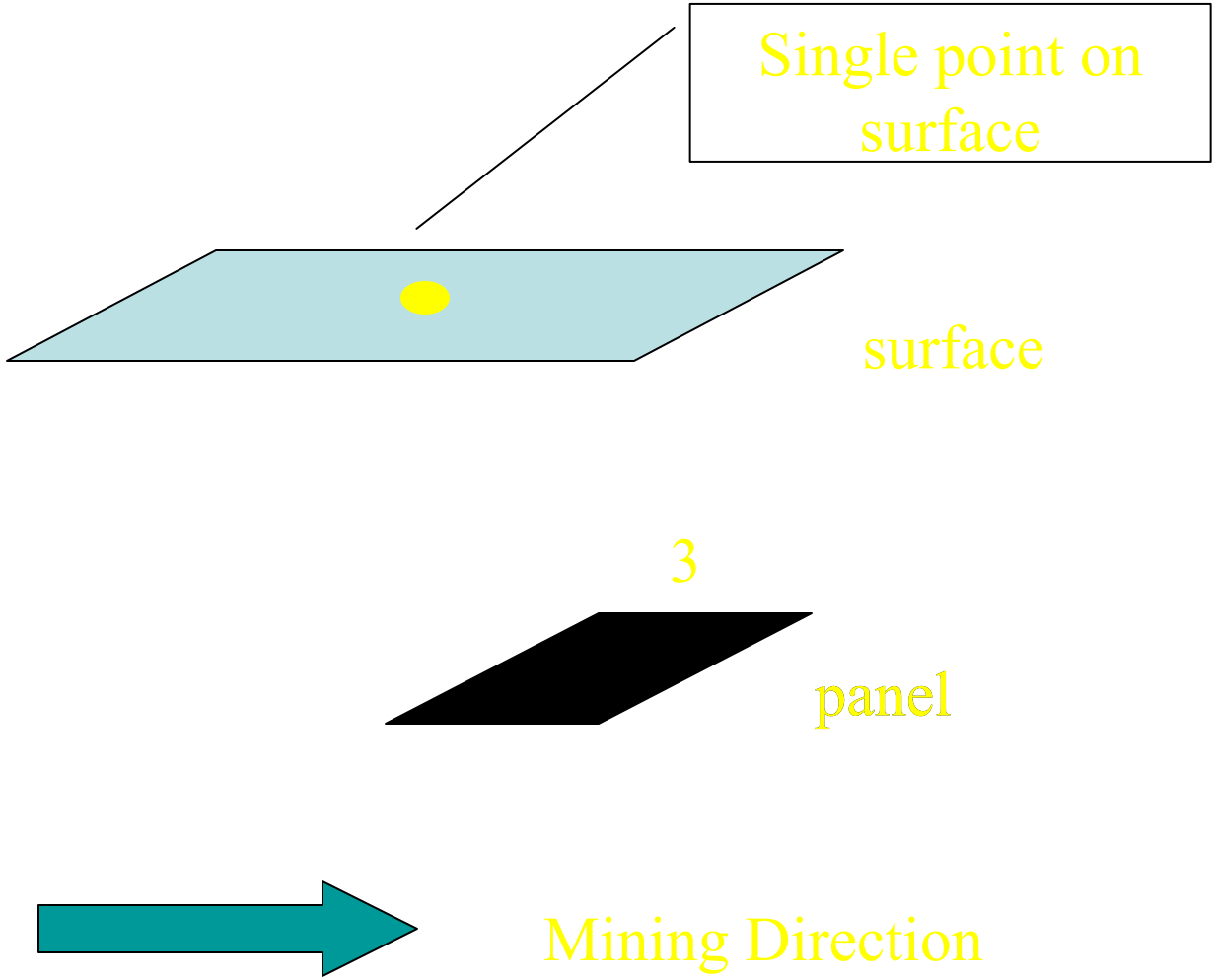

Section View

- Dynamic Subsidence = subsidence movements that occur as a longwall face moves beneath the surface.

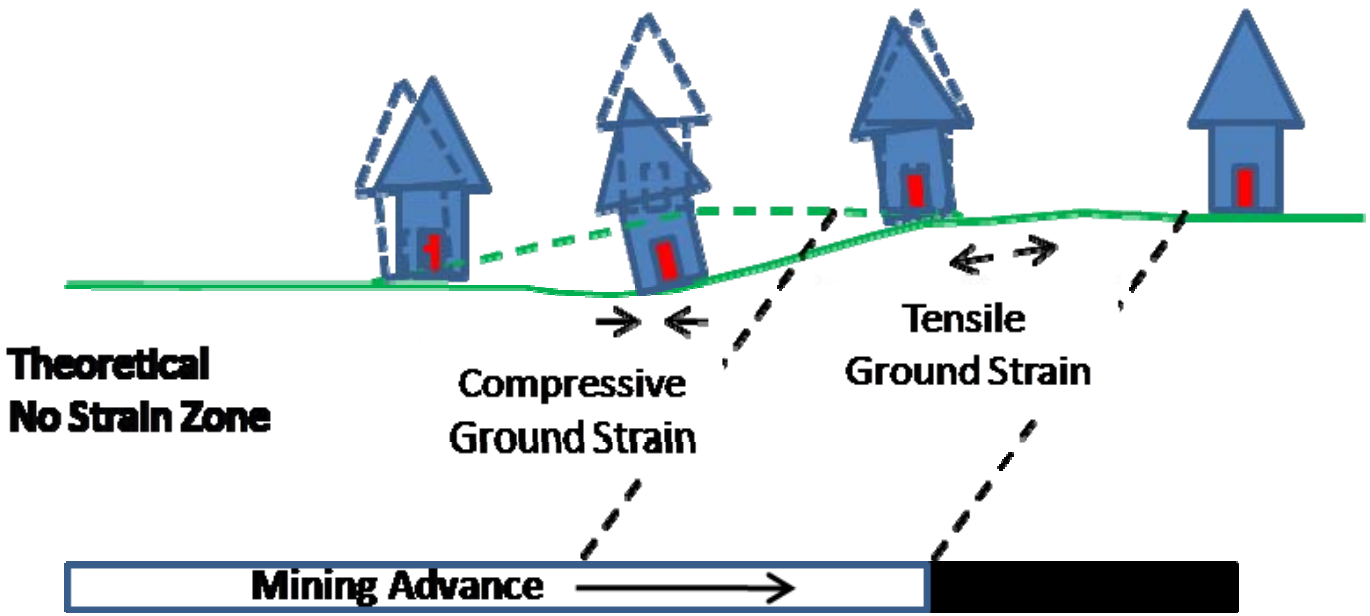

- Surface structures affected by dynamic subsidence experience both tensile and compressive strains.

Image after Geddes and Cooper (1962)

Plan View

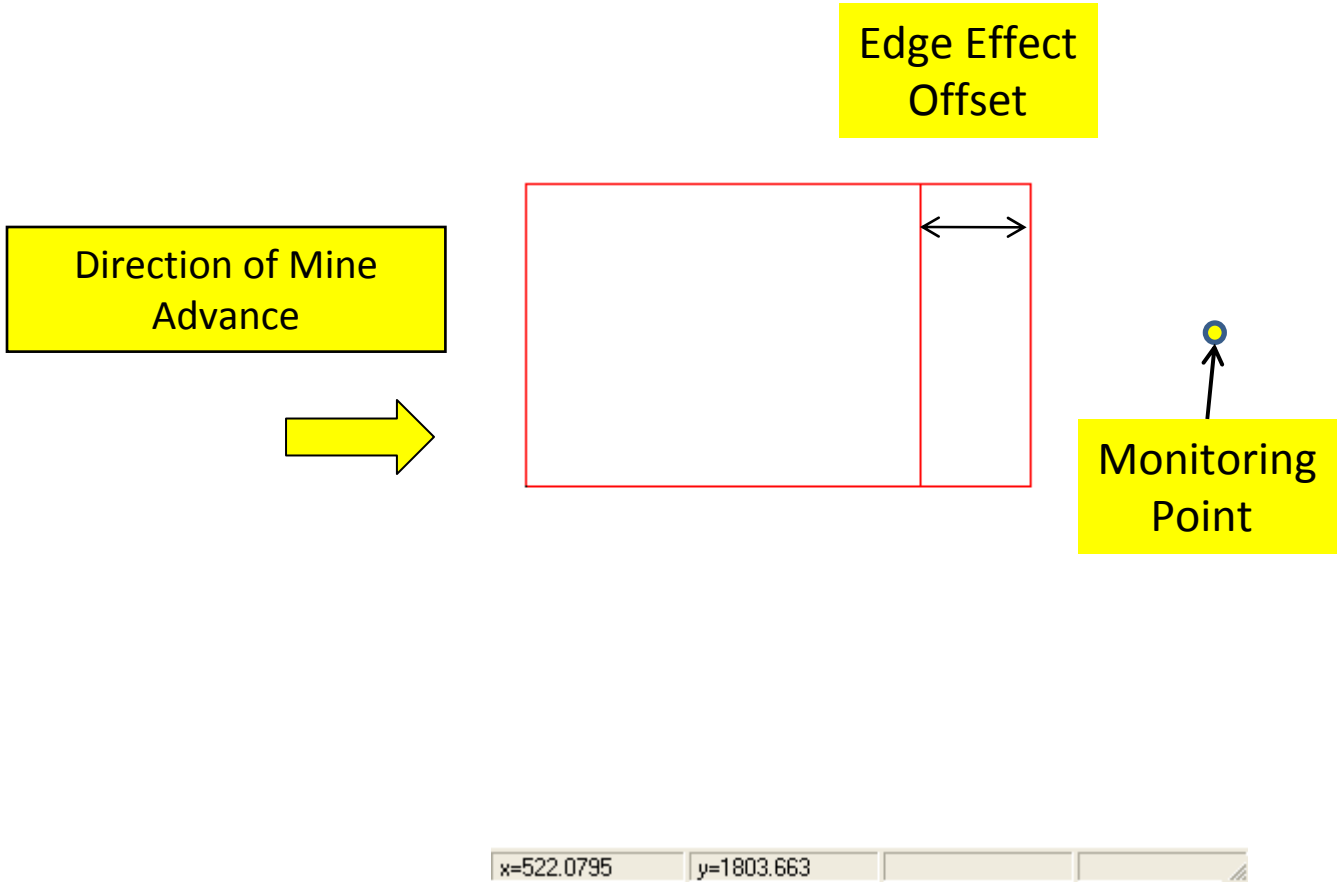
Edge Effect Offset
Direction of Mine Advance
Monitoring Point
x=522.0795
y=1803.663

Dynamic Subsidence Development Example

Dynamic subsidence prediction panel and point layout

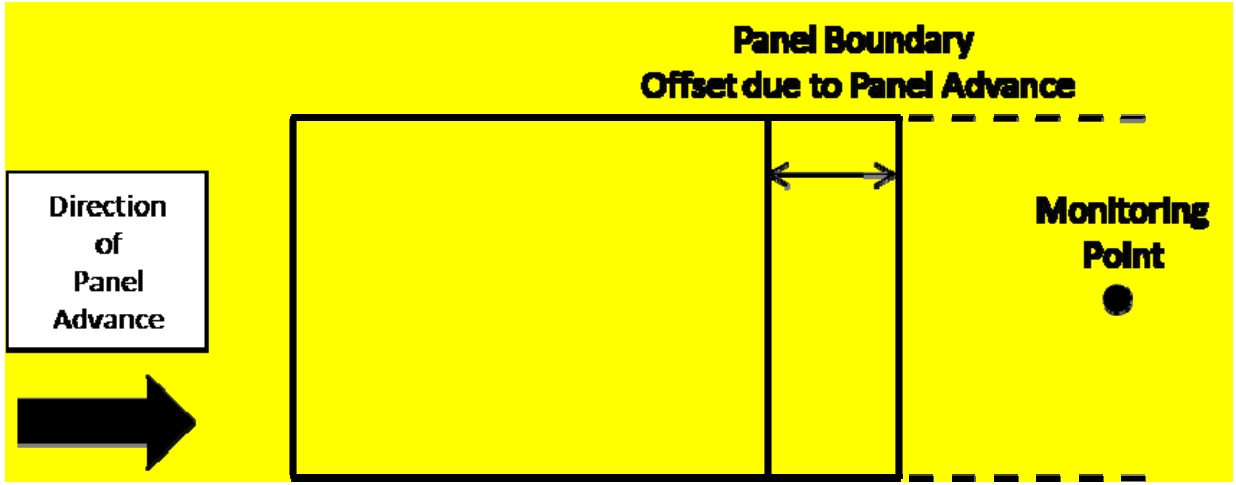

Dynamic subsidence prediction curves

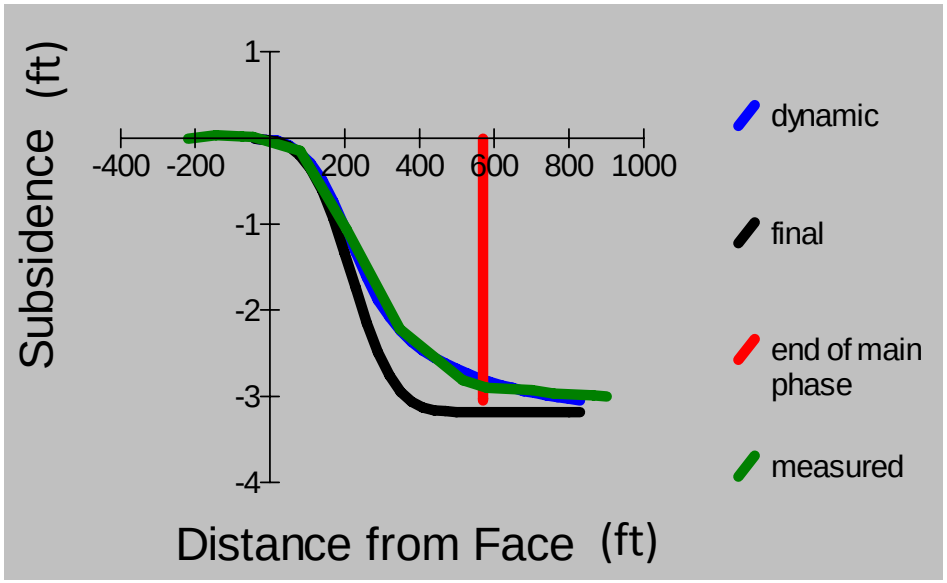

Influence Function Method

- Hands on experience for Dynamic Analysis

Calibration Procedures (1/3)

- Subsidence Calibration
  - Locking procedure when calibrating for subsidence and strain
- Strain Calibration
  - Options for calibrating for average or high values

Calibration Procedures (2/3)

Subsidence Calibration

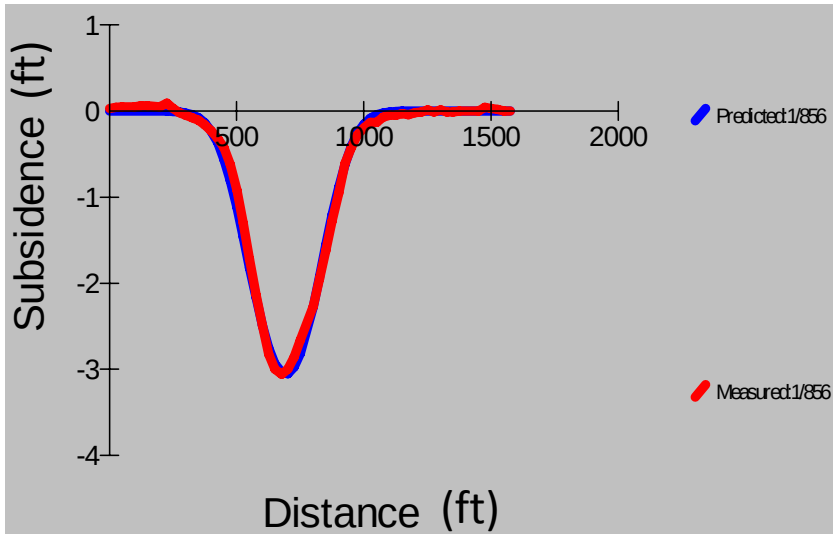

Strain Calibration

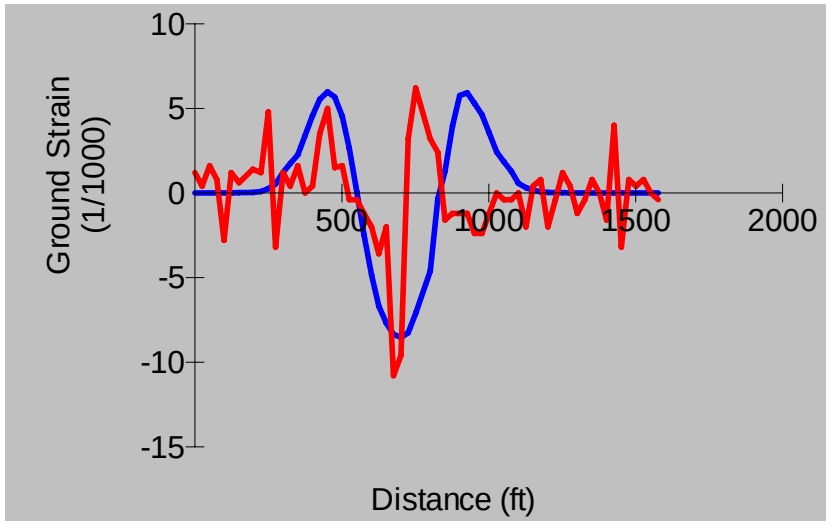

Parameter	Subsidence Calibration	Strain Calibration
Tanb	3.00	3.00
Smax/m	53.0	45.0
EdgeAdjust	167.00	153.50
Perc_Error	13.21	33.58

Calibration Procedures (3/3)

Subsidence Calibration

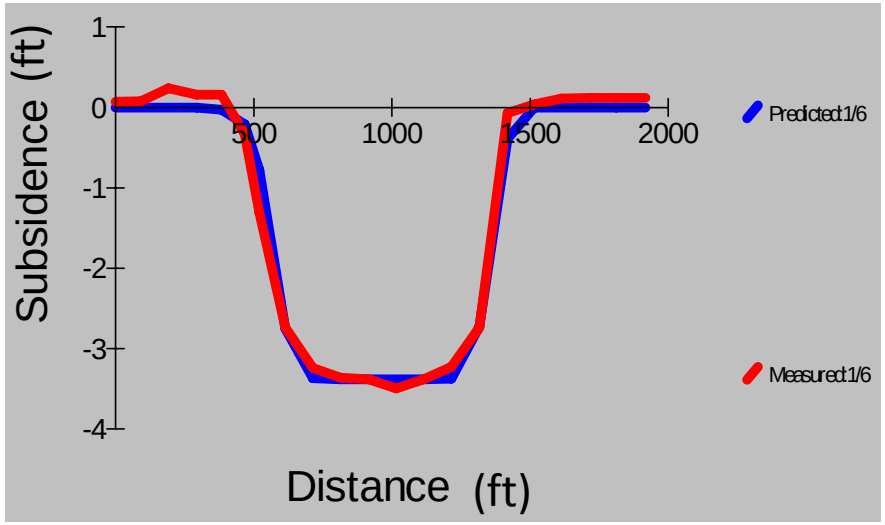

Strain Calibration

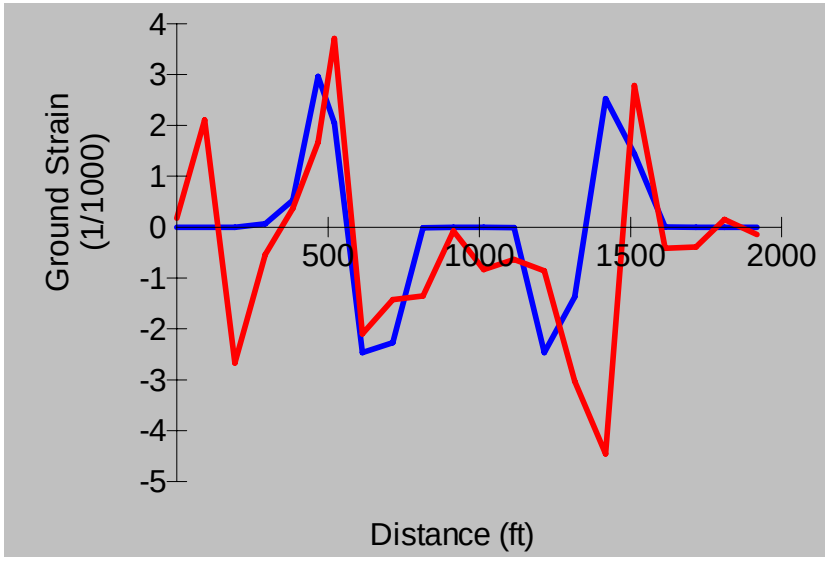

Parameter	Subsidence Calibration	Strain Calibration
Tanb	2.50	3.00
Smax/m	52	45
EdgeAdjust	150	150
Perc_Error	7.90	38.95

Influence Function Method

- Hands on Experience for Calibration Procedures

Risk-Based Assessment for Mine Planning

- Risk-based assessment combines subsidence prediction with surface damage.
- Implementation of a risk-assessment approach to mine planning optimizes mine recovery while providing increased protection of structures.
- Karmis, et al. (1994) provides damage threshold values for subsidence parameters.
- Selecting an appropriate index for assessment purposes is important.
- Contouring of ground strain and other parameters provides a means to create maps delineating high-risk areas.

Risk-Based Assessment for Mine Planning

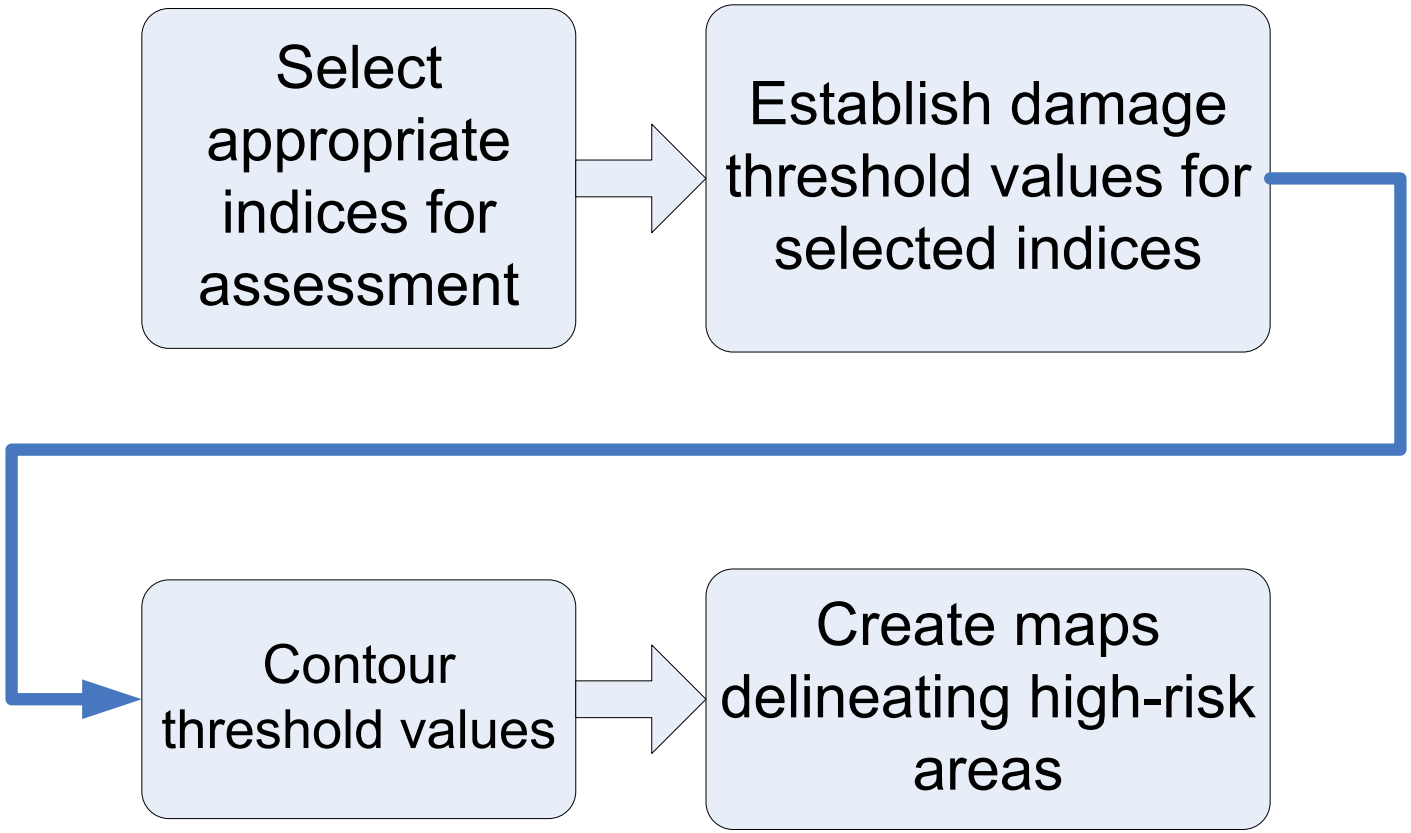

Risk-Based Assessment for Mine Planning

Class of Damage or Severity Level (comparative/comprehensive scheme by Bhattacharya and Singh (1985)/ Singh (1992)) NCB System→SIS→DCS	Horizontal Strain (suggested damage limit values after Singh, 1992)	Angular Distortion (suggested damage-limit values after Singh, 1992)
Negligible→Slight→Architectural	0.5×10^{-3}	1.0×10^{-3}
Slight→Moderate→Functional	$1.5\text{-}2.0 \times 10^{-3}$	$2.5\text{-}3.0 \times 10^{-3}$
Appreciable→Moderate→Functional	$1.5\text{-}2.0 \times 10^{-3}$	$2.5\text{-}3.0 \times 10^{-3}$
Severe→Severe→Structural	3.0×10^{-3}	7.0×10^{-3}
Very Severe→Very Severe→Structural	$>3.0 \times 10^{-3}$	$>7.0 \times 10^{-3}$

Classes of damage and suggested threshold (damage limit) values of horizontal strain and angular distortion (Karmis, et al., 1994)

Ground Deformations over Mined Areas

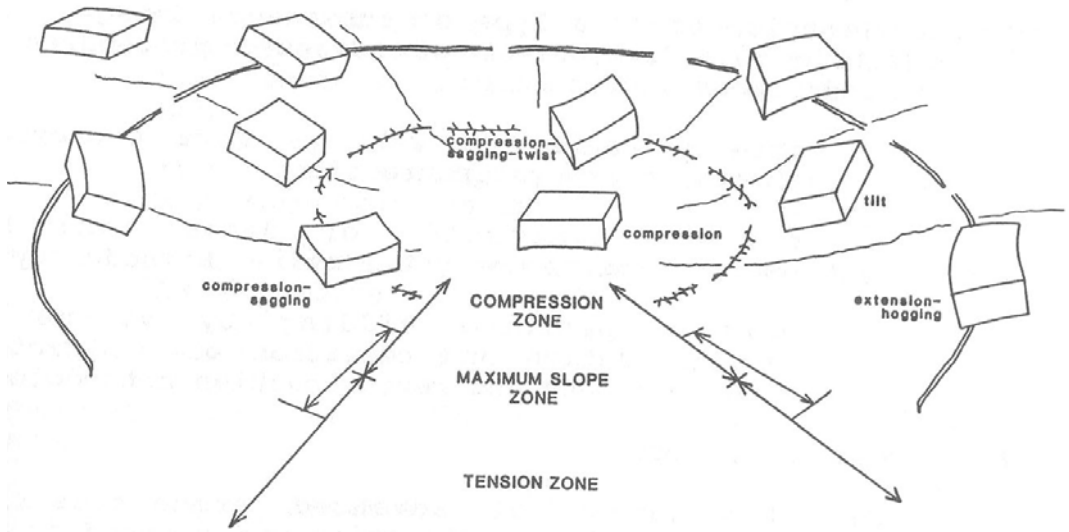

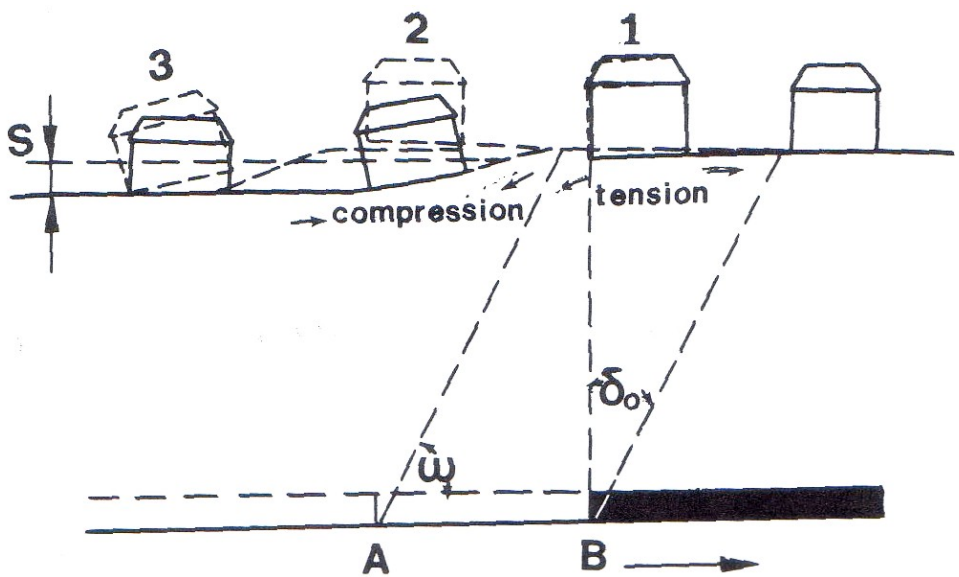

Difference Between a Hazard Map and a Contour Map

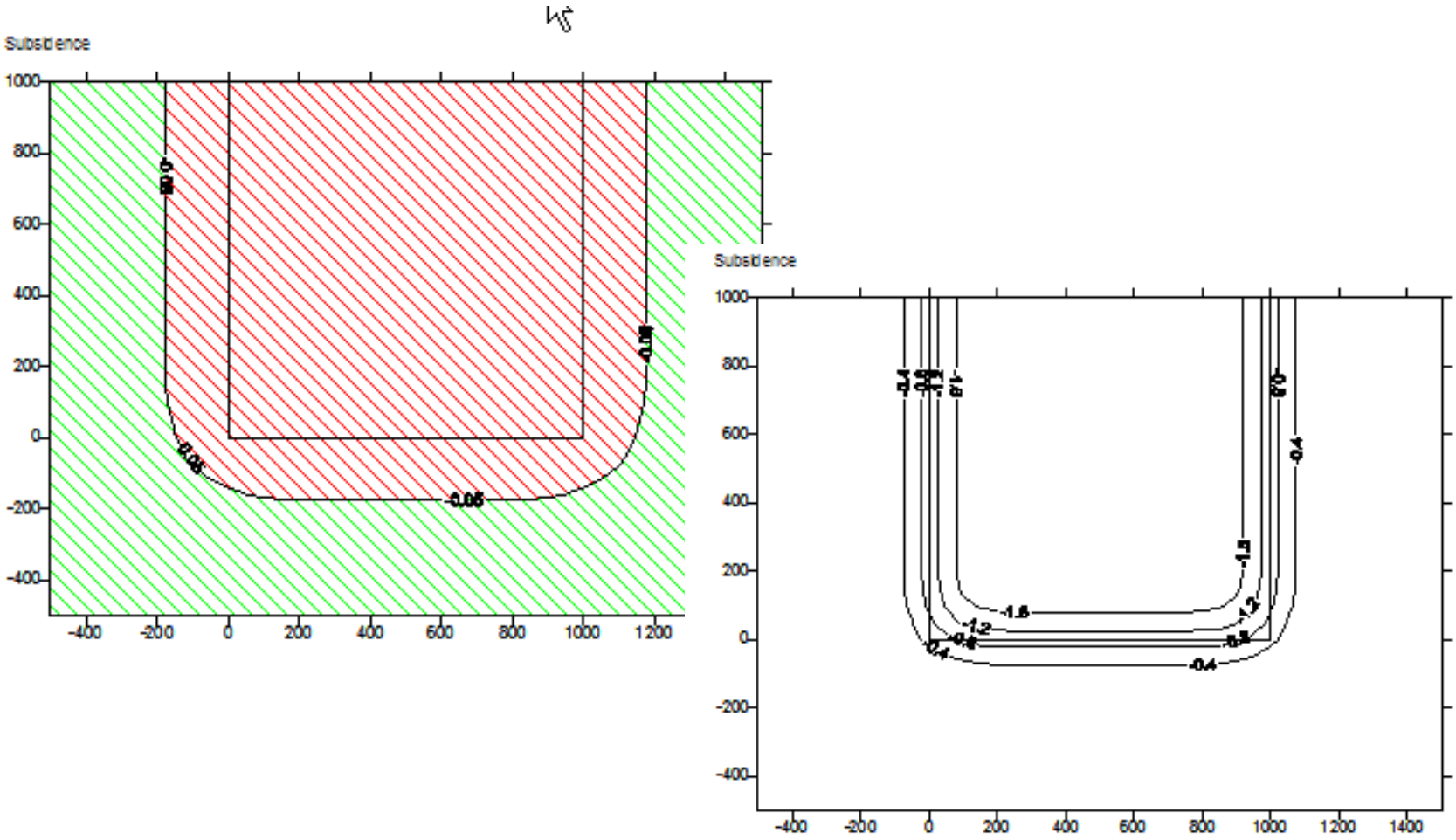

Example of Risk Assessment for Longwall Mine Planning

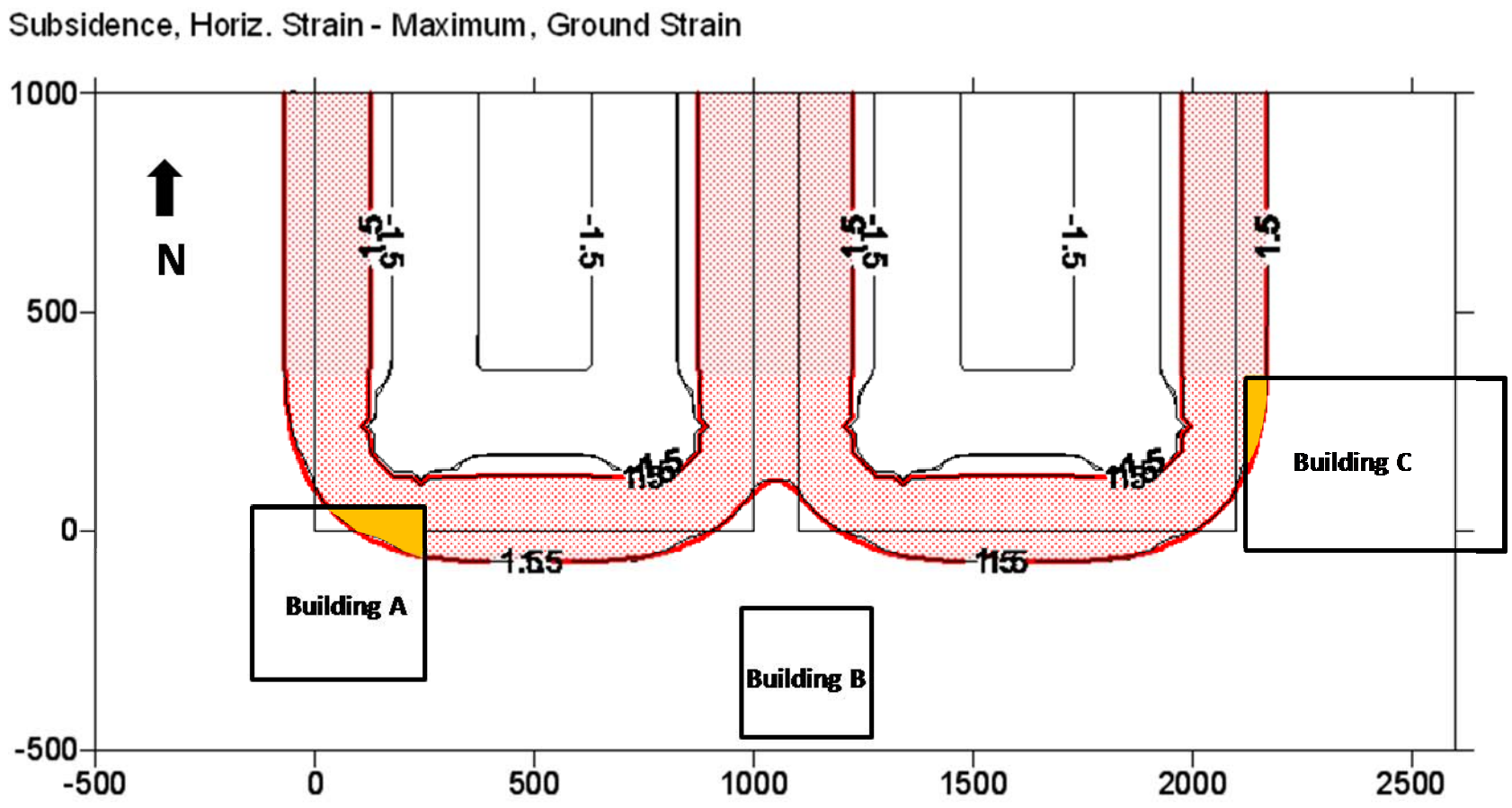

Contoured threshold ground strain values allow for simple risk-based analysis

Prediction of Strain in Steeply-Sloping Terrain – Horizontal Strain

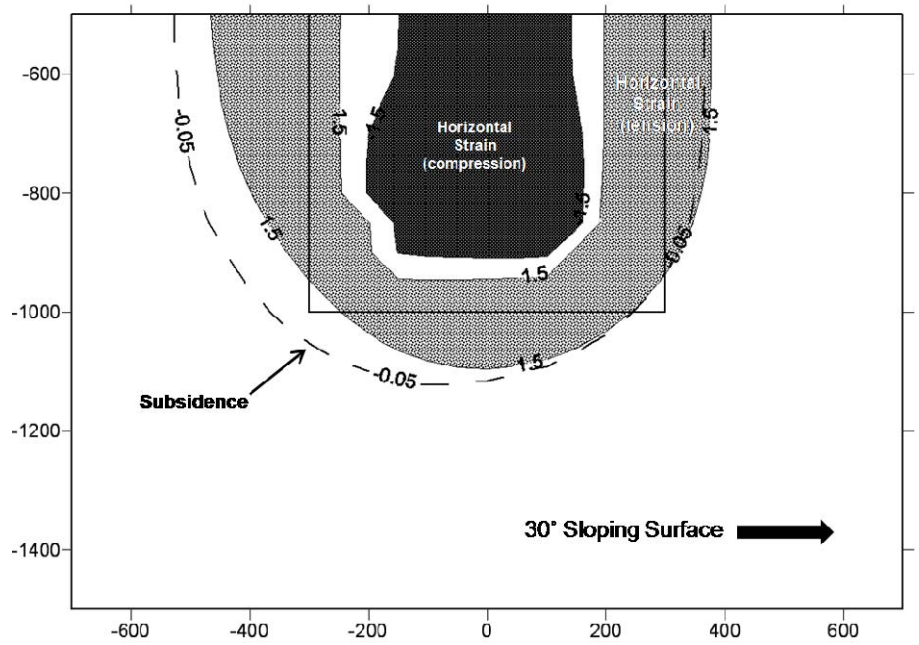

Prediction of Strain in Steeply-Sloping Terrain – Ground Strain

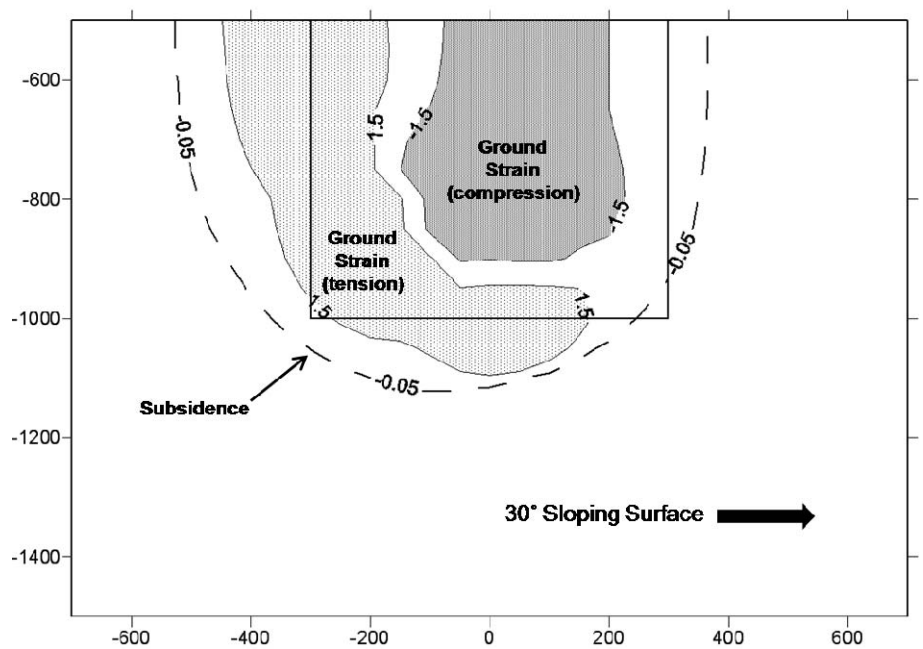

Risk-Based Assessment for Mine Planning

- Edge effect = 140 ft
- Panel Width = 600 ft

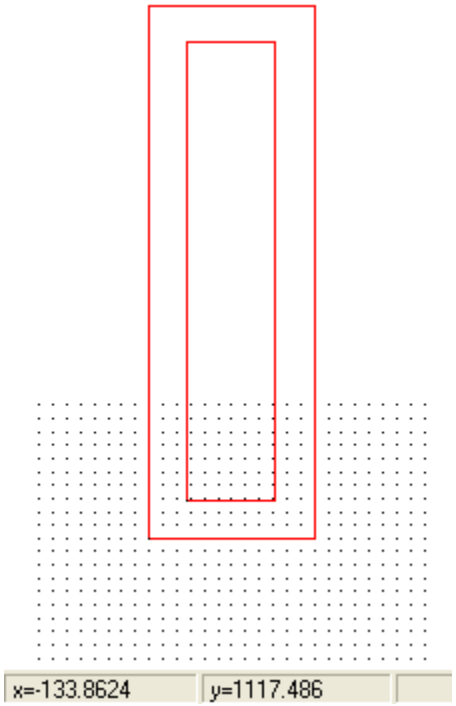

Panel and Points

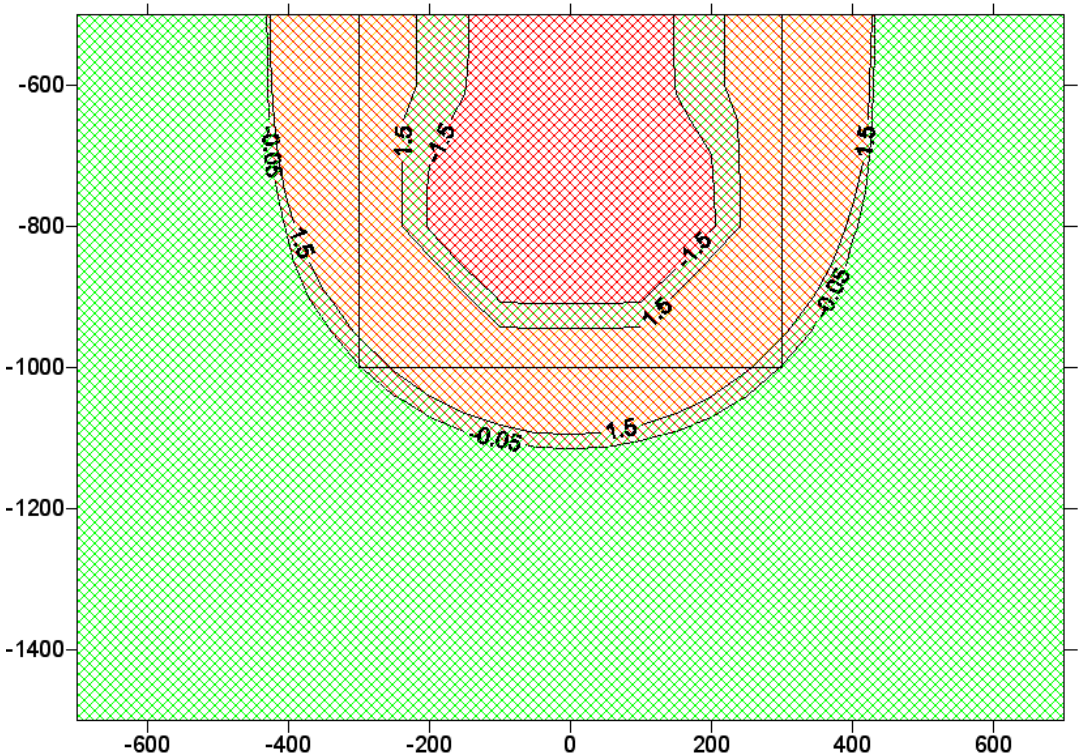

Subsidence and Horizontal Strain Predictions

Example of Risk Assessment for Longwall Mine Planning

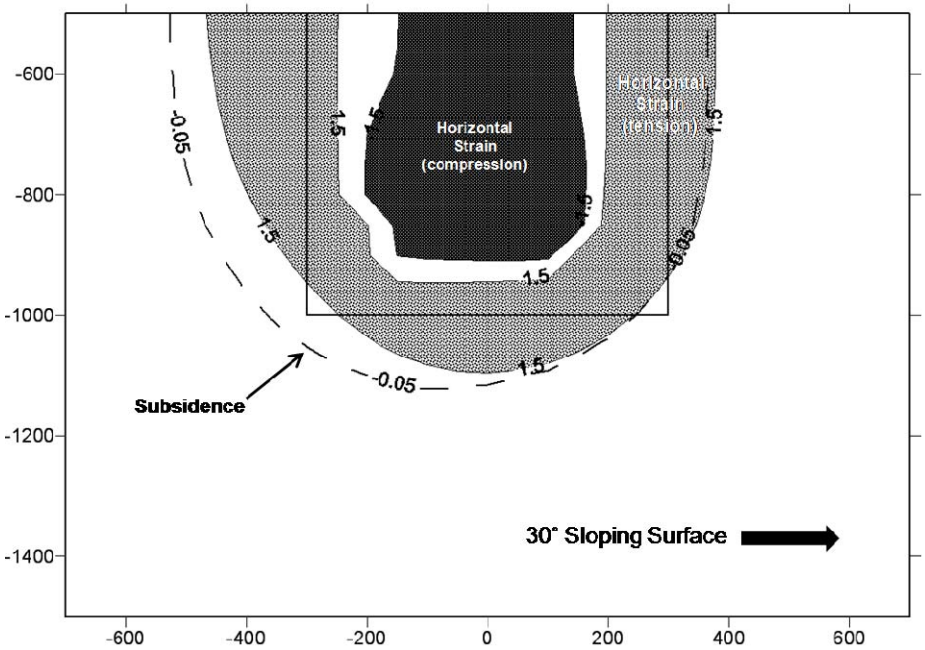

Horizontal strain predictions due to LW mining in 30˚ sloping surface

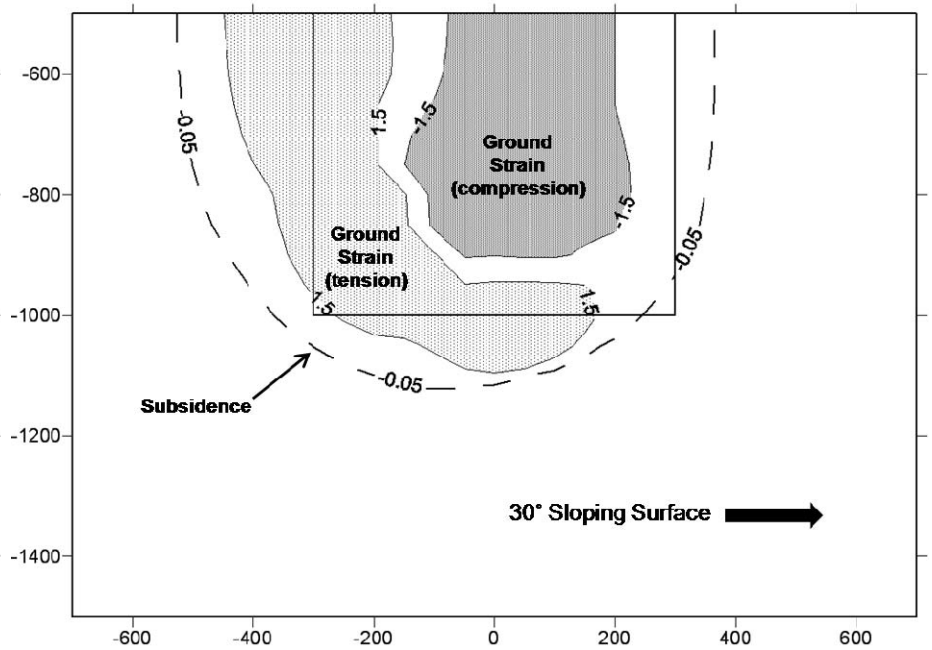

Ground strain predictions due to LW mining in 30˚ sloping surface

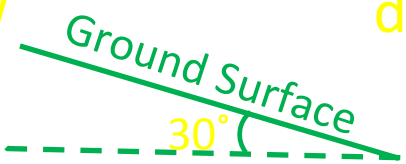

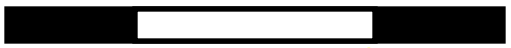

Mine Panel

Risk-Based Assessment for Mine Planning

- Hands on Experience
  - Solution options
  - Threshold limits (user defined and default values)
  - Plot overlays
  - XYZ plots and Grid plots

Risk-Based Assessment for Long-Term Stability

- Assign stability factor to underground workings
- Stability factor applies to pillars
- Stability factor may be arbitrary but consistent in a mineplan.
- Selecting an appropriate index for assessment purposes
- Combine ground deformation prediction with surface damage.

Risk-Based Assessment for Long-Term Stability

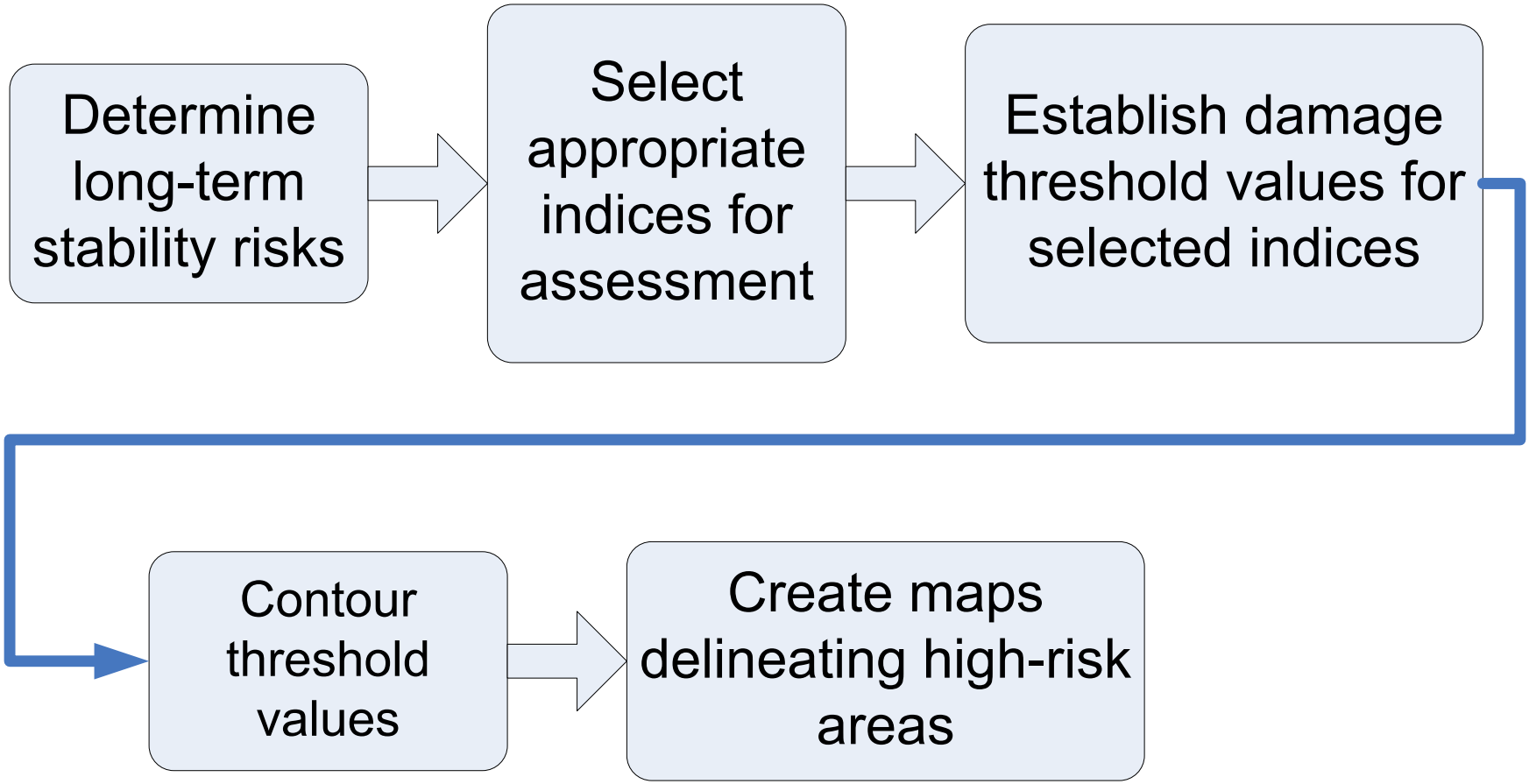

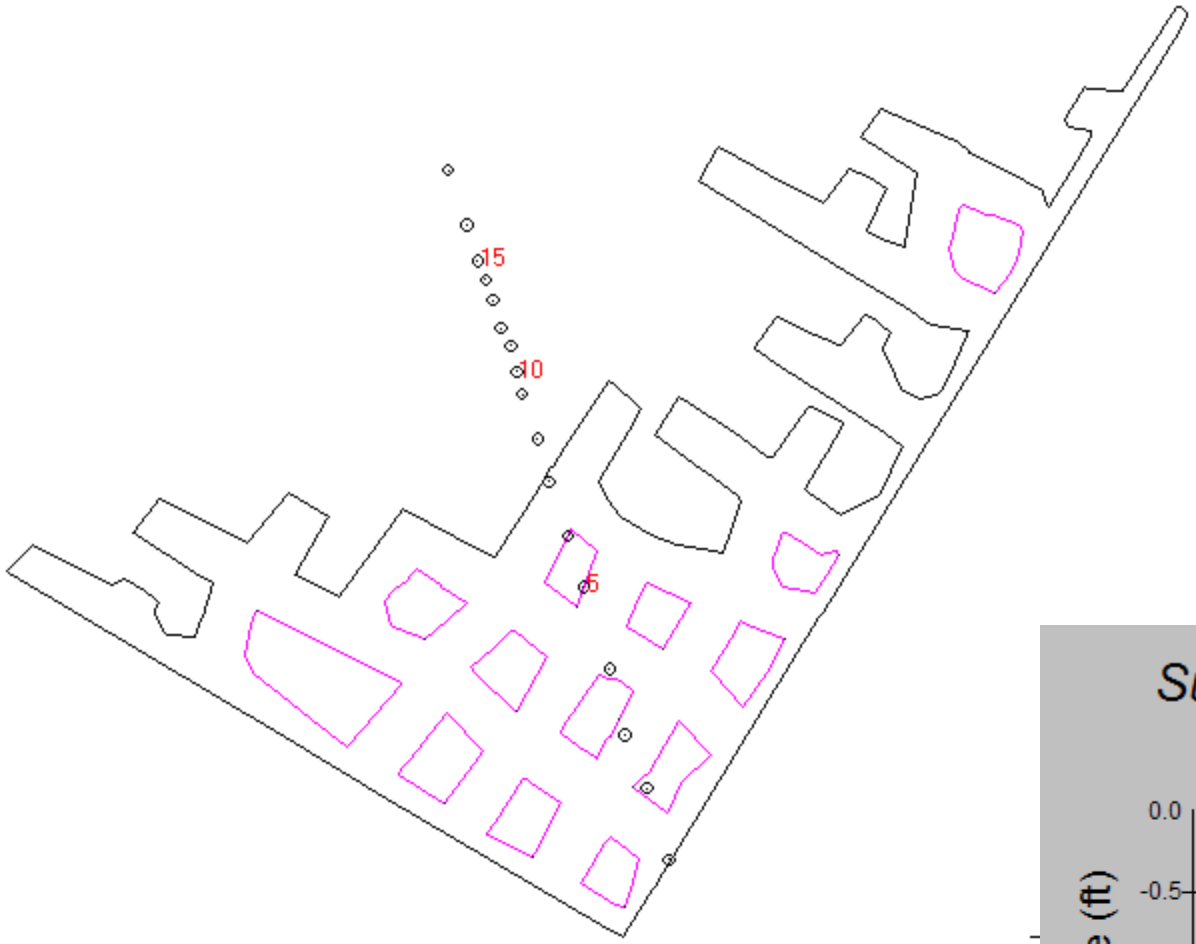

Long-Term Effects for Worst Case Scenario

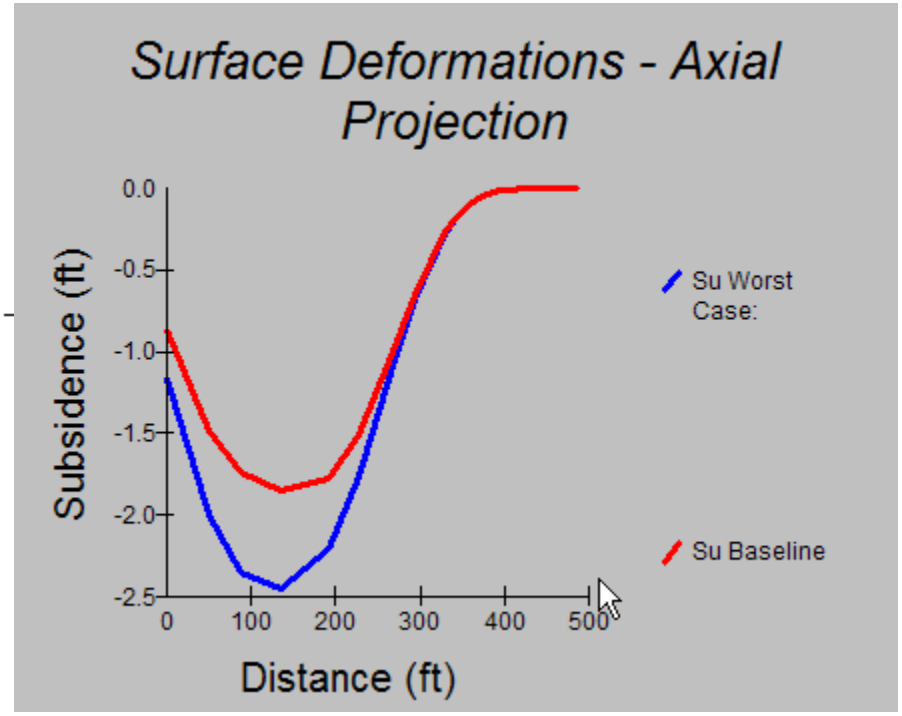

Example of Risk Assessment for Long-Term Stability

Overview of previously mined area and planned landfill development

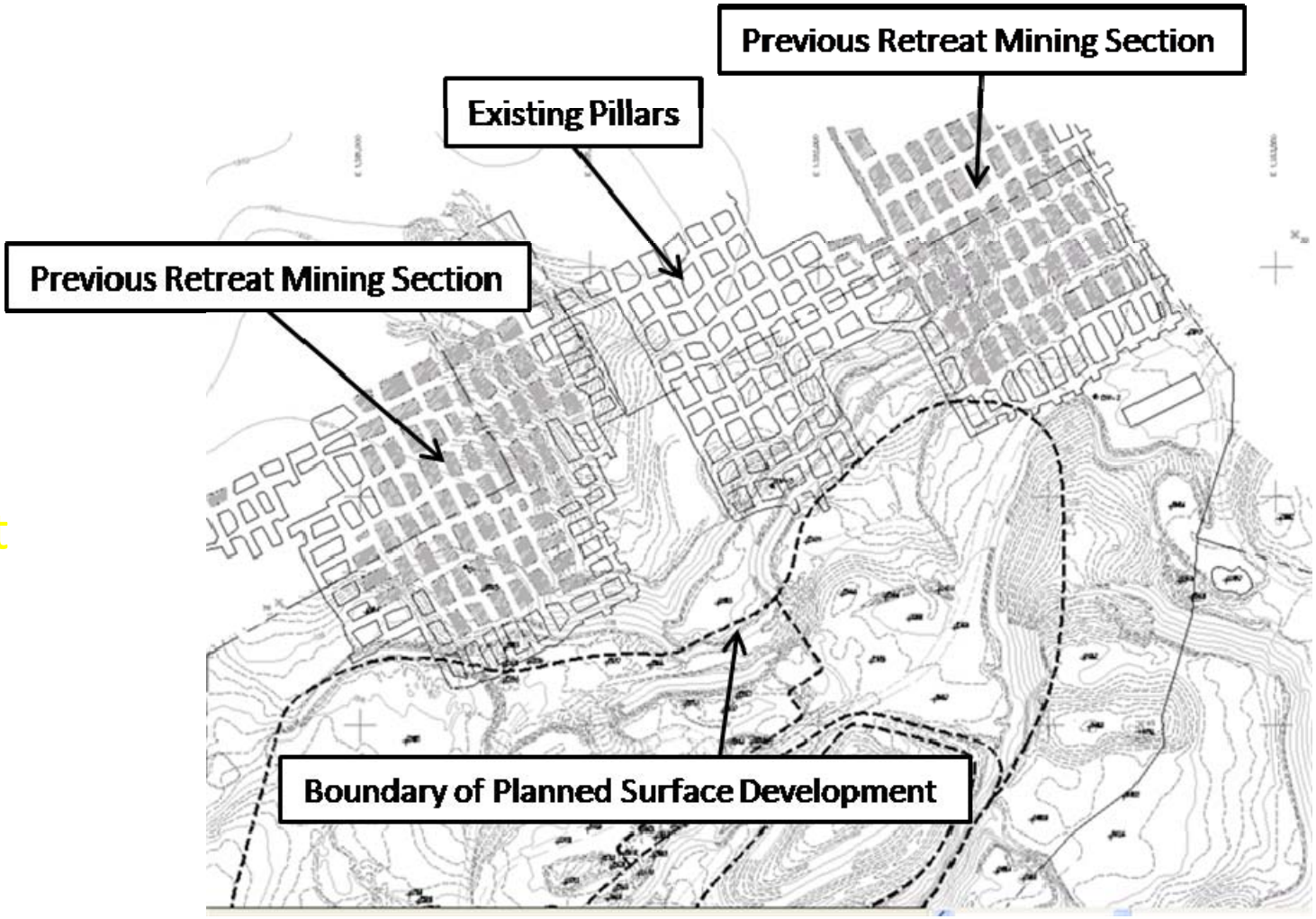

Example of Risk Assessment for Long-Term Stability

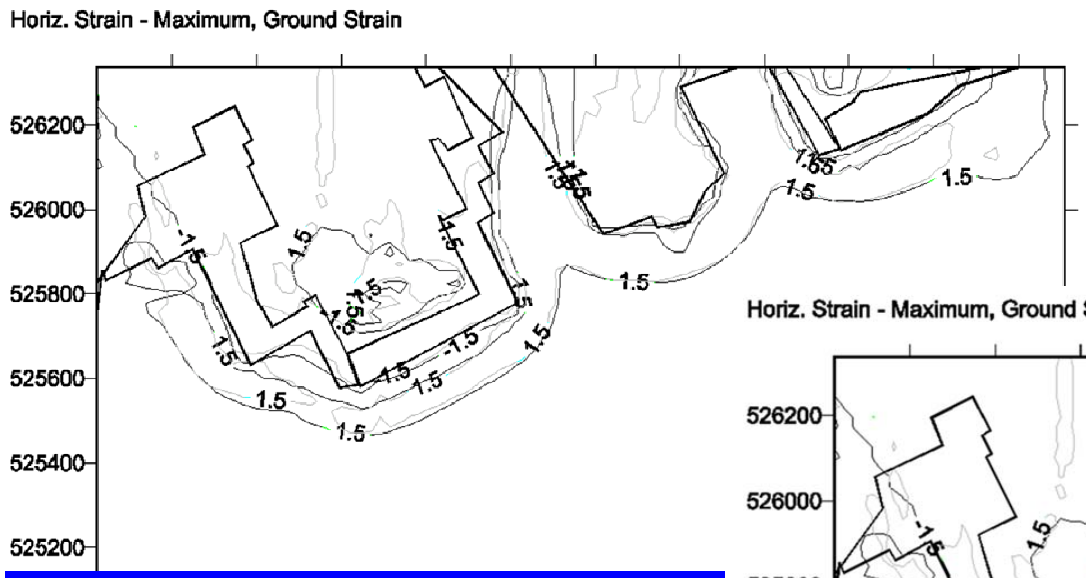

Mine plan with contoured threshold values of horizontal strain and ground strain

Risk assessment map – overlap of threshold strain with planned surface development

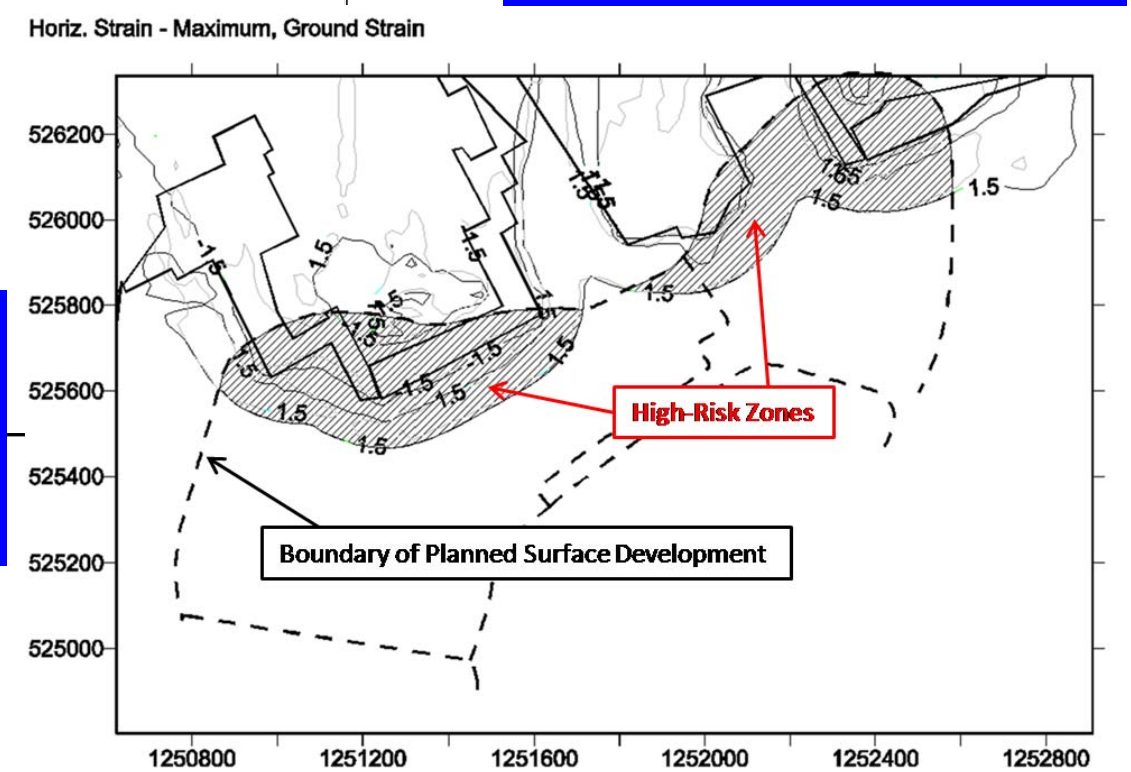

Long-Term Stability Analysis

- Hands on Experience for Long-Term Stability Analysis
  - Stability Factors
  - Solution Options
  - Cross-sectional Plots